Development and Application of Quantitative Liquid Chromatography – Mass Spectrometry Techniques to Facilitate Enhanced Bioprocessing of Therapeutic Proteins

A thesis submitted to Dublin City University for the degree of Ph.D.

By

Amy Farrell BSc. PgDip.

Student Number: 53096777

School of Biotechnology, Faculty of Science and Health

The research described in this thesis was performed under the supervision of

Dr. Jonathan Bones, National Institute for Bioprocessing Research and Training (NIBRT), Co. Dublin and Dr. Niall Barron, School of Biotechnology, DCU.

September 2016

Declaration

I hereby certify that this material, which I now submit for assessment on the programme of study leading to the award of Doctor of Philosophy is entirely my own work, and that I have exercised reasonable care to ensure that the work is original, and does not to the best of my knowledge breach any law of copyright, and has not been taken from the work of others save and to the extent that such work has been cited and acknowledged within the text of my work.

Signed: _____

                   Amy Farrell

Student ID: 53096777

Date: _____

Acknowledgements

First and foremost I would like to express my eternal gratitude to a great supervisor, mentor and friend, Dr. Jonathan Bones. Thank you for entrusting me with this project and for being an endless source of guidance and encouragement, for always having an open door and for saying 'It will be fine!', sorry for having to say it so often! Thanks to both of my co-supervisors, Prof. Ian Marison for your help with the initial stages of the project and to Dr. Niall Barron for all of your advice and assistance.

A huge thank you to all of my NIBRT friends! It has been a pleasure to work with you all. To the research team, thanks for all the coffee, laughs and encouragement that have kept me going over the last four years. Thanks to Brian, Stefan, Csaba and Silvia for all of your analytical-related advice and to Colin, Craig and Krishna in the Bioinformatics team for all of your assistance. I would like to especially thank the training team, past and present, especially Shada, Chris, Gavin, Martin, Stephen and Kate for all of your help with cell culture and bioreactor set-up. Also thanks to my fellow CCL PhD candidates, my weekend companion Josh and neighbour Anne, best of luck!

I am blessed with a wonderful, supportive and encouraging family. Thank you to my brilliant parents, Carmel and Thomas, for years of endless love and reassurance. Thanks to my sisters Lynn and Emily for being best friends as well as sisters and thanks to my big brothers Fergus and Eoin and to my wonderful nephews, Anthony, Luke, Kevin, Aidan and Arthur for always putting a smile on my face.

Thanks to my friends for the little distractions, especially Orla, Ciara and Adrienne. A special thank you to Charissa for inspiring me to start this and for repeatedly telling me it will all come together! Last but by no means least I would like to thank my partner Gary, for all of your love and support and for putting up with my absence and tiredness over the years. This would have been a lot harder with out you. Now that it's done, I can't wait to work on our next project... together! Lots of love xx

Publications and Conference Presentations

Publications

- Farrell, A., McLoughlin, N., Milne, J. J., Marison, I. W., Bones, J., *Application of Multi-Omics Techniques for Bioprocess Design and Optimisation in Chinese Hamster Ovary Cells*. Journal of Proteome Research, 2014. **13**(7): p. 3144-59.

- Farrell, A., Mittermayr, S., Morrissey, B., McLoughlin, N., Navas Iglesias, N., Marison, I. W., Bones, J., *Quantitative Host Cell Protein Analysis using Two Dimensional Data Independent LC-MS^E*. Analytical Chemistry. Submitted Manuscript ID: ac-2015-01377h.

- Millan Martin, S., Delporte, C., Farrell, A., Navas Iglesias, N., McLoughlin, N., Bones, J., *Comparative analysis of monoclonal antibody N-glycosylation using stable isotope labelling and UPLC-fluorescence-MS.* Analyst, 2015. **140**(5): p. 1442-7.

Conference Presentations

- Farrell, A., Bones, J., Host-Cell Protein Analysis of Therapeutic Monoclonal Antibodies Following Protein A Chromatography using Data Independent 2D-LC-MS^E.

  Presented as both an oral and poster presentation at the 11th Symposium on the Practical Applications of Mass Spectrometry in the Biotechnology Industry (CASSS Mass Spec 2014). Napa, California. September 9th to 12th 2014.

- Farrell, A., Mittermayr, S., Morrissey, B., McLoughlin, N., Bones, J., Quantitative Host Cell Protein Analysis using Two Dimensional Data Independent LC-MS^E.

  Presented as a poster presentation at Opportunities in Biopharma Research. NIBRT, 29th September 2015.

- Farrell, A., Scheffler, K., Ho, J., Mowlds, P., Pankert, P., Williamson, A., Cook, K., Bones, J., Application of Quantitative Liquid Chromatography-Mass Spectrometry Techniques to Facilitate Enhanced Bioprocessing of Therapeutic Proteins.

  Accepted: Presentation at the 13th Symposium on the Practical Applications of Mass Spectrometry in the Biotechnology Industry (CASSS Mass Spec 2016) to be held in San Diego, CA, USA from 27th to 30th September 2016.

Awards

- CASSS Travel Reimbursement Grant to facilitate a research presentation at the 11th Symposium on the Practical Applications of Mass Spectrometry in the Biotechnology Industry (CASSS Mass Spec 2014). Napa, California. September 9th to 12th 2014.

- CASSS Travel Reimbursement Grant to facilitate a research presentation at the 13th Symposium on the Practical Applications of Mass Spectrometry in the Biotechnology Industry (CASSS Mass Spec 2014). San Diego, California. September 27th to 30th 2016.

Table of Contents

Abbreviations

2-AA	2-Aminobenzoic Acid
2-AB	2-Aminobenzamide
2D-DIGE	Two-dimensional Difference in Gel Electrophoresis
2-DE	Two-dimensional Gel Electrophoresis
2D-LC-MS	Two-dimensional Liquid Chromatography Mass Spectrometry
ANOVA	Analysis of Variance
Anti-IL8	Anti-interleukin 8
AUC	Analytical Ultracentrifuge
CDR	Complementarity Determining Region
CHO	Chinese Hamster Ovary
CID	Collision Induced Dissociation
CQA	Critical Quality Attribute
DDA	Data Dependent Acquisition
DIA	Data Independent Acquisition
DMSO	Dimethyl Sulfoxide
DNA	Deoxyribonucleic Acid
DO	Dissolved Oxygen
DSP	Downstream Processing
DTT	Dithiothreitol
ELISA	Enzyme-linked Immunosorbent Assay
EPO	Erythropoietin
ESI	Electrospray Ionisation
ETD	Electron Transfer Dissociation
FASP	Filter-aided Sample Preparation
FDA	Food and Drug Administration
FDR	False Discovery Rate
FLR	Fluorescence Detector
FT-ICR	Fourier Transform Ion Cyclotron Resonance
GO	Gene Ontology
GRAVY	Grand Average of Hydropathy
HCD	High Energy Collision Dissociation
HCP	Host Cell Protein
HDX	Hydrogen Deuterium Exchange
HIC	Hydrophobic Interaction Chromatography
HILIC	Hydrophilic Interaction Chromatography
IAA	Iodoacetamide
IEX	Ion Exchange chromatography

IgG	Immunoglobulin G
IL8	Interleukin-8
IMS	Ion Mobility Separation
IPA	Ingenuity Pathway Analysis
iTRAQ	Isobaric Tag for Relative and Absolute Quantitation
LC	Liquid Chromatography
LTQ	Linear Trap Quadrupole Mass Spectrometer
m/z	Mass-to-charge Ratio
MALDI	Matrix Assisted Laser Desorption Ionisation
MS	Mass Spectrometry
MS/MS	Tandem Mass Spectrometry
MWCO	Molecular Weight Cut Off
NMR	Nuclear Magnetic Resonance
PLGS	ProteinLynx Global Server
PTM	Post Translational Modification
QbD	Quality by Design
QLIT	Quadrupole-Linear Ion Trap Mass Spectrometer
qP	Specific Productivity
QQQ	Triple Quadrupole Mass Spectrometer
QTOF	Quadrupole-Time-of-Flight Mass Spectrometer
RNA	Ribonucleic acid
SAX	Strong Anion Exchange
SCX	Strong Cation Exchange
SDS-PAGE	Sodium Dodecyl Sulphate-Polyacrylamide Gel Electrophoresis
SEC	Size Exclusion Chromatography
SELDI	Surface Enhanced Laser Desorption Ionisation
SILAC	Stable Isotope Labelling of Amino Acids in Cell Culture
SPR	Surface Plasmon Resonance
SPS	Synchronous Precursor Selection
SWATH	Sequential Window Acquisition of all Theoretical Spectra
TCEP	Tris(2-carboxyethyl)phosphine
TEAB	Triethylammonium Bicarbonate
Temp.	Temperature
TFA	Trifluoroacetic Acid
TMT	Tandem Mass Tag
TOF	Time-of-Flight
TPP	Trans-Proteomic Pipeline
UPLC	Ultra-high Performance Liquid Chromatography
UV	Ultra-violet

A List of Figures

2.16   Volcano plots showing fold changes plotted against –Log10 of p-values calculated for CHO DP-12 proteins quantified. Significant proteins with fold changes >1.2 and p-value <0.05 are shown in black, green dots represent proteins with p-value >0.05 and >1.2 fold change; blue dots represent proteins with p value >0.05, <1.2 fold change; red dots signify proteins with p value <0.05, <1.2 fold change.

2.17   Volcano plots showing fold changes plotted against –Log10 of p-values calculated for CHO DP-12 proteins quantified. Significant proteins with fold changes >1.2 and p-value <0.05 are shown in blue, red dots represent proteins with p-value >0.05 and >1.2 fold change; green dots represent proteins with p value >0.05, <1.2 fold change; black dots signify proteins with p value <0.05, <1.2 fold change.

2.18   Heat map displaying the top canonical pathways identified for each CHO K1 proteomic sample using IPA. Using IPA, differentially regulated proteins with p values <0.05 and having >1.2 log fold change and associated with different known cellular pathways, were used to identify the top significantly differentially regulated pathways in each of the CHO K1 samples following application of spent media from CHO DP-12 cells cultured under altered bioprocessing conditions.

3.1   Schematic of a mAb, showing sites of potential sequence modifications denoted by symbols outlined in the corresponding legend. The number of modification sites for each half antibody multiplied by the number of possible variations at each site is shown in the parenthesis. Assuming variants on each side of the antibody are independent, each mAb has 10^8 potential variations.

3.2   Chromatograms corresponding to triplicate SCX-UV analysis of **A.** anti-IL8 produced at 39.5°C, **B.** anti-IL8 produced at 32.0°C, **C.** anti-IL8 produced using 110% DO media content. Sample separation was performed using a MAbPac SCX-10 RS analytical column, 5 µm, 2.1 x 50mm, on a Vanquish Flex UHPLC using a diode array detector at 280 nm. Data was acquired using Chromeleon version 7.2 software; peak areas were integrated manually.

3.3   Chromatograms corresponding to SCX-UV analysis (n=3) of **A.** anti-IL8 produced using 60% DO media content, **B.** mAb produced at pH 7.2, **C.** mAb produced at pH 6.8. Sample separation was performed using a MAbPac SCX-10 RS analytical column, 5 µm, 2.1 x 50mm, on a Vanquish Flex UHPLC using a diode array detector at 280 nm. Data was acquired using Chromeleon version 7.2 software; peak areas were integrated manually.

3.4   Chromatograms corresponding to HIC-UV analysis (n=3) of **A.** anti-IL8 produced at 39.5°C, **B.** anti-IL8 produced at 32.0°C, **C.** anti-IL8 produced using 110% DO media content. Sample separation was performed using a MAbPac SEC-1 analytical column, 5 µm, 4.0 x 300mm, on a Vanquish Flex UHPLC using a diode array detector at 280 nm. Data was acquired using Chromeleon version 7.2 software; peak areas were integrated manually.

A List of Tables

Abstract

Title: Development and Application of Quantitative Liquid Chromatography – Mass Spectrometry Techniques to Facilitate Enhanced Bioprocessing of Therapeutic Proteins

Candidate: Amy Farrell

Biopharmaceutical manufacturing is currently the principal growth sector within the pharmaceutical industry. Predominantly formed in mammalian cells, these therapeutic proteins exist as a spectrum of different isoforms and hence pose a unique set of challenges that must be addressed to ensure optimum product quality. To better understand whether the product really is the process, quantitative peptide centred multidimensional liquid chromatography tandem mass spectrometry (LC-MS) based proteomics studies were performed using a Chinese Hamster Ovary (CHO) cell line that expressed an anti-Interleukin-8 IgG1 monoclonal antibody (mAb). Following serum free suspension batch culture under varied bioprocess conditions, quantitative proteomics was completed on the producer CHO cells to elucidate the cellular response to altered culture conditions of pH, temperature and dissolved oxygen. The developed platform was also applied for the analysis of naïve CHO K1 cells following their exposure to spent culture media from the various production runs. Complete characterisation of the expressed mAb was performed, using advanced LC-MS methods including high resolution middle down mass spectrometry; intact protein analysis of critical quality attributes, stable isotope based quantitative glycan analysis and hydrogen deuterium exchange mass spectrometry for structural comparability analysis. In addition data independent LC-MS quantitative proteomics of residual host cell protein impurities was also carried out to evaluate the effect of downstream processing on the quality of the final drug substance. Combined, the findings herein provide a holistic insight into the effect of various upstream and downstream parameters on the quality of therapeutic proteins and facilitate a greater understanding of the molecular mechanisms governing biopharmaceutical production systems, thereby creating a hypothesis for improved future cell line development using various engineering strategies.

1.0

A Review of Analytical Technologies used for Quantitative CHO Cell Proteomics

1.1   Introduction

Chinese hamster ovary (CHO) cell lines are currently the dominant expression system for biotherapeutic proteins produced in mammalian cell lines and are utilised in the production of six of the top ten-selling biopharmaceutical products.[1] CHO cells lines are widely used due to their ability to facilitate correct protein folding and human-like post-translational modifications (*e.g.* glycosylation) of recombinant therapeutic proteins. In addition, CHO cell lines are amenable to serum-free suspension cultivation and are readily adaptable to different media compositions, both critical features for protein production in large-scale bioreactors. Since regulatory approval for the first therapeutic protein, which was produced in a CHO cell line, was achieved, considerable efforts have been made to improve recombinant protein production. Initially the bulk of research was focused on increasing productivity and therapeutic protein quality by altering various bioprocessing parameters. More recently, advances in analytical instrumentation have enabled a deeper understanding of the cellular-level mechanisms that effect protein production in these important cell lines. In particular developments in liquid chromatography (LC) and mass spectrometry (MS) have facilitated the emergence of 'omics' tools which have allowed us to gain a depth of understanding of CHO cell proteomes, the functional units of the cell, that previously had not been possible.

Mass spectrometry coupled with technologies for sample preparation and separation, along with data analysis software for protein identification and quantitation, provide a powerful platform for analysis of proteomes from biologically relevant samples. Traditionally, CHO proteomics was driven by research using two-dimensional gel electrophoresis combined with mass spectrometry. The majority of these studies consisted of separation and isolation of proteins in gel 'spots' and ionisation and detection of peptides using matrix-assisted laser desorption ionisation – Time of flight (MALDI-ToF) mass spectrometry. More recently, major advances in gel-free peptide separation technologies, mass spectrometry and bioinformatics, augmented by the CHO genomic revolution have allowed LC-based proteomics to flourish.

Two-dimensional liquid chromatography coupled to mass spectrometry (2D-LC-MS) now routinely facilitates the identification of thousands of proteins from complex samples.

Due to improvements in MS and bioinformatics, comprehensive characterisation and quantification of proteins within biologically relevant samples using quantitative proteomics is now achievable, enabling the classification of CHO cell proteins that play key roles in recombinant protein production, including those involved in growth, metabolism, protein processing, glycosylation and cell death.[2] Hence, knowledge gained through CHO cell proteomics have the potential to lead to further advances in therapeutic protein production in CHO cells, including improved media and bioprocess development, advanced elimination of bioprocess impurities, characterisation of critical quality attributes and by identifying features that lead to desired phenotypes for biopharmaceutical production of therapeutic proteins. [3]

In Chapter 1, analytical technologies that are currently applied for proteomic profiling of CHO cell line behaviour and characterisation of therapeutic proteins will be discussed. A particular focus is applied to LC-MS separation and detection strategies and related quantitative and bioinformatics tools. Subsequently, a review of the application of these techniques to better understand the CHO cell proteome will be outlined.

1.2   Sample Preparation for Proteome Analysis

Two typical proteomics approaches are used for analysis of large biomolecules by mass spectrometry; these are 'Top-down' and 'Bottom-up' approaches. In a bottom-up strategy, specific peptide bonds are cleaved to produce peptides composed typically of <20 amino acid residues, which are subsequently analysed using a mass spectrometer. Conversely, in a top-down experiment, the complete undigested protein is analysed. In proteomics, the former approach is most frequently used as mass spectrometers are more efficient in deriving sequence information from peptides rather than whole proteins. [4]

Traditionally, a bottom-up proteomic strategy consisted of 'in-gel' digestion, in which proteins were denatured and separated using sodium dodecyl sulphate – polyacrylamide gel electrophoresis (SDS-PAGE), followed by visualisation of proteins in a gel and excising of protein-containing gel plugs before reduction, alkylation, digestion and extraction from the gel matrix for MS analysis. [5] Alternatively 'in-solution digestion' was developed wherein direct solubilisation and denaturation of proteins in a digestion buffer was followed by disulphide reduction and alkylation of free sulfhydryl groups on cysteine residues before digestion with

an endoproteinase. Both 'in-gel' and 'in-solution' sample preparation methods have various advantages and drawbacks, as outlined in Table 1.1.

Table 1.1: Advantages and disadvantages associated with in-gel and in-solution digestion of proteomic samples. [6]

In-gel digestion	Advantages	• Visual indication of relative abundance or proteins in a sample • Robustness against impurities interfering with digestion • Universal solubilisation of proteome using SDS
	Disadvantages	• Proteins trapped in a gel may be inaccessible to digest reagent • Peptide recovery may be hampered by gel matrix
In-solution digestion	Advantages	• No detergents needed • Minimal sample handling • Rapid sample preparation • Easily automated • Reduced sample requirement
	Disadvantages	• Digestion may be inhibited by interfering substances • Risk of incomplete solubilisation of proteome (*e.g.* membrane proteins)

In order to overcome limitations associated with the sample preparation methods outlined, Mann and colleagues developed an alternative method for proteome sample preparation that reportedly combined the advantages of both 'in-gel' and 'in-solution' digestion approaches, known as filter-aided sample preparation (FASP). [7] Using FASP, solubilisation of proteins is achieved using SDS before application of the entire protein sample to a filtration device. The filtration device then serves as a vessel for detergent removal, buffer exchange, reduction and alkylation of proteins and finally protein digestion in solution. FASP therefore combines the solubilisation efficiency of in-gel digestion with the digestion efficiency of in-solution digestion methods.

Several enzymes are available for protein digestion in bottom-up proteomics, however the most commonly used protease in proteomics is Trypsin. Trypsin has a well-defined specificity, hydrolysing only the peptide bonds in which a carbonyl group is followed by either arginine (R) or lysine (K) (except when R or K is N-linked to an aspartic acid residue). Due to the frequency of R and K residues within the proteome, Trypsin generates peptides with the preferred mass range for MS sequencing. [8] Additionally, tryptic peptides terminating in basic R and K

residues form prominent, easily detectable fragment ions. [9] In some instances, additional digestions are required for optimal proteomic sample preparation. The endoprotease Lys-C is often used prior to trypsin digestion producing larger peptide fragments than trypsinization. [10] Similarly, proteases such as Asp-N and Glu-C, may be used to produce peptides complementary to tryptic peptides for MS analysis. [4]

1.3   Separation Technologies

Two-dimensional gel electrophoresis (2-DE) has traditionally been the workhorse for proteomics, facilitating the separation of proteins based on differences in protein size and net charge at different pH values. Although 2-DE is renowned for its excellent resolving power, it has a number of limitations including poor reproducibility, co-migration of proteins, poor representation of low abundant, highly acidic or highly basic proteins and difficulty in automation. [11] To overcome low reproducibility in 2-DE, two-dimensional differential in-gel electrophoresis (2D-DIGE) was developed, allowing for differentially labelled samples to be separated and visualised on the same 2D gel. [12] However like 2-DE, 2D-DIGE is cumbersome and is limited by dynamic range for protein separation. Due to advances in ionisation techniques for mass spectrometry, liquid chromatography has emerged as a leading technique for proteomic separations over the last decade. Reversed phase (RP) chromatography, in which analytes are partitioned based on their interaction with a hydrophobic stationary phase while being carried in a polar hydrophilic mobile phase with increasing organic modifier content, is the most widely used gel-free chromatography method for proteomic sample preparation. [13] Like gel separation technologies, LC approaches often use a two dimensional (2D) separation strategy to ensure sufficient separation of peptides or proteins for detection. Use of orthogonal separation methods permits the resolution of peptides in highly complex samples on the basis of different physiochemical properties, thereby increasing overall peak capacity. [13] Frequently, orthogonal 2D-LC configurations consist of RP, [14] strong cation exchange (SCX), [15] strong anion exchange (SAX), [16] hydrophilic interactions chromatography (HILIC) [17] and other specific chemistries in the first dimension, coupled to RP-nano-LC in the second dimension. The use of nano-LC directly interfaced with MS was of great significance in regards to advances in proteomic analysis, as a reduction in internal diameter of analytical separation columns enabled increased separation efficiency, reduced solvent consumption, smaller sample requirements and ease of coupling to a mass spectrometer. [18] Furthermore, nano-LC systems incorporating split-less pumps ensure a

continuous flow required for electrospray ionisation (ESI) and hence are becoming a mainstay of proteomics research. [19]

1.4   Detection by Mass Spectrometry

MS detection has become a key enabler of in-depth proteomics over the last two decades, resulting from major advancements in mass spectrometry. A mass spectrometer measures the mass-to-charge (m/z) ratio of gas-phase ions, typically consisting of an ion source, for the production of gaseous ions from a sample; a minimum of one mass analyser, for separation of ions based on their m/z ratios and a detector to record ion data. The MS platform is completed by an inlet feature for introduction of sample into the ion source and a computer to process sample information and generate mass spectra.

1.4.1   Ionisation of Biomolecules

The application of MS to the analysis of biomolecules and emergence as an indispensable tool for protein analysis was facilitated by the development of 'soft ionisation' techniques, *e.g.* MALDI or ESI. Proteins and peptides are non-volatile, polar and thermally labile species that, for MS analysis, require an ionisation technique to transfer the analyte to gas phase without resulting in over fragmentation or extensive degradation of the biomolecule. [20] MALDI, classically used in combination with gel-separation strategies, is particularly applicable to top-down analysis of high molecular weight proteins in simple sample mixtures as it predominantly generates singly-charged ions. However, MALDI-associated drawbacks include poor shot-to-shot reproducibility, potential signal suppression, limited detectable mass range and reliance on efficient sample preparation techniques. [20, 21] Due to recent analytical technological advances, LC-ESI-MS capabilities now far surpass those of gel-based MALDI-MS techniques.

The concept of ESI, visualised in Figure 1.1-A, was developed by Fenn *et al.* in 1984 for the MS analysis of biological macromolecules. [22] During ESI, proteins or peptides in solution are pumped through a metal capillary maintained at a high voltage (2-6 kV) and nebulised at the tip of the capillary to produce a fine spray of charged droplets. The charged droplets strongly repel each other to form a conical shape known as a 'Taylor cone' and are quickly evaporated following the application of heat and a nebulising gas. [23] The reduction in droplet size results in a build-up of ions of one polarity on the surface of the drop and, at the point when the

forces of electrostatic repulsion are greater than the surface tension (*i.e.* the 'Rayleigh limit') the droplet explodes, culminating in the production of gas phase ions. The ions are then subsequently transferred into the mass spectrometer. [23, 24]
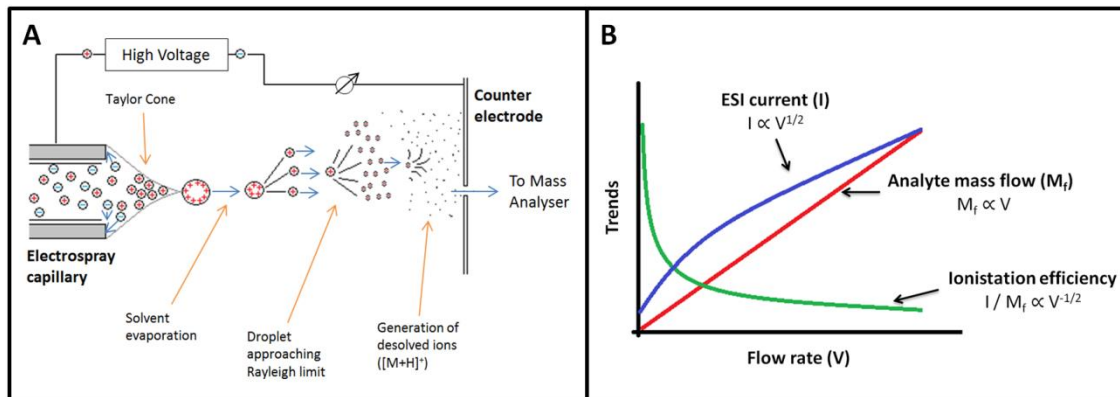
Figure 1.1: A. Schematic diagram of electrospray ionisation process. [25] **B.** The relationship between ionisation efficiency and flow rate. ESI current is directly proportional to the square root of the flow rate (V) while the analyte mass flow (M_f) is directly proportional to V. Hence, the ionisation efficiency (*i.e.* the ratio of the ESI current and mass flow rate) is proportional to the inverse square root of V resulting in a dramatic improvement in ionisation efficiency at very low flow rates. [26, 27]

ESI has a number of advantages rendering the technique particularly suitable for the analysis of biomolecules. Significantly, ESI is carried out at close to ambient temperatures, and hence thermally labile, polar molecules such as proteins and peptides may be ionised without decomposition. In addition as the ions are produced in solution, analytes with several ionisable sites may produce multiply-charged species, successfully extending the effective mass range of the instrument. [23] However, conventional ESI was greatly affected by fluctuation in flow rate and due to the size of the droplets emerging from the ESI capillary and requirement for nebulising gas, only a small portion of the sample is transferred into the mass analyser, as is shown in Figure 1.1-A.

ESI-associated caveats were addressed by Wilm and Mann, when they first described their innovative nano-electrospray ion (nanoESI) source. [28] Wilm and Mann used glass capillaries pulled into sharp tips with a 1-2 µm spraying orifice to reduce the size of droplets formed at the tip of the capillary. Since droplets produced in the nanoESI source are relatively small and have high surface-to-volume ratios, a desolvation gas is not required for solvent evaporation.

[29] Additionally, the small droplet size has resulted in an increased tolerance of buffer salts and other impurities. Use of capillaries with a small spraying orifice also facilitated low flow rates (20 nL.min⁻¹) resulting in increased ionisation efficiency as depicted in Figure 1.1-B. Furthermore, the use of low flow rates permits the positioning of the nanoESI capillary close to the MS inlet orifice, resulting in increased ion transmission in comparison to conventional ESI. Ultimately the use of a nano-scale ESI source resulted in a reportedly 100-fold improvement in ionisation efficiency enabling high sensitivity analysis while using low sample amounts.

Initial use of nanoESI instrumentation involved placing sample into a needle and spraying the sample into the MS inlet. Although this resulted in an increase in overall ionisation efficiency, the absence of analytical separation made manipulation of the ion within the mass spectrometer difficult for MS/MS analysis. Fortuitously, the development of nanoESI coincided with progress in the miniaturisation of LC systems. The suitability of nanoESI for coupling to liquid separation techniques and the development of nano-LC pumps facilitating low flow rates have resulted in greatly advanced separation of peptide ion peaks and hence superior proteome coverage when coupled to mass spectrometers. Due to ease of automation and successful application to highly complex protein samples, integrated nano-LC-ESI-MS systems are now extensively applied in the field of proteomics research.

1.4.2 Mass Analyser Configuration for Quantitative Proteomics and Product Characterisation
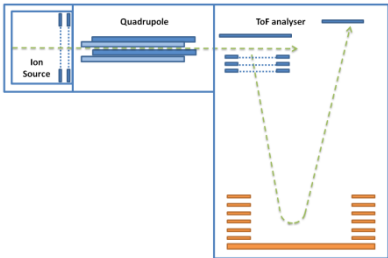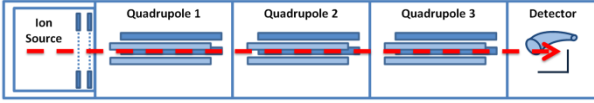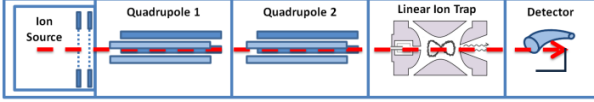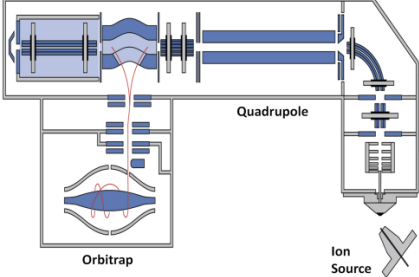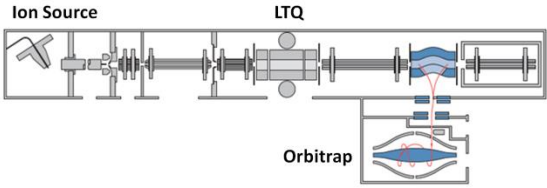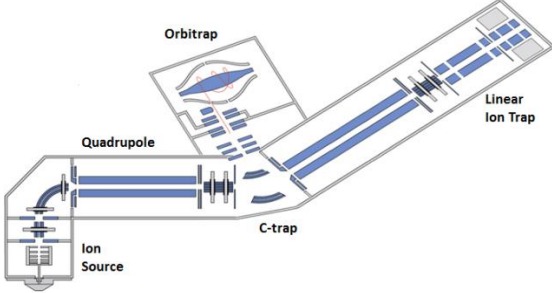
As peptides typically have multiple charge states (z = 2, 3, 4), the ability of the mass analyser to resolve ions with minute differences in m/z is critical for accurate identification of protein and peptide species. Hence, many of the advancements in mass spectrometry in recent years have focused on increasing the resolving power of the mass analyser. Several mass analysers are available, including the first generation low resolution (<10,000) quadrupole, time-of-flight and ion trap mass analysers. However in recent years proteomics has been almost exclusively performed on high resolution hybrid instruments due to their capabilities for high mass accuracy, resolution, sensitivity and extended mass range. Table 1.2 depicts a number of available hybrid instruments, which usually incorporate two or more mass analysers. In these instruments ions from an ion source are focused and transmitted using a quadrupole or linear ion trap and separated and analysed using a ToF, fourier transform ion cyclotron resonance (FT-ICR) or Orbitrap analyser, thereby combining the advantages of each individual mass

analyser. The power of these hybrid instruments is most notably reflected when operated in tandem MS mode, as will be discussed in section 1.4.3.

Due to high resolution and broad mass range capabilities, in addition to more favourable start-up costs in comparison to alternative high resolution instruments, the quadrupole time-of-flight (QToF) mass spectrometer has been widely applied for the identification of CHO cell proteins. A QToF consists of a quadrupole, which serves to selectively transmit ions according to their mass to charge (m/z) ratios by varying the RF potential applied to four parallel poles, into a time-of-flight mass analyser. Ions are then directed towards a detector and measured according to the time taken to move through a field-free region between the inlet and the detector.

High resolution instruments incorporating an Orbitrap mass analyser are capable of achieving the greatest resolving power when compared to other hybrid mass spectrometers. Pioneered by Makarov *et al.*, the Orbitrap is an ion trap mass analyser composed of an outer barrel-like electrode encasing a co-axial spindle-like electrode, which traps ions in an orbital motion. An ion's *m/z* ratio is measured from the frequency of harmonic oscillations undertaken by orbitally trapped ions along the axis of the electric field. [30] In-depth proteomics utilising Orbitrap-containing hybrid MS routinely lead to the identification of >4,000 proteins in a single MS analysis. [31] The concept of hybrid MS has been further expanded by the development of a tribrid MS incorporating three mass analysers (*i.e.* a quadrupole mass filter, an ultra-high field Orbitrap analyser and a dual pressure linear ion trap analyser (Table 1.2). This instrument has significantly improved capabilities for quantitative proteomics as will be discussed in Section 1.6.

Table 1.2: Common hybrid mass spectrometers used in proteomics. [32-35]

Instrument Type	Schematic of MS	Typical Specifications
QTof *e.g.* Waters Xevo G2 QToF		Resolution: 0.04 Δm/z Mass accuracy: <1 ppm m/z range: 50-20,000
QQQ *e.g.* Agilent 6460		Resolution: 0.4 Δm/z Mass accuracy: 5 ppm m/z range: 10-3000
Q-LIT *e.g.* AB SCIEX QTRAP 5500		Resolution: 0.1 Δm/z m/z range: 5-1250
Q-Orbitrap *e.g.* Thermo Fisher Scientific Q Exactive		Resolution: 0.001 Δm/z Mass accuracy: <1 ppm m/z range: 50-4000
LTQ-Orbitrap *e.g.* Thermo Fisher Scientific Orbitrap Elite		Resolution: 0.002 Δm/z Mass accuracy: <1 ppm m/z range: 50-4000
Q-LIT-Orbitrap e.g. Thermo Fisher Scientific Orbitrap Fusion Lumos Tribrid		Resolution: 0.0004 Δm/z Mass accuracy: <1 ppm m/z range: 50-6000

1.4.3   Tandem Mass Spectrometry

Identification of proteins following MS analysis was traditionally achieved using peptide mass fingerprinting, a technique whereby a peptide mass profile detected by MS analysis is compared with all predicted peptide digests in a database of known proteins, to identify the best possible protein match. [36] This method however is not suitable for the analysis of complex protein samples, as frequently common peptide sequences will exist across multiple proteins. The requirement for additional identification methods for analysis of protein mixtures led to the development of tandem MS; (MS/MS), facilitated by the construction of hybrid or tandem mass spectrometers combining two or more mass analysers (section 1.4.2). In MS/MS instrumentation, a single (precursor) ion is selected in the first mass analyser and subsequently fragmented to produce fragment (product) ions which are separated in the second mass analyser according to their mass. Resulting MS/MS spectra consist only of product ions from the selected precursor ion as displayed in Figure 1.2. The mass difference between peaks in the MS/MS spectrum may be correlated to the mass of an amino acid, hence the amino acid sequence of the peptide may be deduced.
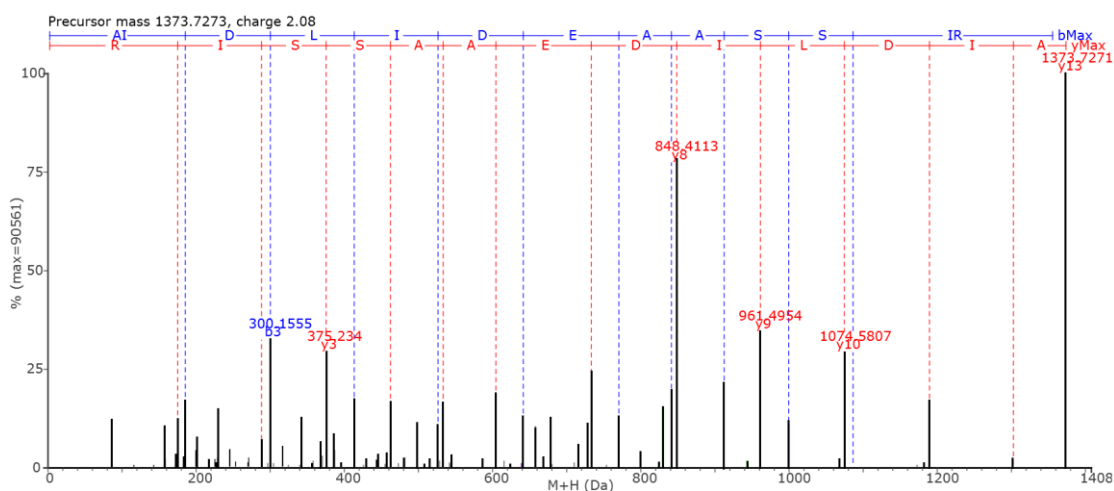
Figure 1.2: MS/MS spectrum generated from tryptic peptide AIDLIDEAASSIR from the *E. coli* protein chaperone ClpB (Hi3 *E. coli* standard peptides purchased from Waters (Dublin, Ireland)). Data was acquired using a Waters Xevo G2 QTof coupled to a Waters nanoAcquity UPLC system equipped with a nanoAcquity UPLC 2G-V/M Trap 5 µm symmetry C18, 180 µm x 20 mm trapping column and a nanoAcquity UPLC 1.8 µm HSS T3, 75 µm x 200 mm analytical column.

Several methods exist for peptide fragmentation; however those most commonly used for proteomics are collision-induced dissociation (CID), electron transfer dissociation (ETD) and high energy collision dissociation (HCD). In CID, peptides are allowed to collide with gas molecules (typically helium, nitrogen or argon), resulting in vibrational excitement of the molecule and subsequent dissociation of the peptide backbone amide bonds located between carbonyl and amide groups. As depicted in Figure 1.3, resulting fragment ions are termed b-ions if they retain the N-terminal part of the peptide or y-ions if they contain the C-terminal portion of the peptide. In addition a-ions may also be formed due to loss of a carbonyl group. [4, 37]
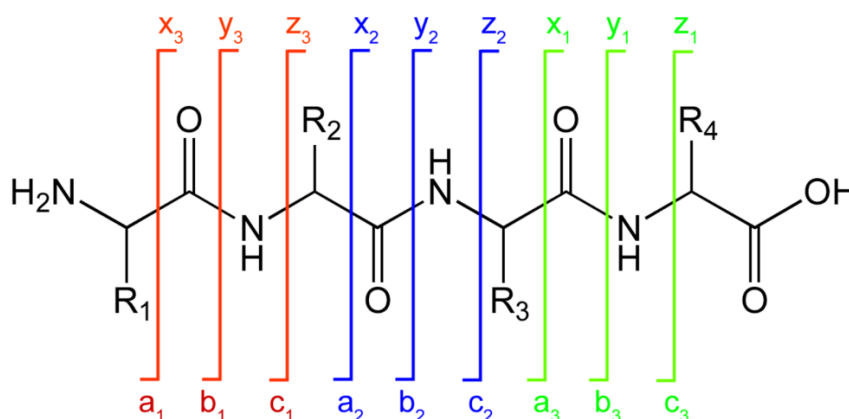
Figure 1.3: Diagram of potential peptide fragmentation pattern following CID (b-, y- and a-ions) and ETD (c-, z- and x-ions).

Although widely applied for global proteomic analysis, CID is known to be unsuitable for analysis of many protein post translational modifications (PTMs) including phosphorylation and glycosylation. [38] CID proceeds *via* fragmentaion of the weakest bond on the peptide (usually between carbonyl and amide groups). However as PTMs tend to be labile, application of CID will result in cleavage of the PTM molecule from the peptide. [37] For phosphorylated peptides, resulting spectra will display a mass shift corresponding to loss of the PTM but will not confirm the peptide sequence. [39] Similarly for glycosylated peptides, the MS/MS spectrum will display characteristic oxonium ions, *e.g. m/z* 204 292, 366, and 657, yielding little or no sequence information. [40]

In ETD, fragmentation is induced by converting positively charged peptides into radicals following transfer of electrons from chemical anions such as anthracene and fluoranthene. [41] Resulting peptide cation radicals are unstable and routinely undergo fragmentation

following dissociation of bonds between amide groups and α-carbons to produce characteristic *c-* and *z*-ions (Figure 1.3). [42] Due to the rapid nature of ETD, it is capable of retaining modifications and hence is ideal for the study of PTMs. [38] Furthermore, as ETD provides information on the location of PTMs, it is an important technique for advanced structural characterisation of proteins.

CID is generally carried out using high energy beam instruments such as QToF and QQQ mass spectrometers for global proteomics, as peptides containing labile PTMs are less amenable to low energy, resonate excitation MS/MS analysis. [43] For this reason Makarov *et al.* developed HCD [44] for use alongside Orbitrap mass analysers to compete with high-beam instruments. In addition to achieving increased fragment ion efficiency when compared to other traditional trapping mass analysers, use of HCD results in an extended detection mass range for MS/MS fragments enabling MS/MS-based quantitation using stable isotopes (to be discussed in section 1.6).

1.4.4   Data dependent versus Data independent Acquisition in Mass Spectrometry

In mass spectrometry, peptide data is acquired in one of two general modes: data dependent acquisition (DDA) or data independent acquisition (DIA) mode. Traditionally DDA has been the gold standard for MS analysis. In DDA ionised peptides are analysed to generate a list of precursor masses then, depending on particular MS settings chosen (*e.g.* peak intensity), a certain number of precursor ions are selected for MS/MS fragmentation. Interpretation of resultant MS/MS spectra yields sequence information which may then be compared with a peptide database for protein identification. [45] As all fragment ions are detected and the precursor ion related to the fragments is known, an analyst may have confidence in the quality of peptide identifications from complex protein mixtures. However, since only a small number of precursor ions are selected in a defined period of time, DDA may display bias towards more abundant proteins in the sample being analysed. As peptides enzymatically derived from proteins will have varying ionisation efficiencies and proteins in a complex sample will have concentrations spanning a wide dynamic range (with the majority existing at concentrations at least two orders of magnitude lower than the most abundant protein), many of the low abundant proteins may not be identified. [46, 47] In order to combat this limitation, dynamic exclusion is often employed wherein previously selected precursor ions are excluded from subsequent ion selection for MS/MS fragmentation, thereby increasing proteome coverage in DDA analysis. [48]

The first DIA method was pioneered by Silva and co-workers, who described a MS acquisition method wherein no selection bias of precursor ions is used, later named MS^E acquisition. [49, 50] In MS^E, the first mass analyser (shown as a quadrupole in Figure 1.4-A) transfers all precursor ions into a collision cell for fragmentation by CID. Collision energy applied is alternated between low and elevated energy, providing precursor (MS 1) and product (MS 2) ion spectra from every ion above the limit of detection of the instrument as low energy scans measure intact peptide ions while fragment ions are measured in high energy scans. [51] Bioinformatics software is then used to correlate fragment ions to their corresponding precursor ions based on retention time, mass accuracy and other physicochemical properties including fragment to precursor ratios and peptide fragmentation prediction. [52]
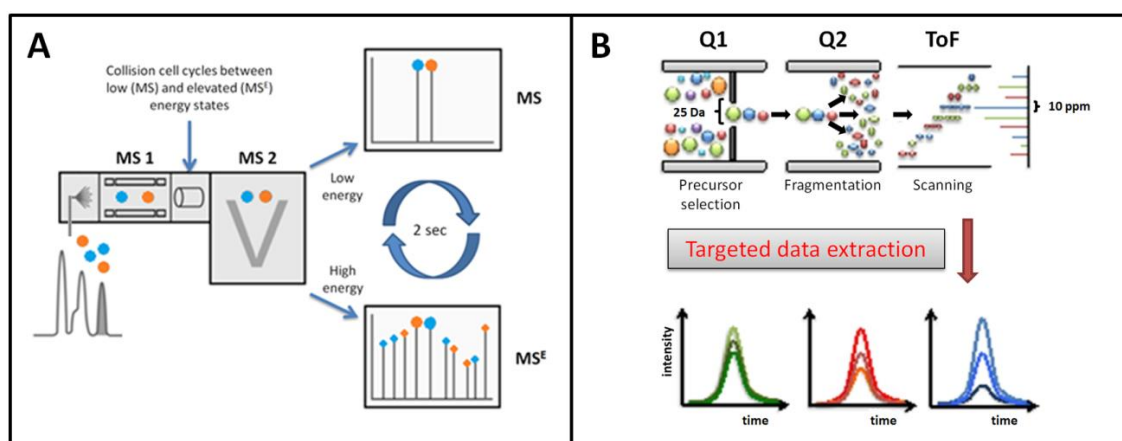
Figure 1.4: A. Depiction of LC-MS^E analysis on a QToF mass spectrometer. All precursor ions are transferred into a collision cell for CID fragmentation using alternated low and elevated collision energy, providing precursor and product ion spectra from every ion above the limit of detection of the MS instrument. [53] **B.** Representation of DIA operating in SWATH mode, adapted from [54]. All precursor ions within successive precursor ion windows over the mass range of the experiment are transmitted into a collision cell for fragmentation by CID.

During MS^E, fragment ions peaks are aligned with the chromatographic profile of the precursor by determination of chromatographic peak characteristics such as apex peak retention time, start and end time of the peak and peak width at half maximum. [47] Therefore the success of the method is highly dependent on chromatographic proficiency. Despite improving the dynamic range for protein identification, limitations of MS^E include its incompatibility with

some quantitative experiments, including those using isobaric tags (to be discussed in section 1.6).

Gillet *et al.* described an alternative strategy for DIA of proteome samples known as SWATH (**s**equential **w**indow **a**cquisition of all **th**eoretical spectra). [55] Similar to MS^E, SWATH also involves the transmission of all precursor ions detected during the MS survey scan (MS 1), for fragmentation by CID. However, in SWATH mode the mass spectrometer repeatedly cycles through a set of precursor acquisition windows over the mass range 400-1200 *m/z* (*i.e.* 32 successive 25 Da precursor isolation windows). As shown in Figure 1.4-B, during each cycle the mass spectrometer fragments all precursor ions in a specific mass range (*e.g.* 400-425 *m/z*, then 425-450 *m/z* etc.) and produces a MS/MS spectrum of all precursors in that isolation window. As the range of precursor ion windows is cycled throughout the entire chromatographic process, fragment ion spectra for all analytes in the specified mass range are also time-resolved.

1.5   Bioinformatics

Widespread use of MS in proteomics would not be possible without the availability of protein sequence databases and bioinformatics tools for protein identification and function assignment. Three main types of search engines for protein identification exist including *de novo* search engines (which derive peptide identifications based on peak patterns in MS/MS spectra without use of reference material, *e.g*. PEAKS [56]); spectral library search engines (that use a library of reference spectra to match MS/MS sample spectra, *e.g.* X!Hunter [57]) and sequence search engines. Various proprietary and non-proprietary sequence search engines are available for protein identification using different algorithms including SEQUEST [58], MASCOT [59], X!Tandem [60], Andromeda [61] and ProteinLynx Global Server [62]. Two main approaches for peptide sequencing using a search engine are shown in Figure 1.5. Probability-based matching is used in many of these (*e.g.* Mascot), where predicted peptide fragments are matched to experimentally observed fragment ion peaks. Alternatively, auto-correlation may be used to determine the over-lap between an experimentally derived spectrum and a theoretical spectrum derived from each sequence in a reference database (*e.g.* SEQUEST). These tools often include the use of decoy databases to estimate false discovery rates for statistical validation of identification results.

As the output of different mass spectrometers and alternative sequence search engines is produced in a variety of proprietary formats, the wide variety of data types produced can be

problematic for comparative analysis of results. In order to facilitate uniform, comparative analysis from a variety of instruments and processing tools, Keller *et al.* developed the Trans-Proteomic Pipeline (TPP) which incorporates various bioinformatics tools and stores data in open XML format. [63] Bioinformatics tools integrated into TPP include PeptideProphet, which validates peptides assigned to MS/MS spectra [64]; XPRESS, used for peptide and protein quantitation [65]; and ProteinProphet for validation of identified proteins. [66]
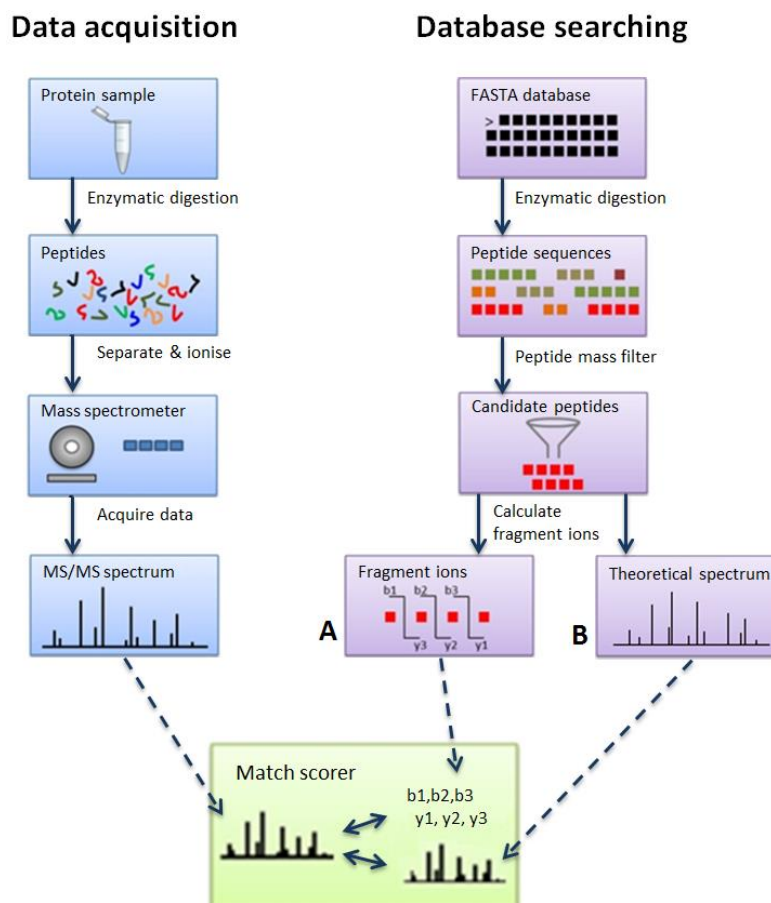
Figure 1.5: Schematic of a data acquisition and database search workflow for proteomics. Experimental MS/MS spectra are matched against (A) predicted fragment ions or (B) theoretical MS/MS spectra from *in-silico* digested proteins, before reporting of best-matched peptides and related score. Adapted from [67].

Once proteins have been identified, it is common-place to use functional assignment bioinformatics tools to gain functional knowledge of entire protein systems composed of protein groups identified. Functional interpretation of identified proteins usually begins with

the association of a protein list with gene ontology (GO) terms that describe related biological processes, molecular functions and cellular components. Following GO term annotation, the abundance of specific GO terms, associated with an identified protein list, is compared with the natural abundance in the organism using a reference database. A probability value (p-value) is then generated to show potential over-representation of a specific GO term in the test sample compared to the reference database [68]. More than 60 tools exist for GO-term enrichment, *e.g.* the **d**atabase for **a**nnotation, **v**isualisation and **i**ntegrated **d**iscovery, DAVID [69, 70]. However care must be taken when choosing a tool for GO annotation as a wide discrepancy in reported GO-terms has been observed when using tools with different algorithms for annotation [71].

Other resources useful for evaluating proteomic results in a biological context include interaction databases for pathway analysis *e.g.* KEGG [72] and Ingenuity pathway analysis (IPA). [73] Proteins that are directly involved or that contribute to regulation of a cellular reaction are contained in pathway databases, [68] which describe a series of cellular reactions that produce an observable biological effect. Using these comprehensive pathway databases, proteomic results may be scrutinised for involvement in biological processes.

1.6   Quantitation

Quantitative information regarding changes in protein expression levels, which may be provoked by pharmacological, environmental or genetic factors, is a key element in understanding disease mechanisms, productivity in bioprocessing and other biological processes. Several strategies for quantitative proteomics, each having specific strengths and limitations, have been described and may be categorised as either label-free or labelling methods.

1.6.1   Label-free Quantitation

Spectral counting and spectral indexing are label-free, relative quantitation strategies for determination of protein concentration by LC-MS/MS, wherein a protein abundance is estimated based on the number of tandem mass spectra obtained for each protein group in a mixture [74, 75]. Spectral counting methods are highly dependent on chromatographic separation reproducibility and require replication of experiments to ensure statistically significant results and hence may be limited by the availability of appropriate instrumentation.

In addition, the potential for detector saturation at high spectral counts and masking of low abundant proteins by high-abundance proteins may lead to erroneous quantitation results [76]. The demonstration of a linear correlation between ion concentration and ion current signal has led to the development of ion accounting based label-free quantitative proteomic methods. Silva *et al.* established a method for absolute quantitation of proteins by LC-MS^E by demonstrating that for all proteins in a sample, the average MS signal for the three most intense tryptic peptides is constant per mole of protein, with a coefficient of variation of less than ± 10% [50]. Hence, using an internal standard of known quantitation, a universal signal response factor may be calculated and subsequently used to accurately determine the absolute quantitation for all proteins in a sample. This approach, known as 'Hi3 quantitation', is capable of accurately quantifying proteins across the entire dynamic range of the mass spectrometer in both simple and complex protein mixtures [77], albeit for data-independent MS analyses only. Label-free quantitative approaches are now commonly applied for clinical proteomics, wherein comparison of >10^2 samples are frequently required. However, excellent reproducibility of all experimental steps is essential for accurate and reliable quantification using label-free methods. [78]

1.6.2   Labelled Quantitation

Labelled quantitation approaches rely on the successful incorporation of a label into multiple protein samples and may be performed in either MS (comparing ion intensities of peptide peaks) or in MS/MS mode (utilising isobaric chemical labels). Quantitative proteomics measured in the MS 1 mode are most accurately achieved using stable isotopes for relative quantitation of identified proteins. Isotopic labelling is based on the assumption that two forms of a molecule, differing only as a result of a stable-isotope substitution, will behave identically in an MS experiment. Hence, the ratio of two sample peaks, separated by a characteristic mass shift equivalent to the difference in isotopic mass, directly indicates the relative concentration of a protein in comparative samples. In stable isotope labelling with amino acids in cell culture (SILAC), cells are grown in medium lacking an essential amino acid but supplemented with an isotopically labelled version of that amino acid, which is incorporated into the cell during culture. [79] Following MS analysis, the relative quantitation of proteins in differently labelled samples may be estimated. Initially, SILAC experiments were limited to samples prepared in cell culture as complete metabolic labelling of the proteome is required. However, since SILAC has proven to be an accurate and robust technique for quantifying proteomes, efforts have been made to extend this powerful technique to higher

organisms. SILAC model systems, which enable the determination of protein functions under complex *in-vivo* conditions, have been prepared by feeding lysine auxotrophic animals with a diet containing the natural or $^{13}C_6$ (and/or $^{15}N_2$)-substituted version of lysine. Reported SILAC model-systems currently available include mouse, [80] fruit fly [81] and zebra-fish. [82] Despite the applicability of available SILAC model systems, these can be costly and time-consuming to prepare. Furthermore, it is unlikely that SILAC-modelling will be extended to human systems. However, Geiger and colleagues developed a novel 'super-SILAC' mix that facilitated the analysis of human tissue samples. [83] By mixing five SILAC-labelled cell lines with a human carcinoma tissue sample, hundreds of thousands of isotopically labelled peptides were incorporated as internal standards facilitating human tumour tissue proteome quantitation, hence broadening the scope of SILAC-based proteomics.

In addition to metabolic-labelled strategies for MS-level quantitation, chemical labelling techniques *e.g.* stable isotope dimethyl labelling, have been applied for quantitative proteomics. Hsu and co-workers first introduced dimethyl-labelling as a quantitative proteomics technology, in which reductive amination using isotopomers of formaldehyde and cyanoborohydride results in highly selective dimethylation of primary amines. [84] A relative mass shift of 4 Da is observed for each derivatised site upon MS analysis in samples treated with formaldehyde and formaldehyde-D_2, thereby facilitating relative quantitation of proteins in two sample populations. Later Boersema *et al.* built upon the dimethylation approach described by additionally labelling a third sample with ^{13}C-formaldehyde-D_2, facilitating the simultaneous analysis of three proteomic samples. [85] In both SILAC and dimethyl-labelling approaches the physicochemical properties of ions are conserved, therefore MS/MS sequence profiling and hence protein identification is not affected. However both methods were limited to three samples for comparative proteomics.

Multiplexed relative quantitation of proteomes within a single MS experiment was first enabled by the development of isobaric tagging methods, *e.g.* iTRAQ and TMT. Isobaric tags for relative and absolute quantitation (iTRAQ) are a set of amine reactive isobaric labels that derivatise peptides in lysine side chains and at the *N*-terminus, hence labelling all peptides in a tryptic digest mixture. [86] Currently iTRAQ reagents are available for 4-plex and 8-plex experiments, composed of a reporter group, a balance group and an amine specific peptide reactive group. [86, 87] In MS 1, peptides labelled with iTRAQ reagents are indistinguishable (isobaric), however upon MS/MS fragmentation, signature ions (*m/z* 114 – 119 and *m/z* 121) are formed which when compared, allow for relative quantitation of all labelled sample peptides. [88] Similar to iTRAQ, tandem mass tags (TMT) are also a commercially available set

of isobaric chemical labels, developed by Thompson and co-workers. [89] TMT reagents, composed of a mass reporter group, a balance group, a cleavable linker and a peptide reactive group, were initially produced as duplex labels but are now available in 6-plex and 10-plex forms. [90] Recently, further extension of multiplexing capabilities have been reported, potentially enabling 16-plex reagents with 1 Da spacing between reporter ions, although these have yet to be commercialised. [91] A typical workflow for quantitative proteomics using TMT reagents is shown in Figure 1.6.

A.

B.
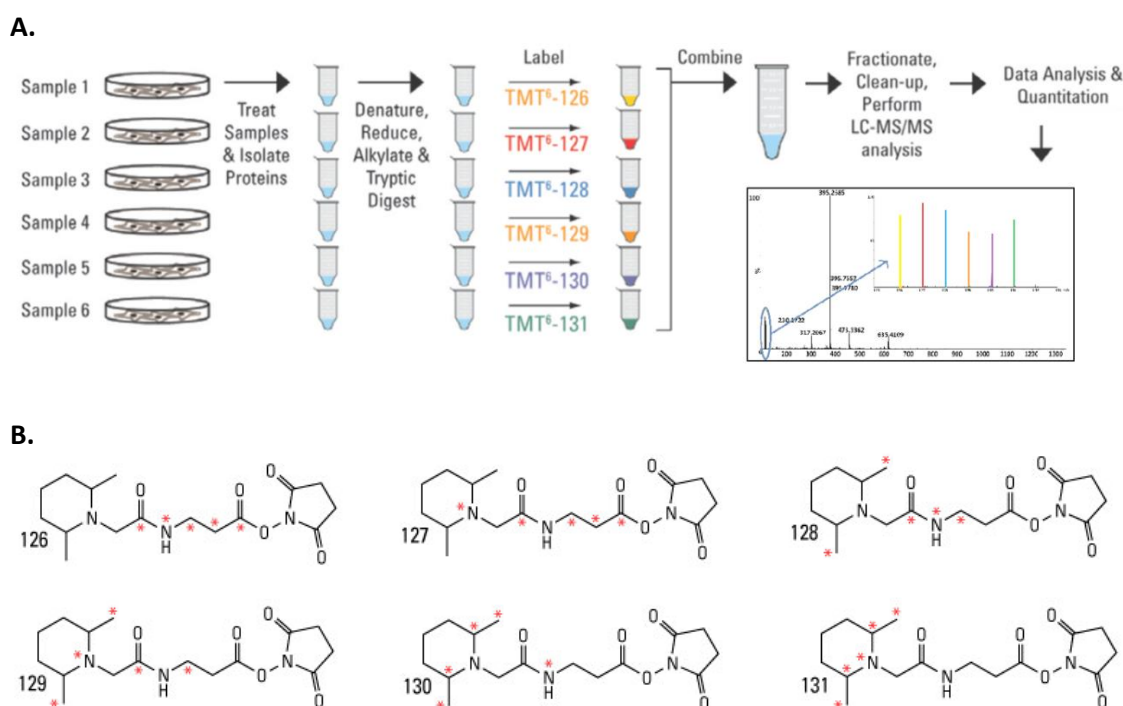
Figure 1.6: A. Schematic of quantitative proteomic analysis workflow using 6-plex TMT reagents. Following sample preparation incorporating TMT reagents, samples are combined before analysis using LC-MS/MS. The ratio of peak heights for reporter fragment ions may then be used to determine the relative quantitation of peptides in the samples under comparison. **B.** Structure of 6-plex TMT reagents. ^{13}C and ^{15}N heavy isotopes are highlighted by red asterisks. [92]

In addition to enabling multiplexing of samples in a single MS experiment, isobaric tagging methods provide potentially increased precision in quantitative proteomics as measurements are performed at the fragment mass spectra level (MS 2). [93] However, the number of labelling reagents that may be used within a single experiment are limited, hence the quantity

of samples that may be compared within a single experiment is also restricted (<10 comparative samples). Furthermore, isobaric tagging methods may potentially be limited by ratio compression, *i.e.* distortion of peptide quantitation ratios due to interference in MS/MS spectra, from multiple precursors within a selected precursor isolation window. Ratio compression has been addressed by combining a narrower precursor isolation window with fragmentation at the LC peak apex, [94] by using a MS3 experiment on an LTQ Orbitrap mass spectrometer [95, 96] and alleviated using high-resolution sample fractionation. [97]

Further improvements were made by McAllister and co-workers by isolating multiple fragment ions in the MS2 spectrum using isolation waveforms with multiple frequency notches (*e.g.* synchronous precursor selection (SPS)). Co-isolation and fragmentation of multiple MS2 fragment ions resulted in a 10-fold increase in reporter ion signals thereby reducing reporter ion variance, enhancing the dynamic range of reporter ion quantitation and ultimately generating better-quality quantitative measurements. [98] The SPS-MS3 method was later applied for a quantitative phosphopeptide analysis incorporating 10-plex TMT labelling and analysed using a tribrid mass spectrometer (Thermo Fisher Scientific Orbitrap Fusion). An enhanced TMT reporter ion intensity and accuracy, with elimination of ratio distortion of reporter ions, was outlined. [99]

Recently, a method for quantitative proteomics has been described that combines the multi-plexing capability of isobaric tags with the accuracy of SILAC methods, termed neutron encoding (NeuCode) SILAC. [100] NeuCode SILAC exploits subtle mass differences in common stable isotopes caused by neutron-binding energy variation, effectively compressing isotopic information into very narrow *m/z* windows, which may be revealed when using ultra-high resolution mass spectrometers. Thus, NeuCode SILAC is capable of high levels of multiplexing (>10 samples) with high accuracy and broad dynamic range but is limited to mass spectrometers with very high resolving power (> 480,000).

1.7   Proteomic Profiling of CHO Behaviour

Reflecting their importance in the biopharmaceutical industry, numerous CHO proteomic studies have been undertaken to better understand these important expression systems. Proteomics has been used to directly identify and measure hundreds to thousands of proteins present in CHO cells that play key roles in recombinant protein production, including those involved in growth, protein processing, metabolism, glycosylation and cell death [2]. CHO cell proteomics can be broadly partitioned into a number of approaches, namely evaluation of

CHO cell proteomes following culture in conditions known to increase specific productivity (qP) or in response to other variations in bioprocessing conditions; profiling of CHO cells with desired phenotypes often following cellular engineering to achieve a desired phenotype; evaluation of secreted proteins and their effect on surrounding cells and to determine host cell protein (HCP) impurities that may be found in purified therapeutic drug substance.

Proteomics can provide powerful insights into alterations in cell physiology following expression of an exogenous recombinant protein or variations in culture conditions, leading to further advancements in CHO cell production through possible genetic or environmental manipulations. As depicted in Table 1.3, many proteomic studies have been performed to determine differential protein expression following cell culture under qP-enhancing conditions compared to standard conditions. These studies aim to identify key regulatory proteins and pathways that may be used as targets for CHO cell engineering to further improve recombinant protein production. Table 1.3 also outlines CHO cell engineering strategies, which have been successfully applied to improve specific productivity in CHO cells. Proteomic approaches have been employed to assess the impact of down-regulation or over-expression of effector proteins used in CHO cell engineering, to enhance biopharmaceutical production [101].

In addition to proteomic studies evaluating changes to protein regulation following culture in conditions that increase qP, numerous studies have been performed to determine molecular changes in response to altered feeding strategies. Metabolic shift through controlled nutrient feeding sustaining low glucose and glutamine concentrations reduces the production of toxic metabolites in cell culture and thereby results in higher viable cell concentrations without impacting qP [102, 103]. Pascoe *et al.* compared two different mAb-producing CHO cell lines with different lactate profiles under the same fed-batch culture conditions to determine changes in the CHO cell proteome linked to metabolism [104]. A substantial proportion of the differentially expressed proteins observed were found to be glycolytic enzymes, although structural proteins and proteins related to mAb production and protein processing were also observed. Notably, a proteomic investigation by Seow and co-workers showed how a feeding strategy, wherein low concentrations of glucose and glutamine were maintained, led to a reduction in metabolite production, altered expression of metabolic enzymes and changes to cellular metabolism. [103] This was further investigated by both Fan *et al.* and Wingens and co-workers who determined the effects of a metabolic shift from glucose surplus to glucose limitation on CHO cellular equipment. [105, 106] Wingens *et al.* found that changes in cellular machinery may be due to epigenetic effects, a conclusion also hinted at by Pascoe and co-

workers who suggested that proteins expressed in cultures, displaying different metabolic profiles, may depend on how the nutrient limited conditions were generated. [104] A more in-depth proteomics investigation of cellular responses to media glucose concentration was recently performed by Liu and colleagues using 2D-LC-MS/MS, resulting in the identification of potential cell engineering targets that may ultimately lead to increased qP along with prevention of apoptosis at standard glucose levels (5 g/L). [107]

The vast majority of CHO proteomic studies have endeavoured to profile CHO proteomes of industrial relevant cell lines, [108, 109] (*e.g.* those exhibiting a high qP, [110, 111] an elevated growth rate phenotype [112]), or to comparatively evaluate various CHO cell lines including high and low recombinant protein producers. [113-115] Additionally research relating to bioprocessing strategies including proteomic profiling of CHO cells undergoing apoptosis during prolonged cultivation or following high passage cultivation have been performed. [116, 117] However, following the publication of the first CHO genome sequenced by Xu *et al.*, [118] Baycin-Hizal and colleagues, published the most significant CHO cell proteomics study of recent years, the first to be published reporting protein groups exclusively identified using a CHO cell genome thereby affording more accurate identification of proteins. [2] Cellular and secreted proteins were isolated by 2D LC and glycoproteins by solid phase extraction prior to LC-MS/MS analysis on an LTQ-Orbitrap Velos mass spectrometer, as depicted in Figure 1.7, yielding a total of 6,164 identified protein groups with a 4.2% false discovery rate. To further enhance knowledge of CHO cell physiology relevant to exogenous protein expression, the codon frequency of all experimentally detected CHO proteins was elucidated. This information facilitates the optimisation of codons for human proteins relevant to the codon frequency of CHO cells and may result in increased recombinant protein expression in CHO cell lines. Analysis of combined transcriptomic and proteomic data sets revealed an enrichment of a number of pathways, including apoptosis and protein processing, and also a reduction in proteins involved in glycosphingolipid and steroid hormone metabolism [2].

Table 1.3: Determination of proteome changes following culture under productivity-enhancing conditions and productivity-enhancing genetic interventions in CHO cells.

Productivity-enhancing condition	Therapeutic Product	Cell line	Analytical Technique	Alterations in Proteome	Reference
Temperature shift (37°C to 30°C)	SEAP	CHO-K1	2DE	Altered expression levels of unidentified proteins following temperature downshift.	[119]
Temperature shift (37°C to 31°C)	-	CHO-K1	2D-DIGE and MALDI-ToF-MS	Differentially expressed protein involved in growth regulation, apoptosis, cap-independent translation and glycoprotein quality control.	[120]
Temperature shift (37°C to 33°C)	EPO	CHO-DUKX	2DE & MALDI-ToF-MS	Increased expression of proteins involved in protein folding and secretion, growth regulation and metabolism. Down regulation of proteins involved in some signalling pathways.	[121]
Temperature shift (37°C to 33°C) & 2mM NaBu	IgG	CHO-EcIn	2DE & nano-LC-MS/MS	Cellular secretory capacity-associated proteins differentially expressed.	[122]
3 mM Sodium butyrate	hTPO	CHO-DUKX-B11	2DE & MALDI-ToF-MS & MS/MS	Proteins associated with protein folding and secretion, growth regulation and metabolism differentially expressed.	[123]
1 mM Sodium butyrate	IFN-γ	CHO- IFN-γ	2DE & nano-LC-MS/MS	Differentially expressed proteins involved in protein metabolism and degradation, translation, apoptosis and fatty acid beta-oxidation.	[124]
0.5mM Sodium butyrate & 80 µM zinc sulphate	hGH	CHO-K1	2D-DIGE and MALDI-Tof-MS	Observed induction of proteins with metabolic and stress protection functions.	[125]
Hyperosmolarity (300 to 450 mOsm/kg)	Antibody	CHO-DG44	2-DE	Up-regulation of glycotic enzymes, resulting in increased metabolic energy for mAb synthesis. Down-regulation of tubulin, reflecting a reduction in growth rate.	[126]

Hyperosmolarity (310 to 510 mOsm/kg)	Antibody	CHO-DUKX-B11	2D-DIGE and MALDI-Tof-MS	Protein involved in cellular metabolism, cellular architecture, protein folding, mRNA processing and protein secretion.	[127]
Hydrolysate addition - 5 g/L of soy hydrolysate, wheat gluten hydrolysate & yeastolate	Antibody	CHO-DG44	2-DE with nano-LC-QToF-MS/MS	Up-regulation of metabolism-associated, proliferation-related and cytoskeleton-associated proteins. Altered expression of several chaperone proteins.	[128]
Bcl-X$_L$ over-expression	Humanised rh fusion protein	CHO-DG44	In-solution digestion & nano LC-MS	Differential expression of metabolism-associated, cytoskeleton-related and transcription-associated proteins and of proteins involved in cell cycle regulation, cell growth and glycolysis.	[129]
Bcl-X$_L$ over-expression	-	-	iTRAQ labelling & 2D-LC-MS	Molecular chaperones, isomerases, cell growth markers and proliferation-associated and apoptosis-related proteins.	[130]
Bcl-X$_L$ over-expression & 3 mM NaBu	EPO	CHO-DUKX-B11	2D-DIGE and MALDI-Tof-MS	Proteins related to apoptotic signalling pathways and proteins associated with cell survival, proliferation and repair of DNA damage.	[131]
Soluble PACEsol over-expression	rh-human bone morphogeneti c protein-2	CHO-DUKX	2D-DIGE and MALDI-Tof-MS	Proteins involved in protein folding, assembly and secretion, chaperone activity and protein translation.	[132]
MicroRNA-7 over-expression	SEAP	CHO-K1	Label-free nano-LC-MS/MS	Down-regulation of proteins relating to protein translation and RNA processing. Up-regulation of proteins involved in apoptosis and cell death	[133]
***C-myc* over-expression**	-	CHO-K1	2DE & LC-MS/MS	Up-regulation of proliferation-related and cytoskeleton-associated proteins and also in proteins involved in energy metabolism and protein biosynthesis. Down-regulation of proteins involved in cell to cell adhesion.	[134]
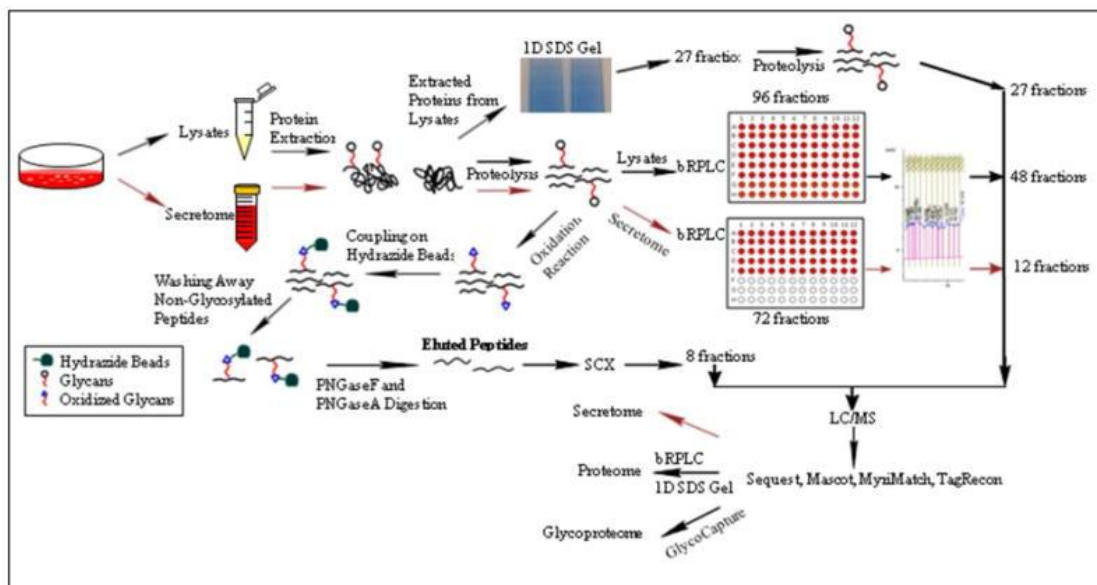
Figure 1.7: Schematic of the CHO proteome sample preparation and analysis approach utilised by Baycin-Hizal *et al.* Proteins were extracted from both cell lysates and spent media prior to in-gel separation and proteolysis or in-solution digestion and reversed phase-LC. Sample fractions were subsequently analysed by LC-MS/MS. In addition glycosylated peptides were analysed by solid phase extraction coupled to LC-MS/MS [2].

Subsequently, Meleady and co-workers generated a translated protein sequence for the CHO-K1 cell line from cDNA sequence information published by Becker *et al.* [135]. This sequence, along with Swissprot data entries for *Mus musculus* and CHO-K1 (derived from the draft genome sequence published by Xu *et al.* [118]) were then used to identify proteins from CHO-SEAP whole cell lysates. Meleady *et al.* demonstrated an improvement in MS-based proteomic identification, noting 282 additionally identified proteins following the use of CHO specific databases when compared to *Mus musculus* Swissprot database entries, despite the high homology between the two species. Importantly, the confidence of identification was heightened as both CHO-K1 databases yielded consistent and congruent results, despite being generated from different sources. [136] Evans and co-workers also endeavoured to generate a protein database for non-model species using expressed mRNA sequences for *de novo* derivation of proteomes. Their technique, proteomics informed by transcriptomics (PIT), was shown to identify >99% of distinct CHO proteins also identified by traditional analysis using cross-species protein sequencing. [137]

Recently, the determination of host cell proteins (HCPs) in purified therapeutic protein sample has gained widespread interest in the biopharmaceutical community. HCP impurities, which

may be introduced into the harvest stream through cell lysis or secretion from host cells and are considered to be process-related impurities. [138, 139] Due to potential adverse clinical reactions in humans relating to HCPs, regulatory requirements necessitate their removal from therapeutic protein preparations to below detectable levels of highly sensitive analytical methods. [140] Although classically measured using immunosorbent assays, (*e.g.* enzyme-linked immunosorbent assay (ELISA), [141]) which have been validated to provide a good quantitative estimation of the total HCP concentration, immunosorbent assays may under-estimate weakly or non-immunoreactive proteins. [142] Proteomic techniques have been utilised to determine HCP profiles to further elucidate cellular processes occurring in CHO cells over the course of a production cycle. The vast advances in analytical technologies have now enabled a more in-depth understanding of the nature of individual HCPs that pass through downstream processing into final drug substances.

Jin *et al.* used 2D-DIGE in a proteomic study to determine changes in HCP profiles following culture under altered upstream processing conditions. [142] Of the upstream processing parameters investigated including cell culture media, feeding strategy, cell viability at harvest and cell duration, cell viability was found to generate the most significant changes in HCP profile. This information could be used to implement upstream process analytical technologies to create more robust upstream process control, assist in the design of downstream purification processes and to ensure greater process consistency. A subsequent study by Tait and co-workers used 2-DE and LC-MS/MS to characterise HCP profiles in the supernatant of mAb-producing and null CHO cell lines, throughout different stages of cell culture. [139] A correlation between the day of harvest and high levels of HCPs present in the process supernatant was observed suggesting the majority of HCPs in the process stream resulted from the lysis of cells associated with viability loss. More recently, Doneanu *et al.* developed an online two-dimensional LC-MS^E method for the analysis of HCPs in biotherapeutic proteins. [143] Using label-free 'Hi3' based quantitation, 33 HCPs with the lowest concentration of 16 ppm, were identified from six IgG preparations. Similarly, Schenauer and co-workers also used 2D-LC-MS^E with label-free 'Hi3' quantitation for the identification and quantification of HCPs in therapeutic proteins. [144] The capability of the method to identify HCPs present at 13 ± 4 ppm, with less than 2-fold quantitative error was demonstrated.

During cell culture various types of proteins that can modify cell growth in culture, including ligands, receptors, waste products and endogenous growth factors, may be secreted by host cells [145, 146]. Accordingly, qualitative and quantitative information regarding secreted proteins at different stages of cell culture may aid bioprocess development. Recognising this

opportunity for improvement in bioprocessing operations, Kumar *et al.* used surface enhanced laser desorption ionisation (SELDI)-Tof MS to monitor secreted proteins in CHO culture media during different stages of the growth cycle [145]. Twenty-four proteins were observed to be differentially expressed over the course of the culture and were also found to accumulate in the process media over time. These secreted proteins represent potential targets for monitoring the removal of host cell proteins (HCPs) from the therapeutic protein product. Woolley and co-workers also evaluated the CHO secretome for possible identification of biomarkers, in this case to serve as an indication of stress and viability loss in CHO culture. [147] Also using SELDI-ToF, the intensity of a peak at 7.7 kDa corresponding to Galectin-1 was found to correlate with the degree of viability loss in triplicate cultures.

Many secreted proteins serve as a mechanism to facilitate communication between cells in culture, with potential positive or negative outcomes. The identification of autocrine growth factors secreted by CHO cells has led to the generation of a protein-free basal media improving cell growth in culture. [148] However, following exposure to detrimental conditions cells may secrete proteins, such as cytokines, that may result in cytotoxicity and genomic instability in surrounding cells. This 'bystander effect' was investigated by Ahram *et al.* who initiated a proteomic study to investigate global changes in secreted proteins collected from conditioned CHO cell culture media samples subsequent to radiation exposure [146]. No evidence of changes in the type of proteins secreted was determined, possibly resulting from a weak response of CHO cells to low amounts of radiation.

Despite many studies investigating the effect of qP enhancing culture conditions and cell engineering strategies on the quality and yield of therapeutic proteins, relatively few studies have examined how physicochemical properties of the recombinant therapeutic protein itself influence the CHO host cell. Sommeregger and colleagues demonstrated how distinct recombinant proteins evoke different proteomic responses within the host cell by performing label-free LC-MS/MS proteomic analysis of different CHO cells prepared from the same expression system but adapted to express different recombinant proteins. [149]

1.8   Future Perspectives

Considerable progress in high-throughput proteomic analysis over the past decade has been fuelled to a large degree by continuous improvements in instrumentation. In particular, the advent of nano-scale separations, high-resolution tandem mass analysers and application of 2D-LC-MS/MS has enabled the optimisation of proteomics. Further improvements in precursor ion resolution will be achievable with the emergence of new capabilities, *e.g.* ion mobility separation (IMS). When coupled to LC, IMS enables an additional dimension of precursor ion separation in the gas-phase, with the potential to increase proteome coverage by enhanced deconvolution of peptides occupying the same retention time and *m/z* space, for instance chimeric peptides. [150] Although the strengths of this technique have potentially not been fully realised, the extra dimension of separation is likely to be more-widely incorporated into future LC-MS configurations. Other emerging techniques for proteome analysis include protein structural characterisation technologies, *e.g.* hydrogen-deuterium exchange (HDX) mass spectrometry. HDX-MS is likely to provide product-quality information regarding protein dynamics, which when combined with functional annotation may potentially enable a more thorough understanding of protein systems. [151] One of the big challenges remaining in proteomics today centres on the processing of vast quantities of data generated using high resolution MS/MS. Improvements to overcome data analysis bottlenecks and ensure the quality of results achieved is likely to remain a focus for improved quantitative proteomics.

1.9   Conclusions

CHO cell expression systems are currently a significant area of research due to their widespread use in the production of therapeutic biomolecules. Although initial improvements in CHO bioprocessing centered on cell and bioprocess engineering strategies, more recent developments have been achieved through greater cellular-level understanding of these important production systems. Much of the knowledge gained has been achieved through in-depth proteomic studies facilitated by key advancements in associated analytical technologies. Future progression in quantitative proteomics will undoubtedly arise from additional advances in instrumentation, data processing and quantitation technologies, allowing us to delve deeper into the proteome, leading to potential improvements in biologically significant areas of research including biopharmaceutical production and therapeutic protein characterisation.

1.10   Associated Publication and Author Contributions

Published in part: Farrell, A., *et al.*, *Application of multi-omics techniques for bioprocess design and optimisation in Chinese hamster ovary cells*. Journal of Proteome Research, 2014, **13**(7):3144-59.

Literature review topic devised by Amy Farrell and Jonathan Bones; Literature review prepared by Amy Farrell and reviewed by Jonathan Bones; Related paper was written by Amy Farrell and reviewed by John J. Milne, Ian W Marison, Niaobh McLoughlin and Jonathan Bones.

1.11   Aims of Thesis

The goals of this work were to determine the impact of variation in the conditions used for bioprocessing of Chinese hamster ovary production cells on both the quality of the therapeutic monoclonal antibody product and on the production cells themselves.

The specific aims of this thesis were:

• To apply state-of-the-art quantitative proteomic techniques to determine potential changes to the proteome of monoclonal antibody producing CHO cells in response to the bioprocessing conditions used for cell culture;

• To determine changes to CHO cells in culture in response to exposure to the secretome of adjacent cells when grown under conditions of altered bioprocessing;

• To develop analytical platforms to extensively characterise differentially produced therapeutic monoclonal antibodies through application of analytical methods for determination of sequence-level modifications, variations in N-glycosylation profile and changes to the structure and function of the therapeutic biomolecules, thereby evaluating alterations in the safety, quality and efficacy of the mAb;

• To develop an analytical platform to enable the identification of host cell proteins in therapeutic monoclonal antibody samples following downstream processing to enable optimisation of processing parameters for clearance of impurities from finished drug substances.

1.12   References

1.   Walsh, G., *Biopharmaceutical benchmarks 2014.* Nat Biotechnol, 2014. **32**(10): p. 992-1000.

2.   Baycin-Hizal, D., et al., *Proteomic analysis of Chinese hamster ovary cells.* J Proteome Res, 2012. **11**(11): p. 5265-76.

3.   Heffner, K.M., et al., *Exploiting the proteomics revolution in biotechnology: from disease and antibody targets to optimizing bioprocess development.* Curr Opin Biotechnol, 2014. **30**: p. 80-6.

4.   Steen, H. and M. Mann, *The ABC's (and XYZ's) of peptide sequencing.* Nat Rev Mol Cell Biol, 2004. **5**(9): p. 699-711.

5.   Shevchenko, A., et al., *Mass spectrometric sequencing of proteins silver-stained polyacrylamide gels.* Anal Chem, 1996. **68**(5): p. 850-8.

6.   Canas, B., et al., *Trends in sample preparation for classical and second generation proteomics.* J Chromatogr A, 2007. **1153**(1-2): p. 235-58.

7.   Wisniewski, J.R., et al., *Universal sample preparation method for proteome analysis.* Nat Methods, 2009. **6**(5): p. 359-62.

8.   Vandermarliere, E., M. Mueller, and L. Martens, *Getting intimate with trypsin, the leading protease in proteomics.* Mass Spectrom Rev, 2013. **32**(6): p. 453-65.

9.   Tabb, D.L., et al., *Influence of basic residue content on fragment ion peak intensities in low-energy collision-induced dissociation spectra of peptides.* Anal Chem, 2004. **76**(5): p. 1243-8.

10.   Washburn, M.P., D. Wolters, and J.R. Yates, 3rd, *Large-scale analysis of the yeast proteome by multidimensional protein identification technology.* Nat Biotechnol, 2001. **19**(3): p. 242-7.

11.   Abdallah, C., et al., *Gel-based and gel-free quantitative proteomics approaches at a glance.* Int J Plant Genomics, 2012. **2012**: p. 494572.

12.   Timms, J.F. and R. Cramer, *Difference gel electrophoresis.* Proteomics, 2008. **8**(23-24): p. 4886-97.

13. Di Palma, S., et al., *Recent advances in peptide separation by multidimensional liquid chromatography for proteome analysis.* J Proteomics, 2012. **75**(13): p. 3791-813.

14. Gilar, M., et al., *Two-dimensional separation of peptides using RP-RP-HPLC system with different pH in first and second separation dimensions.* J Sep Sci, 2005. **28**(14): p. 1694-703.

15. Peng, J., et al., *Evaluation of multidimensional chromatography coupled with tandem mass spectrometry (LC/LC-MS/MS) for large-scale protein analysis: the yeast proteome.* J Proteome Res, 2003. **2**(1): p. 43-50.

16. Ritorto, M.S., et al., *Hydrophilic strong anion exchange (hSAX) chromatography for highly orthogonal peptide separation of complex proteomes.* J Proteome Res, 2013. **12**(6): p. 2449-57.

17. Boersema, P.J., et al., *Evaluation and optimization of ZIC-HILIC-RP as an alternative MudPIT strategy.* J Proteome Res, 2007. **6**(3): p. 937-46.

18. Gama, M.R., C.H. Collins, and C.B. Bottoli, *Nano-liquid chromatography in pharmaceutical and biomedical research.* J Chromatogr Sci, 2013. **51**(7): p. 694-703.

19. Rieux, L., et al., *Nano LC: Principles, Evolution, and State-of-the-Art of the Technique.* LC GC North America, 2011. **29**(10): p. 926-+.

20. Yates, J.R., C.I. Ruse, and A. Nakorchevsky, *Proteomics by mass spectrometry: approaches, advances, and applications.* Annu Rev Biomed Eng, 2009. **11**: p. 49-79.

21. Annesley, T.M., *Ion suppression in mass spectrometry.* Clin Chem, 2003. **49**(7): p. 1041-4.

22. Whitehouse, C.M., et al., *Electrospray interface for liquid chromatographs and mass spectrometers.* Anal Chem, 1985. **57**(3): p. 675-9.

23. Lane, C.S., *Mass spectrometry-based proteomics in the life sciences.* Cell Mol Life Sci, 2005. **62**(7-8): p. 848-69.

24. Pitt, J.J., *Principles and applications of liquid chromatography-mass spectrometry in clinical biochemistry.* Clin Biochem Rev, 2009. **30**(1): p. 19-34.

25.   Banerjee, S. and S. Mazumdar, *Electrospray ionization mass spectrometry: a technique to access the information beyond the molecular weight of the analyte.* Int J Anal Chem, 2012. **2012**: p. 282574.

26.   Schmidt, A., M. Karas, and T. Dulcks, *Effect of different solution flow rates on analyte ion signals in nano-ESI MS, or: when does ESI turn into nano-ESI?* J Am Soc Mass Spectrom, 2003. **14**(5): p. 492-500.

27.   Juraschek, R., T. Dulcks, and M. Karas, *Nanoelectrospray--more than just a minimized-flow electrospray ionization source.* J Am Soc Mass Spectrom, 1999. **10**(4): p. 300-8.

28.   Wilm, M. and M. Mann, *Analytical properties of the nanoelectrospray ion source.* Anal Chem, 1996. **68**(1): p. 1-8.

29.   Wilm, M.S., Mann, M., *Electrospray and Taylor-Cone theory, Dole's beam of macromolecules at last?* International Journal of Mass Spectrometry and Ion Processes, 1994. **136**(2-3): p. 167-180.

30.   Hu, Q., et al., *The Orbitrap: a new mass spectrometer.* J Mass Spectrom, 2005. **40**(4): p. 430-43.

31.   Hebert, A.S., et al., *The one hour yeast proteome.* Mol Cell Proteomics, 2014. **13**(1): p. 339-47.

32.   Holcapek, M., R. Jirasko, and M. Lisa, *Recent developments in liquid chromatography-mass spectrometry and related techniques.* J Chromatogr A, 2012. **1259**: p. 3-15.

33.   *Thermo Fisher Sciencitific Ltd. 2015. LTQ Orbitrap XL Hybrid Ion Trap Mass Spectrometer. [ONLINE] Available at http://planetorbitrap.com/ltq-orbitrap-xl#tab:schematic [Accessed 03 April 2015].*

34.   *Thermo Fisher Sciencitific Ltd. 2015.Q Exactive Hybrid Quadrupole Orbitrap Mass Spectrometer. [ONLINE] Available at http://planetorbitrap.com/q-exactive#tab:schematic [Accessed 03 April 2015].*

35.   Senko, M.W., et al., *Novel parallelized quadrupole/linear ion trap/Orbitrap tribrid mass spectrometer improving proteome coverage and peptide identification rates.* Anal Chem, 2013. **85**(24): p. 11710-4.

36.   Hoffmann, E.d., Stroobant, V., *Mass Spectrometry: Principles and applications*. 3 ed2007, West Sussex, England: Wiley.

37. Jones, A.W. and H.J. Cooper, *Dissociation techniques in mass spectrometry-based proteomics.* Analyst, 2011. **136**(17): p. 3419-29.

38. Mikesh, L.M., et al., *The utility of ETD mass spectrometry in proteomic analysis.* Biochim Biophys Acta, 2006. **1764**(12): p. 1811-22.

39. Zhou, Y., J. Dong, and R.W. Vachet, *Electron transfer dissociation of modified peptides and proteins.* Curr Pharm Biotechnol, 2011. **12**(10): p. 1558-67.

40. Wuhrer, M., et al., *Glycoproteomics based on tandem mass spectrometry of glycopeptides.* J Chromatogr B Analyt Technol Biomed Life Sci, 2007. **849**(1-2): p. 115-28.

41. Syka, J.E., et al., *Peptide and protein sequence analysis by electron transfer dissociation mass spectrometry.* Proc Natl Acad Sci U S A, 2004. **101**(26): p. 9528-33.

42. Molina, H., et al., *Comprehensive comparison of collision induced dissociation and electron transfer dissociation.* Anal Chem, 2008. **80**(13): p. 4825-35.

43. Zhang, Y., et al., *Optimized Orbitrap HCD for quantitative analysis of phosphopeptides.* J Am Soc Mass Spectrom, 2009. **20**(8): p. 1425-34.

44. Olsen, J.V., et al., *Higher-energy C-trap dissociation for peptide modification analysis.* Nat Methods, 2007. **4**(9): p. 709-12.

45. Gillette, M.A. and S.A. Carr, *Quantitative analysis of peptides and proteins in biomedicine by targeted mass spectrometry.* Nat Methods, 2013. **10**(1): p. 28-34.

46. Ishihama, Y., et al., *Exponentially modified protein abundance index (emPAI) for estimation of absolute protein amount in proteomics by the number of sequenced peptides per protein.* Mol Cell Proteomics, 2005. **4**(9): p. 1265-72.

47. Geromanos, S.J., et al., *The detection, correlation, and comparison of peptide precursor and product ions from data independent LC-MS with data dependant LC-MS/MS.* Proteomics, 2009. **9**(6): p. 1683-95.

48. Kohli, B.M., et al., *An alternative sampling algorithm for use in liquid chromatography/tandem mass spectrometry experiments.* Rapid Commun Mass Spectrom, 2005. **19**(5): p. 589-96.

49.   Silva, J.C., et al., *Quantitative proteomic analysis by accurate mass retention time pairs.* Anal Chem, 2005. **77**(7): p. 2187-200.

50.   Silva, J.C., et al., *Absolute quantification of proteins by LCMSE: a virtue of parallel MS acquisition.* Mol Cell Proteomics, 2006. **5**(1): p. 144-56.

51.   Levin, Y., E. Hradetzky, and S. Bahn, *Quantification of proteins using data-independent analysis (MSE) in simple andcomplex samples: a systematic evaluation.* Proteomics, 2011. **11**(16): p. 3273-87.

52.   Li, G.Z., et al., *Database searching and accounting of multiplexed precursor and product ion spectra from the data independent analysis of simple and complex peptide mixtures.* Proteomics, 2009. **9**(6): p. 1696-719.

53.   Chakraborty, A.B., S.J. Berger, and J.C. Gebler, *Use of an integrated MS--multiplexed MS/MS data acquisition strategy for high-coverage peptide mapping studies.* Rapid Commun Mass Spectrom, 2007. **21**(5): p. 730-44.

54.   SWATH quantitative proteomic analysis. http://www.biodiscover.com/product/detail.html?id=322 Accessed 29/03/15 16:16

55.   Gillet, L.C., et al., *Targeted data extraction of the MS/MS spectra generated by data-independent acquisition: a new concept for consistent and accurate proteome analysis.* Mol Cell Proteomics, 2012. **11**(6): p. O111 016717.

56.   Ma, B., et al., *PEAKS: powerful software for peptide de novo sequencing by tandem mass spectrometry.* Rapid Commun Mass Spectrom, 2003. **17**(20): p. 2337-42.

57.   Craig, R., et al., *Using annotated peptide mass spectrum libraries for protein identification.* J Proteome Res, 2006. **5**(8): p. 1843-9.

58.   Eng, J.K., A.L. McCormack, and J.R. Yates, *An approach to correlate tandem mass spectral data of peptides with amino acid sequences in a protein database.* J Am Soc Mass Spectrom, 1994. **5**(11): p. 976-89.

59.   Perkins, D.N., et al., *Probability-based protein identification by searching sequence databases using mass spectrometry data.* Electrophoresis, 1999. **20**(18): p. 3551-67.

60.   Craig, R. and R.C. Beavis, *TANDEM: matching proteins with tandem mass spectra.* Bioinformatics, 2004. **20**(9): p. 1466-7.

61.   Cox, J., et al., *Andromeda: a peptide search engine integrated into the MaxQuant environment.* J Proteome Res, 2011. **10**(4): p. 1794-805.

62.   Waters Corporation. 2006. ProteinLynx Global Server Version 2.2.5 User's Guide. [ONLINE]   Available   at: http://www.embl.de/proteomics/proteomics_services/instrumentation/71500125602 ra.pdf. [Accessed 30 March 15]

63.   Keller, A., et al., *A uniform proteomics MS/MS analysis platform utilizing open XML file formats.* Mol Syst Biol, 2005. **1**: p. 2005 0017.

64.   Keller, A., et al., *Empirical statistical model to estimate the accuracy of peptide identifications made by MS/MS and database search.* Anal Chem, 2002. **74**(20): p. 5383-92.

65.   Han, D.K., et al., *Quantitative profiling of differentiation-induced microsomal proteins using isotope-coded affinity tags and mass spectrometry.* Nat Biotechnol, 2001. **19**(10): p. 946-51.

66.   Nesvizhskii, A.I., et al., *A statistical model for identifying proteins by tandem mass spectrometry.* Anal Chem, 2003. **75**(17): p. 4646-58.

67.   Eng, J.K., et al., *A face in the crowd: recognizing peptides through database search.* Mol Cell Proteomics, 2011. **10**(11): p. R111 009522.

68.   Schmidt, A., I. Forne, and A. Imhof, *Bioinformatic analysis of proteomics data.* BMC Syst Biol, 2014. **8 Suppl 2**: p. S3.

69.   Dennis, G., Jr., et al., *DAVID: Database for Annotation, Visualization, and Integrated Discovery.* Genome Biol, 2003. **4**(5): p. P3.

70.   Huang da, W., B.T. Sherman, and R.A. Lempicki, *Systematic and integrative analysis of large gene lists using DAVID bioinformatics resources.* Nat Protoc, 2009. **4**(1): p. 44-57.

71.   Khatri, P. and S. Draghici, *Ontological analysis of gene expression data: current tools, limitations, and open problems.* Bioinformatics, 2005. **21**(18): p. 3587-95.

72.   Kanehisa, M., et al., *KEGG for integration and interpretation of large-scale molecular data sets.* Nucleic Acids Res, 2012. **40**(Database issue): p. D109-14.

73.   Kumar, A., et al., *Elucidation of the CHO Super-Ome (CHO-SO) by Proteoinformatics.* J Proteome Res, 2015. **14**(11): p. 4687-703.

74.   Liu, H., R.G. Sadygov, and J.R. Yates, 3rd, *A model for random sampling and estimation of relative protein abundance in shotgun proteomics.* Anal Chem, 2004. **76**(14): p. 4193-201.

75.   Cha, S., et al., *In situ proteomic analysis of human breast cancer epithelial cells using laser capture microdissection: annotation by protein set enrichment analysis and gene ontology.* Mol Cell Proteomics, 2010. **9**(11): p. 2529-44.

76.   Elliott, M.H., et al., *Current trends in quantitative proteomics.* J Mass Spectrom, 2009. **44**(12): p. 1637-60.

77.   Bond, N.J., et al., *Improving qualitative and quantitative performance for MS(E)-based label-free proteomics.* J Proteome Res, 2013. **12**(6): p. 2340-53.

78.   Megger, D.A., et al., *Label-free quantification in clinical proteomics.* Biochim Biophys Acta, 2013. **1834**(8): p. 1581-90.

79.   Ong, S.E., et al., *Stable isotope labeling by amino acids in cell culture, SILAC, as a simple and accurate approach to expression proteomics.* Mol Cell Proteomics, 2002. **1**(5): p. 376-86.

80.   Kruger, M., et al., *SILAC mouse for quantitative proteomics uncovers kindlin-3 as an essential factor for red blood cell function.* Cell, 2008. **134**(2): p. 353-64.

81.   Sury, M.D., J.X. Chen, and M. Selbach, *The SILAC fly allows for accurate protein quantification in vivo.* Mol Cell Proteomics, 2010. **9**(10): p. 2173-83.

82.   Westman-Brinkmalm, A., et al., *SILAC zebrafish for quantitative analysis of protein turnover and tissue regeneration.* J Proteomics, 2011. **75**(2): p. 425-34.

83.   Geiger, T., et al., *Super-SILAC mix for quantitative proteomics of human tumor tissue.* Nat Methods, 2010. **7**(5): p. 383-5.

84.   Hsu, J.L., et al., *Stable-isotope dimethyl labeling for quantitative proteomics.* Anal Chem, 2003. **75**(24): p. 6843-52.

85.   Boersema, P.J., et al., *Triplex protein quantification based on stable isotope labeling by peptide dimethylation applied to cell and tissue lysates.* Proteomics, 2008. **8**(22): p. 4624-32.

86.   Ross, P.L., et al., *Multiplexed protein quantitation in Saccharomyces cerevisiae using amine-reactive isobaric tagging reagents.* Mol Cell Proteomics, 2004. **3**(12): p. 1154-69.

87.   Pottiez, G., et al., *Comparison of 4-plex to 8-plex iTRAQ quantitative measurements of proteins in human plasma samples.* J Proteome Res, 2012. **11**(7): p. 3774-81.

88.   Wu, W.W., et al., *Comparative study of three proteomic quantitative methods, DIGE, cICAT, and iTRAQ, using 2D gel- or LC-MALDI TOF/TOF.* J Proteome Res, 2006. **5**(3): p. 651-8.

89.   Thompson, A., et al., *Tandem mass tags: a novel quantification strategy for comparative analysis of complex protein mixtures by MS/MS.* Anal Chem, 2003. **75**(8): p. 1895-904.

90.   Keshishian, H., et al., *Multiplexed, Quantitative Workflow for Sensitive Biomarker Discovery in Plasma Yields Novel Candidates for Early Myocardial Injury.* Mol Cell Proteomics, 2015.

91.   Braun, C.R., et al., *Generation of multiple reporter ions from a single isobaric reagent increases multiplexing capacity for quantitative proteomics.* Anal Chem, 2015. **87**(19): p. 9855-63.

92.   Thermo Fisher Scientific Inc. 2014.Instructions: TMT Mass Tagging Kits and Reagents. [ONLINE] Available at: https://tools.lifetechnologies.com/content/sfs/manuals/MAN0011639_TMT_Mass_Tagging_Reag_UG.pdf [Accessed 01 March 2015]

93.   Savitski, M.M., et al., *Measuring and managing ratio compression for accurate iTRAQ/TMT quantification.* J Proteome Res, 2013. **12**(8): p. 3586-98.

94.   Savitski, M.M., et al., *Delayed fragmentation and optimized isolation width settings for improvement of protein identification and accuracy of isobaric mass tag quantification on Orbitrap-type mass spectrometers.* Anal Chem, 2011. **83**(23): p. 8959-67.

95.   Wenger, C.D., et al., *Gas-phase purification enables accurate, multiplexed proteome quantification with isobaric tagging.* Nat Methods, 2011. **8**(11): p. 933-5.

96.   Ting, L., et al., *MS3 eliminates ratio distortion in isobaric multiplexed quantitative proteomics.* Nat Methods, 2011. **8**(11): p. 937-40.

97.   Ow, S.Y., et al., *Minimising iTRAQ ratio compression through understanding LC-MS elution dependence and high-resolution HILIC fractionation.* Proteomics, 2011. **11**(11): p. 2341-6.

98.   McAlister, G.C., et al., *MultiNotch MS3 enables accurate, sensitive, and multiplexed detection of differential expression across cancer cell line proteomes.* Anal Chem, 2014. **86**(14): p. 7150-8.

99.   Erickson, B.K., et al., *Evaluating multiplexed quantitative phosphopeptide analysis on a hybrid quadrupole mass filter/linear ion trap/orbitrap mass spectrometer.* Anal Chem, 2015. **87**(2): p. 1241-9.

100.   Hebert, A.S., et al., *Neutron-encoded mass signatures for multiplexed proteome quantification.* Nat Methods, 2013. **10**(4): p. 332-4.

101.   Kim, J.Y., Y.G. Kim, and G.M. Lee, *CHO cells in biotechnology for production of recombinant proteins: current state and further potential.* Appl Microbiol Biotechnol, 2012. **93**(3): p. 917-30.

102.   Chee Furng Wong, D., et al., *Impact of dynamic online fed-batch strategies on metabolism, productivity and N-glycosylation quality in CHO cell cultures.* Biotechnol Bioeng, 2005. **89**(2): p. 164-77.

103.   Seow, T.K., et al., *Proteomic investigation of metabolic shift in mammalian cell culture.* Biotechnol Prog, 2001. **17**(6): p. 1137-44.

104.   Pascoe, D.E., et al., *Proteome analysis of antibody-producing CHO cell lines with different metabolic profiles.* Biotechnol Bioeng, 2007. **98**(2): p. 391-410.

105.   Fan, Y., et al., *A multi-pronged investigation into the effect of glucose starvation and culture duration on fed-batch CHO cell culture.* Biotechnol Bioeng, 2015.

106.   Wingens, M., et al., *2D-DIGE screening of high-productive CHO cells under glucose limitation--basic changes in the proteome equipment and hints for epigenetic effects.* J Biotechnol, 2015. **201**: p. 86-97.

107. Liu, Z., et al., *A quantitative proteomic analysis of cellular responses to high glucose media in Chinese hamster ovary cells.* Biotechnol Prog, 2015.

108. Hayduk, E.J., L.H. Choe, and K.H. Lee, *A two-dimensional electrophoresis map of Chinese hamster ovary cell proteins based on fluorescence staining.* Electrophoresis, 2004. **25**(15): p. 2545-56.

109. Lee, J.S., et al., *Protein reference mapping of dihydrofolate reductase-deficient CHO DG44 cell lines using 2-dimensional electrophoresis.* Proteomics, 2010. **10**(12): p. 2292-302.

110. Nissom, P.M., et al., *Transcriptome and proteome profiling to understanding the biology of high productivity CHO cells.* Mol Biotechnol, 2006. **34**(2): p. 125-40.

111. Meleady, P., et al., *Sustained productivity in recombinant Chinese hamster ovary (CHO) cell lines: proteome analysis of the molecular basis for a process-related phenotype.* BMC Biotechnol, 2011. **11**: p. 78.

112. Doolan, P., et al., *Microarray and proteomics expression profiling identifies several candidates, including the valosin-containing protein (VCP), involved in regulating high cellular growth rate in production CHO cell lines.* Biotechnol Bioeng, 2010. **106**(1): p. 42-56.

113. Feng, H.T., et al., *Rapid characterization of high/low producer CHO cells using matrix-assisted laser desorption/ionization time-of-flight.* Rapid Commun Mass Spectrom, 2010. **24**(9): p. 1226-30.

114. Kang, S., et al., *Cell line profiling to improve monoclonal antibody production.* Biotechnol Bioeng, 2014. **111**(4): p. 748-60.

115. Orellana, C.A., et al., *High-antibody-producing Chinese hamster ovary cells up-regulate intracellular protein transport and glutathione synthesis.* J Proteome Res, 2015. **14**(2): p. 609-18.

116. Wei, Y.Y., et al., *Proteomics analysis of chinese hamster ovary cells undergoing apoptosis during prolonged cultivation.* Cytotechnology, 2011. **63**(6): p. 663-77.

117. Beckmann, T.F., et al., *Effects of high passage cultivation on CHO cells: a global analysis.* Appl Microbiol Biotechnol, 2012. **94**(3): p. 659-71.

118. Xu, X., et al., *The genomic sequence of the Chinese hamster ovary (CHO)-K1 cell line.* Nat Biotechnol, 2011. **29**(8): p. 735-41.

119. Kaufmann, H., et al., *Influence of low temperature on productivity, proteome and protein phosphorylation of CHO cells.* Biotechnol Bioeng, 1999. **63**(5): p. 573-82.

120. Kumar, N., et al., *Differential protein expression following low temperature culture of suspension CHO-K1 cells.* BMC Biotechnol, 2008. **8**: p. 42.

121. Baik, J.Y., et al., *Initial transcriptome and proteome analyses of low culture temperature-induced expression in CHO cells producing erythropoietin.* Biotechnol Bioeng, 2006. **93**(2): p. 361-71.

122. Kantardjieff, A., et al., *Transcriptome and proteome analysis of Chinese hamster ovary cells under low temperature and butyrate treatment.* J Biotechnol, 2010. **145**(2): p. 143-59.

123. Baik, J.Y., et al., *Limitations to the comparative proteomic analysis of thrombopoietin producing Chinese hamster ovary cells treated with sodium butyrate.* J Biotechnol, 2008. **133**(4): p. 461-8.

124. Yee, J.C., et al., *Genomic and proteomic exploration of CHO and hybridoma cells under sodium butyrate treatment.* Biotechnol Bioeng, 2008. **99**(5): p. 1186-204.

125. Van Dyk, D.D., et al., *Identification of cellular changes associated with increased production of human growth hormone in a recombinant Chinese hamster ovary cell line.* Proteomics, 2003. **3**(2): p. 147-56.

126. Lee, M.S., et al., *Proteome analysis of antibody-expressing CHO cells in response to hyperosmotic pressure.* Biotechnol Prog, 2003. **19**(6): p. 1734-41.

127. Kim, J.Y., Y.G. Kim, and G.M. Lee, *Differential in-gel electrophoresis (DIGE) analysis of CHO cells under hyperosmotic pressure: osmoprotective effect of glycine betaine addition.* Biotechnol Bioeng, 2012. **109**(6): p. 1395-403.

128. Kim, J.Y., et al., *Proteomic understanding of intracellular responses of recombinant Chinese hamster ovary cells cultivated in serum-free medium supplemented with hydrolysates.* Appl Microbiol Biotechnol, 2011. **89**(6): p. 1917-28.

129. Carlage, T., et al., *Proteomic profiling of a high-producing Chinese hamster ovary cell culture.* Anal Chem, 2009. **81**(17): p. 7357-62.

130. Carlage, T., et al., *Analysis of dynamic changes in the proteome of a Bcl-XL overexpressing Chinese hamster ovary cell culture during exponential and stationary phases.* Biotechnol Prog, 2012. **28**(3): p. 814-23.

131. Baik, J.Y. and G.M. Lee, *A DIGE approach for the assessment of differential expression of the CHO proteome under sodium butyrate addition: Effect of Bcl-x(L) overexpression.* Biotechnol Bioeng, 2010. **105**(2): p. 358-67.

132. Meleady, P., et al., *Proteomic profiling of CHO cells with enhanced rhBMP-2 productivity following co-expression of PACEsol.* Proteomics, 2008. **8**(13): p. 2611-24.

133. Meleady, P., et al., *Impact of miR-7 over-expression on the proteome of Chinese hamster ovary cells.* J Biotechnol, 2012. **160**(3-4): p. 251-62.

134. Kuystermans, D., M.J. Dunn, and M. Al-Rubeai, *A proteomic study of cMyc improvement of CHO culture.* BMC Biotechnol, 2010. **10**: p. 25.

135. Becker, J., et al., *Unraveling the Chinese hamster ovary cell line transcriptome by next-generation sequencing.* J Biotechnol, 2011. **156**(3): p. 227-35.

136. Meleady, P., et al., *Utilization and evaluation of CHO-specific sequence databases for mass spectrometry based proteomics.* Biotechnol Bioeng, 2012. **109**(6): p. 1386-94.

137. Evans, V.C., et al., *De novo derivation of proteomes from transcriptomes for transcript and protein identification.* Nat Methods, 2012. **9**(12): p. 1207-11.

138. Valente, K.N., et al., *Recovery of Chinese hamster ovary host cell proteins for proteomic analysis.* Biotechnol J, 2013.

139. Tait, A.S., et al., *Host cell protein dynamics in the supernatant of a mAb producing CHO cell line.* Biotechnol Bioeng, 2012. **109**(4): p. 971-82.

140. Food and Drug administration. 1997. Points to Consider in the Manufacture and Testing of Monoclonal Antibody Products for Human Use.

141. Krawitz, D.C., et al., *Proteomic studies support the use of multi-product immunoassays to monitor host cell protein impurities.* Proteomics, 2006. **6**(1): p. 94-110.

142. Jin, M., et al., *Profiling of host cell proteins by two-dimensional difference gel electrophoresis (2D-DIGE): Implications for downstream process development.* Biotechnol Bioeng, 2010. **105**(2): p. 306-16.

143. Doneanu, C.E., et al., *Analysis of host-cell proteins in biotherapeutic proteins by comprehensive online two-dimensional liquid chromatography/mass spectrometry.* MAbs, 2012. **4**(1): p. 24-44.

144. Schenauer, M.R., G.C. Flynn, and A.M. Goetze, *Identification and quantification of host cell protein impurities in biotherapeutics using mass spectrometry.* Anal Biochem, 2012. **428**(2): p. 150-7.

145. Kumar, N., et al., *Proteomic profiling of secreted proteins from CHO cells using Surface-Enhanced Laser desorption ionization time-of-flight mass spectrometry.* Biotechnol Prog, 2008. **24**(1): p. 273-8.

146. Ahram, M., et al., *Identification of shed proteins from Chinese hamster ovary cells: application of statistical confidence using human and mouse protein databases.* Proteomics, 2005. **5**(7): p. 1815-26.

147. Woolley, J.F. and M. Al-Rubeai, *The isolation and identification of a secreted biomarker associated with cell stress in serum-free CHO cell culture.* Biotechnol Bioeng, 2009. **104**(3): p. 590-600.

148. Lim, U.M., et al., *Identification of autocrine growth factors secreted by CHO cells for applications in single-cell cloning media.* J Proteome Res, 2013. **12**(7): p. 3496-510.

149. Sommeregger, W., et al., *Proteomic differences in recombinant CHO cells producing two similar antibody fragments.* Biotechnol Bioeng, 2016.

150. Shliaha, P.V., et al., *Effects of traveling wave ion mobility separation on data independent acquisition in proteomics studies.* J Proteome Res, 2013. **12**(6): p. 2323-39.

151. Wales, T.E. and J.R. Engen, *Hydrogen exchange mass spectrometry for the analysis of protein dynamics.* Mass Spectrom Rev, 2006. **25**(1): p. 158-70.

2.0

Quantitative Proteomics Analysis of CHO Cells Following Culture under Altered Bioprocessing Conditions

2.1   Introduction

Chinese hamster ovary (CHO) cell lines are the primary expression system currently used in the biopharmaceutical industry and have been engineered to produce a wide range of recombinant therapeutic biomolecules, including those used to treat cancer, haemophilia, diabetes mellitus, inflammation-related conditions, neutropenia and metabolic disorders. [1] Anti-Interleukin 8 (anti-IL8), a therapeutic monoclonal antibody (mAb), has the potential for use in the treatment and diagnosis of metastatic melanoma and inflammatory disorders, *e.g.* adult respiratory distress syndrome, multiple organ failure and septic shock. [2, 3] Anti-IL8 exerts its effect by binding to the cytokine interleukin 8 (IL8) thereby preventing the activity of IL8 *in-vivo*. IL8 has been shown to contribute to human melanoma advancement by functioning as a mitogenic and angiogenic factor, while IL8 concentration in serum was found to correlate with tumour load. [4-9] Additionally, IL8 is known to be involved in inflammatory responses, possibly due to induction of neutrophils [10] and is associated with adverse dermatological reactions in response to epidermal growth factor receptor inhibitors used in cancer treatment. [11] In this thesis, an anti-IL8 producing CHO DP-12 cell line is used to investigate the impact of altered bioprocessing on both an industrial relevant expression system and on the therapeutic product produced. Although the anti-IL8 IgG1 studied is not currently marketed as a therapeutic biomolecule it is similar to mAbs undergoing biopharmaceutical development for potential pharmacological indications. [12][13]

Since the establishment of the biopharmaceutical industry, great strides have been made for optimisation of CHO cell bioprocessing. Continuous improvements of industrial bioprocesses and associated optimisation in bioreactor design and media formulation has resulted in considerable increases in product yields. [14] Many of the strategies to enhance bioprocessing have incorporated a reduction in temperature from 37°C to 30-32°C, [15-17] an increase in osmolarity, *e.g.* 300 to 450 mOSm.kg^{-1} [18] or a reduction in media pH. [17] Alternative approaches have included the addition of media supplements [19, 20] or the use of a

controlled feeding strategy. [21] These strategies have been shown to result in desirable outcomes with respect to bioprocessing, such as high cell viability, increased specific productivity and reduced accumulation of waste by-products. Cell engineering approaches have also been employed for the optimisation of specific productivity (qP), enhancing culture longevity and improving specific growth rate following CHO bioprocessing. By manipulation of genes involved in growth proliferation, [22] protein secretion, [23, 24] metabolic pathways [25] and apoptosis, [26-30] extended culture viability and increased qP have been achieved.

Traditionally the majority of improvements to CHO bioprocessing have been realised by observing empirical responses to process changes. Despite two decades of CHO bioprocessing, there is still very poor comprehension of the cellular mechanisms that govern recombinant protein production in these important cell lines. Similarly little understanding exists regarding the impact of bioprocessing on the cellular machinery of the production cells. As proteins are the functional components of a cell, they have the potential to change cellular outputs. Hence, characterisation of the fundamental biological mechanisms of CHO cells in industrial cell culture may provide a foundation for further knowledge-driven improvements to manufacturing processes [31]. Increased understanding of the CHO proteome may lead to production of therapeutics that have guaranteed critical quality attributes and consequently reduced attrition rates often associated with biopharmaceutical production and process development.

Recent technological achievements in analytical instrumentation have enabled profiling of the CHO proteome to a depth that was previously not possible. In particular advances in liquid chromatography and mass spectrometry have resulted in the identification of thousands of CHO proteins that play key roles in bioprocessing including those involved in cell growth, protein processing, glycosylation and metabolism. [32] Augmented by the publication of the CHO genome, [33] investigation of the cellular pathways involved in bioprocessing or pathways enhanced in CHO cells with desirable phenotypes is now achievable. As discussed in Chapter 1, use of high resolution hybrid mass spectrometers permit increasingly broad proteome coverage due to the high mass accuracy and resolving power of MS survey scan acquisition combined with fast, sensitive MS/MS analyses. State-of-the-art instruments incorporating a third mass analyser further enhance the dynamic range of detection achievable. By enabling synchronous precursor selection (SPS) prior to MS3 determination, inclusion of multiplexed quantitative strategies in proteomic experiments (*e.g.* use of tandem mass tag (TMT) reagents) has the ability to fully describe the dynamic processes that drive

recombinant protein production. In addition to comprehensively cataloguing proteins within a cell, use of LC-MS[3] may provide insights into molecular interactions within the cell.

In this chapter, a study is described wherein concurrent CHO DP-12 cell cultures, expressing anti-IL8, were initially prepared using standard bioprocessing conditions and later with altered bioprocessing conditions of pH, dissolved oxygen and temperature. Quantitative proteomics analysis of produced CHO cell lysate was performed using a two dimensional high pH low pH reversed phase nano liquid chromatography - mass spectrometry platform to facilitate comparison of the effects of individual culture characteristics on the CHO cell proteome. An Orbitrap Fusion Lumos tribrid mass spectrometer was employed enabling the identification and subsequent relative quantitation of, and hence, determination of altered protein expression in CHO DP-12 cells in response to the bioprocessing conditions utilised. Ingenuity pathway analysis (IPA) was subsequently applied for determination of enriched biological pathways within the differentially bioprocessed CHO cells. Furthermore, the method was also used to determine bystander responses resulting from changes to the secretome of CHO cells following bioprocessing under altered conditions. In this case naïve CHO K1 cultures were prepared and subsequently exposed to spent media from each of the CHO DP-12 cultures. Thus, by evaluating changes to naïve CHO K1 proteomes, a further layer of understanding regarding CHO bioprocessing could be achieved.

2.2 Experimental

2.2.1 Reagents and Consumables

Sodium chloride (NaCl), sodium phosphate monobasic dihydrate (NaH$_2$PO$_4 \cdot$ 2H$_2$O), sodium phosphate dibasic heptahydrate (Na$_2$HPO$_4 \cdot$ 7H$_2$O), sodium hydroxide (NaOH), dithiothreitol (DTT), iodoacetamide (IAA), acetonitrile, formic acid, triethylammonium bicarbonate (TEAB), ammonium hydroxide, L-arginine, phosphate buffered saline, Excell 325 PF CHO media, fetal bovine serum (FBS), methotrexate, recombinant human insulin, trypan blue, dimethyl-sulfoxide, Dulbecco's phosphate buffered saline (D-PBS), Tris buffer, hydrochloric acid, sodium dodecyl sulphate, urea, ammonium bicarbonate, trifluoroacetic acid (TFA), Bradford reagent, Bovine serum albumin (BSA), urea, Trizma-base and Amicon Ultra 0.5 mL centrifugal filters MWCO 10 kDa were purchased from Sigma Aldrich (Wicklow, Ireland). 0.1% formic acid in water (LC-MS Optima), acetonitrile, 0.1% formic acid (LC-MS Optima), 0.1% TFA in water (LC-MS Optima), TMT sixplex isobaric mass tag reagents and penicillin-streptomycin were obtained from Fisher Scientific (Dublin, Ireland). Promega sequencing grade modified trypsin

was from MyBio Ltd. (Kilkenny, Ireland). L-glutamine and trypsin/EDTA solution were purchased from Biosciences Ltd. (Dublin, Ireland). 100% acetic acid (AnalaR NORMAPUR) was obtained from VWR (Dublin, Ireland).

2.2.2 Cell Culture

2.2.2.1 Aseptic Technique

Cell culture work was carried out in a BioAir SafeMate 1.2 class II biological safety cabinet. Prior to use the laminar airflow cabinet was sterilised with UV light for one hour and thoroughly cleaned with 70% (v/v) ethanol. Subsequently, air in the laminar airflow cabinet was to allowed to circulate for a minimum of 15 minutes before cell culture commenced to ensure aseptic conditions were achieved. Any items placed in the cabinet were also swabbed with 70% (v/v) ethanol prior to entry into the cabinet. During use, one cell line only was introduced into the laminar airflow cabinet and upon completion of work with any given cell line, the laminar airflow cabinet was allowed to clear for at least 15 minutes before further use. This was to eliminate any possibility of cross-contamination between cell lines. The cabinets were cleaned weekly with Virkon and operation validated annually by a certified contractor.

2.2.2.2 Adaption of CHO DP-12 to Serum-Free Media and Suspension Culture

A Chinese hamster ovary cell line (CHO DP-12 clone#1934 [CHO DP-12, clone#1934 aIL8.92 NB 28605/14] (ATCC® CRL-12445™) producing recombinant human anti-IL-8 IgG1 antibody, was purchased from LGC standards (Middlesex, UK). Recommended culturing conditions for the CHO DP-12 cell line involved preparing adherent cell culture in DMEM, supplemented with 10% fetal bovine serum (FBS), 200 nM methotrexate and 2 mg.L^{-1} recombinant human insulin in a T75 cm^2 culture flask. As the CHO DP-12 cell line was purchased for use in proteomic studies, adaption of the cell line to grow in protein-free media was required to ensure no impact on proteomic results due to media components and also to facilitate simplified purification of the expressed mAb for subsequent product characterisation as described Chapters 3, 4 and 5. Initially, cells were grown adherently in supplier-recommended media formulation at 37 °C (5% CO$_2$). Adaption to serum-free conditions was achieved by reducing the FBS concentration in the media to 5%, 2.5% and 1% over five passages. Once growing in 1% FBS, the cells were transferred from a T75 cm^2 flask to serum-free conditions in a 125 ml

Erlenmeyer shake flask. In an effort to ensure the growth medium was completely protein-free, cells were subsequently further adapted to grow in a commercially available protein-free media recommended for CHO DP-12 cell cultures, namely Excell™ 325 PF CHO. Adaption to protein-free media was accomplished by altering the composition of the culture medium from 100:0, 75:25, 50:50, 25:75, 0:100 DMEM/ Excell™ 325 PF CHO, over five passages. At each stage, the culture medium was supplemented with 10 mg.L^{-1} recombinant human insulin, 4 mM L-glutamine, 200 nM methotrexate and 20,000 Units of Penicillin-Streptomycin. Finally, to ensure selection pressure for CHO DP-12 clones producing anti-IL-8 IgG1, the concentration of methotrexate was increased from 200 nM to 1 μM over two passages.

2.2.2.3 Thawing of Cryopreserved Cell Banks and Cell Culture of Fully-Adapted CHO DP-12 Cell Lines in Protein-Free, Suspension Culture

CHO DP-12 cells, from a working cell bank stored at -196 °C, were rapidly thawed at 37 °C. Cells were re-constituted in 10 mL of pre-warmed complete media (Excell™ 325 PF CHO, 10 mg.L^{-1} recombinant human Insulin, 4 mM L-glutamine, 1 μM methotrexate and 20,000 Units of Penicillin-Streptomycin), before centrifugation at 800 rpm for five minutes. The resultant cell pellet was re-suspended in a 10 mL aliquot of fresh complete media, before cell counting using the trypan blue exclusion method and a haemocytometer. Cells were seeded at an initial viable cell density of 3 x 10^5 cells per mL of complete media in a 125 mL Erlenmeyer shake flask and were incubated at 37°C (5% CO_2, 125 rpm). Passaging of cells was performed while cell cultures were in an exponential growth phase.

2.2.2.4 Maintenance of the Cell Lines

Cells for cryopreservation were harvested in the exponential phase of growth. Cell pellets were re-suspended in a suitable volume of Excell™ 325 PF CHO supplemented with 10 mg.L^{-1} recombinant human insulin, 4 mM L-glutamine and 5% DMSO and 1 mL aliquots of the suspension were placed in cryovials. Vials were then placed in a slow-freezing container at -80°C to achieve cooling of cells at a rate of approximately -1°C per minute. After a period of five hours, vials were transferred to a Dewar containing liquid nitrogen for storage (-196°C). Cell lines were tested in-house for possible mycoplasma contamination using a Roche MycoTool mycoplasma real-time polymerase chain reaction kit with MagNa Pure LC2.0 and

the Roche LightCycler 480 instrumentation. No mycoplasma infection was determined in samples analysed.

2.2.2.5 Cell Culture using Disposable Single Use Bioreactors

All bioprocessing studies were performed using Sartorius Stedim Cultibag systems equipped with a 2L Optical Cultibag single use bioreactor. Bioreactors were placed on temperature controlled rocker stations and fitted with a gas line, dissolved oxygen and pH sensors and a base addition line. pH was initially set to pH 7.0 and maintained by the automated addition of sterile 1 M sodium hydroxide or by purging 0.22 µm sterile filtered CO_2 gas into the head-space of the disposable bioreactor. The rocker station angle was set to 7.0^o. Gas flow was set to 0.3 L.min^{-1}. The rocker also served as a heating element used to maintain the culture at the initial set-point of 37.0^oC. Dissolved oxygen (DO) levels were maintained by purging a mixture of purified air and oxygen into the head-space of the bioreactor and also by altering the rocking speed of the disposable bioreactor (3 to 14 rocks per minute). 950 mL of media, composed of Excell^{TM} 325 PF CHO, 10 mg.L^{-1} recombinant human Insulin, 4 mM L-glutamine, 1 µM methotrexate and 20,000 Units of Penicillin-Streptomycin, was added to each of three disposable bioreactors and were allowed to equilibrate to initial conditions of 37.0^oC, pH 7.0 and 85% DO overnight. Prior to inoculation with 50 mL of CHO DP-12 culture, pH readings were verified by removing an aliquot of media from the bioreactor and measuring the pH value using a calibrated pH electrode. CHO DP-12 cells were inoculated at a starting viable cell density of 3 x 10^5 cells.mL^{-1}. Cell culture harvest was performed after 7 days of culture. Culture harvest was completed by transferring each culture into a sterile 1 L Duran bottle, before sub-dividing the cultures into sterile falcon tubes and centrifuging at 125 x g for 5 minutes. Spent media was subsequently pipetted into fresh sterile falcon tubes. 50 mL aliquots of the spent media were retained for subsequent application to naïve CHO K1 cell cultures. The remaining spent media and all CHO DP-12 cell pellets were immediately placed at -80°C pending further analysis.

2.2.2.6 Determination of Nutrient and Metabolite Concentration, Cell Count and Cell Viability

A 5 mL aliquot of cell culture was removed from each of the bioreactors daily. Cell counting was performed using the trypan blue exclusion method and a haemocytometer. 1 mL of each

culture was centrifuged (5,000 x g, 10 minutes) to remove cellular material before measurement of IgG, L-glutamine, glucose, glutamate, ammonia and lactate concentration and also LDH activity in the clarified culture media using a Cedex Bioanalyser *via* photometric analysis.

2.2.2.7 Culture of Naïve CHO K1 Cells

A non-recombinant protein producing cell line (CHO K1 - ATCC® CCL-61^{TM}) was purchased from LGC standards (Middlesex, UK). Initially grown in recommended F-12K media supplemented with 10% FBS and 4 mM L-glutamine, adaption to serum-free conditions was achieved by reducing the FBS concentration in the media to 5%, 2.5% and 1% over five passages. Once growing in 1% FBS, the cells were transferred from a T75 cm^2 flask to serum-free conditions in a 125 ml Erlenmeyer shake flask. The CHO K1 cells were adapted to growth in commercial protein-free media by altering the composition of the culture medium from 100:0, 75:25, 50:50, 25:75, 0:100 F-12K/ Excell^{TM} 325 PF CHO over five passages. For each bioprocess parameter studied, CHO K1 cultures were seeded in 12 x 125 mL Erlenmeyer culture flasks and allowed to grow for two days in Excell 325 PF medium supplemented with 10 mg.L^{-1} recombinant human insulin, 4 mM L-glutamine, 200 nM methotrexate and 20,000 Units of Penicillin-Streptomycin. Once in the exponential growth phase spent media from each CHO DP-12 altered bioprocessing culture were applied to one of nine CHO K1 cultures. Three remaining CHO K1 cell cultures were maintained using the same media components but not exposed to spent media samples. The cells were exposed to the spent media for 24 hours before harvest *via* centrifugation (125 x g, 5 minutes). Cell pellets were immediately frozen at -80°C pending further analysis.

2.2.3   Proteomic Analysis of CHO Cells using High pH- Low pH 2D-LC-MS/MS
2.2.3.1 CHO Proteome Sample Preparation

Cell pellets were thawed on ice and rinsed with three 1 mL aliquots of PBS to ensure complete removal of culture medium. Freshly prepared 8M Urea in 100 mM Tris, pH 8.0 was added to reconstitute each cell pellet to an approximate final concentration of 1×10^7 cells.mL^{-1}. Subsequently cells were homogenised *via* sonication for 30 seconds using a sonic dismembrator (Fisher Scientific) set to 20 V and centrifuged (16,000 x g, 10 minutes). Supernatant was placed in a fresh tube and assayed for protein content using a Bradford

protein assay, wherein samples were diluted 50-fold with Bradford reagent and incubated for 30 minutes at room temperature before recording the sample absorbance using a spectrophotometer at 595 nm. Sample concentration was calculated using a standard curve prepared from BSA standards of known concentration, diluted with Bradford reagent and inclubated concurrent to the CHO protein samples. Proteomic samples were prepared using the filter-aided sample preparation (FASP) method described previously. [34] Briefly, 100 µg of CHO cell lysate was added to a pre-rinsed 10 kDa MWCO filters and reduced with 5 mM DTT at 25°C for 30 minutes, before alkylation with 15 mM IAA for 30 minutes at 20°C in darkness. Following buffer exchange into 100 mM TEAB, enzymatic digestion was performed overnight with trypsin at 37°C using a 1:50 (w/w, enzyme: protein) ratio. Subsequently sample peptides were retrieved from the filters by centrifugation before labelling with TMT-sixplex reagents as per manufacturer's instructions. [35] 0.8 mg of each TMT labelling reagent dissolved in 41 µL of anhydrous acetonitrile was added to 100 µg of CHO tryptic peptides, before incubation for one hour at room temperature. The reaction was quenched by addition of 8 µL of 5% hydroxylamine prior to incubation for 15 minutes. Tryptic peptide samples from CHO DP-12 and CHO K1 cultures were labelled as per the experimental design outlined in Tables 2.2 and 2.3, respectively. Samples labelled with each set of TMT-sixplex labels were pooled into eight combined samples sets and reduced to dryness *via* vacuum centrifugation.

2.2.3.2 First Dimensional Fractionation

First dimensional separation of the peptide sample sets was carried out using high pH (pH 10) reversed-phase chromatography on a Waters Acquity H-Class UPLC instrument with UV detection. Separations were performed on an Acquity UPLC BEH 130 C18 1.7 µm 2.1 x 150 mm analytical column using a binary gradient of 10 mM ammonium formate in water, pH 10 (A) and 10 mM ammonium formate in 95% acetonitrile, pH 10 (B). Before separation analysis, samples were diluted to 500 µL with 0.1% formic acid and loaded onto the analytical column, using 3% B, over three injections. Sample separation was accomplished using gradient conditions as follows: 3% B initially for 2 minutes, increased to 10% B in 2 minutes with a further increase to 45% B over 33 minutes followed by a final increase to 100% B in two minutes with a two minute isocratic hold. Initial conditions were restored in one minute and held for an additional 10 minutes to ensure column re-equilibration. The column temperature was maintained at 40°C throughout and UV absorbance recorded at 214 nm. The flow rate was sustained at 200 µL.min^{-1}. Sample eluate was collected at minute intervals over the course of the gradient and subsequently recombined to 10 sample fractions of equal concentration as

estimated based on the UV response. Finally sample fractions obtained for each sample set were reduced to dryness *via* vacuum centrifugation.

2.2.3.3 Second Dimension nano-LC-MS Method Development

All spectra were acquired on an Orbitrap Fusion Lumos (Thermo Fisher Scientific) coupled to a Dionex Ultimate® 3000 RSLCnano system. Peptides were separated on an Acclaim PepMap RSLC C18, 100 Å, 75µm x 50 cm, easy-spray column (Thermo Fisher Scientific) using a binary gradient of 0.1% (v/v) formic acid in water (C) and 0.1% (v/v) formic acid in acetonitrile (D). Gradient conditions were as follows: 5% D initially for 5 minutes, increased to 25% D in 85 minutes with a further increase to 60% D over 20 minutes followed by a final increase to 90% D in 5 minutes with a 5 minute isocratic hold. Initial conditions were restored in one minute and held for an additional 29 minutes to ensure column re-equilibration. The column temperature was maintained at 40°C and the flow rate was 300 µL.min^{-1}. Injection volume was 1 µL, corresponding to 1 µg of labelled tryptic peptides.

The mass spectrometer was operated in data dependent mode. Survey scans of peptide precursors were performed from 350 to 1500 m/z at 120,000 FWHM resolution (at 200 m/z) in the Orbitrap with a 4 x 10^5 ion count target and a maximum injection time of 50 ms. The instrument was set to run in top speed mode (considering only the most intense charge state for fragmentation) with 3 second cycles for the survey and the MS/MS scans. Following a survey scan, tandem MS was performed on the most intense precursors exhibiting a charge state from 2 to 7 and of greater than 5 x 10^3 intensity by isolation in the quadrupole using a mass filter width of 0.7 Th. Dynamic exclusion was set to each precursor for 60 seconds subsequent to acquisition ensuring a 10 ppm mass tolerance around the precursor and its isotopes. CID fragmentation was applied with 35% normalised collision energy and resulting fragments were detected using the turbo scan rate in the ion trap mass analyser. The AGC target for MS/MS was set to 10^4 and the maximum injection time limited to 50 ms. Precursor selection mass range was performed from 400 to 1200 m/z for MS2 and isobaric tag loss exclusion set for TMT. Synchronous precursor selection was enabled to include the top five fragment ions for the MS3 scan using an isolation window of 0.7 m/z. HCD fragmentation was applied with 65% collision energy to ensure maximal TMT reporter ion yield and resulting fragments were detected using the Orbitrap from 100 to 500 m/z at 30,000 FWHM resolution (at 200 m/z). The AGC target for MS/MS was set to 10^5 and the maximum injection time limited to 105 ms.

2.2.3.4 Bioinformatics

Raw data was processed using Thermo Scientific™ Proteome Discoverer™ software version 2.1.0.81. Proteome Discoverer™ software is a bioinformatics tool used to interpret Thermo Fisher Scientific mass spectrometry data acquired from complex biological samples. Proteome Discoverer™ software enables the identification and quantitation of proteins using various database search algorithms, *e.g.* Mascot and SEQUEST®, and supports multiple dissociation techniques, *e.g.* collision induced dissocation. MS2 spectra were searched with the SEQUEST® HT engine against the *Cricetulus griseus*, NCBI FASTA database (http://www.ncbi.nlm.nih.gov/assembly/GCF_000419365.1/, downloaded 12th August 2015) and also a CHO DG44 proteome database, translated from CHO DG44 transcriptome sequences, additionally annotated with *mus musculus* RefSeq notation. [36] Search parameters included an *in silico* tryptic digestion permitting ≤2 missed cleavages, fixed modifications including carbamidomethylation (+57.021 Da) of cysteine residues and TMT sixplex (+229.163 Da) of the N-terminus and K side chain and a variable modification set to oxidation of methionine residues (+15.9949 Da). Mass tolerances were set to 10 ppm for precursors and 0.6 Da for product ions. Peptide spectral matches (PSM) were validated using the Percolator® algorithm, based on q-values at a 1% FDR. For both the CHO DP-12 and CHO K1 studies, each set of 10 samples were grouped as fractions using Proteome Discoverer™ software and subsequent data merged to produce a single result file outlining all peptides and protein groups identified along with corresponding TMT reporter abundance values and sequence information.

TMT reporter intensity values relating to peptides from each culture prepared under altered bioprocessing conditions were compared to corresponding TMT reporter abundances from peptides prepared under standard culture conditions. Log fold changes and p-values for the CHO DG44 proteome database-searched data were determined using InfernoRDN version 1.1.5970.31895. [37] InfernoRDN is a statistical tool for quantitative analysis of 'omics' data sets and may be applied for normalisation of data, hypothesis testing, clustering and generation of heat-maps. Using InfernoRDN, peptide level abundance values corresponding to the TMT reporter ion for each peptide were log 2 transformed, median centered and grouped together according to their related protein group using the 'ZRollup' function. ANOVA analysis was performed at the protein level to determine related p-values and fold changes were calculated. Proteins with a p-value <0.05 and greater than 1.2 log fold change in the test samples compared to the control standard samples were listed as differentially regulated in the samples produced under altered bioprocessing conditions

Gene Ontology (GO) annotation terms of cell components were determined for identified proteins using the online tool, the database for annotation, visualisation and integrated discovery (DAVID) (http://david.abcc.ncifcrf.gov). [38, 39] DAVID is a bioinformatics tool that enables functional annotation of lists of genes or proteins to facilitate a better understanding of biological function relating to large protein data sets or list of genes. Mouse homologue RefSeq annotation correlating to identified CHO proteins, were used to determine the function of quantified CHO cell proteins in DAVID. Gene ontology terms, obtained using DAVID software, were visualised using REVIGO online software. REVIGO functions as a tool to summarise and interpret lists of GO terms through use of a clustering algorithm, which relies on semantic similarity measurements (http://revigo.irb.hr). [40] Ingenuity Pathway Analysis (IPA) version 27216297 (QIAGEN, Redwood City, CA, USA) was utilised to map significantly differentially regulated proteins into biological networks and pathway maps. IPA is a tool for analysis, modelling and understanding of complex biological systems through provision of insights into potential relationships, mechanisms, functions and relevant molecular and protein pathways.   In this work, experimental data from human, mouse and rat were used for determination of protein pathways and networks in IPA, incorporating a significance threshold of $p<0.01$ and greater than 1.2 log fold change of test samples compared to the control standard samples. Biological functions for proteins statistically significant with a |Z score| ≥ 1.0 for activation or repression were reported

2.3   Results and Discussion.

2.3.1 Experimental Design for Anti-IL8 Production under Altered Bioprocessing Conditions

Since the realisation of CHO cells as recombinant protein expression systems for the biopharmaceutical industry, vast improvements in production strategies have resulted in high product titres and improved therapeutic protein quality in response to empirical improvements following measured changes to bioprocessing. In particular, changes to culture temperature, pH, dissolved oxygen, osmolarity and feeding strategies have been effective approaches used to halt apoptosis, stimulate protein secretion and alter cellular metabolism. [17, 41-44] Several studies have endeavoured to understand the cellular processes that effect change to protein secretion from CHO cells in response to some of the known productivity-enhancing culture conditions. [36, 45-49] By investigating changes to the proteome of recombinant protein producing cells, various differentially regulated proteins have been identified which suggest potential pathways that may be in play when bioreactor settings have been optimised for protein production. However, advances in analytical technology,

supplemented by the recent sequencing of the *Cricetulus griseus* genome, have now enabled profiling of the CHO proteome at a depth that was previously not possible.

A major aim of this work was to apply state of the art analytical technology to determine systematic responses of CHO cells to altered bioprocessing conditions. In this study multiple bioprocess production sequences were prepared to study the effects of pH, temperature and dissolved oxygen (DO) on the production of biotherapeutics as depicted in Figure 2.1. By preparing CHO cell cultures using disposable bioreactors commonly used in industrial settings a high level of process control could be achieved while closely mimicking a genuine production process. For each of the parameters under study, three concurrent cell cultures were prepared. Following inoculation of Sartorius Cultibag disposable bioreactors, batch culture of CHO DP-12 cells was performed at standard culture settings of 37.0^{o}C, pH 7.0 and 85% DO. As the cell cultures began to enter the stationary phase of cell growth (equivalent to day 5 of cell culture), one parameter in two of the bioreactors was changed as shown in Table 2.1. The parameters selected reflect settings commonly used in bioprocessing, chosen to represent the outer limits of a design space used in biopharmaceutical production of CHO cell culture. Hence any changes that are identified may reflect tangible alterations in CHO cell proteomes that may occur in routine production in the biopharmaceutical industry. Cultures were allowed to proceed for 48 hours at altered bioprocessing conditions, at which stage the cultures were harvested (culture day 7) as outlined in Section 2.2.2.5. All cell cultures were harvested prior to entry into the logarithmic decline phase of cell growth, ensuring high viability at the time of culture harvest. In addition to production of CHO DP-12 batch culture, naïve CHO K1 cell cultures were also prepared concurrently. Following harvest of conditioned spent media from CHO DP-12 studies, aliquots of each of the spent media samples were applied to CHO K1 cell culture for approximately 24 hours before CHO K1 cell harvest. This step was performed to evaluate any potential changes to CHO cells in response to signalling factors in the secretome of production cells present due to the use of altered bioprocessing conditions. Additionally full characterisation of anti-IL8 expressed from CHO DP-12 cells during each of the studies described will be outlined in Chapters 3, 4 and 5.
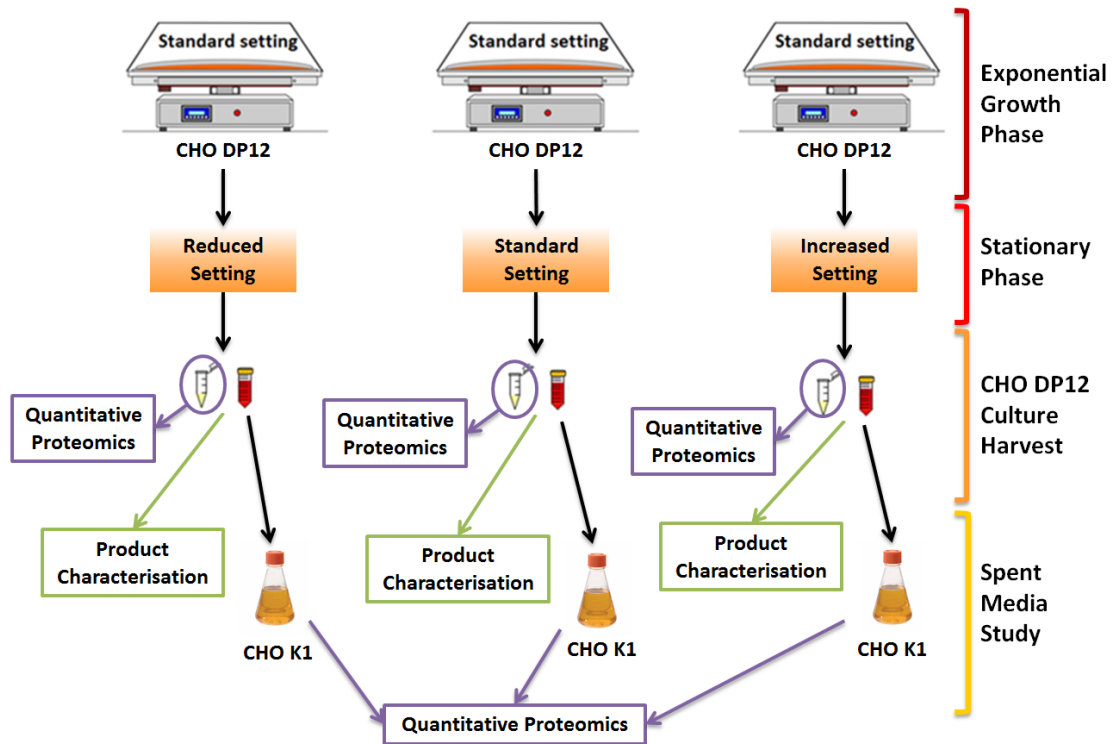
Figure 2.1: Experimental design for the determination of changes to CHO cell proteome in response to altered bioprocessing. For each parameter studied (temperature, pH, dissolved oxygen (DO)), three concurrent cultures were prepared and maintained at standard culture conditions (37.0°C, pH 7.0, 85% DO) for the duration of th exponential growth phase. When cultures entered the stationary phase of cell growth (Day 5), one parameter was altered in two of the cultures as outlined in Table 2.1. Bioprocessing was continued for a further 2 days before harvesting of the cultures and separation of cells from spent cuture medium. An aliquot of media was then applied for culture or naïve CHO-K1 cells for a period of 24 hours. Anti-IL8 IgG1 was purified from the remaining media samples using Protien A affinity chromatography.

Table 2.1: Bioprocessing conditions used to prepare CHO DP-12 cell cultures in Sartorius Cultibag Disposable Bioreactors.

Parameter Studied	Bioreactor Settings applied for Stationary Phase Growth		
	A	**B**	**C**
Temperature	**High Temperature**: 39.5°C, pH 7.0, 85% DO	**Standard 1**: 37.0°C, pH 7.0, 85% DO	**Low Temperature**: 32.0°C, pH 7.0, 85% DO
pH	**High pH**: 37.0°C, pH 7.2, 85% DO	**Standard 2**: 37.0°C, pH 7.0, 85% DO	**Low pH**: 37.0°C, pH 6.8, 85% DO
Dissolved Oxygen	**High DO**: 37.0°C, pH 7.0, 110% DO	**Standard 3**: 37.0°C, pH 7.0, 85% DO	**Low DO**: 37.0°C, pH 7.0, 60% DO

2.3.2   Bioprocess Monitoring

Throughout the duration of CHO DP-12 batch culture, aliquots of cell culture were sampled daily for determination of cell count, viability and concentration of nutrients and metabolites in each bioreactor; corresponding results are displayed in Figures 2.2 to 2.4. As the Figures show, high cell viability was maintained for the duration of batch culture (>85%). Viable cell count (cells.mL^{-1}) and nutrient concentration profiles were found to follow expected trends based on published literature. The influence of temperature on growth rate, recombinant protein quality and expression, nutrient consumption and metabolite production in CHO cells has been intensively studied. [16, 42, 43, 50-52] As a consequence it is now widely accepted that a biphasic approach to setting culture temperature, incorporating initial culture at 37°C to increase cell density, followed by a reduction in culture temperature, results in inhibited growth rate, maintenance of high cell viability, reduced nutrient consumption, decreased metabolite production and ultimately enhanced specific productivity of recombinant proteins. Although there are some exceptions to these observations, [53] the current study was found to be in-line with general trends as following application of a temperature shift from 37.0°C to 32.0°C, IgG concentration increased, glucose and glutamine consumption was reduced and ammonia and lactate production decreased. Additionally, the viable cell count did not change considerably when compared to an increase in viable cell count observed for cultures maintained at 37°C or increased to 39.5°C. Conversely, CHO DP-12 cells prepared at 39.5°C were found to have an elevation in nutrient consumption and metabolite production. These observations suggest the cellular machinery shifted towards cell growth rather than recombinant protein expression at elevated temperatures compared to reduced settings.

Cell growth, metabolism and recombinant protein production are known to be significantly influenced by culture pH, [17] however variations in the observed effects have been reported, including optimum growth at pH 7.6, [54] or conversely between pH 6.8 -7.0 [55] and between pH 7.0 - 7.2. [44] In this case the viable cell count for cultures maintained at pH 6.8 was found to be lower than that of cultures processed using higher pH settings. IgG concentration was increased following culture at pH 6.8 compared to pH 7.0-7.2, whilst a reduction in glucose and glutamine consumption and associated reduction in ammonia and lactate production were also observed. In correlation with reduced lactate concentration, lactate dehydrogenase (LDH) activity was also decreased at pH 6.8 when compared to pH 7.0 – 7.2. While distinct differences could be noted in viable cell count, IgG concentration and nutrient and metabolite profiles whilst altering pH and temperature settings, variation in DO content of culture media between 60 and 110% DO was not perceived to result in any distinct elevated or reduced trends for the analytes measured. This finding is in accordance with observations made by Trummer and co-workers, who found no significant impact to culture performance when DO levels were maintained between 30 and 90% of air saturation. [17]
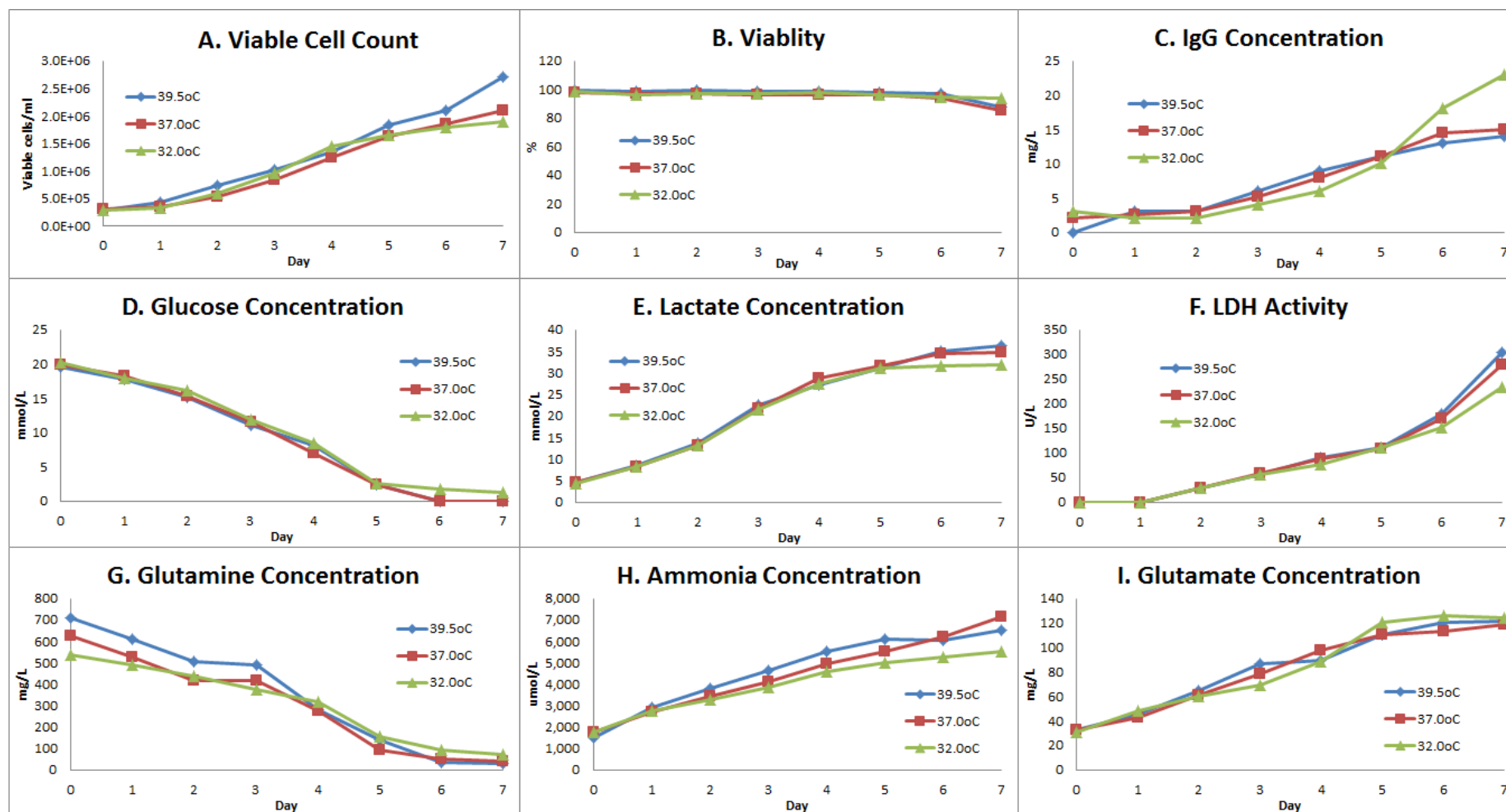
Figure 2.2: Graphs showing cell viability and viable cell counts and also metabolite and nutrient concentrations recorded for CHO DP-12 cultures prepared to study the effects of culture temperature. All measurements were performed using a Cedex Bioanalyser *via* photometric analysis (n=1).
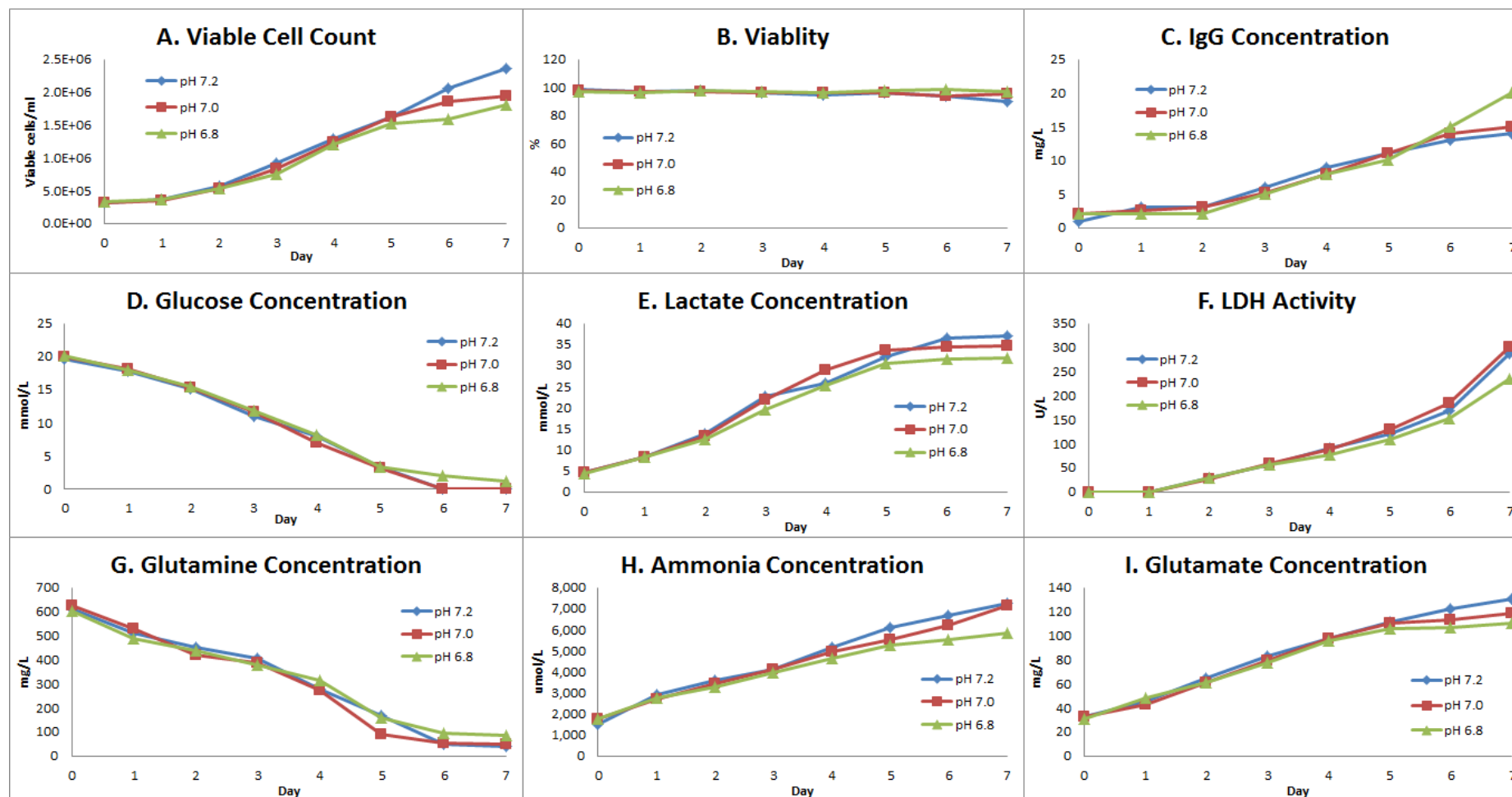
Figure 2.3: Graphs showing cell viability and viable cell counts and also metabolite and nutrient concentrations recorded for CHO DP-12 cultures prepared to study the effects of culture pH. All measurements were performed using a Cedex Bioanalyser *via* photometric analysis (n=1).
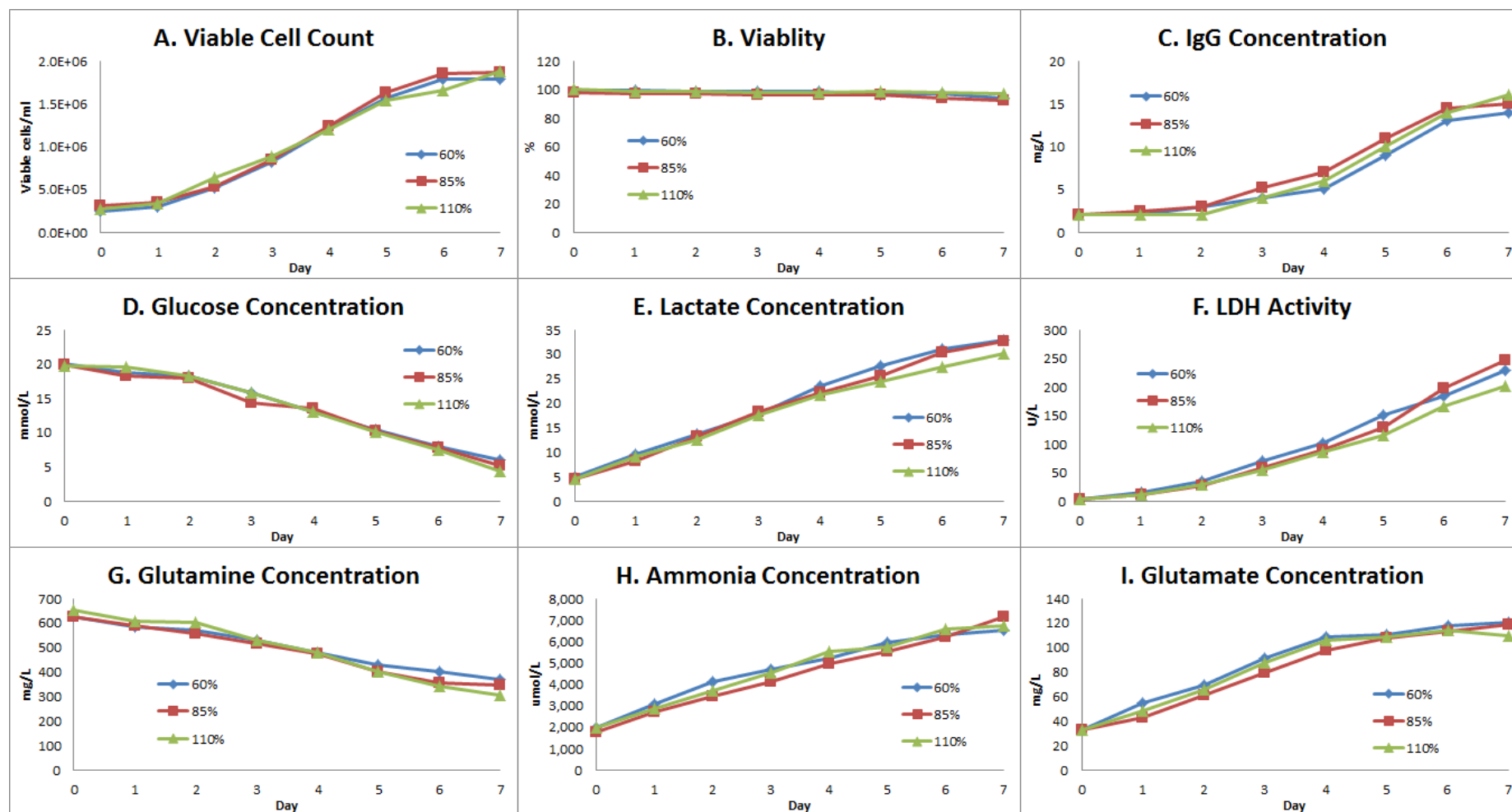
Figure 2.4: Graphs showing cell viability and viable cell counts and also metabolite and nutrient concentrations recorded for CHO DP-12 cultures prepared to study the effects of dissolved oxygen content of culture media. All measurements were performed using a Cedex Bioanalyser *via* photometric analysis (n=1).

2.3.3   Proteomic Method Performance

The instrument set-up applied herein employs numerous separation and detection components to enable deep proteome identification and subsequent quantitation, which has recently become feasible due to the extensive capabilities of modern analytical instrumentation. In the first instance, sample complexity was reduced using off line basic pH reversed phase LC separation, which has proven to be successful for proteome sample separation when followed by orthogonal low pH reversed phase nano-LC. [32, 36] Subsequently, a mass spectrometer incorporating three mass analysers was used wherein ionised peptide precursors are selected during an MS1 survey scan in an Orbitrap for subsequent fragmentation in an ion trap mass analyser, before further fragmentation to cleave TMT reporter ions from corresponding peptides in the Orbitrap. Significantly the mass spectrometer, an Orbitrap Fusion Lumos (Thermo Fisher Scientific), is capable of performing synchronous precursor selection to co-isolate and co-fragment multiple MS2 fragment ions, which has been shown to significantly extend the dynamic range for reporter ion quantitation, hence increasing confidence in peptide quantitation when using multiplexing strategies with isobaric labelling reagents. [56] Thus, the analytical platform has the potential to not only permit global proteome identification but also to enable deep quantitative proteomics and, significantly, facilitate the study of enriched biological pathways that have been altered in response to different bioprocessing parameters applied during cell culture.

2.3.3.1 Evaluation of Method Reproducibility

Prior to application for analysis of CHO cell lysates from differentially produced cultures as outlined in Section 2.3.1, the reproducibility of the high pH low pH reversed phase nano-LC-MS^3 proteomic platform was evaluated. Technical replicate samples were prepared from a single CHO DP-12 cell lysate sample (Standard 1, Table 2.1). Following tryptic digestion, differential labelling using TMT-sixplex reagents and 2D-LC-MS^3 analysis, resulting data was processed and abundance values obtained for TMT report ions corresponding to each identified protein group. Abundance values were then plotted to evaluate the performance of the proteomic platform. As displayed in Figure 2.5, exceptional correlation (R^2>0.999) between different sample preparations was observed, demonstrating high performance consistency of the sample preparation and subsequent 2D-LC-MS^3 analysis methods.
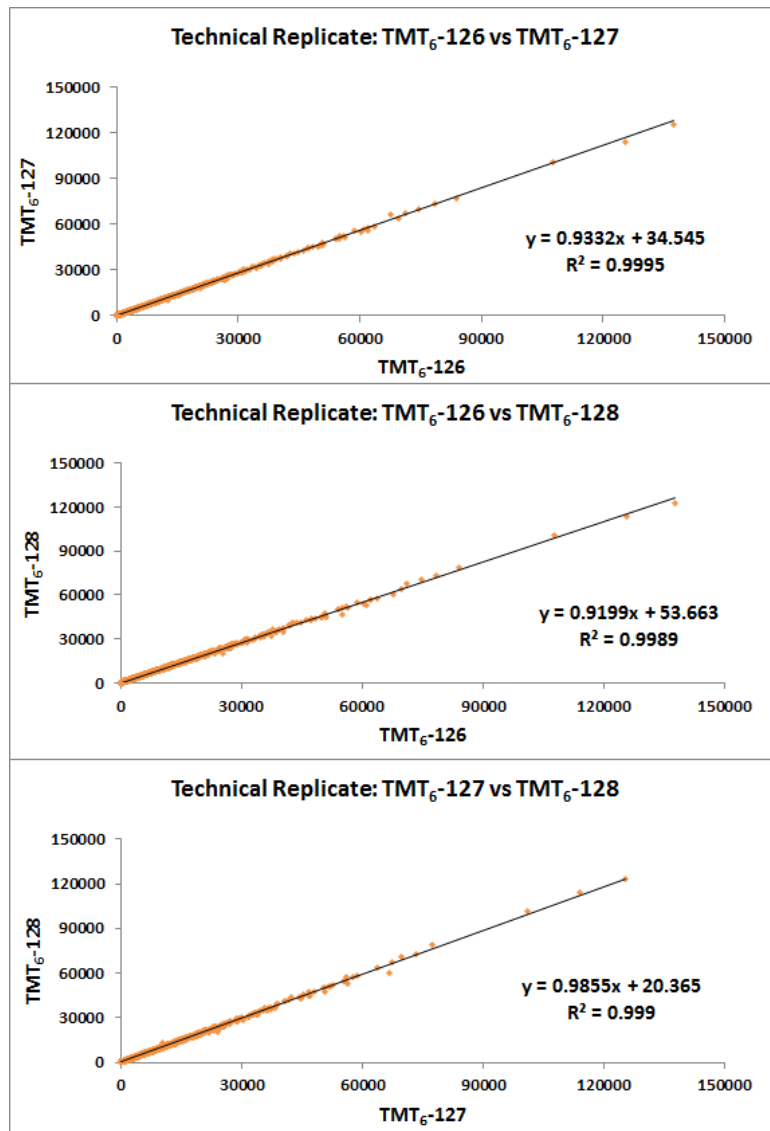
Figure 2.5: Scatter plots prepared from TMT abundance data for identified and quantified proteins from CHO DP-12 cell lysate, analysed using the 2D-LC-MS^3 method, showing linear correlation between triplicate technical replicates prepared.

2.3.3.2 Quantitative Proteomics Experimental Design and Platform Performance

Having confirmed the reproducibility of the proteomic platform, samples were subsequently prepared from each of the CHO DP12 cultures as outline in Table 2.2. Each sample was prepared in duplicate and labelled in a manner which allowed for each condition (*i.e.* an elevated or reduced setting for each parameter) to be compared to a proteome sample from CHO DP-12 cells cultured in parallel using standard conditions. In addition, proteomic samples prepared from biological replicate cultures, produced under standard bioprocessing conditions during each study, were also included in the experimental design in order to establish

consistency of the proteomic platform from upstream bioprocessing of CHO cell cultures to the final data analysis steps of the proteomic platform. Using this approach for combination of differentially labelled samples, the method consistency could be evaluated by determining variation within each combined set of TMT-sixplex labelled samples and also between sets, *e.g.* by comparison of TMT^6-127 abundance values corresponding to Standards 1 – 3 (Table 2.2). Furthermore, duplicate samples prepared from altered bioprocessing conditions were included in different sample sets to add further confidence by ensuring results were not impacted by variations in instrument performance from day to day. As displayed in Figures 2.6 and 2.7, high consistency in relative quantitation was demonstrated both within the same 2D-LC-MS^3 analysis (R^2>0.98) and across different 2D-LC-MS^3 analysis (R^2>0.95). Figure 2.8 shows examples of first and second dimensional chromatograms acquired during 2D-LC-MS^3 analysis, showing broad separation over the gradients applied as was typical of all samples analysed.

Table 2.2: Experimental design for CHO DP-12 cultures prepared in Cultibag disposable bioreactors. CHO-DP12 culture conditions are outlined in more detail in Table 2.1.

TMT label applied	TMT^6-126	TMT^6-127	TMT^6-128	TMT^6-129	TMT^6-130	TMT^6-131
Set A	High Temp. Study: 39.5°C	Standard 1	Low Temp. Study: 32.0°C	Standard 1	Standard 2	Standard 3
Set B	High pH Study: pH 7.2	Standard 2	Low pH Study: pH 6.8	High Temp. Study: 39.5°C	Standard 1	Low Temp. Study: 32.0°C
Set C	High DO Study: 110% DO	Standard 3	Low DO Study: 60% DO	High pH Study: pH 7.2	Standard 2	Low pH Study: pH 6.8
Set D	Standard 1	Standard 2	Standard 3	High DO Study: 110% DO	Standard 3	Low DO Study: 60% DO
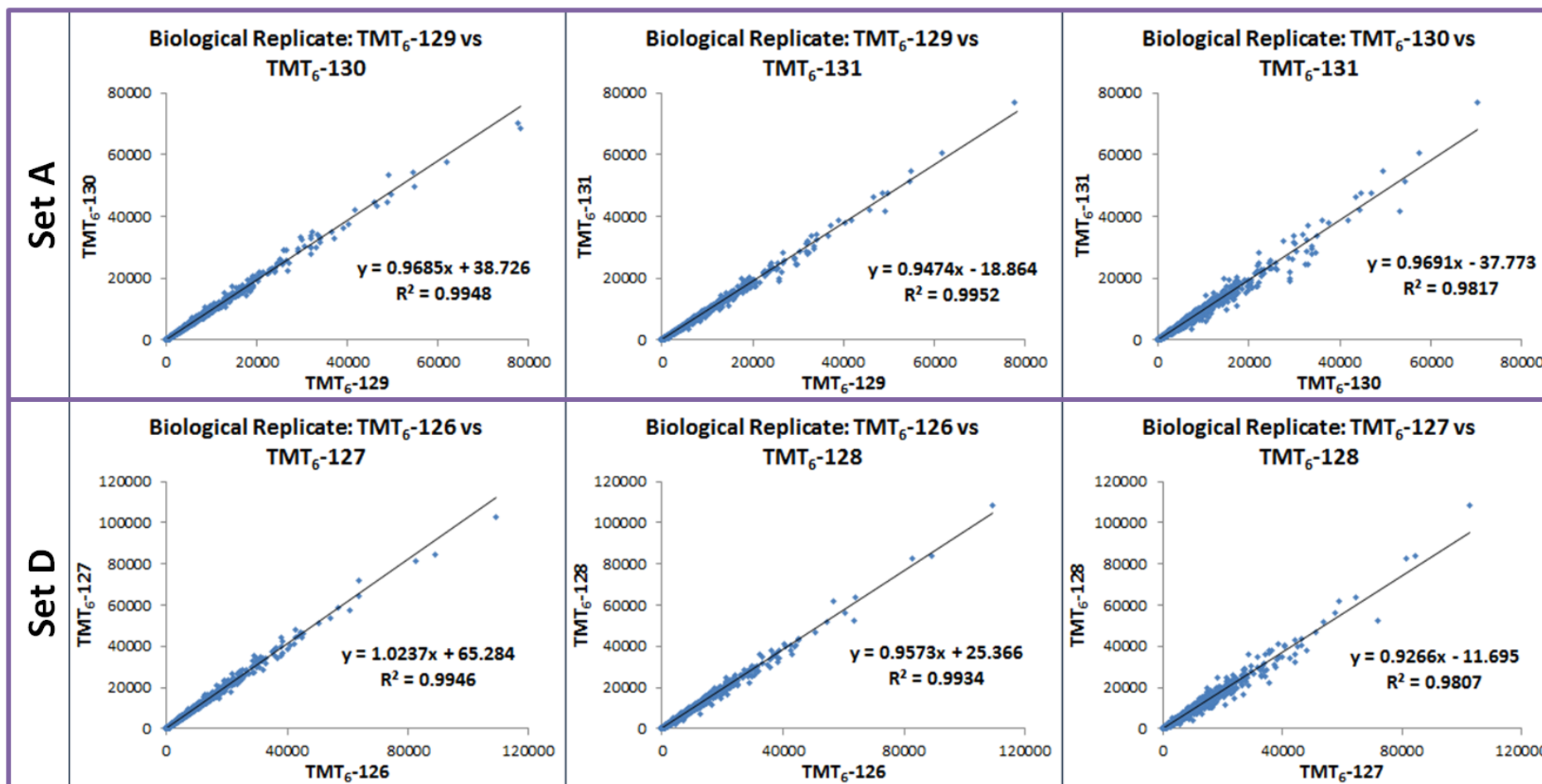
Figure 2.6: Scatter plots showing linear correlation between biological triplicate replicates prepared from different CHO DP-12 cell samples, cultured using identical bioprocess conditions, and subsequently TMT labelled and analysed as part of Set A or Set D (Table 2.2) using the 2D-LC-MS^3 method described.
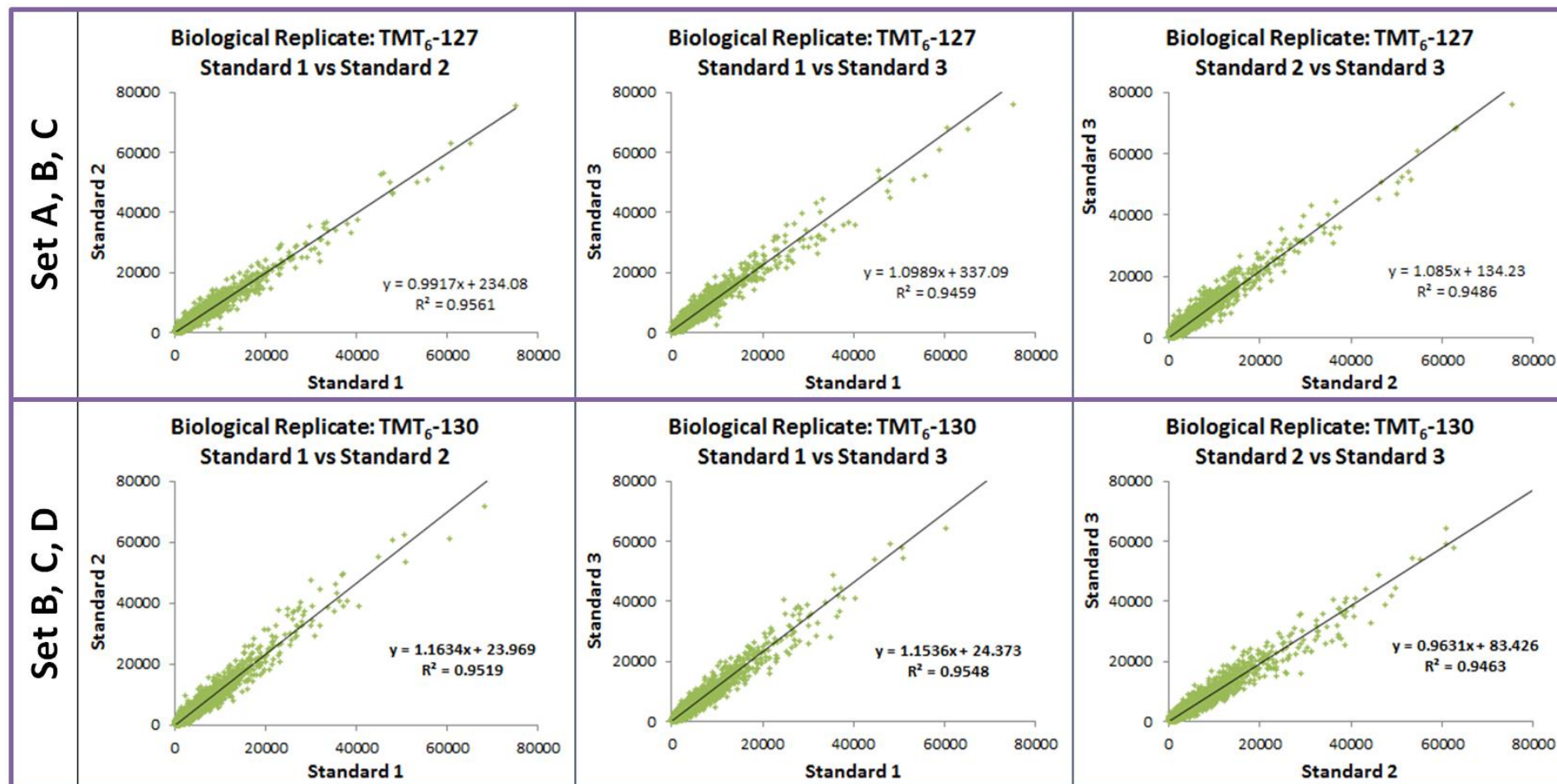
Figure 2.7: Scatter plots showing linear correlation between biological triplicate replicates prepared from different CHO DP-12 cell samples, cultured using identical bioprocess conditions, and subsequently TMT labelled and analysed using different 2D-LC-MS^3 runs.
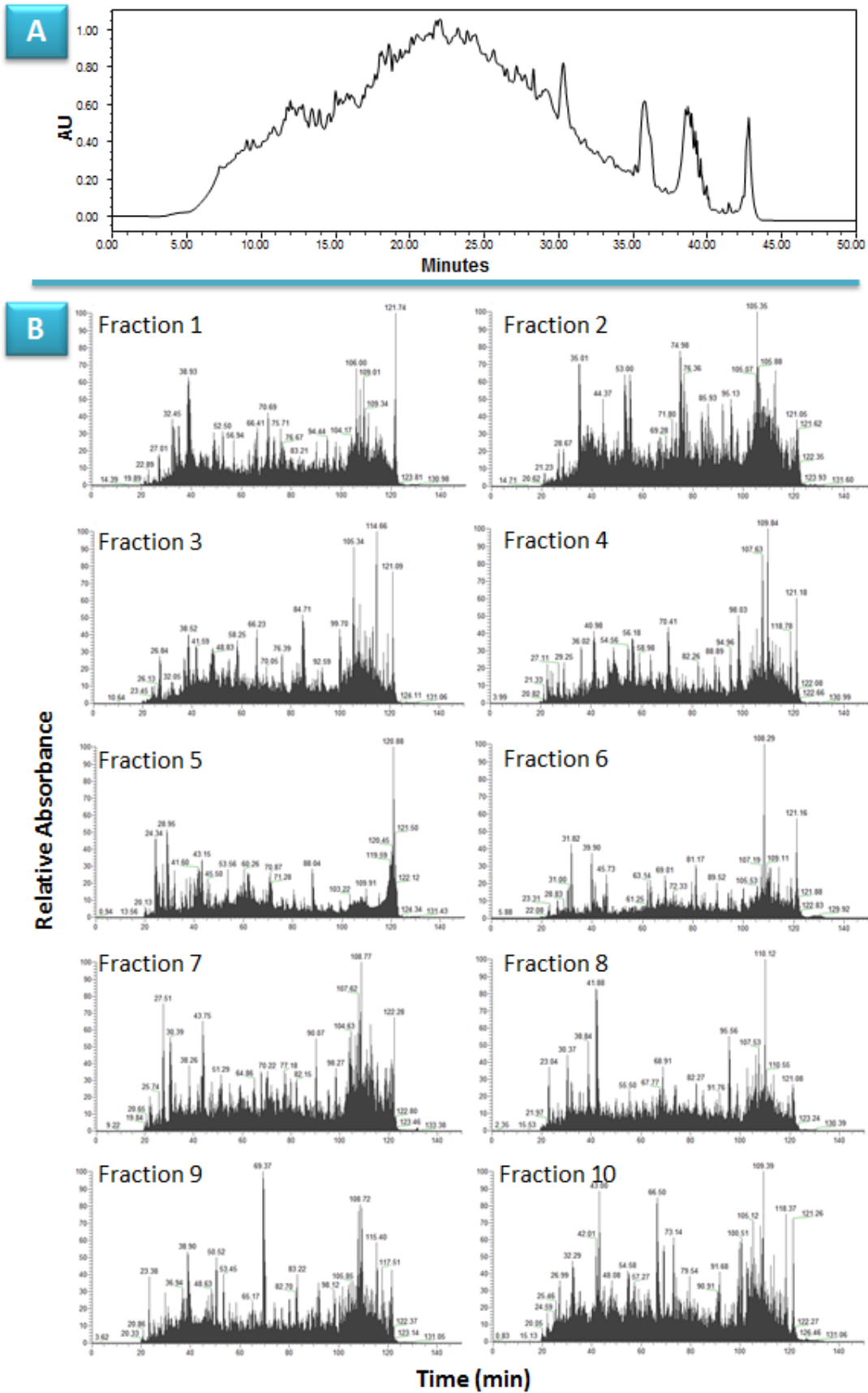
Figure 2.8: A. First dimensional chromatogram showing high pH reversed phase separation of sample peptides from Set D. **B.** Total ion chromatograms obtained during second-dimensional LC-MS³ analysis of Set D sample fractions.

A similar experimental approach was employed for proteomic analysis of naïve CHO K1 cells which were exposed to conditioned media samples, as displayed in Table 2.3. However, in this instance, only one set of biological replicates (to be analysed using the same 2D-LC-MS³ analysis run) were generated. Three CHO K1 cultures that were prepared alongside cultures exposed to spent media were also analysed, these are described as Blank 1 to 3 in Table 2.3. The method performance was further confirmed by determining the correlation of abundance values obtained for reporter ions associated with protein groups identified and quantified in CHO K1 samples. Scatter plots were prepared using TMT ion abundances reported for untreated CHO K1 cultures revealing high correlation between quantified protein groups (Figure 2.9, $R^2 > 0.99$). Furthermore, samples cultured using spent media produced in CHO DP-12 cultures prepared under standard conditions, also displayed high levels of correlation both within the same 2D-LC-MS³ analysis (Figure 10, $R^2 > 0.99$) and across different experiments (Figure 11, $R^2 > 0.95$).

Table 2.3: Experimental design for CHO K1 cultures treated with conditioned media obtained from CHO DP-12 cultures. Three untreated 'blank' CHO K1 cultures were also prepared.

TMT label applied	TMT⁶-126	TMT⁶-127	TMT⁶-128	TMT⁶-129	TMT⁶-130	TMT⁶-131
Set E	High Temp. Study: 39.5ºC	Standard 1	Low Temp. Study: 32.0ºC	Blank 1	Blank 2	Blank 3
Set F	High pH Study: pH 7.2	Standard 2	Low pH Study: pH 6.8	High Temp. Study: 39.5ºC	Standard 1	Low Temp. Study: 32.0ºC
Set G	High DO Study: 110% DO	Standard 3	Low DO Study: 60% DO	High pH Study: pH 7.2	Standard 2	Low pH Study: pH 6.8
Set H	Standard 1	Standard 2	Standard 3	High DO Study: 110% DO	Standard 3	Low DO Study: 60% DO
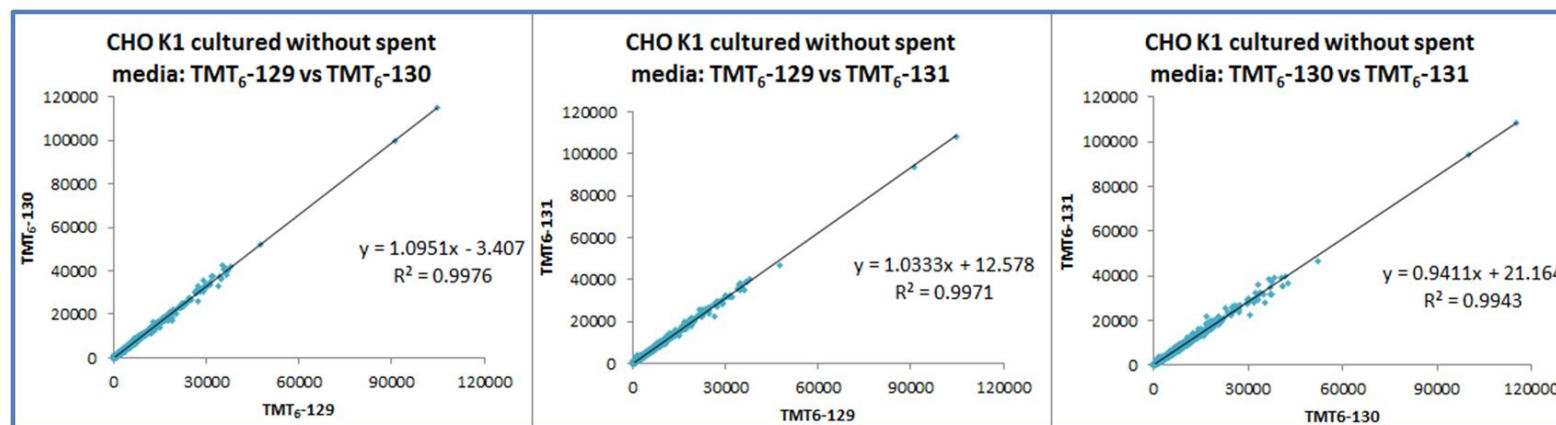
Figure 2.9: Scatter plots showing linear correlation between biological triplicate replicates prepared from different CHO K1 cell samples, cultured without application of conditioned media samples, and subsequently TMT labelled and analysed using the 2D-LC-MS^3 method described.
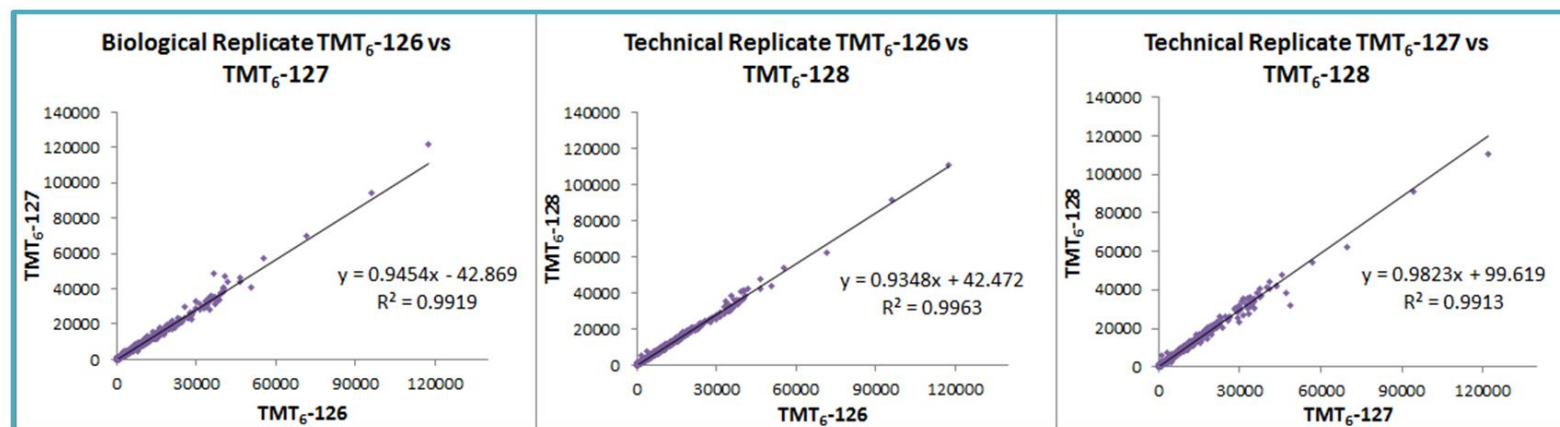
Figure 2.10: Scatter plots showing linear correlation between biological triplicate replicates prepared from different CHO K1 cell samples, cultured using CHO DP-12 spent media produced under identical bioprocess conditions, and subsequently TMT labelled and analysed using the 2D-LC-MS^3 method described.
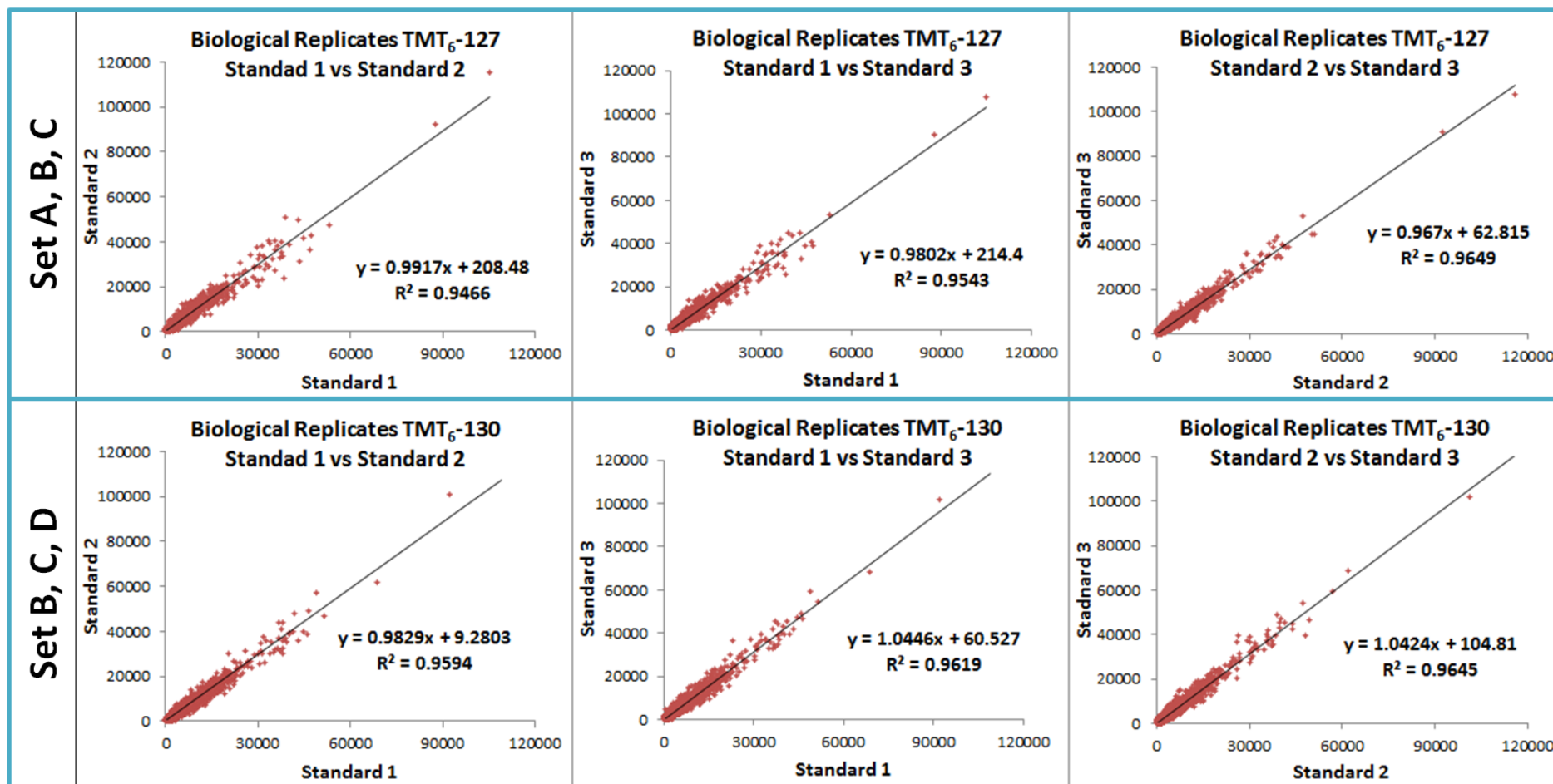
Figure 2.11: Scatter plots showing linear correlation between biological triplicate replicates prepared from different CHO K1 cell samples cultured using CHO DP-12 spent media produced under identical bioprocess conditions, and subsequently analysed using the 2D-LC-MS^3 method described.

2.3.3.3 Identification of CHO Cell Proteins

In total 6,821 CHO DP-12 protein groups and 7,082 CHO K1 protein groups were identified and quantified across all proteomic analyses with <1% false discovery rate (FDR) and using a minimum of 2 peptides for protein identification. Within CHO DP-12 data sets the number of protein groups quantified ranged from 6,276 to 6,503, whilst the amount of protein groups measured within sets of CHO K1 proteomes ranged from 6,703 to 6,835. The majority of peptides identified had charges states of +2, +3 or +4, as is typical of tryptic peptides (Figure 2.12). Broad sequence coverage was also achieved for the majority of protein groups quantified, >84% of proteins were identified using more than four peptides while >10% sequence coverage was achieved for over 83% of the protein groups determined for all sample sets (Figure 2.12). The CHO cell proteome coverage attained represents a significant extension to the number of CHO cell proteins that have been identified in previous CHO quantitative proteomics studies. Baycin-Hizal *et al.* identified 5,782 grouped proteins in the first proteomic analysis of CHO cells using the CHO genome exclusively, [32] however 48 first dimensional fractions were required for LC-MS/MS analysis, compared to ten used in this study, and a quantitative strategy was not incorporated into the method design. Quantitative proteomics of CHO cells was performed by Liu and co-workers used an mRNA CHO DG44 database for protein identification. [36] Using 22 fractions, separated over a 260 minute LC-MS/MS gradient, 4,986 CHO protein groups were identified; including 2,800 proteins quantified with a minimum of two peptides. In the current study, use of a tribrid mass spectrometer permits the use of a reduced first dimensional sample fractionation as the unmatched mass accuracy, resolution and detectable mass range capabilities of the instrument enables in-depth proteome coverage without extensive first dimensional fractionation.
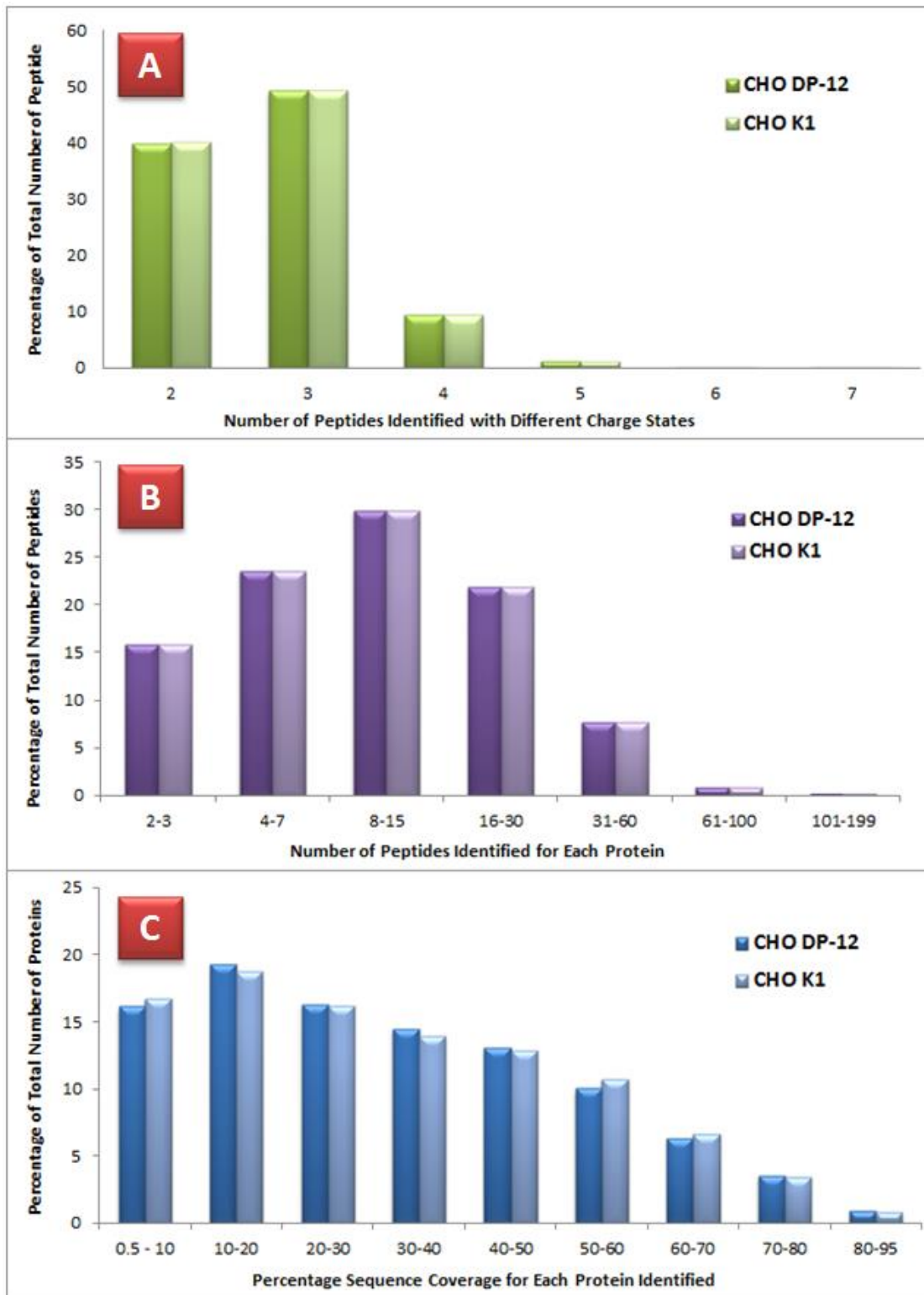
Figure 2.12: 2D-LC-MS³ method performance. A. Charge state distribution of peptides used for identification of grouped proteins; **B.** Number of peptides identified for each CHO protein reported; **C.** Sequence coverage profile for all protein groups determined.

2.3.3.4 Gene Ontology Analysis

In an effort to investigate if any bias exists in proteome coverage for proteins identified using the high pH low pH 2D-LC-MS[3] method, the DAVID bioinformatics resource was used to determine gene ontology (GO) terms associated with the identified CHO DP-12 protein groups. [38, 39] Associated GO terms with <1% FDR were visualised using REVIGO and resultant interaction graphs representing enriched biological processes and molecular functions are shown in Figures 2.13 and 2.14, respectively, and a scatter plot showing related cellular compartments is displayed in Figure 2.15.
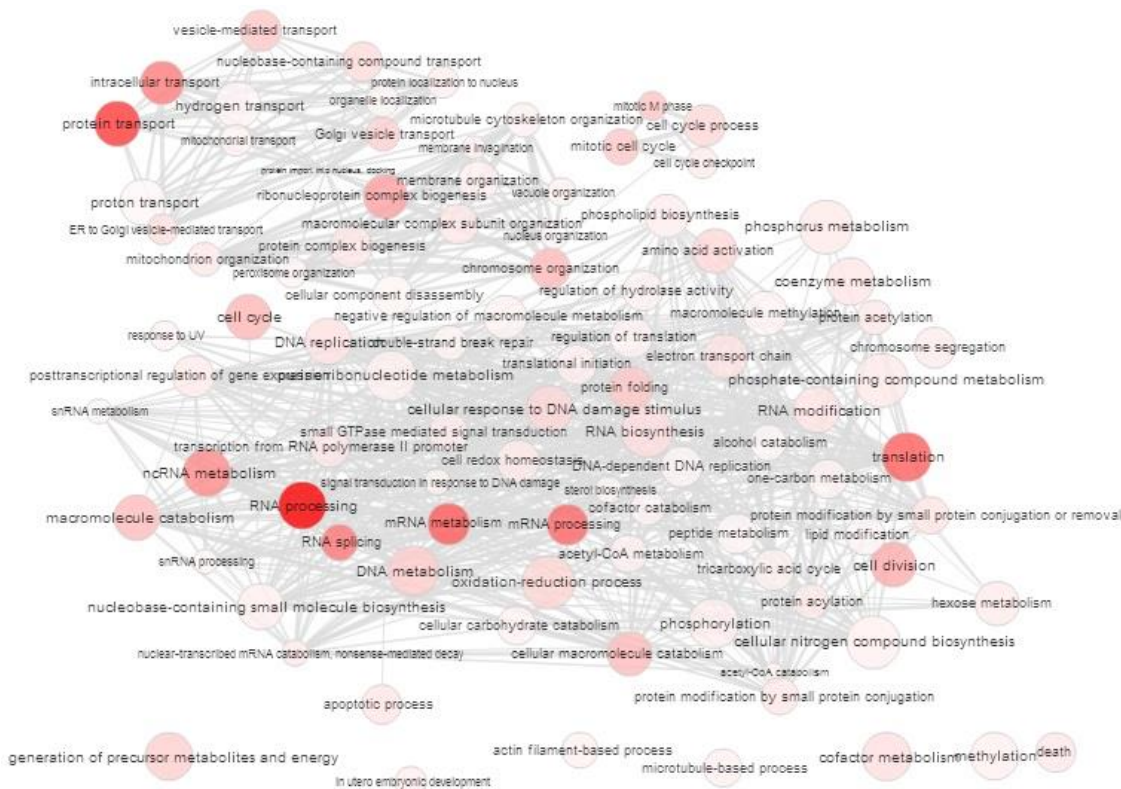
Figure 2.13: Identified CHO DP-12 proteins were processed using DAVID for determination of potential associated biological functions. Enriched biological processes associated with proteins identified in CHO DP-12 cell lysate, identified using DAVID with p-values >0.05 and <1% FDR, were visualised using REVIGO. [38-40] The complexity of the graph and absence of clustering signifys the broad proteome coverage achieved.

From the complexity of the graph showing biological processes related to protein groups identified and the absence of clustering of GO terms in this graph, it may be deduced that broad proteome coverage was achieved. Furthermore, all components of the cell, including nuclear, cytosolic and membrane compartments are well represented, as depicted in Figure

2.15. In terms of molecular function, a number of distinct clusters were observed (Figure 2.14), including RNA/DNA binding, ATPase and helicase activity, kinase and ligase activity and oxidoreductase activity, all of which are functions of growing cells. Hence it was deduced that wide proteome coverage was achieved using the optimised proteomic 2D-LC-MS[3] platform.
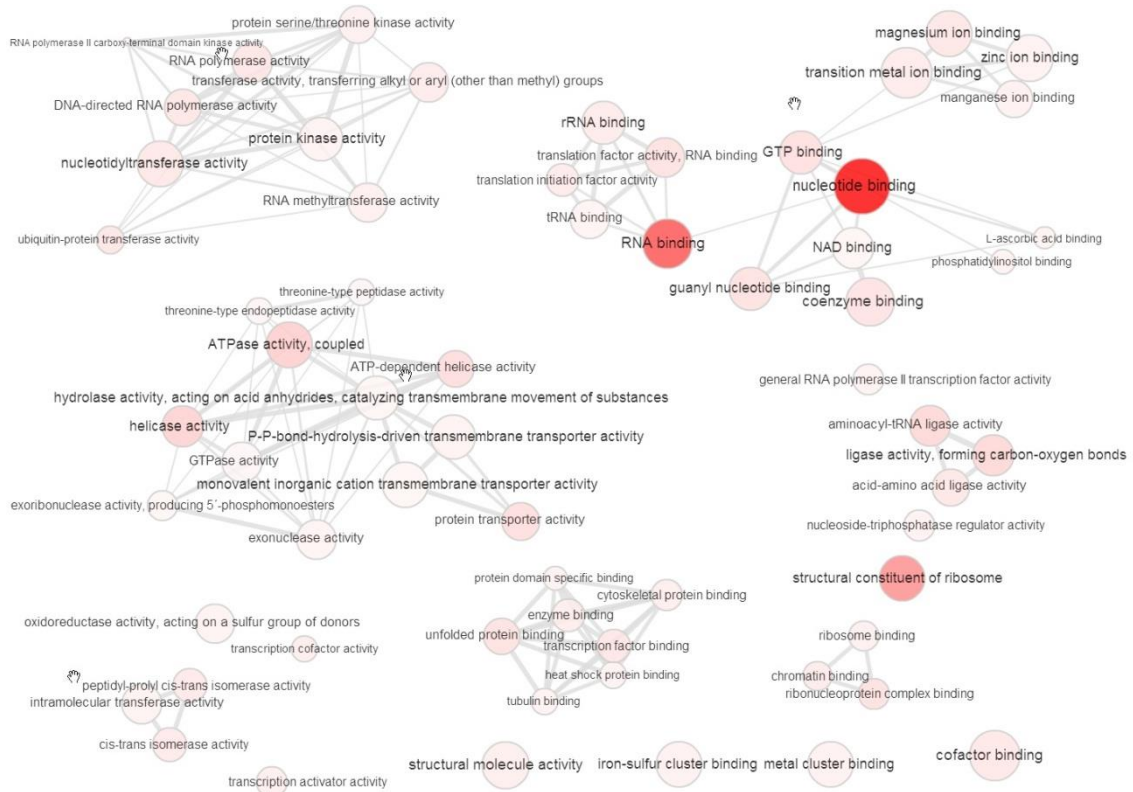
Figure 2.14: Identified CHO DP-12 proteins were processed using DAVID for determination of potential associated biological functions. Enriched molecular functions associated with proteins identified in CHO DP-12 cell lysate, identified using DAVID with results set to a 1% FDR and P-value > 0.05, were visualised using REVIGO. [38-40] A number of distinct clusters were observed, all of which were found to be functions of growing cells.
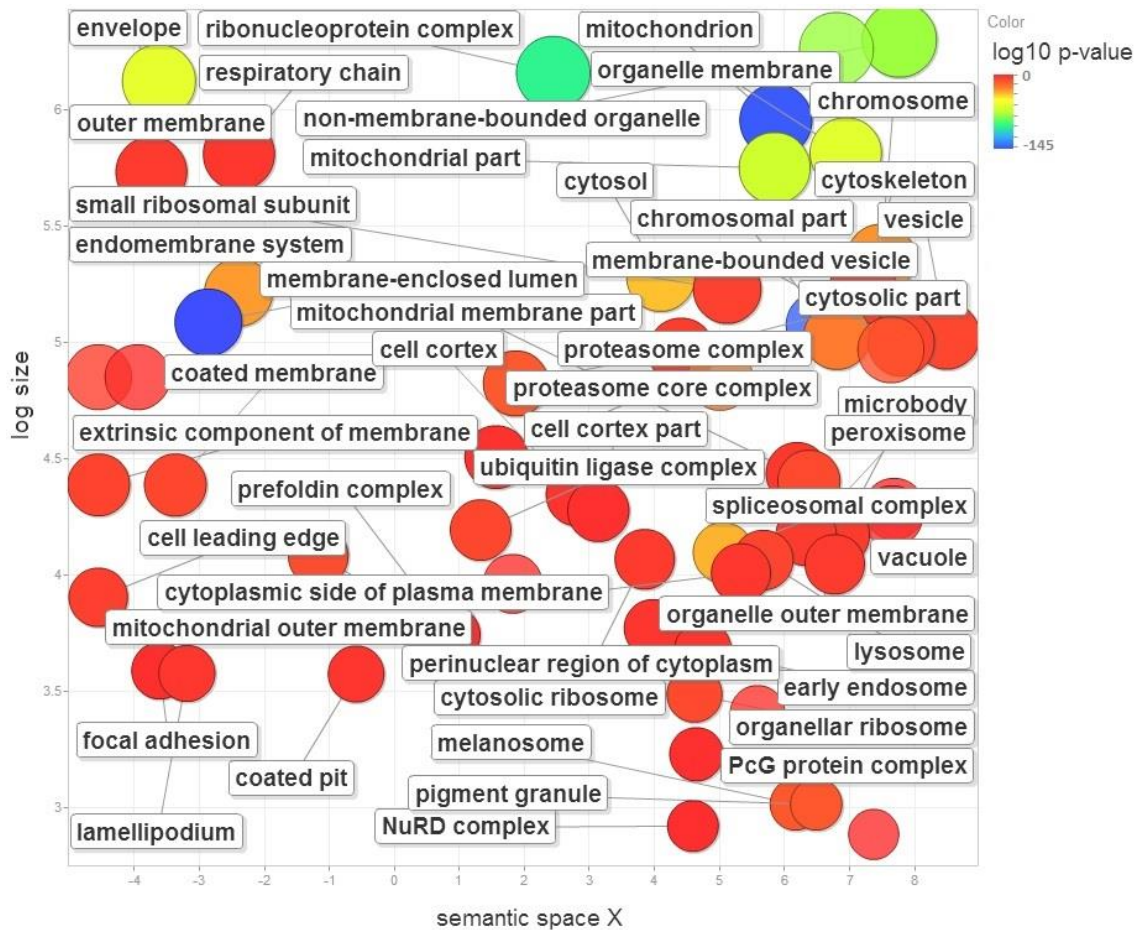
Figure 2.15: Identified CHO DP-12 proteins were processed using DAVID for determination of potential associated biological functions. Enriched cellular compartments associated with proteins identified in CHO DP-12 cell lysate, identified usign DAVID with results set to 1% FDR and P-vallue >0.05, are depicted. A description of a portion of the annotated cellular compartments are shown. Cellular compartments were visualised using REVIGO. [38-40] For each cellular compartment shown, the colour of the represenatative circle depicts Log 10 of the related p-value, as shown in the legend.

2.3.4   Quantitative CHO DP-12 Proteomics Following Altered Bioprocessing

For each altered bioprocessing condition studied, peptide abundance data was compared to corresponding proteome samples produced from CHO cell lysate subsequent to culture under standard bioprocessing conditions. Using InfernoRDN fold changes and p-values were calculated and subsequently used to prepare volcano plots to investigate differential expression as shown in Figure 2.16. In order to evaluate differentially regulated proteins, a frequently selected threshold for significant change, within samples derived from the same cell line, of 1.2 fold change was utilised. [45, 47, 48, 57] As the overall number of proteins was so large, the individual protein data for all identified protein groups are not included in this thesis. Identified grouped proteins that were found to be differentially regulated are listed in Appendix 1. A range of 175 – 788 differentially regulated grouped proteins were determined in CHO DP-12 samples cultured under the altered bioprocessing conditions studied. Complete proteome data may be accessed on the National Institute of Bioprocessing Research and Training (NIBRT) server.
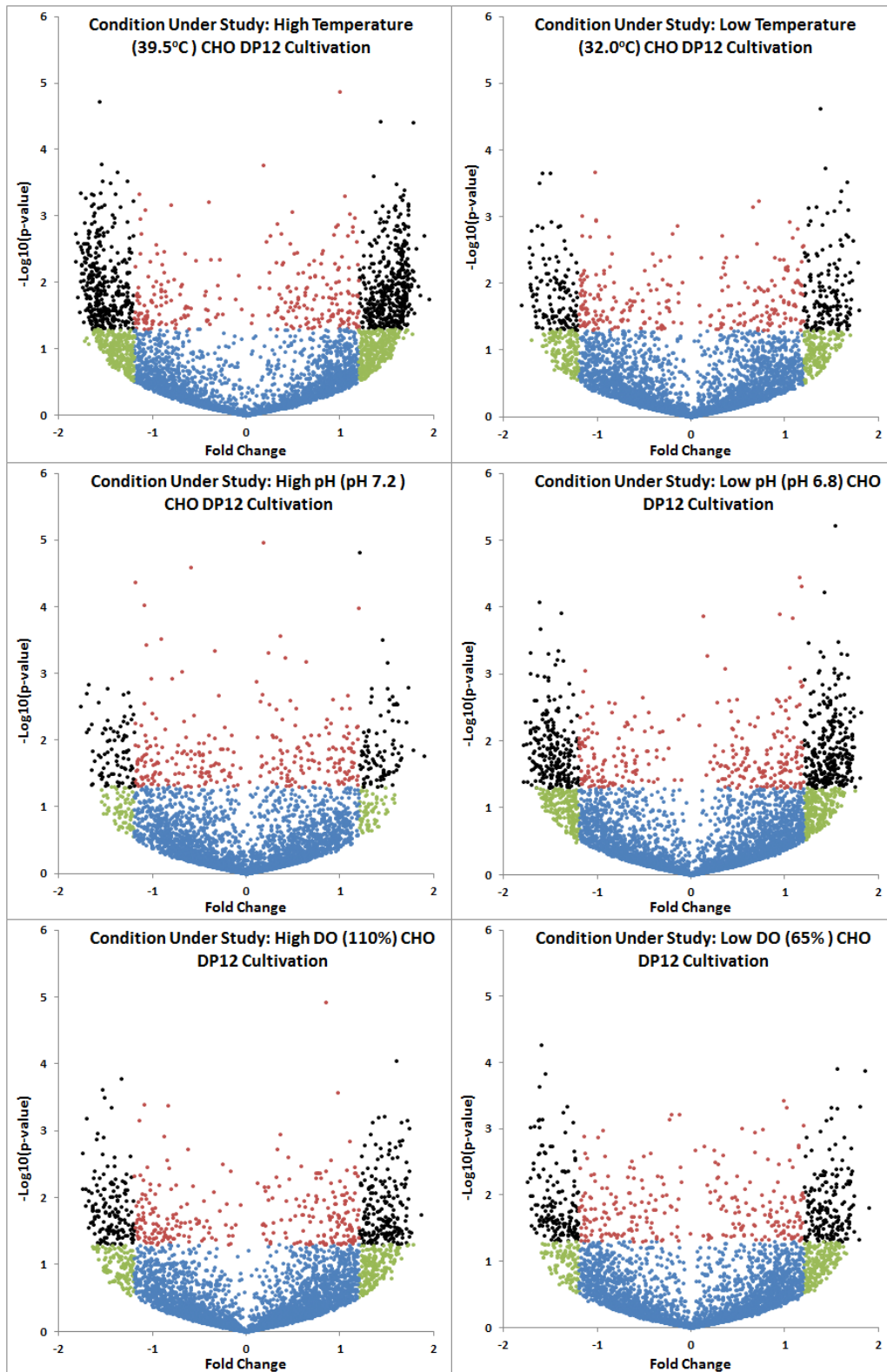
Figure 2.16: Volcano plots showing fold changes plotted against –Log10 of p-values calculated for CHO DP-12 proteins quantified. Significant proteins with fold changes >1.2 and p-value <0.05 are shown in black, green dots represent proteins with p-value >0.05 and >1.2 fold change; blue dots represent proteins with p value >0.05, <1.2 fold change; red dots signify proteins with p value <0.05, <1.2 fold change.

Significant proteins identified for each study were correlated with potential cellular pathways using Ingenuity pathway analysis (IPA) for determination of enriched or decreased pathways as a consequence of CHO DP-12 cell culture under conditions of altered bioprocessing. IPA uses information stored in a knowledgebase to generate cellular and molecular networks for identified proteins and uses a statistical algorithm to assign a significance score for the association (Z-score). [34] A higher score signifies greater statistical significance to support the correlation of those proteins in the network. For each study, the top three positively or negatively altered pathways having a |Z score| ≥ 1.0, and identified using a minimum of four proteins were determined and are reported in Table 2.4. The vast majority of potentially altered pathways determined across all samples were found to be involved in cellular signalling, *e.g.* PTEN signalling, NF-kappa-B signalling and 14-3-3-mediated signalling. Reflecting the high cell viability at the point of cell harvest, the majority of the cells were not found to have apoptotic activity. However, proteome samples generated from cells produced at pH 7.2 displayed down-regulation of prostaglandin G/H synthase 2 (PTGS2), which is involved in apoptosis resistance and up-regulation of tumour necrosis factor receptor superfamily member 3 (LTBR), an apoptotic promoter. These proteins may be related to a reduction in viability in cells cultured at pH 7.2 when compared to those maintained at pH 7.0. The CHO DP-12 cells produced at 60% DO were found to have increased signalling activity by Rho family GTPases, which are involved in a variety of cellular activities including actin cytoskeleton reorganisation and transcriptional regulation. Interestingly, NADPH oxidase 4 (NOX4), which may function as an oxygen sensor, was found to be up-regulated. Potentially related to excess oxygen levels in the culture media, the oxidoreductase, superoxide dismutase (SOD1) was observed to be up-regulated (fold change = 1.609) in CHO DP-12 proteome corresponding to cell culture at 110% DO. Unsurprisingly, a large number of heat shock proteins were up-regulated in CHO DP-12 cells produced at 39.5°C, including the DnaJ heat shock protein family members A1, C3, C8, C13, C16, C17 (DNAJA1, DNAJC3, DNAJC8, DNAJC13, DNAJC16, DNAJC17) and heat shock protein HSP 90-α (HSP90AA1). Conversely, heat shock protein HSP 90-β (HSP90AB1) was down-regulated (fold change = -1.217) in CHO cells produced at 32°C.

Table 2.4: Top up- or down-regulated pathways for CHO DP-12 cells cultured under various altered bioprocessing conditions, as determined using IPA. The top three pathways with an absolute z-score of >1.0 and identified using a minimum of 4 proteins are shown; gene names coloured green were found to be up-regulated whereas those in red were identified as being down-regulated.

Sample	Pathway	Change to Pathway	Z-Score	Molecules
Low pH mAb	PTEN Signalling	Up-regulated	2.333	CHUK, GSK3A, IKBKB, ILK, MAP2K1, PDGFRB, PDPK1, TGFBR1, TGFBR2
	NGF Signalling	Down-regulated	-2.121	CHUK, IKBKB, MAP2K1, PDPK1, PIK3C3, ROCK2, RPS6KA1, RPS6KA3, SMPD1
	EIF2 Signalling	Down-regulated	-2.000	eif2b5 eif2s1, eif2s3, eif3i, eif3l, eif4g2, map2k1, pdpk1, PIK3C3, RPS18, RPS21, RPS28
	FLT3 Signalling in hematopoietic progenitor cells	Down-regulated	-2.236	MAP2K1, PDPK1, PIK3C3, RPS6KA1, RPS6KA3
High pH mAb	NF-kB Signalling	Up-regulated	1.342	FGFR1, LTBR, PIK3C3, TGFBR1, TGFBR2
	Stat3 pathway	Up-regulated	1.000	FGFR1, MAP2K1, TGFBR1, TGFBR2
	Colorectal cancer metastasis Signalling	Down-regulated	-2.646	MAP2K1, MMP12, MMP19, MSH2, PIK3C3, PTGS2, TGFBR1, TGFBR2
	neutotrophin/TRK Signalling	Down-regulated	-2.000	MAP2K1, PDPK1, PIK3C3, RPS6KA1
	FLT3 Signalling in hematopoietic progenitor cells	Down-regulated	-2.000	MAP2K1, PDPK1, PIK3C3, RPS6KA1
Low DO mAb	Signalling by Rho Family GTPases	Up-regulated	2.646	BAIAP2, CDC42EP1, EZR, GNA12, GNAQ, GNAS, NFKB2, NOX4, RAC1
	IL-1 Signalling	Up-regulated	2.449	ADCY9, GNA12, GNAQ, GNAS, IL1RAP, NFKB2
	Colorectal cancer metastasis signalling	Up-regulated	2.333	ADCY9, GNAS, IFNGR1, JAK1, MMP12, NFKB2, RAC1, STAT1, STAT3
	LXR/RXR Activation	Down-regulated	-2.236	CD36, CLU, CYP51A1, ECHS1, FASN, FDFT1, HADH, IL1RAP, LPL, NFKB2, PLTP
	PPARa/RXRa Activation	Down-regulated	-2.121	ACVR1, ADCY9, AIP, CD36, CHD5, FASN, GNAQ, GNAS, IL1RAP, LPL, MED12, NFKB2
High DO mAb	14-3-3-mediated Signalling	Up-regulated	1.000	GSK3A, GSK3B, MAP2K1, PDCD6IP, YWHAG
	Cell cycle: G2/M DNA Damage Checkpoint Regulation	Down-regulated	-2.236	CUL1, PLK1, PTPMT1, TOP2A, TOP2B, YWHAG
	EIF2 Signalling	Down-regulated	-1.342	EIF2B5, EIF2S3, EIF3C, EIF3L, EIF3M, EIF4G2, GSK3B, MAP2K1, RPL11, RPL24, RPS15, RPS16
	NRF2-mediated oxidative stress	Down-regulated	-1.342	CBR1, CCT7, GSK3B, GSTM5, MAP2K1, SOD1, USP14, VCP

	Pathway	Regulation	Score	Genes
Low T. mAb	PPARa/RXRa Activation	Up-regulated	1.134	ACAA1, ACOX1, CD36, GNAS, HSP90AB1, IKBKB, IL1RAP, TGFB1
	LXR/RXR Activation	Down-regulated	-2.000	CD36, CLU, FDFT1, IL1RAP, SERPINF1
	PI3K/AKT Signalling	Down-regulated	-1.000	HSP90AB1, IKBKB, ILK, MCL1, OCRL
High T. mAb	NRF2-mediated oxidative stress response	Up-regulated	1.667	AKR7A2, ATM, CLPP, DNAJA1, DNAJC3, DNAJC8, DNAJC13, DNAJC16, DNAJC17, ERP29, FTH1, GSTO1, GSTT2/GSTT2B, KEAP1, MAFG, PIK3R4, PRDX1, SQSTM1, STIP1, UBE2K
	PTEN Signalling	Up-regulated	1.732	CSNK2B, IGF2R, IKBKB, ILK, INSR, ITGA5, OCRL, PDGFRA, PDGFRB, PTK2, RELA, TGFBR2
	PPaR Signalling	Up-regulated	1.667	HSP90AA1, IKBKB, IL1RAP, IL1RL1, INSR, PDGFRA, PDGFRB, RELA, TRAF6
	IL-6 Signalling	Down-regulated	-3.317	ABCB1, ATM, CSNK2B, IKBKB, IL1RAP, IL1RL1, MCL1, PIK3R4, RELA, TRAF6, VEGFA
	Signalling by Rho Family GTPases	Down-regulated	-2.711	ACTR3, ARFIP2, ARHGEF2, ARHGEF6, ARPC1B, ATM, BAIAP2, CDC42EP1, CFL1, CLIP1, CYFIP1, GNA11, IQGAP1, ITGA5, MYL12A, PIK3R4, PTK2, RELA, RHOA, ROCK2, SEPT2, SEPT5, SEPT9, SEPT11, STMN1
	Thrombin Signalling	Down-regulated	-2.714	ARHGEF2, ARHGEF6, ATM, GNA11, IKBKB, MYL12A, PIK3R4, PTK2, RELA, RHOA, ROCK2, SRC

In addition to cellular pathways, individual proteins that were found to be significantly differentially altered across the different samples analysed, were also investigated. In this case, proteins determined to have an absolute Z-score > 2.0 were highlighted are shown in Table 2.5. A large proportion of differentially regulated proteins identified are thought to be involved in transcription and phosphorylation mechanisms associated with actively growing and protein producing cells, illustrating the activity of the cell undergoing normal processes during production. These observations reflect the results obtained while monitoring IgG and metabolite production and growth trends during CHO DP-12 bioprocessing as the cells were actively growing and expressing recombinant therapeutic proteins at the time of culture harvest. These findings indicate the ruggedness of the bioprocess in response to the induced pH, temperature and DO variations. However, the minor changes that were applied were not designed to induce stress, but rather to mimic an industrial process in an attempt to decipher what cellular-level changes have occurred and may occur in routine biopharmaceutical manufacture. Of the bioprocess parameters studied temperature shift is one of the most widely used methods in bioprocessing for induction of recombinant protein expression. [16, 17, 41-44, 58] In this study differential expression on a cellular level appeared to be low for proteins that could be correlated with cellular pathways for CHO DP-12 cells produced at 32.0°C when compared to those produced at 37.0°C. Despite the vastness of the dataset for quantitative proteomics, showing high reproducibility and incorporating high quantitation confidence due to the use of SPS-MS^3, no obvious pathways that could be correlated with increased recombinant protein expression were determined. However, a number of caveats regarding data processing with IPA may be noted. Firstly, human, mouse and rat models were used for determination of protein pathways as no Chinese hamster model is available. Secondly, there were many proteins which were not assigned a Z-score and could not be correlated with pathways using IPA. Hence, it is possible that further data mining may yield additional information regarding the cellular activity of the CHO cells studied.

Table 2.5: Differentially regulated proteins identified in CHO DP-12 proteomes following 2D-LC-MS[3] and IPA analysis using an absolute Z-score > 2.0.

Bioprocess Condition	Upstream Regulator	Molecule Type	Predicted Activation State	Activation z-score
Low pH	SSMAD4	Transcription regulator	Inhibited	-2.224
	OLR1	Transmembrane receptor	Inhibited	-2.000
	MGEA5	Deglycosylation enzyme	Activated	2.673
	RIPK2	Kinase	Activated	2.213
	ACOX1	Enzyme	Activated	2.621
	LEP	Growth factor	Activated	2.372
	INSR	Kinase	Activated	2.164
	LGALS3	Involved in differentiation	Activated	2.219
	MAPK1	Kinase	Activated	3.208
High pH	RICTOR	Subunit of mTORC2	Inhibited	-2.236
	SYVN1	Component of ER-associated degradation	Activated	2.236
Low DO	Lh	Complex (proliferation, transcription, apoptosis)	Inhibited	-2.000
	PTEN	phosphatase	Inhibited	-2.415
	NUPR1	Transcription regulator	Inhibited	-2.138
	NFE2L2	Transcription regulator	Inhibited	-2.054
	APOE	Transporter	Inhibited	-2.423
	RB1	Transcription regulator	Inhibited	-2.828
	RICTOR	Subunit of mTORC2	Activated	3.162
	RABL6	cellular proliferation	Activated	2.449
	ATP7B	copper transport	Activated	2.236
	CCND1	cell division	Activated	2.200
	MTOR	serine threonine protein kinase, up regulates protein synthesis	Activated	2.236
	PTGER2	cell signalling, proliferation	Activated	2.236
	CEBPB	transcription factor	Activated	2.359
	KDM5A	transcription regulator	Activated	2.449
	PLAU	cellular response to fluid shear stress and glucose stimulus	Activated	2.000
	CSF2	cytokine - kinase activity	Activated	3.146
	MITF	transcription factor	Activated	2.720
	MAP4K4	serine threonine protein kinase, response to environmental stress and cytokines	Activated	2.132
High DO	NUPR1	Transcription regulator	Inhibited	-2.668
	CD38	Enzyme	Inhibited	-2.219
	CST5	Cysteine protease inhibitor	Inhibited	-2.333
	EBF1	Transcription regulator	Inhibited	-2.449
	IGF1R	Transmembrane receptor	Activated	2.138

	ATP7B	Transporter	Activated	2.000
	CEBPB	Transcription regulator	Activated	2.547
	TFAM	Transcription regulator	Activated	2.000
	EIF4E	Translation regulator	Activated	2.200
	Esrra	Transcription regulator	Activated	2.000
Low T.	MYD88	Signalling innate immune response	Inhibited	-2.000
	NFE2L2	Transcription regulator	Inhibited	-2.158
	CST5	Cysteine protease inhibitor	Inhibited	-3.000
	WT1	Transcription regulator	Inhibited	-2.000
High T.	P38 MAPK	Serine/threonine kinase	Inhibited	-2.404
	MTORC1	Serine/threonine kinase	Inhibited	-2.034
	PRKCD	Kinase	Inhibited	-2.000
	NR1H3	Ligand-dependent nuclear receptor	Inhibited	-2.183
	SCAP	Cholesterol/lipid metabolism	Inhibited	-2.941
	IKBKB	Kinase	Inhibited	-2.029
	SP1	Transcription regulator	Inhibited	-2.156
	NUPR1	Transcription regulator	Inhibited	-2.746
	CD44	Enzyme	Inhibited	-2.339
	SREBF1	Transcription regulator	Inhibited	-3.423
	TNF	Cytokine	Inhibited	-3.093
	KRAS	Enzyme	Inhibited	-2.464
	IL6R	Transmembrane receptor	Inhibited	-2.415
	SYVN1	Transporter	Inhibited	-2.982
	CST5	Cysteine protease inhibitor	Inhibited	-3.182
	EGR1	Transcription regulator	Inhibited	-2.200
	TCF7L2	Transcription regulator	Inhibited	-2.500
	SREBF2	Transcription regulator	Inhibited	-2.184
	CTNNA1	Role in apoptosis, adhesion, growth, proliferation	Activated	2.215
	26s Proteasome non-ATPase regulatory subunit 1	Role in degradation in, expression in, binding, apoptosis	Activated	2.236
	ESRI1	Complex (proliferation, transcription, apoptosis)	Activated	2.345
	ACOX1	Enzyme	Activated	2.043
	COL18A1	Endostatin	Activated	2.219
	FLI1	Transcription regulator	Activated	2.000
	INSIG1	Control of cholesterol synthesis	Activated	2.567
	LEPR	Transcription regulator	Activated	2.137
	EIF4E	Translation regulator	Activated	2.132
	Esrra	Transcription regulator	Activated	2.630

2.3.5 Application of Quantitative Proteomics to Determine Bystander Response: Naïve CHO K1

In addition to evaluating changes to proteomes of recombinant protein expressing CHO cells in response to altered bioprocessing conditions, a further study was performed wherein the media obtained from CHO DP-12 cell culture post-harvest was applied to non-producing CHO K1 cell culture. By identifying cellular-level variations in CHO K1 proteomes, an assessment regarding the impact of the secretome of production cells following altered bioprocessing may be made. For this study CHO K1 cell culture was prepared and treated with spent media, before proteomic analysis using the optimised 2D-nano-LC-MS^3 platform and data processing methods as outlined in Section 2.2. InfernoRDN software was utilised for the determination of p-values and fold changes for CHO K1 proteins treated with media from altered bioprocessing CHO DP-12 cell cultures, compared to media used for culture under standard bioprocessing conditions. Significance thresholds for differentially regulated proteins were set to |fold change| > 1.2 and p-value < 0.05. Corresponding data, illustrated in volcano plots in Figure 2.17, detail a high level of differentially regulated proteins in CHO K1 cells treated with media used to culture CHO DP-12 cells at 39.5°C (352 significant proteins) and at 110% DO (399 significant proteins), compared to other samples (57 – 187 significant proteins determined). All differentially regulated CHO K1 protein groups identified are listed in Appendix 2. To evaluate potential cellular pathways that may be associated with differentially regulated proteins in all CHO K1 proteome samples investigated, data was processed using IPA. The top 30 altered pathways determined following IPA analysis, with an absolute Z-score >1.0 and requiring a minimum of four proteins for pathway identification, are displayed in Figure 2.18. A high number of signalling pathways appear to have been activated in the CHO K1 cell cultures, in particular for the samples treated with media from high DO and high temperature culture studies. However, upon closer inspection it was noted that a number of up-regulated proteins are associated with multiple pathways. Proteins contributing to the Z-score of >10 pathways identified are outlined in Table 2.6.
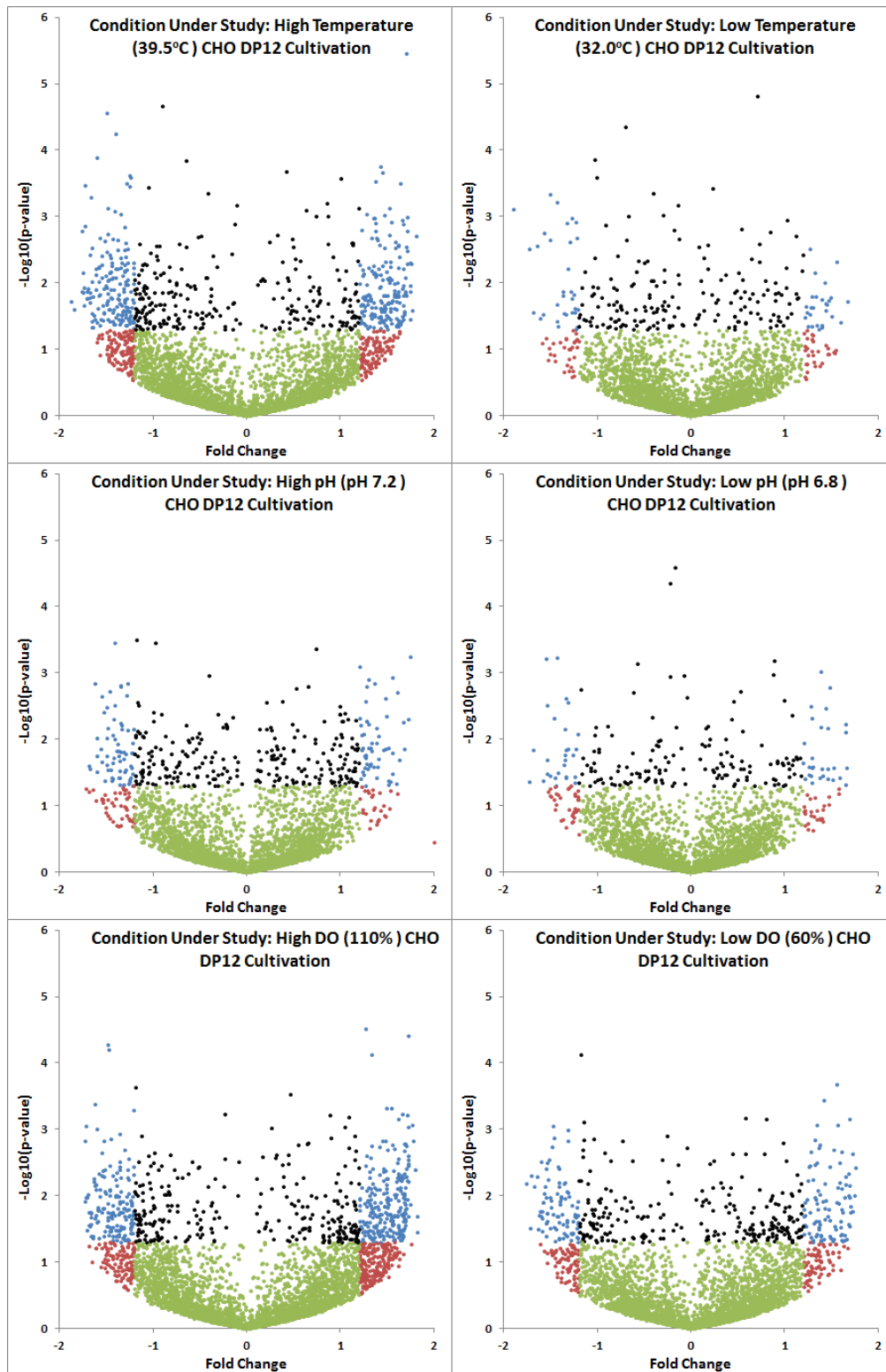
Figure 2.17: Volcano plots showing fold changes plotted against –Log10 of p-values calculated for CHO DP-12 proteins quantified. Significant proteins with fold changes >1.2 and p-value <0.05 are shown in blue, red dots represent proteins with p-value >0.05 and >1.2 fold change; green dots represent proteins with p value >0.05, <1.2 fold change; black dots signify proteins with p value <0.05, <1.2 fold change.

Figure 2.18: Heat map displaying the top canonical pathways identified for each CHO K1 proteomic sample using IPA. Using IPA, differentially regulated proteins with p values <0.05 and having >1.2 log fold change and associated with different known cellular pathways, were used to identify the top significantly differentially regulated pathways in each of the CHO K1 samples following application of spent media from CHO DP-12 cells cultured under altered bioprocessing conditions.

Table 2.6: Individual protein (|Z-score|> 2.0) associated with >10 differentially regulated pathways observed following IPA analysis of CHO K1 proteomic data.

Gene	Protein	Biological Activity
NFKB1	Nuclear factor NF-kappa-B p 105 subunit	Transcription factor, endpoint of signal transduction
RRAS2	Ras-related protein R-Ras2	GTPase activity, intracellular protein transport
GNAI2	Guanine nucleotide-binding protein G (i) subunit alpha-2	Transmembrane signalling, GTP-binding
GNAQ	Guanine nucleotide-binding protein G (q) subunit alpha	Transmembrane signalling, GTP-binding
GNB2	Guanine nucleotide-binding protein G(1)/G(S)/G(T) subunit beta-2	Transmembrane signalling, GTP-binding
GNB4	Guanine nucleotide-binding protein subunit beta-4	Transmembrane signalling, GTP-binding
PPP2R2A	Serine-threonine-protein phosphatase 2A 55 kDa regulatory subunit B alpha	Protein de-phosphorylation

2.4   Conclusions and Future Work

In this Chapter, a high pH low pH 2D LC-MS^3 proteomic platform incorporating SPS-MS^3 for identification and quantitation of TMT sixplex labelled proteomic samples was applied for determination of differentially regulated proteins and cellular pathways in CHO cells undergoing altered bioprocessing. The platform was found to be highly reproducible and capable of identification and quantitation of >6,200 protein groups with >1% FDR for all sample sets, ensuring high confidence in the data acquired. However, based on the pathways identified as having increased or decreased activity, it appears that proteomic analysis on its own may not provide enough of an insight into the molecular activities of these CHO cells. Many of the pathway changes observed were related to the activity of kinases, transcription factors whose activity may be modulated by phosphorylation. Despite determination of physical changes to their concentration, in the absence of phosphoproteome analysis an assumption must be made in regards to their activity. Thus to truly understand the cellular level activities of CHO cells producing recombinant therapeutics, a more global omics approach would be useful, in particular the addition of metabolomics and phosphoproteomics would be highly beneficial to gain a more in-depth understanding of these important production systems. Furthermore, augmentation of bioinformatics resources for CHO, in line with model systems such as human, mouse and rat, may enable more relevant biological findings to be made. Finally, in order to determine whether the product is the process, complementary characterisation of the therapeutic protein produced is required for a more

thorough assessment of the impact of altered bioprocessing on therapeutic protein production from CHO cell lines.

2.5   Author Contributions

Research study devised by Amy Farrell and Jonathan Bones; Bioprocessing of cell cultures performed by Amy Farrell; Sample preparation performed by Amy Farrell; LC-MS analysis of samples performed by Amy Farrell and Jenny Ho (Thermo Fisher Scientific, Hemel Hempstead, UK); CHO DG44 proteome database was supplied by Somak Ray and Barry Karger (Barnett Institute, Northeastern University, Boston, USA); Data analysis performed by Amy Farrell; Chapter written by Amy Farrell and reviewed by Jonathan Bones.

2.6   References

1.   Walsh, G., *Biopharmaceutical benchmarks 2014.* Nat Biotechnol, 2014. **32**(10): p. 992-1000.

2.   Huang, S., et al., *Fully humanized neutralizing antibodies to interleukin-8 (ABX-IL8) inhibit angiogenesis, tumor growth, and metastasis of human melanoma.* Am J Pathol, 2002. **161**(1): p. 125-34.

3.   Gonzalez, T.N., Leong, S. R., Presta, L. G., *Humanized Anti-IL8 monoclonal antibodies. September 12th 2000. [Accessed from http://www.google.com/patents/US6117980 on 12th June 2016.].* 2000.

4.   Bar-Eli, M., *Role of interleukin-8 in tumor growth and metastasis of human melanoma.* Pathobiology, 1999. **67**(1): p. 12-8.

5.   Nurnberg, W., et al., *Expression of interleukin-8 detected by in situ hybridization correlates with worse prognosis in primary cutaneous melanoma.* J Pathol, 1999. **189**(4): p. 546-51.

6.   Scheibenbogen, C., et al., *Serum interleukin-8 (IL-8) is elevated in patients with metastatic melanoma and correlates with tumour load.* Melanoma Res, 1995. **5**(3): p. 179-81.

7.   Singh, R.K., et al., *Expression of interleukin 8 correlates with the metastatic potential of human melanoma cells in nude mice.* Cancer Res, 1994. **54**(12): p. 3242-7.

8.   Singh, R.K., et al., *Expression of interleukin-8 in primary and metastatic malignant melanoma of the skin.* Melanoma Res, 1999. **9**(4): p. 383-7.

9.   Ugurel, S., et al., *Increased serum concentration of angiogenic factors in malignant melanoma patients correlates with tumor progression and survival.* J Clin Oncol, 2001. **19**(2): p. 577-83.

10.   Yang, X.D., et al., *Fully human anti-interleukin-8 monoclonal antibodies: potential therapeutics for the treatment of inflammatory disease states.* J Leukoc Biol, 1999. **66**(3): p. 401-10.

11.   Bangsgaard, N., et al., *Neutralization of IL-8 prevents the induction of dermatologic adverse events associated with the inhibition of epidermal growth factor receptor.* PLoS One, 2012. **7**(6): p. e39706.

12.   Tappeiner, C., et al., *New biologic drugs: anti-interleukin therapy.* Dev Ophthalmol, 2012. **51**: p. 79-89.

13.   US National Institute of Health. ClinicalTrials.gov Identifier NCT02536469 - HuMax-IL8 (Interleukin8) in Patients with Advanced Malignant Solid Tumors. [Information accessed from https://clinicaltrials.gov/ct2/show/NCT02536469 on 12th June 2016].

14.   Wurm, F.M., *Production of recombinant protein therapeutics in cultivated mammalian cells.* Nat Biotechnol, 2004. **22**(11): p. 1393-8.

15.   Furukawa, K. and K. Ohsuye, *Enhancement of productivity of recombinant alpha-amidating enzyme by low temperature culture.* Cytotechnology, 1999. **31**(1-2): p. 85-94.

16.   Moore, A., et al., *Effects of temperature shift on cell cycle, apoptosis and nucleotide pools in CHO cell batch cultues.* Cytotechnology, 1997. **23**(1-3): p. 47-54.

17.   Trummer, E., et al., *Process parameter shifting: Part I. Effect of DOT, pH, and temperature on the performance of Epo-Fc expressing CHO cells cultivated in controlled batch bioreactors.* Biotechnol Bioeng, 2006. **94**(6): p. 1033-44.

18. Zhu, M.M., et al., *Effects of elevated pCO2 and osmolality on growth of CHO cells and production of antibody-fusion protein B1: a case study.* Biotechnol Prog, 2005. **21**(1): p. 70-7.

19. Xie, L. and D.I. Wang, *High cell density and high monoclonal antibody production through medium design and rational control in a bioreactor.* Biotechnol Bioeng, 1996. **51**(6): p. 725-9.

20. Castro, P.M., et al., *Application of a statistical design to the optimization of culture medium for recombinant interferon-gamma production by Chinese hamster ovary cells.* Appl Microbiol Biotechnol, 1992. **38**(1): p. 84-90.

21. Sellick, C.A., et al., *Metabolite profiling of recombinant CHO cells: designing tailored feeding regimes that enhance recombinant antibody production.* Biotechnol Bioeng, 2011. **108**(12): p. 3025-31.

22. Kuystermans, D., M.J. Dunn, and M. Al-Rubeai, *A proteomic study of cMyc improvement of CHO culture.* BMC Biotechnol, 2010. **10**: p. 25.

23. Ku, S.C., et al., *Effects of overexpression of X-box binding protein 1 on recombinant protein production in Chinese hamster ovary and NS0 myeloma cells.* Biotechnol Bioeng, 2008. **99**(1): p. 155-64.

24. Ku, S.C., et al., *Regulation of XBP-1 signaling during transient and stable recombinant protein production in CHO cells.* Biotechnol Prog, 2010. **26**(2): p. 517-26.

25. Baik, J.Y., et al., *Metabolic engineering of Chinese hamster ovary cells: towards a bioengineered heparin.* Metab Eng, 2012. **14**(2): p. 81-90.

26. Carlage, T., et al., *Proteomic profiling of a high-producing Chinese hamster ovary cell culture.* Anal Chem, 2009. **81**(17): p. 7357-62.

27. Lee, Y.Y., et al., *Overexpression of heat shock proteins (HSPs) in CHO cells for extended culture viability and improved recombinant protein production.* J Biotechnol, 2009. **143**(1): p. 34-43.

28. Lim, S.F., et al., *RNAi suppression of Bax and Bak enhances viability in fed-batch cultures of CHO cells.* Metab Eng, 2006. **8**(6): p. 509-22.

29. Wong, D.C., et al., *Targeting early apoptotic genes in batch and fed-batch CHO cell cultures.* Biotechnol Bioeng, 2006. **95**(3): p. 350-61.

30. Yun, C.Y., et al., *Specific inhibition of caspase-8 and -9 in CHO cells enhances cell viability in batch and fed-batch cultures.* Metab Eng, 2007. **9**(5-6): p. 406-18.

31. Meleady, P., et al., *Utilization and evaluation of CHO-specific sequence databases for mass spectrometry based proteomics.* Biotechnol Bioeng, 2012. **109**(6): p. 1386-94.

32. Baycin-Hizal, D., et al., *Proteomic analysis of Chinese hamster ovary cells.* J Proteome Res, 2012. **11**(11): p. 5265-76.

33. Xu, X., et al., The genomic sequence of the Chinese hamster oveary (CHO)-K1 cell line. *Nature Biotechnology,* 2011. **29**(8):p. 735-41.

34. Tambor, V., et al., *Proteomics and bioinformatics analysis reveal underlying pathways of infection associated histologic chorioamnionitis in pPROM.* Placenta, 2013. **34**(2): p. 155-61.

35. Thermo Fisher Scientific Inc. 2014. Instructions: TMT mass tagging kits and reagents. [ONLINE] Available at https://tools.lifetechnologies.com/content/sfs/manuals/MAN0011639_TMT_Mass_Tagging_Reag_UG.pdf [Accessed 09 April 2015].

36. Liu, Z., et al., *A quantitative proteomic analysis of cellular responses to high glucose media in Chinese hamster ovary cells.* Biotechnol Prog, 2015. **31**(4): p. 1026-38.

37. Pacific Northwest National Laboratory. InfernoRDN v 1.1.5970. Downloaded from https://omics.pnl.gov/software/infernordn on 20th May 2016.

38. Wu, S., et al., *Employment of tandem mass spectrometry for the accurate and specific identification of oligosaccharide structures.* Anal Chem. **84**(17): p. 7456-62.

39. Huang da, W., B.T. Sherman, and R.A. Lempicki, *Bioinformatics enrichment tools: paths toward the comprehensive functional analysis of large gene lists.* Nucleic Acids Res, 2009. **37**(1): p. 1-13.

40. Supek, F., et al., *REVIGO summarizes and visualizes long lists of gene ontology terms.* PLoS One, 2011. **6**(7): p. e21800.

41. Chuppa, S., et al., *Fermentor temperature as a tool for control of high-density perfusion cultures of mammalian cells.* Biotechnol Bioeng, 1997. **55**(2): p. 328-38.

42.   Fogolin, M.B., et al., *Impact of temperature reduction and expression of yeast pyruvate carboxylase on hGM-CSF-producing CHO cells.* J Biotechnol, 2004. **109**(1-2): p. 179-91.

43.   Fox, S.R., et al., *Maximizing interferon-gamma production by Chinese hamster ovary cells through temperature shift optimization: experimental and modeling.* Biotechnol Bioeng, 2004. **85**(2): p. 177-84.

44.   Kaufmann, H., et al., *Influence of low temperature on productivity, proteome and protein phosphorylation of CHO cells.* Biotechnol Bioeng, 1999. **63**(5): p. 573-82.

45.   Moulder, R., et al., *Quantitative proteomics analysis of the nuclear fraction of human CD4+ cells in the early phases of IL-4-induced Th2 differentiation.* Mol Cell Proteomics, 2010. **9**(9): p. 1937-53.

46.   Link, T., et al., *Bioprocess development for the production of a recombinant MUC1 fusion protein expressed by CHO-K1 cells in protein-free medium.* J Biotechnol, 2004. **110**(1): p. 51-62.

47.   Unwin, R.D., et al., *Quantitative proteomics reveals posttranslational control as a regulatory factor in primary hematopoietic stem cells.* Blood, 2006. **107**(12): p. 4687-94.

48.   Salem, M., et al., *Proteomic signature of muscle atrophy in rainbow trout.* J Proteomics, 2010. **73**(4): p. 778-89.

49.   Dowling, P., et al., *Proteomic screening of glucose-responsive and glucose non-responsive MIN-6 beta cells reveals differential expression of proteins involved in protein folding, secretion and oxidative stress.* Proteomics, 2006. **6**(24): p. 6578-87.

50.   Borys, M.C., D.I. Linzer, and E.T. Papoutsakis, *Culture pH affects expression rates and glycosylation of recombinant mouse placental lactogen proteins by Chinese hamster ovary (CHO) cells.* Biotechnology (N Y), 1993. **11**(6): p. 720-4.

51.   Baik, J.Y., et al., *Initial transcriptome and proteome analyses of low culture temperature-induced expression in CHO cells producing erythropoietin.* Biotechnol Bioeng, 2006. **93**(2): p. 361-71.

52.   Kantardjieff, A., et al., *Transcriptome and proteome analysis of Chinese hamster ovary cells under low temperature and butyrate treatment.* J Biotechnol, 2010. **145**(2): p. 143-59.

53. Yoon, S.K., S.H. Kim, and G.M. Lee, *Effect of low culture temperature on specific productivity and transcription level of anti-4-1BB antibody in recombinant Chinese hamster ovary cells.* Biotechnol Prog, 2003. **19**(4): p. 1383-6.

54. Yee, J.C., et al., *Genomic and proteomic exploration of CHO and hybridoma cells under sodium butyrate treatment.* Biotechnol Bioeng, 2008. **99**(5): p. 1186-204.

55. Lee, M.S., et al., *Proteome analysis of antibody-expressing CHO cells in response to hyperosmotic pressure.* Biotechnol Prog, 2003. **19**(6): p. 1734-41.

56. McAlister, G.C., et al., *MultiNotch MS3 enables accurate, sensitive, and multiplexed detection of differential expression across cancer cell line proteomes.* Anal Chem, 2014. **86**(14): p. 7150-8.

57. Rathore, A.S. and H. Winkle, *Quality by design for biopharmaceuticals.* Nat Biotechnol, 2009. **27**(1): p. 26-34.

58. Furukawa, K. and K. Ohsuye, *Effect of culture temperature on a recombinant CHO cell line producing a C-terminal alpha-amidating enzyme.* Cytotechnology, 1998. **26**(2): p. 153-64.

3.0

Characterisation of Monoclonal Antibodies Following Production under Altered Bioprocessing Conditions

3.1   Introduction

Recombinant monoclonal antibodies (mAbs) are well-established pharmacological therapeutics featuring high specificity to target antigens, long serum half-life in humans and capabilities for the treatment of a wide range of ailments, such as inflammatory diseases and cancer. MAbs are large tetrameric glycoproteins, structurally composed of four polypeptide chains: two identical heavy chains (~50 kDa in size) and two identical light chains (~25 kDa in size), connected *via* disulfide bonds at their hinge region. Each mAb comprises of two variable antigen-binding fragments (Fab) and a crystallisable fragment (Fc), responsible for effector function *via* interaction with the Fc_γ receptor family. [1] Inherently heterogeneous biomolecules, mAbs may undergo a broad range of both enzymatic and non-enzymatic modifications during biopharmaceutical production. [2] Protein modifications have the potential to alter the safety and efficacy profile of mAbs by impacting protein binding, reducing drug activity and giving rise to adverse toxicological and immunological responses *in-vivo*. [3] Consequently, therapeutic protein characterisation is an essential component of drug development and manufacture, as outlined in the U.S. Food and Drug Administration's initiatives including pharmaceutical cGMPs for the 21st century [4], process analytical technology (PAT) [5] and the International Conference on Harmonisation (ICH) tripartite guidelines on product development and quality. [6, 7] Critical quality attributes (CQAs) that must be determined include protein identity (primary sequence), and frequently encountered host cell- and process-related modifications including deamidation, oxidation, N-terminal glutamine cyclization, C-terminal lysine truncation, glycosylation, isomerisation and incomplete disulfide bond formation. [8] Combinations of these modifications have been theorised to result in 10^8 potential mAb variants for each therapeutic mAb, [9] resulting in biomolecules with differences in size, charge, hydrophobicity, structure and potentially, therapeutic function. As no single analytical technique exists to determine all of these

attributes, a wide range of analytical technologies are required for the complete characterisation of therapeutic mAbs.

Biophysical properties, including heterogeneity in size, net charge of the biomolecule and hydrophobic properties are most commonly determined using chromatographic techniques coupled with ultra-violet (UV) detection. Size exclusion chromatography (SEC-UV) is the most widely applied method for the determination of protein aggregation and formation of particles in response to structural, environmental and bioprocessing factors. [10] Concerns regarding the potential of protein aggregates to produce immunogenic reactions and alter the actual dosing concentration of drug substances, have led to interest in alternative methods for evaluating aggregation concentrations. [3] Hence complementary techniques, such as analytical ultracentrifugation (AUC) and hydrophobic interaction chromatography (HIC-UV) have been evaluated. HIC has shown promise for the determination of mAb isoforms including small aggregates (1- 10 μm), which are undetectable using SEC-UV. [11] Additionally, HIC has been applied for monitoring of modifications such as methionine or tryptophan oxidations, which result in a change in mAb hydrophobicity. [11] Ion exchange chromatography (IEX-UV), or more frequently, cation exchange chromatography (SCX-UV) using either a salt or pH separation gradient, is the gold standard for determination of the charge variant profile of therapeutic mAbs. [12] Different charge variants of mAbs may be formed as a result of a variety of modifications including C-terminal lysine processing of the mAb heavy chain, deamidation of asparagine or glutamine, cyclisation of N-terminal glutamic acid to form pyroglutamate and peptide bond cleavage. [2]

Although chromatographic techniques are useful for the evaluation of potential changes to mAb sequence, they are not capable of identifying exact sequence changes, determining alterations to protein mass or of evaluating the relative concentration of mAb variants. High resolution mass spectrometry (MS) is a key technique for biotherapeutic characterisation, capable of providing sequence-level information that is crucial for the evaluation of therapeutic protein quality. Three general approaches are used for reversed-phase liquid chromatography-mass spectrometry, namely top-down, middle-down and peptide mapping strategies. Top-down approaches involve the analysis of intact mAb species and are capable of evaluating changes to protein mass caused by sequence modification and determination of post-translational modifications, *e.g.* glycosylation. However, top-down strategies frequently suffer from low sensitivity due to poor ionisation efficiencies of large biomolecules and low sequence coverage caused by poor fragmentation of peptide bonds in complex biotherapeutics. [13-15] Middle-down analysis of mAbs refers to the mass measurements of

mAb subunits following limited proteolysis to generate polypeptides that are more amenable to chromatographic separation and have higher MS ionisation efficiencies when compared to the large intact biomolecule (~150 kDa). Proteolytic enzymes Lys-C [16] and papain [17] have been applied for mAb subunit generation, however, the recently discover IdeS (immunoglobulin-degrading enzyme of *Streptococcus pyrogenes*) is fast becoming the go-to protease for middle-down analysis due to its simple, rapid and robust digestion procedure and high specificity, cleaving at the mAb hinge region between two glycine amino acid residues in IgG1. [18, 19] IdeS digestion is frequently followed by disulfide bond reduction to generate light chain (LC), scFc and Fd' fragments as depicted in Figure 3.6. Middle down analysis may be applied for determination of changes to mAbs, wherein protein mass has been altered (*e.g.* from amino acid insertions or deletions or following sequence level modifications).

Peptide mapping of mAbs is the most common approach for determination of protein amino acid sequence, [20] and generally involves initial protein denaturation using reagents such as guanidine-HCl, dithiothreitol or tris(2-carboxyethyl)phosphine (TCEP), followed by digestion with one or more proteases (*e.g.* trypsin or Lys-C). [12] Resulting peptides may be analysed using LC-MS/MS, enabling the identification of sequence-level modifications that result in distinctive mass shifts upon data analysis (*e.g.* N-terminal pyroglutamate results in a mass reduction of 17 Da). [2] Recent advances in high resolution MS instrumentation have significantly increased the power of this technique by enabling the determination of small mass shifts corresponding to peptide modifications that may impact product quality, such as an increase in peptide mass of 0.984 Da corresponding to deamidation of an amino acid residue. [21] Using peptide mapping, the quantity of a modified peptide relative to the total amount of that peptide in a therapeutic protein sample may be deduced.

In this Chapter, characterisation of anti-interleukin 8 IgG1 (anti-IL8) produced from CHO DP-12 cells processed under altered conditions of temperature, pH or dissolved oxygen (DO), is described. Comparative analysis of anti-IL8 produced under altered conditions and anti-IL8 produced using standard bioprocessing conditions, may reveal changes to the primary sequence of recombinant mAbs that could be attributed to the change in the bioprocess used for their production. Hence application of chromatographic and mass spectrometry techniques may enable a better understanding of the role of bioprocessing in achieving desired protein critical quality attributed essential for recombinant therapeutic protein safety, quality and efficacy.

3.2 Experimental

3.2.1 Reagents and Consumables

Phosphate buffered saline (PBS), dithiothreitol (DTT), iodoacetamide (IAA), ammonium bicarbonate (ABC), L-arginine, guanidine-hydrochloride, tris(2-carboxyethyl)phosphine (TCEP), Trizma-hydrochloride (Tris), sodium phosphate dibasic (Na_2HPO_4), sodium phosphate monobasic (NaH_2PO_4), sodium chloride (NaCl), ammonium sulphate (($NH_4)_2SO_4$) and Amicon Ultra centrifugal filter units 10 kDa MWCO were obtained from Sigma Aldrich (Wicklow, Ireland). Water (LC-MS Optima), water, 0.1% (v/v) formic acid (LC-MS Optima) and acetonitrile, 0.1% (v/v) formic acid (LC-MS Optima) were purchased from Fisher Scientific. CX-1, pH gradient buffer A (pH 5.6), CX-1, pH gradient buffer B (pH 10.2), BCA assay kit and 0.45 μm and 0.2 μm bottle top filter units were acquired from Thermo Fisher Scientific (Dublin, Ireland). Promega sequencing grade modified trypsin was from MyBio Ltd. (Kilkenny, Ireland). FabRICATOR (IdeS) was purchased from Genovis (Lund, Sweden).

3.2.2 Purification of Anti-IL 8 from CHO DP12

Anti-IL8 mAb was produced in Sartorius Cultibag disposable bioreactors as outlined in Chapter 2, Section 2.2.2.5. Spent media from CHO DP-12 cell culture were retrieved from -80°C freezer and thawed before clarification of media samples by sequential filtration through 0.45 μm and 0.2 μm syringe filters (VWR). Samples of clarified media were then passed through a HiTrap Protein A column (GE Healthcare) at a flow rate of 1 mL.min^{-1} and subsequently washed with PBS to ensure complete removal of all unretained material. Elution of anti-IL8 from the Protein A column was performed using 100 mM arginine, pH 3.5. The pH of eluate, collected in Amicon Ultra centrifugal filter units with a 10 kDa cut-off membrane (Sigma Aldrich), was neutralized using 0.5 M Tris buffer and buffer-exchanged into PBS (4,000 rpm for 20 min). An aliquot of the concentrated and buffer exchanged IgG1 sample was assayed for IgG content using a BCA protein assay. The remainder of the samples were divided into 100 μg portions and stored at -30°C pending further analysis.

3.2.3 Size Exclusion Chromatography

SEC-UV analysis was performed on a Vanquish Flex UHPLC (Thermo Scientific) using a diode array detector at 280 nm. The presence protein aggregates, monomers and fragment moieties

was determined using a MAbPac^{TM} SEC-1, 5 µm, 300 Å, 4.0 x 300 mm analytical column (Thermo Scientific) under isocratic conditions of 50mM sodium phosphate buffer, 300 mM NaCl, pH 6.8 at 0.2 mL.min^{-1} for 25 minutes. The column temperature was 30°C. Triplicate analysis of 10 µg of each mAb sample was performed. Chromeleon version 7.2 software was used for data acquisition and analysis.

3.2.4   Cation Exchange Chromatography

Charge variant analysis of intact mAb was performed using a Vanquish Flex UHPLC using a diode array detector at 280 nm. pH gradient based separation on a MAbPac^{TM} SCX-10 RS analytical column, 5 µm, 2.1 x 50 mm (Thermo Scientific) using CX-1 pH gradient buffer A, pH 5.6 and CX-1 pH gradient buffer B, pH 10.2 (Thermo scientific). Elution of sample peaks was achieved using a linear gradient of 35 - 55% CX-1 pH gradient buffer B, pH 10.2 in 30 minutes. Column temperature was 25°C and flow rate was 0.5 mL.min^{-1}. Chromeleon version 7.2 software was used for data acquisition and analysis.

3.2.5   Hydrophobic Interaction Chromatography

HIC-UV analysis was performed on a Vanquish Flex UHPLC using a diode array detector at 280 nm. To achieve sufficient separation of mAb species, two MabPac^{TM} HIC-10, 5 µm, 4.6 x 100 mm analytical columns (Thermo Scientific) were set up in sequence. Separation buffers used were 2 M ammonium sulphate, 100 mM sodium phosphate, pH 7.0 (A) and 100 mM sodium phosphate, pH 7.0 (B). Gradient conditions were as follows: 60% B for 2 minutes followed by an increase to 100% B over 38 minutes; solvent composition was maintained at 100% B for 5 minutes before reduction to 60% B in 0.1 minute; column equilibration was achieved over 6 minutes. Column temperature was maintained at 30°C. Flow rate was 1.0 mL.min^{-1}. Triplicate analysis of 25 µg of each mAb sample was performed. Chromeleon version 7.2 software was used for data acquisition and analysis.

3.2.6   Middle Down Analysis of IdeS-digested mAb

One µL of the FacRICATOR enzymatic digestion solution (67 units IdeS µL^{-1} in Optima grade water) was combined with 50 µL of anti-IL8 in PBS (~100 µg) and incubated at 37°C for 2 hours at 500 rpm using an Eppendorf Thermomixer. Reduction of disulphide bonds was achieved

with 4 M guanidine hydrochloride/ 50 mM TCEP for 45 minutes at 56°C. Following incubation, samples were reduced to dryness *via* vacuum centrifugation. Each sample was reconstituted in 100 µL 0.1% formic acid in water. Middle down analyses were perfromed using a MabPac™ RP, 4 µm, 2.1 x 100 mm analytical column on a Vanquish UHPLC coupled to a Q Exactive HF mass spectrometer (Thermo Fisher Scientific, Bremen, Germany). Separation of mAb subunits was performed using a binary gradient of 0.1% (v/v) formic acid in water (C) and 0.1% (v/v) formic acid in acetonitrile (D). Gradient conditions were as follows: 25% D initially for one minute, increased to 32% D in 15 minutes with a further increase to 80% D in one minute with a one minute isocratic hold. Initial conditions were restored in 0.5 minutes and held for an additional 9.5 minutes to ensure column re-equilibration. The column temperature was maintained at 80°C throughout and flow rate was sustained at 250 µL.min^{-1}. The mass spectrometer was operated in positive ion mode with MS scans ranging from 600 to 2400 m/z with a mass resolution of 240,000 at m/z 400. Briefly, MS instrumental paramters were set as follows: spray voltage was 3.8 kV sheath gas flow rate was 25 arbitrary units (AU), auxillary gas flow rate was 10 AU, spray current was 13 µA, capillary temperature was 320°C. Data was processed using Biopharma Finder version 1.0.76.10, using the Auto Xtract algorithm set to deconvolute spectra with a charge of 5 to 50 in the range 600 to 2000 m/z. Biopharma Finder software is an informatics platform used for the analysis of protein characterisation data acquired on Thermo Fisher Scientific mass spectrometers. Biopharma Finder enables the confirmation of amino acid sequence, identification of the site and type of post translational modifications and facilitates the determintion of relative amounts of mAb peptide varients.

3.2.7 Peptide Mapping

Peptide sequence mapping of anti-IL-8 IgG1 samples was performed on a Vanquish UHPLC coupled to a Q Exactive Plus mass spectrometer (Thermo Fisher Scientific, Bremen, Germany). Sample preparation was performed using the filter-aided sample preparation (FASP) method described previously. [22] 50 µg of mAb was diluted in 8 M urea in 100 mM Tris-HCl and added to a pre-rinsed 10 kDa MWCO filters. Samples were reduced with 5 mM DTT at 65°C for 30 minutes, before alkylation with 15 mM IAA for 30 minutes at 20°C in darkness. Following buffer exchange into 50 mM ABC, enzymatic digestion was performed overnight with trypsin at 37°C using a 1:50 (w/w, enzyme: protein) ratio. Samples were eluted from the filters by centrifugation and subsequently reduced to dryness *via* vacuum centrifugation.

Tryptic peptides were reconstituted in 0.1% (v/v) formic acid in water and separated using an Acclaim 120 C18, 5µm, 2.1 x 250 mm analytical column (Thermo Fisher Scientific) with a binary gradient of 0.1% (v/v) formic acid in water (C) and 0.1% (v/v) formic acid in acetonitrile (D). Gradient conditions were as follows: 2% D increased to 30% D in 40 minutes with a further increase to 80% D over 3 minutes with a 3.5 minute isocratic hold. Initial conditions were restored in 0.5 minutes and held for an additional 18 minutes to ensure column re-equilibration. The column temperature was maintained at 60°C throughout and flow rate was sustained at 250 µL.min^{-1}. The mass spectrometer was operated in positive ion data dependent mode. Survey full-scan MS spectra (m/z 200-2000) were acquired in the Orbitrap with a mass resolution of 70,000 at m/z 400. The spray voltage was 3.5 kV. The top five most intense precursors were selected for MS^2 fragmentation, using an isolation window of 2.0 m/z. Other MS parameters used included a capillary temperature of 320°C, sheath gas set to 20 AU and auxillary gas of 8 AU. Resultant data were processed using Biopharma Finder version 1.0.76.10, using the following workflow parameters: mass accuracy = 5 ppm, maximum number of modifications per peptide = 1, protease = trypsin, specificity set to high, variable modifications: N-terminal pyro-glutamine, C-terminal lysine clipping, side chain carbamidomethylation and carboxymethylation, asparagine deamidation, glutamine deamidation and oxidation of methionine and tryptophan. Data was searched against a FASTA file composed of the anti-IL-8 IgG1 sequence taken from US Patent 6117980. [23]

3.3   Results and Discussion

Unlike small molecule chemical drug substances that may be produced showing consistent conformity between manufacturing batches, routine bioprocessing can result in the production of heterogeneous mAb products due to inherent difficulties in achieving consistency while producing large biomolecules from living cells. A huge number of potential mAb variants may be generated, as outlined in Figure 3.1 and may result in undesired negative effects on the safety, efficacy and stability profile of therapeutic biomolecules. However, using appropriate analytical techniques changes to the primary sequence of mAbs may be determined by evaluating differences in the mass, charge and hydrophobicity of proteins or peptides generated from those proteins. In this work, anti-IL8 IgG1 was produced under standard bioprocessing conditions and also in batch culture wherein one of the parameters studied was increased or decreased, thereby resulting in the acquisition of a range of mAb samples that may undergo comparability assessment to identify changes potentially attributed to the application of a particular bioprocess setting (Table 3.1). Various analytical techniques

were applied for characterisation and comparability assessment of the therapeutic mAb produced, including SEC-UV for determination of protein aggregation, SCX-UV for analysis of mAb charge variants and HIC-UV for evaluation of changes to the hydrophobicity of the mAb produced. Subsequently, existing modifications were further investigated using middle-down and peptide mapping strategies for sequence and domain-level characterisation of anti-IL8, produced under altered bioprocessing conditions.

Table 3.1: Description of anti-IL8 samples for product characterisation analysis.

mAb Sample Name	Conditions used for batch culture of Anti-IL8
Standard 1-3 mAb	37.0°C, pH 7.0, 85% DO
High Temperature mAb	39.5°C, pH 7.0, 85% DO
Low Temperature mAb	32.0°C, pH 7.0, 85% DO
High pH mAb	37.0°C, pH 7.2, 85% DO
Low pH mAb	37.0°C, pH 6.8, 85% DO
High DO mAb	37.0°C, pH 7.0, 110% DO
Low DO mAb	37.0°C, pH 7.0, 65% DO
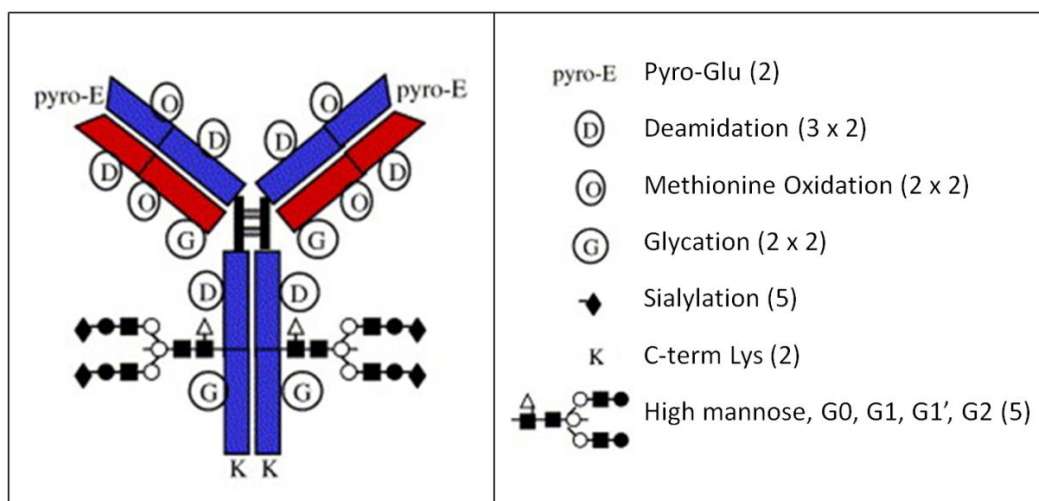
Figure 3.1: Schematic of a mAb, showing sites of potential sequence modifications denoted by symbols outlined in the corresponding legend. The number of modification sites for each half antibody multiplied by the number of possible variations at each site is shown in the parenthesis. Assuming variants on each side of the antibody are independent, each mAb has 10^8 potential variations. [9]

3.3.1 Intact Anti-IL8 Analysis

Size exclusion chromatography (SEC) is frequently applied for the evaluation of protein aggregation due to its simplicity, low cost and low sample requirements. [24-26] Administration of protein aggregates have the potential to cause adverse immune responses in patients and hence levels of protein aggregation is a CQA that must be monitored in biotherapeutic proteins. [27] Cleavage of peptide bonds to produce smaller subunit fragments and/or subsequent erroneous re-formation of mAb tertiary structure and creation of dimers or trimers may be indicated by separation of non-monomeric species using SEC. [28] Other sequence-level modifications that may be highlighted using SEC include the oxidation of tryptophan residues, which reportedly result in the earlier elution of mAbs from SEC columns, attributed to a reduction in non-specific hydrophobic stationary phase interactions rather than a change in mAb size. [29] To determine changes to the aggregation profile of anti-IL8 in response to altered bioprocessing conditions, triplicate analysis of each of the samples produced were performed using the method outlined in Section 3.2.3. Following SEC analysis, chromatographic peaks were integrated to determine the % area of the monomer and aggregate peaks. Corresponding results are shown in Table 3.2. Size-related heterogeneity observed across all samples following SEC-UV analysis was found to be comparable, with levels of differentially sized species ranging from 0.18 – 0.34% of the entire mAb sample. From the results obtained using SEC analysis it may deduced that the levels of protein aggregation are not widely impacted by production within the range of bioprocessing parameters investigated.

Table 3.2: Results from SEC-UV analysis of differentially produced mAb samples (n=3).

Sample	Replicate 1		Replicate 2		Replicate 3	
	% Area of Monomer	% Area of Aggregate	% Area of Monomer	% Area of Aggregate	% Area of Monomer	% Area of Aggregate
Standard 1	99.72	0.28	99.73	0.27	99.72	0.28
Standard 2	99.75	0.25	99.75	0.25	99.74	0.26
Standard 3	99.70	0.30	99.70	0.30	99.70	0.30
High T mAb	99.68	0.32	99.67	0.33	99.66	0.34
Low T mAb	99.72	0.28	99.72	0.28	99.73	0.27
High DO mAb	99.69	0.31	99.70	0.30	99.70	0.30
Low DO mAb	99.77	0.23	99.76	0.24	99.77	0.23
High pH mAb	99.70	0.30	99.71	0.29	99.69	0.31
Low pH mAb	99.82	0.18	99.80	0.20	99.78	0.22

Charge-related microheterogeneity of mAbs is frequently observed following bioprocessing due to both enzymatic processes and non-enzymatic degradation of therapeutic proteins. [30] Chemical modifications, such as deamidations and impart a negative charge onto mAbs thereby decreasing their isoelectric point (pI) and resulting in the formation of acidic mAb variants. [31, 32] Similarly, C-terminal cleavage of lysine residues results in the loss of positively charged amino acids on the mAb also creating acidic protein variants. [33] Conversely, the presence of one or more lysine amino acids or oxidation of mAb residues may result in an increase in mAb pI value and thus in the formation of basic mAb variants. [34, 35] To determine the charge variant profile of anti-IL8 IgG1 samples following production using different bioprocessing parameters, triplicate SCX-UV analysis of each mAb sample was performed enabling the separation of species according to differences in their pI. A number of distinct peaks, in addition to the main mAb peak, were observed in resulting chromatograms indicating the existence of greater than seven mAb variants within each sample, (Figures 3.2 and 3.3). Chromatographic peaks were integrated manually and the area of each peak as a percentage of the total area was calculated (Table 3.3). Large disparities between the charge variant profiles for all of the samples were observed potentially relating to a variety of mAb modifications including asparagine deamidation, oxidation of methionine, tryptophan oxidation, glycation, sialylation and non-classical disulfide bond formation. [36] Two likely mAb variants include moieties incorporating either one or two C-terminal lysine residues, which are known to produce distinctive peaks eluting after the main mAb peak upon SCX analysis, such as those observed in the chromatograms shown in Figures 3.2 and 3.3. [37] Samples produced at pH 7.2 displayed higher levels of both acidic and basic variants, while samples produced at 110% DO, pH 6.8 and 39.5°C resulted in an observed reduction in both acidic and basic variants when compared to mAb produced at standard conditions. In agreement with Zhang *et al.* [38] we determined a decrease in acidic variants and an increase in basic variant profile in mAb produced from batch culture maintained at 32.0°C when compared to mAb generated in culture at 37.0°C.

Table 3.3: Percentage area of peaks observed following SCX-UV analysis and manual integration of differentially produced anti-IL8; standard deviation between triplicate replicates is shown in the parenthesis.

Sample	Combined % area of peaks corresponding to acidic variants	% Area of Main mAb peak	Combined % area of peaks corresponding to basic variants
Standard 1	6.82 (0.08)	76.25 (0.18)	16.68 (0.19)
Standard 2	7.06 (0.14)	75.34 (0.27)	17.36 (0.10)
Standard 3	6.66 (0.12)	76.58 (0.15)	16.70 (0.06)
Low DO mAb	9.04 (0.21)	72.33 (0.13)	18.06 (0.42)
High DO mAb	3.80 (0.18)	83.81 (0.21)	12.14 (0.05)
Low pH mAb	3.41 (0.14)	85.88 (0.05)	10.47 (0.11)
High pH mAb	9.12 (0.10)	64.10 (0.04)	26.53 (0.06)
Low Temp. mAb	5.90 (0.14)	68.89 (0.18)	24.82 (0.42)
High Temp. mAb	3.07 (0.09)	82.52 (0.34)	14.13 (0.13)
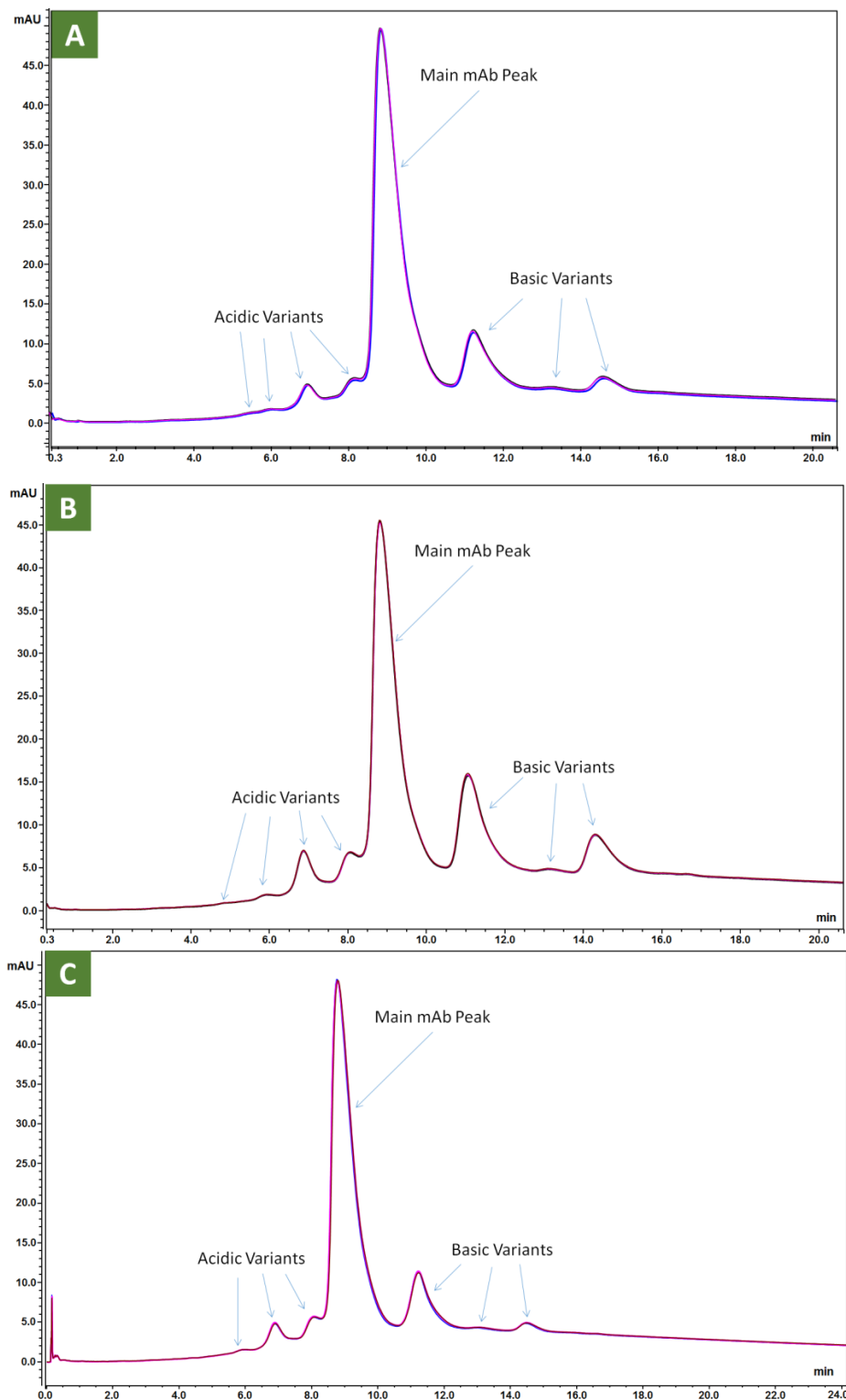
Figure 3.2: Chromatograms corresponding to triplicate SCX-UV analysis of **A.** anti-IL8 produced at 39.5°C, **B.** anti-IL8 produced at 32.0°C, **C.** anti-IL8 produced using 110% DO media content. Sample separation was performed using a MAbPac SCX-10 RS analytical column, 5 µm, 2.1 x 50mm, on a Vanquish Flex UHPLC using a diode array detector at 280 nm. Data was acquired using Chromeleon version 7.2 software; peak areas were integrated manually.
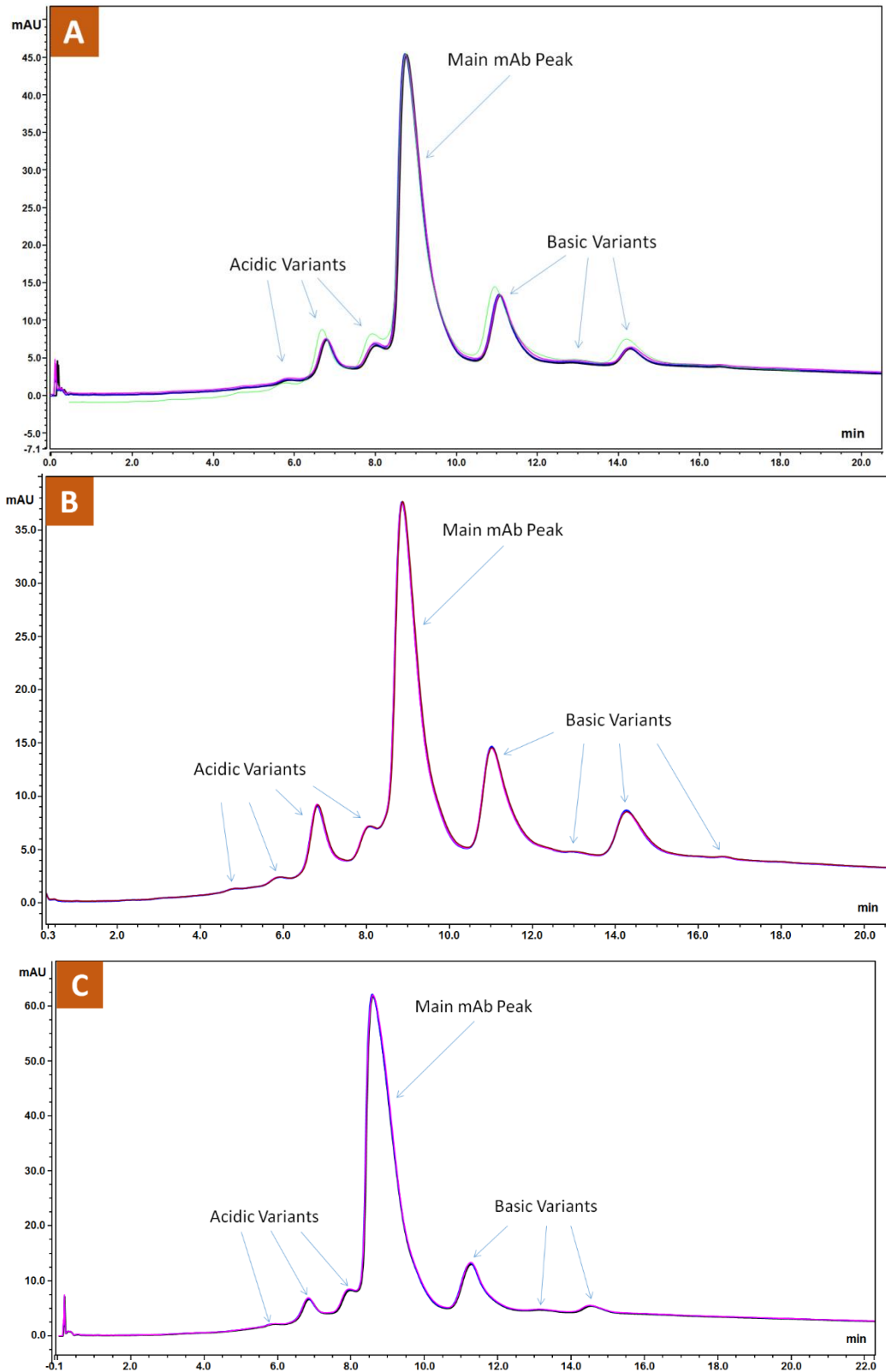
Figure 3.3: Chromatograms corresponding to SCX-UV analysis (n=3) of **A.** anti-IL8 produced using 60% DO media content, **B.** mAb produced at pH 7.2, **C.** mAb produced at pH 6.8. Sample separation was performed using a MAbPac SCX-10 RS analytical column, 5 μm, 2.1 x 50mm, on a Vanquish Flex UHPLC using a diode array detector at 280 nm. Data was acquired using Chromeleon version 7.2 software; peak areas were integrated manually.

In addition to evaluating mAb microheterogeneity in terms of charge and size, separation of mAb variants according to their over-all hydrophobicity is now commonly applied for characterisation of therapeutic mAb products. Unlike reversed-phase chromatography, which also separates molecules based on hydrophobicity, HIC enables the elucidation of additional mAb characteristics as retention of biomolecules on the HIC column matrix is solely attributed to interaction with amino acid residues on the surface of the molecule and hence differences in HIC retention profile may allude to changes in mAb tertiary structure. [11] Many common modifications may potentially alter mAb hydrophobicity, most notable oxidation of methionine or tryptophan, [39, 40] but also aspartic acid isomerization, formation of cyclic imide and domain misfolding. [11] To determine the hydrophobicity profile of anti-IL8 mAb in response to altered bioprocessing conditions of temperature, pH and DO, triplicate analysis of all produced mAb samples (Table 3.1) were performed using the method outlined in Section 3.2.5. Resulting chromatograms produced for each of the mAb samples cultured under altered bioprocessing conditions are shown in Figures 3.4 and 3.5. Peaks were integrated to determine the percentage area of the main peak relative to all peaks in the chromatogram; corresponding data is shown in Table 3.4. The most notable changes were observed for anti-IL8 produced at 110% DO and pH 6.8, both of which showed less heterogeneity in mAb hydrophobicity than mAb produced under standard conditions, and also for mAb produced at pH 7.2, as this sample was found to contain species with a wide range of hydrophobicities when compared to mAb generated from standard cell culture conditions. These differences may signify changes to the levels of amino acid oxidations or possible changes to mAb higher order structure. When combined with SEC analysis findings, it may be deduced that changes observed following HIC-UV analysis may not be attributed to variations in mAb aggregation/higher order structure profile thereby suggesting that the differences observed are a result of post translational modification of the primary sequence.

Table 3.4: Percentage area of main mAb peak observed following HIC-UV analysis of differentially produced anti-IL8 IgG1. Sample separation was performed using a MAbPac SEC-1 analytical column, 5 μm, 4.0 x 300mm, on a Vanquish Flex UHPLC using a diode array detector at 280 nm. Data was acquired using Chromeleon version 7.2 software; peak areas were integrated manually.

mAb sample analysed	% Area of main peak				
	Analysis 1	Analysis 2	Analysis 3	Average	Standard deviation
Standard 1 mAb	86.93	87.38	87.84	87.38	0.46
Standard 2 mAb	85.42	85.78	85.35	85.52	0.23
Standard 3 mAb	86.65	87.23	87.53	87.14	0.45
Low DO mAb	86.38	85.45	86.02	85.95	0.47
High DO mAb	92.97	91.69	93.68	92.78	1.01
Low pH mAb	93.66	92.54	92.47	92.89	0.67
High pH mAb	77.48	77.47	81.11	78.69	2.10
Low Temp. mAb	86.10	84.61	84.76	85.16	0.82
High Temp. mAb	90.55	89.82	89.25	89.87	0.65
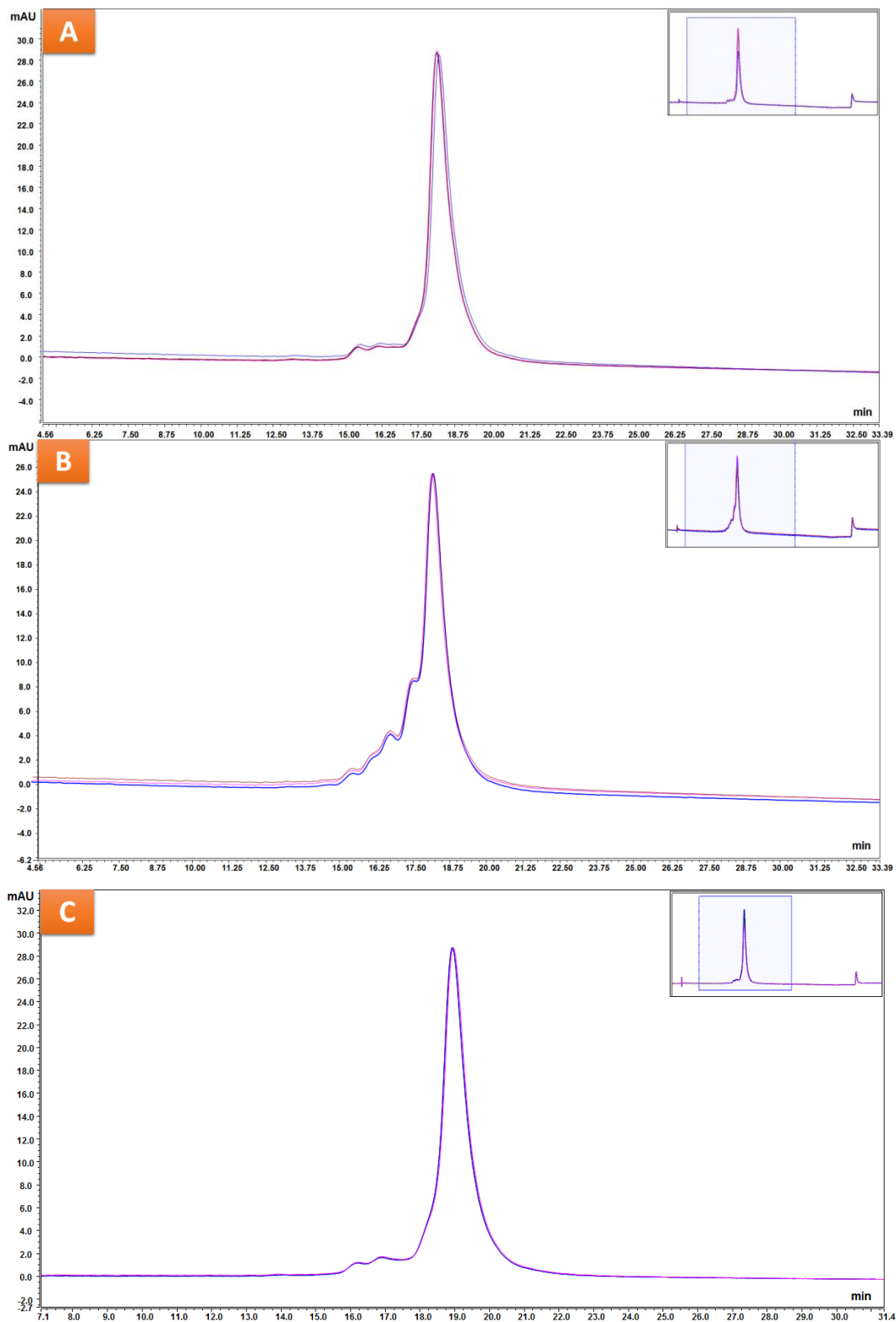
Figure 3.4: Chromatograms corresponding to HIC-UV analysis (n=3) of **A.** anti-IL8 produced at 39.5°C, **B.** anti-IL8 produced at 32.0°C, **C.** anti-IL8 produced using 110% DO media content. Sample separation was performed using a MAbPac SEC-1 analytical column, 5 µm, 4.0 x 300mm, on a Vanquish Flex UHPLC using a diode array detector at 280 nm. Data was acquired using Chromeleon version 7.2 software; peak areas were integrated manually.
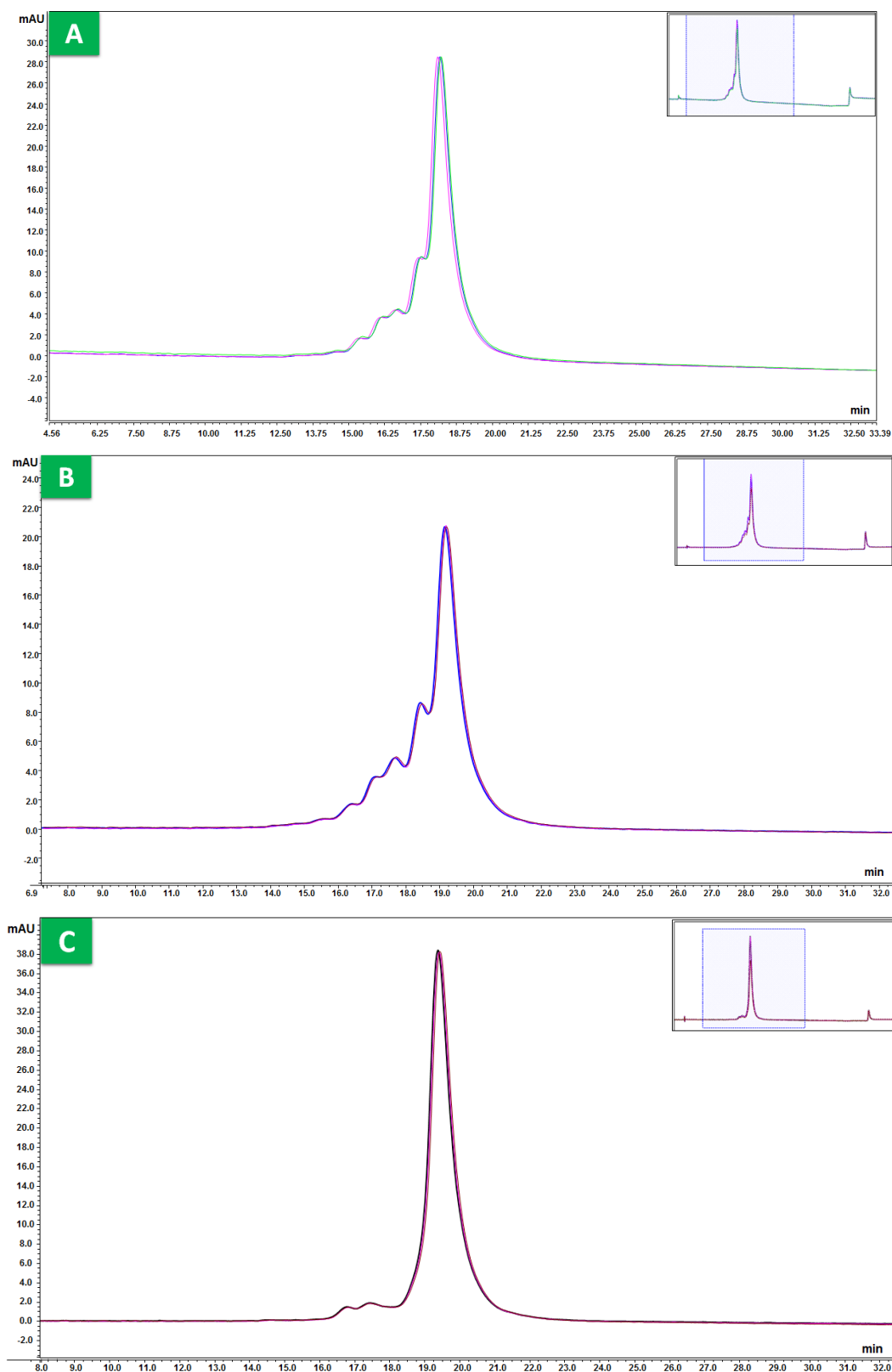
Figure 3.5: Chromatograms corresponding to HIC-UV analysis (n=3) of **A.** anti-IL8 produced using 60% DO media content, **B.** mAb produced at pH 7.2, **C.** mAb produced at pH 6.8. Sample separation was performed using a MAbPac SEC-1 analytical column, 5 μm, 4.0 x 300mm, on a Vanquish Flex UHPLC using a diode array detector at 280 nm. Data was acquired using Chromeleon version 7.2 software; peak areas were integrated manually.

3.3.2 Middle-down Analysis of IdeS Digested Anti-IL8 IgG1

Despite the wide range of information regarding mAb heterogeneity that may be attained using HPLC-UV, mass spectrometry (MS) is required to provide essential information regarding mAb primary structure including amino acid sequence, protein mass and sequence-level modifications. Like top-down analysis of intact biomolecules, middle-down MS approaches enable the determination of protein mass and sequence modifications, by identification of differences in mass upon MS analyses. However, in contrast to top-down methodology, limited proteolysis of proteins incorporated into middle-down approaches results in the generation of polypeptides which are more suited to MS detection than intact biomolecules. To evaluate protein mass and domain-level changes to differentially produced anti-IL8 mAb under study (Table 3.1), antibody samples were digested using IdeS (FabRICATOR, Genovis), a cysteine protease with high specificity for the hinge region of IgG. [41, 42] IdeS cleaves IgG1 at the linkage between (ELL)G and G(PSVF) on the mAb heavy chain, as illustrated in Figure 3.6. [18] Following subsequent disulfide bond reduction, three polypeptide populations are formed: the intact light chain (LC), a heavy chain fragment containing the N-terminus (Fd') and the remaining heavy chain portion containing the asparagine-293 N-glycosylation site and the C-terminus (scFc). In addition to determination of the exact mass for each of these subunits, MS analysis may also reveal potential modifications on each of these polypeptide fragments, *e.g.* different N-glycosylation moieties on scFC and various other enzymatic and non-enzymatic modifications that produce distinctive mass shifts upon MS analysis.
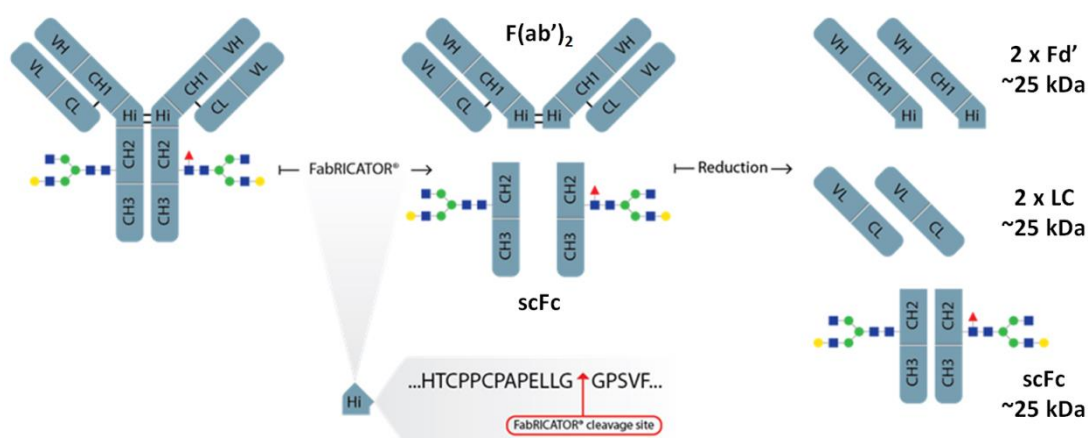
Figure 3.6: Limited proteolysis of IgG1 by IdeS (FabRICATOR). [43] FabRICATOR cleaves IgG1 with high specificity at the hinge region between two glycine residues. Subsequent disulfide bond reduction results in the formation of three polypeptide populations of approximately 25 kDa in size.

Anti-IL8 IgG1 produced under standard and altered bioprocess conditions (Table 3.1) were prepared as described in Section 3.2.6. In an effort to evaluate method performance, standard 1 mAb was prepared in triplicate and analysed in conjunction with the remaining mAb samples. Following MS acquisition, data was processed using the AutoExtract algorithm in BioPharma Finder (Thermo Fisher Scientific). Deconvolution of mass spectra obtained for each peak in the total ion chromatogram (TIC) acquired resulted in the generation of spectra corresponding to each of the mAb subunits produced following IdeS digestion. The mass of the polypeptide and related variants in each of the samples could then be deduced from the deconvoluted spectra. TIC traces, spectra showing charge envelope profiles corresponding to each peak and deconvoluted mass spectra for each sample analysis are shown in Figures 3.7 to 3.17. As the figures show, interpretation of the deconvoluted mass spectra confirms the identity of three polypeptides corresponding to the mass of the LC, scFc and Fd' mAb subunits. For each technical replicate, the difference in mass for each subunit identified was found to be < 2 ppm (0.99, 1.13 and 1.78 ppm, respectively for scFc, LC and Fd' mAb subunits) showing good precision across all experimental analyses. Various other peaks were observed in the spectra confirming the existence of modified versions of these polypeptides. The monoisotopic mass of the scFc fragment (~25220 Da) corresponds to the theoretical mass of this subunit combined with the mass of FA2 (~1462.5 Da), the most abundant *N*-glycan moiety attached to humanised IgG1. Other variants that may be deduced from the deconvoluted spectra include scFc with N-glycan species including FA2G1 (~25383 Da), FA2G2 (~25545 Da), A2 (~25073 Da) and Man5 (~24991 Da). Due to the importance of glycosylation in modulating the structural stability and functional activity of mAbs, [44, 45] and because of the huge variation in potential *N*-glycans present on the mAb Fc region, the *N*-glycosylation profile of anti-IL8 is specifically investigated in more detail in Chapter 4. Modifications observed across all samples for the LC and Fd' subunits were not as easily deduced, as common mass shifts, such as those outlined in Table 3.5 were not observed. For example, the peak of mass 24000.888 Da observed in the deconvoluted mass spectrum corresponding to LC of Standard 2 (Figure 3.10) was ~59.0 Da greater in mass than the main LC peak, possibly corresponding to multiple modifications on the same mAb fragment. Hence, for thorough evaluation of the exact modifications that are present on the mAb samples analysed peptide mapping analysis must be performed. However, as the reported masses for the most abundant peak in each of the deconvoluted mass spectra was not significantly changed across all samples analysed, it may be concluded that the application of different bioprocess parameters during batch culture of CHO DP-12 cells did not result in alterations to the primary sequence of the anti-IL8 IgG1 produced.
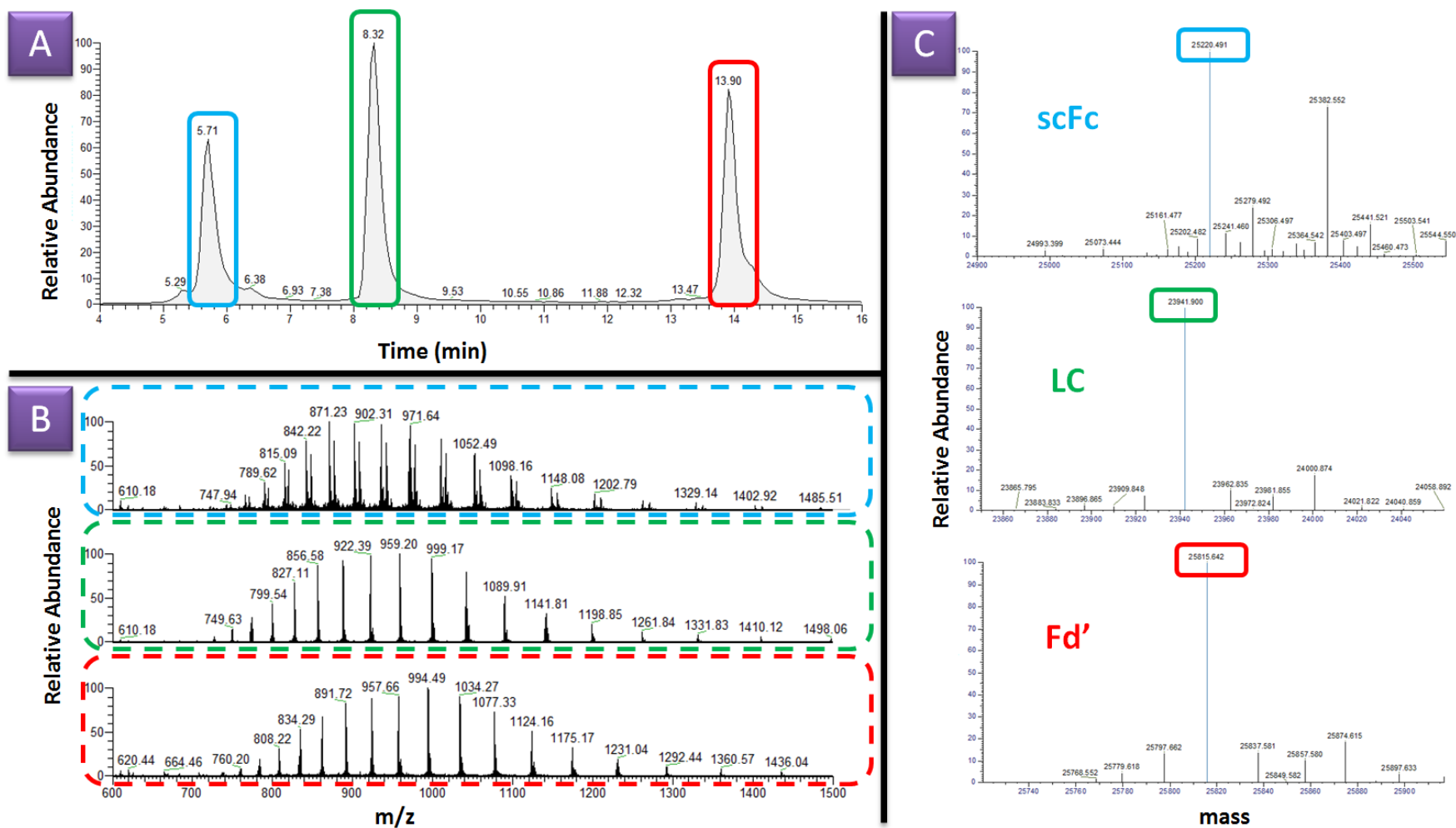
Figure 3.7: Middle down analysis of Standard 1, replicate 1. **A.** Total Ion Chromatogram (TIC); **B.** MS spectra corresponding to each highlighted TIC peak; **C.** Deconvolution of charge envelopes shown in MS spectra to reveal monoisotopic masses of mAb species.
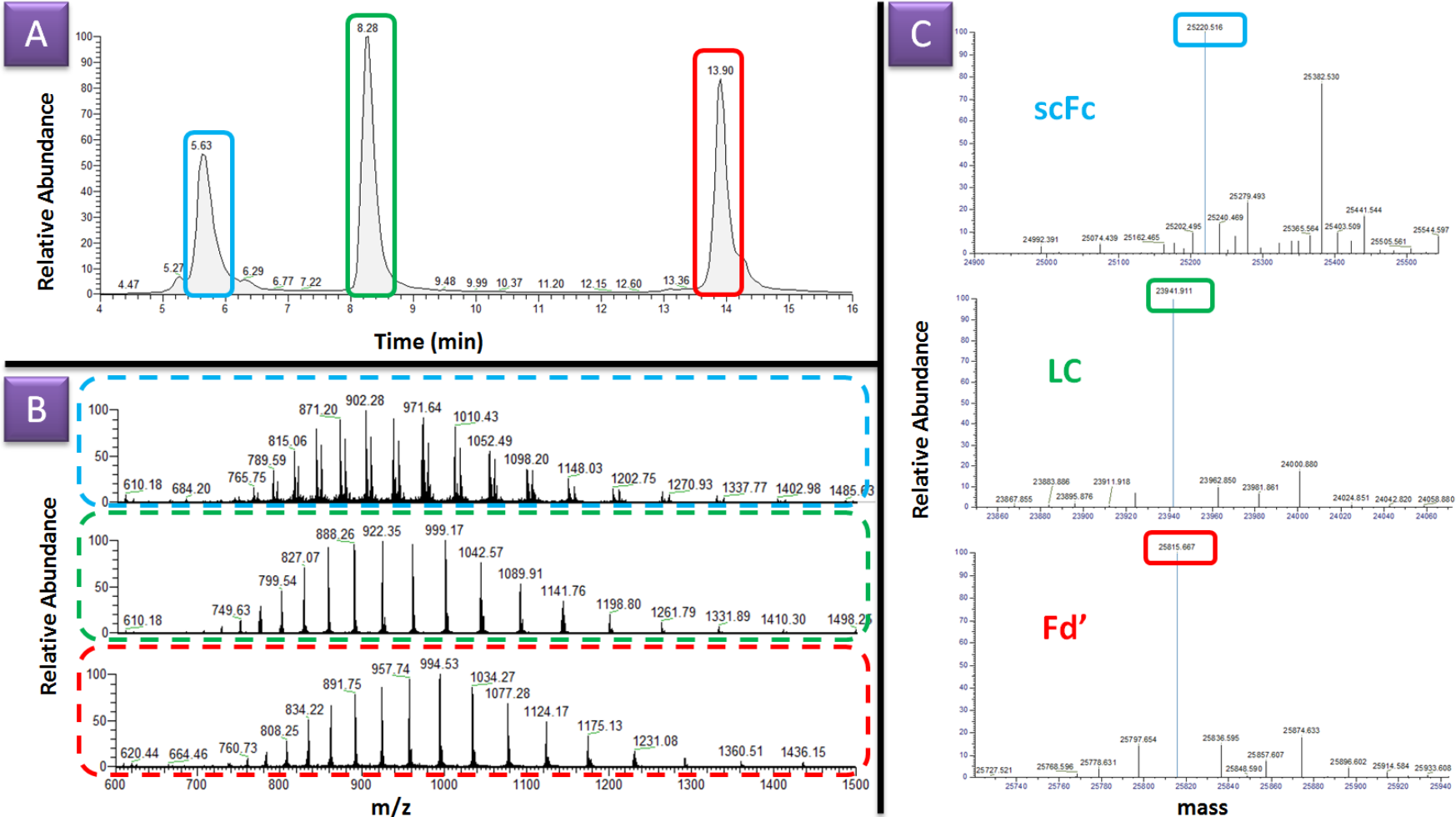
Figure 3.8: Middle down analysis of Standard 1, replicate 2. **A.** Total Ion Chromatogram (TIC); **B.** MS spectra corresponding to each highlighted TIC peak; **C.** Deconvolution of charge envelopes shown in MS spectra to reveal monoisotopic masses of mAb species.
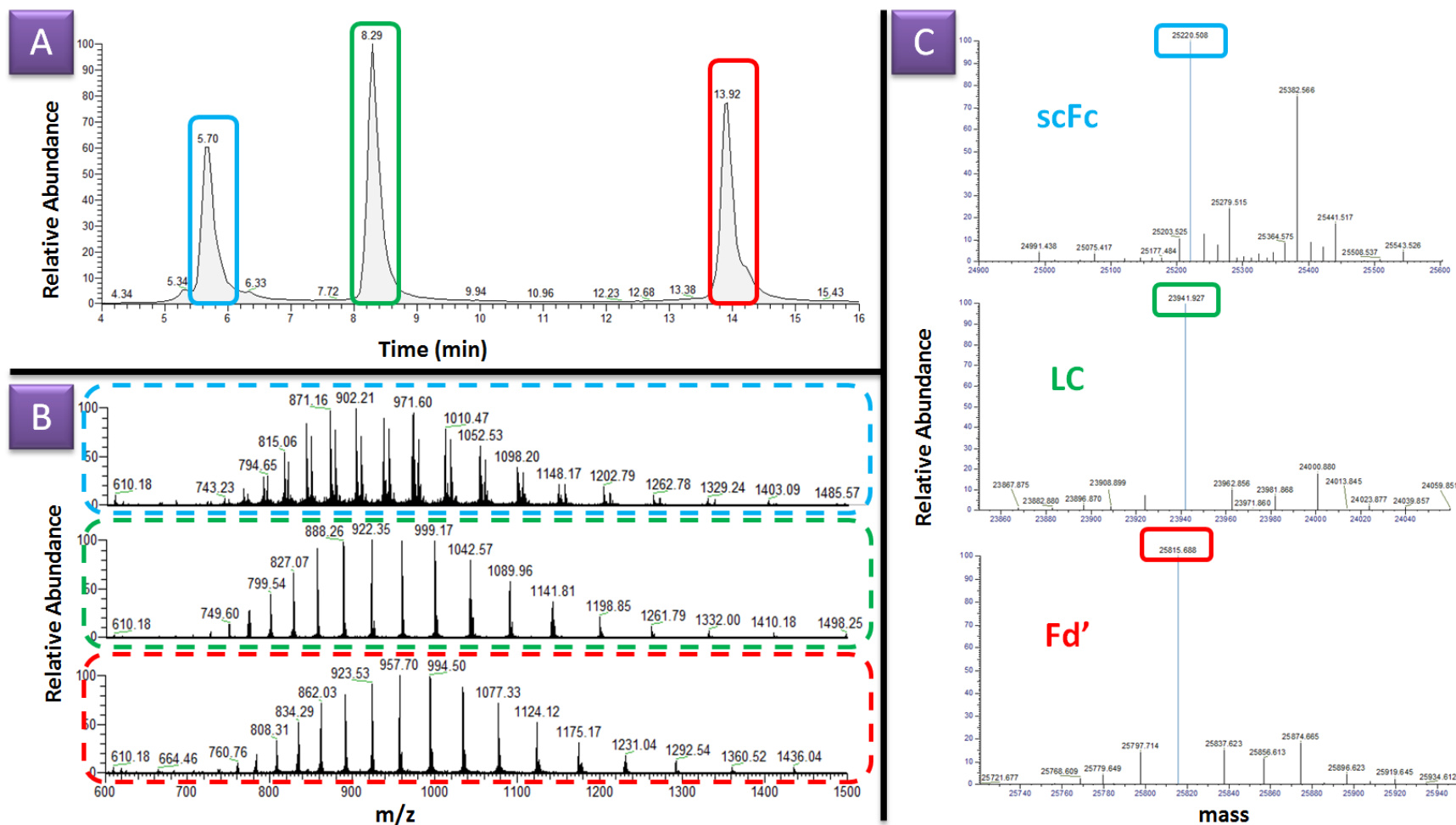
Figure 3.9: Middle down analysis of Standard 1, replicate 3. **A.** Total Ion Chromatogram (TIC); **B.** MS spectra corresponding to each highlighted TIC peak; **C.** Deconvolution of charge envelopes shown in MS spectra to reveal monoisotopic masses of mAb species.
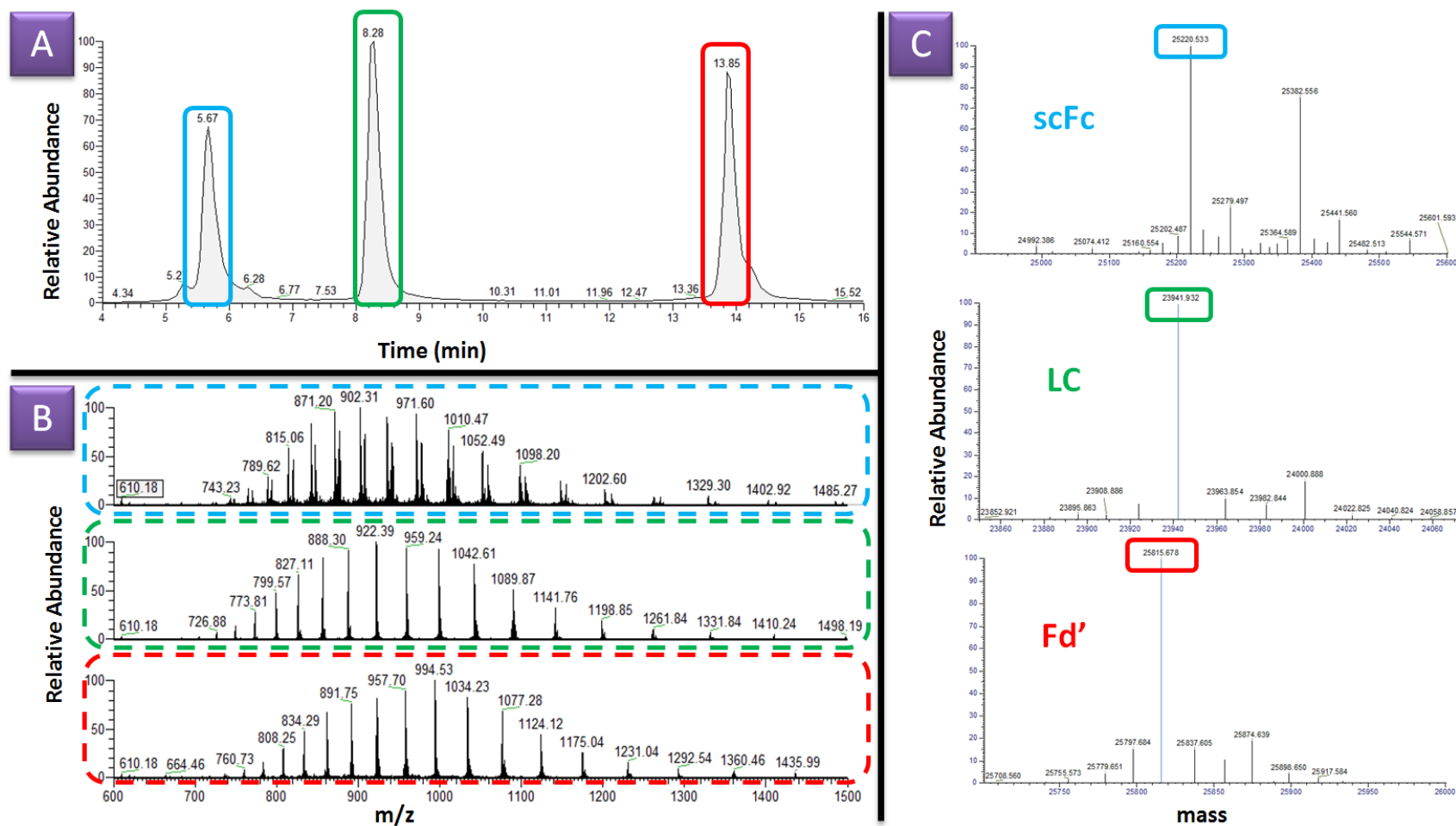
Figure 3.10: Middle down analysis of Standard 2. **A.** Total Ion Chromatogram (TIC); **B.** MS spectra corresponding to each highlighted TIC peak; **C.** Deconvolution of charge envelopes shown in MS spectra to reveal monoisotopic masses of mAb species.
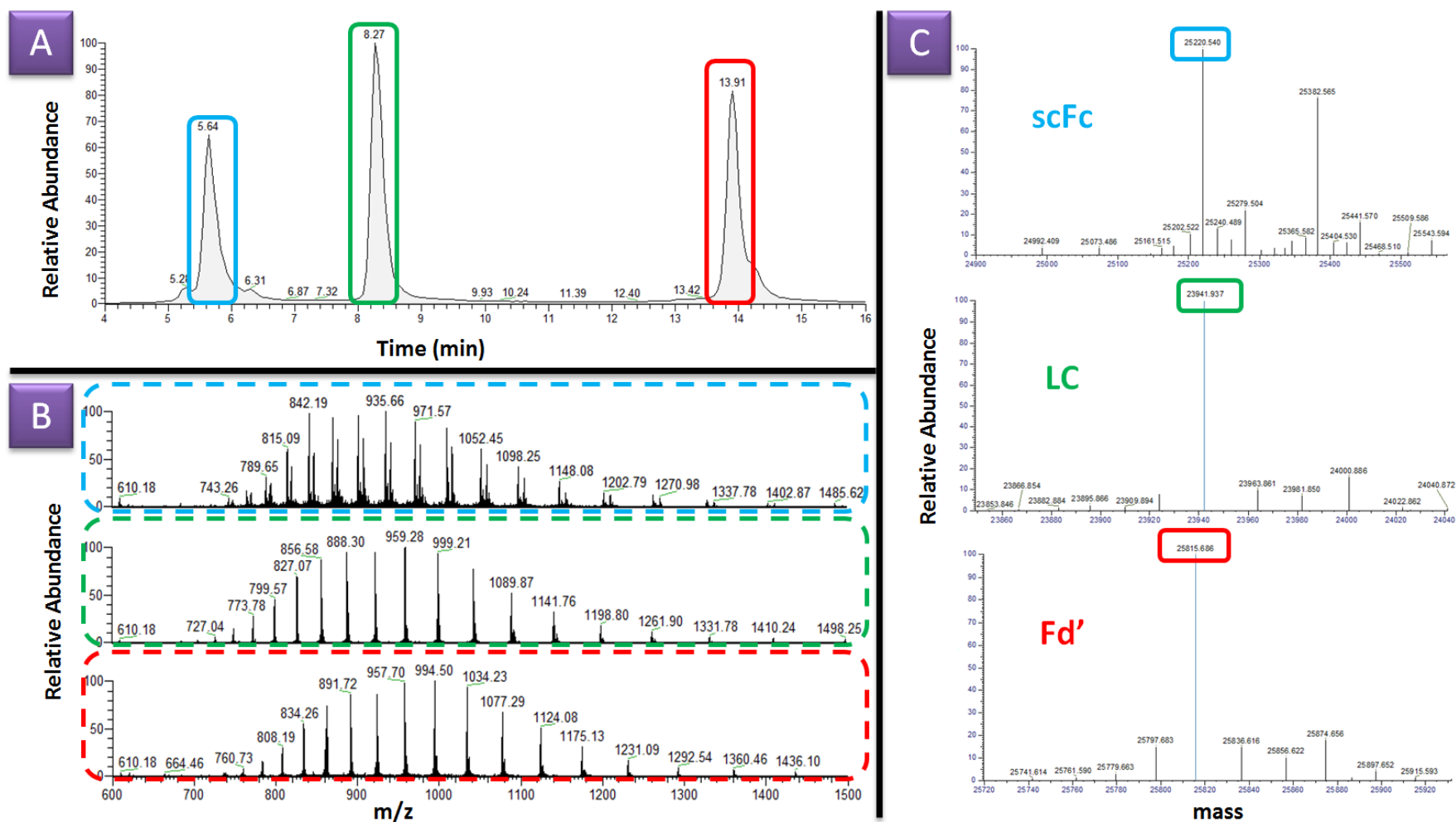
Figure 3.11: Middle down analysis of Standard 3. **A.** Total Ion Chromatogram (TIC); **B.** MS spectra corresponding to each highlighted TIC peak; **C.** Deconvolution of charge envelopes shown in MS spectra to reveal monoisotopic masses of mAb species.
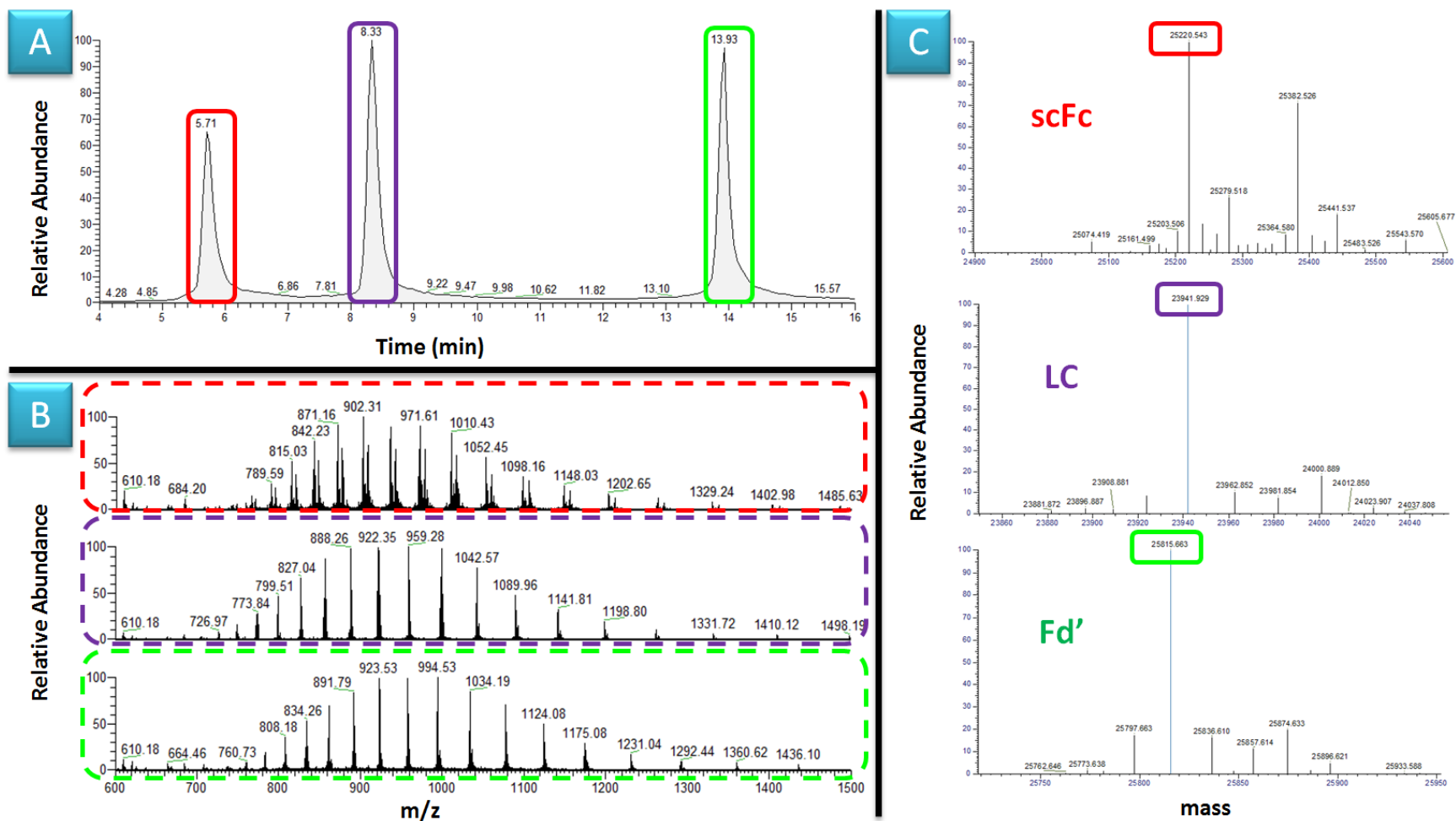
Figure 3.12: Middle down analysis of anti-IL8 produced in culture maintained at 110% DO. **A.** Total Ion Chromatogram (TIC); **B.** MS spectra corresponding to each highlighted TIC peak; **C.** Deconvolution of charge envelopes shown in MS spectra to reveal monoisotopic masses of mAb species.
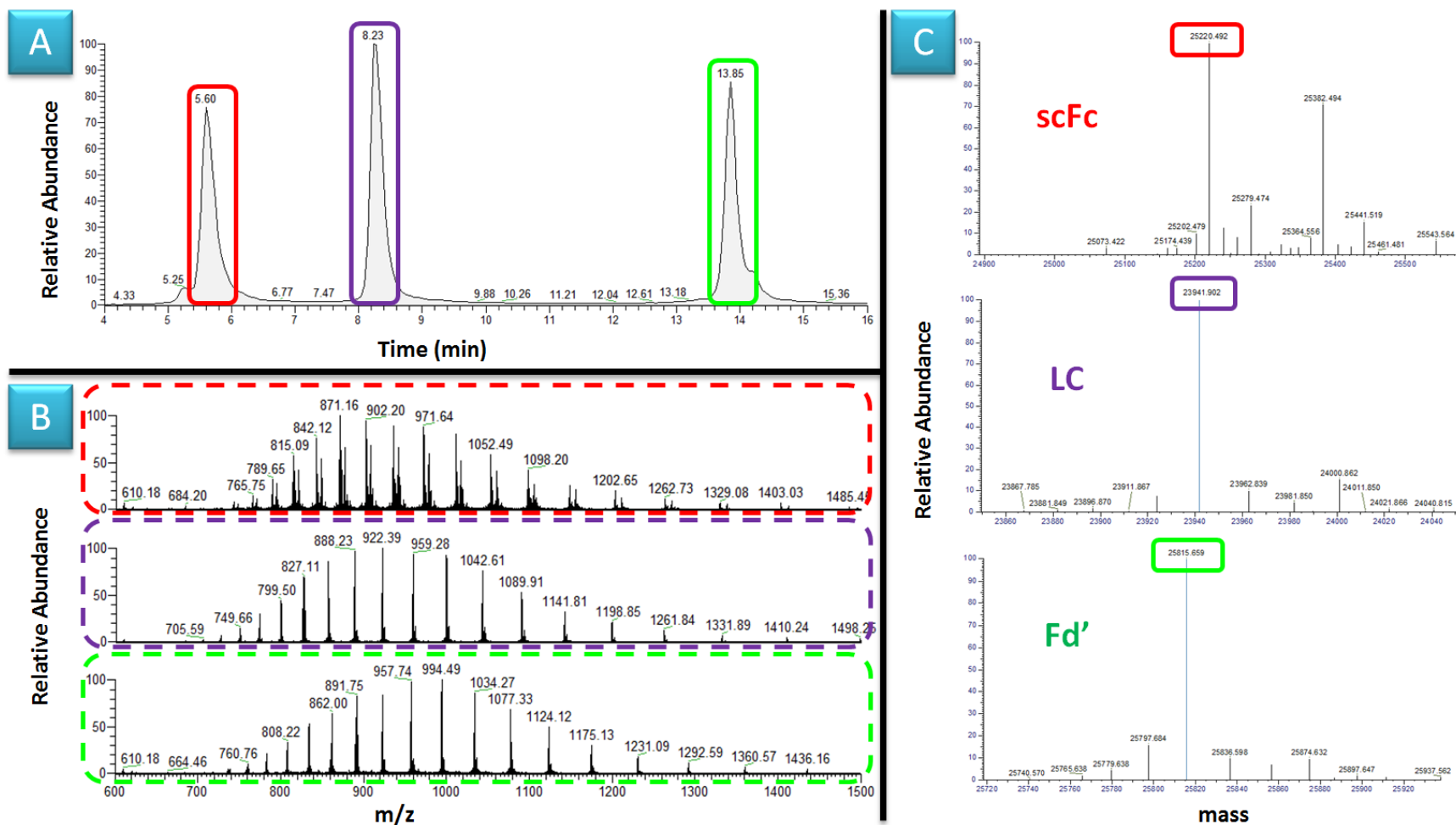
Figure 3.13: Middle down analysis of anti-IL8 produced in culture maintained at 60% DO. **A.** Total Ion Chromatogram (TIC); **B.** MS spectra corresponding to each highlighted TIC peak; **C.** Deconvolution of charge envelopes shown in MS spectra to reveal monoisotopic masses of mAb species.
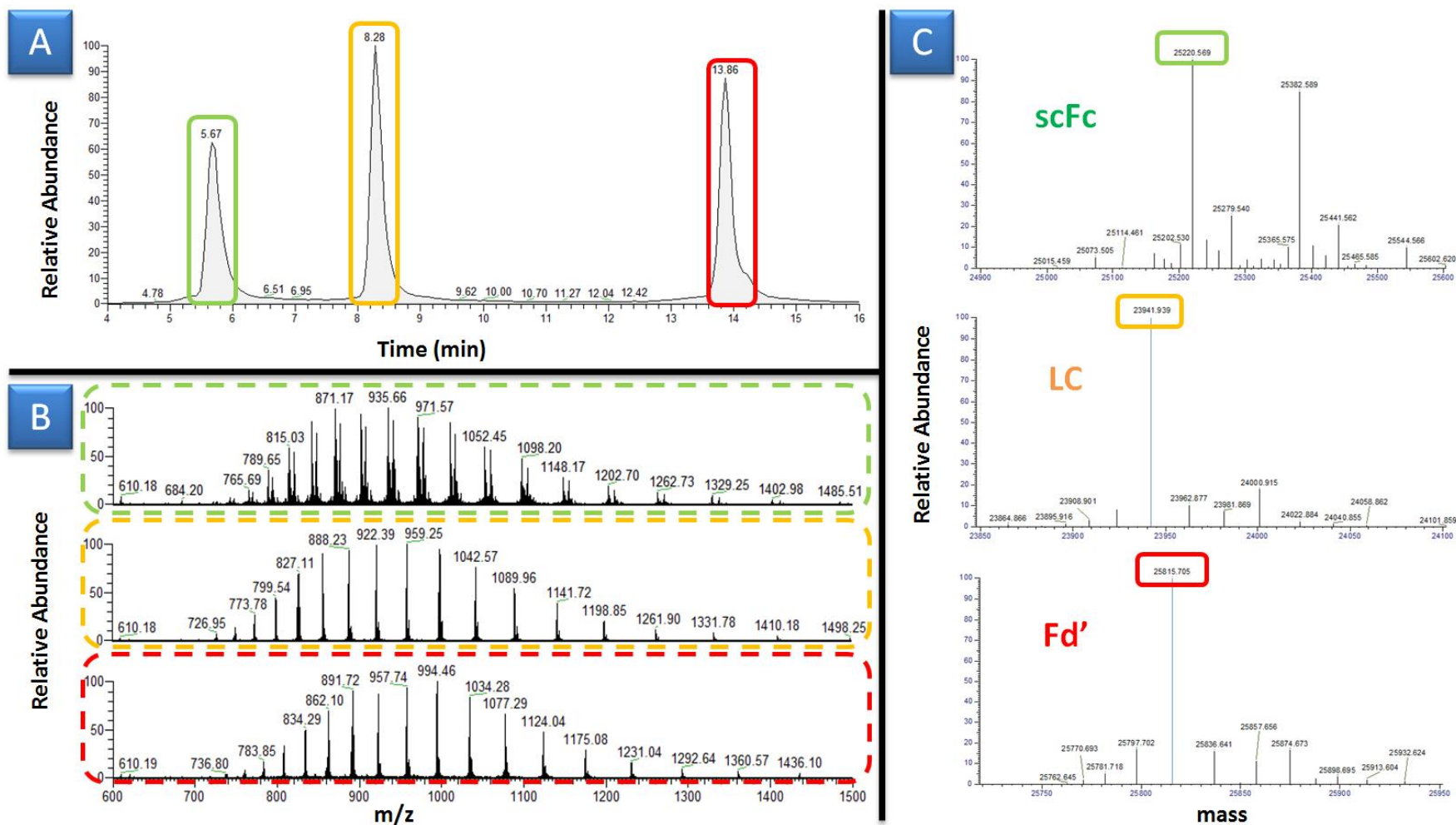
Figure 3.14: Middle down analysis of anti-IL8 produced using increased culture temperature of 39.5°C. **A.** Total Ion Chromatogram (TIC); **B.** MS spectra corresponding to each highlighted TIC peak; **C.** Deconvolution of charge envelopes shown in MS spectra to reveal monoisotopic masses of mAb species.
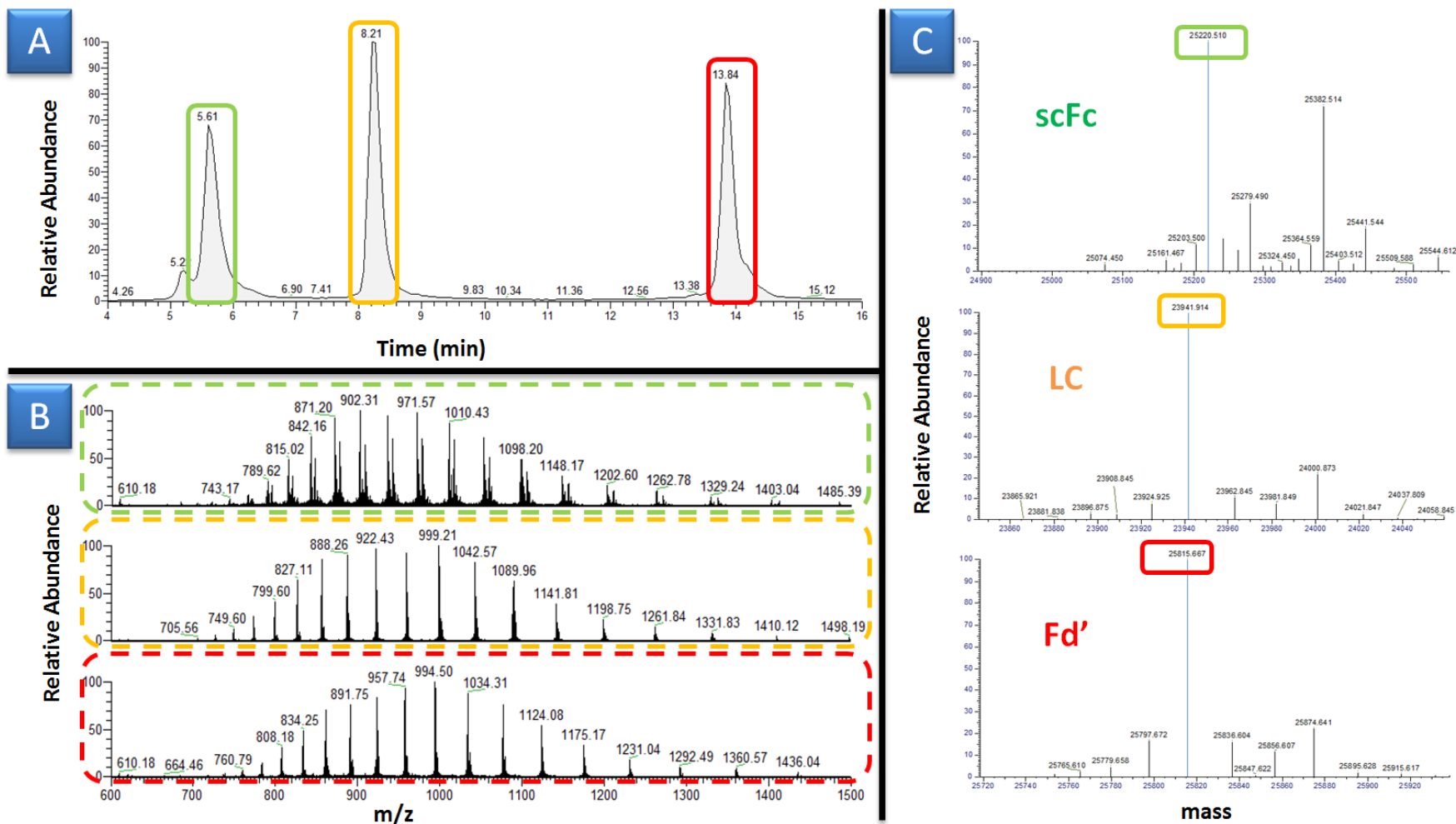
Figure 3.15: Middle down analysis of anti-IL8 produced using increased culture temperature of 32.0°C. **A.** Total Ion Chromatogram (TIC); **B.** MS spectra corresponding to each highlighted TIC peak; **C.** Deconvolution of charge envelopes shown in MS spectra to reveal monoisotopic masses of mAb species.
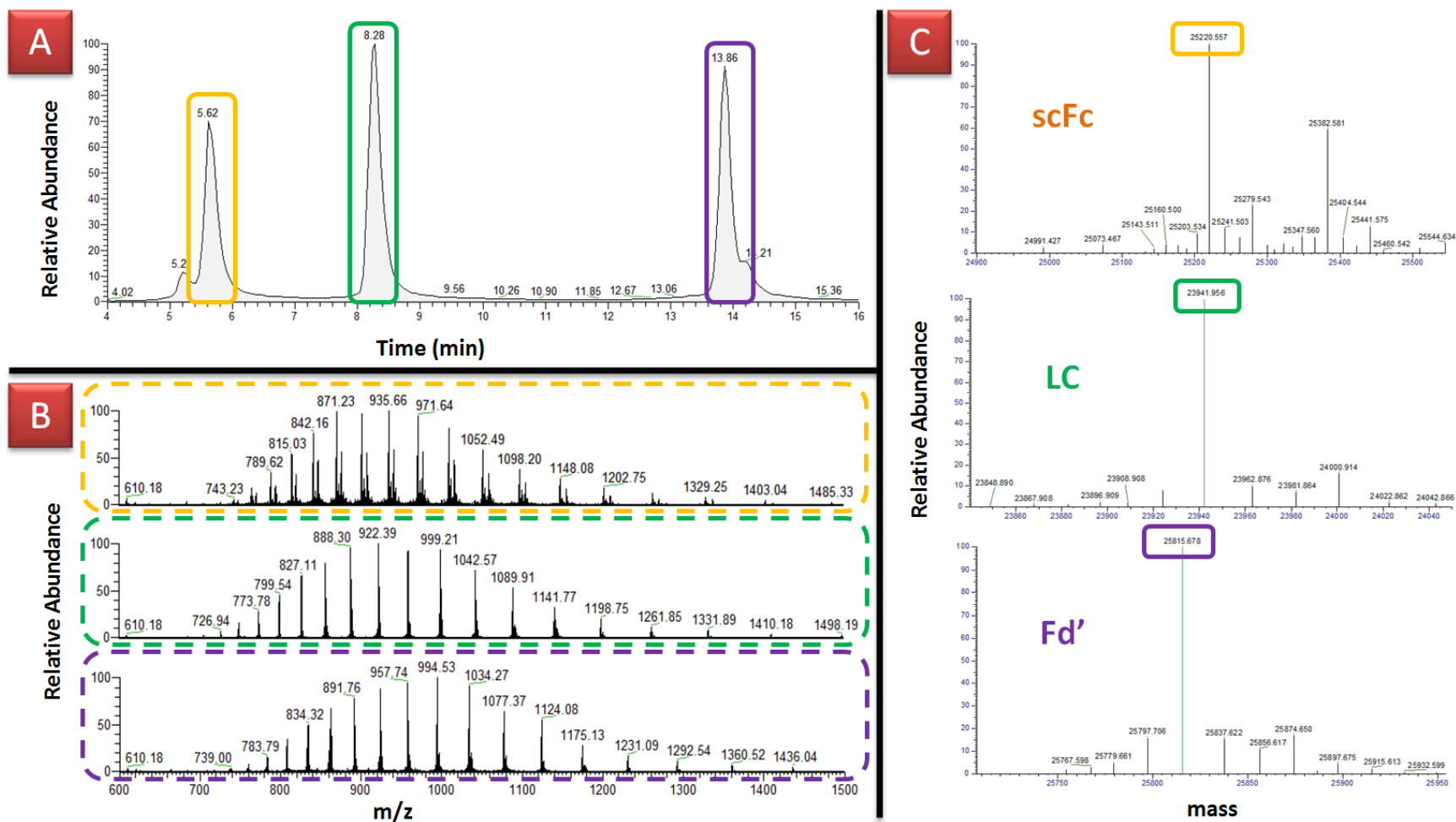
Figure 3.16: Middle down analysis of anti-IL8 produced in culture maintained at pH 7.2. **A.** Total Ion Chromatogram (TIC); **B.** MS spectra corresponding to each highlighted TIC peak; **C.** Deconvolution of charge envelopes shown in MS spectra to reveal monoisotopic masses of mAb species.
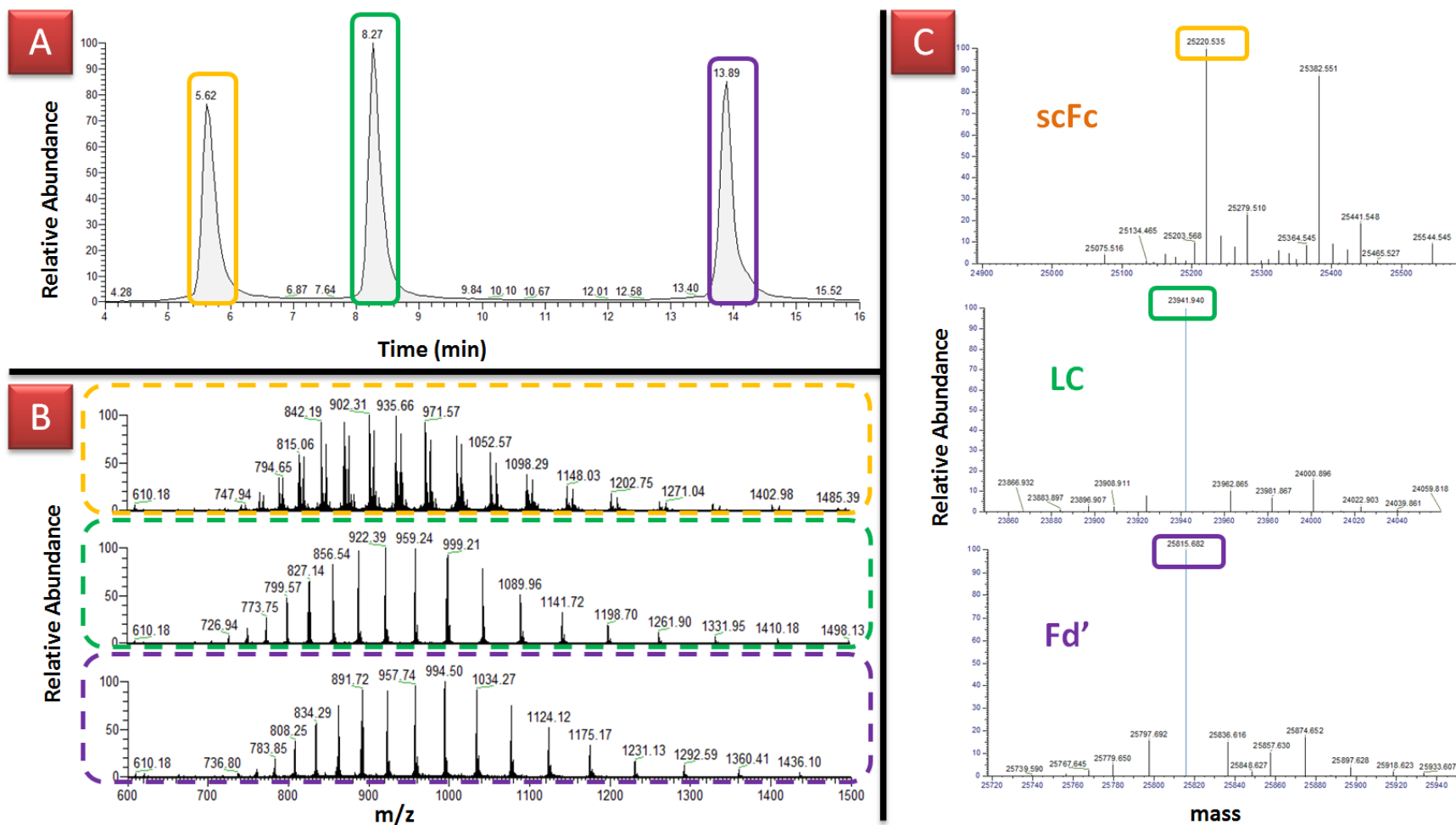
Figure 3.17: Middle down analysis of anti-IL8 produced in culture maintained at pH 6.8. **A.** Total Ion Chromatogram (TIC); **B.** MS spectra corresponding to each highlighted TIC peak; **C.** Deconvolution of charge envelopes shown in MS spectra to reveal monoisotopic masses of mAb species.

3.3.3 Peptide Mapping Analysis of Anti-IL8 Produced Under Altered Bioprocessing Conditions

Peptide mapping analysis using liquid chromatography and mass spectrometry is a powerful strategy capable of simultaneously identifying and quantifying sequence variants, low abundance impurities and site-specific modifications of a protein primary sequence. [46] Frequently, peptide mapping involves protein denaturation, reduction of disulfide bonds, alkylation of cysteine resides and digestion with a protease to produce peptide fragments appropriate for MS detection. Subsequent data processing is generally facilitated by data analysis algorithms used to compare experimental data with a known protein sequence. In addition to identification of expected peptides based on comparison with the primary sequence, peptides found to have an increased or decreased mass may be correlated with having a known modification. Furthermore, the abundance of a modified peptide relative to the unmodified peptide may be deduced. This approach is especially useful for comparative analysis of protein samples, *e.g.* for analysis of biosimilars, evaluation of protein stability or when determining the impact of an upstream or downstream process change during protein manufacture.

Here, peptide mapping analysis is used to determine the protein sequence of anti-IL8 IgG1 and to evaluate the incidence of protein modifications as a result of bioprocessing parameters used for CHO DP-12 culture during recombinant antibody expression. LC-MS analysis of tryptic peptides generated from each mAb sample was performed as outlined in Section 3.2.7, resulting in the acquisition of spectra showing excellent peak resolution as may be seen in Figure 3.18. Processing of MS data yielded 100% sequence coverage of all samples analysed (Figure 3.19). All of the data was searched against the light and heavy chain sequences for anti-IL8 (Figure 3.20) with potential variable modifications as outlined in Table 3.5.

Table 3.5: Common modifications observed for monoclonal antibodies and applied for peptide mapping analysis of anti-IL8. [2, 21]

Modification	Monoisotopic Mass Shift (Da)	Average Mass Shift (Da)
C-terminal lysine clipping	-128.095	-128.174
Glutamic acid to Pyroglutamate	-17.027	-17.031
Deamidation of asparagine or glutamine	0.984	0.985
Oxidation of methionine or tryptophan	15.995	15.999
Carbamidomethylation	57.021	57.051
Carboxymethylation	58.005	58.036
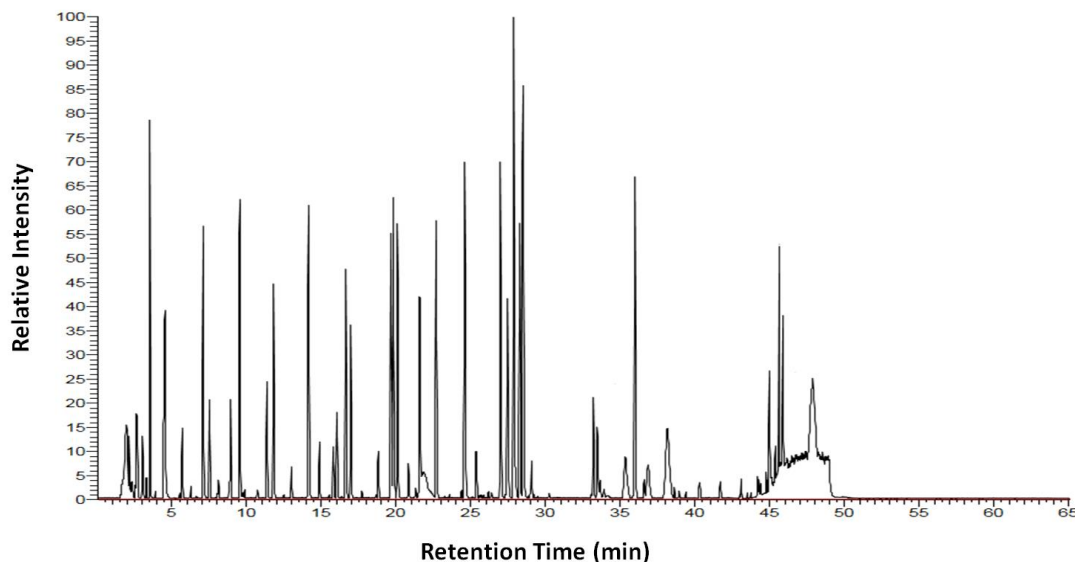
Figure 3.18: Base peak chromatogram corresponding to **LC-MS** peptide mapping analysis of tryptic peptides prepared from anti-IL8 mAb produced using 110% DO in culture media.

Identical modifications were observed on the heavy chain and light chain of each of the samples analysed. The amount of modified peptide relative to corresponding unmodified peptide was determined and is reported in Tables 3.6 and 3.7. The light chain of anti-IL8 has three potential oxidation sites, one methionine and two tryptophan residues, each of which displayed low levels of oxidation across all samples. Additionally, four of six asparagine residues showed varying levels of deamidation in the different mAb samples analysed. Deamidation of glutamine is known to be kinetically slower than that of asparagine and hence is not widely reported. [47] Correspondingly, despite the presence of a large number of glutamine amino acids in the anti-IL8 sequence, only one glutamine residue was found to be deamidated. Modification of the heavy chain primary sequence *via* oxidation of methionine and tryptophan and also deamination of asparagine amino acid was also observed. In addition, high concentrations of the modified form of the peptide corresponding to the C-terminal of the heavy chain (SLSLSPGK) were determined, indicating that the C-terminal lysine truncated version of the mAb is the most abundant form in all samples analysed. Surprisingly, modification of the N-terminal glutamine residue was not determined in any of the mAb samples as is commonly reported for humanised monoclonal antibodies. [48] However, N-terminal cyclization of glutamine to pyro-glutamic acid is reportedly a slow process when proceeding non-enzymatically at neutral pH [49] and may be more noticeably present for mAb that is produced in cultures maintained for long periods or after pro-longed storage. [50]

Figure 3.19: Sequence coverage obtained following peptide mapping analysis of Standard 1 sample, injection 1. **A:** Light chain peptides identified, **B:** Heavy chain peptides identified. Following LC-MS analysis of tryptic peptides, resultant data was searched using Biopharma Finder software for identification and visualisation of peptides. Each peptide identified is signified by a coloured bar. Red bars represent peptides with a signal intensity of > 4.9 x 10^6;

Yellow bars represent peptides with a signal intensity of $> 1.4 \times 10^5$; Green bars represent peptides with a signal intensity of $> 3.8 \times 10^3$. Each number shown within each bar equals to the retention time of that peptide.

Table 3.6: Average percentage abundance values for light chain mAb modifications determined following peptide mapping analysis; standard deviation between replicate analyses is shown in the parenthesis (n=2). Values were determined following data analysis using Biopharma Finder software.

Residue	Modification	Peptide Sequence	Standard 1	Standard 2	Standard 3	High Temp. mAb	Low Temp. mAb	High DO mAb	Low DO mAb	High pH mAb	Low pH mAb
M4	Oxidation	DIQMTQSPSS LSASVGDR	1.05 (0.03)	1.09 (0.04)	1.21 (0.02)	1.16 (0.05)	1.71 (0.02)	1.24 (0.03)	1.11 (0.03)	1.12 (0.02)	1.18 (0.00)
W40	Oxidation	SSQSLVHGIGETYLHWYQQK PGK	0.04 (0.00)	0.03 (0.00)	0.04 (0.01)	0.05 (0.00)	0.05 (0.00)	0.06 (0.01)	0.04 (0.00)	0.04 (0.00)	0.04 (0.00)
W153	Oxidation	VQWK	0.06 (0.00)	0.05 (0.00)	0.07 (0.00)	0.06 (0.00)	0.09 (0.03)	0.08 (0.02)	0.07 (0.01)	0.06 (0.01)	0.07 (0.00)
N58	Deamidation	VSNR	0.76 (0.04)	0.86 (0.02)	0.64 (0.04)	0.71 (0.09)	0.36 (0.01)	0.75 (0.04)	0.74 (0.12)	0.73 (0.05)	0.70 (0.00)
N157	Deamidation	VDNALQSGNS QESVTEQDSK	0.77 (0.06)	0.74 (0.03)	0.78 (0.06)	0.79 (0.06)	0.62 (0.04)	0.71 (0.00)	0.82 (0.01)	0.76 (0.09)	0.74 (0.00)
Q160	Deamidation	VDNALQSGNSQESVTEQDSK DSTYSLSSTL TLSK	4.10 (0.04)	4.25 (0.17)	3.67 (0.03)	4.85 (0.38)	2.65 (0.35)	3.73 (0.02)	4.09 (0.16)	4.09 (0.24)	4.08 (0.00)
N163	Deamidation	VDNALQSGNS QESVTEQDSK	4.03 (0.14)	3.99 (0.01)	3.91 (0.01)	4.53 (0.09)	3.07 (0.43)	4.05 (0.22)	4.11 (0.08)	4.05 (0.02)	3.74 (0.00)
N215	Deamidation	SFNR	0.26 (0.00)	0.30 (0.01)	0.26 (0.01)	0.30 (0.01)	0.27 (0.00)	0.26 (0.02)	0.27 (0.01)	0.26 (0.01)	0.25 (0.00)

Table 3.7: Average percentage abundance values for heavy chain mAb modifications determined following peptide mapping analysis; standard deviation between replicate analyses is shown in the parenthesis (n=2). Values were determined following data analysis using Biopharma Finder software.

Residue	Modification	Sequence	Standard 1	Standard 2	Standard 3	High Temp. mAb	Low Temp. mAb	High DO mAb	Low DO mAb	High pH mAb	Low pH mAb
K452	Lysine Clipping	SLSLSPGK	90.53 (0.17)	89.89 (0.25)	90.32 (0.21)	97.79 (0.05)	85.49 (0.18)	97.29 (0.47)	94.24 (0.35)	85.54 (0.04)	98.79 (0.00)
N55	Deamidation	GLEWVGYIDP SNGETTYNQK	38.80 (0.48)	39.75 (0.01)	36.57 (0.05)	38.33 (0.25)	37.31 (0.63)	39.24 (0.26)	38.50 (0.97)	39.11 (0.29)	38.89 (0.00)
N74	Deamidation	DNSKNTAYLQ MNSLR	8.74 (0.04)	9.34 (0.39)	8.90 (0.81)	9.18 (0.35)	3.63 (0.05)	8.22 (0.25)	8.91 (0.15)	8.63 (0.40)	9.51 (0.00)
N77	Deamidation	NTAYLQMNSL R	1.90 (0.02)	1.73 (0.03)	2.02 (0.01)	1.68 (0.02)	1.99 (0.01)	2.18 (0.04)	1.74 (0.05)	2.01 (0.01)	1.98 (0.00)
N84	Deamidation	NTAYLQMNSL R	6.03 (0.01)	5.48 (0.06)	6.05 (0.05)	5.04 (0.13)	7.19 (0.10)	6.52 (0.01)	5.57 (0.24)	6.51 (0.03)	6.52 (0.00)
N104	Deamidation	GDYRYNGDWFFDVWGQGTLV TVSSASTK	88.05 (0.65)	91.74 (0.10)	68.75 (3.53)	89.53 (1.70)	30.42 (7.24)	61.95 (5.46)	91.92 (1.47)	79.00 (1.36)	69.62 (0.00)
N291	Deamidation	FNWYVDGVEV HNAK	4.05 (0.14)	3.97 (0.07)	3.94 (0.01)	3.91 (0.09)	4.05 (0.05)	4.27 (0.10)	3.96 (0.02)	4.17 (0.06)	4.06 (0.00)
N320	Deamidation	VVSVLTVLHQ DWLNGKEYK	73.77 (0.17)	69.61 (0.35)	75.01 (0.15)	69.16 (0.67)	66.44 (0.16)	72.19 (0.11)	68.01 (0.05)	71.00 (0.55)	74.74 (0.00)
N389	Deamidation	GFYPSDIAVE WESNGQPENN YK	16.35 (0.14)	16.35 (0.57)	15.51 (0.29)	15.97 (0.20	13.91 (0.22)	15.34 (0.33)	15.67 (0.18)	15.95 (0.36)	14.53 (0.00)
M83	Oxidation	NTAYLQMNSL R	1.45 (0.04)	1.34 (0.05)	1.92 (0.01)	1.37 (0.01)	2.78 (0.13)	1.92 (0.03)	1.26 (0.01)	1.51 (0.01)	1.65 (0.00)
M257	Oxidation	DTLMISR	1.67 (0.07)	1.72 (0.01)	1.75 (0.02)	1.55 (0.00)	2.49 (0.08)	1.87 (0.11)	1.58 (0.03)	1.65 (0.00)	1.64 (0.00)
W282	Oxidation	FNWYVDGVEV HNAK	0.10 (0.01)	0.09 (0.00)	0.15 (0.00)	0.14 (0.00)	0.15 (0.01)	0.15 (0.01)	0.11 (0.00)	0.11 (0.00)	0.10 (0.00)

In order to estimate potential changes to the concentrations of sequence-level modifications in response to the conditions used for mAb production, the percentage abundance of each of the modifications in samples produced under altered bioprocess conditions were compared to the levels of corresponding modifications in mAb samples produced using standard bioprocess conditions. For each of the modifications the ratio of the percentage abundance of that modification in the differentially produced mAb compared to the average percentage abundance of that modification found in the standard cultured-mAb samples was determined and is reported in Table 3.8. The mAb samples produced at pH 6.8, pH 7.2 and at 60% DO did not appear to have greatly altered levels of amino acid modifications for the heavy or light chain of anti-IL8. Deamidation of glutamine appeared to be increased in mAb produced at 39.5°C but reduced at 32.0°C, suggesting a possible effect on the kinetics of glutamine deamidation due to culture temperature. An increase in the methionine and tryptophan oxidation levels in mAb produced at 110% compared to mAb produced at 85% was not reflected in the corresponding HIC or SCX traces possibly signifying the conformation of the modified residues is contained within the internal part of the mAb tertiary structure. The most pronounced change in sequence-level modifications were found to exist in mAb samples expressed in media maintained at 32°C, which showed comparatively low levels of deamidated peptides on the mAb light chain and on the N74 residue on the mAb heavy chain. Conversely, the levels of methionine and tryptophan oxidation were elevated on both the heavy and light chain sequences. Although the high levels of primary sequence oxidation observed for the mAb produced at low temperature may appear to correlate with the HIC and SCX data, showing both greater levels of basic and polar species, the same levels of oxidation were not observed for the mAb produced at pH 7.2, despite a similar charge and hydrophobic variant profile. Hence it is possible that there are additional factors at play that may influence the critical quality attributes of the mAb produced.

Although sequence level modifications frequently are present on therapeutic proteins, the goal of product characterisation is to ensure that existing variants do not alter the safely, potency and efficacy profile of the drug substance. A modification to the primary sequence of a mAb may potentially impact the proteins CQAs if that modification occurs in one of the complementarity determining regions (CDR) of the antibody, which are responsible for target antigen binding and hence mAb therapeutic function. [51] Following peptide mapping analysis one modified amino acid residue, namely N55, which formed part of a CDR was identified. Although studies have revealed that deamidation of N55 may reduce ligand binding activity resulting in reduced mAb potency, [52] the levels of deamidation of N55 were not found to be relatively altered in the mAb samples determined.

Table 3.8: Ratio of light chain and heavy chain modifications determined in mAb produced under different bioprocessing conditions relative to average % abundance of each modification in mAb produced under standard conditions.

	Residue	Modification	Sequence	High DO mAb	High pH mAb	High Temp. mAb	Low DO mAb	Low pH mAb	Low Temp. mAb
Light Chain	N58	Deamidation	VSNR	1.00	0.97	0.95	0.98	0.94	0.48
	N157	Deamidation	VDNALQSGNSQESVTEQDSK	0.93	0.99	1.04	1.08	0.97	0.82
	Q160	Deamidation	VDNALQSGNSQESVTEQDSKDSTYSLSSTLTLSK	0.93	1.02	1.21	1.02	1.02	0.66
	N163	Deamidation	VDNALQSGNSQESVTEQDSK	1.02	1.02	1.14	1.03	0.94	0.77
	N215	Deamidation	SFNR	0.95	0.96	1.10	1.01	0.91	1.02
	M4	Oxidation	DIQMTQSPSSLSASVGDR	1.10	1.00	1.04	0.99	1.06	1.52
	W40	Oxidation	SSQSLVHGIGETYLHWYQQKPGK	1.57	1.12	1.24	1.02	1.07	1.26
	W153	Oxidation	VQWK	1.34	1.07	1.01	1.16	1.13	1.60
Heavy Chain	N55	Deamidation	GLEWVGYIDPSNGETTYNQK	1.02	1.02	1.00	1.00	1.01	0.97
	N74	Deamidation	DNSKNTAYLQMNSLR	0.91	0.96	1.02	0.99	1.06	0.40
	N77	Deamidation	NTAYLQMNSLR	1.16	1.07	0.89	0.92	1.05	1.06
	N84	Deamidation	NTAYLQMNSLR	1.11	1.11	0.86	0.95	1.11	1.23
	N291	Deamidation	FNWYVDGVEVHNAK	1.07	1.05	0.98	0.99	1.02	1.02
	N320	Deamidation	VVSVLTVLHQDWLNGKEYK	0.99	0.98	0.95	0.93	1.03	0.91
	N389	Deamidation	GFYPSDIAVEWESNGQPENNYK	0.95	0.99	0.99	0.98	0.90	0.87
	M83	Oxidation	NTAYLQMNSLR	1.22	0.96	0.87	0.80	1.05	1.77
	M257	Oxidation	DTLMISR	1.09	0.96	0.90	0.92	0.96	1.45
	W282	Oxidation	FNWYVDGVEVHNAK	1.27	0.94	1.23	0.94	0.90	1.30
	K452	Lysine clipping	SLSLSPGK	1.08	0.95	1.08	1.04	1.09	0.95

Anti-IL8 Light Chain

```
            10          20          30          40          50          60
DIQMTQSPSS  LSASVGDRVT  ITCRSSQSLV  HGIGETYLHW  YQQKPGKAPK  LLIYKVSNRF

            70          80          90         100         110         120
SGVPSRFSGS  GSGTDFTLTI  SSLQPEDFAT  YYCSQSTHVP  LTFGQGTKVE  IKRTVAAPSV

           130         140         150         160         170         180
FIFPPSDEQL  KSGTASVVCL  LNNFYPREAK  VQWKVDNALQ  SGNSQESVTE  QDSKDSTYSL

           190         200         210
SSTLTLSKAD  YEKHKVYACE  VTHQGLSSPV  TKSFNRGEC
```

Anti-IL8 Heavy Chain

```
            10          20          30          40          50          60
EVQLVQSGGG  LVQPGGSLRL  SCAASGYSFS  SHYMHWVKQA  PGKGLEWVGY  IDPSNGETTY

            70          80          90         100         110         120
NQKFKGRFTL  SRDNSKNTAY  LQMNSLRAED  TAVYYCARGD  YRYNGDWFFD  VWGQGTLVTV

           130         140         150         160         170         180
SSASTKGPSV  FPLAPSSKST  SGGTAALGCL  VKDYFPEPVT  VSWNSGALTS  GVHTFPAVLQ

           190         200         210         220         230         240
SSGLYSLSSV  VTVPSSSLGT  QTYICNVNHK  PSNTKVDKKV  EPKSCDKTHT  CPPCPAPELL

           250         260         270         280         290         300
GGPSVFLFPP  KPKDTLMISR  TPEVTCVVVD  VSHEDPEVKF  NWYVDGVEVH  NAKTKPREEQ

           310         320         330         340         350         360
YNSTYRVVSV  LTVLHQDWLN  GKEYKCKVSN  KALPAPIEKT  ISKAKGQPRE  PQVYTLPPSR

           370         380         390         400         410         420
DELTKNQVSL  TCLVKGFYPS  DIAVEWESNG  QPENNYKTTP  PVLDSDGSFF  LYSKLTVDKS

           430         440         450
RWQQGNVFSC  SVMHEALHNH  YTQKSLSLSP  GK
```

Figure 3.20 Anti-IL-8 IgG1 heavy and light chain protein sequence. Amino acid residues that were determined to have been modified following peptide mapping analysis are highlighted: deamidation residues are coloured green; oxidised residues are red; C-terminal truncated lysine is blue. CDR regions are underlined. [23]

3.4   Conclusions

Monoclonal antibodies are highly complex biomolecules, which have the potential to undergo a range of modifications resulting in extensive microheterogeneity for each mAb entity. Since the incidence of primary structure modification may be impacted by environmental factors, *e.g.* bioprocessing, wide-ranging characterisation of therapeutic protein samples are required. In this study, domain and sequence-level characterisation of differentially produced anti-IL8 IgG1 was performed. Although SEC-UV and middle down MS analysis did not signify changes to the mass of protein samples analysed, application of SCX-UV and HIC-UV for intact protein analysis and also use of high resolution MS instrumentation for peptide mapping of the protein primary sequence, revealed differences in peptide-level modifications, protein variant charge and hydrophobicity. Interestingly, previously reported correlations between peptide level modifications, *e.g.* oxidation and deamidation, and changes to the hydrophobicity and charge characteristics of the IgG1 samples analysed were not clear-cut. These findings suggest that there is a fundamental need to further evaluate therapeutic mAbs, as improvements in chromatographic stationary phases and in high resolution MS analysis may reveal new features of therapeutic biomolecules that have not previously been determined. With the advent of increasing complex biotherapeutics, such as biosimilars, bispecific antibodies, antibody drug conjugates and other new drug therapies, it is now increasingly important to apply intuitive orthogonal analytical technologies to achieve a deeper understanding of therapeutic biomolecules at the sequence level. The results herein show, that in order to predict the safety, quality and efficacy of a therapeutic protein sample, a more holistic approach must be taken as prediction of potential protein properties based on sequence quality assessment may not be appropriate. Ultimately to fully characterise a proteins CQAs, a thorough evaluation of sequence and domain-level features, combined with structural and functional characterisation must be performed.

3.5   Author Contributions

Research study devised by Amy Farrell and Jonathan Bones; Sample preparation performed by Amy Farrell; Chromatography analysis performed by Amy Farrell; Mass spectrometry analysis performed by Amy Farrell and Kai Scheffler; Data analysis performed by Amy Farrell; Data reviewed by Jonathan Bones.

3.6   References

1.   Stracke, J., et al., *A novel approach to investigate the effect of methionine oxidation on pharmacokinetic properties of therapeutic antibodies.* MAbs, 2014. **6**(5): p. 1229-42.

2.   Liu, H., et al., *Heterogeneity of monoclonal antibodies.* J Pharm Sci, 2008. **97**(7): p. 2426-47.

3.   Berkowitz, S.A., et al., *Analytical tools for characterizing biopharmaceuticals and the implications for biosimilars.* Nat Rev Drug Discov, 2012. **11**(7): p. 527-40.

4.   US Food and Drug Administration. September 2004. Pharmaceutical cGMPs for the 21st century - A risk based approach. [Retrieved 14 June 2016 from http://www.fda.gov/downloads/Drugs/DevelopmentApprovalProcess/Manufacturing/QuestionsandAnswersonCurrentGoodManufacturingPracticescGMPforDrugs/UCM176374.pdf.]

5.   US Food and Drug Administration. September 2004. Guidance for Industry, PAT -A framework for innovative pharmaceutical development, manufacturing and quality assurance. [Retrieved 14 June 2016 from http://www.fda.gov/downloads/Drugs/GuidanceComplianceRegulatoryInformation/Guidances/UCM070305.pdf.]

6.   *International Conference on Harmonisation. ICH Harmonised Tripartite Guideline, Pharmaceutical Development Q8 (R2). [Retrieved 14 June 2016 from http://www.ich.org/fileadmin/Public_Web_Site/ICH_Products/Guidelines/Quality/Q8_R1/Step4/Q8_R2_Guideline.pdf].* August 2009.

7.   *International Conference on Harmonisation. ICH Harmonised Tripartite Guideline, Comparability of biotechnological/biological products subject to changes in their manufacturing process Q5E. [Retrieved 14 June 2016 from http://www.ich.org/fileadmin/Public_Web_Site/ICH_Products/Guidelines/Quality/Q5E/Step4/Q5E_Guideline.pdf].* November 2004.

8.   Rathore, A.S., *Roadmap for implementation of quality by design (QbD) for biotechnology products.* Trends Biotechnol, 2009. **27**(9): p. 546-53.

9.   Kozlowski, S. and P. Swann, *Current and future issues in the manufacturing and development of monoclonal antibodies.* Adv Drug Deliv Rev, 2006. **58**(5-6): p. 707-22.

10.   Kunert, R. and D. Reinhart, *Advances in recombinant antibody manufacturing.* Appl Microbiol Biotechnol, 2016. **100**(8): p. 3451-61.

11.   Haverick, M., et al., *Separation of mAbs molecular variants by analytical hydrophobic interaction chromatography HPLC: overview and applications.* MAbs, 2014. **6**(4): p. 852-8.

12.   Parr, M.K., O. Montacir, and H. Montacir, *Physicochemical characterization of biopharmaceuticals.* J Pharm Biomed Anal, 2016.

13.   Liu, Z. and K.L. Schey, *Fragmentation of multiply-charged intact protein ions using MALDI TOF-TOF mass spectrometry.* J Am Soc Mass Spectrom, 2008. **19**(2): p. 231-8.

14.   Valeja, S.G., et al., *New reagents for enhanced liquid chromatographic separation and charging of intact protein ions for electrospray ionization mass spectrometry.* Anal Chem, 2010. **82**(17): p. 7515-9.

15.   Wu, S., et al., *Top-Down Characterization of the Post-Translationally Modified Intact Periplasmic Proteome from the Bacterium Novosphingobium aromaticivorans.* Int J Proteomics, 2013. **2013**: p. 279590.

16.   Gadgil, H.S., et al., *Identification of cysteinylation of a free cysteine in the Fab region of a recombinant monoclonal IgG1 antibody using Lys-C limited proteolysis coupled with LC/MS analysis.* Anal Biochem, 2006. **355**(2): p. 165-74.

17.   Yan, B., et al., *Analysis of post-translational modifications in recombinant monoclonal antibody IgG1 by reversed-phase liquid chromatography/mass spectrometry.* J Chromatogr A, 2007. **1164**(1-2): p. 153-61.

18.   Wang, B., et al., *Structural comparison of two anti-CD20 monoclonal antibody drug products using middle-down mass spectrometry.* Analyst, 2013. **138**(10): p. 3058-65.

19.   An, Y., et al., *A new tool for monoclonal antibody analysis: application of IdeS proteolysis in IgG domain-specific characterization.* MAbs, 2014. **6**(4): p. 879-93.

20.   Bongers, J., et al., *Validation of a peptide mapping method for a therapeutic monoclonal antibody: what could we possibly learn about a method we have run 100 times?* J Pharm Biomed Anal, 2000. **21**(6): p. 1099-128.

21.   Yang, H. and R.A. Zubarev, *Mass spectrometric analysis of asparagine deamidation and aspartate isomerization in polypeptides.* Electrophoresis, 2010. **31**(11): p. 1764-72.

22. Wisniewski, J.R., et al., *Universal sample preparation method for proteome analysis.* Nat Methods, 2009. **6**(5): p. 359-62.

23. Gonzalez, T.N., Leong, S. R., Presta, L. G., *Humanized Anti-IL-8 Monoclonal Antibodies. US Patent 6117980.* 12 September 2000.

24. den Engelsman, J., et al., *Strategies for the assessment of protein aggregates in pharmaceutical biotech product development.* Pharm Res, 2011. **28**(4): p. 920-33.

25. Philo, J.S., *A critical review of methods for size characterization of non-particulate protein aggregates.* Curr Pharm Biotechnol, 2009. **10**(4): p. 359-72.

26. Yang, R., et al., *High resolution separation of recombinant monoclonal antibodies by size-exclusion ultra-high performance liquid chromatography (SE-UHPLC).* J Pharm Biomed Anal, 2015. **109**: p. 52-61.

27. Carpenter, J.F., et al., *Overlooking subvisible particles in therapeutic protein products: gaps that may compromise product quality.* J Pharm Sci, 2009. **98**(4): p. 1201-5.

28. Szabolcs Fekete, A.-L.G., Serge Rudaz, Julie Schappler, Davy Guillarme, *Analytical strategies for the characterization of therapeutic monoclonal antibodies.* Trends in Analytical Chemistry, 2013. **42**: p. 74-83.

29. Yang, J., et al., *Determination of tryptophan oxidation of monoclonal antibody by reversed phase high performance liquid chromatography.* J Chromatogr A, 2007. **1156**(1-2): p. 174-82.

30. Khawli, L.A., et al., *Charge variants in IgG1: Isolation, characterization, in vitro binding properties and pharmacokinetics in rats.* MAbs, 2010. **2**(6): p. 613-24.

31. Zheng, J.Y. and L.J. Janis, *Influence of pH, buffer species, and storage temperature on physicochemical stability of a humanized monoclonal antibody LA298.* Int J Pharm, 2006. **308**(1-2): p. 46-51.

32. Huang, L., et al., *In vivo deamidation characterization of monoclonal antibody by LC/MS/MS.* Anal Chem, 2005. **77**(5): p. 1432-9.

33. Antes, B., et al., *Analysis of lysine clipping of a humanized Lewis-Y specific IgG antibody and its relation to Fc-mediated effector function.* J Chromatogr B Analyt Technol Biomed Life Sci, 2007. **852**(1-2): p. 250-6.

34.   Chumsae, C., et al., *Comparison of methionine oxidation in thermal stability and chemically stressed samples of a fully human monoclonal antibody.* J Chromatogr B Analyt Technol Biomed Life Sci, 2007. **850**(1-2): p. 285-94.

35.   Johnson, K.A., et al., *Cation exchange-HPLC and mass spectrometry reveal C-terminal amidation of an IgG1 heavy chain.* Anal Biochem, 2007. **360**(1): p. 75-83.

36.   Du, Y., et al., *Chromatographic analysis of the acidic and basic species of recombinant monoclonal antibodies.* MAbs, 2012. **4**(5): p. 578-85.

37.   Dick, L.W., Jr., et al., *C-terminal lysine variants in fully human monoclonal antibodies: investigation of test methods and possible causes.* Biotechnol Bioeng, 2008. **100**(6): p. 1132-43.

38.   Zhang, X., et al., *Culture temperature modulates monoclonal antibody charge variation distribution in Chinese hamster ovary cell cultures.* Biotechnol Lett, 2015. **37**(11): p. 2151-7.

39.   Lam, X.M., J.Y. Yang, and J.L. Cleland, *Antioxidants for prevention of methionine oxidation in recombinant monoclonal antibody HER2.* J Pharm Sci, 1997. **86**(11): p. 1250-5.

40.   Boyd, D., T. Kaschak, and B. Yan, *HIC resolution of an IgG1 with an oxidized Trp in a complementarity determining region.* J Chromatogr B Analyt Technol Biomed Life Sci, 2011. **879**(13-14): p. 955-60.

41.   Vincents, B., et al., *Enzymatic characterization of the streptococcal endopeptidase, IdeS, reveals that it is a cysteine protease with strict specificity for IgG cleavage due to exosite binding.* Biochemistry, 2004. **43**(49): p. 15540-9.

42.   Chevreux, G., N. Tilly, and N. Bihoreau, *Fast analysis of recombinant monoclonal antibodies using IdeS proteolytic digestion and electrospray mass spectrometry.* Anal Biochem, 2011. **415**(2): p. 212-4.

43.   Graphic created by Genovis. Accessed from http://www.genovis.com/antibody-oxidation on 26th June 2016.

44.   Nimmerjahn, F. and J.V. Ravetch, *Fcgamma receptors as regulators of immune responses.* Nat Rev Immunol, 2008. **8**(1): p. 34-47.

45.   Walsh, G. and R. Jefferis, *Post-translational modifications in the context of therapeutic proteins.* Nat Biotechnol, 2006. **24**(10): p. 1241-52.

46.   Xie, H., et al., *Rapid comparison of a candidate biosimilar to an innovator monoclonal antibody with advanced liquid chromatography and mass spectrometry technologies.* MAbs, 2010. **2**(4): p. 379-94.

47.   Robinson, A.B., J.W. Scotchler, and J.H. McKerrow, *Rates of nonenzymatic deamidation of glutaminyl and asparaginyl residues in pentapeptides.* J Am Chem Soc, 1973. **95**(24): p. 8156-9.

48.   Liu, Y.D., et al., *N-terminal glutamate to pyroglutamate conversion in vivo for human IgG2 antibodies.* J Biol Chem, 2011. **286**(13): p. 11211-7.

49.   Dick, L.W., Jr., et al., *Determination of the origin of the N-terminal pyro-glutamate variation in monoclonal antibodies using model peptides.* Biotechnol Bioeng, 2007. **97**(3): p. 544-53.

50.   Yu, L., et al., *Investigation of N-terminal glutamate cyclization of recombinant monoclonal antibody in formulation development.* J Pharm Biomed Anal, 2006. **42**(4): p. 455-63.

51.   Haberger, M., et al., *Assessment of chemical modifications of sites in the CDRs of recombinant antibodies: Susceptibility vs. functionality of critical quality attributes.* MAbs, 2014. **6**(2): p. 327-39.

52.   Yan, B., et al., *Succinimide formation at Asn 55 in the complementarity determining region of a recombinant monoclonal antibody IgG1 heavy chain.* J Pharm Sci, 2009. **98**(10): p. 3509-21.

4.0

Comparative Analysis of Monoclonal Antibody *N*-Glycosylation using Stable Isotope Tagging and UPLC-Fluorescence-MS

4.1   Introduction

Monoclonal antibody (mAb) *N*-glycosylation is a common post-translational modification, present on each mAb heavy chain at the highly conserved asparagine 297 residue in the CH2 region of the Fc portion of mAbs. [1-3] In addition to preserving structural stability of the CH2 domain, glycosylation has been shown to play a critical role in the effector function of mAbs, facilitating interaction with Fc*γ* receptors present on cells of the innate immune system. [4, 5] Hence *N*-glycans are important in modulating therapeutic mAb efficacy *e.g.* by facilitating antibody-dependent cell-mediated cytotoxicity, complement-dependent cytotoxicity and by extending serum half-life. [6, 7] As glycosylation is a critical quality attribute (CQA), quantitative structural characterisation of *N*-glycans present on antibody therapeutics is a regulatory requirement as outlined in ICH Q6B. [8] Characterisation of *N*-glycans is normally performed using liquid phase separation techniques with optical detection following enzymatic liberation of *N*-glycans from the antibody and derivatisation with a fluorophore to increase detection sensitivity. [9, 10] Despite recent advances in separation chemistries for oligosaccharides, peak area based quantitation remains a subjective and laborious process due to integration challenges for distorted peaks containing poorly or partially resolved *N*-glycans, or due to the presence of multiple glycans within a single chromatographic peak. [11] Such effects can result in either under reporting of a particular *N*-glycan or difficulties in the alignment of data for subsequent statistical evaluation.

Relative or absolute quantitation, for the elucidation of protein differential expression, using stable isotope labelling technology has become widely used in proteomics. Methods employed include those in which a heavy analogue is either incorporated into the peptide metabolically, *e.g.* stable isotope labelling with amino acids in cell culture (SILAC), or *via* chemical derivatisation, *e.g.* stable isotope dimethylation of peptides. [12, 13] Quantitation is performed by determining the levels of 'light' and 'heavy' analyte pairs present following a single stage mass spectrometric analysis (MS1). Alternatively, isobaric tagging of analytes may

be performed, wherein analytes are derivatised with reagents bearing the same nominal mass. Using isobaric mass tags, quantitation is facilitated following the release of low mass reporter ions during tandem mass spectrometric analysis of the precursor ion. [14] Isobaric tagging offers the ability to multiplex higher numbers of experiments, however, problems with the associated quantitative performance have been reported in cases where multiple ions with mass to charge ratios (m/z) within the isolation window are selected and fragmented simultaneously. [15, 16] Application of stable isotope methods for quantitative glycomics has attracted attention with many published reports focusing upon heavy isotope incorporation during permethylation of oligosaccharides prior to MALDI-MS analysis. [17-19] This approach may be limited due to potential variance in light-heavy mass difference resulting from inconsistencies in the number of available methylation sites for isotope incorporation on the oligosaccharide. Recently, this limitation has been overcome by labelling of oligosaccharide samples for comparison with either $^{13}CH_3I$ or $^{12}CH_2DI$, respectively, which introduces a mass difference of 2.922 mDa per methylation site. [20, 21] High resolution mass analysis using FT-ICR or Orbitrap mass analysers are required to distinguish the resulting isotopic pair. Stable isotope incorporation using reductive amination has also been reported prior to MALDI-MS analysis using $^{13}C_6$ or deuterated analogues of commonly used reagents for high sensitivity fluorescence detection. [22-29]

In this Chapter, the development of a two-plex method for the quantitative analysis of *N*-glycans present on a chimeric IgG1 monoclonal antibody is described, wherein released oligosaccharides are labeled with light ($^{12}C_6$) or heavy ($^{13}C_6$) 2-aminobenzoic acid (2-AA) prior to ultra-performance liquid chromatography (UPLC) with sequential fluorescence and accurate mass quadrupole time of flight (QToF) mass spectrometric detection. Optimisation and evaluation of the $^{12/13}C_6$ 2-AA tag was performed, which revealed a high level of technical precision determined using both *N*-glycan standards and oligosaccharides released from complex glycoproteins. The combination of isotopic labelling, UPLC separation and MS detection facilitated full quantitative evaluation and structural annotation of *N*-glycans present within the glycan pool under investigation. Minimisation of technical variation and operator subjectivity is achieved through multiplexing reference and analytical samples into a single LC-MS injection, demonstrating the suitability of the developed method for comparability analysis of *N*-glycosylation on therapeutic glycoproteins.

The developed method was applied for comparability assessment of different commercial lots of a chimeric IgG1 mAb. Comparison of different lots revealed notable differences in the levels of sialylated *N*-glycans and *N*-glycans bearing galactose α1-3 linked galactose (α-gal) epitopes.

Finally, considering the importance of N-glycosylation on the structural stability and effector function of therapeutic mAbs, the developed method was also applied to determine potential variations of the *N*-glycan profile on anti-Interleukin 8 (anti-IL8), a recombinant humanised IgG1, following production under varied culture conditions. Variation of bioprocessing conditions was found to results in changes to the glycoform profile, in particular changes to galactosylation in response to culture pH and changes to fucosylation levels following alterations in culture temperature.

4.2 Experimental

4.2.1 Reagents and Consumables

Standard *N*-glycans (A2F, NA2F, Man5, NA2) and Peptide-*N*-glycosidase F (PNGase F) were purchased from Prozyme (San Leandro, CA). Bovine ribonuclease B (RNase B), Bovine fetuin, Human serum IgG, $^{12}C_6$ 2-aminobenzoic acid, $^{13}C_6$ 2-aminobenzoic acid, Dimethyl sulfoxide (DMSO), Acetic acid, Dithiothreitol (DTT), Iodoacetamide (IAA), and Formic acid were purchased from Sigma-Aldrich (Wicklow, Ireland). Sodium cyanoborohydride, Water, 0.1 % formic acid (LC-MS Optima), Acetonitrile, 0.1 % formic acid (LC-MS Optima) were purchased from Fisher Scientific, (Dublin, Ireland). Nanosep 10 kDa centrifugal devices were obtained from Pall (Port Washington, NY). Promega sequencing grade modified trypsin was from MyBio Ltd. (Kilkenny, Ireland). Different commercial lots of the chimeric IgG1 monoclonal antibody (mAb) for analysis were generously provided by San Cecilio University Hospital (Granada, Spain).

4.2.2 Glycoprotein Deglycosylation

100 μg aliquots of each standard glycoprotein (RNase B, bovine fetuin and human serum IgG), 500 μg aliquots of commercial chimeric IgG1 and 250 μg aliquots of anti-IL8 IgG1 (produced in-house using CHO DP12 cells and purified using Protein A affinity chromatography - Chapter 2, Section 2.2.2.5), were reduced with 1 mM DTT for 10 minutes at 65°C and alkylated by incubation with 5 mM IAA at room temperature in the dark for 30 minutes. *N*-glycans were enzymatically released by overnight (16 hour) incubation with 500 Units of PNGase F at 37 °C in 20 mM sodium bicarbonate buffer pH 7.0. The deglycosylation mixture was then centrifuged through a 10 kDa molecular weight cut-off (MWCO) to remove the protein. The filtrate containing the released glycans was reduced to dryness *via* vacuum centrifugation.

Once dry, the released glycans were treated with 50 μL of 1% v/v aqueous formic acid to ensure complete conversion to the reducing sugar form prior to derivatisation.

4.2.3   Derivatisation of free glycans with $^{12}C_6$/$^{13}C_6$ 2-aminobenzoic acid

Glycan samples were derivatised with either light or heavy 2-AA by reductive amination in the presence of sodium cyanoborohydride. 5 μL of a freshly prepared solution of 0.37M $^{12}C_6$ 2-AA or $^{13}C_6$ 2-AA containing 1 M NaCNBH$_3$ prepared in DMSO/acetic acid (70:30), were added to the dried glycans and incubated for 5 hours at 65 °C. Following labelling the light and heavy samples were mixed together and prepared with 5 μL of purified water and 85 μL of acetonitrile. *N*-glycans were purified by HILIC chromatography using a Thermo Ultimate 3000 RS UHPLC equipped with a BEH Glycan 2.1 x 50 mm, 1.7 μm analytical column (Waters). Briefly samples were introduced onto the column using a mobile phase composition of 32.5% 50 mM Ammonium formate, pH 4.5 and 67.5% acetonitrile. Following removal of excess fluorophore, the gradient composition was switched to 20% acetonitrile to enable elution of 2-AA derivatised *N*-glycans. Subsequently samples were dried *via* vacuum centrifugation. The cleaned *N*-glycans were re-suspended in 25 μL of purified water and stored at -40 °C pending analysis.

4.2.4   Separation of 2AA-labeled glycans UPLC-FLR-MS

Labeled *N*-glycans were separated using a Waters Acquity UPLC BEH Amide (1.0 x 150 mm, 1.7 μm) column coupled to an Acquity UPLC equipped with online fluorescence detection (Waters Corporation, Milford, MA, USA). The fluorescence excitation and emission wavelength parameters were 350 and 425 nm, respectively. The flow rate was 0.150 mL.min^{-1} and column temperature was maintained at 60°C. A binary gradient of 50 mM ammonium formate, pH 4.4 (A) and acetonitrile (B) was used as follows: 28% A for 1 min, 28-43% A for 30 minutes, 43-70 % A for 1 minute, 70 % A for 3 min, 70-28% solvent A for 1 min and finally 28 % A for 4 minutes. Samples were diluted in 75% acetonitrile prior to analysis and sample injection volume was 8 μL. The outlet of the chromatographic system was directly coupled to a Waters Xevo G2 QToF mass spectrometer (Milford, MA, USA) equipped with an electrospray ionisation interface. The instrument was operated in negative ion mode with a capillary voltage of 1.80 kV. The ion source and nitrogen desolvation gas temperatures were set at 120°C and 400°C, respectively. The desolvation gas flow rate was 600 L/h. The cone voltage was maintained at

50 V. Full-scan MS data was acquired over the range of 450 to 2500 m/z. Data collection and processing was controlled using MassLynx version 4.1 (Waters Corporation, Milford, MA, USA). To avoid contamination of the instrument, the column flow was diverted to waste for the first 1.2 minutes and after 32 minutes of the chromatographic run.

4.2.5   Determination of Glycosylation Site Occupancy using LC-MS^E

Determination of glycosylation site occupancy was performed on a Waters Acquity UPLC instrument coupled to a Xevo G2 QToF mass spectrometer (Millford, MA, USA). 50 µg aliquots of commercial chimeric IgG1 were reduced with 5 mM DTT at 65°C for 15 minutes, before alkylation with 15 mM IAA for 30 minutes at 20°C in darkness. Following reduction and alkylation, enzymatic digestion was performed overnight with trypsin at 37°C using a 1:50 (w/w, enzyme: protein) ratio. In addition, where required, commercial chimeric IgG1 tryptic digests were de-glycosylated by incubation with 500 Units of PNGase F. Tryptic peptides were subsequently separated using a BEH 130 C18 2.1 x 150 mm analytical column (Waters) with a binary gradient of 0.1% formic acid in water (C) and 0.1% formic acid in acetonitrile (D). Gradient conditions were as follows: 2% D initially for 2 minutes, increased to 10% D in 3 minutes with a further increase to 35% D over 40 minutes followed by a final increase to 90% D in two minutes with a two minute isocratic hold. Initial conditions were restored in one minute and held for an additional 10 minutes to ensure column re-equilibration. The column temperature was maintained at 40°C throughout and flow rate was sustained at 200 µL.min^{-1}. The mass spectrometer was operated in positive ion data independent mode with one second sequential low and high energy scans in the range of 50 to 2,000 Da. The spray voltage was 3 kV. A collision energy ramp from 20 to 45 V was used for the high energy function. Leucine enkephalin (m/z 556.2771, z=1) was used as lock mass solution, recorded at 30 second intervals. Resultant data were processed using ProteinLynx Global Server (PLGS) version 3.0.1, using the following workflow parameters: automatic peptide and fragment tolerances with lockmass correction of all doubly charged masses, minimum number of fragment ion matches per peptide = 3, minimum number of fragment ion matches per protein = 7, minimum number of unique peptides per protein = 2, primary digest reagent trypsin, with maximum number of one missed cleavage, fixed modification: carbamidomethyl C, variable modifications: oxidation M and deamidation N, Q, false discovery rate maintained at 1% FDR. Data was searched against a fasta file composed of the known sequence for the chimeric IgG1.

4.3   Results and Discussion

Quantitative structural analysis of *N*-glycans present on therapeutic glycoproteins is required by regulatory agencies for new drug applications and to demonstrate correlation between different manufacture batches, biosimilars or following changes to a bioprocess. Despite advances in separation chemistries for glycosylation profiling, the presence of multiple glycan structures in a single peak or peak distortion as a result of partial or poor resolution of closely eluting oligosaccharide structures, can affect relative peak area based quantitation. Although LC-MS analysis of *N*-glycans may overcome these challenges, potential differences with ionisation efficiencies or instrument response factors may lead to distorted results. These issues may be circumvented using stable isotope tagging methods as comparative samples are combined following labelling and analysed in a single LC-MS injection. Hence, technical variation of the measurement is minimized and comparability assessment based upon the relative ratio of the light and heavy peaks for each glycan present may be facilitated. In this Chapter, the development and application of a two-plex stable isotope labelling strategy for the comparability assessment of *N*-glycans present on commercial chimeric IgG1 using $^{12/13}C_6$ 2-AA labelling prior to hydrophilic interaction UPLC with sequential fluorescence and accurate mass QToF-MS detection is described. Application of the method for the determination of lot-to-lot consistency of the *N*-glycans present on the chimeric IgG1 and to evaluate changes to the *N*-glycan profile on anti-IL8 IgG1 following culture under varied bioprocessing conditions is described.

4.3.1   Optimisation and Evaluation of $^{12/13}C_6$ 2-AA Performance

Initial investigations focused upon the optimisation of the 2-AA conjugation reaction to ensure complete *N*-glycan derivatisation. Glycans are labelled using a two-step reductive amination reaction, wherein the primary amide group of 2-AA reacts with the aldehyde group of a glycan in a condensation reaction to form a Schiff's base. The resulting imine group is then reduced using sodium cyanoborohydride to form a stable labeled glycans, as shown in Figure 4.1.
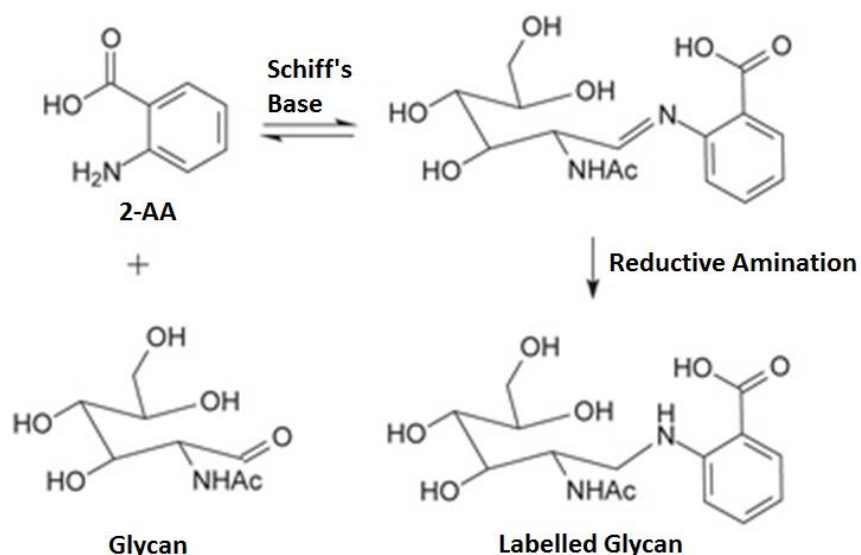
Figure 4.1: Labelling of glycans using 2-aminobenzoic acid (2-AA). Glycans are labelled using a two-step reductive amination reaction, wherein the primary amide group of 2-AA reacts with the aldehyde group of a glycan in a condensation reaction to form a Schiff's base. The resulting imine group is then reduced using sodium cyanoborohydride to form a stable labeled glycans.

Hydrophilic interaction UPLC with sequential fluorescence and MS detection was employed to facilitate the detection of the fluorescent oligosaccharide 2-AA conjugate and also any underivatised *N*-glycans present following the derivatisation reaction. Reaction time was systematically optimised using a combination of oligomannose *N*-glycans release from RNase B and complex sialylated *N*-glycans released from bovine fetuin to ensure complete derivatisation whilst maintaining oligosaccharide integrity. Figure 4.2 shows the determined conjugation efficiency following incubation for various reaction times. From this data it was determined that the optimum incubation time for labelling was 5 hours at 65°C in 0.37 M 2-AA containing 1 M sodium cyanoborohydride in 70:30 DMSO acetic acid.
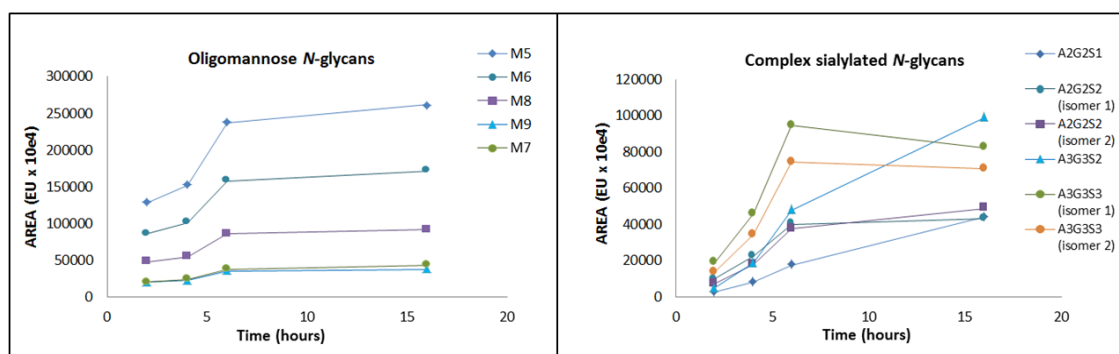
Figure 4.2: Optimisation of 2-AA labelling reaction time. Oligomannose *N*-glycans released from RNase B and complex sialylated *N*-glycans released from bovine fetuin were incubated with 0.37 M 2-AA containing 1 M sodium cyanoborohydride in 70:30 DMSO acetic acid using a range of incubation times. The optimum incubation time determined was 5 hours at 65 °C. Above this time desialylation of sialylated *N*-glycans was observed.

Following optimisation of the *N*-glycan derivatisation conditions, the quantitative response of the $^{12/13}C_6$ 2-AA analogues was then determined using *N*-glycan standards labeled and mixed in a 1:1 light: heavy molar ratio. Quantitation of the resulting LC-MS, *i.e.* the ratio of the sum of the extracted mass chromatogram peak areas generated using the combination of the $^{12}C_6$ isotopes relative to the $^{13}C_6$ isotopic data for the $[M-2H]^{2-}$ pseudomolecular ion, [25] did not provide the expected 1:1 ratio. To investigate the root cause of this observation the purity of the $^{12}C_6$ 2-AA and the $^{13}C_6$ 2-AA reagents was evaluated using reversed phase liquid chromatography with UV and MS detection which revealed the presence of an impurity in the $^{13}C_6$ 2-AA reagent (~33%). This impurity exhibited low solubility in 70:30 DMSO/acetic acid and did not react with the *N*-glycans to form a conjugated product. Correction for the purity of the $^{13}C_6$ 2-AA reagent facilitated the experimental achievement of the expected 1:1 ratio for equimolar concentrations of *N*-glycan standards labeled with the light and heavy reagents (Figure 4.3-A).
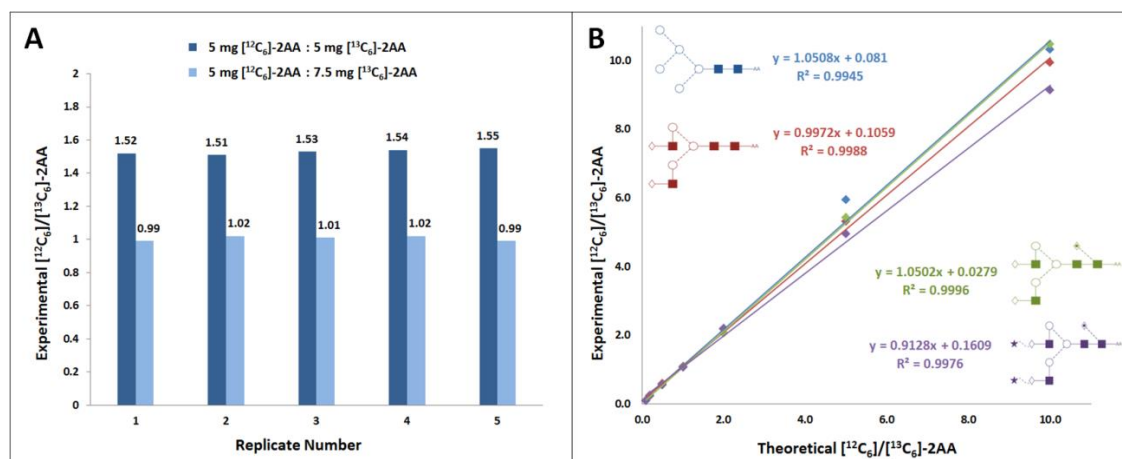
Figure 4.3: A. Evaluation of the purity of the $^{13}C_6$ 2-AA reagent. The graph shows the relative response of *N*-glycan samples labelled with the same concentration of the heavy or light 2-AA labelling reagent (dark blue) and relative response of samples labelled with light label and increased concentration of the heavy label to account for label purity (light blue); **B.** Evaluation of relative quantitation performance using stable isotope tagging.

In order to evaluate quantitation performance, a variety of labelled *N*-glycan standards were prepared (bi-antennary *N*-glycans with and without core fucose, antennary galactose and sialic acid residues) to assess linearity and accuracy of the quantitative response. The molar ratios of the light and heavy labelled *N*-glycan standards were mixed in theoretical ratios of 1:1, 2:1, 5:1 and 10:1. Quantitation was performed by determining the ratio of the sum of the extracted mass chromatogram peak areas generated using the combination of the $^{12}C_6$ isotopes relative to the $^{13}C_6$ isotopic data for the [M–2H]$^{2-}$ pseudomolecular ion. Evaluation of the experimental data revealed close agreement of the experimental ratios with the theoretically mixed values. As shown in Figure 4.3-B, translation of the data into linearity plots resulted in correlation coefficients for fitted least squares regression trend lines of $R^2 > 0.99$ for all glycan standards tested indicating excellent linear quantitative performance of the $^{12/13}C_6$ 2-AA reagents.

Quantitative precision of the $^{12/13}C_6$ 2-AA labelling method was next established using IgG *N*-glycans released from polyclonal IgG that was extracted from healthy human control serum using Protein A affinity chromatography. Normalisation was performed based upon the total amount of IgG taken for each deglycosylation (250 μg). Six technical replicate pairs were prepared with an expected light heavy ratio of 1:1 for all *N*-glycans. Each technical replicate was analysed using hydrophilic interaction UPLC-fluorescence-MS, the mean and standard

deviation of the six technical replicates was determined, resulting data is depicted in Figure 4.4.
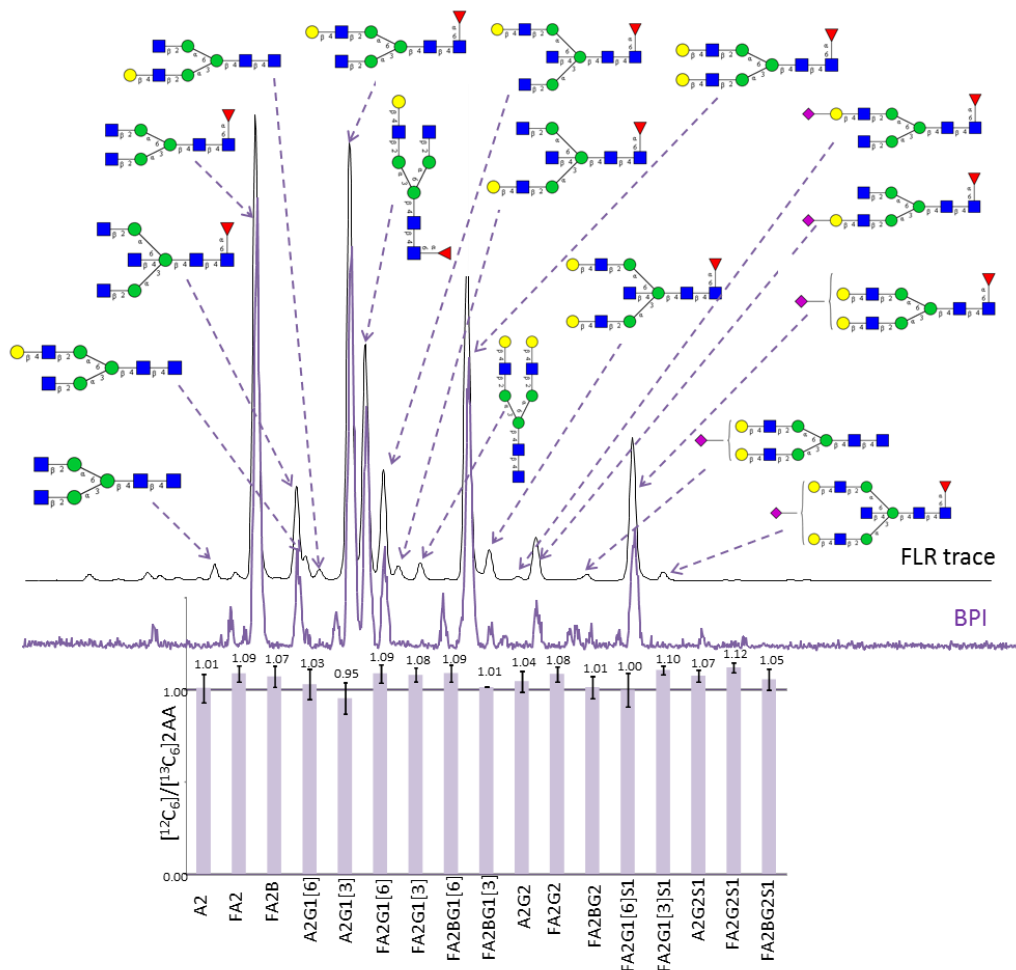
Figure 4.4: Annotated fluorescence and base peak intensity chromatograms for *N*-glycans released from polyclonal human serum IgG. The bar chart underneath the chromatograms depicts the mean light to heavy relative ratio as experimentally determined for the six technical replicates analyzed, y-error bars are also included at ± the standard deviation of the six technical replicates.

Annotation of the *N*-glycans present in each chromatographic peak was based upon the oligosaccharide composition as derived from the *m/z* value, expression of the retention time as a glucose unit value, comparison with an in-house database and MS/MS analysis for structural confirmation where required. Excellent precision was established for the six replicate analysis of the light heavy pairs with the expected 1:1 light-heavy ratio obtained and

with an average percentage error of ~5% across all *N*-glycans annotated, (range 2-9%), demonstrating the excellent precision of the described approach.

4.3.2 Comparability Assessment of Different Lots of a Commercial mAb using $^{12/13}C_6$ 2-AA *N*-Glycan UPLC-Fluorescence-MS

The developed two-plex $^{12/13}C_6$ 2-AA labelling hydrophilic interaction UPLC-fluorescence-MS approach was applied to investigate the consistency of *N*-glycans present on two different commercial lots of a chimeric IgG1 mAb. To ensure validity of the generated data, the experimental design focused upon triplicate analysis of technical replicates (lot 1 *versus* lot 1, lot 2 *versus* lot 2 and finally, lot 1 *versus* lot 2), with each comparison normalised based upon the amount of mAb taken for deglycosylation (500 µg). Twenty four structures were annotated and relative quantitation was inferred from the light to heavy ratios for each oligosaccharide present. Resulting data is displayed in Table 4.1, which lists the mean light-heavy ratio for each *N*-glycan and the standard deviation of the triplicate measurement (displayed in parenthesis).

Table 4.1: Relative light to heavy ratios determined for the analysis of the individual lots of mAb analysed as indicated in the table header.

Glycan Structure	Ratio ($^{12}C_6$) Lot 1: ($^{13}C_6$) Lot 1	Ratio ($^{12}C_6$) Lot 2: ($^{13}C_6$) Lot 2	Ratio ($^{12}C_6$) Lot 1: ($^{13}C_6$) Lot 2
A1	0.96 (0.02)	1.03 (0.04)	0.92 (0.03)
FA1	1.00 (0.01)	0.98 (0.08)	1.00 (0.03)
A2	0.95 (0.01)	1.03 (0.06)	0.82 (0.06)
M4A1	0.97 (0.04)	0.95 (0.07)	1.00 (0.04)
FA2	0.99 (0.02)	0.99 (0.08)	0.81 (0.02)
M5	0.96 (0.04)	0.97 (0.08)	0.88 (0.06)
FA1G1	0.97 (0.01)	1.00 (0.04)	0.80 (0.01)
M5A1/M4A1G1	0.96 (0.01)	1.02 (0.06)	1.00 (0.07)
FA2G1 [6]	0.98 (0.01)	0.98 (0.06)	0.59 (0.07)
FA2G1 [3]	1.00 (0.01)	0.96 (0.06)	0.69 (0.02)
FM5A1/FM4A1G1	0.99 (0.00)	0.98 (0.05)	0.99 (0.01)
FA1G1Gal1	0.95 (0.02)	0.97 (0.09)	0.64 (0.01)
M5A1G1/M4A1G1Gal1	0.96 (0.02)	1.02 (0.13)	0.75 (0.05)
FA2G2	0.94 (0.04)	1.00 (0.05)	0.44 (0.03)
FM5A1G1	0.99 (0.06)	1.02 (0.09)	0.72 (0.04)
FA1G1Sg1	1.03 (0.03)	1.01 (0.08)	0.72 (0.03)
FA2G1Sg1	1.02 (0.01)	1.05 (0.11)	0.54 (0.01)
FA2G2Gal1	0.95 (0.08)	0.94 (0.13)	0.39 (0.01)
FA2G1Sg1	1.02 (0.06)	0.97 (0.16)	0.63 (0.08)
FM4A1G1Sg1	1.04 (0.02)	0.98 (0.10)	0.66 (0.02)
FA2G2Sg1	0.96 (0.02)	0.99 (0.06)	0.41 (0.02)
M5A1G1Sg1	0.94 (0.02)	0.96 (0.10)	0.65 (0.04)
FM5A1G1Sg1	0.99 (0.03)	0.98 (0.09)	0.66 (0.02)
FA2G2Sg1Gal1	0.99 (0.01)	1.02 (0.04)	0.41 (0.02)

As seen from Table 5.1, the replicate analysis of individual lots (lot 1 *versus* lot 1 and lot 2 *versus* lot 2) indicated excellent and precise quantitative performance of the developed platform, with ratios near unity, as expected, for each *N*-glycan annotated. Interestingly, when the two lots were compared against each other distinct differences in the levels of certain glycans present were easily identified. The relative ratios of the majority of high mannose and hybrid oligosaccharides present on both lots were highly comparable with relative light heavy ratios of unity observed for many of these structures. Notably, the relative light heavy ratios for the complex biantennary glycans, particularly sialylated glycans and those containing a galactose α1-3 linked galactose residue, showed a dramatic difference between the two lots.

Glycosylation site occupancy was also determined using LC-MS^E (Figure 4.5) by subjecting aliquots of both lots of mAb to trypsin (Sequence coverage: Lot 1; 69.9% light chain, 66.0%

heavy chain, Lot 2; 66.2% light chain, 56.2% heavy chain) and PNGase F followed by trypsin (Sequence coverage: Lot 1; 50.9% light chain, 52.0% heavy chain, Lot 2; 44.4% light chain, 39.1% heavy chain). The relative peak area of the unoccupied glycopeptide (EEQYNSTYR) and the deamidated glycopeptide (EEQYDSTYR) generated following enzymatic deglycosylation were evaluated, enabling *N*-glycosylation site occupancy of 99.92 and 99.90% to be determined for lot 1 and lot 2, respectively. The reason for the difference in *N*-glycosylation between the two commercial lots is unclear but may be process related, for example, cellular age at time of harvest has been previously demonstrated to exhibit a similar effect of the glycosylation of an IgG4 mAb produced in CHO. [30] Process manufacturing changes have also been shown to be detectable through the analysis of different lots of drug product. [31] It is acknowledged that many more drug product lots would need to be analysed to deduce such a conclusion; however, the presented two-plex $^{12/13}C_6$ 2-AA labelling method represents a simple and eloquent solution for glycosylation comparability analysis, capable of detecting substantial differences between products as demonstrated due to the minimisation of technical variability and operator subjectivity from the analysis.
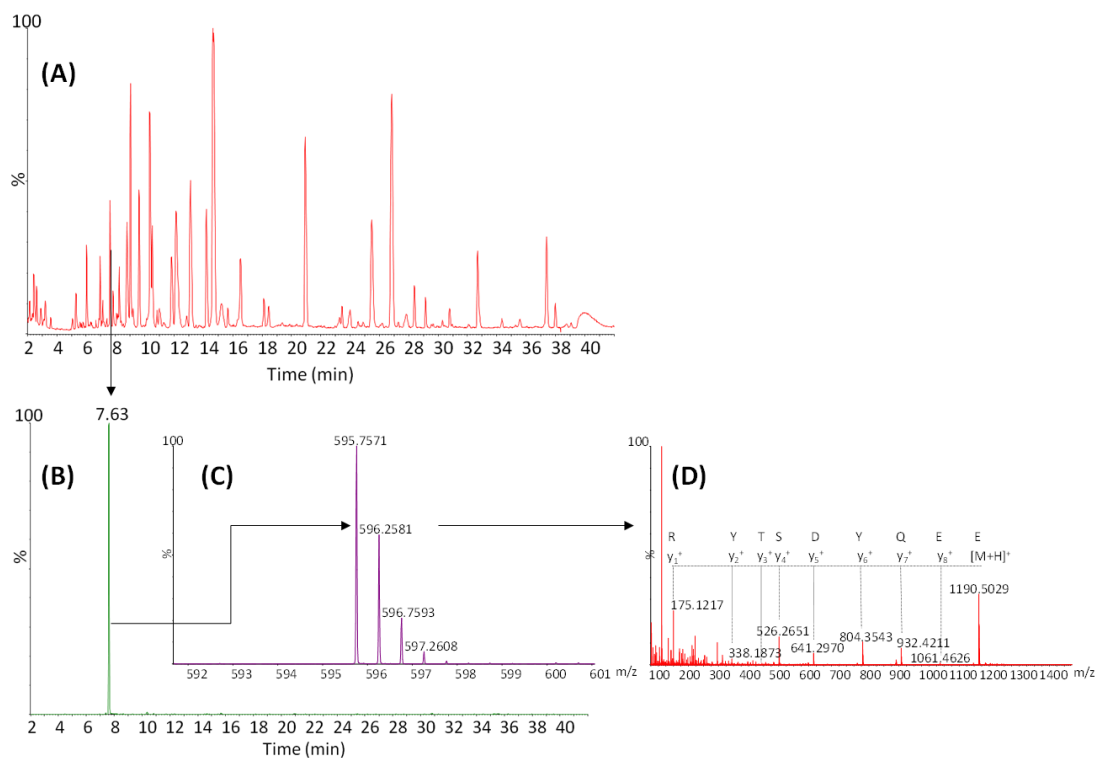
Figure 4.5: Determination of glycosylation site occupancy. **A.** Representative base peak chromatogram obtained following LC-MSE analysis of tryptic peptides, **B.** Extracted ion chromatogram for EEQYDSTYR, **C.** MS spectrum corresponding to EEQYDSTYR**, D.** MS/MS spectrum for EEQYDSTYR showing identified b and y ions and amino acid sequence.

4.3.3   Comparability Assessment of Anti-IL8 IgG1 *N*-glycan Profile in Response to Conditions of Altered Bioprocessing Using $^{12/13}$C$_6$ 2-AA *N*-Glycan UPLC-Fluorescence-MS

Glycosylation is a CQA of therapeutic proteins, which can modulate the efficacy of mAbs *in-vivo,* hence an ability to achieve a consistent glycoform profile is desired in biopharmaceutical production. In recent times, regulatory agencies including the U.S. Food and Drug Administration (FDA) have suggested a quality by design (QbD) approach to biopharmaceutical manufacture, wherein quality is designed into a drug product through greater understanding of the processes that are used in their manufacture. [32] In the QbD paradigm, a product is produced using process parameters that are maintained within a 'design space', in which the CQA's of a drug product are consistently achieved. In this section the developed $^{12/13}$C$_6$ 2-AA *N*-Glycan UPLC-Fluorescence-MS platform was applied to evaluate changes to the N-glycosylation profile of a mAb that has been produced under bioprocessing conditions that were altered but maintained within typical limits of a design-space for upstream

bioprocessing. Anti-IL8 was produced in CHO DP-12 cells that were prepared in cultures maintained at various pH, temperature and dissolved oxygen (DO) settings as described in Chapter 2, Section 2.2. *N*-glycans released from Protein A-purified mAb produced in each of these cultures were prepared as described in section 4.2.

Method performance of the $^{12/13}C_6$ 2-AA *N*-Glycan UPLC-Fluorescence-MS platform was confirmed using mAb *N*-glycans released from anti-IL8 that had been secreted from CHO DP12 cells cultured using standard conditions (pH 7.0, 85% DO, 37°C). Normalisation was performed based upon the total amount of IgG used for each deglycosylation (250 μg). Five technical replicate pairs were prepared with an expected light heavy ratio of 1:1 for all *N*-glycans. Each technical replicate was analysed using hydrophilic interaction UPLC-fluorescence-MS and the mean and standard deviation of the five technical replicates was determined (data shown in Figure 4.6). Composition of *N*-glycans present in each chromatographic peak was derived from the *m/z* value, expression of the retention time as a glucose unit value and comparison with an in-house database. Acceptable accuracy and precision was established for the five replicate analyses with the expected 1:1 light-heavy ratio obtained for all *N*-glycans annotated with the exception of one species, namely MAN5. MAN5 was present at levels that were too low to facilitate accurate quantitation and hence this species will not be considered for quantitation when reporting *N*-glycan species present in anti-IL8 IgG1 samples. The remaining annotated *N*-glycan species were found to have an average percentage error of <3% (range 1-8%) confirming excellent method performance.
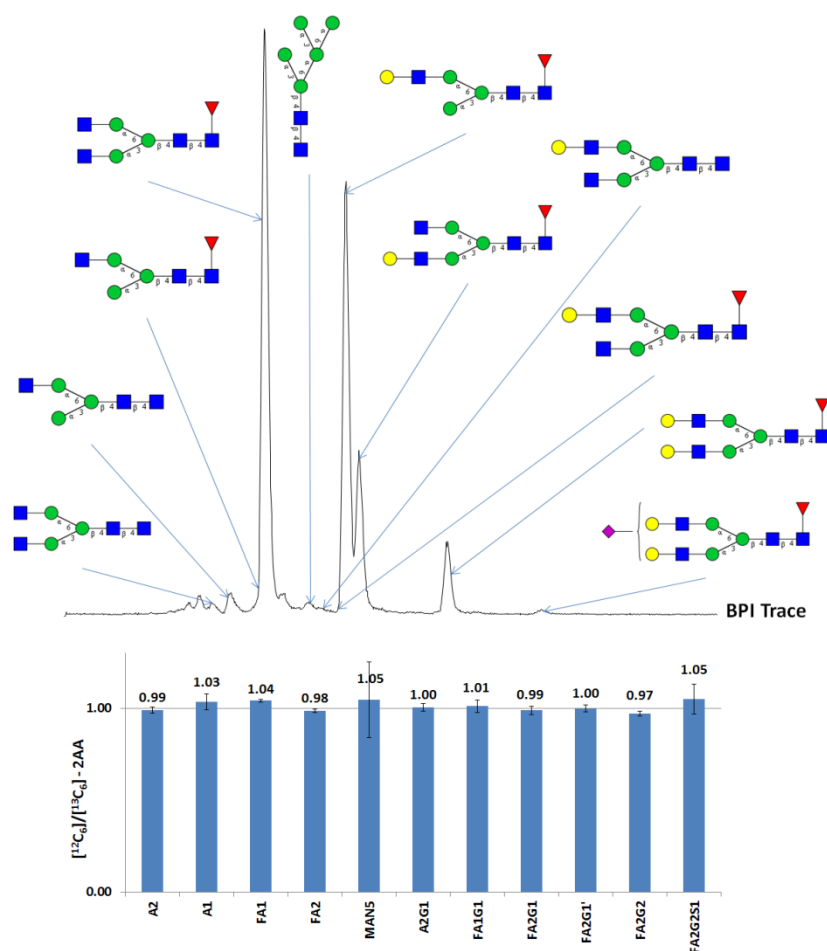
Figure 4.6: Annotated fluorescence and base peak intensity chromatograms for *N*-glycans released from anti-IL8 IgG1. The bar chart underneath the chromatograms depicts the mean light to heavy relative ratio as experimentally determined for the five technical replicates analysed, y-error bars are also included at ± the standard deviation of the five technical replicates.

For each set of anti-IL8 mAb produced, three replicate preparations of the mAb were prepared and labelled using $^{13}C_6$ 2-AA. Each of these was combined with the equivalent amount of mAb produced under standard bioprocessing conditions, labelled using $^{12}C_6$ 2-AA. The pooled *N*-glycan samples were then analysed using UPLC-Fluorescence-MS as described in section 4.2.4. Ten oligosaccharises were annotated and relative quantitation was inferred from the heavy to light ratios for each *N*-glycan structure present. The mean heavy-light ratio for each *N*-glycan, and the standard deviation of the triplicate measurement (displayed in the parenthesis), are presented in Table 4.2.

Distinct differences in the *N*-glycoform profile of anti-IL8 were observed following production in a range of bioprocessing conditions. The most obvious trend in glycoform profile changes were observed for those mAbs that were cultured with increased or decreased pH settings. Anti-IL8 produced in culture maintained at pH 7.2 was found to contain higher levels of galactosylation compared to cultures maintained at pH 7.0, whereas a shift towards decreased galactosylation of glycan chains was observed at pH 6.8. Both cell culture at 39.5°C and also at 110% DO resulted in higher proportions of afucosylated species.

Changes to the levels of therapeutic protein *N*-glycans in response to bioprocessing conditions has been a focus of several studies, most notably for erythropoietin (EPO) producing cell lines due to potential effect on serum half-life of EPO. [2] In this study, the greatest proportion of sialylated *N*-glycans were observed on anti-IL8 mAb produced at pH 7.2 when compared to those secreted at pH 7.0, whereas a reduction in sialylated species was observed for mAb samples produced at a higher temperature (39.5°C) or at higher DO levels (110%). Trummer *et al*. [33] found the highest concentration of sialylated species at pH 7.0, on CHO-produced homodimeric fusion protein Epo-Fc, compared to those produced at higher and lower pH settings. A reduction in sialic acid content of the glycoform profile for EPO under conditions of both reduced temperature (30-35°C) and high dissolved oxygen (70-100%) were also noted. Conversely, Yoon *et al.* [34] detected a decrease in sialic acid content as pH was increased in EPO-producing CHO cultures.

As trends in glycoprofile changes observed herein, and changes in glycan profiles in response to variations in bioprocess conditions reported in the literature do not correlate, it may be suggested that the effects of alterations of various bioprocess parameters are cell line or product dependent rather than exclusively bioprocess dependent. Hence, incorporation of QbD into a final drug product may require a more holistic understanding of the effects of culture process, cell type and the therapeutic protein itself, along with a greater understanding of metabolic pathways to gain physiological insights.

Table 4.2: Relative light to heavy ratios determined for the analysis of anti-IL8 IgG1. *N*-glycan species released from IgG1 cultured under standard conditions with one parameter varied, as outline in the table header information, were labelled using $^{12}C_6$ 2-AA, while those from cultures maintained at standard conditions (37°C, 85% DO, pH7.0) were labelled using $^{13}C_6$ 2-AA.

Glycan Structure	m/z	Altered Bioprocessing Condition					
		High T. mAb (39.5°C)	Low T. mAb (32.0°C)	High pH mAb (pH 7.2)	Low pH mAb (pH 6.8) (pH 6.8)	High DO mAb (110%)	Low DO mAb (65%)
A1	616.230	1.09 (0.09)	0.90 (0.11)	0.98 (0.04)	0.84 (0.02)	1.15 (0.07)	1.01 (0.11)
FA1	689.259	0.82 (0.05)	1.03 (0.05)	0.96 (0.01)	0.78 (0.01)	0.89 (0.01)	1.05 (0.02)
FA1G1	770.285	0.97 (0.10)	0.95 (0.02)	1.16 (0.04)	0.95 (0.03)	0.91 (0.07)	0.92 (0.15)
A2	717.770	1.17 (0.12)	0.93 (0.05)	0.91 (0.02)	0.84 (0.03)	1.21 (0.03)	1.17 (0.15)
FA2	790.799	0.89 (0.04)	1.12 (0.06)	0.87 (0.00)	0.86 (0.01)	0.96 (0.03)	1.16 (0.04)
A2G1	798.796	1.07 (0.04)	0.87 (0.09)	1.11 (0.12)	1.00 (0.02)	1.18 (0.05)	0.82 (0.06)
FA2G1	871.825	0.99 (0.05)	1.08 (0.06)	1.09 (0.01)	0.99 (0.01)	0.95 (0.03)	1.06 (0.03)
FA2G1'	871.825	0.96 (0.06)	1.03 (0.03)	1.13 (0.05)	0.98 (0.04)	1.00 (0.05)	1.04 (0.04)
FA2G2	952.851	1.18 (0.06)	1.02 (0.03)	1.26 (0.02)	1.07 (0.04)	0.92 (0.02)	1.01 (0.04)
FA2G2S1	1098.392	0.83 (0.05)	1.07 (0.17)	1.35 (0.04)	1.09 (0.06)	0.84 (0.07)	1.09 (0.01)

4.4   Conclusions

The development and application of a two-plex method for comparative glycomics of *N*-glycosylation present on mAbs, based upon the differential labelling of samples for comparison with either 'light' $^{12}C_6$ 2-AA or 'heavy' $^{13}C_6$ 2-AA prior to hydrophilic interaction UPLC with sequential fluorescence and accurate mass QToF-MS detection, is described. Optimisation of 2-AA conjugation was investigated followed by an evaluation of the quantitative performance of the $^{12/13}C_6$ 2-AA labeled *N*-glycans. The method was found to be linear, evaluated using reference *N*-glycan standards, and precise with expected light heavy relative ratios of approximately unity determined for six technical replicate analyses of the *N*-

glycans present on polyclonal serum IgG. Application of the method for lot-to-lot comparability analysis of a commercial chimeric IgG1 mAb revealed alterations in the levels of certain glycans, in particular sialylated bi-antennary glycans and glycans bearing galactose α1-3 linked galactose residues between the two drug product lots. Additionally a comparability assessment of anti-IL8 IgG1 *N*-glycan profile in response to conditions of altered bioprocessing using the developed platform revealed changes to the glycoform profile of anti-IL8, notably for galactose-containing *N*-glycans produced in cultures at pH 7.2 and afucosylated species produced in cultures maintained at 110% DO.

The presented method is ideally suited for comparability analyses due to the minimisation of technical variation and operator subjectivity from the analysis, combined with the ability to perform full quantitative structural characterisation of all oligosaccharides, including isomeric species, present in the glycan pool. The method builds on widely used and understood chemistry and concepts but adds an additional dimension through the application of the stable isotope labelling based quantitation. The described platform can be readily employed for physiochemical demonstration of molecular comparability following process or manufacturing changes, or for the assessment of similarity between innovator and biosimilar candidate molecules.

4.5   Associated Publication and Author Contributions

Published in part: Millán Martín, S., et al., *Comparative analysis of monoclonal antibody N-glycosylation using stable isotope labelling and UPLC-fluorescence-MS.* Analyst, 2015, **140**(5): 1442-7.

Research study devised by Amy Farrell, Silvia Millán Martín and Jonathan Bones; Research performed by Amy Farrell, Silvia Millán Martín and Cedric Delporte; Natalia Navas Iglesias provided commercial samples; Data and related paper were reviewed by Jonathan Bones and Niaobh McLoughlin.

4.6 References

1. Nimmerjahn, F. and J.V. Ravetch, *Fcgamma receptors as regulators of immune responses.* Nat Rev Immunol, 2008. **8**(1): p. 34-47.

2. Walsh, G. and R. Jefferis, *Post-translational modifications in the context of therapeutic proteins.* Nat Biotechnol, 2006. **24**(10): p. 1241-52.

3. Zheng, K., C. Bantog, and R. Bayer, *The impact of glycosylation on monoclonal antibody conformation and stability.* MAbs, 2011. **3**(6): p. 568-76.

4. Arnold, J.N., et al., *The impact of glycosylation on the biological function and structure of human immunoglobulins.* Annu Rev Immunol, 2007. **25**: p. 21-50.

5. Krapp, S., et al., *Structural analysis of human IgG-Fc glycoforms reveals a correlation between glycosylation and structural integrity.* J Mol Biol, 2003. **325**(5): p. 979-89.

6. Hodoniczky, J., Y.Z. Zheng, and D.C. James, *Control of recombinant monoclonal antibody effector functions by Fc N-glycan remodeling in vitro.* Biotechnol Prog, 2005. **21**(6): p. 1644-52.

7. Elliott, S., et al., *Enhancement of therapeutic protein in vivo activities through glycoengineering.* Nat Biotechnol, 2003. **21**(4): p. 414-21.

8. International Conference on Harmonisation, 2012, ICH Harmonised Tripartite Guideline, Development and Manufacture of Drug Substances (Chemical Entities and Biotechnological/Biological Entities) Q11. Retrieved 28 May 2016 from http://www.ich.org/fileadmin/Public_Web_Site/ICH_Products/Guidelines/Quality/Q11/Q11_Step_4.pdf.

9. Marino, K., et al., *A systematic approach to protein glycosylation analysis: a path through the maze.* Nat Chem Biol, 2010. **6**(10): p. 713-23.

10. Mittermayr, S., et al., *Multiplexed analytical glycomics: rapid and confident IgG N-glycan structural elucidation.* J Proteome Res, 2011. **10**(8): p. 3820-9.

11. Zauner, G., A.M. Deelder, and M. Wuhrer, *Recent advances in hydrophilic interaction liquid chromatography (HILIC) for structural glycomics.* Electrophoresis, 2011. **32**(24): p. 3456-66.

12.	Boersema, P.J., et al., *Triplex protein quantification based on stable isotope labeling by peptide dimethylation applied to cell and tissue lysates.* Proteomics, 2008. **8**(22): p. 4624-32.

13.	Ong, S.E., et al., *Stable isotope labeling by amino acids in cell culture, SILAC, as a simple and accurate approach to expression proteomics.* Mol Cell Proteomics, 2002. **1**(5): p. 376-86.

14.	Christoforou, A.L. and K.S. Lilley, *Isobaric tagging approaches in quantitative proteomics: the ups and downs.* Anal Bioanal Chem, 2012. **404**(4): p. 1029-37.

15.	Ow, S.Y., et al., *iTRAQ underestimation in simple and complex mixtures: "the good, the bad and the ugly".* J Proteome Res, 2009. **8**(11): p. 5347-55.

16.	Savitski, M.M., et al., *Measuring and managing ratio compression for accurate iTRAQ/TMT quantification.* J Proteome Res, 2013. **12**(8): p. 3586-98.

17.	Alvarez-Manilla, G., et al., *Tools for glycomics: relative quantitation of glycans by isotopic permethylation using 13CH3I.* Glycobiology, 2007. **17**(7): p. 677-87.

18.	Kang, P., et al., *Comparative glycomic mapping through quantitative permethylation and stable-isotope labeling.* Anal Chem, 2007. **79**(16): p. 6064-73.

19.	Hu, Y., J.L. Desantos-Garcia, and Y. Mechref, *Comparative glycomic profiling of isotopically permethylated N-glycans by liquid chromatography/electrospray ionization mass spectrometry.* Rapid Commun Mass Spectrom, 2013. **27**(8): p. 865-77.

20.	Atwood, J.A., 3rd, et al., *Quantitation by isobaric labeling: applications to glycomics.* J Proteome Res, 2008. **7**(1): p. 367-74.

21.	Botelho, J.C., et al., *Quantification by isobaric labeling (QUIBL) for the comparative glycomic study of O-linked glycans.* International Journal of Mass Spectrometry, 2008. **278**: p. 137–142.

22.	Gimenez, E., V. Sanz-Nebot, and A. Rizzi, *Relative quantitation of glycosylation variants by stable isotope labeling of enzymatically released N-glycans using [12C]/[13C] aniline and ZIC-HILIC-ESI-TOF-MS.* Anal Bioanal Chem, 2013. **405**(23): p. 7307-19.

23.	Hitchcock, A.M., C.E. Costello, and J. Zaia, *Glycoform quantification of chondroitin/dermatan sulfate using a liquid chromatography-tandem mass spectrometry platform.* Biochemistry, 2006. **45**(7): p. 2350-61.

24. Hitchcock, A.M., et al., *Optimized extraction of glycosaminoglycans from normal and osteoarthritic cartilage for glycomics profiling.* Glycobiology, 2007. **17**(1): p. 25-35.

25. Prien, J.M., et al., *Mass spectrometric-based stable isotopic 2-aminobenzoic acid glycan mapping for rapid glycan screening of biotherapeutics.* Anal Chem, 2010. **82**(4): p. 1498-508.

26. Tep, S., M. Hincapie, and W.S. Hancock, *The characterization and quantitation of glycomic changes in CHO cells during a bioreactor campaign.* Biotechnol Bioeng, 2012. **109**(12): p. 3007-17.

27. Tep, S., M. Hincapie, and W.S. Hancock, *A general approach for the purification and quantitative glycomic analysis of human plasma.* Anal Bioanal Chem, 2012. **402**(9): p. 2687-700.

28. Xia, B., et al., *Glycan reductive isotope labeling for quantitative glycomics.* Anal Biochem, 2009. **387**(2): p. 162-70.

29. Yuan, J., et al., *Isotope tag method for quantitative analysis of carbohydrates by liquid chromatography-mass spectrometry.* J Chromatogr A, 2005. **1067**(1-2): p. 145-152.

30. Reid, C.Q., et al., *Rapid whole monoclonal antibody analysis by mass spectrometry: An ultra scale-down study of the effect of harvesting by centrifugation on the post-translational modification profile.* Biotechnol Bioeng, 2010. **107**(1): p. 85-95.

31. Schiestl, M., et al., *Acceptable changes in quality attributes of glycosylated biopharmaceuticals.* Nat Biotechnol, 2011. **29**(4): p. 310-2.

32. Rathore, A.S. and H. Winkle, *Quality by design for biopharmaceuticals.* Nat Biotechnol, 2009. **27**(1): p. 26-34.

33. Trummer, E., et al., *Process parameter shifting: Part I. Effect of DOT, pH, and temperature on the performance of Epo-Fc expressing CHO cells cultivated in controlled batch bioreactors.* Biotechnol Bioeng, 2006. **94**(6): p. 1033-44.

34. Yoon, S.K., et al., *Effect of culture pH on erythropoietin production by Chinese hamster ovary cells grown in suspension at 32.5 and 37.0 degrees C.* Biotechnol Bioeng, 2005. **89**(3): p. 345-56.

5.0

Structural and Functional Characterisation of Monoclonal Antibodies Following Production under Altered Bioprocessing Conditions

5.1   Introduction

Therapeutic monoclonal antibodies (mAbs) are large, complex macromolecules, consisting of thousands of atoms intricately connected to form unique three-dimensional structures. Conformation of protein higher order structure may have a profound effect on the mAb function as conformational changes have the potential to alter the accessibility of binding sites to cellular or antigen targets. Protein structure is maintained by various interactions, including hydrogen bonds and electrostatic forces, which impart significant structural flexibility enabling dynamic motion in solution. [1] Sequence-level protein modifications may interrupt the interactions that are critical to protein structure and, hence, may affect the functional activity of mAbs *in-vivo*. In particular, changes to mAb higher order structure may alter the accessibility of the Fc binding site, responsible for non-antigen binding activity and *in vivo* half-life, or similarly may modify the complementarity-determining regions (CDRs) leading to a reduction in antigen binding affinity, ultimately affecting potency and therapeutic efficacy of mAbs. Consequently, in addition to primary sequence characterisation, elucidation of the structure and structure-function relationship for a protein should be determined during product or bioprocess development, when evaluating biosimilar therapeutic proteins or following changes to a bioprocess. [2] Regulatory agencies recommend for comparability purposes, that an attempt should be made to determine the higher order structure of a protein. Alternatively if structural characterisation is not possible, changes to a protein tertiary structure should be assessed by determining the biological activity of the therapeutic drug substance. [3]

Numerous techniques are available for structural characterisation of proteins, including the well-established nuclear magnetic resonance (NMR) spectroscopy [4, 5] and X-ray crystallography. [6] Although widely applied, practical limitations exist for the application of

NMR to intact protein characterisation, including difficult spectral annotation attributed to the large molecule size and a requirement for isotopic labelling. [7] X-ray crystallography applications may be limited due to the necessity for generation of antibody crystals and also resulting from reservations regarding the impact of complex sample preparation buffers on the protein under analysis. [8] Other biophysical characterisation techniques are available, including analytical ultracentrifugation (AUC), size exclusion chromatography (SEC), differential scanning calorimetry and circular dichroism. [8] However these methods only provide limited data and are incapable of providing information regarding the location of a change on a protein molecule or of identifying subtle alterations to a protein's higher order structure. Hydrogen deuterium exchange mass spectrometry (HDX-MS) has become an increasingly popular alternative technique for determination of protein structure. Backbone amide hydrogen's located at the surface of the protein or involved in weak hydrogen bonds exchange rapidly with deuterium when place in a deuterated solvent, whereas those contained within the interior of the protein structure or forming stabilising hydrogen bonds exchange at a much slower rate. [9] Following HDX, the labelling reaction may be quenched using a low pH denaturation buffer and the protein digested by means of an acid-resistant protease (*e.g.* pepsin). Analysis of resulting peptides is performed using a rapid liquid chromatography separation method followed by mass spectrometry detection for evaluation of deuterium uptake and hence determination of protein tertiary structure. A typical HDX-MS workflow is illustrated in Figure 5.1.

Analysis of chemical composition (amino acid sequence) and higher order structure may provide extensive information regarding potential changes to a therapeutic mAb, *e.g.* in response to bioprocess changes or for biosimilar comparability. However, to fully characterise a mAb the functional capabilities of the protein must also be assessed. Antibody therapeutics may be classified as having two general mechanisms of action. Therapeutic mAbs may exert their effect by binding directly to their cellular target (*e.g.* cell surface tumour antigens), thereby enabling immune mediated effects to take place. Alternatively, mAbs may be directed against soluble molecules (*e.g.* cytokines) and function by binding to and inhibiting the action of the target molecule. [10] In this work, a humanised anti-interleukin 8 (anti-IL8) IgG1 was produced from CHO DP-12 culture. Anti-IL8 IgG1 functions in humans by binding to the cytokine interleukin-8 forming a complex which may be recognised by the immune system thereby facilitating clearance from the body. Hence, for anti-IL8 IgG1 to produce a pharmacological effect, the antibody must be allowed to circulate for a sufficient period of time in human serum. Fortuitously, the success of IgG1 mAbs as drug therapies may in part be attributed to a long serum half-life in humans as a result of their ability to bind to the neonatal

Fc receptor (FcRn), a soluble receptor expressed by cells of endothelial, epithelial and myeloid lineages. [11, 12] Binding of IgG1 to FcRn is exquisitely pH dependent: FcRn forms a complex with IgG1 at acidic pH (<pH 6.5) protecting mAbs from degradation inside the endosomal compartment and facilitating recycling of the mAb to the cell surface, where upon the FcRn-IgG1 complex dissociates at neutral pH (or higher). [13] Many new drug therapies, *e.g.* antibody drug conjugates and Fc-fusion proteins, have been engineered to exploit the high binding specificity of FcRn-IgG1 and hence, create a long serum half-life. [14, 15]

FcRn-IgG binding has also been widely applied for the evaluation of IgG antibody pharmacokinetics in drug development, to estimate the serum half-life of new drug products and for comparability assessment of mAbs following process changes. [16, 17]   Different analytical strategies exist for the determination of IgG binding and function, including cell-based assays or ligand binding assays. As a general rule-of-thumb, mAbs that function by binding to cellular targets are usually assessed using cell based assays while those that interact with soluble receptors are determined using a technique based on ligand binding wherein ligand interaction is normally the first step in protein-induced cellular response. [18] Since anti-IL8 IgG1 functions by binding to soluble interleukin-8, and is circulated in the body as a result of binding to soluble FcRn receptors, determination of ligand binding is an appropriate strategy to investigate its functional activity. Surface plasmon resonance (SPR) biosensor binding assays are widely applied for the determination of mAb functional activity. In SPR, changes in reflected polarised light are measured following binding of analytes to ligands embedded in a dextran matrix on the surface of a gold plated sensor chip. [19] Using SPR the rate of association and dissociation of an antigen to a mAb and also their binding affinity may be assessed. Thus, structural alterations to a therapeutic protein impacting antigen binding, which transpire following environmental changes, degradation or exist between biosimilar products, may be identified by measuring the binding affinity or binding rates of the therapeutic protein.

In this chapter, potential changes to the structural conformation and the function of anti-IL8 mAb produced from CHO DP-12 cells under conditions of altered bioprocessing, as outlined in Chapter 2 (pH, temperature, dissolved oxygen (DO)), are investigated. HDX-MS^E is applied to identify which regions, if any, of the mAb higher order structure are potentially altered as a result of variations in bioprocessing parameters. In addition SPR-based binding assays are applied to determine potential changes to serum half-life caused by culture under different conditions by evaluating the binding affinity of FcRn to differentially cultured mAbs.

Additionally, by determining the binding dynamics of anti-IL8 IgG1 to interleukin 8, possible changes to the function of anti-IL8 mAbs are evaluated.

5.2   Experimental

5.2.1   Reagents and Consumables

Deuterium oxide (D_2O), Deuterium chloride (DCl), Potassium phosphate dibasic, Potassium phosphate monobasic, Tris(2-carboxyethyl)phosphine (TCEP), Guanidine hydrochloride, Hydrochloric acid, [Glu^1]-Fibrinopeptide B, Monosodium phosphate monohydrate, Tris(hydroxymethyl)-aminomethane (Tris), Sodium chloride (NaCl), Acetonitrile, Formic acid and Methanol were obtained from Sigma Aldrich (Wicklow, Ireland). Sodium iodide and Leucine enkephalin were received from Waters (Dublin, Ireland). Water, 0.1% formic acid (LC-MS Optima), Acetonitrile, 0.1% formic acid (LC-MS Optima), and Water, 0.1% TFA (LC-MS Optima) were obtained from Fisher Scientific (Dublin, Ireland). Recombinant human CXCL8/IL-8 protein and Recombinant human FcRn protein were purchased from R&D systems (Minnesota, USA). Biacore series S sensor chip CM5, Biacore series S Protein A sensor chip, 10 mM sodium acetate, pH 5.0, Glycine-hydrochloride, HBS-EP+ buffer and amine coupling reagents (1-ethyl-3-(3-dimethylaminopropyl)carbodimide hydrochloride (EDC), N-hydroxysuccinimide (NHS) and 1.0 M ethanolamine-HCL pH 8.5) were obtained from GE Healthcare (Dublin, Ireland).

5.2.2   Hydrogen-Deuterium Exchange Mass Spectrometry

Hydrogen-Deuterium Exchange Mass Spectrometry (HDX-MS) was performed using a nanoAcquity UPLC M-class system with a LEAP HDX automation manager coupled to a Waters Synapt G2 HDMS QToF. The HDX-MS platform was equipped with an Enzymate BEH pepsin column, 2.1 x 30 mm (Waters), an Acquity UPLC BEH C18 1.7 μm VanGuard Pre-Column, 2.1 x 5 mm (Waters) and an Acquity UPLC BEH C18 1.7 μm, 1.0 x 100 mm analytical column (Waters). Purified anti-IL8 IgG1 produced under conditions of altered bioprocessing (Section 2.2.2.5) and later purified and quantified (Section 3.2.2) were diluted to a concentration of 5 mg. mL^{-1} in 10 mM potassium phosphate, pH 7.0. For each labelling time point, 4.8 μL of anti-IL8 IgG1 was diluted with 20-fold 10 mM potassium phosphate in D_2O, pH 6.6 at room temperature and incubated for a pre-defined time (20 s, 1 min, 2 min, 10 min, 30 min, 1 hr, 2 hr, 4 hr). Following incubation, the reaction was quenched by the addition of 50 mM

potassium phosphate, 2 M guanidine-HCl, 200 mM TCEP, pH 2.30 before on-line pepsin digestion. The digestion temperature was set to 20°C. All subsequent chromatographic separations were performed in a cooling chamber maintained at 0.0 ± 0.1°C to prevent back exchange of deuterium. To minimise carry-over between each sample preparation, a blank injection and a pepsin column wash, using 1.5 M guanidine-HCl, 4% acetonitrile, 0.8% formic acid, 200 mM TCEP, pH 2.5, were performed.

Eluting peptides were loaded *via* trapping column for 3 minutes at 200 µL.min⁻¹, using an isocratic gradient of 0.1% (v/v) formic acid in water (A) and 0.1% (v/v) formic acid in acetonitrile (B). Peptides were subsequently directly sampled onto a C_{18} analytical column and separated using the following gradient conditions: 5% to 35% B in 6 minutes, followed by a further increase to 95% B over 1 minute and a 3 minute isocratic hold. Subsequently the column was washed three times by decreasing mobile phase composition to 5% B in 1 minute followed by increase to 95% B. Initial conditions were restored in one minute and held for an additional 2 minutes to ensure column re-equilibration. The flow rate was 40 µL.min⁻¹. Eluate from the chromatographic system was sampled directly into a Synapt G2 HDMS QTof mass spectrometer (Millford, MA, USA) *via* an electrospray ion source. The mass spectrometer was operated in positive ion data independent resolution mode with 0.3 second sequential low and high energy scans in the range of 50 to 2,000 Da. The spray voltage was 3 kV. A collision energy ramp from 15 to 35 V was used for the high energy function. Glu-fibrinopeptide (m/z 785.8426, z=2) was used as lockmass solution, recorded at 30 second intervals. Non-deuterated control experiments were also carried out to identify all peptides produced during enzymatic digestion.

Following analysis unlabelled samples were processed using ProteinLynx Global Server software (PLGS, version 3.0.1) for identification of sample peptides. Workflow parameters used include automatic peptide and fragment tolerances with lockmass correction of all doubly charged masses, minimum number of fragment ion matches per peptide = 2, minimum number of fragment ion matches per protein = 5, minimum number of unique peptides per protein = 1, primary digest reagent trypsin, with maximum number of one missed cleavage, fixed modification: carbamidomethyl C, variable modifications: oxidation M, deamidation N and deamidation Q, false discovery rate maintained at 1% FDR. Data was searched against a fasta file composed of known mAb sequence described in US patent 6117980 A. [20] All HDX-MS data were processed using DynamX® HDX data analysis software version 3.0.0 (Waters) with additional manual verification of the raw spectra. DynamX® is a software tool designed to automate visualisation and sorting of data acquired using a Waters HDX-MS platform. The

following settings were used for filtering of the data: minimum intensity of 1000, minimum sequence length of 6, maximum sequence length of 30, file threshold = 3 and retention time RSD of 5%. Deuterium uptake for each peptide was calculated by subtracting the centroid of the isotopic distribution for non-labelled peptide ions from the centroid of the isotopic distribution for peptide ions for each deuterated sample. A minimum sequence coverage of 70% and average redundancy of <5 was required for all data. HDX comparability profiles were plotted using an algorithm developed by Houde *et al.* incorporated into DynamX software. [1]

5.2.3   Surface Plasmon Resonance

All SPR experiments were carried out on a Biacore T100 instrument (GE Healthcare, Uppsala, Sweden) using Biacore T100 Control Software version 2.0.4. Processing of acquired data was perfumed using Biacore Evaluation software version 2.0.4.

5.2.3.1 Determination of FcRn-Anti-IL8 Binding Affinity

Standard amine coupling was performed to immobilise FcRn on to the surface of a Series S CM5 chip. Briefly, the dextran surface of two flow cells was activated by injecting a 1:1 solution of EDC/NHS for 420 s at 10 μL.min^{-1}. FcRn molecules were diluted to 2.5 μg.mL^{-1} in 10 mM sodium acetate, pH 5.0 and injected at a flow rate of 5 μL.min^{-1} (onto the test flow cell only) until the target response level of 500 RU was reached. Subsequently, the surface of both flow cells was blocked by injecting 1 M ethanolamine pH 8.5 for 420 s at 10 μL.min^{-1}. The running buffer, 50 mM sodium phosphate/150 mM NaCl, pH 6.0, was allowed to flow at a rate of 30 μL.min^{-1}. For each anti-IL8 sample studied, a range of concentrations of the mAb were prepared in triplicate in running buffer (0, 10, 25, 50, 100, 150 and 200 μg.mL^{-1}) and injected at 25°C using a multi-cycle approach. Regeneration of the immobilised FcRn surface was achieved following each mAb sample introduction using 100 mM Tris/200 mM NaCl, pH 8.0, injected for 60 seconds at 30 μL.min^{-1}. For each analysis, the response was calculated at a position 4 seconds before the injection stop, with a 5 second window. A steady state affinity fit model was applied for determination of the dissociation constant.

5.2.3.2 Evaluation of Anti-IL8 – Interleukin 8 Binding Kinetics

A Series S Protein A chip was utilised for the determination of changes to the binding kinetics of anti-IL8 IgG1 to the cytokine interleukin-8 using a single-cycle kinetics procedure. Before use the Protein A chip was primed with HBS-EP+ running buffer and conditioned *via* triplicate injection of 10 mM glycine, pH 1.5 for 60 seconds using a flow rate of 30 µL.min^{-1}. For each analysis, a 10 µg.mL^{-1} solution of mAb was passed over the active sample flow cell for 30 s at 5 µL.min^{-1} to enable capture of the protein on the protein A chip surface. Interleukin 8, prepared at a range of concentrations (0.625, 1.25, 2.5, 5 and 10 nM), was then injected in order of increasing concentration over reference and active flow cell using five 150 s injections at 30 µL.min^{-1}, applying a single cycle kinetics approach. [21] Following the final interleukin-8 injection, a 1200 s dissociation time was applied. Regeneration of the chip surface was achieved using a 30 s injection of 10 mM glycine, pH 1.5 at 30 µL.min^{-1}. Data was referenced by subtraction of the response from the reference flow cell before kinetic fit analysis was performed *via* Biacore Evaluation software using a 1:1 binding fit model.

5.3   Results and Discussion

5.3.1   HDX-MS

Hydrogen/deuterium exchange-mass spectrometry (HDX-MS) is a useful method for structural characterisation of therapeutic mAbs, as it may potentially generate information regarding locations of conformation differences and conformational dynamics of proteins in solution. [1, 22-27] By monitoring the HDX of a protein's backbone amide hydrogen for deuterium as a function of time, information regarding the protein structure and conformation in solution may be deduced. HDX-MS poses a number of significant analytical challenges. Firstly, due to the labile nature of the deuterium label, a quenching step must be incorporated into the analytical workflow to ensure no back-exchange of deuterium occurs. Frequently, the HDX reaction is quenched *via* a reduction in solution temperature and pH (<pH 3) as other methods such as use of organic solvents may be incompatible with biomolecules or with subsequent analytical steps. [28-30] Secondly, protein digestion must be performed under quench conditions; hence a protease that exhibits activity at low temperature and in low pH conditions is required. Pepsin fulfils these criteria, while additionally enabling automation of HDX-MS experiments as it is commercially available immobilised on analytical columns. However, sequence coverage obtained following MS analyses of peptic digests can be suboptimal depending on conditions used (*e.g.* temperature, exposure time, enzyme-protein

ratio) and most importantly on the protein itself. [31] Unlike other frequently used proteases for sample preparation prior to MS analyses (*e.g.* Trypsin, Lys-C, Asp-N) pepsin does not cleave with high specificity. [31, 32] Although pepsin tends to cleave after bulky hydrophobic amino acid residues (*e.g.* phenylalanine), the digestion pattern of pepsin is reportedly most influenced by the molten globule conformation of a protein in acidic conditions. [31] Various approaches to improving sequence coverage achievable have been reported, including the use of denaturants (*e.g.* guanidine hydrochloride) and reducing agents (*e.g.* TCEP), and increasing back pressure to facilitate enhanced digestion efficiency. [30, 33] In this study, HDX-MS was employed for the comparative structural evaluation of anti-IL8 IgG1 following production using a variety of bioprocessing conditions frequently used in therapeutic Chinese hamster ovary (CHO) cell culture (described in Chapter 2). Conformational changes in protein therapeutics are reportedly triggered by a variety of factors including chemical modification, thermal or pH denaturation and mutation caused by disparities in bioprocessing and may occur with or without a change in primary structure. [9] Hence, by determination of protein high order structure for each anti-IL8 IgG1 sample produced, potential changes to mAb tertiary structure caused by alterations in bioprocessing may be deduced. For each mAb sample analysed, triplicate HDX samples were prepared for each time-point, digested and separated using a short chromatographic gradient before undergoing MS^E analysis, as described in Section 5.2.2. Data generated was subsequently analysed for determination of changes to the mass of peptides in samples exposed to deuterated buffer for increasing periods of time. Peptides found to have exchanged deuterium in place of hydrogen atoms produced a MS spectrum showing distinctive mass shifts corresponding to the levels of deuterium incorporated into each peptide, as shown in Figure 5.2.
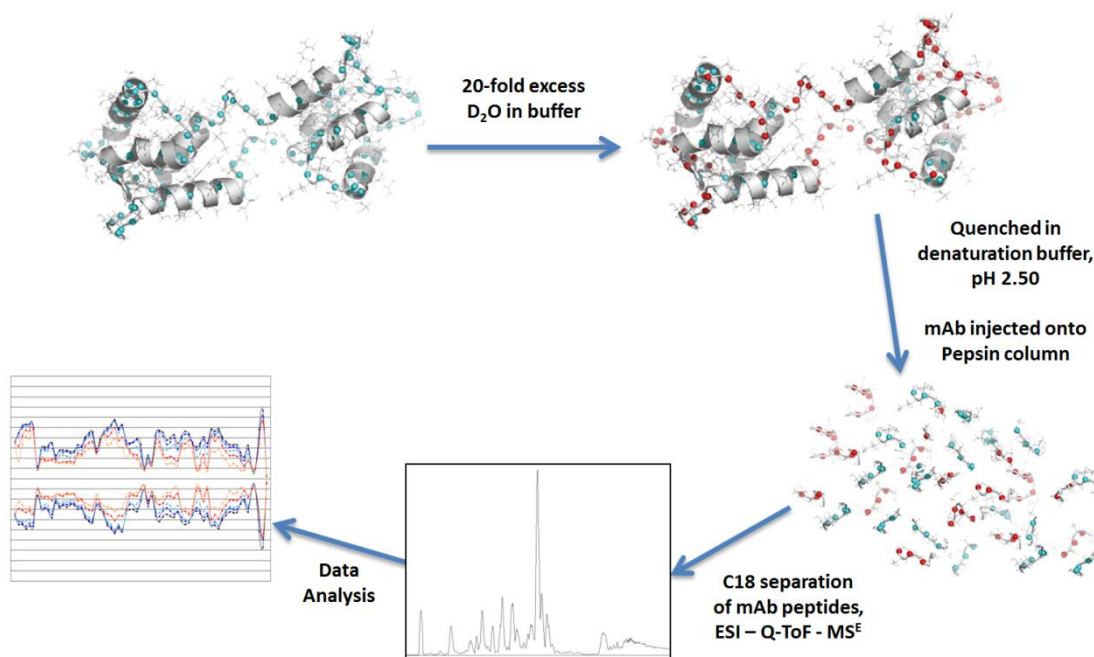
Figure 5.1: Typical HDX-MS workflow, adapted from [30]. Proteins in solution at room temperature are diluted in excess deuterated solution and HDX is allowed to occur for a specified amount of time before the reaction is quenched in a low pH denaturation buffer. Protein sample is then injected into a pepsin column for low temperature digestion. Resultant peptides are separated using a fast separation gradient and detected *via* mass spectrometry. Finally the mass shift of analysed peptides due to deuterium uptake is determined and information regarding higher order structure of the protein may be deduced.
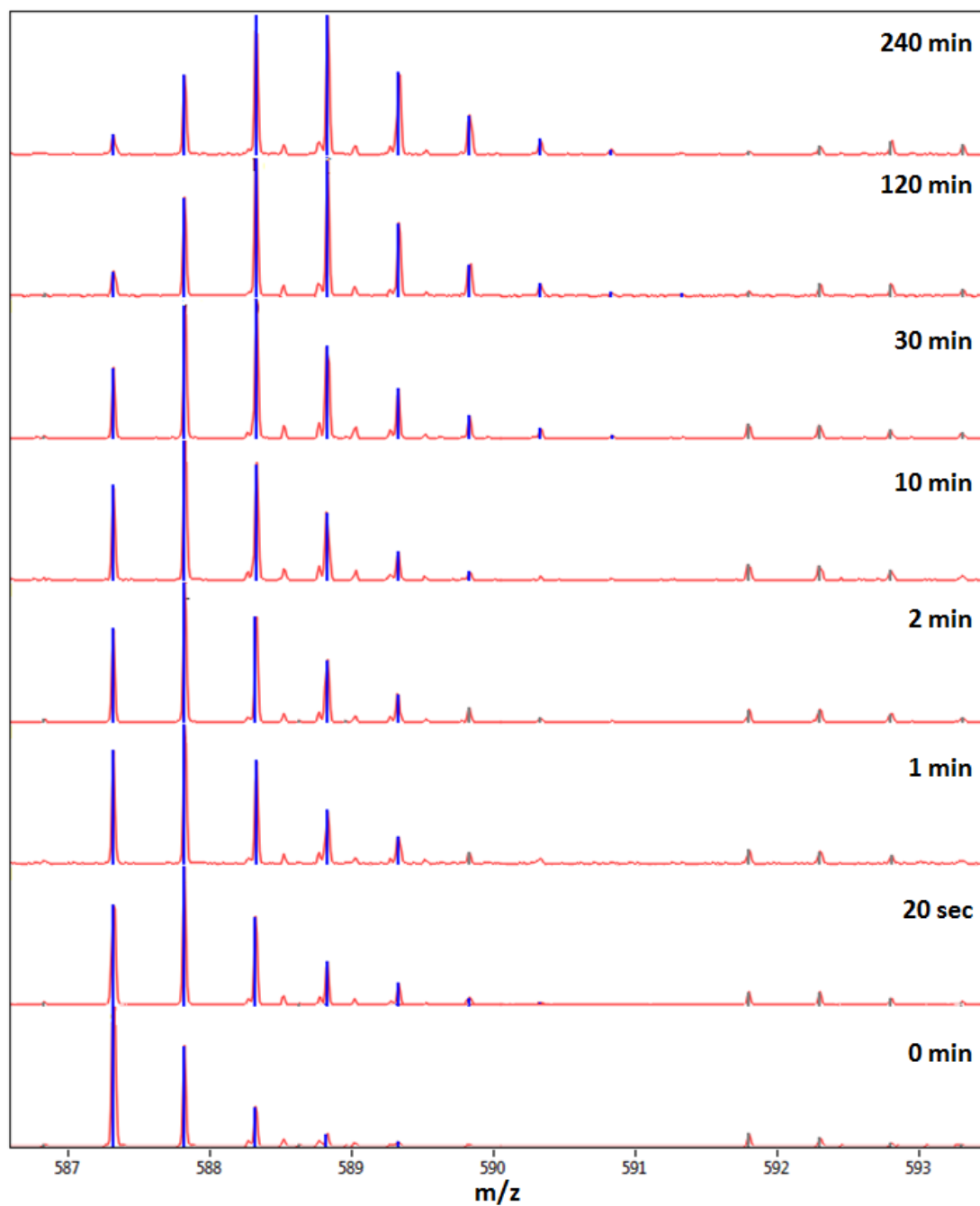
Figure 5.2: Deuterium uptake chart for FPPKPKDTLM (low temperature mAb - one MS spectrum from each time-point only is shown for brevity). Each IgG1 sample analysed was exposed to deuterated buffer for different lengths of time ranging from 0 to 240 minutes, before undergoing proteolysis and MS analysis. MS spectra corresponding to the same peptide (FPPKPKDTLM) determined in the same sample that had been exposed to deuterated buffer for various durations are shown. A characteristic mass shift is observed in the spectra following HDX corresponding to the increased peptide mass, resulting from the replacement of the peptide's backbone amide hydrogen atoms with deuterium.

Initial experiments resulted in poor mAb digestion efficiencies for samples analysed (~65% sequence coverage for mAb light chain, ~70% sequence coverage for mAb heavy chain). To ensure as broad coverage as possible for the mAb samples studied, optimisation of the experimental platform was achieved by increasing the TCEP concentration of the quench buffer from 50 M to 200 M, increasing the digestion temperature from 15°C to 20°C and by placing a BEH C18, 1.7 μm, 2.1 x 50 mm analytical column on the UPLC waste line for the purposes of increasing back-pressure to the pepsin column. Following these modifications the sequence coverage achievable was increased to >72% for mAb light chain and >83% for mAb heavy chain. Similar peptides were generated across all experiments, showing reproducible peptic digestion profiles for anti-IL8 IgG1 within different sample preparations; sequence coverage maps displaying peptides produced are shown in Figures 5.3 to 5.5. In each experiment, a minimum of 147 peptic peptides were unambiguously identified with a maximum redundancy of 4.12, representing a minimum of 72.6% of the total light chain and 81.2% of the total heavy chain amino acid sequence for anti-IL8 IgG1.
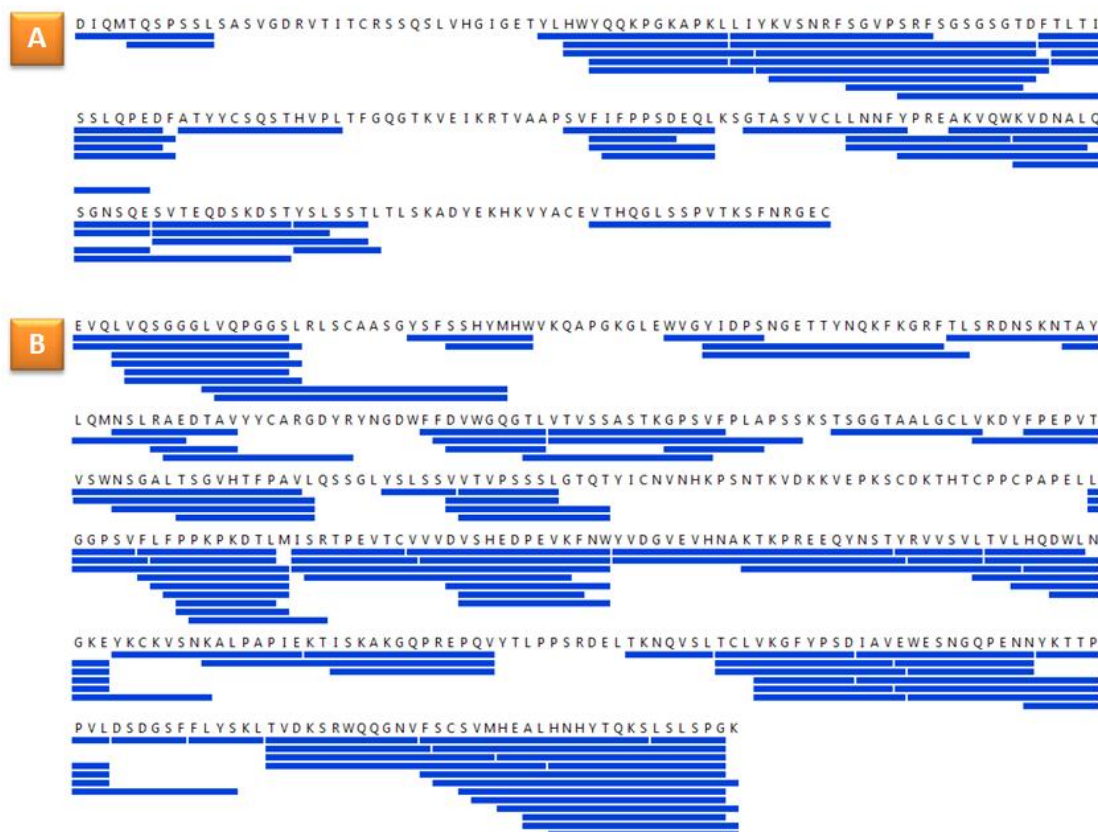
Figure 5.3: Peptic peptides identified across all experiments for anti-IL8 IgG1 produced at standard conditions, 110% DO and 60% DO in mAb **A.** light chain and **B.** heavy chain. Each peptide is represented by a blue bar.
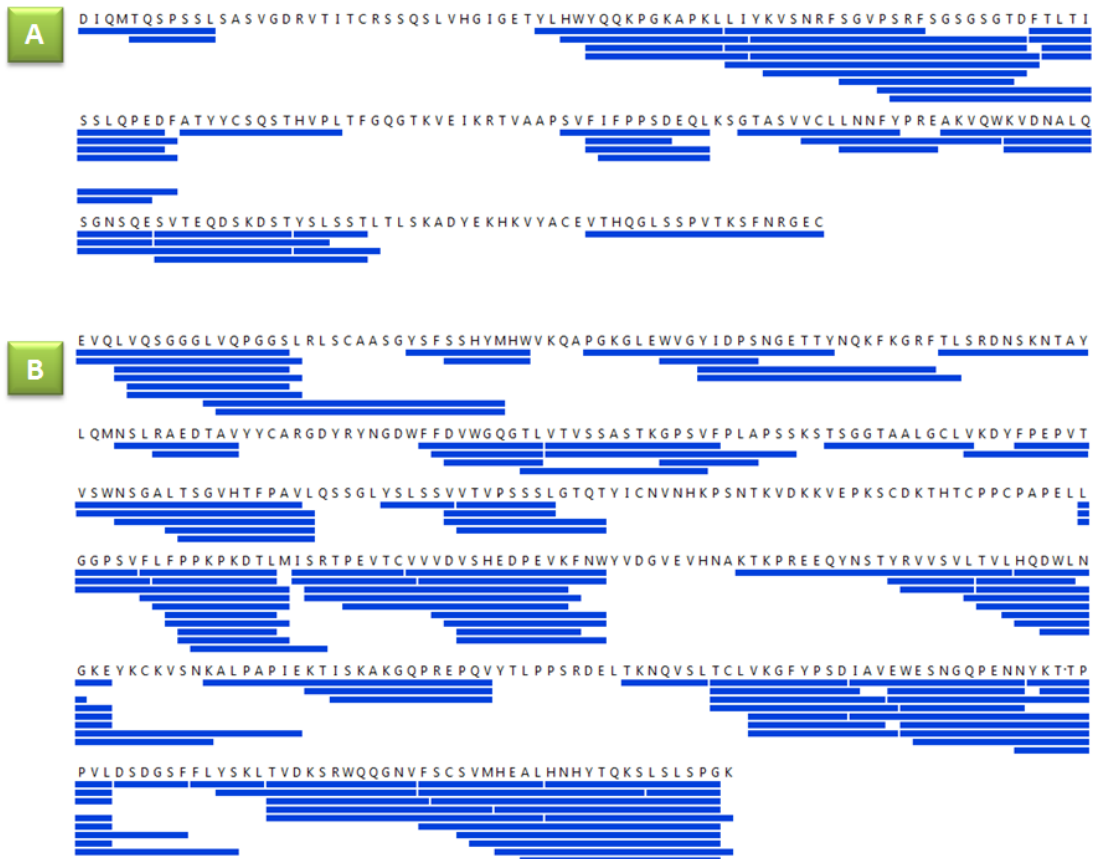
Figure 5.4: Peptic peptides identified across all experiments for anti-IL8 IgG1 produced at standard conditions, pH 7.2 and pH 6.8 in mAb **A.** light chain and **B.** heavy chain. Each peptide is represented by a blue bar.

Figure 5.5: Peptic peptides identified across all experiments for anti-IL8 IgG1 produced at

standard conditions, 32.0°C and 39.5°C in mAb **A.** light chain and **B.** heavy chain. Each peptide is represented by a blue bar.

The relative fractional uptake of deuterium for peptides produced from mAb cultures from each study (*i.e.* DO, pH and temperature study cultures) at each time-point was determined by comparison of the centroid mass from peptides produced at each time-point to the mass of un-deuterated peptide ions. To evaluate deuterium incorporation in different parts of the mAb structure, heat maps and mirror plots showing the relative fractional uptake of deuterium for a particular peptide as a function of time were generated. Figures 5.6 to 5.8 show corresponding heat-maps for each study. Peptides that are enclosed within the protein structure and therefore, not exposed to deuterium do not undergo HDX and, hence, do not exhibit an increase in relative fractional uptake for deuterium over-time. Conversely peptides on the outer part of the mAb higher order structure readily exchange their backbone amide hydrogen atoms for deuterium and thus display a high deuterium fractional uptake relative to un-deuterated samples. Finally, peptides that are partially exposed to the deuterated buffer undergo a slower rate of HDX and hence produce a relative fractional uptake profile wherein the uptake of deuterium is observed to increase as a function of time. Heat maps corresponding to anti-IL8 produced in each study clearly visualise the regions of the mAb that are encased within the protein structure as these show poor uptake of deuterium overall the time-points analysed, appearing as green in the heat maps, whereas portions of IgG1 that comprise the outer part of the structure readily incorporate deuterium across the time-points and are displayed in red. Portions of mAb that are partially enclosed within the mAb higher order structure display increased deuterium uptake over time, displayed as changing colour over time according to the scale shown in the corresponding figures.
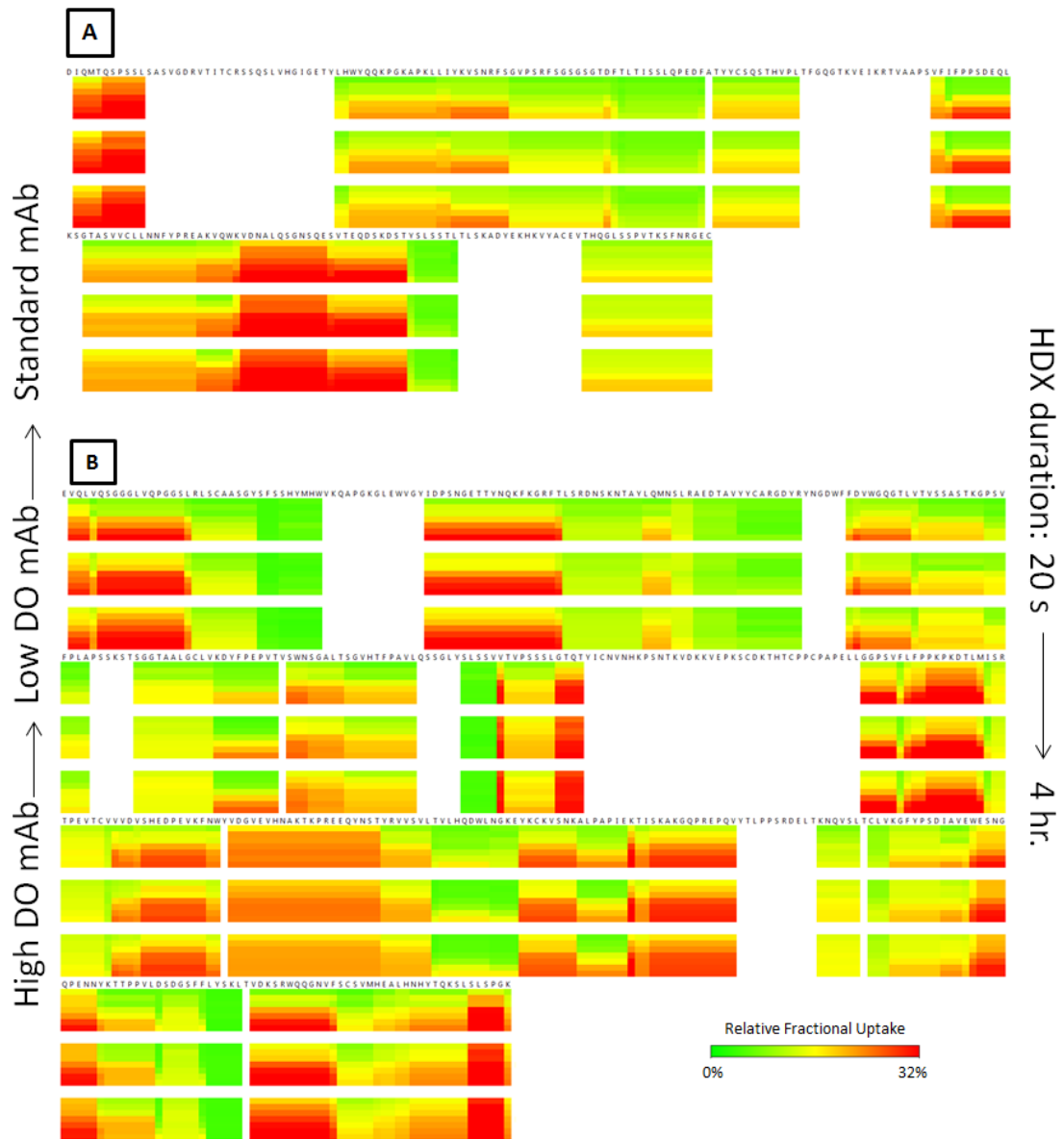
Figure 5.6: Relative fractional uptake of deuterium for **A.** light chain and **B.** heavy chain anti-IL8, produced under standard (85% DO), low DO (60% DO) and high DO (110% DO) bioprocess conditions.
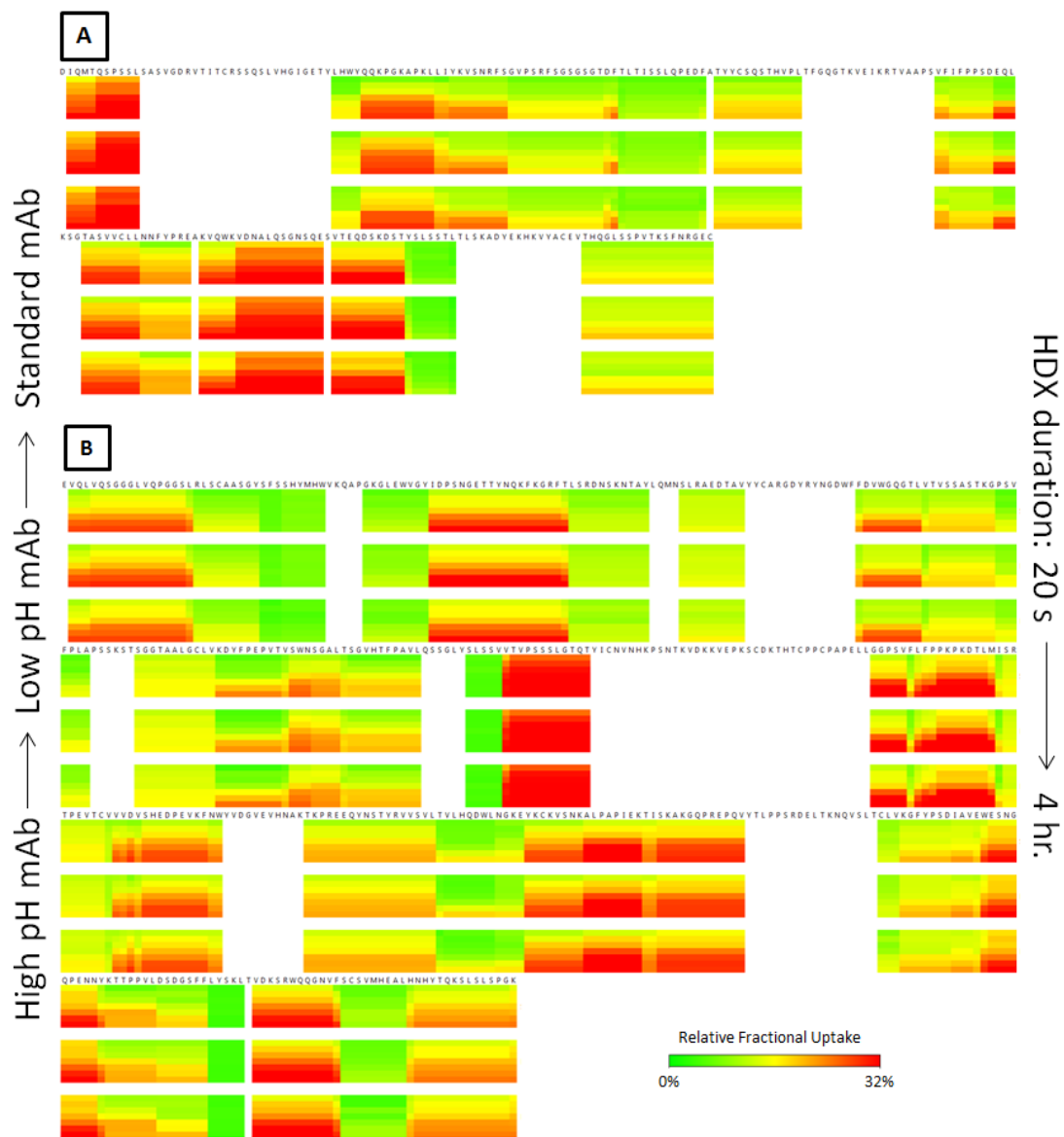
Figure 5.7: Relative fractional uptake of deuterium for **A.** light chain and **B.** heavy chain anti-IL8, produced under standard (pH 7.0), low pH (pH 6.8) and high pH (pH 7.2) bioprocess conditions.
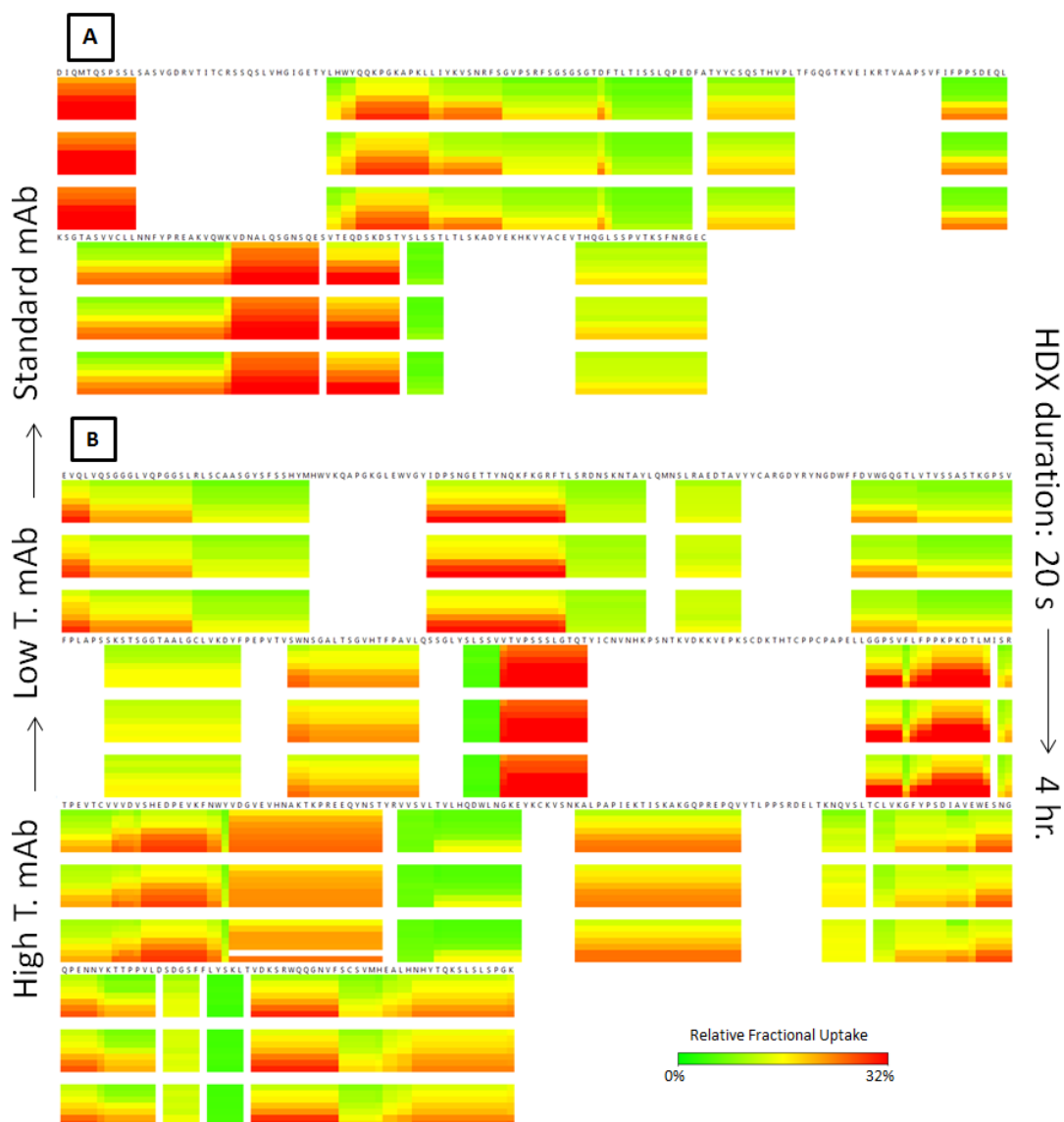
Figure 5.8: Relative fractional uptake of deuterium for **A.** light chain and **B.** heavy chain anti-IL8, produced under standard (37.0°C), low temperature (32.0°C) and high temperature (39.5°C) bioprocess conditions.

Figures 5.9 to 5.14 show mirror plots depicting the average relative fractional uptake for heavy or light chain mAb from each condition compared to standard mAb that was produced during the same production run. In all mirror plots the horizontal axis denotes each peptide, shown as differentially coloured dots each colour representing the duration of HDX as shown in the accompanying legend, sorted in ascending order from the N-terminus to the C-terminus for each mAb chain. Distance from the mid-point represents increased deuterium uptake, described as the ratio of the mass of the deuterated peptide relative to the mass of the corresponding un-deuterated sample. The grey area depicts the standard deviation for relative fractional uptake for each peptide across all time-points.
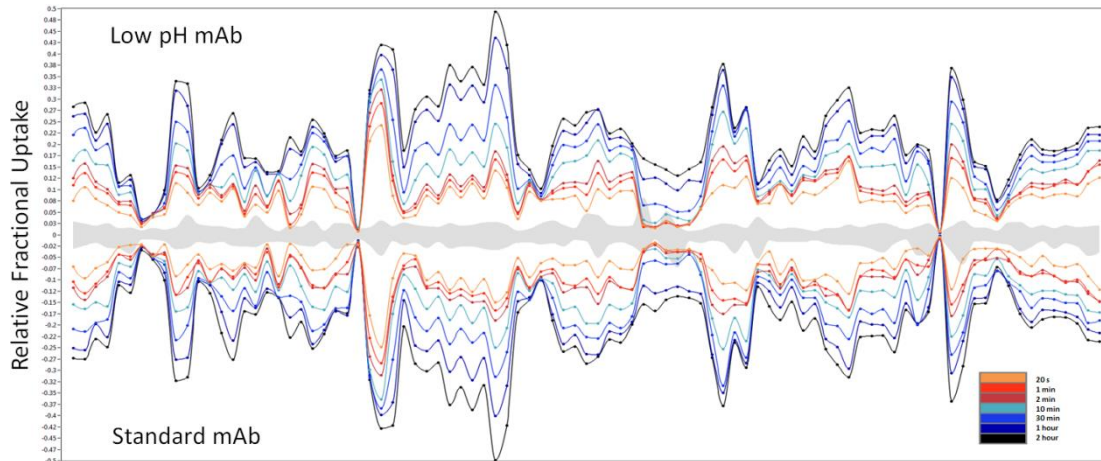
Figure 5.9: Mirror plot showing the relative fractional uptake for mAb heavy chain from samples produced using standard and altered bioprocess conditions of pH 6.8.
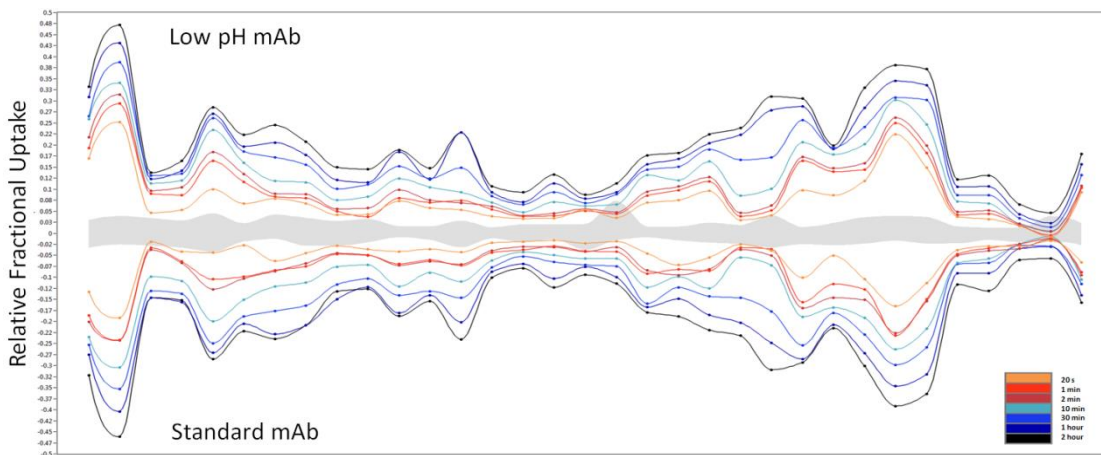
Figure 5.10: Mirror plot showing the relative fractional uptake for mAb light chain from samples produced using standard and altered bioprocess conditions of pH 6.8.
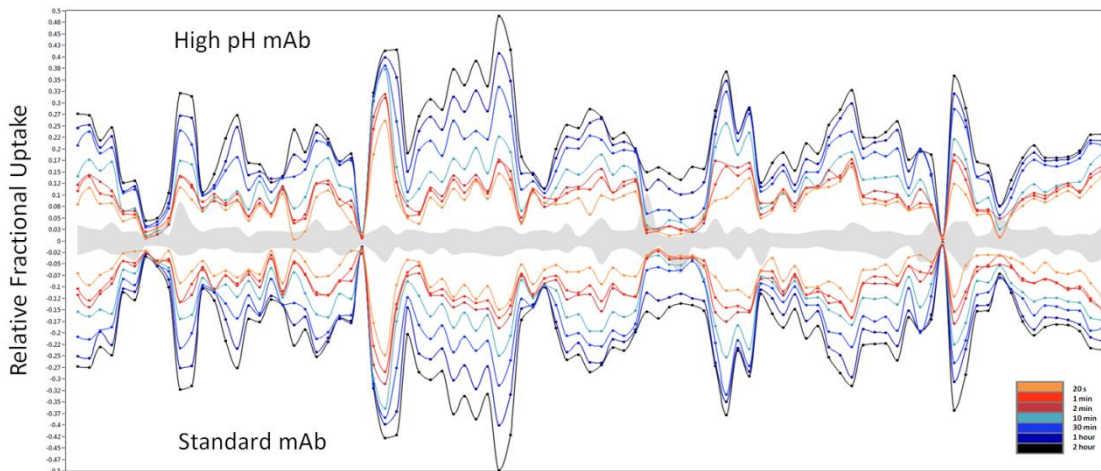
Figure 5.11: Mirror plot showing the relative fractional uptake for mAb heavy chain from samples produced using standard and altered bioprocess conditions of pH 7.2.
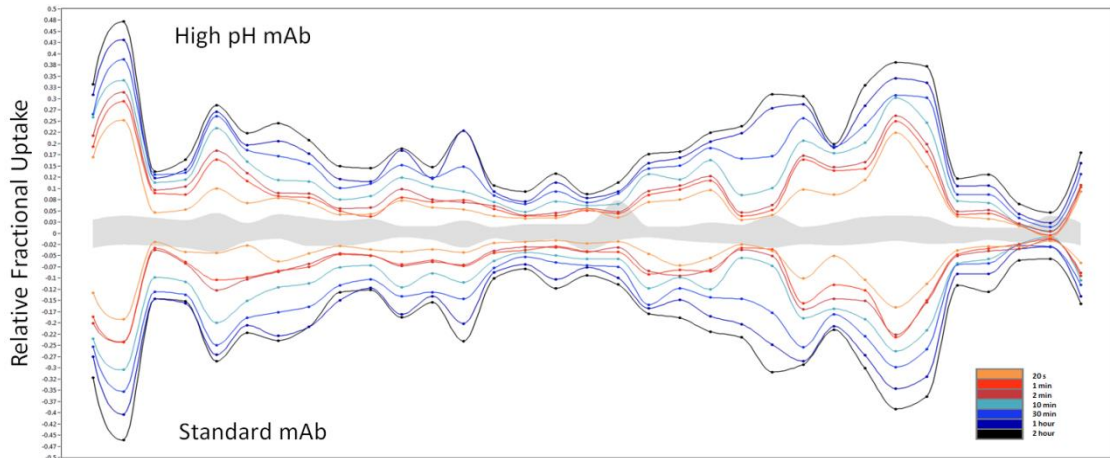
Figure 5.12: Mirror plot showing the relative fractional uptake for mAb light chain from samples produced using standard and altered bioprocess conditions of pH 7.2.
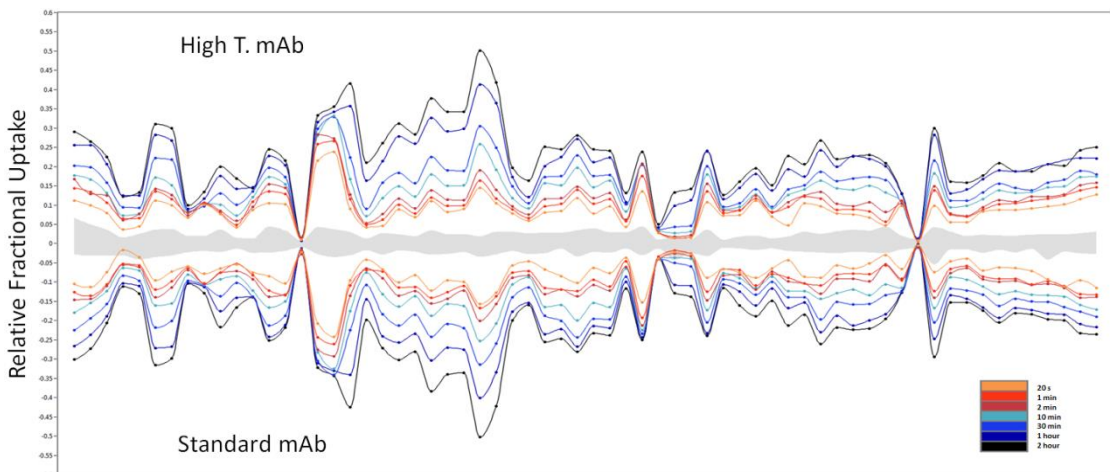
Figure 5.13: Mirror plot showing the relative fractional uptake for mAb heavy chain from samples produced using standard and altered bioprocess conditions of 39.5°C.
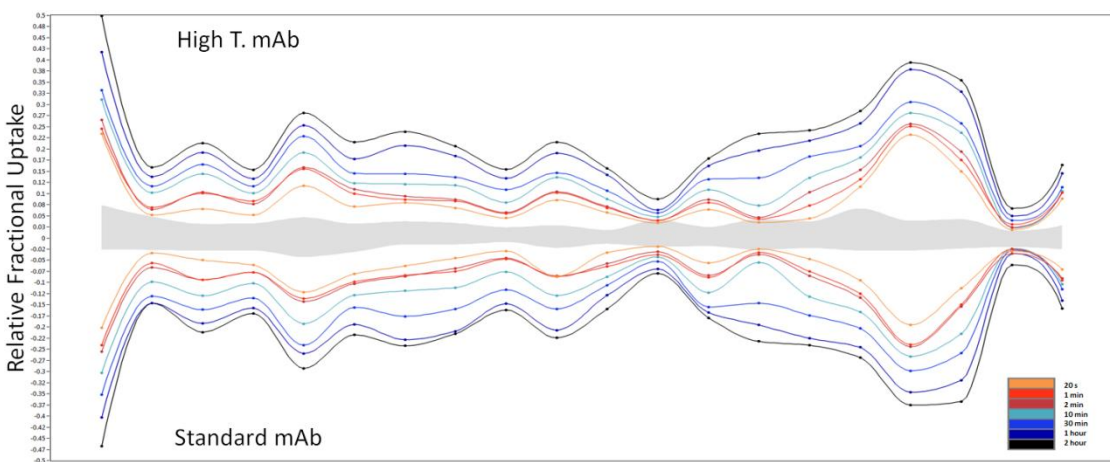
Figure 5.14: Mirror plot showing the relative fractional uptake for mAb light chain from samples produced using standard and altered bioprocess conditions of 39.5°C.
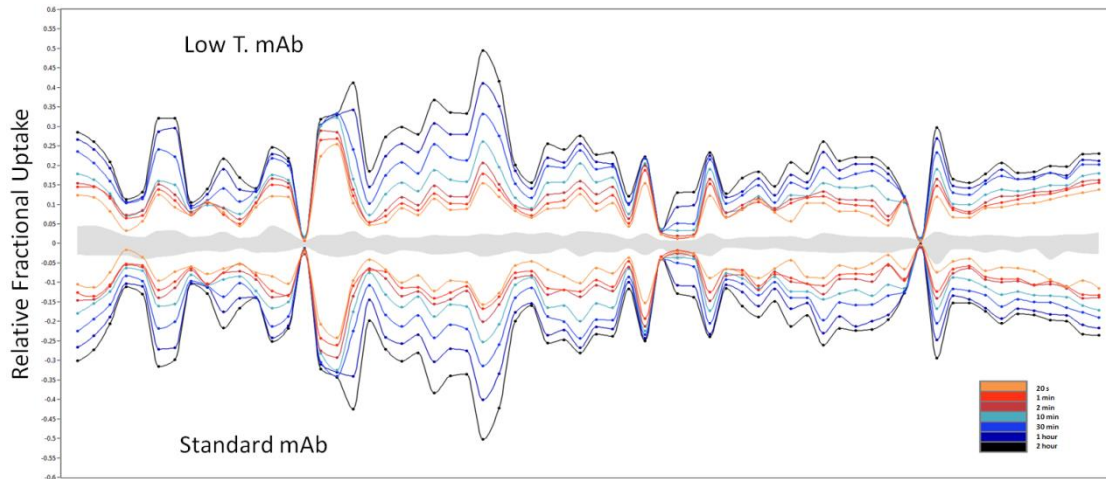
Figure 5.15: Mirror plot showing the relative fractional uptake for mAb heavy chain from samples produced using standard and altered bioprocess conditions of 32.0°C.
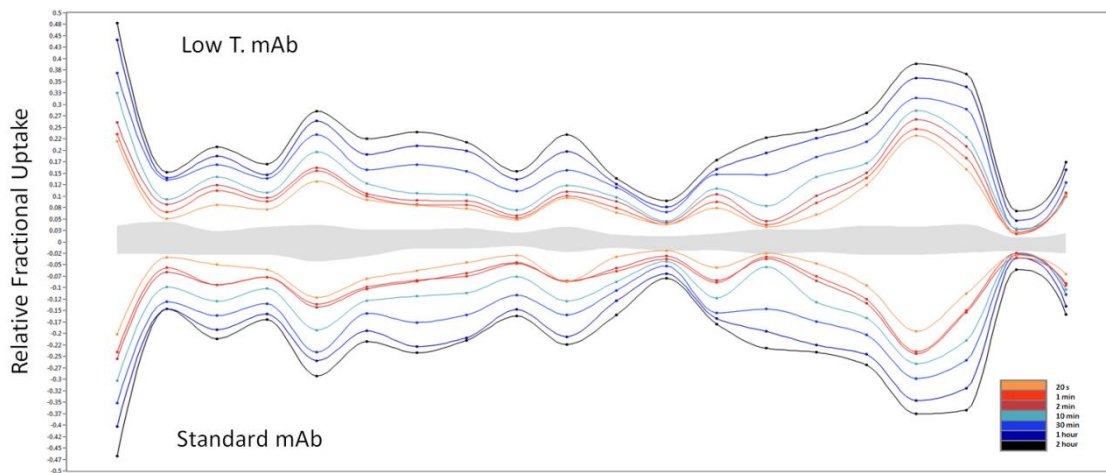
Figure 5.16: Mirror plot showing the relative fractional uptake for mAb light chain from samples produced using standard and altered bioprocess conditions of 32.0°C.
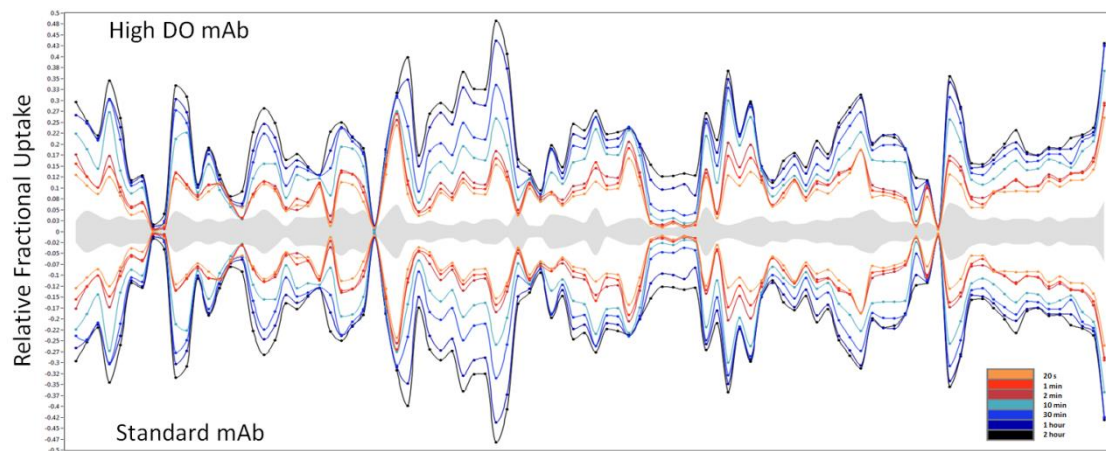
Figure 5.17: Mirror plot showing the relative fractional uptake for mAb heavy chain from samples produced using standard and altered bioprocess conditions of 110% DO.
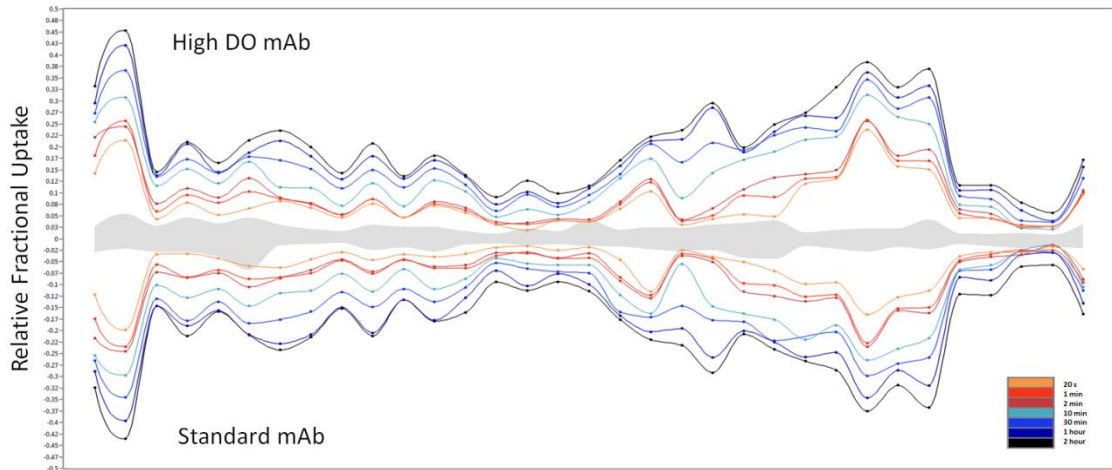
Figure 5.18: Mirror plot showing the relative fractional uptake for mAb light chain from samples produced using standard and altered bioprocess conditions of 110% DO.
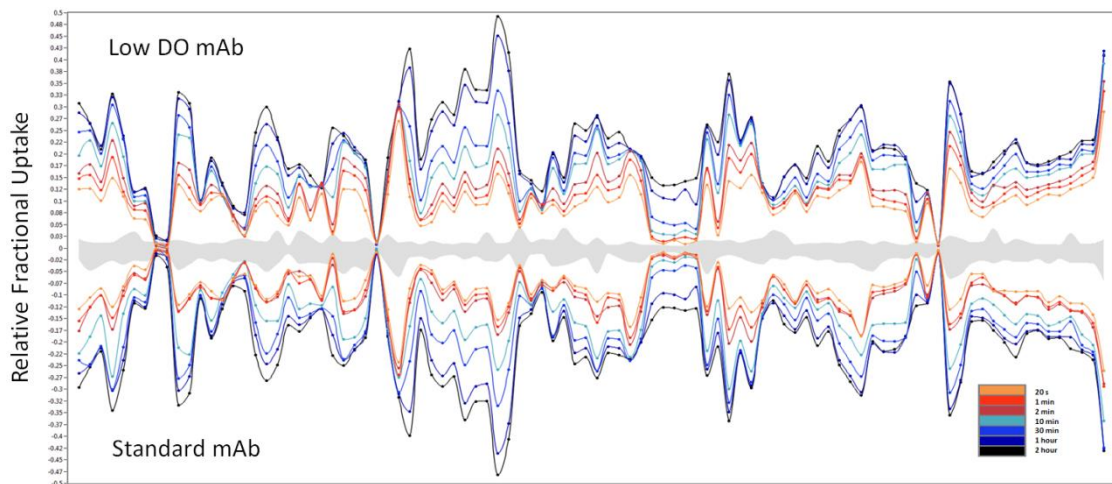
Figure 5.19: Mirror plot showing the relative fractional uptake for mAb heavy chain from samples produced using standard and altered bioprocess conditions of 60% DO.
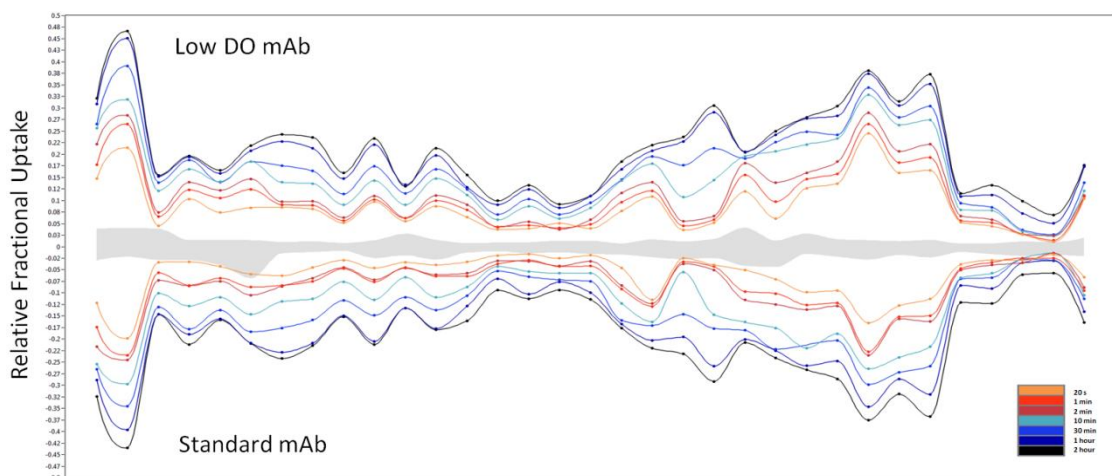
Figure 5.20: Mirror plot showing the relative fractional uptake for mAb light chain from samples produced using standard and altered bioprocess conditions of 60% DO.

Finally, to determine whether the relative fractional uptake of each peptide was changed between mAb produced at standard conditions and mAb produced under conditions of altered bioprocessing, the difference in deuterium incorporation for peptides in comparative samples were determined and used to prepare difference index plots as shown in Figures 5.21 to 5.23. The differential value for each peptide (shown along x-axis) for each HDX reaction was calculated by subtracting the deuterium uptake value of the altered bioprocessing sample from that of the mAb produced under standard bioprocess conditions. The summed difference for all HDX time-points for all peptides are signified by the vertical grey bars in each difference index plot. Criteria for determining statistically significant HDX differences between the peptides from altered bioprocessing and standard mAb samples were evaluated as described previously. [25] The standard deviation (SD) of summed difference values for each peptide across different experiments was determined and averaged; 3 × average SD was set as the difference limit for significance determination. As the average SD of summed difference values for each peptide was calculated to be 0.37 Da, the limit outside of which difference values were deemed to be significant was set as ±1.1 Da (represented by dashed lines in Figures 5.21 to 5.23). Positive difference index values signify increased HDX in anti-IL8 IgG1 samples produced under altered bioprocessing conditions compared to samples produced under standard conditions, while negative values represent decreased relative HDX for altered mAb samples. For each of the samples determined no distinct regions were found to be significantly changed in mAb produced under altered bioprocessing conditions compared to mAb produced at standard conditions. However, a number of individual peptides, detailed in Table 5.1, displayed alterations in deuterium uptake which were found to be different based on the significance criteria applied. Three of the seven peptides identified as having altered conformation within the mAb higher order structure, across all experiments, were found to incorporate amino acids previously determined to contain sequence-level modifications (Chapter 3). However, those regions of the mAb that were found to contain both alterations to the the mAb structure and also a primary sequence modification were identified solely on the light chain of anti-IL8 IgG1 samples produced under low temperature conditions of 32.0°C. Interestingly, three peptides determined for mAb heavy chain for anti-IL8 IgG1 produced at 32.0°C displayed altered deuterium uptake but were not correlated with having sequence-level modifications. However, the low temperature mAb sample was found to exhibit the greatest changes to levels of modified amino acids when compared to other samples analysed. Thus, it is possible that changes in protein conformation, may not necessarily result from changes to protein primary sequence at the site of conformational change, but may be an outcome of modifications to adjacent or spatially close sequence-level modifications.

Table 5.1: Peptides displaying altered deuterium uptake compared to standard mAb samples analysed and related peptide modifications identified.

Sample	mAb Chain	Peptide	Position	Peptide Modification
Low T mAb	Light	HWYQQKPGKAPKLLI	H39-I53	Oxidation W40
High pH mAb	Light	AKVQWKVDNALQSGNSQE	A149-E166	Oxidation W153, Deamidation N157, Deamidation Q160, Deamidation Q163
High DO mAb	Heavy	VQSGGGLVQPGGS	V5-S17	n/a
Low DO mAb	Heavy	TLSRDNSKNTAY	T69-Y80	Deamidation N74, Deamidation N77
Low T mAb	Heavy	VSWNSGALTSGVHTFPAVL	V161-L179	n/a
Low T mAb	Heavy	NSGALTSGVHTFPAVL	N164-L179	n/a
Low T mAb	Heavy	TVDKSRWQQGNVFSCSVM	T416-M433	n/a

It has been been widely reported that changes to a the higher order structure of a therapeutic protein have the potential to alter the safety, potency and efficiacy characteristics of that protein by reducing or inhibiting accessibility to mAb binding sites. [23, 25, 26, 34] Hence for IgG1, sequence or structural modificiations of CDRs or the highly conserved C_H3 domain, responsible for FcRn binding, may have a profound effect on the physiological activities of therapeutic mAbs. Changes in the primary sequence or higher order structure may allude to alterations in the physiological activity of a therapeutic mAb, however, to confidently assess the impact of these CQAs to protein activity determination of the functional activity must be performed.
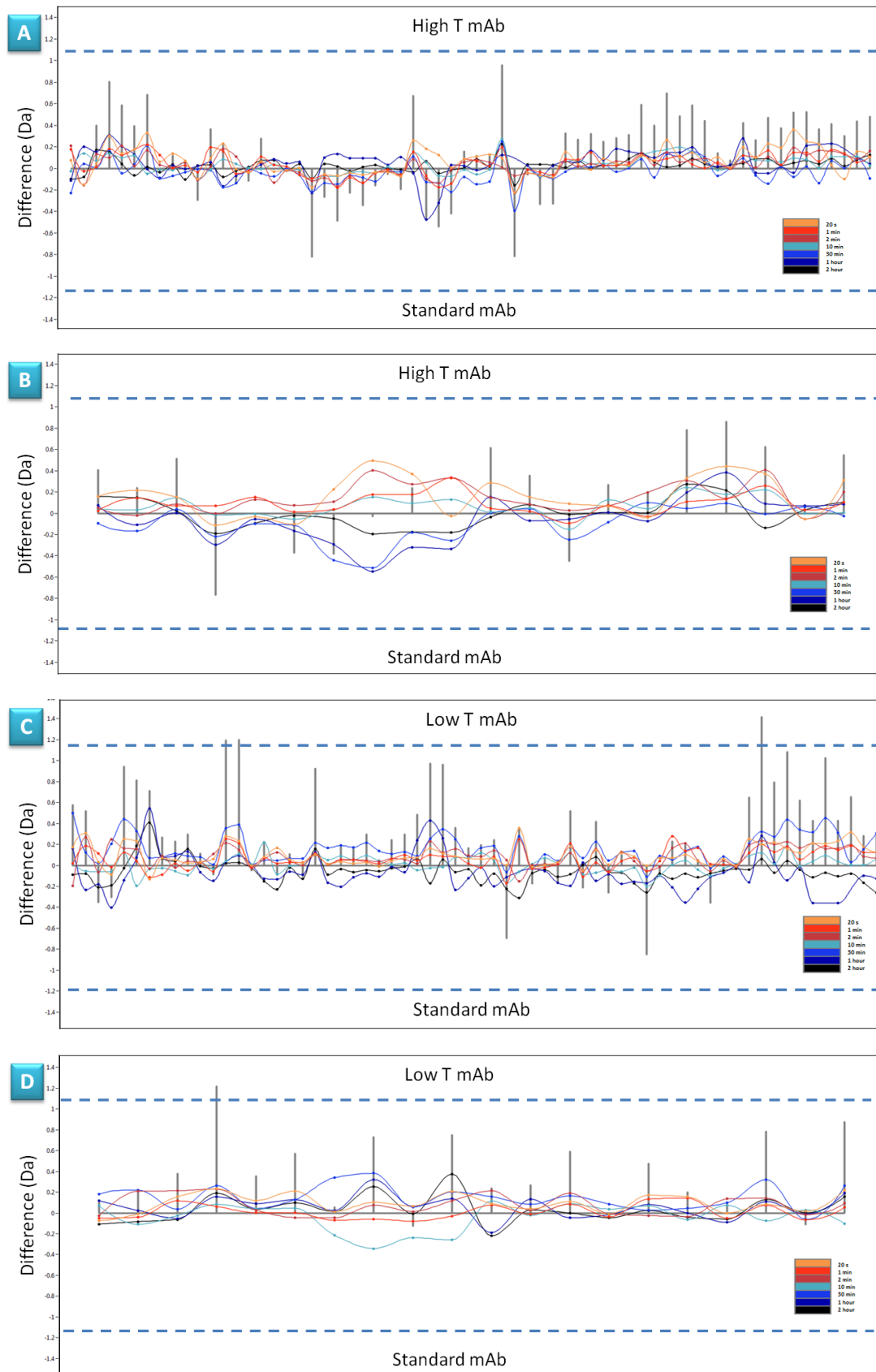
Figure 5.21: Difference index plots showing differences in deuterium uptake between standard mAb and **A.** high temperature mAb heavy chain, **B.** high temperature mAb light chain, **C.** low temperature mAb heavy chain and **D.** low temperature mAb light chain.
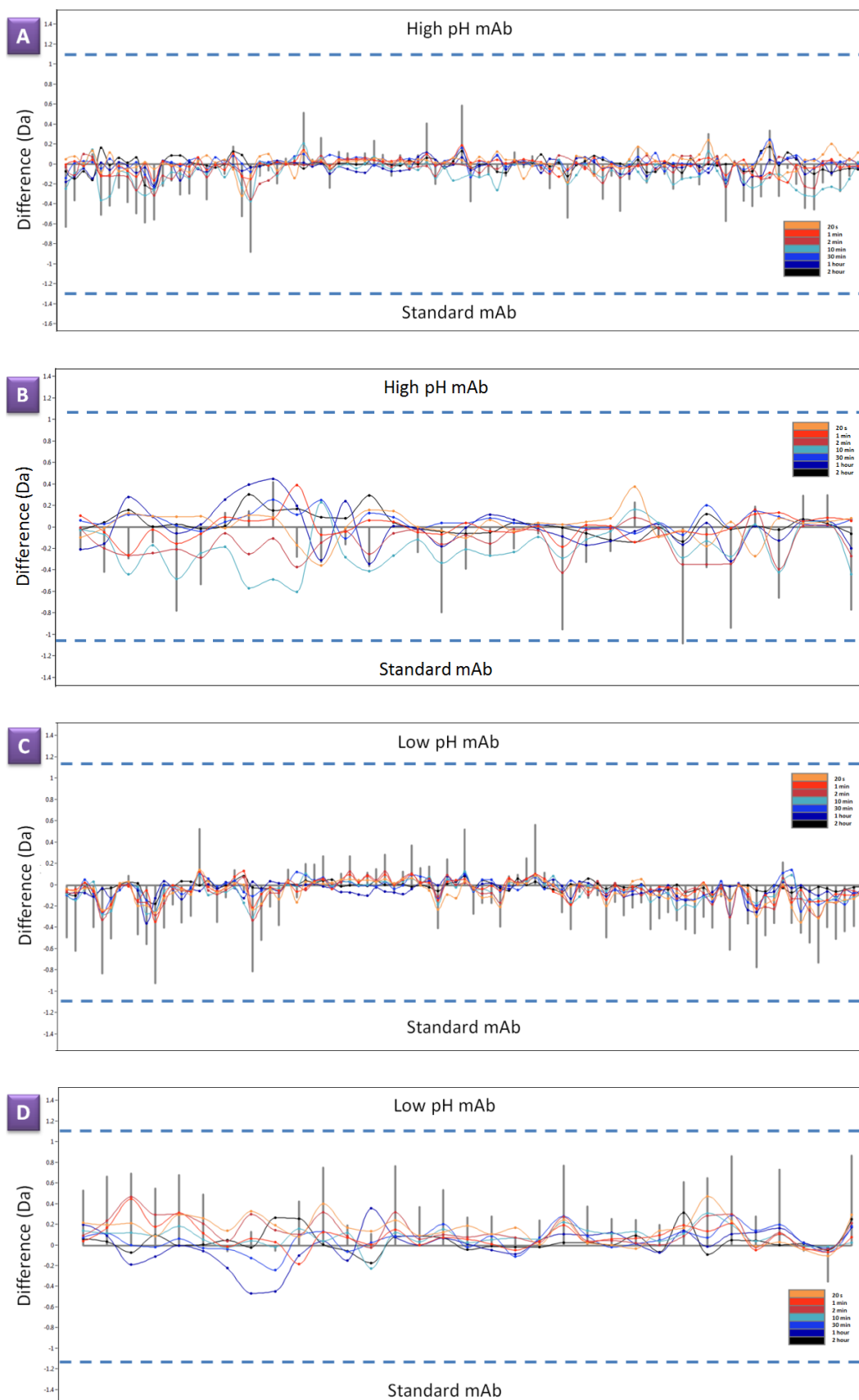
Figure 5.22: Difference index plots showing differences in deuterium uptake between standard mAb and **A.** high temperature mAb heavy chain, **B.** high temperature mAb light chain, **C.** low temperature mAb heavy chain and **D.** low temperature mAb light chain.
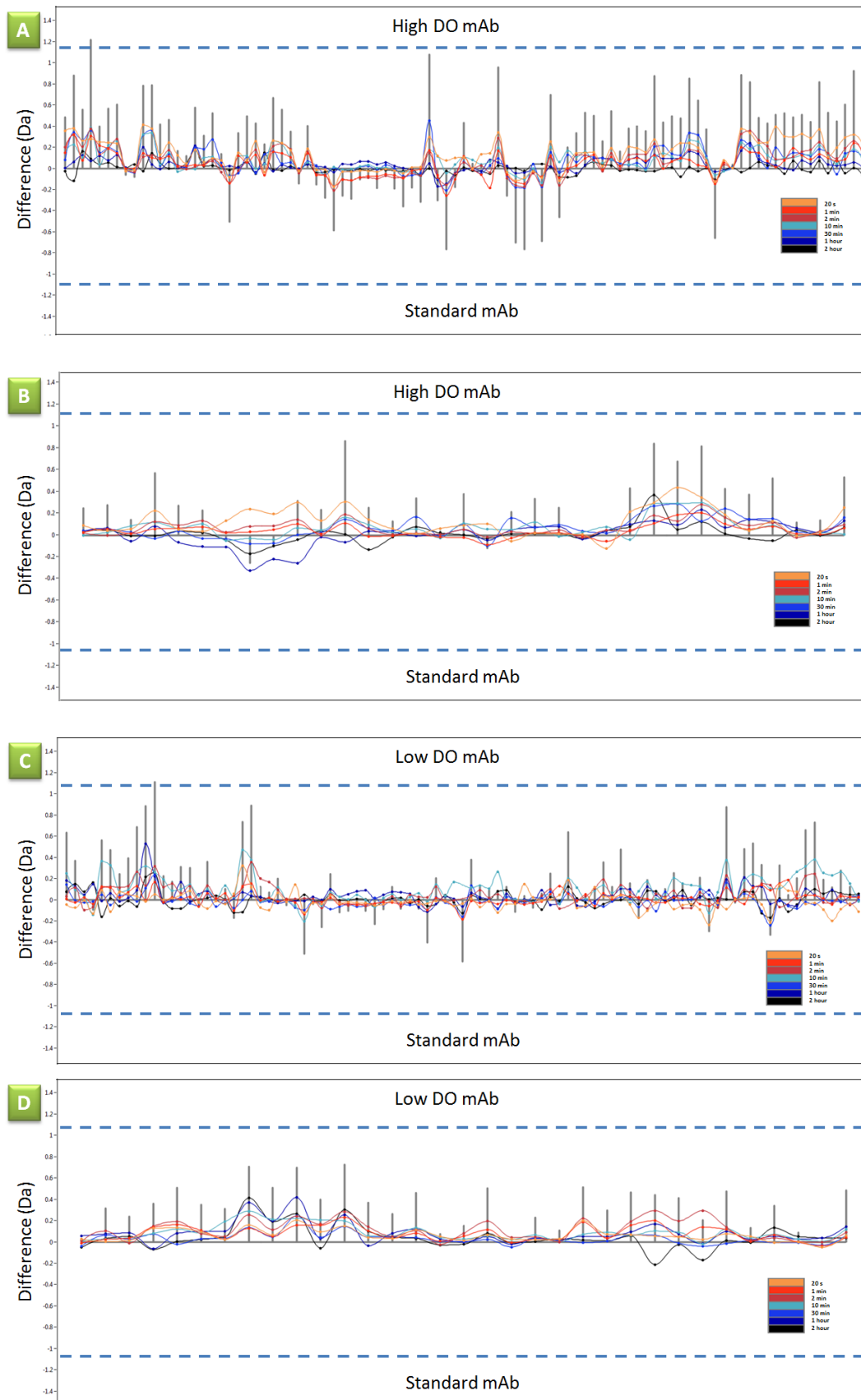
Figure 5.23: Difference index plots showing differences in deuterium uptake between standard mAb and **A.** high DO mAb heavy chain, **B.** high DO mAb light chain, **C.** low DO mAb heavy chain and **D.** low DO mAb light chain.

5.3.2 SPR Analysis Using Biacore

Surface plasmon resonance (SPR) enables the elucidation of alterations in the binding capabilities of proteins by measuring the affinity, or rate of association and dissociation, of a protein to a target antigen which has been immobilised onto a gold-plated sensor chip. Conversely, a protein may be captured onto a surface and the rate of an antigen binding to the protein determined. By measuring changes in reflected polarised light following protein-antigen binding, changes to binding characteristics may be assessed. Anti-IL8 IgG1 is pharmacologically active due to its ability to bind to interleukin-8 facilitating its removal from the body, and to bind to the neonatal Fc receptor, ensuring extended serum half-life in humans. Both of these features were evaluated to assess changes to the functional characteristics of anti-IL8 IgG1 following production under conditions of altered bioprocessing.

5.3.2.1 Determination of FcRn-Anti-IL8 IgG1 Binding for Anti-IL8 IgG1 Produced Using Altered Bioprocessing

FcRn is a heterodimeric protein consisting of a major histocompatibility complex class 1-like protein and a β2-microglobulin subunit. [13, 16] It is expressed by endothelial, epithelial and myeloid cells, which internalise serum constituents including mAbs from the blood stream by pinocytosis. [13] FcRn binds with high affinity to the Fc domain of IgG1 at the highly conserved C_H2-C_H3 region in a strictly pH dependent manner, resulting in a 2:1 stoichiometry. [11, 16, 35] The pH dependent nature of the interaction enables the FcRn-mediated protection of IgG1 from intracellular degradation by binding to the receptor within the acidic endosomal environment. Subsequently, FcRn facilitates the recycling of IgG to the cell surface and release into the blood stream for re-circulation. As FcRn is strongly correlated with serum half-life of IgG1 *in-vivo*, it is frequently used during drug development for *in-vitro* assessment of the pharmacokinetic capabilities of therapeutic mAbs. [12] Additionally, lab-based evaluation of the effects of primary sequence modifications on IgG-FcRn binding affinities have been studied, *e.g.* charge heterogeneity was found to have little or no effect on IgG1-FcRn binding, [36] whereas methionine oxidation in mAb C_H2-C_H3 regions significantly reduced IgG1-FcRn binding. [34, 37] In the current study, determination of FcRn binding affinity to anti-IL8 IgG1 is used to assess changes to the functional capabilities of mAb that has been produced under conditions of altered pH, temperature and DO. Using multi-cycle affinity SPR analysis, FcRn was immobilised onto a Biacore CM5 chip before passing over different concentrations of anti-IL8 IgG1. The affinity constants (KD) for each triplicate analysis of the IgG1-FcRn binding

interaction were determined and are reported in Table 5.2. Increasing KD values signify low affinity and hence weak binding interactions. Corresponding sensograms and steady state fit graphs for triplicate analysis of mAb samples produced under standard and altered bioprocessing conditions are shown in Figures 5.24 to 5.28.

Table 5.2: Dissociation constants determined following SPR binding affinity analysis of anti-IL8 IgG1 and FcRn.

Anti-IL8 sample	Analysis 1 - KD (nM)	Analysis 2 - KD (nM)	Analysis 3 - KD (nM)
Low DO mAb	697.6	736.2	677.9
High DO mAb	742.2	728.4	687.7
Low pH mAb	675.2	704.2	665.7
High pH mAb	695.1	703.0	725.0
Low T mAb	819.1	807.0	858.2
High T mAb	739.7	718.2	712.8
Standard 1	694.8	675.0	756.1
Standard 2	691.8	699.5	680.8
Standard 3	686.2	738.0	698.0

A box-plot depicting the binding affinity values determined for each IgG1 sample analysed is displayed in Figure 5.29. A distinct difference in the binding affinity for anti-IL8 IgG1 produced at 32.0°C compared to mAb expressed in CHO DP-12 culture using all other parameters investigated was observed. It is possible that a correlation between the reduction in FcRn binding affinity and heavy chain conformational changes for mAb produced at 32.0°C may exist. Furthermore, primary sequence modifications determined for mAb produced at 32.0°C may also play a role in the reduced FcRn affinity for this IgG1 sample. Anti-IL8 IgG1 produced at 32.0°C was determined to have a higher proportion of oxidised methionine-257 when compared to other mAb samples analysed (Chapter 3). This would appear to correlate with the findings of Bertolotti-Ciarlet *et al.* and Pan and colleagues, who associated a reduction in FcRn binding affinity with methionine oxidation on mAb heavy chain. [37, 38]
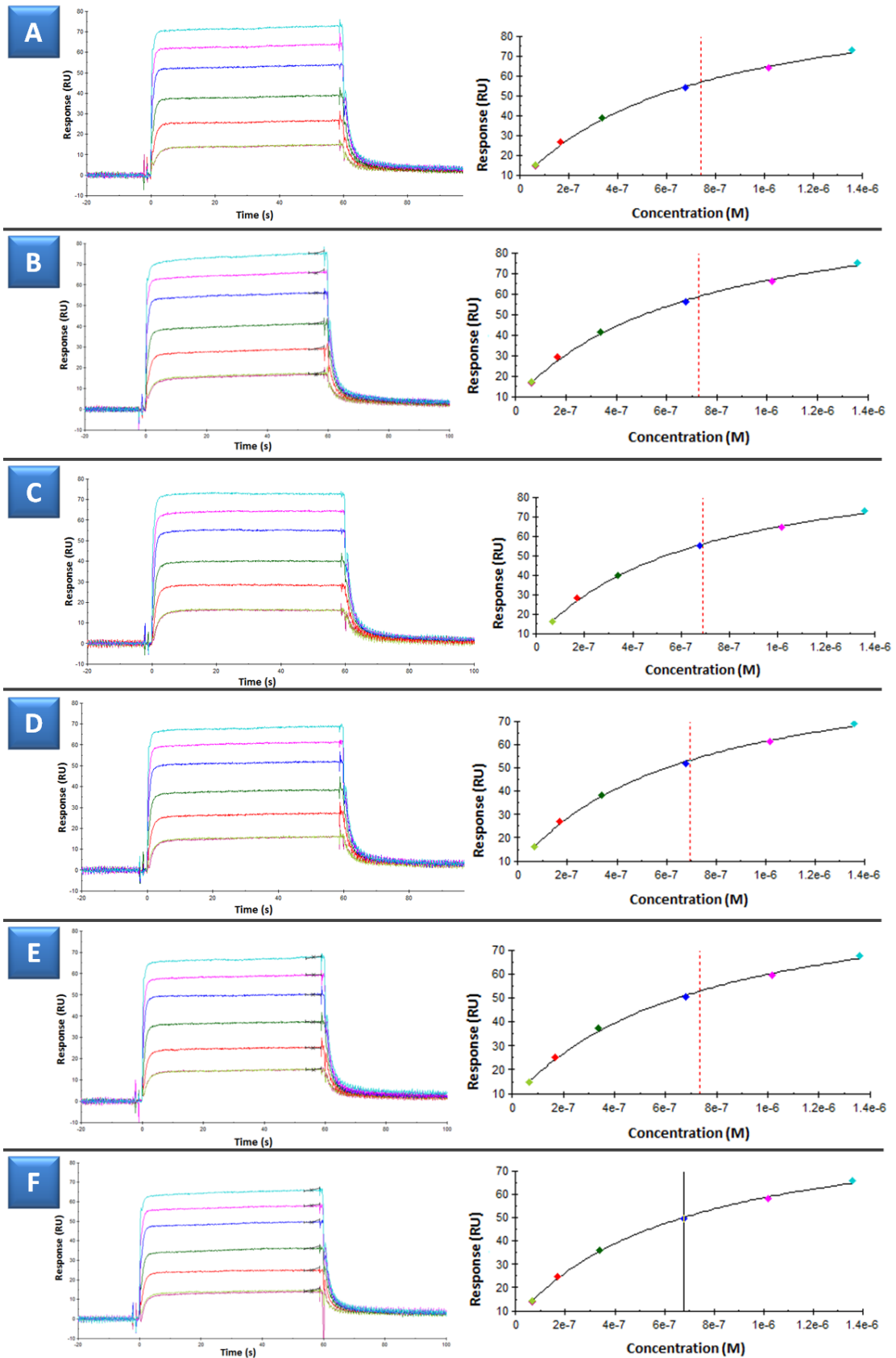
Figure 5.24: Sensograms and residual plots from triplicate affinity analysis of FcRn binding to anti-IL8 IgG1 produced in cell culture maintained at 110% DO (A-C) and 60% DO (D-F).
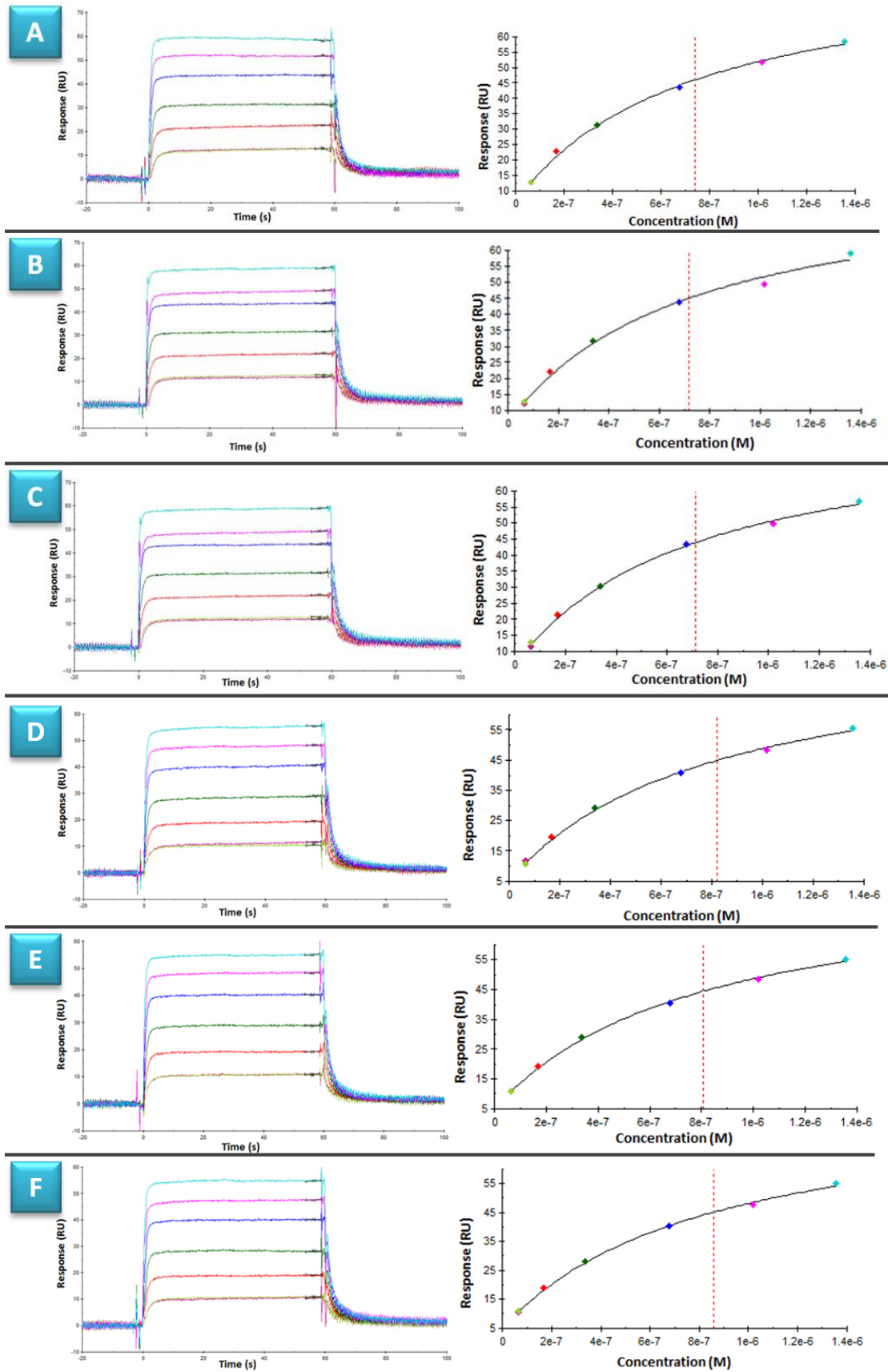
Figure 5.25: Sensograms and residual plots from triplicate affinity analysis of FcRn binding to anti-IL8 IgG1 produced in cell culture maintained at 39.5°C (A-C) and 32.0°C (D-F).
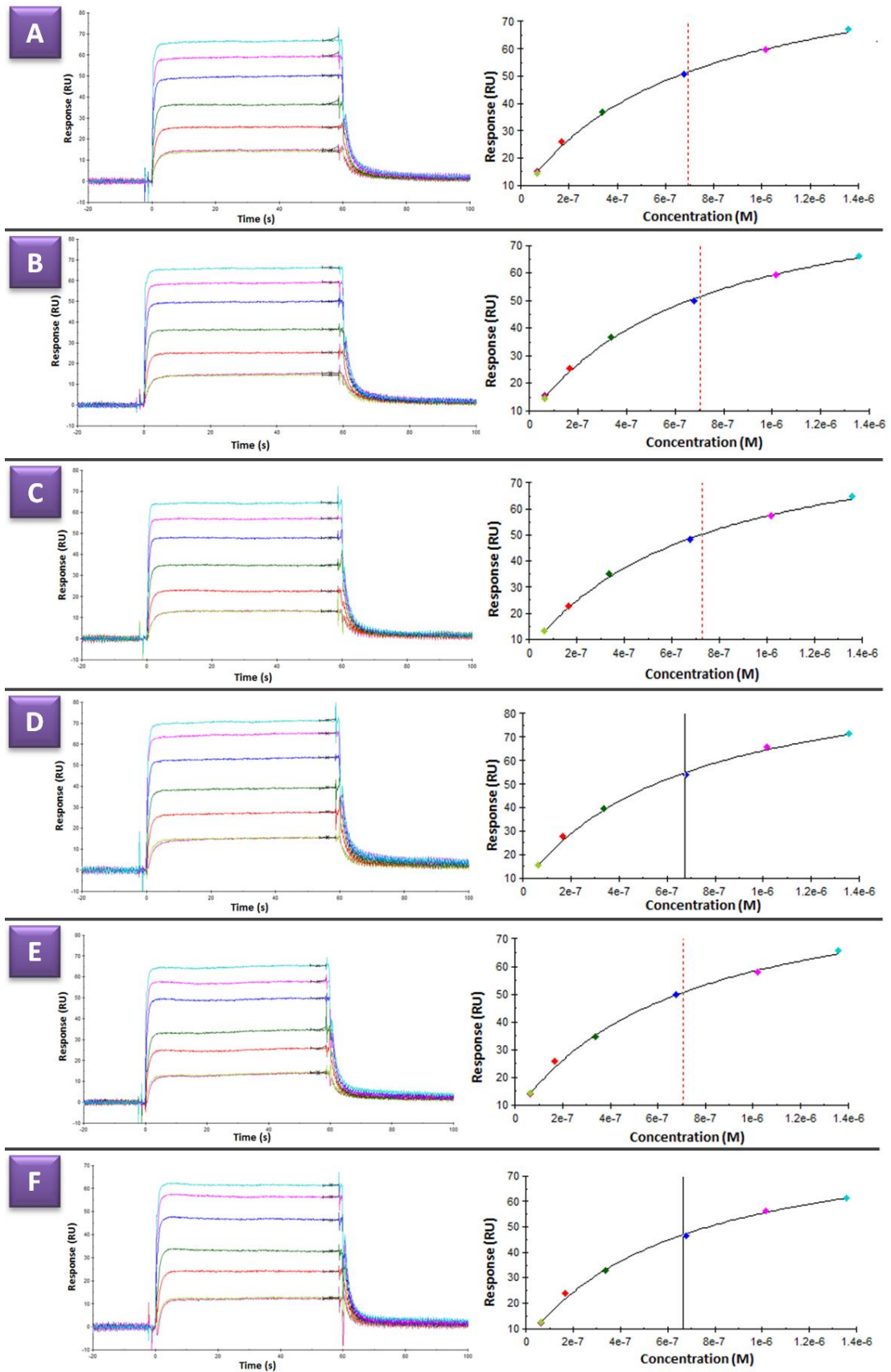
Figure 5.26: Sensograms and residual plots from triplicate affinity analysis of FcRn binding to anti-IL8 IgG1 produced in cell culture maintained at pH 7.2 (A-C) and pH 6.8 (D-F).
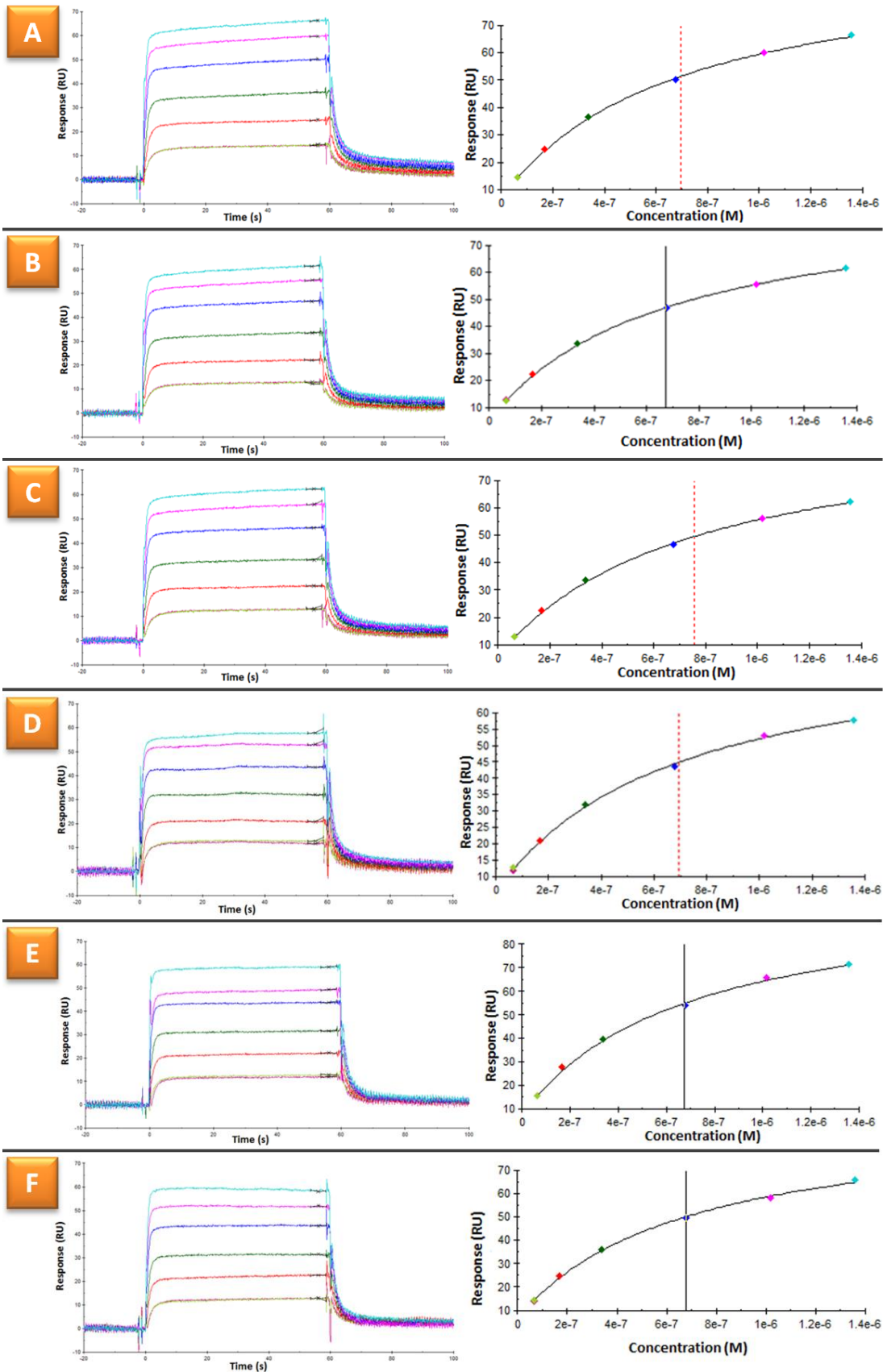
Figure 5.27: Sensograms and residual plots from triplicate affinity analysis of FcRn binding to anti-IL8 IgG1 produced in cell culture maintained at standard conditions: standard 1 (A-C), standard 2 (D-F).
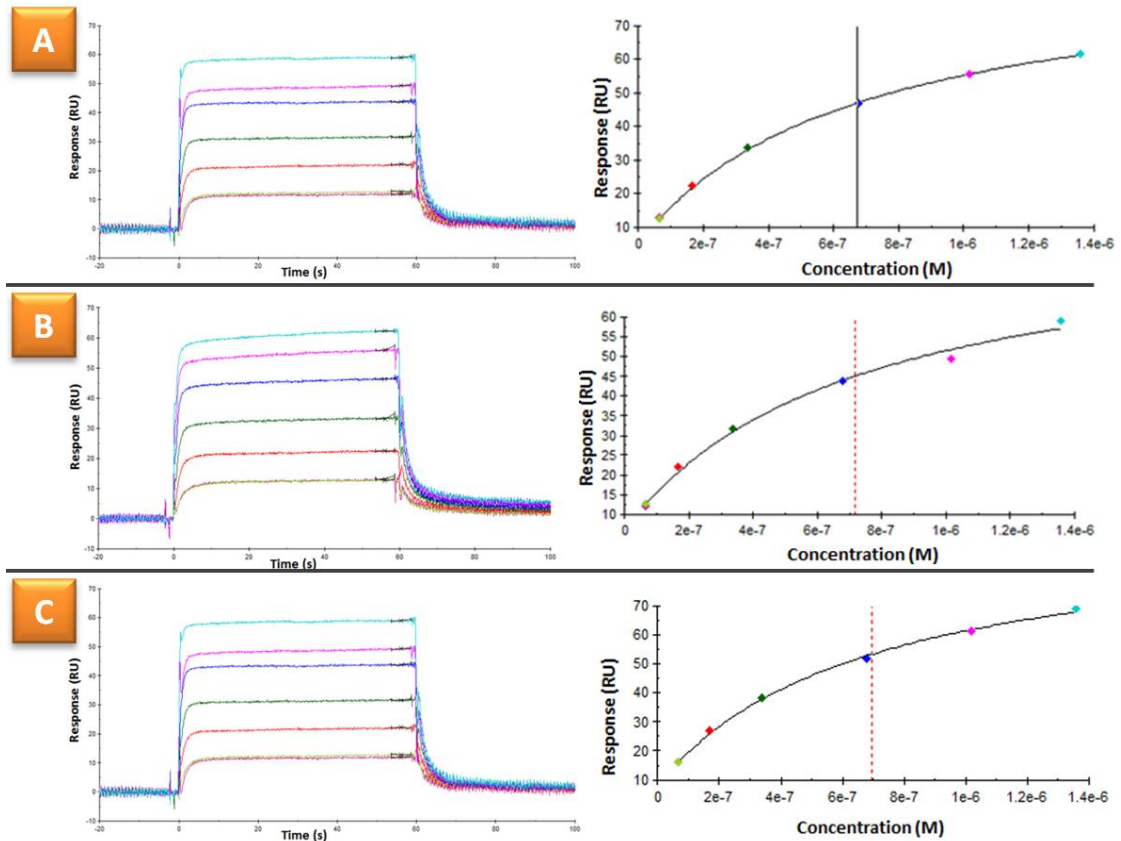
Figure 5.28: Sensograms and residual plots from triplicate affinity analysis of FcRn binding to anti-IL8 IgG1 produced in cell culture maintained at standard conditions: standard 3 (A-C).
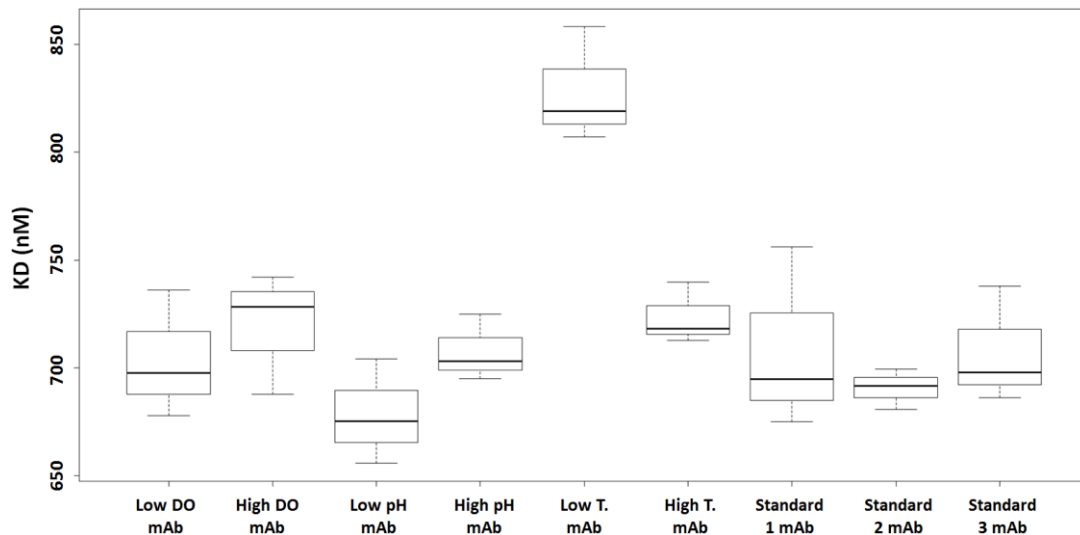
Figure 5.29: Box-plot showing FcRn binding dissociation constants determined for anti-IL8 IgG1 produced using different bioprocessing conditions of pH, DO and temperature (T).

5.3.2.2 Determination of Binding Kinetics for Interleukin-8 and Anti-IL8 IgG1 Produced Using Altered Bioprocessing Conditions

Having assessed the binding affinity to its cellular receptor FcRn, changes to the binding affinity of anti-IL8 IgG1 following production under altered bioprocess conditions to the target antigen interleukin-8 were assessed. In this instance a single-cycle SPR analysis approach was used, wherein the anti-IL8 samples under study were captured onto a Protein a SPR chip before the introduction of interleukin-8 for determination of binding affinity. Affinity constants determined following single-cycle SPR analysis of anti-IL8 IgG1 and interleukin-8 binding kinetics are displayed in Table 5.3. Corresponding sensograms and residual plots for each analysis are shown in Figures 5.30 to 5.34. Finally, box-plots depicting the data displayed in Table 5.3 are presented in Figure 5.35. The box plot shows a slight decrease in the binding affinity of anti-IL8 IgG1 produced in culture maintained at 110% DO. It is possible that this change in binding affinity may be related to a change in the conformation of the mAb heavy chain adjacent to the CDR1 region, observed for the anti-IL8 sample produced at 110% DO. An observed increase in the proportion of oxidised tryptophan-40 residues, located close to the CDR1 and CDR2 regions of the light chain for this sample, may also potentially have contributed to the altered binding affinity of anti-IL8 IgG1 to interleukin-8.

Table 5.3: Affinity constants obtained following single-cycle SPR analysis of anti-IL8 IgG1 and interleukin-8 binding kinetics.

Anti-IL8 sample	Analysis 1 - KD (nM)	Analysis 2 - KD (nM)	Analysis 3 - KD (nM)
Low DO mAb	18.0	19.4	17.9
High DO mAb	27.3	28.7	25.4
Low pH mAb	17.2	17.5	17.6
High pH mAb	21.1	20.4	18.7
Low T mAb	19.5	22.4	20.8
High T mAb	18.2	18.0	16.5
Standard 1	21.5	21.8	20.3
Standard 2	22.4	23.4	22.5
Standard 3	22.2	22.8	21.0
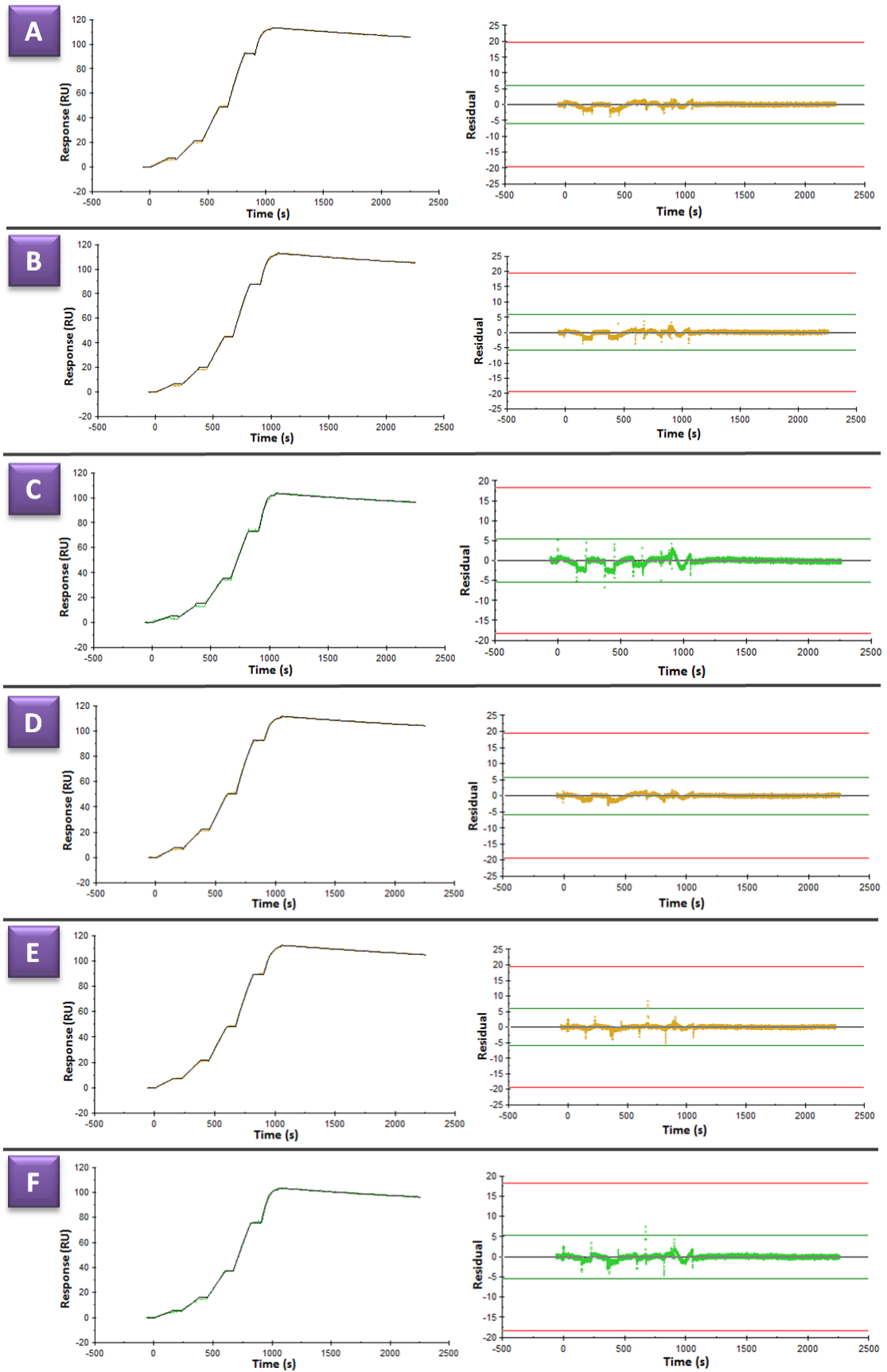
Figure 5.30: Resulting Sensograms and residual plots from triplicate affinity analysis of interleukin 8 binding to anti-IL8 IgG1 produced in cell culture maintained at 39.5°C (A-C) and 32.0°C (D-F).
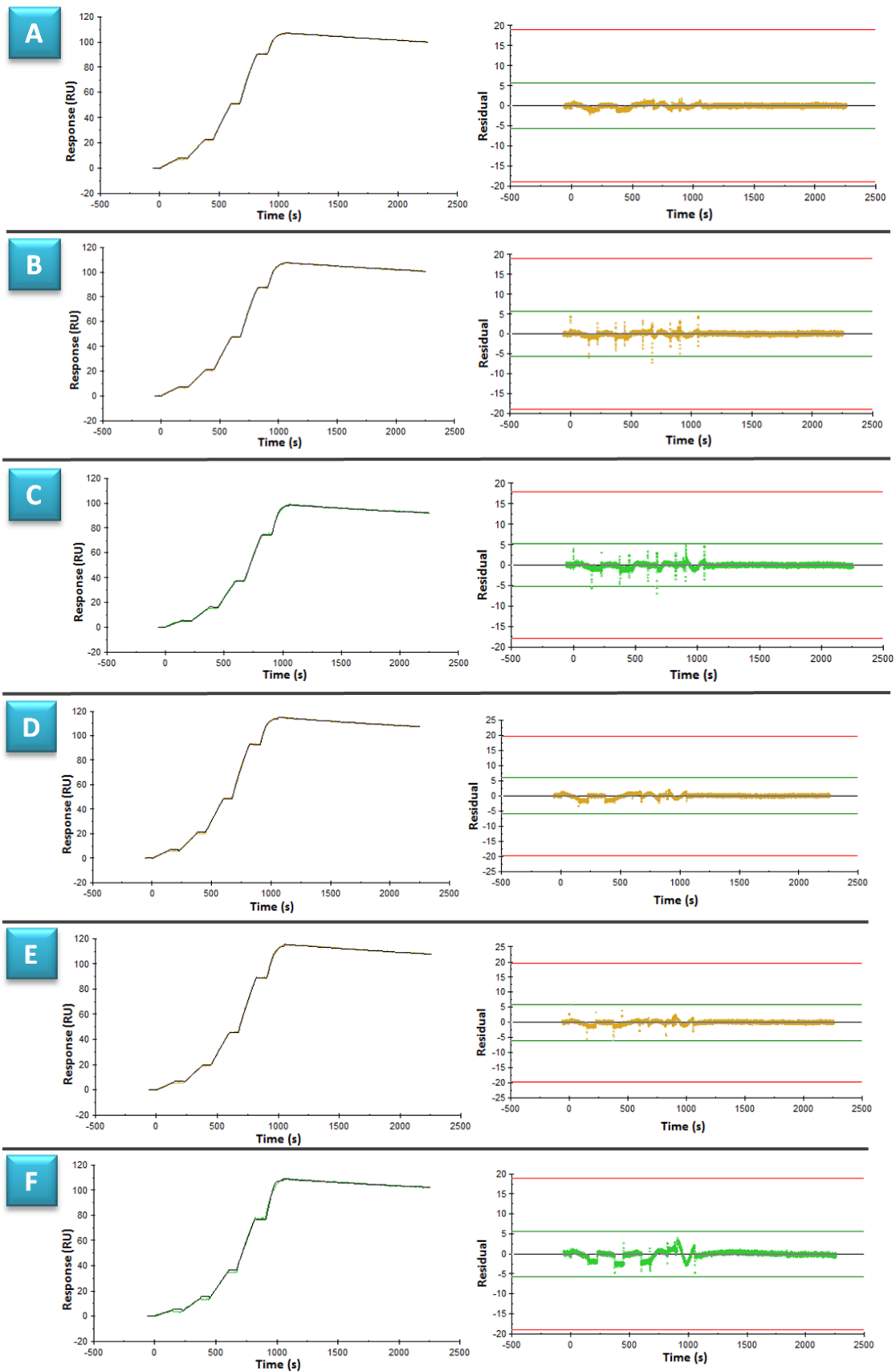
Figure 5.31: Resulting Sensograms and residual plots from triplicate affinity analysis of interleukin 8 binding to anti-IL8 IgG1 produced in cell culture maintained at pH 7.2 (A-C) and pH 6.8 (D-F).
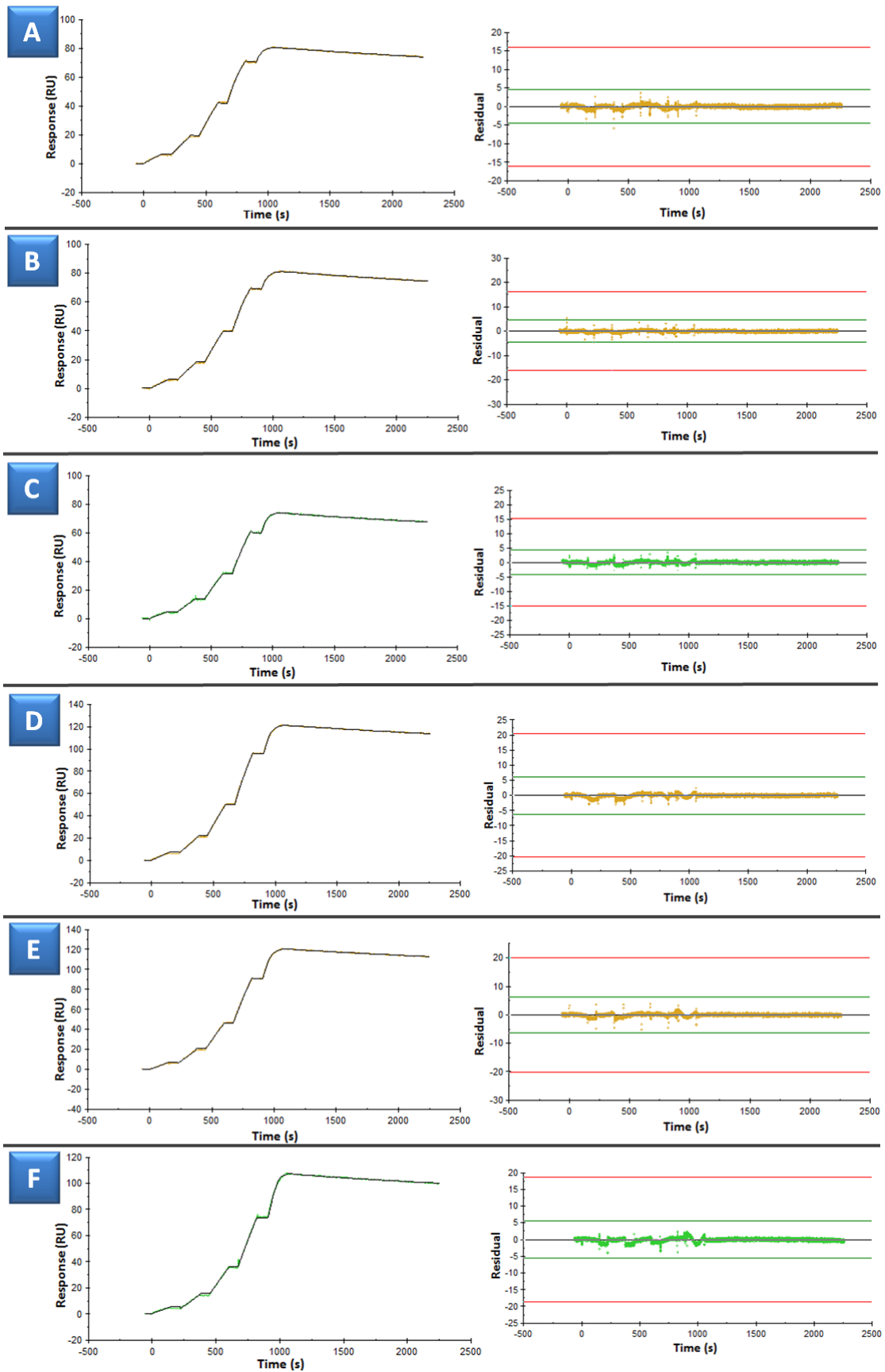
Figure 5.32: Resulting Sensograms and residual plots from triplicate affinity analysis of interleukin 8 binding to anti-IL8 IgG1 produced in cell culture maintained at 110% DO (A-C) and 60% DO (D-F).
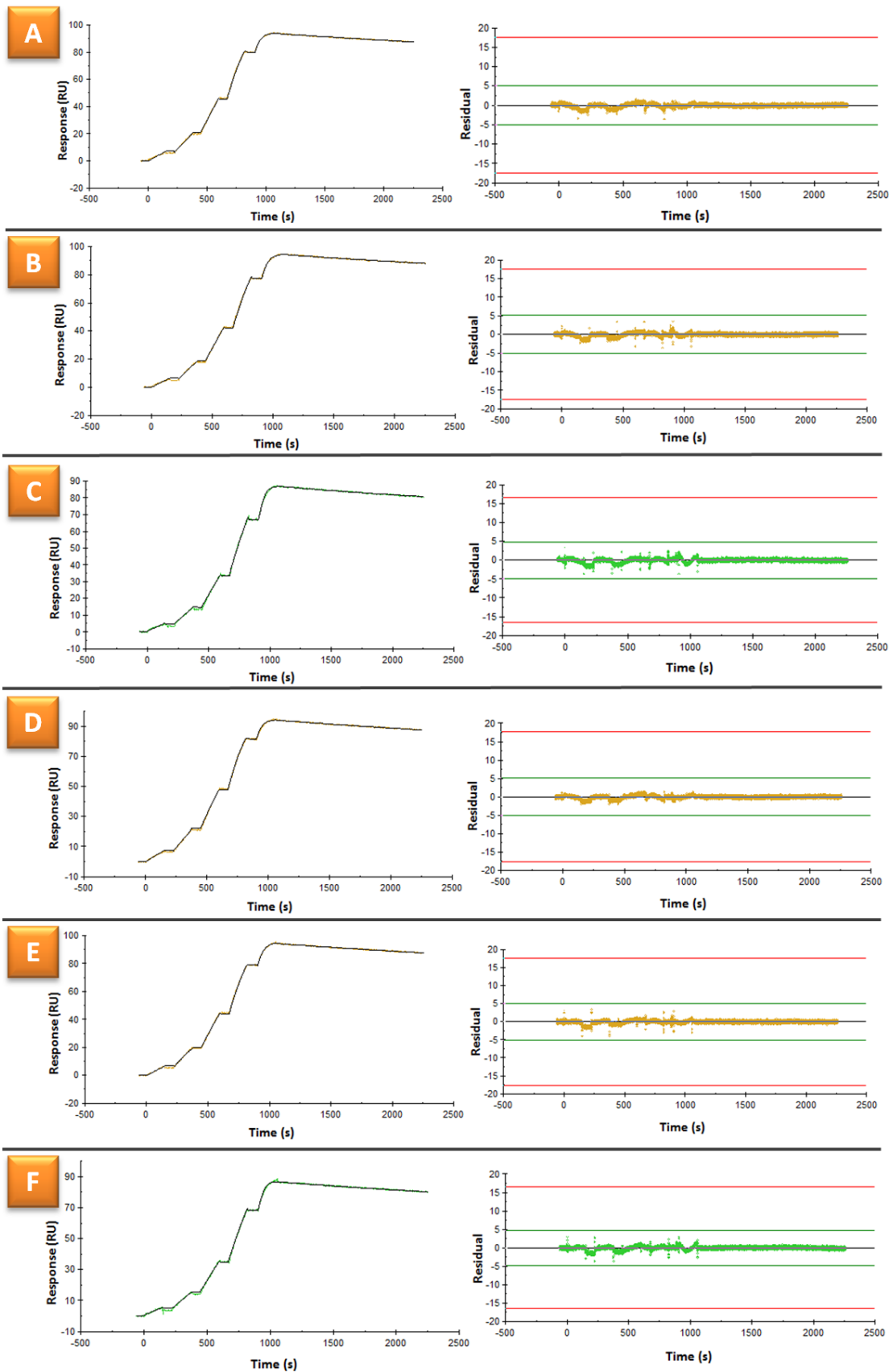
Figure 5.33: Resulting Sensograms and residual plots from triplicate affinity analysis of interleukin 8 binding to anti-IL8 IgG1 produced in cell culture maintained at standard conditions: standard 1 (A-C), standard 2 (D-F).
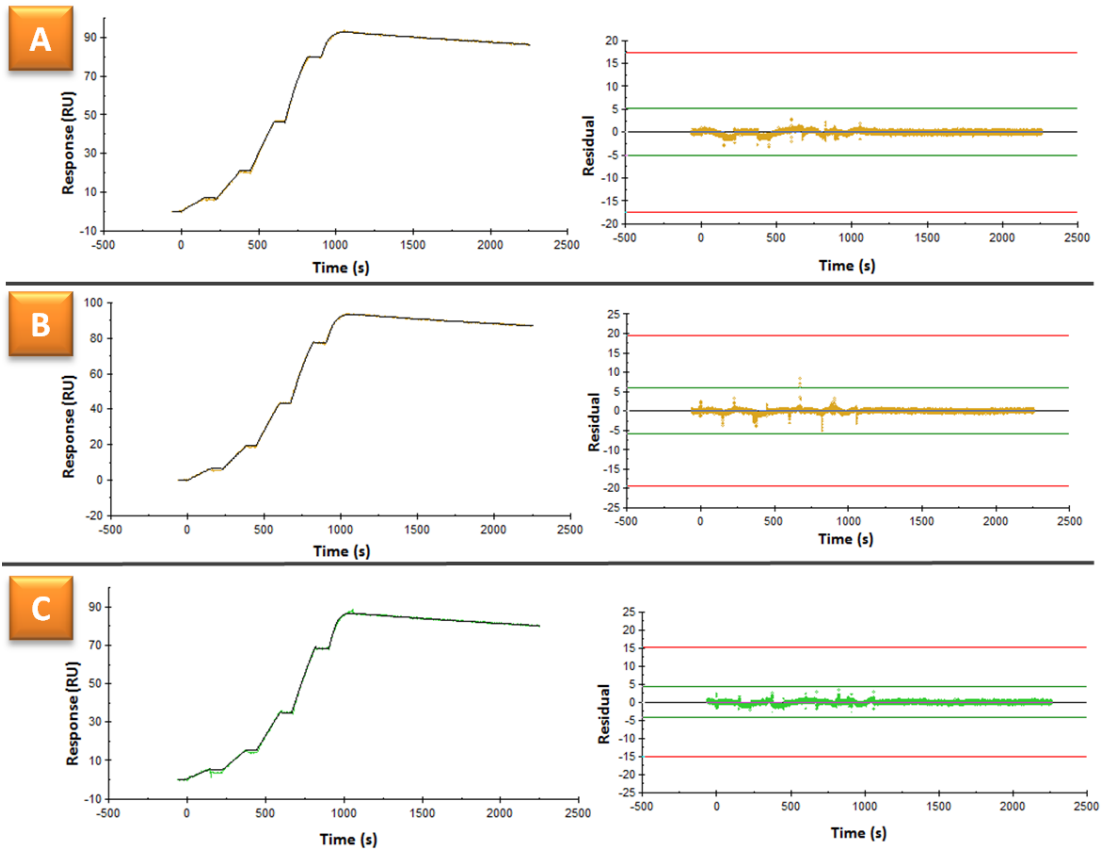
Figure 5.34: Resulting Sensograms and residual plots from triplicate affinity analysis of interleukin 8 binding to anti-IL8 IgG1 produced in cell culture maintained at standard conditions: standard 3 (A-C).
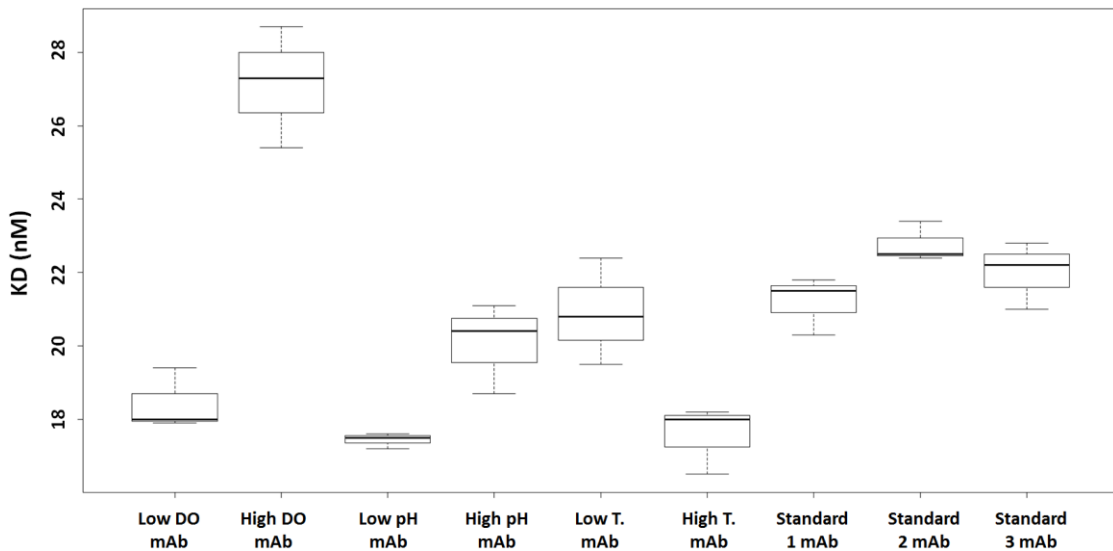
Figure 5.35: Box-plot showing interleukin-8 binding dissociation constants determined for anti-IL8 IgG1 produced using different bioprocessing conditions of pH, DO and temperature (T).

5.4   Conclusions

In this Chapter, the effect of altering bioprocess conditions of pH, temperature and DO on the structure and function of therapeutic anti-IL8 IgG1 was evaluated. HDX-MS was used for in-depth structural characterisation of the biomolecule revealing conformational changes to some portions of anti-IL8 IgG1 in response to expression in CHO DP-12 culture maintained under different bioprocess parameters, namely 32.0°C, pH 7.2, 60% DO and 110% DO. Almost half of these observed structural modifications could be aligned with sequence level modifications determined previously. Although structural changes at both primary sequence level and to the higher order structure may indicate potential variations in therapeutic mAb function, to fully characterise the potential effects of altered bioprocessing on the quality of the mAb, a functional assessment using SPR analysis was also performed. Following SPR analysis to determine mAb binding to FcRn, the cellular receptor responsible for re-circulation of mAb in the body and hence serum half-life of mAbs, variations in the binding affinities of FcRn and mAb produced at 32.0°C were determined. These results indicate a possible reduction in serum half-life for anti-IL8 IgG1 produced at 32.0°C and may be potentially related to conformational changes and primary sequence changes observed for this mAb sample. Additional SPR analysis to assess the binding characteristics of anti-IL8 IgG1 produced using different bioprocessing conditions to the target antigen interleukin-8 revealed an observed change in binding affinity for mAb produced using 110% DO content of culture media. Despite scope for improvement, in particular for HDX digestion efficiency, these two techniques epitomise powerful analytical tools that may be applied for comparability assessment of biosimilars or to determine changes to function, efficacy and safety of protein biopharmaceuticals in response to changes in production. Furthermore, the combined results highlight the need for multiple analytical strategies to fully evaluate changes to recombinant protein products in response to manufacture changes.

5.5   Author Contributions

Research study devised by Amy Farrell and Jonathan Bones; research performed by Amy Farrell; Chapter written by Amy Farrell and reviewed by Jonathan Bones.

5.6   References

1.   Houde, D., S.A. Berkowitz, and J.R. Engen, *The utility of hydrogen/deuterium exchange mass spectrometry in biopharmaceutical comparability studies.* J Pharm Sci, 2011. **100**(6): p. 2071-86.

2.   International Conference on Harmonisation, 2012, ICH Harmonised Tripartite Guideline, Development and Manufacture of Drug Substances (Chemical Entities and Biotechnological/Biological Entities) Q11. Retrieved 10 June 2016 from http://www.ich.org/fileadmin/Public_Web_Site/ICH_Products/Guidelines/Quality/Q11/Q11_Step_4.pdf.

3.   International Conference on Harmonisation, 2004, ICH Harmonised Tripartite Guideline, Comparability of Biotechnological/Biological Products Subject to Changes in Their Manufacturing Process Q5E. Retrieved 10 June 2016 from http://www.ich.org/fileadmin/Public_Web_Site/ICH_Products/Guidelines/Quality/Q5E/Step4/Q5E_Guideline.pdf.

4.   Panjwani, N., et al., *Assessment of the effects of pH, formulation and deformulation on the conformation of interferon alpha-2 by NMR.* J Pharm Sci, 2010. **99**(8): p. 3334-42.

5.   Amezcua, C.A. and C.M. Szabo, *Assessment of higher order structure comparability in therapeutic proteins using nuclear magnetic resonance spectroscopy.* J Pharm Sci, 2013. **102**(6): p. 1724-33.

6.   Norrman, M. and G. Schluckebier, *Crystallographic characterization of two novel crystal forms of human insulin induced by chaotropic agents and a shift in pH.* BMC Struct Biol, 2007. **7**: p. 83.

7.   Majumdar, R., et al., *Hydrogen-deuterium exchange mass spectrometry as an emerging analytical tool for stabilization and formulation development of therapeutic monoclonal antibodies.* J Pharm Sci, 2015. **104**(2): p. 327-45.

8.   Berkowitz, S.A., et al., *Analytical tools for characterizing biopharmaceuticals and the implications for biosimilars.* Nat Rev Drug Discov, 2012. **11**(7): p. 527-40.

9.   Wei, H., et al., *Hydrogen/deuterium exchange mass spectrometry for probing higher order structure of protein therapeutics: methodology and applications.* Drug Discov Today, 2014. **19**(1): p. 95-102.

10.   Golay, J. and M. Introna, *Mechanism of action of therapeutic monoclonal antibodies: promises and pitfalls of in vitro and in vivo assays.* Arch Biochem Biophys, 2012. **526**(2): p. 146-53.

11.   Roopenian, D.C. and S. Akilesh, *FcRn: the neonatal Fc receptor comes of age.* Nat Rev Immunol, 2007. **7**(9): p. 715-25.

12.   Abdiche, Y.N., et al., *The neonatal Fc receptor (FcRn) binds independently to both sites of the IgG homodimer with identical affinity.* MAbs, 2015. **7**(2): p. 331-43.

13.   Neuber, T., et al., *Characterization and screening of IgG binding to the neonatal Fc receptor.* MAbs, 2014. **6**(4): p. 928-42.

14.   Hamblett, K.J., et al., *Altering antibody drug conjugate binding to the Neonatal Fc Receptor impacts efficacy and tolerability.* Mol Pharm, 2016.

15.   Suzuki, T., et al., *Importance of neonatal FcR in regulating the serum half-life of therapeutic proteins containing the Fc domain of human IgG1: a comparative study of the affinity of monoclonal antibodies and Fc-fusion proteins to human neonatal FcR.* J Immunol, 2010. **184**(4): p. 1968-76.

16.   Schlothauer, T., et al., *Analytical FcRn affinity chromatography for functional characterization of monoclonal antibodies.* MAbs, 2013. **5**(4): p. 576-86.

17.   Wu, Q., et al., *Development and applications of AlphaScreen-based FcRn binding assay to characterize monoclonal antibodies.* J Immunol Methods, 2015. **420**: p. 31-7.

18.   Manta, B., et al., *Tools to evaluate the conformation of protein products.* Biotechnol J, 2011. **6**(6): p. 731-41.

19.   Leonard, P., S. Hearty, and R. O'Kennedy, *Measuring protein-protein interactions using Biacore.* Methods Mol Biol, 2011. **681**: p. 403-18.

20.   US patent 6117980 A, Humanized anti-IL-8 monoclonal antibodies. [http://www.google.com/patents/US6117980

21.   Karlsson, R., et al., *Analyzing a kinetic titration series using affinity biosensors.* Anal Biochem, 2006. **349**(1): p. 136-47.

22. Iacob, R.E., et al., *Investigating monoclonal antibody aggregation using a combination of H/DX-MS and other biophysical measurements.* J Pharm Sci, 2013. **102**(12): p. 4315-29.

23. Houde, D., et al., *Post-translational modifications differentially affect IgG1 conformation and receptor binding.* Mol Cell Proteomics, 2010. **9**(8): p. 1716-28.

24. Houde, D., et al., *Characterization of IgG1 conformation and conformational dynamics by hydrogen/deuterium exchange mass spectrometry.* Anal Chem, 2009. **81**(7): p. 2644-51.

25. Yan, Y., et al., *Isomerization and Oxidation in the Complementarity-Determining Regions of a Monoclonal Antibody: A Study of the Modification-Structure-Function Correlations by Hydrogen-Deuterium Exchange Mass Spectrometry.* Anal Chem, 2016. **88**(4): p. 2041-50.

26. Jensen, P.F., et al., *Investigating the interaction between the neonatal Fc receptor and monoclonal antibody variants by hydrogen/deuterium exchange mass spectrometry.* Mol Cell Proteomics, 2015. **14**(1): p. 148-61.

27. Fang, J., et al., *Effect of Fc-Glycan Structure on the Conformational Stability of IgG Revealed by Hydrogen/Deuterium Exchange and Limited Proteolysis.* Biochemistry, 2016. **55**(6): p. 860-8.

28. Klotz, I.M. and D.D. Mueller, *Local environment effects on hydrogen--deuterium exchange.* Biochemistry, 1969. **8**(1): p. 12-6.

29. Venable, J.D., et al., *Subzero temperature chromatography for reduced back-exchange and improved dynamic range in amide hydrogen/deuterium exchange mass spectrometry.* Anal Chem, 2012. **84**(21): p. 9601-8.

30. Engen, J.R. and T.E. Wales, *Analytical Aspects of Hydrogen Exchange Mass Spectrometry.* Annu Rev Anal Chem (Palo Alto Calif), 2015. **8**: p. 127-48.

31. Ahn, J., et al., *Accessing the reproducibility and specificity of pepsin and other aspartic proteases.* Biochim Biophys Acta, 2013. **1834**(6): p. 1222-9.

32. Dykstra, A.B., M. Chen, and K.D. Cook, *Complementary peptide sequence coverage using alternative enzymes for on-line digestion with a triaxial electrospray probe.* J Am Soc Mass Spectrom, 2009. **20**(11): p. 1983-7.

33. Ahn, J., et al., *Pepsin immobilized on high-strength hybrid particles for continuous flow online digestion at 10,000 psi.* Anal Chem, 2012. **84**(16): p. 7256-62.

34. Wang, W., et al., *Impact of methionine oxidation in human IgG1 Fc on serum half-life of monoclonal antibodies.* Mol Immunol, 2011. **48**(6-7): p. 860-6.

35. Goebl, N.A., et al., *Neonatal Fc receptor mediates internalization of Fc in transfected human endothelial cells.* Mol Biol Cell, 2008. **19**(12): p. 5490-505.

36. Khawli, L.A., et al., *Charge variants in IgG1: Isolation, characterization, in vitro binding properties and pharmacokinetics in rats.* MAbs, 2010. **2**(6): p. 613-24.

37. Bertolotti-Ciarlet, A., et al., *Impact of methionine oxidation on the binding of human IgG1 to Fc Rn and Fc gamma receptors.* Mol Immunol, 2009. **46**(8-9): p. 1878-82.

38. Pan, H., et al., *Methionine oxidation in human IgG2 Fc decreases binding affinities to protein A and FcRn.* Protein Sci, 2009. **18**(2): p. 424-33.

6.0

Identification and Quantitation of Bioprocess-related Host Cell Protein Impurities following Downstream Processing of Therapeutic Monoclonal Antibodies

6.1   Introduction

Monoclonal antibodies (mAbs), the largest class of recombinant biotherapeutic proteins currently marketed, are secreted from host cells during fermentation and subsequently purified using an optimised downstream processing (DSP) platform. Host cell proteins (HCPs) may be co-purified with therapeutic mAbs and hence are considered as a major class of bioprocess-related impurities and categorised as a critical quality attribute in the International Conference on Harmonisation (ICH) guideline Q11 - Development and manufacture of drug substances. [1] Due to their potential impact on drug product safety, including their potential to cause adverse events or antigenic effects in patients, it is a regulatory requirement to remove these impurities from therapeutic mAb products to below detectable levels when measured using highly sensitive analytical methods. [2][3] As HCPs have a diverse range of immunological and physiochemical properties, downstream processing (DSP) of mAbs requires multiple orthogonal purification steps, often comprised of Protein A affinity capture followed by additional chromatographic polishing. [4, 5] Protein A chromatography is capable of removing >98% of HCPs directly from the product stream and hence has become a standard component of downstream processing platforms for monoclonal antibodies and Fc fusion proteins. HCPs that are not removed *via* Protein A affinity chromatography have been shown to be retained due to their interaction with bound mAb rather than association with the Protein A resin itself. [6] The concentration and composition of HCPs in the harvest stream has been shown to be dependent on the host cell line and culturing process, cell viability at the time of harvest, the choice of downstream processing techniques and on the sequence of mAb under production. [4, 7-11] Considerable work has been undertaken to develop robust and sensitive analytical methods for HCP detection and quantitation due to the importance in

detecting HCPs during process development, biopharmaceutical production and in the final drug product.

The HCP content of in-process and final mAb drug product samples are typically quantified using anti-HCP enzyme-linked immuno-sorbent assays (ELISA). However, as the generation of antibodies used for ELISA is dependent on the immune response of the species used for anti-HCP antibody generation, HCPs that do not provoke an immune response or that produce a low immune response may not be detected. [9] Nevertheless, anti-HCP ELISA is highly sensitive (1-100 ppm) and is recommended by regulatory agencies for quantitation of total HCP content within in-process samples and in final drug product. [12] While quantitative information of the total HCP content provided by ELISA analysis is currently acceptable for lot-release, it does not provide any information on the profile or properties of HCPs, which may be used for process design improvement. Hence methods that facilitate identification of individual HCPs have gained prominence in recent years, most notable those incorporating mass spectrometry-based detection. Two dimensional gel electrophoresis (2-DE) with subsequent mass spectrometry-based protein identification has been used to determine HCPs present in products produced by different CHO cell lines.[6, 13-15] While more recently, LC-MS techniques have been applied to evaluate the clearance of HCPs from the process stream following various downstream processing steps. [16-18]

Quantitative proteomic approaches involving liquid chromatography coupled to mass spectrometry (LC-MS) operated in the data dependent acquisition (DDA) mode are widely used for detection of proteins in complex biological mixtures. However, as mAb concentration in biopharmaceutical samples are typically more than three orders of magnitude greater than HCP species, low intensity HCP peptides are not selected for fragmentation by DDA due to the intensity bias of the mAb peptides. Consequently, data independent acquisition (DIA) modes, such as multiplexed data acquisition (MS^E), have proven to be more suitable for the detection and quantitation of low abundance HCPs. [3, 19-22] The use of multidimensional chromatographic separation methods, in conjunction with MS^E detection allows for the analysis of a broad dynamic range of proteins [23] and when combined with label free Hi3 quantitation, [24] LC-MS^E represents a powerful approach for the quantitative analysis of HCPs. [19] Unlike alternative proteomic methods for HCP analysis that require the incorporation of a HCP enrichment step, [3, 25, 26] the 2D-LC-MS^E method has the added advantage of enabling the analysis of HCPs in the presence of the biotherapeutic protein product.

In this study, we applied an offline 2D-LC-MS^E proteomic platform with Hi3 quantitation to evaluate the suitability of four different elution buffers for the removal of HCPs from mAb samples following Protein A purification. In the first dimension a high pH reversed-phase HPLC method was used to generate a peptide map. Collected fractions were subsequently further separated using low pH reversed-phase nano-LC with hyphenated MS detection operated in the data independent MS^E mode. The effect of elution buffer choice on the quality of the therapeutic protein was evaluated by determination of critical quality attributes (CQAs) including aggregation profile, charge variant analysis and *N*-glycosylation analysis. In addition, the developed proteomic platform was used to investigate the impact of the time of cell culture harvest on the HCP repertoire of a therapeutic protein following Protein A purification. Subsequently, the incorporation of additional DSP procedures to compliment Protein A purification in removing HCPs from the product stream was evaluated.

6.2 Experimental

6.2.1 Reagents and Consumables

Dithiothreitol (DTT), Iodoacetamide (IAA), Acetonitrile, Formic acid, Triethylammonium bicarbonate (TAB), Ammonium hydroxide, Sodium acetate, Trisodium citrate dehydrate, L-arginine, Phosphate buffered saline, [Glu^1]-Fibrinopeptide B, Trifluoroacetic acid (TFA), Sodium hydroxide (NaOH), Acetone, Acetic acid, Trichloroacetic acid (TCA), Ammonium Bicarbonate, Sodium chloride (NaCl), dimethyl sulfoxide (DMSO), 2-aminobenzamide (2-AB), Sodium Cyanoborohydride, Phosphate Buffered Saline (PBS), Sodium phosphate monobasic dihydrate (NaH$_2$PO$_4 \cdot$ 2H$_2$O) and Sodium phosphate dibasic heptahydrate (Na$_2$HPO$_4 \cdot$ 7H$_2$O) were purchased from Sigma Aldrich and were ACS reagent grade or better (Wicklow, Ireland).

Water, 0.1 % formic acid (LC-MS Optima), Acetonitrile, 0.1 % formic acid (LC-MS Optima) and Water, 0.1 % TFA (LC-MS Optima) were obtained from Fisher Scientific (Dublin, Ireland). pH gradient buffers CX-1, pH gradient buffer A (pH 5.6) and CX-1, pH gradient buffer B (pH 10.2) were acquired from Thermo Scientific. Promega sequencing grade modified trypsin was from MyBio Ltd. (Kilkenny, Ireland). New England Biolabs Glycerol Free PNGase F, (exoglycosidase enzymes) were purchased from Brennan and Co. (Dublin, Ireland). Glycine was obtained from USB Corporation (Ohio, USA). A BioRad QuickStart^{TM} Bradford Protein Assay Kit with Bovine γ-globulin standard sets was acquired from Fannin Ltd. (Dublin, Ireland). A CHO HCP ELISA kit was purchased from Cygnus Technologies (North Carolina, USA). 100% Acetic acid (AnalaR NORMAPUR) was from VWR (Dublin, Ireland). RapiGest SF surfactant and Hi3 *E. coli* standard

peptides were purchased from Waters (Dublin, Ireland). New Objectives Silica Tip Pico Tip emitters were obtained from Aquilant scientific UK Ltd. (Hampshire, UK).

6.2.2   Cell Culture

A Chinese hamster ovary cell line (CHO DP-12 clone#1934 [CHO DP-12, clone#1934 aIL8.92 NB 28605/14] (ATCC® CRL-12445^{TM}) producing recombinant human anti-interleukin 8 IgG1 antibody, mAb1, was purchased from LGC standards (Middlesex, UK) and adapted to grow in serum-free suspension culture. CHO DP-12 cells were grown in 200 mL (shake flask, 125 rpm) of Excell 325 PF CHO serum-free cell culture medium (Sigma Aldrich) supplemented with 10 mg.L^{-1} recombinant human Insulin (Sigma Aldrich), 1 µM Methotrexate (Sigma Aldrich), 4 mM L-glutamine (Biosciences) and 20,000 Units of Penicillin-Streptomycin (Fisher Scientific) at 37 °C (5% CO_2). Viability and viable cell density were measured using the trypan blue exclusion method and a haemocytometer. Culture supernatant was obtained by centrifuging the cell suspension (4000 rpm, 5 minutes) and was stored at -30°C pending further analysis.

6.2.3   IgG Purification

6.2.3.1 Protein A Affinity Chromatography

Aliquots of cell culture supernatant were clarified prior to Protein A purification by sequential filtration through 0.45 µm and 0.2 µm syringe filters (VWR). Samples were then purified *via* Protein A chromatography using a 1 mL HiTrap Protein A column (GE Healthcare). Samples of clarified media were passed through the Protein A column at a flow rate of 1 mL.min^{-1} and subsequently washed with PBS to ensure complete removal of all un-retained material. Elution of mAb1 from the Protein A column was performed using one of four buffers, namely 100 mM sodium acetate, pH 3.5; 100 mM glycine, pH 3.5; 100 mM citrate, pH 3.5 or 100 mM arginine, pH 3.5. The pH of eluate, collected in Amicon Ultra centrifugal filter units with a 10 kDa cut-off membrane (Sigma Aldrich), was neutralized using 0.5 M Tris and buffer-exchanged into PBS (4,000 rpm for 20 min). An aliquot of the concentrated and buffer exchanged mAb1 sample was assayed for IgG content using the Bradford assay, wherein samples were diluted 50-fold with Bradford reagent and incubated for 30 minutes at room temperature before recording the sample absorbance using a spectrophotometer at 595 nm. Sample concentration was calculated using a standard curve prepared from BSA standards of known concentration

prepared at the same time The remainder of the samples were stored at -30°C pending further analysis.

6.2.3.2 Multimodal Chromatography Purification *via* Capto^TM Adhere ImpRes

Following Protein A purification, 2 mg of mAb1 was further purified using a multimodal strong anion exchange resin, Capto^TM adhere ImpRes (GE Healthcare), operating in flow-through mode. Following sample application, the column was washed with PBS until mAb1 had fully eluted from the column. Adsorbed material was eluted using 100 mM acetic acid, pH 3.0. The flow-through mAb1 was collected in Amicon Ultra 10 kDa centrifugal filter units (Sigma Aldrich) and centrifuged (4,000 rpm for 20 min). An aliquot of mAb1 sample was assayed for IgG content using the Bradford assay. The remainder of the sample was stored at -30°C pending further analysis.

6.2.4   High pH- Low pH 2D-LC-MS^E Analysis of HCPs

1 mg of mAb was denatured with 0.1% (w/v) Rapigest, reduced with 5 mM DTT for 60 minutes at 20°C, alkylated with 15 mM IAA for 30 minutes at 20°C in darkness and enzymatically digested overnight (37 °C) with trypsin using a 1:50 (w/w, enzyme: protein) ratio. Following digestion the Rapigest surfactant was hydrolysed by the addition of an equal volume of 1% (v/v) formic acid in 10% acetonitrile. Samples were incubated for 10 minutes at 20°C and centrifuged (10 minutes, 16,000 x g) for removal of the insoluble constituent of the hydrolysed Rapigest. The supernatant was reduced to dryness *via* vacuum centrifugation.

Dried peptides were reconstituted in 500 µL of 0.1% formic acid and analysed using a Waters 2695 Alliance HPLC instrument with UV detection for first dimension separation. Peptide separations were performed on a Waters XBridge BEH 130 C18 3.5 µm 2.1 x 150 mm analytical column using a binary gradient of 20 mM ammonium formate in water, pH 10 (A) and 20 mM ammonium formate in 90% acetonitrile, pH 10 (B). Gradient conditions were as follows: 3% B initially for 2 minutes, increased to 10% B in 2 minutes with a further increase to 45% B over 33 minutes followed by a final increase to 100% B in two minutes with a two minute isocratic hold. Initial conditions were restored in one minute and held for an additional 10 minutes to ensure column re-equilibration. The column temperature was maintained at 40°C and the flow rate was 200 µL.min^-1. Sample fractions were collected at minute intervals over the course of the gradient and subsequently recombined to 20 samples in such a way as to ensure that

resulting samples contained peptides with a range of hydrophobicity and a similar peptide concentration, estimated based on UV absorbance at 214 nm. Resulting samples were reduced to dryness *via* vacuum centrifugation.

A Waters nanoAcquity™ UPLC® instrument equipped with a nanoAcquity UPLC 2G-V/M Trap 5 µm symmetry C18, 180 µm x 20 mm trapping column and a nanoAcquity UPLC 1.8 µm HSS T3, 75 µm x 200 mm analytical column was used for the second dimension low pH LC-MS separation of peptides. Prior to loading, peptide samples were reconstituted in 1.6 µL 0.1% FA and 6.4 µL of 1 pmol.µL^{-1} Hi3 *E. coli* standard peptides and loaded onto the trapping column at a flow rate of 10 µL.min^{-1} using 0.1% (v/v) formic acid in water (C) and 0.1% (v/v) formic acid in acetonitrile (D). Trapping conditions were maintained at 99.9% C for 5 minutes. Subsequent analytical separation of peptides was achieved using the following gradient conditions: 3% D initially for 2 minutes, increased to 6% D in 2 minutes with a further increase to 25% D over 88 minutes followed by a final increase to 85% B in two minutes with a two minute isocratic hold. Initial conditions were restored in 11 minutes and held for an additional 15 minutes to ensure column re-equilibration. The column temperature was maintained at 30°C throughout and the flow rate at 0.3 µL.min^{-1}. Injection volume was 2.5 µL.

Eluate from the chromatographic system was sampled directly into a Synapt G2 HDMS QTof mass spectrometer (Millford, MA, USA) via a NanoLockSpray™ dual electrospray ion source equipped with a nanoflow sprayer using 10 ± 1 µm PicoTip emitters. The mass spectrometer was operated in positive ion data independent mode with one second sequential low and high energy scans in the range of 50 to 2,000 Da. The spray voltage was 3 kV. A collision energy ramp from 20 to 45 V was used for the high energy function. Glu-fibrinopeptide (m/z 785.8426, z=2) was used as lockmass solution, recorded at 30 second intervals.

Resultant data were processed using ProteinLynx Global Server (PLGS) version 3.0.1. for identification and quantitation of HCPs, using the following workflow parameters: automatic peptide and fragment tolerances with lockmass correction of all doubly charged masses, minimum number of fragment ion matches per peptide = 3, minimum number of fragment ion matches per protein = 7, minimum number of unique peptides per protein = 2, primary digest reagent trypsin, with maximum number of one missed cleavage, fixed modification: carbamidomethyl C, variable modifications: oxidation M and deamidation N, Q, false discovery rate maintained at 1% FDR. Data was searched against the *Cricetulus griseus*, NCBI FASTA database (http://www.ncbi.nlm.nih.gov/assembly/GCF_000419365.1/, downloaded 12th June 2015), appended with Hi3 standard protein sequence (*E. coli* chaperone protein ClpB) and the known mAb sequence. Processing parameters were optimized using Waters PLGS Threshold

Inspector software version 2.0. Processed data for each sample fraction were combined using the 'Merge data' function in PLGS. A minimum of two unique peptides was required for protein identification. Three unique peptides were necessary for Hi3 quantitation of individual proteins. For each identified protein, PLGS software reported absolute quantitation in terms of femtomoles and nanograms of protein in each sample. Given that one milligram of mAb was prepared; it was possible to determine the amount of each HCP expressed in nanograms per milligram of mAb, i.e. ppm of HCP in mAb sample.

6.2.5 Intact Protein Analysis of mAb Critical Quality Attributes

MAb critical quality attributes (CQAs) including aggregation profile and charge variant analysis were determined using a Waters Acquity H-Class Bio UPLC instrument with UV detection at 280 nm. The presence of protein aggregates and higher order structures was determined *via* size exclusion chromatography, SEC-UV, using an Acquity UPLC BEH200 SEC 1.7 µm, 2.1 x 150 mm (Waters) column under isocratic conditions of 100 mM sodium phosphate buffer, 150 mM NaCl, pH 6.8 at 0.3 mL.min^{-1}. Charge variant analysis of intact mAb was performed using a pH gradient based separation on a MAbPac SCX-10 RS analytical column, 5 µm, 2.1 x 50 mm (Thermo Scientific) using CX-1 pH gradient buffer A, pH 5.6 and CX-1 pH gradient buffer B, pH 10.2 (Thermo scientific). Elution of sample peaks was achieved using a linear gradient of 37 - 55% CX-1 pH gradient buffer B, pH 10.2 in 10 minutes.

6.2.6 Glycan Analysis

50 µg of Protein A purified mAb1 was prepared in 50 mM ammonium bicarbonate, reduced with 1 mM DTT for 10 minutes at 65°C and alkylated by incubation with 5 mM IAA at room temperature in the dark for 30 minutes. *N*-glycans were enzymatically released by overnight (16 hour) incubation with 500 Units of PNGase F. Following digestion, the mAb was removed from solution using ice cold ethanol precipitation. The liquid phase containing the glycans was reduced to dryness *via* vacuum centrifugation. Released glycans were then fluorescently derivatised *via* reductive amination using 5 µL of 0.37 M 2-aminobenzamide (2AB) and 0.95 M sodium cyanoborohydride in 30% v/v acetic acid in DMSO at 65°C for two hours. Upon completion of the labelling reaction, 10 µL of water and 85 µL of acetonitrile were added to the sample. Excess fluorophore was removed by HILIC chromatography using a Thermo Ultimate 3000 RS HPLC equipped with an Acquity BEH Glycan analytical column, 1.7 µm, 2.1 x

50 mm (Waters). Purified *N*-glycans were collected and reduced to dryness by vacuum centrifugation. 2AB-derivatised *N*-glycan samples were subsequently reconstituted in 50 µL of 80% acetonitrile and analysed using a Waters Acquity I-Class UPLC instrument with fluorescence detection. Separations were performed using a BEH Glycan, 1.7 µm, 2.1 x 100 mm analytical column using a gradient of 50 mM ammonium formate, pH 4.5 and acetonitrile, 70 to 53% acetonitrile at 0.561 mL.min^{-1} in 15.5 minutes. Column temperature was maintained at 40°C. Excitation and emission wavelengths for fluorescence detection were λ_{ex} = 330 nm and λ_{em} = 420 nm. Exoglycosidase digestion of *N*-glycans was performed using an adaption of the method described by Royle and co-workers. [27]

6.2.7   Anti-Host Cell Protein ELISA

HCPs were quantified by ELISA using a CHO HCP ELISA kit (Cygnus technologies) according to the high sensitivity protocol recommended by the manufacturer. Optical density was measured using a Perkin Elmer Victor X3 Multi-label plate reader at 450 nm.

6.3   Results and Discussion

6.3.1   Analytical Platform Performance
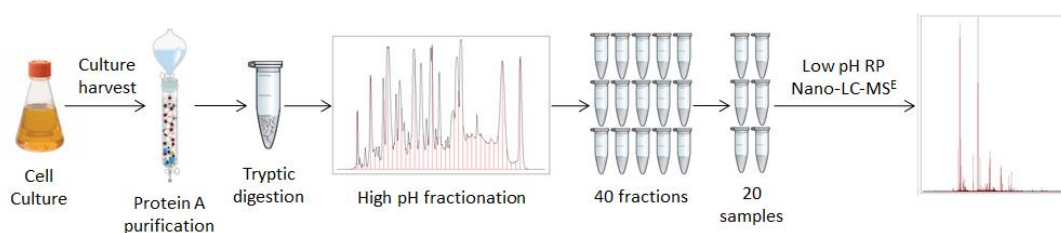
Figure 6.1: Schematic of workflow for discovery proteomic analysis of HCPs in biotherapeutic protein samples.

A standard schematic of the workflow used for processing of HCP samples is shown in Figure 6.1. To determine the performance of the proteomic platform, cell culture media containing mAb1, HCPs and other contaminants was harvested and processed using Protein A affinity chromatography. In total 1 mg of mAb1 was reduced, alkylated and digested with trypsin before undergoing offline 2D high pH/low pH reversed phase separation. Unlike previous

studies which utilised online 2D-LC-MS^E for the analysis of HCPs in biopharmaceutical samples, [19, 28] the use of offline high pH separation in the first dimension allows for the generation of a high performance peptide map at pH 10. As will be discussed later in this Section, the formation of a peptide separation map permits the subsequent investigation of potential sites of interaction between HCPs and individual mAb peptides. Following high pH fractionation, the sample fractions were combined such that approximately the same amount of peptides was contained in each of 20 samples for low pH nano-LC-MS^E analysis. As previously noted the use of the data independent MS^E approach allows us to investigate the HCPs attached to the actual therapeutic protein itself, by enabling a broad dynamic range for protein detection and by eliminating any selection bias for ions as is characteristic of data dependent MS acquisition modes. Due to the complexity of the method, incorporating multi-dimensional separation and long run times, the precision of the proteomic method was evaluated in terms of repeatability, based on the response of Hi3 standard peptides added to each of the prepared samples. Following MS analysis, the peak heights of five Hi3 standard peptides in extracted ion chromatograms for each of 20 second dimensional LC-MS^E injections across three experiments, shown in Figure 6.2, were evaluated using the ANOVA statistical test. Using ANOVA it was determined that at 95% confidence level, no significant difference (P-value > 0.05) in the peak heights of the Hi3 standards was determined across multiple experiments. Actual P-values from ANOVA analysis of standard peptide ion peak height in different samples and experiments are displayed in Table 6.1. The Hi3 quantitation method was used to ensure stringency with the resultant proteomic data, wherein a minimum requirement of three unique identified peptides per protein was needed for quantitation. In addition to ensuring the accurate quantitation of proteins, previously proven by Silva *et al.*[24], the necessity for a minimum of three unique peptides also ensures specificity of protein identifications.
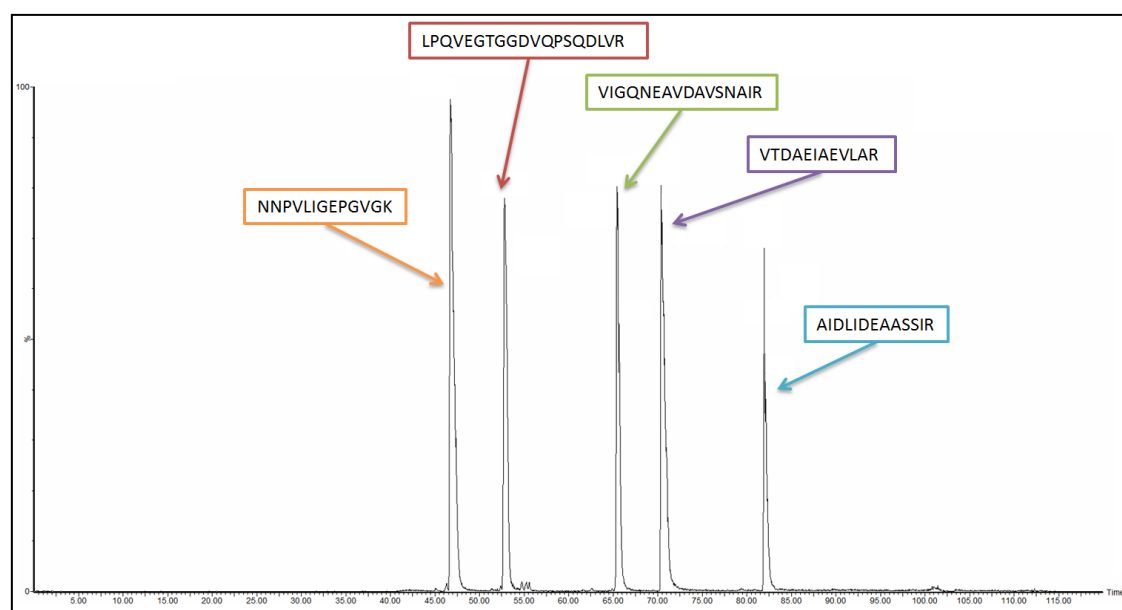
Figure 6.2: Extracted ion chromatogram displaying ion peaks for each of the standard peptides used for Hi3 quantitation.

Table 6.1: Resulting P-values from ANOVA determination of peak heights for each standard peptide ion in extracted ion chromatograms analysed.

Hi3 Standard Peptide Sequence	Average Molecular Weight	m/z	P-value
NNPVLIGEPGVGK	1293.4863	647.38	0.13770
LPQVEGTGGDVQPSQDLVR	1995.1776	998.54	0.12817
VIGQNEAVDAVSNAIR	1655.8292	828.47	0.07979
VTDAEIAEVLAR	1286.4484	643.88	0.55885
AIDLIDEAASSIR	1373.5266	687.39	0.14309

6.3.2   Evaluation of Protein A Elution Buffers on mAb HCP Load

DSP of mAbs generally involves the use of Protein A affinity chromatography in the first stage of the purification process, wherein the mAb is retained and washed at neutral pH and subsequently eluted from the Protein A resin by exposure to low pH (2.8-4.0) elution buffers. A variety of elution buffers for Protein A purification are frequently used in industry including acetate, arginine, citrate and glycine based buffers. [29, 30] The choice of elution buffer and also pH and volume of elution buffer form a large portion of DSP development. [31]

To determine the criticality of the Protein A elution buffer for elimination of HCPs from the product stream, the developed proteomic platform was applied to evaluate the effect of

different Protein A elution buffers commonly used in DSP on the resulting mAb HCP load. Suspension batch culture of CHO DP12 cells expressing a human anti-interleukin 8 IgG1 antibody, mAb1, was prepared using batch culture as described in Section 6.2.2. Following entry into the stationary phase of cell growth, the culture was harvested and subsequently divided into four equal volumes of spent media, which were individually filtered and purified using HiTrap Protein A affinity chromatography in accordance with the procedure outlined in Section 6.2.3.1. For each of the four samples, mAb1 was eluted from the Protein A resin using one of the following buffers: 100 mM sodium acetate, pH 3.5; 100 mM arginine, pH 3.5; 100 mM citrate, pH 3.5 or 100 mM glycine, pH 3.5. Following buffer exchange into PBS, the samples were assayed for protein content and analysed for HCP concentration using high pH/low pH reversed phase 2D-LC-MS^E method described previously. HCPs that were found to have co-purified with mAb1 following Protein A chromatography are depicted in Figure 6.3. The description and quantity of the HCPs identified in each of the samples is outlined in Table 6.2.
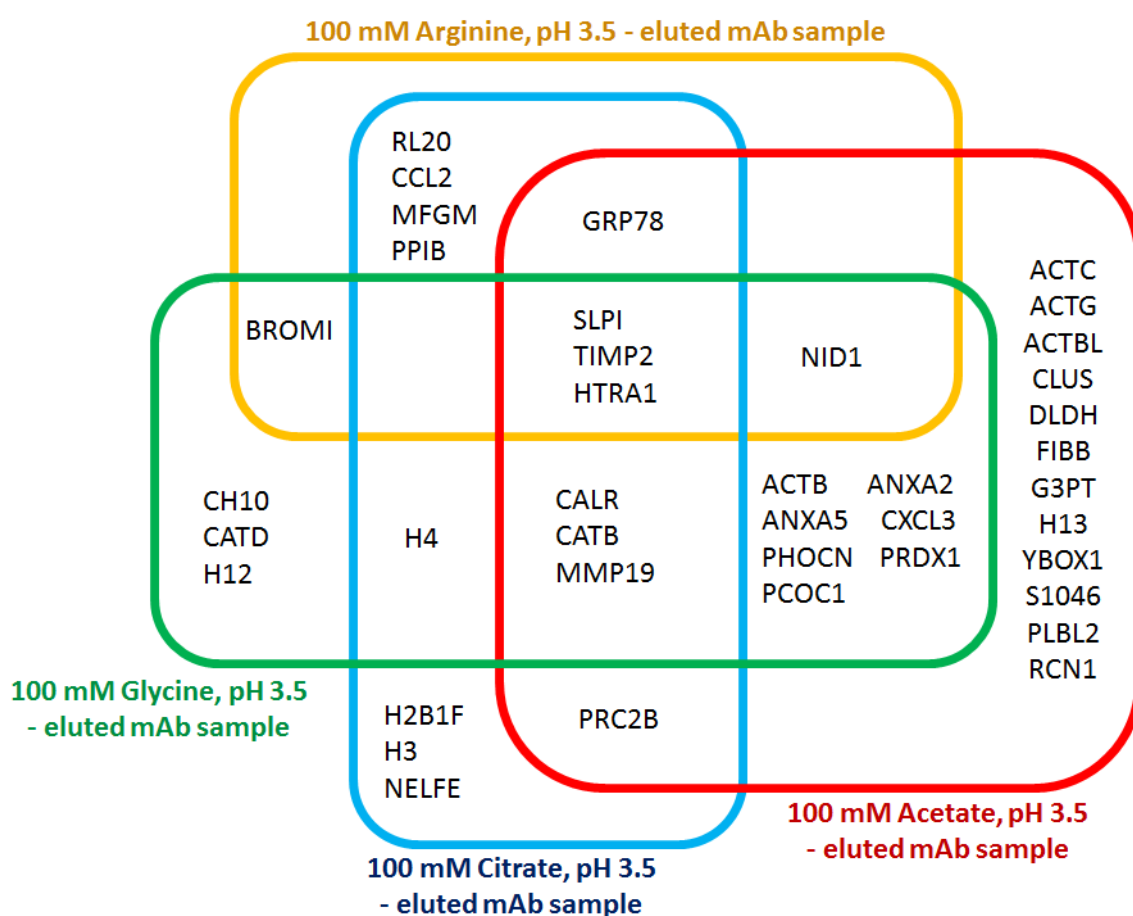
Figure 6.3: Venn diagram showing the distribution of HCPs identified in mAb samples eluted from Protein A resin using various buffers under study. A description of the protein entries shown in the Venn diagram may be found in Table 6.2.

Table 6.2: Summary of identified HCPs and related concentrations in combined sample sets processed from Protein A resin with different elution buffers.

Protein Entry	Protein Description	100 mM Acetate	100 mM Arginine	100 mM Citrate	100 mM Glycine	PLGS protein score Range	Protein average mass (kDa)	Protein Sequence Coverage Range (%)	Number of Peptides Identified
	List of HCPs identified with >2 unique peptides	Concentration of HCP in combined sample sets (ppm - ng/mg)							
CH10	10 kDa heat shock protein mitochondrial	ND	ND	ND	*	542.0	11.032	23.53	2
RL20	60S ribosomal protein L30	ND	44.1	*	ND	780.6 - 2090.1	12.955	20.80 - 26.09	2 – 3
GRP78	78 kDa glucose-regulated protein	73.7	126.3	205.6	ND	419.3 - 503.4	72.550	11.93 - 14.53	7 – 12
ACTC	Actin alpha cardiac muscle 1	*	ND	ND	ND	307.7	42.361	14.59	2
ACTB	Actin cytoplasmic 1	*	ND	ND	113.7	470.9 - 569.6	42.080	20.27 - 36.27	2 – 11
ACTG	Actin cytoplasmic 2	19.5	ND	ND	ND	627.4	33.391	17.69	7
ANXA2	Annexin A2	*	ND	ND	232.6	396.4 - 771.0	38.946	9.73 - 25.37	2 – 5
ANXA5	Annexin A5	95.1	ND	ND	*	346.7 - 536.4	36.122	10.28 - 19.31	2 – 6
SLPI	Antileukoproteinase	1088.3	819.4	3727.5	4528.7	2531.1 - 21214.76	16.745	30.56 - 59.72	4 – 10
ACTBL	Beta-actin-like protein 2	153.0	ND	ND	ND	257.1	37.484	15.57	5
CALR	Calreticulin	208.1	ND	360.8	380.5	819.7 - 1882.2	48.414	30.46 - 37.41	8 – 13
CATB	Cathepsin B	99.4	ND	*	261.1	479.2 - 2732.9	38.417	10.03 - 40.12	2 – 8
CATD	Cathepsin D	ND	ND	ND	951.6	285.7	44.567	7.60	8
CCL2	C-C motif chemokine 2	ND	*	*	ND	635.6 - 703.7	16.201	5.59	2
CLUS	Clusterin	445.9	ND	ND	ND	535	52.385	20.58	12
CXCL3	C-X-C motif chemokine 3	72.7	ND	ND	*	2258.0 - 3765.8	11.264	40.59	2 - 5
DLDH	Dihydrolipoyl dehydrogenase mitochondrial	*	ND	ND	ND	342.5	54.702	5.89	2
FIBB	Fibrinogen beta chain	*	ND	ND	ND	335.0	54.893	3.55	2
G3PT	Glyceraldehyde-3-phosphate dehydrogenase	*	ND	ND	ND	407.4	35.976	6.91	2

H12	Histone H1.2	ND	ND	ND	82	1212.3	21.285	17.92	5
H13	Histone H1.3	*	ND	ND	ND	1196.2	20.512	17.87	2
H2B1F	Histone H2B type 1-F/J/L	ND	ND	*	ND	2297.5	11.158	27.45	2
H3	Histone H3	ND	ND	*	ND	951.4	24.371	11.93	2
H4	Histone H4	ND	ND	*	86.3	782.6 - 1301.0	8.983	24.69 - 37.04	2 – 3
MFGM	Lactadherin	ND	207.1	419.6	ND	2639.8 - 3598.1	48.284	43.56 - 52.22	9 – 15
MMP19	Matrix metalloproteinase-19	*	ND	210.0	449.8	462.7 - 584.3	59.170	12.57 - 20.38	2 – 8
TIMP2	Metalloproteinase inhibitor 2	358.7	298.0	346.9	1583.4	507.5 - 2285.2	27.486	17.62 - 52.46	6 – 9
PHOCN	MOB-like protein phocein isoformX2	627.4	ND	ND	*	540.8 - 2205.8	32.759	20.28 - 25.17	2 – 8
NELFE	Negative elongation factor E	ND	ND	*	ND	755.8	42.788	26.26	2
NID1	Nidogen-1	3357.9	*	ND	2516	308.9 - 744.5	135.143	14.19 - 25.91	2 – 26
YBOX1	Nuclease-sensitive element-binding protein 1	318.6	ND	ND	ND	565.7	32.776	31.03	8
PPIB	Peptidyl-prolyl cis-trans isomerase B	ND	*	85.3	ND	619.8 - 1464.6	23.692	21.76 - 22.22	2 – 6
PRDX1	Peroxiredoxin-1	*	ND	ND	*	210.0 - 653.6	22.548	9.17 - 16.08	2
PCOC1	Procollagen C-endopeptidase enhancer	98.8	ND	ND	1210	222.8 - 1109.1	51.131	16.45 - 33.55	7 – 11
PRC2B	Proline-rich protein 2-like	1940.1	ND	*	ND	1310.9 - 1512.2	52.585	62.63 - 63.93	2 - 52
BROMI	Protein Broad minded isoform X3	ND	*	ND	*	374.5 - 415.7	146.423	4.77 - 5.16	2
S1046	Protein S100-A6	1.4	ND	ND	ND	1187.4	10.108	61.80	6
PLBL2	Putative phospholipase B-like 2	*	ND	ND	ND	313.2	65.940	9.40	2
RCN1	Reticulocalbin-1	*	ND	ND	ND	741.6	19.539	55.76	2
HTRA1	Serine Protease HTRA1	247.6	781.0	1247.9	2119.5	592.1.2 - 1530.7	48.697	24.94 - 38.98	7 - 13
	Total concentration (ppm - ng HCP/mg IgG)	**9206.2**	**2275.9**	**6603.6**	**14515.2**				

HCPs identified using a minimum of 2 peptides are denoted by the symbol '*', while undetected HCPs are represented by 'ND'.

A total of 40 individual HCPs were identified across the four samples. The highest overall HCP concentration was quantified in the mAb1 sample eluted from Protein A resin with a glycine-based buffer. This is in agreement with total HCP concentration values obtained following sample determination using HCP ELISA, namely 169.36 ppm, 139.21 ppm, 156.45 ppm and 216.12 ppm for mAb1 processed using acetate-, arginine-, citrate- and glycine-based buffers respectively. Although the actual HCP concentration values recovered using ELISA was less than those quantified using the 2D-LC-MS^E method, the quantified total concentration for sample purified using a glycine-based buffer was notably higher for both methods. Deviations between results obtained for HCP concentration using ELISA and 2D-LC-MS^E methods were investigated using CHOPPI, a web based tool for determination of immunogenicity potential of CHO proteins. [32] Using CHOPPI, many of the HCPs identified and quantified in mAb samples purified with the different buffer systems outlined, were predicted to be immunologically inert (immunogenicity score < -20), as shown in Table 6.3. Therefore many of the HCPs identified potentially will not illicit an immune response during the generation of antibodies used for anti-HCP ELISA. Hence anti-HCP ELISA may underestimate the total concentration of HCPs in a mAb samples.

In the remaining samples eluted from Protein A resin using acetate, arginine and citrate-based buffers, the total HCP concentrations determined were 9206.2, 2275.9, and 6603.6 ppm, respectively. The most abundant HCPs quantified were proline rich protein 2, nidogen-1, antileukoproteinase, metalloproteinase inhibitor 2, and serine protease HTRA1, the latter three contaminants being common to all four samples. Several of the HCPs identified, including the most abundant HCPs outlined, were in agreement with those identified in other studies investigating HCP content of biotherapeutic mAb samples produced in CHO cells. [4, 16, 19, 33, 34] Interestingly, some of the HCPs identified in the mAb1 samples processed using the different Protein A elution buffers investigated are those that are known to impact DSP and the quality of therapeutic protein products, *e.g.* purative phospholipase B-like 2 and various histones. Purative phospholipase B-like 2 has been shown to catalyse the breakdown of Polysorbate 20, a non-ionic surfactant frequently used in biopharmaceutical formulation to prevent protein aggregation and denaturation. [35, 36] Histones are the primary component of Chromatin, which bind Protein A *via* their nucleosomal histone components thereby inhibiting access of mAb to Protein A, reducing the binding capacity of Protein A and ultimately decreasing the overall yield of therapeutic mAbs. [37]

Table 6.3: Whole protein immunogenicity score reported by the CHOPPI web tool for assessment of immunogenicity risk from HCPs in CHO-based protein production. Proteins with an immunogenicity score of > 20 are considered to be a high risk for immunogenicity, while proteins with a score < -20 are reportedly immunologically inert.

Protein Entry	Protein Description	CHOPPI Immunogenicity Score
YBOX1	Nuclease-sensitive element-binding protein 1	-65.86
RCN1	Reticulocalbin-1	-57.94
PRDX1	Peroxiredoxin-1	-51.76
GRP78	78 kDa glucose-regulated protein	-48.51
G3PT	Glyceraldehyde-3-phosphate dehydrogenase	-39.89
H13	Histone H1.3	-39.18
CALR	Calreticulin	-37.79
ACTB	Actin cytoplasmic 1	-34.19
CATB	Cathepsin B	-32.6
NID1	Nidogen-1	-32.42
ACTC	Actin alpha cardiac muscle 1	-32.34
H12	Histone H1.2	-28.81
PCOC1	Procollagen C-endopeptidase enhancer	-28.49
ACTBL	Beta-actin-like protein 2	-26.78
TIMP2	Metalloproteinase inhibitor 2	-25.28
FIBB	Fibrinogen beta chain	-24.24
DLDH	Dihydrolipoyl dehydrogenase mitochondrial	-22.06
PPIB	Peptidyl-prolyl cis-trans isomerase B	-13.65
HTRA1	Serine Protease HTRA1	-13.02
CATD	Cathepsin D	-11.36
ACTG	Actin cytoplasmic 2	-9.36
MFGM	Lactadherin	-9.16
CH10	10 kDa heat shock protein mitochondrial	-7.1
CLUS	Clusterin	-3.55
MMP19	Matrix metalloproteinase-19	-2.49
SLPI	Antileukoproteinase	0.01
PHOCN	MOB-like protein phocein isoform X2	4.44
H2B1F	Histone H2B type 1-F/J/L	6.77
H4	Histone H4	7.67
NELFE	Negative elongation factor E	10.59
ANXA2	Annexin A2	14.87
CCL2	C-C motif chemokine 2	18.31
H3	Histone H3	25.79
PLBL2	Putative phospholipase B-like 2	32.89
S1046	Protein S100-A6	52.84
ANXA5	Annexin A5	52.91
RL20	60S ribosomal protein L30	57.41
CXCL3	C-X-C motif chemokine 3	91.84

ICH guideline Q5E outlines a requirement to ensure that any alterations in a bioprocess should not have an adverse impact on the safety, quality and efficacy of a therapeutic drug product. [38] In addition to examining the impact of Protein A elution buffer selection on the HCP load of the mAb product, additional CQAs were also examined, including protein aggregation profile, *N*-glycosylation analysis, charge variants and levels of oxidation and deamidation of the mAb product.

Charge variant analysis and determination of protein aggregation were performed as described in Section 6.2.5 and resulting chromatographic profiles are shown in Figure 6.4. Comparable aggregation profiles were observed for all samples. In agreement with previous studies, which have shown IgG1 to be resistant to low pH aggregation, [29] the results herein demonstrate low concentration of protein aggregation following Protein A purification with each of the buffer systems under evaluation. The SEC and charge variant analysis results are presented in Table 6.4. For both charge variant analysis and SEC, the mAb1 sample purified from Protein A using citrate buffer was found to contain the highest concentration of variants and aggregation although these values were to not found to be statistically significantly higher than those purified with alternative elution buffers.
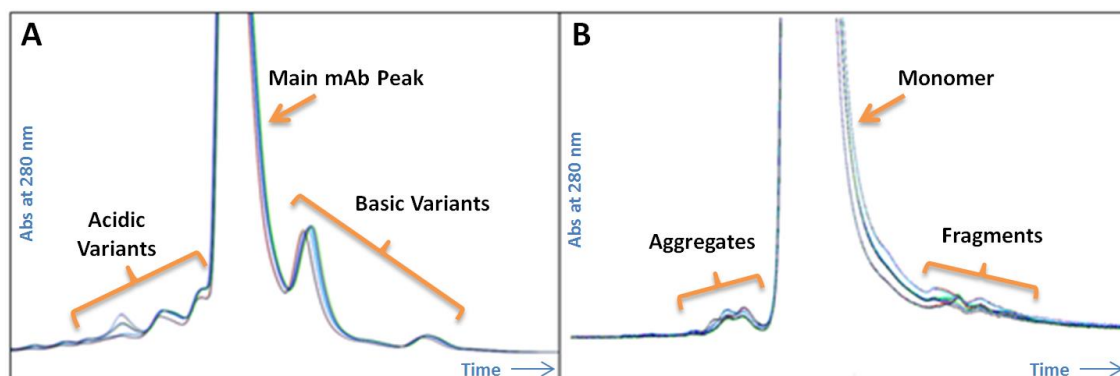
Figure 6.4: Chromatographic profiles obtained from (A) charge variant analysis and (B) SEC, both shown in expanded scale, for mAb1 samples purified from Protein A resin using acetate-, arginine-, citrate- and glycine-based buffers. Reference Table 6.4 for numerical values obtained from these analyses.

Table 6.4: Analytical results from charge variant and size exclusion analysis of intact mAb1.

Buffer under evaluation	Charge variant analysis			Size exclusion analysis		
	% acidic variants	% main	% basic variants	% aggregates	% monomer	% fragment
100 mM sodium acetate, pH3.5	2.75 ± 0.23	87.61 ± 0.14	9.64 ± 0.94	0.10 ± 0.94	99.87 ± 0.12	0.03 ± 10.57
100 mM arginine, pH3.5	2.14 ±1.64	88.72 ± 0.14	9.14 ±0.59	0.10 ± 3.08	99.87 ± 0.06	0.03 ± 15.59
100 mM citrate, pH3.5	3.43 ± 1.36	87.21 ± 0.21	9.37 ± 0.26	0.19 ± 0.95	99.76 ± 0.10	0.05 ± 13.74
100 mM glycine, pH3.5	1.94 ± 2.15	88.76 ± 0.22	9.30 ± 0.57	0.12 ± 3.24	99.84 ± 0.05	0.04 ± 3.49

Analysis of *N*-glycans present on mAb1 samples eluted from Protein A resin with the different buffer systems was also performed as per Section 6.2.6; resulting chromatograms are shown in Figure 6.5. Peaks corresponding to the *N*-glycans released from the mAb1 samples were integrated and compared based on relative percentage areas. Differences in the levels of certain *N*-glycans identified using a panel of exoglycosidase digestions were found to be those bearing terminal galactose residues, Figure 6.5, between the mAbs eluted using the different buffers. Although galactosylation has not been correlated with adverse events in patients treated with biotherapeutic mAb products, it may impact mAb effector functions [39] and hence these results suggest, for this particular mAb, the use of glycine-based buffers in DSP may have an effect on product efficacy.

Levels of deamidation and oxidation on the mAb peptide identified following LC-MS^E analysis of Protein A purified mAb1 samples eluted with the four aforementioned buffer systems were also examined. A total of 13, 10, 10 and 9 modified peptides were identified in mAb1 samples processed using acetate-, arginine- citrate- and glycine-based buffers, respectively, eight of which were common to all samples (data not shown).

| Main Buffer Constituent | % Area of Integrated Peak in Total Chromatogram | | | | | | | | | | | | | |
	Peak 1	Peak 2	Peak 3	Peak 4	Peak 5	Peak 6	Peak 7	Peak 8	Peak 9	Peak 10	Peak 11	Peak 12	Peak 13	Peak 14
Acetate	2.38	48.58	0.13	0.58	0.26	30.14	10.84	0.50	5.52	0.61	0.08	0.12	0.20	0.06
	2.37	48.17	0.14	0.59	0.27	30.26	10.89	0.50	5.72	0.61	0.08	0.13	0.20	0.07
	2.35	47.99	0.14	0.58	0.26	30.31	11.01	0.50	5.78	0.61	0.08	0.13	0.19	0.07
Arginine	2.69	50.68	0.05	0.59	0.28	29.21	10.64	0.45	4.59	0.51	0.03	0.05	0.16	0.07
	2.58	50.22	0.05	0.60	0.28	29.37	10.85	0.45	4.76	0.52	0.03	0.06	0.16	0.07
	2.56	50.16	0.05	0.59	0.28	29.42	10.85	0.45	4.82	0.51	0.03	0.05	0.16	0.07
Citrate	2.28	50.11	0.19	0.54	0.26	29.26	10.61	0.48	5.20	0.60	0.04	0.11	0.21	0.11
	2.27	49.83	0.19	0.55	0.27	29.30	10.71	0.48	5.31	0.60	0.03	0.12	0.22	0.12
	2.27	49.78	0.19	0.55	0.27	29.31	10.73	0.48	5.34	0.61	0.03	0.12	0.21	0.11
Glycine	3.74	58.78	0.05	0.69	0.31	24.47	8.68	0.37	2.45	0.30	0.01	0.03	0.06	0.06
	3.39	58.68	0.06	0.69	0.31	24.61	8.83	0.36	2.55	0.31	0.01	0.03	0.08	0.09
	3.38	58.52	0.06	0.69	0.31	24.75	8.82	0.36	2.57	0.33	0.01	0.03	0.08	0.09

Figure 6.5: Overlay of chromatgrams displaying *N*-glycan profiles of mAb1 processed from Protein A resin using elution buffers 100 mM sodium acetate, pH 3.5, 100 mM arginine, pH 3.5, 100 mM citrate, pH 3.5 and 100 mM glycine, pH 3.5.

As each of the mAb1 samples purified using Protein A resin were produced using the same cell culture, resulting data from HCP analysis and determination of CQAs should in theory be identical across all samples. As the difference in Protein A elution buffer remained the single variable in DSP of the mAbs, any disparity in HCP profile or quality attributes of the mAb could be associated with the choice of the Protein A elution buffer. The glycine elution buffer resulted in the highest overall concentration of HCPs and also revealed a negative impact on mAb CQAs relative to the other buffers investigated. The greatest number of individual HCPs identified and the highest number of modified mAb1 peptides were found in mAb1 purified using an acetate buffer. Samples purified using the arginine buffer were found to contain fewer individual HCP species and a considerably lower overall concentration of HCPs when compared to othe purified mAb1 samples. Arginine buffers have recently attracted increased interest for the elution of mAbs from Protein A resins due to their ability to suppress protein-protein interactions and protein-surface interactions [40] resulting in desirable characteristics including enhancement of virus inactivation. [41] The arginine-based elution buffer was used for all subsequent Protein A purifications of mAb1 in this study.

As offline high performance peptide maps were generated while fractionating the mAb1 samples, the possibility of relating the carriage of HCP through DSP to specific portions of the mAb itself was investigated. Calreticulin, a HCP identified in multiple samples, was selected for further investigation to determine possible interactions with mAb1. Calreticulin was identified and quantified in a single fraction of three of the mAb samples analysed using 2D-LC-MS^E. MAb1 peptides also contained within these fractions were noted and are highlighted in Figure 6.6. As the Figure shows, the peptides contained within the fractions are not confined to one particular portion of the mAb, inhibiting any potential correlation of interaction of Calreticulin with a specific mAb sequence region. Grand average of hydropathy (GRAVY) score for each of the mAb1 and HCP peptides was also evaluated resulting in no significant enrichment of GRAVY scores suggesting that the retention of HCPs is not hydrophobicity based (data not shown).
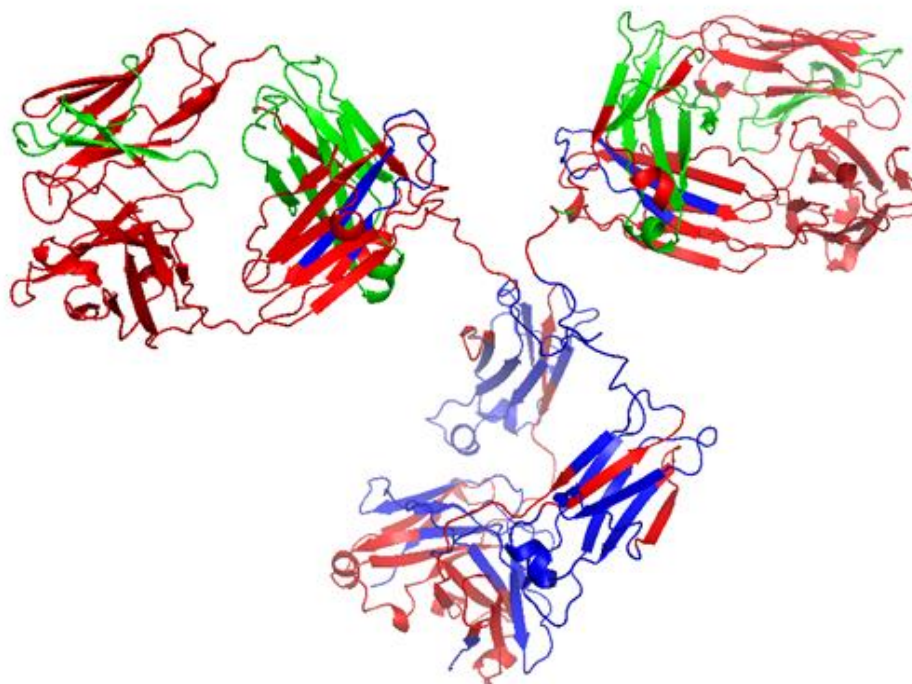
Figure 6.6: Graphic of anti-Interleukin 8 IgG1 (mAb1) structure. MAb1 peptides, which were identified in sample fractions also containing Calreticulin peptides, are highlighted in the heavy chain (blue) and light chain (green) portions of the structure. [42]

6.3.3   Evaluation of Impact of Harvest Time on HCP Repertoire

Cell culture duration and cell viability are interrelated factors that may have a significant effect on the composition and quantity of HCPs in biotherapeutic products. [9, 14, 15, 34] To investigate the impact of cell culture harvest time, the developed 2D-LC-MS^E proteomic platform was applied in a temporal manner to determine changes in the HCP repertoire of purified mAb samples, following harvest at different stages of cell culture. Replicate cell cultures producing mAb1 were prepared concurrently and batch cultured under identical conditions for five days. On day five, having reached the stationary phase of cell growth, the first culture was harvested. The second cell culture was continued for a further two days, until such a time as the culture had reached the end of the stationary phase of cell growth and at which time the viability of the cells had begun to decrease. Resultant mAb1 samples were analysed for HCP content using the high pH low pH 2D-LC-MS^E method described in Section 6.2.4. Identified and quantified HCPs in the mAb1 samples are outlined in Table 6.5.

HCPs identified at the onset of stationary phase samples are predominantly secreted proteins while the majority (>70%) of HCPs identified in the end of stationary phase samples are characterised as intracellular proteins. [43] In addition, the mAb1 samples, from culture harvested at the beginning of the stationary phase were found to contain lower levels of HCPs when compared to mAb harvested at the end of the stationary phase. The increased instances of intracellular proteins in mAb1 samples harvested at the end of the stationary phase may be attributed to a loss in viability of cell culture (98.5% to 90.8%) likely resulting from lysis or rupture of cells rather than secretion of protein material from within the cell.

Table 6.5: Host cell proteins identified and quantified in Protein A purified mAb1 samples harvested at different stages of cell culture growth.

Protein Entry	Protein Description	Cellular Location	Cell Culture Harvest time	
			HCP concentration (ppm) - Start of stationary phase	HCP concentration (ppm) - End of stationary phase
GRP78	78 kDa glucose-regulated protein	Cytoplasm, Endoplasmic reticulum	ND	329.6
ACTB	Actin (cytoplasmic 1)	Cytoplasm	ND	83.5
ATL4	ADAMTS-like protein 4	Secreted	*	
SLPI	Antileukoproteinase	Secreted	*	25.9
ABCG3	ATP-binding cassette sub-family G member 3	Cell membrane	ND	*
DHX8	ATP-dependent RNA helicase DHX8	Nucleus, cytoplasm	ND	*
CALR	Calreticulin	Endoplasmic reticulum	ND	*
CLUS	Clusterin	Secreted, nucleus, cytoplasm	*	288.6
G3P	Glyceraldehyde-3-phosphate dehydrogenase	Cytoplasm, nucleus	ND	67.7
H2AX	Histone H2AX	Nucleus, chromosome	ND	*
MFGM	Lactadherin	Secreted	21.3	ND
MMP19	Matrix metalloproteinase-19	Secreted	43.5	*
TIMP2	Metalloproteinase inhibitor 2	Secreted	ND	*
NID1	Nidogen-1	Secreted	1189.7	772.3
PRDX1	Peroxiredoxin-1	Cytoplasm, nucleus	559.8	343.2
PAIRB	Plasminogen activator inhibitor 1 RNA-binding protein	Cytoplasm, nucleus	*	ND
PCOC1	Procollagen C-endopeptidase enhancer	Secreted	*	ND
HTRA1	Serine Protease HTRA1	Secreted, cytoplasm	ND	111.2
TPA	Tissue-type plasminogen activator	Secreted, cytoplasm	*	ND
Total HCP concentration (ppm - ng of HCP/ mg of mAb)			**1814**	**2022**

HCPs identified using a minimum of 2 peptides are denoted by the symbol '*', while undetected HCPs are represented by 'ND'.

6.3.4 Evaluation of Additional Downstream Processing Steps

Purification of mAbs requires multiple complimentary DSP steps to remove HCPs and other contaminants with potentially wide ranging physicochemical and physiological properties. As previously discussed, the first step usually involves the use of Protein A resin to extract mAbs from the harvest stream. Subsequently, the product undergoes one or two additional chromatography polishing steps to guarantee a highly pure product. These additional steps are aimed at reducing HCPs, host cell DNA, low molecular weight clipped species, high molecular weight aggregates and also leached Protein A resin, to acceptable levels. [31] Common polishing steps include cation exchange chromatography, anion exchange chromatography, hydrophobic interaction chromatography or a combination of multiple chromatographic resin interactions known as mixed mode chromatography. The choice of chromatography mode depends on the properties of the host expression system and the biotherapeutic protein, the impurities that require clearance and difficulty involved in impurity removal. [44] As common DSP unit operations for mAbs dictate the use of subsequent chromatographic steps to compliment Protein A purification, the effect of integrating a multi-modal chromatography step on the profile and concentration of HCPs in a purified mAb sample was evaluated. A mixed mode strong anion exchange resin with hydrophobic properties, Capto Adhere ImpRes^{TM} (GE Healthcare), was incorporated as a second DSP step to evaluate the capability of this additional DSP step for removal of HCP impurities. Capto Adhere ImpRes^{TM} resin contains a quaternary ammonium group for anion exchange mediated retention of negatively charged sample components such as host cell DNA, an aromatic functionality and small alkyl chain that may facilitate retention of sample components through hydrophobic interactions. [5]

To evaluate the effect of the additional multi-modal step, an aliquot of mAb1-containing culture harvest was purified using Protein A chromatography. Subsequently, a portion of the purified mAb1 was further processed using mixed-mode Capto Adhere ImpRes^{TM} chromatography conducted in flow-through mode as outlined in Section 6.2.3.2. Comparative analysis of both samples was then performed by 2D-LC-MS^E. HCPs identified and quantified in samples taken before and after the multi-modal chromatography step are shown in Table 6.6.

Unsurprisingly, the addition of the second purification step resulted in a dramatic reduction in HCP profile concentration. A singular HCP, namely Histone H2AX, was found to be present in the Capto Adhere ImpRes^{TM}-purified mAb1 sample but not at levels that could facilitate quantitation.

Table 6.6: Host cell protein profile of mAb1 samples taken before and after mixed-mode chromatographic polishing using Capto Adhere ImpRes™.

Protein Entry	Protein Description	Concentration of HCP in combined sample sets (ppm - ng/mg)	
		Following Protein A purification	Following Protein A and Capto adhere ImpRes purification
GRP78	78 kDa glucose-regulated protein	329.6	ND
ACTB	Actin (cytoplasmic 1)	83.5	ND
SLPI	Antileukoproteinase	25.9	ND
ABCG3	ATP-binding cassette sub-family G member 3	*	ND
DHX8	ATP-dependent RNA helicase DHX8	*	ND
CALR	Calreticulin	*	ND
CLUS	Clusterin	288.6	ND
G3P	Glyceraldehyde-3-phosphate dehydrogenase	67.7	ND
H2AX	Histone H2AX	*	*
MMP19	Matrix metalloproteinase-19	*	ND
TIMP2	Metalloproteinase inhibitor 2	*	ND
NID1	Nidogen-1	772.3	ND
PRDX1	Peroxiredoxin-1	343.2	ND
HTRA1	Serine Protease HTRA1	111.2	ND
Total HCP concentration (ppm - ng of HCP/ mg of mAb)		**2022**	ND

HCPs identified using a minimum of 2 peptides are denoted by the symbol '*', while undetected HCPs are represented by 'ND'.

6.4 Conclusions

A high pH/low pH reversed phase nano-2D-LC-MS^E method with Hi3 quantitation for the determination of HCPs in purified mAb samples is described. The use of off-line high pH fractionation facilitates a more thorough investigation of potential interactions that may have resulted in the carriage of HCPs through Protein A purification during DSP. No specific correlations of HCPs with regions of the mAb were identified; however, presented data suggests that the interaction of HCPs with mAb was not hydrophobicity based. The choice of Protein A elution buffer was demonstrated to exhibit a potential impact on the HCP repertoire of purified mAb samples. A link between the time of culture harvest and the abundance of HCPs present following a Protein A affinity capture step was verified, and is thought to result from a loss of cell viability in samples harvested at a later stage of cell culture. Inclusion of additional DSP demonstrated how complementary polishing successfully removed HCPs in the process stream to very low levels. Taken together these results show the importance in optimising components of downstream processing including choice of buffers used for purification and viability or age of cell culture at the time of harvest. This data shows how mass spectrometry methods are capable of providing a wealth of information that provides valuable insights for DSP. Compared to ELISA, mass-spectrometry-based methods may provide a more comprehensive characterisation of HCPs, not only facilitating a more efficient removal strategy for DSP, but also allowing for a more rational assessment of potential safety risks posed by individual HCPs.

6.5 Associated Publication and Author Contributions

Adapted from Farrell, A., et al., *Quantitative host cell protein analysis using two dimensional data independent LC-MS^E*. Analytical Chemistry, 2015, **87**(18):9186-93.

Research study devised by Amy Farrell and Jonathan Bones; research performed by Amy Farrell; Stefan Mittermayr contributed to *N*-glycan analysis; Brian Morrissey and Niaobh McLoughlin provided advice regarding industrial relevance; Natalia Navas Iglesias provided commercial samples that were not included in the final study; data and related paper were reviewed by Jonathan Bones, Ian Marison, Brian Morrissey and Niaobh McLoughlin.

6.6 References

1. International Conference on Harmonisation, 2012, ICH Harmonised Tripartite Guideline, Development and Manufacture of Drug Substances (Chemical Entities and Biotechnological/Biological Entities) Q11. Retrieved 28 May 2016 from http://www.ich.org/fileadmin/Public_Web_Site/ICH_Products/Guidelines/Quality/Q11/Q11_Step_4.pdf.

2. U.S. Food and Drug Administration. 1997. Points to Consider in the Manufacture and Testing of Monoclonal Antibody Products for Human Use. Centre for Biologics Evaluation and Research, Food and Administration.

3. Thompson, J.H., et al., *Improved detection of host cell proteins (HCPs) in a mammalian cell-derived antibody drug using liquid chromatography/mass spectrometry in conjunction with an HCP-enrichment strategy.* Rapid Commun Mass Spectrom, 2014. **28**(8): p. 855-60.

4. Levy, N.E., et al., *Identification and characterization of host cell protein product-associated impurities in monoclonal antibody bioprocessing.* Biotechnol Bioeng, 2014. **111**(5): p. 904-12.

5. Pezzini, J., et al., *Antibody capture by mixed-mode chromatography: a comprehensive study from determination of optimal purification conditions to identification of contaminating host cell proteins.* J Chromatogr A, 2011. **1218**(45): p. 8197-208.

6. Tarrant, R.D., et al., *Host cell protein adsorption characteristics during protein A chromatography.* Biotechnol Prog, 2012. **28**(4): p. 1037-44.

7. Sisodiya, V.N., et al., *Studying host cell protein interactions with monoclonal antibodies using high throughput protein A chromatography.* Biotechnol J, 2012. **7**(10): p. 1233-41.

8. Hogwood, C.E., D.G. Bracewell, and C.M. Smales, *Measurement and control of host cell proteins (HCPs) in CHO cell bioprocesses.* Curr Opin Biotechnol, 2014. **30**: p. 153-60.

9. Tait, A.S., et al., *Host cell protein dynamics in the supernatant of a mAb producing CHO cell line.* Biotechnol Bioeng, 2012. **109**(4): p. 971-82.

10. Hogwood, C.E., et al., *The dynamics of the CHO host cell protein profile during clarification and protein A capture in a platform antibody purification process.* Biotechnol Bioeng, 2013. **110**(1): p. 240-51.

11. Hogwood, C.E., et al., *An ultra scale-down approach identifies host cell protein differences across a panel of mAb producing CHO cell line variants.* Biotechnol J, 2016. **11**(3): p. 415-24.

12. International Conference on Harmonisation. 1999. ICH Harmonised Tripartite Guideline, Specifications: Test Procedures and Acceptance Criteria for Biotechnological/ Biological Products Q6B. Retrieved 28 May 2016 from http://www.ich.org/fileadmin/Public_Web_Site/ICH_Products/Guidelines/Quality/Q6 B/Step4/Q6B_Guideline.pdf.

13. Krawitz, D.C., et al., *Proteomic studies support the use of multi-product immunoassays to monitor host cell protein impurities.* Proteomics, 2006. **6**(1): p. 94-110.

14. Jin, M., et al., *Profiling of host cell proteins by two-dimensional difference gel electrophoresis (2D-DIGE): Implications for downstream process development.* Biotechnol Bioeng, 2010. **105**(2): p. 306-16.

15. Grzeskowiak, J.K., et al., *2-D DIGE to expedite downstream process development for human monoclonal antibody purification.* Protein Expr Purif, 2009. **66**(1): p. 58-65.

16. Zhang, Q., et al., *Comprehensive tracking of host cell proteins during monoclonal antibody purifications using mass spectrometry.* MAbs, 2014. **6**(3): p. 659-70.

17. Levy, N.E., et al., *Host cell protein impurities in chromatographic polishing steps for monoclonal antibody purification.* Biotechnol Bioeng, 2016. **113**(6): p. 1260-72.

18. Chiverton, L.M., et al., *Quantitative definition and monitoring of the host cell protein proteome using iTRAQ - a study of an industrial mAb producing CHO-S cell line.* Biotechnol J, 2016.

19. Doneanu, C.E., et al., *Analysis of host-cell proteins in biotherapeutic proteins by comprehensive online two-dimensional liquid chromatography/mass spectrometry.* MAbs, 2012. **4**(1): p. 24-44.

20. Geromanos, S.J., et al., *The detection, correlation, and comparison of peptide precursor and product ions from data independent LC-MS with data dependant LC-MS/MS.* Proteomics, 2009. **9**(6): p. 1683-95.

21. Silva, J.C., et al., *Quantitative proteomic analysis by accurate mass retention time pairs.* Anal Chem, 2005. **77**(7): p. 2187-200.

22. Levin, Y., E. Hradetzky, and S. Bahn, *Quantification of proteins using data-independent analysis (MSE) in simple andcomplex samples: a systematic evaluation.* Proteomics, 2011. **11**(16): p. 3273-87.

23. Schenauer, M.R., G.C. Flynn, and A.M. Goetze, *Identification and quantification of host cell protein impurities in biotherapeutics using mass spectrometry.* Anal Biochem, 2012. **428**(2): p. 150-7.

24. Silva, J.C., et al., *Absolute quantification of proteins by LCMSE: a virtue of parallel MS acquisition.* Mol Cell Proteomics, 2006. **5**(1): p. 144-56.

25. Bomans, K., et al., *Identification and monitoring of host cell proteins by mass spectrometry combined with high performance immunochemistry testing.* PLoS One, 2013. **8**(11): p. e81639.

26. Zhu, G., et al., *Absolute quantitation of host cell proteins in recombinant human monoclonal antibodies with an automated CZE-ESI-MS/MS system.* Electrophoresis, 2014. **35**(10): p. 1448-52.

27. Royle, L., et al., *Detailed structural analysis of N-glycans released from glycoproteins in SDS-PAGE gel bands using HPLC combined with exoglycosidase array digestions.* Methods Mol Biol, 2006. **347**: p. 125-43.

28. Schenauer, M.R., G.C. Flynn, and A.M. Goetze, *Profiling the effects of process changes on residual host cell proteins in biotherapeutics by mass spectrometry.* Biotechnol Prog, 2013. **29**(4): p. 951-7.

29. Hari, S.B., et al., *Acid-induced aggregation of human monoclonal IgG1 and IgG2: molecular mechanism and the effect of solution composition.* Biochemistry, 2010. **49**(43): p. 9328-38.

30. Wang, S. and A. Raghani, *Arginine as an eluent for automated on-line Protein A/size exclusion chromatographic analysis of monoclonal antibody aggregates in cell culture.* J Chromatogr B Analyt Technol Biomed Life Sci, 2014. **945-946**: p. 115-20.

31. Shukla, A.A., et al., *Demonstration of robust host cell protein clearance in biopharmaceutical downstream processes.* Biotechnol Prog, 2008. **24**(3): p. 615-22.

32. Bailey-Kellogg, C., et al., *CHOPPI: a web tool for the analysis of immunogenicity risk from host cell proteins in CHO-based protein production.* Biotechnol Bioeng, 2014. **111**(11): p. 2170-82.

33. Joucla, G., et al., *Cation exchange versus multimodal cation exchange resins for antibody capture from CHO supernatants: identification of contaminating host cell proteins by mass spectrometry.* J Chromatogr B Analyt Technol Biomed Life Sci, 2013. **942-943**: p. 126-33.

34. Valente, K.N., A.M. Lenhoff, and K.H. Lee, *Expression of difficult-to-remove host cell protein impurities during extended Chinese hamster ovary cell culture and their impact on continuous bioprocessing.* Biotechnol Bioeng, 2014.

35. Li, Y., et al., *Characterization and stability study of polysorbate 20 in therapeutic monoclonal antibody formulation by multidimensional ultrahigh-performance liquid chromatography-charged aerosol detection-mass spectrometry.* Anal Chem, 2014. **86**(10): p. 5150-7.

36. Dixit, N., et al., *Residual Host Cell Protein Promotes Polysorbate 20 Degradation in a Sulfatase Drug Product Leading to Free Fatty Acid Particles.* J Pharm Sci, 2016. **105**(5): p. 1657-66.

37. Gagnon, P., et al., *Nonspecific interactions of chromatin with immunoglobulin G and protein A, and their impact on purification performance.* J Chromatogr A, 2014. **1340**: p. 68-78.

38. International Conference on Harmonisation, Note for guidance on biotechnological/biological products subject to changes in their manufacturing process (CP<P/ICH/5721/03) June 2005. Retrieved 12 February 2015 from http://www.ema.europa.eu/docs/en_GB/document_library/Scientific_guideline/2009/09/WC500002805.pdf.

39. Raju, T.S. and R.E. Jordan, *Galactosylation variations in marketed therapeutic antibodies.* MAbs, 2012. **4**(3): p. 385-91.

40. Arakawa, T. and Y. Kita, *Multi-faceted arginine: mechanism of the effects of arginine on protein.* Curr Protein Pept Sci, 2014. **15**(6): p. 608-20.

41. Yamasaki, H., et al., *Arginine facilitates inactivation of enveloped viruses.* J Pharm Sci, 2008. **97**(8): p. 3067-73.

42. PyMOL molecular visualisation system version 1.3r1. Downloaded from http://pymol.org/educational/ on 01 December 2014.

43. *UniProt: a hub for protein information.* Nucleic Acids Res, 2015. **43**(Database issue): p. D204-12.

44. Wang, X., A.K. Hunter, and N.M. Mozier, *Host cell proteins in biologics development: Identification, quantitation and risk assessment.* Biotechnol Bioeng, 2009. **103**(3): p. 446-58.

7.0

Overall Conclusions and Future Research Direction

7.1   Overall Conclusions

CHO cells are important expression systems currently used in the biopharmaceutical industry for the production of a wide range of therapeutic proteins and thus represent a significant area of interest for biopharmaceutical research. Although specific production of biomolecules in CHO cells has previously been optimised using cell and bioprocess engineering strategies, current and future advances in analytical instrumentation are theorised to contribute to increased cellular-level understanding of CHO cells and ultimately result in improvements in biotherapeutic production and product quality. The goals of this work were to apply state-of-the-art analytical techniques to gain a greater understanding of recombinant protein producing CHO cells during routine bioprocessing. By preparing concurrent identical CHO DP-12 cell cultures, in highly controlled bioreactor systems, and altering one bioprocessing parameter, *e.g.* pH, temperature or dissolved oxygen, potential changes to the CHO cell proteomes in response to that particular condition could be identified. Subsequently, through application of spent media to naïve CHO cells, a further goal to evaluate the effects of CHO secretome during bioprocessing could be assessed. In addition to evaluation of CHO cells, extensive product characterisation techniques were developed and applied for determination of the impact of altered bioprocessing on the therapeutic protein produced. Furthermore, since the presence of host cell protein (HCP) impurities in therapeutic drug products has the potential to cause adverse events in patients, a final goal was to develop an analytical method that could identify HCP impurities in purified drug product.

Chapter 2 focused on the development and application of a state-of-the-art quantitative proteomics platform, incorporating two dimensional high pH-low pH reversed phase nano liquid chromatography mass spectrometry with SPS-MS^3 detection of TMT-sixplex labelled proteome samples, to facilitate comparison of the effects of individual culture characteristics on a CHO cell proteome. In addition to profiling the changes to a recombinant monoclonal antibody producing CHO cell line, caused by alterations in bioprocessing parameters typically applied during biopharmaceutical production, the platform was also applied for the evaluation

of the bystander response of CHO cells in culture, to the secretome of production cells maintained at different bioprocess conditions. The developed proteomic platform displayed excellent performance capabilities, enabling the identification and relative quantitation of thousands of proteins with relatively low first dimensional pre-fractionation. Application of the method for the evaluation of CHO DP-12 cells producing anti-interleukin 8 IgG1 enabled the realisation of a snapshot into CHO production cells responding to altered bioprocessing, illustrating the robustness of the bioprocess in terms of the effect on recombinant protein expressing CHO cells. Observation of increased activity for proteins involved in signalling pathways for both CHO production cells, and also for naïve CHO cells in response to CHO secretome, signified a high level of activity within the cells relating to normal growth but also highlighted the benefit of investigating the cell as a whole, *i.e.* to use a multi-omics approach incorporating phosphoproteomics, metabolomics and product characterisation, to obtain a full picture of the molecular level manifestations within the cell in response to the altered bioprocessing conditions applied.

The proteomics study was complemented by sequence level characterisation of recombinant anti-interleukin 8 IgG1 produced during CHO DP-12 culture maintained under different bioprocessing settings. This work, described in Chapter 3, involved the determination of the size, hydrophobicity and charge variant profile of mAb samples *via* evaluation of intact mAb species using various chromatographic approaches. Although miniscule changes to the size profile were observed, variations in the hydrophobicity and charge of some mAb samples were determined. High resolution mass spectrometry analysis was applied for the evaluation of protein mass following limited proteolysis to produce mAb subunits more amenable to mass spectrometry detection. Changes to the mass of the most abundant mAb species were not observed, however mAb heterogeneity was illustrated by the existence of low levels of species with variations in polypeptide mass, potentially corresponding to differently *N*-glycan moieties and sequence-level modifications. Protein heterogeneity was further investigated by high resolution LC-MS analysis of tryptic peptides for identification of modifications to mAb primary sequence. Varying levels of modified species were observed for various samples, most notably for anti-IL8 IgG1 produced at 32.0°C.

Due to the importance of mAb *N*-glycosylation in regards to the therapeutic function of mAbs *in-vivo*, variations in the *N*-glycosylation profile of anti-IL 8 IgG1 were investigated in Chapter 4. A twoplex method for comparative glycomics of *N*-glycans present on IgG1 was developed, based upon the differential labelling of samples for comparison with either 'light' $^{12}C_6$ 2-AA or 'heavy' $^{13}C_6$ 2-AA prior to hydrophilic interaction UPLC with sequential fluorescence and

accurate mass QToF-MS detection. Application of the developed method for the relative quantitation of *N*-glycans attached to mAbs produced under altered bioprocessing conditions revealed changes to the levels of some *N*-glycan species, in particular those attached to anti-IL 8 IgG1 produced at pH 7.2 and 110% dissolved oxygen.

The purpose of product characterisation is to estimate potential changes to the therapeutic function and safety of a drug substance, hence to thoroughly evaluate the effect of altered bioprocessing on the therapeutic protein produced, characterisation of the changes to the structure and function of the IgG was performed. In Chapter 5, a developed HDX-MS platform for the determination of conformation changes to therapeutic mAbs was described. Identification of changes to the uptake of deuterium by backbone amide hydrogen atoms of differentially produced anti-IL8 IgG1 as a function of time *via* MS^E detection of peptic peptides produced form samples following HDX, a number of conformational changes were detected in mAbs produced under altered conditions of 32.0^{o}C, pH 7.2, 60% DO and 110%DO. Subsequent surface plasmon resonance analysis of anti-IL8 samples revealed changes to the binding affinity of mAb produced at 32.0^{o}C for FcRn, the mAb cellular receptor, indicating a potential alteration in the serum half-life of anti-IL8 IgG1 resulting from low temperature production. Further surface plasmon resonance analysis to determine changes in the binding affinity of anti-IL8 to its target antigen interleukin 8 signified a negative impact on the therapeutic efficacy of mAbs produced using culture media with a dissolved oxygen concentration of 110%.

Finally, in addition to assessing the impact of upstream bioprocessing on therapeutic biomolecules, the identification and quantitation of bioprocess-related host cell protein impurities following downstream processing is described in Chapter 6. In this case a high pH low pH reversed phase nano-liquid chromatography mass spectrometry platform was developed and applied to evaluate different features of downstream processing including the choice of buffer used during Protein A purification, influence of multiple downstream processing steps and the effect of harvest time on the profile of HCPs detected. The developed platform may be of significance for product and process development as unlike many other methods described in the literature for HCP analysis, the method described is capable of identification of low levels of HCP impurities without the requirement for extraction or pre-concentration, which may artificially alter the actual HCP profile of therapeutic mAbs. Thus improvements to downstream processing may be made by targeting of HCPs identified using the platform described.

7.2   Future Research Direction

The following areas have been identified as potential avenues for future research:

- The developed high performance analytical platform, capable of quantitative proteomic analysis of thousands of proteins within a cellular sample, highlighted the ruggedness of the bioprocess used for CHO DP-12 culture. However, application of the platform to other molecules could be more informative, in particular for manufacturing processes wherein product critical quality attributes are difficult to control. This method could potentially form a key component of process optimisation and application of quality by design during product development.

- Proteomic analysis of CHO DP-12 cells and naïve CHO K1 cells revealed significant differential regulation of signalling pathways within the cell. Application of a combination of other omics strategies may provide an enhanced view of the molecular events within the cells. Specifically use of metabolomics, for determination of cellular outputs and phosphoproteomics, to evaluate whether variations in protein regulation observed in this study are attributed to differential signalling or differential expression, would be beneficial. Should additional markers be identified, a potential for cellular engineering for phenotype modification may arise, now possible using technologies such as CRISPR-Cas9.

- The advanced mass spectrometry-based analytical platforms developed for product characterisation were applied exclusively to monoclonal antibody samples, however as these methods use high resolution accurate mass technology, they may be used for the characterisation of any molecular entity. Application of the developed methods to new therapeutic entities, such as Fc fusion proteins, bispecific antibodies and antibody drug conjugates may be of particular interest. However, despite providing crucial information, the methods described were based on middle-down and bottom-up approaches to product characterisation. An ability to acquire high resolution mass spectrometric data of intact biomolecules could provide additional information regarding the causes of observed structural, functional or primary sequence modifications, *i.e.* to determine if a specific structural modification is a result of a sequence-level modification or vice versa.

- The HCP platform developed, based on MS^E, was highly conservative due to criteria required for Hi3 quantitation (>3 identified peptides for each protein). Future work to advance the platform further using either an improvement in the informatics platform to remove any potential bias for spectral intensity or a transformation of the platform

to higher resolution accurate mass platforms *e.g.* parallel reaction monitoring using an Orbitrap mass analyser, where accurate quantitation could be acquired based solely on the precursor may enable further confidence in the data acquired.

- The HCP analysis platform could enable the development of targeted analytical methods that may be used in a Quality Control laboratory to facilitate process monitoring and process improvements thereby potentially reducing high product attrition rates often associated with biopharmaceutical production. Skyline, a software application for building multiple reaction monitoring (MRM) quantitiative MS methods (https://skyline.gs.washington.edu), may enable the utilisation of data (generated using the HCP platform described in Chapter 6) for design of targeted MRM methods. These methods may then be further optimised using a triple-Quadrupole MS instrument, *e.g.* Agilent 6460.

- HDX is capable of providing useful information regarding protein higher order structure, however it is based on the reaction of amide hydrogen atoms only, thus facilitating tertiary structure determination only. If this method was complemented by the application of biophysical technology *e.g.* light scattering, fast photochemical oxidation of proteins (FPOP) or other spectroscopy-based methods, a deeper level of structural characterisation could be achieved.

- Despite some degree of resolution between intact protein species using available technologies, *e.g.* hydrophobic interaction and ion exchange chromatography, poor resolution attributable to low diffusion coefficients is observed. Scope for improvement exists for chromatographic methods available for intact protein analysis, in particular to enable efficient mass spectrometry analysis of intact protein species.

Supplementary Data

Appendix A

CHO DP-12 Proteins determined to be significantly differentially regulated in CHO DP-12 cultures prepared at altered Bioprocessing conditions when compared to CHO DP-12 cells cultured under standard Bioprocessing conditions. Proteomic samples were analysed using 2D-LC-MS^3 and data analysed using Thermo Fisher Scientific Proteome Discoverer version 2.1.0.81 and InfernoRDN version 1.1.5970.31895.

Table 1-A: Differentially regulated CHO DP-12 proteins determined in samples corresponding to culture using an increased bioprocessing temperature of 39.5°C.

RefSeq Annotation	Description	Fold Change	p-value
NM_001081242	talin 2	1.944	0.018
NM_144857	cDNA sequence BC011248	1.895	0.002
NM_010480	predicted gene 5511; heat shock protein 90, alpha (cytosolic), class A member 1	1.853	0.015
NM_133726	suppression of tumorigenicity 13	1.835	0.011
NP_001162071	guanine nucleotide binding protein-like 3 (nucleolar)-like	1.814	0.003
NM_027852	retinoic acid receptor responder (tazarotene induced) 2	1.794	0.029
NM_010729	lysyl oxidase-like 1	1.789	0.009
NM_010893	neuraminidase 1	1.782	0.000
NP_001135450	TPX2, microtubule-associated protein homolog	1.780	0.007
NM_011933	2-4-dienoyl-Coenzyme A reductase 2, peroxisomal	1.768	0.009
NM_001001491	tropomyosin 4; predicted gene 7809	1.764	0.006
NM_001082961	small nuclear ribonucleoprotein N; SNRPN upstream reading frame; predicted gene 5802; similar to SNRPN upstream reading frame protein	1.762	0.011
NM_021895	actinin alpha 4	1.760	0.025
NM_145392	BCL2-associated athanogene 2	1.759	0.010
NM_144937	ubiquitin specific peptidase 3	1.737	0.007
NM_145150	protein regulator of cytokinesis 1	1.733	0.021
NM_024223	cysteine rich protein 2	1.731	0.001
NM_016906	Sec61 alpha 1 subunit (S. cerevisiae)	1.730	0.001
NM_019772	predicted gene 9169; RIKEN cDNA 1110004F10 gene	1.730	0.001
NM_009297	suppressor of Ty 6 homolog	1.730	0.027
NM_009048	RalBP1 associated Eps domain containing protein	1.730	0.001
NM_001001491	tropomyosin 4; predicted gene 7809	1.729	0.001
NM_054043	Musashi homolog 2 (Drosophila)	1.729	0.002
NM_011175	Legumain	1.729	0.012
NM_025591	RIKEN cDNA 2010309E21 gene; similar to CG5323-PA	1.727	0.003
NM_025364	predicted gene 6563; SAP domain containing ribonucleoprotein	1.723	0.023
NM_024428	dpy-30 homolog (C. elegans); predicted gene 2059; similar to RIKEN cDNA 2810410M20 gene	1.723	0.005

NM_008972	predicted gene 12504; predicted gene 9800; predicted gene 4617; predicted gene 6625; predicted gene 7614; similar to prothymosin alpha; prothymosin alpha; predicted gene 9009	1.723	0.006
NM_028871	predicted gene 6159; heterogeneous nuclear ribonucleoprotein R	1.722	0.009
NM_026842	ubiquilin 1	1.719	0.007
NM_011070	prefoldin 2	1.719	0.043
NM_012021	peroxiredoxin 5	1.719	0.031
NM_013897	translocase of inner mitochondrial membrane 8 homolog b (yeast)	1.719	0.008
NM_008866	lysophospholipase 1	1.717	0.005
NM_026572	predicted gene 3672; similar to Glycine cleavage system H protein, mitochondrial precursor; glycine cleavage system protein H (aminomethyl carrier)	1.716	0.009
NM_026623	nudix (nucleoside diphosphate linked moiety X)-type motif 21	1.715	0.004
NM_008683	neural precursor cell expressed, developmentally down-regulated gene 8	1.714	0.011
NM_130889	acidic (leucine-rich) nuclear phosphoprotein 32 family, member B	1.713	0.011
NM_016786	ubiquitin-conjugating enzyme E2K (UBC1 homolog, yeast)	1.713	0.011
NM_133716	stromal membrane-associated GTPase-activating protein 2	1.709	0.005
NM_007466	apoptosis inhibitor 5	1.706	0.002
NM_144897	apolipoprotein A-I binding protein	1.706	0.017
NP_001136216	RIKEN cDNA 2610110G12 gene	1.706	0.003
NM_026020	similar to LOC665931 protein; ribosomal protein, large P2; predicted gene 7852; WD repeat domain 89	1.705	0.016
NM_025657	leucine rich repeat containing 57	1.705	0.043
NM_011801	craniofacial development protein 1	1.703	0.017
NM_172262	amine oxidase, flavin containing 1	1.703	0.014
NM_008520	latent transforming growth factor beta binding protein 3	1.700	0.018
NM_026988	Parathymosin	1.698	0.005
NM_008638	methylenetetrahydrofolate dehydrogenase (NAD+ dependent), methenyltetrahydrofolate cyclohydrolase	1.698	0.018
NM_010023	dodecenoyl-Coenzyme A delta isomerase (3,2 trans-enoyl-Coenzyme A isomerase)	1.693	0.005
NM_133934	ISY1 splicing factor homolog (S. cerevisiae)	1.693	0.012
NM_198937	hematological and neurological expressed 1-like	1.692	0.023
NM_080419	immunoglobulin superfamily, member 8	1.692	0.001
NM_023397	RIKEN cDNA 1810034K20 gene	1.692	0.023
NM_011418	SWI/SNF related, matrix associated, actin dependent regulator of chromatin, subfamily b, member 1	1.692	0.023
NM_025337	aldo-keto reductase family 7	1.691	0.015
NM_010479	heat shock protein 1B; heat shock protein 1A	1.691	0.007
NM_010361	glutathione S-transferase, theta 2	1.691	0.024
NM_011623	topoisomerase (DNA) II alpha	1.688	0.000
NM_133795	tetratricopeptide repeat domain 1	1.686	0.002
NM_029752	Bri3 binding protein	1.685	0.010
NM_010398	histocompatibility 2, T region locus 23; similar to RT1 class Ib, locus H2-Q-like, grc region	1.685	0.003
NM_026280	matrix-remodelling associated 7	1.683	0.013
NM_028871	predicted gene 6159; heterogeneous nuclear ribonucleoprotein R	1.683	0.017
NM_176968	5'-nucleotidase domain containing 1	1.682	0.018
NM_172572	rhomboid 5 homolog 2 (Drosophila)	1.682	0.011
NM_011752	zinc finger protein 259	1.682	0.041
NP_001157185	predicted gene 9755; Tu translation elongation factor,	1.681	0.002

	mitochondrial		
NM_053104	RNA binding motif protein 9	1.680	0.021
NM_023232	diablo homolog (Drosophila)	1.680	0.008
NM_019641	stathmin 1; predicted gene 11223; predicted gene 6393	1.677	0.021
NM_025299	thioredoxin-like 4A	1.677	0.003
NM_001029844	vaccinia related kinase 1	1.676	0.016
NM_029250	ethanolamine kinase 1	1.676	0.010
NP_001157583	nuclear factor of activated T-cells, cytoplasmic, calcineurin-dependent 1	1.675	0.006
NM_012047	bromodomain containing 7	1.675	0.010
NM_028870	clathrin, light polypeptide (Lcb)	1.674	0.032
NM_153552	THO complex 1	1.674	0.003
NM_001168382	PHD finger protein 14	1.674	0.001
NM_027296	tRNA nucleotidyl transferase, CCA-adding, 1	1.674	0.012
NM_023735	ARP3 actin-related protein 3 homolog (yeast)	1.674	0.001
NM_145955	RIKEN cDNA 1110007A13 gene	1.673	0.000
NM_021315	nucleolar complex associated 3 homolog (S. cerevisiae)	1.673	0.027
NM_021604	Agrin	1.671	0.008
NM_008234	helicase, lymphoid specific	1.668	0.013
NM_008408	STT3, subunit of the oligosaccharyltransferase complex	1.667	0.004
NM_198645	coiled-coil domain containing 58	1.666	0.038
NM_145588	kinesin family member 22	1.666	0.038
NM_133783	prostaglandin E synthase 2	1.665	0.005
NM_025315	mediator complex subunit 21	1.665	0.026
NM_015774	ERO1-like (S. cerevisiae)	1.664	0.019
NM_026522	chitinase domain containing 1	1.664	0.029
NM_028312	coiled-coil domain containing 12; predicted gene 8518	1.663	0.030
NM_145620	RRP9, small subunit (SSU) processome component, homolog (yeast)	1.663	0.004
NM_020584	telomeric repeat binding factor 2, interacting protein	1.663	0.027
NM_026195	5-aminoimidazole-4-carboxamide ribonucleotide formyltransferase/IMP cyclohydrolase; similar to 5-aminoimidazole-4-carboxamide ribonucleotide formyltransferase/IMP cyclohydrolase	1.663	0.011
NM_021895	actinin alpha 4	1.662	0.003
NM_010948	nuclear distribution gene C homolog (Aspergillus), pseudogene 1; nuclear distribution gene C homolog (Aspergillus)	1.662	0.001
NM_013902	FK506 binding protein 3	1.662	0.006
NM_011768	zinc finger protein X-linked; similar to zinc finger protein	1.661	0.033
NM_146154	protein phosphatase 1, regulatory (inhibitor) subunit 8	1.659	0.035
NM_008251	predicted gene 11663; predicted gene 2992; predicted gene 7862; high mobility group nucleosomal binding domain 1; similar to high mobility group nucleosomal binding domain 1	1.659	0.003
NM_009408	topoisomerase (DNA) I	1.657	0.004
NM_009346	TEA domain family member 1	1.656	0.010
NM_029802	ADP-ribosylation factor interacting protein 2	1.656	0.006
NM_013716	Ras-GTPase-activating protein SH3-domain binding protein 1	1.656	0.008
NM_016784	pleiotropic regulator 1, PRL1 homolog (Arabidopsis)	1.656	0.035
NM_145414	NOL1/NOP2/Sun domain family, member 5	1.656	0.022
NM_007971	enhancer of zeste homolog 2 (Drosophila)	1.656	0.004
NM_026487	ATPase family, AAA domain containing 1	1.655	0.017
NM_017477	coatomer protein complex, subunit gamma	1.654	0.003
NM_025776	RNA binding motif protein 22	1.654	0.038
NM_026602	breast carcinoma amplified sequence 2	1.649	0.010
NM_029293	phosphohistidine phosphatase 1	1.648	0.048

NM_016844	similar to 40S ribosomal protein S28; predicted gene 10443; predicted gene 12943; predicted gene 13192; similar to ribosomal protein S28; predicted gene 10263; predicted gene 3511; ribosomal protein S28	1.648	0.033
NM_019673	actin-like 6A	1.648	0.024
NM_026040	serum response factor binding protein 1; similar to SRF-dependent transcription regulation associated protein	1.647	0.003
NM_001013616	tripartite motif-containing 6; similar to Tripartite motif protein 6	1.646	0.046
NM_001033273	RIKEN cDNA 5031439G07 gene	1.646	0.049
NM_008012	aldo-keto reductase family 1, member B8	1.646	0.001
NM_026631	NHP2 ribonucleoprotein homolog (yeast)	1.646	0.002
NM_008249	transcription factor B2, mitochondrial; predicted gene 1818	1.645	0.005
NM_028767	forkhead box P4	1.645	0.020
NM_010756	similar to mafG; v-maf musculoaponeurotic fibrosarcoma oncogene family, protein G (avian)	1.644	0.034
NM_148930	RNA binding motif protein 5	1.644	0.040
NM_015816	LSM4 homolog, U6 small nuclear RNA associated (S. cerevisiae)	1.643	0.031
NM_138599	translocase of outer mitochondrial membrane 70 homolog A	1.642	0.005
NM_153516	BCL2-like 13 (apoptosis facilitator)	1.640	0.038
NM_028597	THO complex 3	1.639	0.017
NM_026120	RIKEN cDNA 2410127L17 gene; predicted gene 7622	1.638	0.021
NM_008907	predicted gene 9234; peptidylprolyl isomerase A	1.638	0.001
NM_030109	splicing factor 3b, subunit 2	1.638	0.007
NM_026063	hypothetical protein LOC675054; RIKEN cDNA 2900010M23 gene	1.635	0.023
NM_021433	syntaxin 6	1.635	0.044
NM_026023	NudC domain containing 2	1.635	0.002
NM_023215	predicted gene 6365; RIKEN cDNA 2500003M10 gene	1.633	0.032
NM_008854	protein kinase, cAMP dependent, catalytic, alpha	1.633	0.039
NM_016737	stress-induced phosphoprotein 1	1.632	0.027
NM_010917	similar to Nidogen precursor (Entactin); nidogen 1; similar to Nid1 protein	1.632	0.004
NM_009786	calcyclin binding protein	1.632	0.004
NM_026422	mitochondrial ribosome recycling factor; similar to mitochondrial ribosome recycling factor; predicted gene 6374	1.631	0.047
NP_085112	histone cluster 1, H1a	1.628	0.020
NM_138747	NOP2 nucleolar protein homolog (yeast)	1.628	0.023
NM_133815	lamin B receptor	1.627	0.008
NM_133757	phosphatidylglycerophosphate synthase 1	1.627	0.004
NM_011958	origin recognition complex, subunit 4-like (S. cerevisiae)	1.626	0.007
NM_022023	glia maturation factor, beta	1.626	0.044
NM_172400	DnaJ (Hsp40) homolog, subfamily C, member 8; predicted gene 4928	1.626	0.008
NM_008881	plexin A1	1.626	0.007
NM_011034	peroxiredoxin 1; predicted gene 7204	1.626	0.046
NM_030721	acyl-Coenzyme A oxidase 3, pristanoyl	1.625	0.004
NM_001044751	Corticosteroid 11-beta-dehydrogenase isozyme 1	1.624	0.010
NM_025351	coiled-coil-helix-coiled-coil-helix domain containing 6	1.623	0.010
NM_008704	similar to Nucleoside diphosphate kinase A (NDK A) (NDP kinase A) (Tumor metastatic process-associated protein) (Metastasis inhibition factor NM23) (NDPK-A) (nm23-M1); non-metastatic cells 1, protein (NM23A) expressed in	1.623	0.007
NP_083939	predicted gene 11675; eukaryotic translation elongation factor 1 delta (guanine nucleotide exchange protein)	1.623	0.010
NM_053179	N-acetylneuraminic acid synthase (sialic acid synthase)	1.620	0.013
NM_010931	ubiquitin-like, containing PHD and RING finger domains, 1;	1.619	0.016

	predicted gene 5648; similar to nuclear zinc finger protein Np95		
NM_025814	serpine1 mRNA binding protein 1	1.618	0.003
NP_001258827	Peroxisomal acyl-coenzyme A oxidase 1	1.618	0.001
NM_007624	predicted gene 6917; similar to chromobox homolog 3; predicted gene 5792; predicted gene 7469; predicted gene 6901; predicted gene 7721; predicted gene 5196; complement component 7; chromobox homolog 3 (Drosophila HP1 gamma)	1.617	0.030
NM_020506	exportin 4	1.611	0.010
NM_027478	RIKEN cDNA 5730494N06 gene; predicted gene 7368	1.611	0.015
NM_011306	retinoid X receptor beta	1.611	0.045
NP_951062	DEAD (Asp-Glu-Ala-Asp) box polypeptide 17	1.611	0.017
NM_023479	elaC homolog 2 (E. coli)	1.610	0.005
NM_001177658	39S ribosomal protein L15, mitochondrial	1.609	0.001
NM_027226	forty-two-three domain containing 1	1.609	0.019
NM_027219	CDC42 effector protein (Rho GTPase binding) 1	1.609	0.026
NM_011750	splicing factor 1	1.608	0.042
NM_027044	prefoldin 5	1.608	0.041
NM_019796	synaptotagmin binding, cytoplasmic RNA interacting protein	1.607	0.007
XP_619909	predicted gene 5449; small nuclear ribonucleoprotein D2; predicted gene 5848; predicted gene 10120	1.607	0.013
NM_018888	ubiquinol-cytochrome c reductase complex chaperone, CBP3 homolog (yeast)	1.605	0.002
NM_022988	Ngg1 interacting factor 3-like 1 (S. pombe)	1.604	0.003
NM_025994	similar to EF hand domain containing 2; EF hand domain containing 2	1.604	0.038
NM_207176	testis derived transcript	1.601	0.030
NM_021336	small nuclear ribonucleoprotein polypeptide A'	1.601	0.008
NM_019813	drebrin 1	1.600	0.001
NM_134122	nurim (nuclear envelope membrane protein)	1.599	0.018
NP_598452	poly-U binding splicing factor 60	1.599	0.023
NM_011327	sterol carrier protein 2, liver	1.598	0.003
NM_001093753	splicing factor, arginine/serine-rich 11	1.597	0.000
NM_175465	SEC14 and spectrin domains 1; predicted gene 9165	1.595	0.014
NM_146036	AHA1, activator of heat shock protein ATPase homolog 1 (yeast)	1.593	0.001
NM_008991	ATP-binding cassette, sub-family D (ALD), member 3	1.592	0.002
NM_019537	proteasome (prosome, macropain) assembly chaperone 1	1.592	0.036
NM_054081	similar to metastasis-associated protein; metastasis associated 1; similar to MTA1	1.591	0.011
NM_001037756	breast cancer metastasis-suppressor 1-like	1.589	0.015
NM_010219	FK506 binding protein 4	1.588	0.001
NM_008305	perlecan (heparan sulfate proteoglycan 2)	1.587	0.003
NM_172288	nucleoporin 133	1.586	0.009
NM_144930	expressed sequence AU018778	1.585	0.015
NM_023402	Myosin regulatory light chain 12B	1.585	0.003
NM_018868	NOP58 ribonucleoprotein homolog (yeast)	1.582	0.030
NM_021559	zinc finger protein 191	1.581	0.040
NM_053183	predicted gene 8228; DEAD (Asp-Glu-Ala-Asp) box polypeptide 50	1.580	0.001
NM_025292	RIKEN cDNA 1810020G14 gene; synaptojanin 2 binding protein; predicted gene 4116	1.579	0.028
NM_026503	RIKEN cDNA 1110058L19 gene	1.579	0.002
NP_033898	Basigin	1.576	0.022
NM_139236	nucleolar protein family 6 (RNA-associated)	1.576	0.049
NM_025281	Ly1 antibody reactive clone	1.574	0.050
NM_025375	Williams Beuren syndrome chromosome region 22	1.571	0.044

NM_145556	predicted gene 13886; TAR DNA binding protein	1.570	0.008
NM_009881	chromodomain protein, Y chromosome-like; predicted gene 7584	1.569	0.022
NM_152807	coiled-coil domain containing 137	1.568	0.027
NM_013559	heat shock 105kDa/110kDa protein 1	1.564	0.007
NM_020027	HLA-B associated transcript 2	1.561	0.010
NM_134080	filamin, beta	1.560	0.007
NM_025996	translocase of outer mitochondrial membrane 34	1.559	0.011
NM_153571	HscB iron-sulfur cluster co-chaperone homolog (E. coli)	1.559	0.012
NM_021465	stromal antigen 2	1.557	0.036
NM_025349	predicted gene 13182; LSM7 homolog, U6 small nuclear RNA associated (S. cerevisiae); predicted gene 10146	1.554	0.020
NM_026532	similar to Chain A, D92n,D94n Double Point Mutant Of Human Nuclear Transport Factor 2 (Ntf2); predicted gene 10349; predicted gene 4682; nuclear transport factor 2; similar to nuclear transport factor 2; predicted gene 9386; predicted gene 10333	1.552	0.006
NM_053089	NMDA receptor-regulated gene 1	1.551	0.007
NM_009295	syntaxin binding protein 1	1.550	0.012
NM_001081196	heterogeneous nuclear ribonucleoprotein U-like 2	1.549	0.011
NM_001033270	solute carrier family 4, sodium bicarbonate cotransporter, member 7	1.549	0.007
NM_010324	similar to Aspartate aminotransferase, cytoplasmic (Transaminase A) (Glutamate oxaloacetate transaminase 1); glutamate oxaloacetate transaminase 1, soluble	1.548	0.015
NM_007951	predicted gene 6941; predicted gene 10131; enhancer of rudimentary homolog (Drosophila)	1.546	0.007
NM_026483	M-phase phosphoprotein 10 (U3 small nucleolar ribonucleoprotein)	1.545	0.033
NM_010015	defender against cell death 1	1.544	0.046
NM_013492	similar to clusterin; clusterin	1.543	0.014
NM_029688	sulfiredoxin 1 homolog (S. cerevisiae)	1.543	0.040
NM_025507	SNW domain containing 1	1.543	0.009
NM_008722	predicted gene 6477; predicted gene 9118; nucleophosmin 1; similar to Nucleophosmin (NPM) (Nucleolar phosphoprotein B23) (Numatrin) (Nucleolar protein NO38); predicted gene 7289; predicted gene 5611	1.542	0.036
NM_001081071	lysocardiolipin acyltransferase 1	1.542	0.011
NM_023731	coiled-coil domain containing 86	1.541	0.015
NM_133933	ribophorin I	1.539	0.002
NM_145417	arginyl aminopeptidase (aminopeptidase B)	1.535	0.025
NM_078478	growth hormone inducible transmembrane protein	1.534	0.046
NM_015824	origin recognition complex, subunit 3-like (S. cerevisiae)	1.530	0.026
NM_144885	cDNA sequence BC005624; predicted gene 5904	1.530	0.013
NM_010579	eukaryotic translation initiation factor 6	1.528	0.020
NM_008549	mannosidase 2, alpha 1	1.525	0.018
NM_010368	glucuronidase, beta	1.525	0.020
NM_021714	WW domain binding protein 11	1.524	0.033
NM_001078167	splicing factor, arginine/serine-rich 1 (ASF/SF2); similar to splicing factor, arginine/serine-rich 1 (splicing factor 2, alternate splicing factor)	1.523	0.029
NM_019648	methionine aminopeptidase 2	1.523	0.023
NM_144861	regulation of nuclear pre-mRNA domain containing 1A	1.521	0.033
NM_023140	predicted gene 12669; glutaredoxin 3	1.520	0.030
NM_009278	Sjogren syndrome antigen B	1.518	0.013

NM_029157	splicing factor 3a, subunit 3	1.517	0.009
NM_007453	similar to Peroxiredoxin-6 (Antioxidant protein 2) (1-Cys peroxiredoxin) (1-Cys PRX) (Acidic calcium-independent phospholipase A2) (aiPLA2) (Non-selenium glutathione peroxidase) (NSGPx); peroxiredoxin 6	1.517	0.005
NM_016777	nuclear autoantigenic sperm protein (histone-binding); similar to nuclear autoantigenic sperm protein; NASP	1.516	0.043
NM_024448	RAB12, member RAS oncogene family	1.516	0.001
NM_133976	IMP3, U3 small nucleolar ribonucleoprotein, homolog (yeast); RIKEN cDNA 4933427G23 gene	1.515	0.013
NP_001029080	mediator complex subunit 22	1.513	0.041
NM_172666	alkylglycerone phosphate synthase	1.512	0.001
NM_026780	SYF2 homolog, RNA splicing factor (S. cerevisiae)	1.512	0.018
NM_009981	phosphate cytidylyltransferase 1, choline, alpha isoform	1.510	0.039
NP_001095925	amyloid beta (A4) precursor-like protein 2	1.510	0.003
NM_023130	RIKEN cDNA C130057N11 gene; hnRNP-associated with lethal yellow	1.509	0.005
NM_010911	nitrogen fixation gene 1 (S. cerevisiae); similar to Nitrogen fixation gene 1 (S. cerevisiae)	1.508	0.011
NM_026742	NADH dehydrogenase (ubiquinone) 1 alpha subcomplex, assembly factor 4	1.507	0.016
NM_007512	ATPase inhibitory factor 1	1.507	0.043
NP_001158082	sphingomyelin phosphodiesterase 4	1.506	0.033
NM_009033	RNA binding motif protein, X chromosome retrogene	1.505	0.033
NM_178647	CGG triplet repeat binding protein 1	1.503	0.002
NM_021512	nucleoporin 160	1.503	0.006
NM_001103165	poly(rC) binding protein 2	1.503	0.042
NM_001081164	OTU domain containing 4	1.501	0.012
NM_016884	heterogeneous nuclear ribonucleoprotein C	1.499	0.035
NM_198090	predicted gene 7498; hypothetical protein LOC635773; predicted gene 9242; predicted gene 6793; predicted gene 14730; predicted gene 7551; predicted gene 14398; predicted gene 6528; predicted gene 6641; hypothetical protein LOC630507; predicted gene 5550;	1.494	0.008
NM_133780	similar to nuclear pore complex-associated intranuclear coiled-coil protein TPR; translocated promoter region	1.493	0.012
NM_173763	cysteine conjugate-beta lyase 2	1.489	0.011
NP_904359	phospholipase A2, group XIIA	1.489	0.040
NM_010447	heterogeneous nuclear ribonucleoprotein A1-like 2; similar to heterogeneous nuclear ribonucleoprotein A1; predicted gene 13418; predicted gene 5461; predicted gene 8652; predicted gene 5643; similar to Heterogeneous nuclear ribonucleoprotein A1 (Helix-des	1.489	0.001
NM_194342	unc-84 homolog B (C. elegans)	1.488	0.037
NM_134138	proteasome (prosome, macropain) assembly chaperone 2; similar to Clast3 protein	1.485	0.014
NM_198326	NSFL1 (p97) cofactor (p47)	1.483	0.006
NM_031165	similar to heat shock protein 8; heat shock protein 8	1.479	0.021
NM_019816	apoptosis antagonizing transcription factor	1.475	0.045
NM_001013374	lectin, mannose-binding 2-like	1.475	0.018
NM_028599	WD repeat domain 75	1.474	0.015
NM_017374	similar to protein phosphatase 2a, catalytic subunit, beta isoform; protein phosphatase 2 (formerly 2A), catalytic subunit, beta isoform	1.473	0.012
NM_001024806	CCAAT/enhancer binding protein zeta	1.473	0.045

NM_026276	aminoadipate-semialdehyde dehydrogenase-phosphopantetheinyl transferase; hypothetical protein LOC100044211	1.470	0.013
NM_133242	RNA binding motif protein 39	1.469	0.014
NM_008618	malate dehydrogenase 1, NAD (soluble)	1.468	0.034
NM_016776	MYB binding protein (P160) 1a	1.468	0.015
NM_145415	expressed sequence AA408296	1.467	0.002
NM_001127346	NADH dehydrogenase (ubiquinone) 1 alpha subcomplex, assembly factor 2	1.466	0.026
NM_001033297	predicted gene 561	1.464	0.004
NM_175639	WD repeat domain 43; RIKEN cDNA 2610029G23 gene; hypothetical protein LOC674157	1.463	0.004
NM_001081028	signal-induced proliferation-associated 1 like 3	1.463	0.018
NM_138607	family with sequence similarity 50, member A	1.462	0.048
NM_080560	ubiquitin-conjugating enzyme E2N; similar to ubiquitin-conjugating enzyme E2 UbcH-ben; similar to ubiquitin-conjugating enzyme E2N; predicted gene 5943	1.462	0.025
NM_009634	adenylosuccinate lyase	1.462	0.012
NM_053186	cyclin M3	1.461	0.049
NM_027091	predicted gene 4353; nucleoporin 35	1.460	0.001
NM_009025	RAS p21 protein activator 3	1.458	0.025
NM_009798	capping protein (actin filament) muscle Z-line, beta	1.456	0.016
NM_019562	ubiquitin carboxyl-terminal esterase L5	1.456	0.021
NM_001163300	scaffold attachment factor B	1.456	0.016
NM_010752	mitotic arrest deficient 1-like 1	1.455	0.028
NM_134255	ELOVL family member 5, elongation of long chain fatty acids (yeast)	1.455	0.001
NM_007690	chromodomain helicase DNA binding protein 1	1.453	0.002
NM_010613	KH-type splicing regulatory protein	1.453	0.003
NM_026673	similar to Novel transmembrane domain containing protein; apolipoprotein O	1.453	0.041
NM_009089	polymerase (RNA) II (DNA directed) polypeptide A	1.451	0.036
NM_009825	serine (or cysteine) peptidase inhibitor, clade H, member 1	1.450	0.029
NM_024434	leucine aminopeptidase 3	1.448	0.010
NM_001002929	nucleoporin 85	1.447	0.011
NM_008828	phosphoglycerate kinase 1; predicted gene, EG668435	1.446	0.022
NM_025820	Crn, crooked neck-like 1 (Drosophila)	1.446	0.020
NM_026041	ribosomal RNA processing 15 homolog (S. cerevisiae)	1.444	0.014
NM_008774	poly(A) binding protein, cytoplasmic 1	1.443	0.021
NM_026270	AKT1 substrate 1 (proline-rich)	1.440	0.019
NM_178918	UTP15, U3 small nucleolar ribonucleoprotein, homolog (yeast)	1.440	0.013
NM_133928	coiled-coil-helix-coiled-coil-helix domain containing 4	1.439	0.016
NM_024166	coiled-coil-helix-coiled-coil-helix domain containing 2; predicted gene 13202; similar to coiled-coil-helix-coiled-coil-helix domain containing 2; predicted gene 12350	1.438	0.024
NM_001001932	early endosome antigen 1	1.435	0.013
NM_019869	RNA binding motif protein 14	1.433	0.024
NM_008669	N-acetyl galactosaminidase, alpha	1.431	0.047
NP_033778	A kinase (PRKA) anchor protein 1	1.428	0.034
NM_145431	notchless homolog 1 (Drosophila)	1.428	0.010
NM_030743	ring finger protein 114	1.428	0.000
NM_007626	chromobox homolog 5 (Drosophila HP1a)	1.427	0.001
NM_033526	ubiquilin 4	1.427	0.005
NM_026075	SFRS12-interacting protein 1	1.425	0.046
NM_023374	succinate dehydrogenase complex, subunit B, iron sulfur (Ip);	1.423	0.048

	similar to succinate dehydrogenase Ip subunit		
NM_026305	predicted gene 11401; similar to transcription elongation factor B (SIII), polypeptide 2; predicted gene 8971; transcription elongation factor B (SIII), polypeptide 2	1.422	0.007
NM_007801	cathepsin H	1.421	0.021
NM_016891	protein phosphatase 2 (formerly 2A), regulatory subunit A (PR 65), alpha isoform	1.420	0.022
NM_017393	caseinolytic peptidase, ATP-dependent, proteolytic subunit homolog (E. coli)	1.420	0.023
NM_025700	phosphoglucomutase 1	1.419	0.001
NM_029631	abhydrolase domain containing 14b	1.419	0.023
NM_008292	hydroxysteroid (17-beta) dehydrogenase 4	1.418	0.039
NP_001092280	peptidyl-tRNA hydrolase 2	1.417	0.027
NM_139139	DnaJ (Hsp40) homolog, subfamily C, member 17; predicted gene 6257	1.416	0.030
NM_023153	CWC15 homolog (S. cerevisiae)	1.416	0.005
NM_145706	nucleoporin 43	1.415	0.013
NM_010568	insulin receptor	1.414	0.044
NM_145627	RNA binding motif protein 10; predicted gene 12799	1.410	0.030
NM_011431	elongation factor Tu GTP binding domain containing 2	1.409	0.011
NM_001111279	WD repeat and FYVE domain containing 1	1.408	0.002
NM_009383	Tia1 cytotoxic granule-associated RNA binding protein-like 1	1.404	0.011
NM_172410	similar to nucleoporin 93; nucleoporin 93	1.403	0.008
NM_019758	mitochondrial carrier homolog 2 (C. elegans); predicted gene, 100039384; predicted gene, 100039506	1.401	0.024
NM_028766	transmembrane protein 43	1.397	0.029
NM_025374	glyoxalase 1	1.395	0.019
NM_177420	similar to Phosphoserine aminotransferase 1; phosphoserine aminotransferase 1	1.395	0.028
NM_001045523	bromo adjacent homology domain containing 1	1.392	0.045
NM_001033268	family with sequence similarity 120, member A	1.390	0.002
NM_178216	histone cluster 2, H3b; histone cluster 1, H3f; histone cluster 1, H3e; histone cluster 2, H3c1; histone cluster 1, H3d; histone cluster 1, H3c; histone cluster 1, H3b; histone cluster 2, H3c2; histone cluster 2, H2aa1; histone cluster 2, H2aa2	1.388	0.033
NM_025616	translocase of inner mitochondrial membrane 50 homolog (yeast)	1.387	0.046
NM_010722	lamin B2	1.386	0.045
NM_001005419	2-aminoethanethiol (cysteamine) dioxygenase	1.385	0.026
NM_145575	caldesmon 1	1.382	0.014
NM_026439	coiled-coil domain containing 80	1.382	0.008
NM_011508	predicted gene 5265; similar to suppressor of initiator codon mutations, related sequence 1; predicted gene 4017; predicted gene 6913; predicted gene 7688; predicted gene 6535; predicted gene 6900; predicted gene 5471; predicted gene 7845; predicted gene	1.380	0.021
NM_001013375	UTP18, small subunit (SSU) processome component, homolog (yeast)	1.378	0.001
NM_008388	eukaryotic translation initiation factor 3, subunit E	1.372	0.009
NM_172532	aldhehyde dehydrogenase family 5, subfamily A1	1.371	0.042
NM_027250	RIKEN cDNA 2010305A19 gene	1.369	0.026
NM_016692	inner centromere protein	1.364	0.012
NM_026438	pyrophosphatase (inorganic) 1	1.363	0.002
NM_010322	glyceronephosphate O-acyltransferase	1.361	0.047
NM_019765	CAP-GLY domain containing linker protein 1	1.359	0.032

NM_144804	DEP domain containing 7	1.358	0.018
NM_028112	SEH1-like (S. cerevisiae	1.357	0.023
NP_733486	RNA binding motif protein 12	1.357	0.000
NM_138659	pre-mRNA processing factor 8	1.356	0.007
NM_177253	cleavage stimulation factor, 3' pre-RNA, subunit 3	1.355	0.018
NM_183017	tubulin tyrosine ligase-like family, member 12	1.354	0.005
NM_025860	predicted gene 16433; similar to DEAD (Asp-Glu-Ala-Asp) box polypeptide 18; predicted gene 9214; predicted gene 8173; DEAD (Asp-Glu-Ala-Asp) box polypeptide 18	1.352	0.021
NM_019553	DEAD (Asp-Glu-Ala-Asp) box polypeptide 21	1.345	0.014
NM_011814	fragile X mental retardation, autosomal homolog 2	1.344	0.016
NM_028381	coiled-coil domain containing 94	1.343	0.030
NM_026077	RIKEN cDNA 3110040N11 gene	1.342	0.038
NM_023733	carnitine O-octanoyltransferase	1.342	0.021
NM_026318	RIKEN cDNA 2310003F16 gene	1.341	0.038
NP_001106817	similar to Transcriptional repressor p66 alpha (GATA zinc finger domain-containing protein 2A); GATA zinc finger domain containing 2A	1.340	0.046
NM_009672	acidic (leucine-rich) nuclear phosphoprotein 32 family, member A	1.338	0.027
NM_001080948	La ribonucleoprotein domain family, member 4; predicted gene 14373; predicted gene 8177	1.337	0.044
NM_025482	tumor protein D52-like 2	1.336	0.014
NM_027513	nucleoporin 205	1.335	0.014
NM_025430	mitochondrial ribosomal protein L35	1.334	0.012
NM_178707	zinc finger protein 592	1.334	0.020
NM_001161816	predicted gene 15455	1.333	0.005
NM_026313	RIKEN cDNA 3300001P08 gene	1.330	0.003
NM_183020	ataxin 2-like	1.328	0.028
NM_001081056	exportin, tRNA (nuclear export receptor for tRNAs)	1.328	0.029
NM_009668	bridging integrator 1	1.328	0.004
NM_023142	actin related protein 2/3 complex, subunit 1B	1.326	0.035
NM_009975	casein kinase 2, beta polypeptide	1.325	0.032
NM_028372	metallo-beta-lactamase domain containing 2	1.325	0.039
NM_026452	coenzyme Q9 homolog (yeast)	1.324	0.044
NM_009009	RAD21 homolog (S. pombe)	1.324	0.017
NM_172404	cysteine conjugate-beta lyase 1	1.321	0.012
NM_026578	GAR1 ribonucleoprotein homolog (yeast)	1.319	0.024
NM_009471	uridine monophosphate synthetase	1.317	0.042
NM_178625	transmembrane protein 209	1.317	0.003
NM_001171147	yes-associated protein 1	1.316	0.033
NM_016764	peroxiredoxin 4	1.316	0.021
NM_010726	phytanoyl-CoA hydroxylase	1.314	0.019
NM_007991	similar to Fibrillarin; fibrillarin	1.314	0.029
NM_010123	eukaryotic translation initiation factor 3, subunit A	1.314	0.006
NM_001164671	predicted gene 15542; predicted gene 7816; similar to DnaJ-like protein; predicted gene 6335; DnaJ (Hsp40) homolog, subfamily A, member 1, pseudogene; DnaJ (Hsp40) homolog, subfamily A, member 1	1.313	0.040
NM_133885	oxysterol binding protein-like 9	1.302	0.048
NM_134077	RNA binding motif protein 26	1.301	0.010
NM_026768	mitochondrial ribosomal protein S18A	1.299	0.030
NM_013511	erythrocyte protein band 4.1-like 2	1.296	0.024
NM_009456	predicted gene 7423; predicted gene 5858; predicted gene 6562; similar to ubiquitin-conjugating enzyme UbcH7; predicted gene	1.293	0.026

	3076; ubiquitin-conjugating enzyme E2L 3; predicted gene 15267; predicted gene 9057; predicted gene 10705; predicted gene 10145		
NM_177214	small nuclear ribonucleoprotein 200 (U5)	1.290	0.020
NM_009938	coatomer protein complex subunit alpha	1.289	0.036
NM_172924	RIKEN cDNA C230081A13 gene	1.275	0.012
NM_001017429	cytochrome c oxidase, subunit XVII assembly protein homolog (yeast)	1.274	0.028
NM_133953	splicing factor 3b, subunit 3	1.273	0.018
NM_153126	N-acetyltransferase 10	1.268	0.033
NM_009536	tyrosine 3-monooxygenase/tryptophan 5-monooxygenase activation protein, epsilon polypeptide	1.262	0.010
NM_001045529	microrchidia 3	1.261	0.025
NM_016926	squamous cell carcinoma antigen recognized by T-cells 3	1.255	0.026
NM_007687	cofilin 1, non-muscle; similar to Cofilin-1 (Cofilin, non-muscle isoform); predicted gene 6180	1.252	0.004
NM_026129	endoplasmic reticulum protein 29	1.251	0.010
NM_001077529	predicted gene 7730; non-metastatic cells 2, protein (NM23B) expressed in; predicted gene 5566; predicted gene 5425; similar to Nucleoside diphosphate kinase B (NDK B) (NDP kinase B) (P18)	1.250	0.008
NM_001033300	guanine monphosphate synthetase; predicted gene 7282	1.249	0.006
NM_009082	similar to ribosomal protein; predicted gene 6344; predicted gene 11449; predicted gene 13841; predicted gene 8210; hypothetical protein LOC675793; ribosomal protein L29; predicted gene 12704; predicted gene 7252; predicted gene 8965; predicted gene 13213	1.245	0.032
NM_021299	adenylate kinase 3	1.243	0.039
NP_001268984	Probable ATP-dependent RNA helicase DDX46	1.240	0.008
NM_144560	growth arrest-specific 2 like 1	1.236	0.046
NM_016805	heterogeneous nuclear ribonucleoprotein U	1.235	0.002
NM_010135	enabled homolog (Drosophila)	1.228	0.039
NM_183392	nucleoporin 54	1.227	0.023
NP_001157089	threonyl-tRNA synthetase 2, mitochondrial (putative)	1.213	0.017
NM_028044	similar to calponin 3, acidic; predicted gene 4815; calponin 3, acidic	1.211	0.021
NM_001024205	nuclear fragile X mental retardation protein interacting protein 2	1.210	0.009
NM_019489	peptidylprolyl isomerase E (cyclophilin E)	1.209	0.006
NM_145610	peter pan homolog (Drosophila)	1.206	0.008
NM_134010	nucleoporin 107	1.203	0.014
NM_023764	toll interacting protein	-1.203	0.016
NM_009424	TNF receptor-associated factor 6	-1.205	0.001
NM_025691	signal recognition particle 72	-1.208	0.048
NM_175546	WD repeat and FYVE domain-containing protein 2	-1.211	0.041
NM_175313	RIKEN cDNA A130022J15 gene	-1.213	0.002
NM_012001	COP9 (constitutive photomorphogenic) homolog, subunit 4 (Arabidopsis thaliana)	-1.217	0.021
NM_175244	HECT domain containing 3	-1.217	0.027
NM_181594	enhancer of mRNA decapping 4	-1.218	0.048
NM_009418	tripeptidyl peptidase II	-1.219	0.020
NM_029746	component of oligomeric golgi complex 2	-1.229	0.024
NM_011370	cytoplasmic FMR1 interacting protein 1	-1.231	0.035
NM_181413	ankyrin repeat and SAM domain containing 1	-1.231	0.004
NM_133913	RIKEN cDNA 2010209O12 gene	-1.232	0.023
NP_001185841	Rho guanine nucleotide exchange factor 2	-1.236	0.025
NM_007381	acyl-Coenzyme A dehydrogenase, long-chain	-1.249	0.003

NM_027185	differentially expressed in FDCP 6	-1.250	0.003
NM_138749	plexin B2	-1.250	0.033
NM_175145	transmembrane protein 127	-1.251	0.007
NM_146001	huntingtin interacting protein 1	-1.253	0.004
NM_172338	DnaJ (Hsp40) homolog, subfamily C, member 16	-1.254	0.029
NM_019760	serine incorporator 1	-1.255	0.020
NM_133717	RAB43, member RAS oncogene family	-1.257	0.039
NM_007438	aldolase A, fructose-bisphosphate; predicted gene 8767; predicted gene 7556	-1.258	0.012
NM_024465	abhydrolase domain containing 12	-1.258	0.048
NM_021420	serine/threonine kinase 4	-1.262	0.018
NM_012042	cullin 1	-1.268	0.007
NM_008564	minichromosome maintenance deficient 2 mitotin (S. cerevisiae)	-1.268	0.007
NM_178645	bleomycin hydrolase	-1.270	0.000
NM_008929	DnaJ (Hsp40) homolog, subfamily C, member 3	-1.270	0.011
NM_001136075	numb gene homolog (Drosophila)	-1.270	0.016
NM_011130	polymerase (DNA directed), beta	-1.275	0.001
NM_201226	leucine rich repeat containing 47; similar to leucine rich repeat containing 47	-1.275	0.014
NM_010301	guanine nucleotide binding protein, alpha 11	-1.276	0.021
NM_001113413	ring finger protein 13	-1.278	0.010
NM_019826	isovaleryl coenzyme A dehydrogenase	-1.279	0.038
NM_033477	DNA segment, Chr 17, human D6S53E	-1.286	0.005
NM_030035	golgi autoantigen, golgin subfamily b, macrogolgin 1	-1.287	0.018
NM_001034085	protein phosphatase 2 (formerly 2A), regulatory subunit A (PR 65), beta isoform	-1.287	0.020
NM_026061	NADH dehydrogenase (ubiquinone) 1 beta subcomplex 8	-1.293	0.019
NM_009103	ribonucleotide reductase M1	-1.294	0.011
NP_001153189	septin 2	-1.294	0.023
NM_008184	glutathione S-transferase, mu 6	-1.296	0.039
NM_009680	adaptor-related protein complex 3, beta 1 subunit	-1.297	0.040
NM_025835	propionyl Coenzyme A carboxylase, beta polypeptide	-1.297	0.044
NM_184053	calumenin	-1.298	0.005
NM_007598	CAP, adenylate cyclase-associated protein 1 (yeast)	-1.298	0.022
NM_024267	importin 4	-1.314	0.015
NM_001163026	DnaJ (Hsp40) homolog, subfamily C, member 13	-1.315	0.012
NM_028782	lon peptidase 1, mitochondrial	-1.325	0.023
NM_016802	ras homolog gene family, member A; similar to aplysia ras-related homolog A2; predicted gene 12844	-1.327	0.037
NM_027707	Nipped-B homolog (Drosophila)	-1.328	0.005
NM_008136	guanine nucleotide binding protein-like 1	-1.329	0.011
NM_025429	serine (or cysteine) peptidase inhibitor, clade B, member 1a	-1.333	0.030
NM_009812	caspase 8	-1.335	0.023
NP_035932	caseinolytic peptidase X (E.coli)	-1.337	0.028
NM_007861	dihydrolipoamide dehydrogenase	-1.338	0.015
NM_009072	Rho-associated coiled-coil containing protein kinase 2	-1.341	0.010
NM_178589	tumor necrosis factor receptor superfamily, member 21	-1.342	0.048
NM_007754	carboxypeptidase D; similar to carboxypeptidase D	-1.343	0.026
NM_011706	transient receptor potential cation channel, subfamily V, member 2	-1.343	0.043
NM_001077411	glucosidase, beta, acid	-1.348	0.026
NM_027270	exocyst complex component 1	-1.349	0.028
NM_023525	carbamoyl-phosphate synthetase 2, aspartate transcarbamylase, and dihydroorotase	-1.350	0.001

NM_010163	exostoses (multiple) 2	-1.355	0.028
NM_007399	a disintegrin and metallopeptidase domain 10	-1.362	0.005
NM_008293	hydroxy-delta-5-steroid dehydrogenase, 3 beta- and steroid delta-isomerase 1	-1.363	0.013
NM_007499	ataxia telangiectasia mutated homolog (human)	-1.366	0.036
NM_134100	major facilitator superfamily domain containing 5	-1.366	0.014
NM_001081309	phosphatidylinositol 3 kinase, regulatory subunit, polypeptide 4, p150	-1.368	0.011
NM_080287	engulfment and cell motility 2, ced-12 homolog (C. elegans)	-1.371	0.015
NM_011874	proteasome (prosome, macropain) 26S subunit, ATPase, 4	-1.376	0.008
NM_007999	flap structure specific endonuclease 1	-1.379	0.029
NM_009373	transglutaminase 2, C polypeptide	-1.379	0.004
NM_027357	proteasome (prosome, macropain) 26S subunit, non-ATPase, 1	-1.381	0.000
NM_008947	similar to peptidase (prosome, macropain) 26S subunit, ATPase 1; protease (prosome, macropain) 26S subunit, ATPase 1	-1.384	0.014
NM_178029	SET domain containing 1A	-1.385	0.014
NM_213614	similar to CDCrel-1AI; septin 5	-1.387	0.015
NP_001185796	Dynactin subunit 1	-1.390	0.027
NM_001013371	deltex 3-like (Drosophila)	-1.395	0.026
NM_007908	eukaryotic elongation factor-2 kinase	-1.397	0.035
NM_172767	von Willebrand factor A domain containing 5A	-1.397	0.026
NM_011602	talin 1	-1.400	0.009
NM_198249	RIKEN cDNA E130112L23 gene	-1.400	0.023
NM_153592	ER lipid raft associated 2	-1.400	0.000
NP_001005331	eukaryotic translation initiation factor 4, gamma 1	-1.401	0.007
NM_011875	proteasome (prosome, macropain) 26S subunit, non-ATPase, 13	-1.403	0.006
NM_133794	glutaminyl-tRNA synthetase	-1.404	0.025
NM_013657	sema domain, immunoglobulin domain (Ig), short basic domain, secreted, (semaphorin) 3C	-1.405	0.009
NM_023644	methylcrotonoyl-Coenzyme A carboxylase 1 (alpha)	-1.406	0.006
NM_030262	protein O-fucosyltransferase 2	-1.407	0.001
NM_144941	microtubule-associated protein 7 domain containing 1	-1.409	0.001
NM_130862	brain-specific angiogenesis inhibitor 1-associated protein 2	-1.410	0.006
NM_010620	kinesin family member 15	-1.411	0.022
NM_172827	leucyl/cystinyl aminopeptidase	-1.414	0.045
NM_153569	cyclin G associated kinase	-1.415	0.024
NM_025692	ubiquitin-like modifier activating enzyme 5	-1.415	0.032
NM_008565	minichromosome maintenance deficient 4 homolog (S. cerevisiae)	-1.415	0.022
NM_010763	mannosidase, alpha, class 1A, member 2	-1.416	0.035
NM_011723	xanthine dehydrogenase	-1.418	0.026
NM_133995	ureidopropionase, beta	-1.418	0.025
NM_008788	procollagen C-endopeptidase enhancer protein	-1.420	0.038
NM_080638	major vault protein	-1.420	0.018
NM_008149	glycerol-3-phosphate acyltransferase, mitochondrial	-1.422	0.034
NM_009795	calpain, small subunit 1	-1.422	0.048
NM_028662	solute carrier family 35, member B2	-1.423	0.032
NM_020332	progressive ankylosis	-1.426	0.034
NM_181395	peroxidasin homolog (Drosophila)	-1.428	0.001
NM_011787	autocrine motility factor receptor	-1.429	0.016
NM_026079	inhibitor of kappa light polypeptide enhancer in B-cells, kinase complex-associated protein	-1.430	0.001
NM_026644	1-acylglycerol-3-phosphate O-acyltransferase 4 (lysophosphatidic acid acyltransferase, delta)	-1.430	0.037
NM_010941	NAD(P) dependent steroid dehydrogenase-like	-1.432	0.007

NM_030253	poly (ADP-ribose) polymerase family, member 9	-1.432	0.008
NM_008984	protein tyrosine phosphatase, receptor type, M	-1.434	0.035
NM_053110	glycoprotein (transmembrane) nmb	-1.435	0.026
NM_011312	S100 calcium binding protein A5	-1.442	0.009
NM_008448	kinesin family member 5B	-1.445	0.003
NM_009212	immunoglobulin mu binding protein 2	-1.446	0.044
NM_053262	hydroxysteroid (17-beta) dehydrogenase 11	-1.449	0.044
NM_001160330	molybdenum cofactor synthesis 3	-1.452	0.000
NM_008481	laminin, alpha 2	-1.456	0.022
NM_021429	HCLS1 binding protein 3	-1.456	0.005
NM_001033167	solute carrier family 22, member 23	-1.456	0.048
NM_026545	proteasome (prosome, macropain) 26S subunit, non-ATPase, 8	-1.460	0.027
NM_019519	Rab geranylgeranyl transferase, a subunit	-1.462	0.041
NM_133907	ubiquitin protein ligase E3C	-1.467	0.031
NM_139144	O-linked N-acetylglucosamine (GlcNAc) transferase (UDP-N-acetylglucosamine:polypeptide-N-acetylglucosaminyl transferase)	-1.469	0.030
NM_023420	collagen, type IV, alpha 3 (Goodpasture antigen) binding protein	-1.472	0.029
NM_008364	interleukin 1 receptor accessory protein	-1.476	0.025
NM_175193	golgi integral membrane protein 4	-1.477	0.041
NM_030238	dynein cytoplasmic 1 heavy chain 1	-1.477	0.011
NM_013700	ubiquitin specific peptidase 5 (isopeptidase T)	-1.483	0.025
NM_013796	N-acetylglucosamine-1-phosphodiester alpha-N-acetylglucosaminidase	-1.484	0.035
NM_008328	similar to Interferon-activatable protein 203 (Ifi-203) (Interferon-inducible protein p203); similar to interferon activated gene 203; interferon activated gene 203	-1.484	0.009
NM_008566	minichromosome maintenance deficient 5, cell division cycle 46 (S. cerevisiae)	-1.487	0.038
NM_198007	activating signal cointegrator 1 complex subunit 3	-1.488	0.002
NM_173443	valosin containing protein (p97)/p47 complex interacting protein 1	-1.495	0.034
NM_010708	lectin, galactose binding, soluble 9	-1.495	0.026
NM_011696	predicted gene 7591; voltage-dependent anion channel 3	-1.498	0.015
NM_177876	vacuolar protein sorting 37B (yeast)	-1.500	0.029
NM_009045	v-rel reticuloendotheliosis viral oncogene homolog A (avian)	-1.506	0.024
NM_001080968	golgi autoantigen, golgin subfamily a, 2	-1.507	0.028
NM_029572	endoplasmic reticulum protein 44	-1.512	0.014
NM_008255	3-hydroxy-3-methylglutaryl-Coenzyme A reductase	-1.514	0.049
NM_133224	ATPase type 13A1	-1.516	0.008
NP_001020566	Rous sarcoma oncogene	-1.517	0.015
NM_172769	sterol-C5-desaturase (fungal ERG3, delta-5-desaturase) homolog (S. cerevisae)	-1.517	0.010
NM_026171	nuclear VCP-like	-1.517	0.010
NM_198163	RAB35, member RAS oncogene family	-1.518	0.013
NM_183106	tetratricopeptide repeat domain 17	-1.518	0.023
NM_010562	integrin linked kinase; predicted gene 6263	-1.518	0.048
NM_013472	annexin A6	-1.519	0.001
NM_001081193	LEM domain containing 3	-1.519	0.006
NM_028264	transmembrane protein 55A	-1.520	0.006
NM_013495	carnitine palmitoyltransferase 1a, liver	-1.520	0.049
NM_001163126	component of oligomeric golgi complex 5	-1.522	0.024
NM_001081252	UDP-glucose ceramide glucosyltransferase-like 2	-1.522	0.013
NP_001240821	Anion exchange protein 2	-1.522	0.048
NM_013528	glutamine fructose-6-phosphate transaminase 1	-1.523	0.002

NM_027677	G protein-coupled receptor 39	-1.523	0.002
NM_007842	DEAH (Asp-Glu-Ala-His) box polypeptide 9	-1.524	0.026
NM_028817	acyl-CoA synthetase long-chain family member 3	-1.526	0.034
NM_177215	oculocerebrorenal syndrome of Lowe	-1.527	0.003
NM_027127	glutathione peroxidase 8 (putative)	-1.527	0.036
NM_009112	S100 calcium binding protein A10 (calpactin)	-1.527	0.036
NM_011026	purinergic receptor P2X, ligand-gated ion channel 4	-1.528	0.048
NM_009755	bone morphogenetic protein 1	-1.528	0.012
NM_172381	expressed sequence AI314180	-1.530	0.031
NM_001013380	dynein, cytoplasmic 1 light intermediate chain 2	-1.532	0.020
NM_008684	neogenin	-1.533	0.008
NM_008562	similar to myeloid cell leukemia sequence 1; myeloid cell leukemia sequence 1	-1.534	0.011
NM_008512	low density lipoprotein receptor-related protein 1	-1.534	0.027
NM_025816	Tax1 (human T-cell leukemia virus type I) binding protein 1	-1.536	0.035
NM_027815	RIKEN cDNA 9030624J02 gene	-1.536	0.009
NM_144792	sphingomyelin synthase 1	-1.538	0.044
NM_010261	Rab acceptor 1 (prenylated)	-1.539	0.000
NM_011018	sequestosome 1	-1.541	0.039
NM_133838	EH-domain containing 4	-1.541	0.006
NM_010515	insulin-like growth factor 2 receptor	-1.543	0.001
NM_025551	NADH dehydrogenase (ubiquinone) 1 alpha subcomplex, 12	-1.544	0.018
NM_013795	predicted gene 10221; predicted gene 4602; predicted gene 9391; ATP synthase, H+ transporting, mitochondrial FO complex, subunit G2, pseudogene; predicted gene 11477; predicted gene 9712; ATP synthase, H+ transporting, mitochondrial F0 complex, subunit g;	-1.546	0.000
NM_145543	chloride channel CLIC-like 1	-1.546	0.001
NM_009794	calpain 2	-1.548	0.011
NM_008826	phosphofructokinase, liver, B-type	-1.550	0.027
NM_025550	proteasome (prosome, macropain) 26S subunit, non-ATPase, 6	-1.552	0.036
NM_008482	laminin B1 subunit 1	-1.552	0.000
NM_022009	flightless I homolog (Drosophila); similar to cytoskeletal actin-modulating protein	-1.553	0.003
NM_001146268	platelet derived growth factor receptor, beta polypeptide	-1.554	0.015
NM_145558	predicted gene 13910; similar to Hydroxyacyl-Coenzyme A dehydrogenase/3-ketoacyl-Coenzyme A thiolase/enoyl-Coenzyme A hydratase (trifunctional protein), beta subunit; hydroxyacyl-Coenzyme A dehydrogenase/3-ketoacyl-Coenzyme A thiolase/enoyl-Coenzyme A hyd	-1.555	0.044
NM_025586	similar to ribosomal protein L15; predicted gene 8420; predicted gene 6937; predicted gene 4581; predicted gene 5613; predicted gene 7287; predicted gene, 674243; predicted gene 4607; predicted gene 10224; predicted gene 8037; predicted gene 4294; predict	-1.557	0.044
NM_021557	retinol dehydrogenase 11	-1.558	0.000
NM_027992	transmembrane protein 106B	-1.558	0.032
NM_026610	NADH dehydrogenase (ubiquinone) 1 beta subcomplex 4; predicted gene 3873; predicted gene 3244	-1.560	0.028
NM_145506	erythrocyte protein band 4.1-like 5	-1.560	0.013
NM_009149	golgi apparatus protein 1	-1.561	0.025
NM_134083	regulator of chromosome condensation (RCC1) and BTB (POZ) domain containing protein 2	-1.562	0.014
NM_024436	RAB22A, member RAS oncogene family	-1.563	0.003
NM_010890	neural precursor cell expressed, developmentally down-	-1.564	0.002

	regulated 4		
NM_176860	ubiquitin associated and SH3 domain containing, B	-1.564	0.037
NM_007988	fatty acid synthase	-1.565	0.000
NM_030013	cytochrome P450, family 20, subfamily A, polypeptide 1	-1.566	0.015
NM_007508	ATPase, H+ transporting, lysosomal V1 subunit A	-1.569	0.010
NM_024226	reticulon 4	-1.569	0.011
NM_010875	neural cell adhesion molecule 1	-1.572	0.002
NM_020586	HERPUD family member 2	-1.572	0.002
NM_173013	microtubule-associated protein 1S	-1.573	0.007
NM_011313	S100 calcium binding protein A6 (calcyclin)	-1.575	0.043
NM_178772	arylacetamide deacetylase-like 1	-1.575	0.031
NM_011704	vanin 1	-1.577	0.002
NM_001045489	milk fat globule-EGF factor 8 protein	-1.577	0.020
NM_152801	Rac/Cdc42 guanine nucleotide exchange factor (GEF) 6	-1.578	0.021
NM_009842	CD151 antigen	-1.579	0.029
NM_007509	ATPase, H+ transporting, lysosomal V1 subunit B2	-1.579	0.006
NM_012002	COP9 (constitutive photomorphogenic) homolog, subunit 6 (Arabidopsis thaliana)	-1.579	0.026
NM_010546	inhibitor of kappaB kinase beta	-1.580	0.019
NM_080445	similar to UDP-Gal:betaGal beta 1,3-galactosyltransferase, polypeptide 6; UDP-Gal:betaGal beta 1,3-galactosyltransferase, polypeptide 6	-1.582	0.016
NM_008898	P450 (cytochrome) oxidoreductase	-1.582	0.008
NM_019703	phosphofructokinase, platelet	-1.583	0.004
NM_009530	alpha thalassemia/mental retardation syndrome X-linked homolog (human)	-1.583	0.001
NM_016721	IQ motif containing GTPase activating protein 1	-1.584	0.002
NM_009371	transforming growth factor, beta receptor II	-1.585	0.002
NM_011311	hippocampus abundant transcript-like 1; S100 calcium binding protein A4	-1.586	0.007
NM_009933	collagen, type VI, alpha 1	-1.586	0.013
NM_178376	Ras-related GTP binding A	-1.591	0.025
NM_175229	serine/arginine repetitive matrix 2; similar to Serine/arginine repetitive matrix protein 2; similar to retinitis pigmentosa GTPase regulator	-1.592	0.012
NM_027410	tectonin beta-propeller repeat containing 1	-1.592	0.011
XM_001475417	similar to cytochrome c oxidase, subunit Vb; predicted gene 11273; cytochrome c oxidase, subunit Vb	-1.592	0.022
NM_138579	TRIO and F-actin binding protein	-1.592	0.002
NM_145138	NIMA (never in mitosis gene a)-related expressed kinase 9	-1.593	0.018
NM_008948	proteasome (prosome, macropain) 26S subunit, ATPase 3	-1.595	0.005
NM_011504	syntaxin binding protein 3A	-1.596	0.017
NM_025515	similar to Coiled-coil domain containing 90B; coiled-coil domain containing 90B	-1.596	0.031
NM_001081066	DENN/MADD domain containing 3	-1.598	0.006
NM_183162	cDNA sequence BC006779	-1.598	0.039
NM_009465	AXL receptor tyrosine kinase	-1.599	0.003
NM_009481	ubiquitin specific peptidase 9, X chromosome	-1.601	0.006
NM_008133	glutamate dehydrogenase 1; predicted gene 5902	-1.602	0.002
NM_008325	iduronidase, alpha-L-	-1.603	0.008
NM_008451	kinesin light chain 2	-1.604	0.014
NM_010046	diacylglycerol O-acyltransferase 1	-1.605	0.036
NM_175126	zinc finger, CCHC domain containing 3	-1.606	0.043
NM_023220	RIKEN cDNA 2010106G01 gene	-1.607	0.012
NM_028248	transmembrane protein 87B	-1.608	0.022

NM_021607	nicastrin	-1.608	0.047
NM_022563	discoidin domain receptor family, member 2	-1.610	0.020
NM_145925	pituitary tumor-transforming 1 interacting protein	-1.612	0.003
NM_144922	heterogeneous nuclear ribonucleoprotein U-like 1	-1.613	0.002
NM_019811	acyl-CoA synthetase short-chain family member 2	-1.613	0.039
NM_033320	glucuronyl C5-epimerase	-1.613	0.037
NM_178070	vacuolar protein sorting 33B (yeast)	-1.614	0.006
NM_029005	mixed lineage kinase domain-like	-1.614	0.004
NM_007502	ATPase, Na+/K+ transporting, beta 3 polypeptide	-1.615	0.016
NM_172935	amidohydrolase domain containing 2	-1.618	0.030
NM_010577	integrin alpha 5 (fibronectin receptor alpha)	-1.619	0.025
NM_011989	solute carrier family 27 (fatty acid transporter), member 4	-1.621	0.035
NM_013587	low density lipoprotein receptor-related protein associated protein 1	-1.623	0.001
NM_133348	acyl-CoA thioesterase 7	-1.623	0.001
NM_009269	serine palmitoyltransferase, long chain base subunit 1	-1.626	0.008
NM_016709	AU RNA binding protein/enoyl-coenzyme A hydratase	-1.627	0.001
NM_001033284	cDNA sequence BC026585	-1.627	0.006
NM_010362	glutathione S-transferase omega 1	-1.630	0.033
NM_029091	kinesin light chain 4	-1.630	0.005
NM_019861	cathepsin F	-1.633	0.013
NM_009294	syntaxin 4A (placental)	-1.633	0.006
NM_175438	aldehyde dehydrogenase 4 family, member A1	-1.633	0.001
NM_011654	predicted gene 3756; tubulin, alpha 1B; predicted gene 5620; similar to alpha-tubulin isotype M-alpha-2; predicted gene 14150; predicted gene 3226	-1.635	0.000
NM_144825	TAO kinase 1	-1.637	0.009
NM_016679	kelch-like ECH-associated protein 1	-1.639	0.049
NM_139272	UDP-N-acetyl-alpha-D-galactosamine:polypeptide N-acetylgalactosaminyltransferase 2	-1.640	0.032
NM_207298	cerebral endothelial cell adhesion molecule	-1.641	0.005
NM_010684	lysosomal-associated membrane protein 1	-1.642	0.048
NM_198105	family with sequence similarity 120, member C	-1.643	0.009
NM_172380	KTEL (Lys-Tyr-Glu-Leu) containing 1	-1.644	0.009
NM_010233	fibronectin 1	-1.645	0.025
NM_001004156	pleckstrin homology domain containing, family G (with RhoGef domain) member 5	-1.646	0.048
NM_001025250	vascular endothelial growth factor A	-1.646	0.050
NM_054097	phosphatidylinositol-5-phosphate 4-kinase, type II, gamma	-1.647	0.006
NM_139307	vasorin	-1.647	0.012
NM_007530	B-cell receptor-associated protein 29	-1.648	0.007
NM_019802	gamma-glutamyl carboxylase	-1.649	0.031
NM_053181	pyridoxal-dependent decarboxylase domain containing 1	-1.649	0.038
NM_026719	LMBR1 domain containing 1	-1.650	0.001
NM_172687	coenzyme Q3 homolog, methyltransferase (yeast)	-1.650	0.041
NM_024281	ribosome binding protein 1	-1.654	0.008
NM_001083316	platelet derived growth factor receptor, alpha polypeptide	-1.655	0.001
NM_172557	RUN and FYVE domain containing 1	-1.656	0.027
NM_017380	septin 9	-1.658	0.000
NM_030210	acetoacetyl-CoA synthetase	-1.658	0.031
NM_015742	myosin IXb	-1.659	0.004
NM_017472	sorting nexin 3	-1.660	0.038
NM_001009818	septin 11	-1.662	0.040
NM_153774	importin 9	-1.663	0.010

NM_153125	SEC16 homolog A (S. cerevisiae)	-1.664	0.017
NM_026698	transmembrane protein 129	-1.665	0.028
NM_011170	prion protein	-1.666	0.006
NM_029841	RIKEN cDNA 2510039O18 gene; similar to RIKEN cDNA 2510039O18 gene	-1.666	0.022
NM_011076	ATP-binding cassette, sub-family B (MDR/TAP), member 1A	-1.666	0.022
NM_010117	rhomboid family 1 (Drosophila)	-1.669	0.036
NM_177304	ectonucleotide pyrophosphatase/phosphodiesterase 6	-1.670	0.003
NM_146121	RAB GTPase activating protein 1	-1.670	0.008
NP_001240839	Protein Nat8f7	-1.671	0.021
NP_001070732	adaptor protein complex AP-2, alpha 1 subunit	-1.671	0.022
NM_026228	solute carrier family 39 (metal ion transporter), member 8	-1.672	0.002
NM_133826	ATPase, H+ transporting, lysosomal V1 subunit H	-1.674	0.012
NM_001033293	UDP-N-acteylglucosamine pyrophosphorylase 1-like 1	-1.676	0.003
NM_001033202	ubiquitin specific peptidase 30	-1.677	0.006
NM_145619	poly (ADP-ribose) polymerase family, member 3	-1.678	0.008
NM_001081306	protein tyrosine phosphatase, receptor type Z, polypeptide 1	-1.678	0.021
NM_194334	TBC1 domain family, member 2B	-1.678	0.017
NM_144878	flavin containing monooxygenase 4	-1.679	0.016
NM_010239	ferritin heavy chain 1	-1.680	0.008
NM_153800	Rho GTPase activating protein 22	-1.682	0.009
NM_011400	solute carrier family 2 (facilitated glucose transporter), member 1	-1.683	0.002
NM_026677	RAB13, member RAS oncogene family	-1.683	0.002
NM_053014	1-acylglycerol-3-phosphate O-acyltransferase 3	-1.684	0.002
NM_028428	fucosyltransferase 11	-1.684	0.033
NM_021534	peroxisomal membrane protein 4	-1.685	0.026
NM_009288	serine/threonine kinase 10	-1.687	0.004
NM_010049	dihydrofolate reductase	-1.691	0.003
NM_145960	mitochondrial translational release factor 1	-1.692	0.010
NM_172570	tripartite motif-containing 47	-1.693	0.024
NM_024436	RAB22A, member RAS oncogene family	-1.697	0.003
NM_133921	nuclear transcription factor, X-box binding-like 1	-1.697	0.012
NM_029884	heparan-alpha-glucosaminide N-acetyltransferase	-1.698	0.003
NM_175121	solute carrier family 38, member 2	-1.702	0.011
NM_145540	integrator complex subunit 3	-1.708	0.004
NM_001033534	layilin	-1.708	0.016
NM_007653	CD63 antigen	-1.711	0.017
NP_001116240	leucine rich repeat containing 8D	-1.712	0.006
NM_008980	protein tyrosine phosphatase, receptor type, A	-1.712	0.003
NM_008175	granulin	-1.713	0.015
NP_062718	Nuclear receptor coactivator 4	-1.713	0.005
NM_013792	alpha-N-acetylglucosaminidase (Sanfilippo disease IIIB)	-1.715	0.026
NM_027379	fatty acyl CoA reductase 1	-1.716	0.001
NM_080555	phosphatidic acid phosphatase type 2B	-1.725	0.001
NM_153198	high mobility group box transcription factor 1	-1.725	0.004
NM_026825	leucine rich repeat containing 16A	-1.727	0.013
NM_008608	matrix metallopeptidase 14 (membrane-inserted)	-1.730	0.005
NM_022018	family with sequence similarity 129, member A	-1.735	0.003
NM_007387	acid phosphatase 2, lysosomal	-1.738	0.009
NM_011577	transforming growth factor, beta 1	-1.739	0.007
NM_007874	receptor accessory protein 5	-1.741	0.040
NP_001258788	Beta-adducin	-1.744	0.012
NM_007643	CD36 antigen	-1.752	0.004

NM_010106	predicted gene 5869; predicted gene 7161; predicted gene 7105; predicted gene 5822; similar to eukaryotic translation elongation factor 1 alpha 1; predicted gene 6192; predicted gene 6392; predicted gene 6767; predicted gene 6170; predicted gene 6548; pre	-1.754	0.005
NM_010441	predicted gene 7996; high mobility group AT-hook 2	-1.755	0.005
NM_010212	four and a half LIM domains 2	-1.757	0.007
NM_029600	ATP-binding cassette, sub-family C (CFTR/MRP), member 3	-1.758	0.003
NM_031871	GH3 domain containing	-1.768	0.003
NM_178337	tubulin-specific chaperone E	-1.770	0.000
NP_034873	interleukin 1 receptor-like 1	-1.772	0.010
NM_030201	heat shock protein 70 family, member 13	-1.784	0.027
NM_007982	PTK2 protein tyrosine kinase 2	-1.797	0.002
NM_028431	peptidase (mitochondrial processing) beta	-1.803	0.017
NM_172456	endo/exonuclease (5'-3'), endonuclease G-like	-1.818	0.005
NM_013477	ATPase, H+ transporting, lysosomal V0 subunit D1	-1.822	0.002

Table 1-B: Differentially regulated CHO DP-12 proteins determined in samples corresponding to culture using a reduced bioprocessing temperature of 32.0°C

RefSeq Annotation	Description	Fold Change	P-Value
NM_011638	transferrin receptor	1.792	0.025
NM_008881	plexin A1	1.782	0.005
NM_023130	RIKEN cDNA C130057N11 gene; hnRNP-associated with lethal yellow	1.728	0.002
NP_001103445	synaptopodin	1.713	0.009
NM_146090	zinc binding alcohol dehydrogenase, domain containing 2	1.701	0.017
NM_011170	prion protein	1.697	0.007
NM_028870	clathrin, light polypeptide (Lcb)	1.692	0.028
NM_026159	retinol saturase (all trans retinol 13,14 reductase)	1.691	0.023
NM_021895	actinin alpha 4	1.680	0.042
NM_008558	similar to Myn protein; Max protein	1.680	0.026
NM_026041	ribosomal RNA processing 15 homolog (S. cerevisiae)	1.679	0.010
NM_025788	nucleus accumbens associated 1, BEN and BTB (POZ) domain containing	1.675	0.002
NM_130862	brain-specific angiogenesis inhibitor 1-associated protein 2	1.673	0.001
NM_011544	transcription factor 12	1.670	0.026
NM_001163662	nucleobindin 1	1.665	0.047
NM_019772	predicted gene 9169; RIKEN cDNA 1110004F10 gene; similar to small acidic protein	1.662	0.033
NM_026277	NIN1/RPN12 binding protein 1 homolog (S. cerevisiae)	1.661	0.000
NM_175126	zinc finger, CCHC domain containing 3	1.660	0.042
NM_009264	small proline-rich protein 1A	1.658	0.043
NM_026623	nudix (nucleoside diphosphate linked moiety X)-type motif 21	1.656	0.002
NM_016844	similar to 40S ribosomal protein S28; predicted gene 10443; predicted gene 12943; predicted gene 13192; similar to ribosomal protein S28; predicted gene 10263; predicted gene 3511; ribosomal protein S28	1.654	0.018
NM_172943	similar to AlkB, alkylation repair homolog 5 (E. coli); alkB, alkylation repair homolog 5 (E. coli)	1.654	0.022
NM_009032	RNA binding motif protein 4	1.653	0.038

NM_008980	protein tyrosine phosphatase, receptor type, A	1.649	0.031
NM_023731	coiled-coil domain containing 86	1.644	0.008
NM_026732	mitochondrial ribosomal protein L14	1.633	0.037
NM_133887	syntaxin 12	1.624	0.015
NM_019813	drebrin 1	1.610	0.003
NM_021895	actinin alpha 4	1.610	0.010
NM_027044	prefoldin 5	1.602	0.040
NM_001033284	cDNA sequence BC026585	1.600	0.000
NM_183020	ataxin 2-like	1.594	0.003
NM_011197	prostaglandin F2 receptor negative regulator	1.591	0.022
NM_008562	similar to myeloid cell leukemia sequence 1; myeloid cell leukemia sequence 1	1.590	0.002
NM_080555	phosphatidic acid phosphatase type 2B	1.587	0.001
NM_033526	ubiquilin 4	1.583	0.029
NM_016690	heterogeneous nuclear ribonucleoprotein D-like	1.580	0.042
NM_021557	retinol dehydrogenase 11	1.576	0.004
NM_010213	four and a half LIM domains 3	1.572	0.018
NM_021336	small nuclear ribonucleoprotein polypeptide A'	1.571	0.039
NM_024166	coiled-coil-helix-coiled-coil-helix domain containing 2; predicted gene 13202; similar to coiled-coil-helix-coiled-coil-helix domain containing 2; predicted gene 12350	1.569	0.047
NM_008972	predicted gene 12504; predicted gene 9800; predicted gene 4617; predicted gene 6625; predicted gene 7614; similar to prothymosin alpha; prothymosin alpha; predicted gene 9009	1.568	0.018
NM_025587	predicted gene 5963; ribosomal protein S21	1.568	0.050
NM_020506	exportin 4	1.561	0.024
NM_010875	neural cell adhesion molecule 1	1.560	0.012
NM_011312	S100 calcium binding protein A5	1.560	0.021
NM_025682	paraspeckle protein 1	1.554	0.006
NM_025315	mediator complex subunit 21	1.552	0.008
NM_016786	ubiquitin-conjugating enzyme E2K (UBC1 homolog, yeast)	1.552	0.029
NM_026677	RAB13, member RAS oncogene family	1.552	0.034
NM_025430	mitochondrial ribosomal protein L35	1.550	0.009
NP_001129553	structure specific recognition protein 1	1.550	0.022
NM_001171147	yes-associated protein 1	1.547	0.041
NM_153787	BCL2-associated transcription factor 1	1.546	0.006
NM_026538	DEAD (Asp-Glu-Ala-Asp) box polypeptide 56	1.546	0.015
NM_172769	sterol-C5-desaturase (fungal ERG3, delta-5-desaturase) homolog (S. cerevisae)	1.541	0.017
NM_144560	growth arrest-specific 2 like 1	1.539	0.016
NM_001024205	nuclear fragile X mental retardation protein interacting protein 2	1.534	0.013
NM_009643	AHNAK nucleoprotein (desmoyokin)	1.521	0.001
NM_144930	expressed sequence AU018778	1.520	0.005
NM_008155	glucose phosphate isomerase 1	1.517	0.013
NM_016696	glypican 1	1.512	0.022
NM_007705	cold inducible RNA binding protein	1.505	0.034
NM_019975	2-hydroxyacyl-CoA lyase 1	1.495	0.014
NM_001080926	low density lipoprotein receptor-related protein 8, apolipoprotein e receptor	1.494	0.038
NM_007840	DEAD (Asp-Glu-Ala-Asp) box polypeptide 5; predicted gene 12183	1.486	0.038
NM_025697	RIKEN cDNA 6330409N04 gene	1.485	0.025
NM_027000	GTP binding protein 4	1.484	0.022
NM_001163540	plectin 1	1.482	0.003
NM_199323	transforming, acidic coiled-coil containing protein 1	1.481	0.041
NM_026228	solute carrier family 39 (metal ion transporter), member 8	1.474	0.011

NM_011768	zinc finger protein X-linked; similar to zinc finger protein	1.472	0.029
NM_026602	breast carcinoma amplified sequence 2	1.469	0.005
NM_153419	glutamate-rich WD repeat containing 1	1.463	0.038
NM_009933	collagen, type VI, alpha 1	1.461	0.006
NM_009295	syntaxin binding protein 1	1.459	0.007
NM_130864	acetyl-Coenzyme A acyltransferase 1A	1.452	0.001
NM_009881	chromodomain protein, Y chromosome-like; predicted gene 7584	1.450	0.026
NM_026020	similar to LOC665931 protein; ribosomal protein, large P2; predicted gene 7852; WD repeat domain 89	1.446	0.028
NM_009510	ezrin; hypothetical protein LOC100044177	1.445	0.024
NM_008684	neogenin	1.445	0.015
NM_025884	zinc finger protein 830	1.437	0.022
NM_026503	RIKEN cDNA 1110058L19 gene	1.429	0.000
NM_025551	NADH dehydrogenase (ubiquinone) 1 alpha subcomplex, 12	1.423	0.013
NM_009048	RalBP1 associated Eps domain containing protein	1.422	0.022
NM_011925	CD97 antigen	1.419	0.020
NM_001082961	small nuclear ribonucleoprotein N; SNRPN upstream reading frame; predicted gene 5802; similar to SNRPN upstream reading frame protein	1.407	0.026
NM_009112	S100 calcium binding protein A10 (calpactin)	1.407	0.039
NM_018796	eukaryotic translation elongation factor 1 beta 2	1.402	0.049
NM_028871	predicted gene 6159; heterogeneous nuclear ribonucleoprotein R	1.400	0.003
NM_011917	5'-3' exoribonuclease 2	1.399	0.033
NM_011479	serine palmitoyltransferase, long chain base subunit 2	1.397	0.011
NM_020586	HERPUD family member 2	1.396	0.021
NM_026737	PHD finger protein 5A	1.393	0.001
NM_145610	peter pan homolog (Drosophila)	1.388	0.029
NM_008133	glutamate dehydrogenase 1; predicted gene 5902	1.386	0.007
NM_080558	sperm specific antigen 2	1.382	0.015
NP_062718	Nuclear receptor coactivator 4	1.377	0.037
NM_001080794	GTPase activating protein (SH3 domain) binding protein 2	1.375	0.016
NM_001037756	breast cancer metastasis-suppressor 1-like	1.374	0.000
NM_017382	RAB11a, member RAS oncogene family	1.372	0.012
NM_008638	methylenetetrahydrofolate dehydrogenase (NAD+ dependent), methenyltetrahydrofolate cyclohydrolase	1.372	0.046
NM_008364	interleukin 1 receptor accessory protein	1.370	0.038
NM_010191	predicted gene 6781; farnesyl diphosphate farnesyl transferase 1	1.370	0.046
NM_026988	parathymosin	1.369	0.022
NM_016753	latexin	1.366	0.028
NM_025814	serpine1 mRNA binding protein 1	1.366	0.020
NM_011327	sterol carrier protein 2, liver	1.363	0.011
NM_023536	predicted gene 9178; MRT4, mRNA turnover 4, homolog (S. cerevisiae); predicted gene 5633	1.361	0.010
NM_011300	similar to 40S ribosomal protein S7 (S8); predicted gene 6252; predicted gene 5055; predicted gene 4761; ribosomal protein S7; predicted gene 7351; predicted gene 6472	1.358	0.046
NM_025864	transmembrane protein 206	1.352	0.007
NM_023144	non-POU-domain-containing, octamer binding protein; predicted gene 8806	1.352	0.029
NP_001158005	death associated protein 3	1.343	0.004
NM_011189	predicted gene 7776; proteasome (prosome, macropain) 28 subunit, alpha	1.342	0.019
NM_026933	TP53 regulated inhibitor of apoptosis 1	1.338	0.049
NM_007842	DEAH (Asp-Glu-Ala-His) box polypeptide 9	1.338	0.019
NM_009530	alpha thalassemia/mental retardation syndrome X-linked homolog	1.337	0.001

	(human)		
NM_026482	ATPase, Ca++ transporting, plasma membrane 1	1.331	0.050
NM_145431	notchless homolog 1 (Drosophila)	1.331	0.004
NM_010117	rhomboid family 1 (Drosophila)	1.324	0.043
NM_023764	toll interacting protein	1.320	0.037
NM_023603	splicing factor proline/glutamine rich (polypyrimidine tract binding protein associated); similar to PTB-associated splicing factor	1.319	0.041
NM_011287	predicted gene 13573; predicted gene 15451; ribosomal protein L10A; predicted gene 7695; similar to ribosomal protein L10a	1.318	0.023
NM_007840	DEAD (Asp-Glu-Ala-Asp) box polypeptide 5; predicted gene 12183	1.316	0.043
NM_019869	RNA binding motif protein 14	1.309	0.021
NM_009125	ataxin 2	1.304	0.013
NM_001081293	regulation of nuclear pre-mRNA domain containing 2	1.293	0.045
NM_025331	guanine nucleotide binding protein (G protein), gamma 11	1.282	0.050
NP_598452	poly-U binding splicing factor 60	1.281	0.046
NM_172666	alkylglycerone phosphate synthase	1.275	0.007
NM_008364	interleukin 1 receptor accessory protein	1.274	0.009
NM_134080	filamin, beta	1.268	0.008
NM_001081267	remodeling and spacing factor 1	1.268	0.001
NM_024436	RAB22A, member RAS oncogene family	1.265	0.008
NM_178216	histone cluster 2, H3b; histone cluster 1, H3f; histone cluster 1, H3e; histone cluster 2, H3c1; histone cluster 1, H3d; histone cluster 1, H3c; histone cluster 1, H3b; histone cluster 2, H3c2; histone cluster 2, H2aa1; histone cluster 2, H2aa2	1.254	0.030
NM_029157	splicing factor 3a, subunit 3	1.254	0.005
NM_008882	plexin A2	1.253	0.001
NM_026171	nuclear VCP-like	1.247	0.001
NM_010726	phytanoyl-CoA hydroxylase	1.241	0.004
NM_028264	transmembrane protein 55A	1.241	0.036
NM_153567	SLAIN motif family, member 2	1.237	0.044
NM_016888	UDP-GlcNAc:betaGal beta-1,3-N-acetylglucosaminyltransferase 2	1.232	0.045
NM_011605	thymopoietin	1.229	0.041
NM_011076	ATP-binding cassette, sub-family B (MDR/TAP), member 1A	1.228	0.026
NM_013902	FK506 binding protein 3	1.220	0.004
NM_001081164	OTU domain containing 4	1.216	0.014
NP_963910	GNAS (guanine nucleotide binding protein, alpha stimulating) complex locus	1.215	0.041
NM_001163300	scaffold attachment factor B	1.215	0.042
NP_001258827	Peroxisomal acyl-coenzyme A oxidase 1	1.208	0.011
NM_020027	HLA-B associated transcript 2	1.206	0.023
NM_133947	nuclear mitotic apparatus protein 1	1.202	0.015
NM_009338	acetyl-Coenzyme A acetyltransferase 2	1.202	0.003
NM_008477	kinectin 1	1.200	0.025
NM_027901	general transcription factor IIIC, polypeptide 2, beta; Mpv17 transgene, kidney disease mutant	-1.206	0.042
NM_008302	heat shock protein 90 alpha (cytosolic), class B member 1	-1.217	0.050
NM_010239	ferritin heavy chain 1	-1.219	0.007
NM_133348	acyl-CoA thioesterase 7	-1.223	0.016
NM_001025947	dynamin 1-like	-1.224	0.014
NM_175438	aldehyde dehydrogenase 4 family, member A1	-1.224	0.036
NM_031843	dipeptidylpeptidase 7	-1.229	0.005
NM_025343	required for meiotic nuclear division 1 homolog (S. cerevisiae); predicted gene 5512	-1.229	0.021
NM_025845	PRP38 pre-mRNA processing factor 38 (yeast) domain containing B; similar to PRP38 pre-mRNA processing factor 38 (yeast) domain	-1.231	0.030

	containing B		
NM_019770	transmembrane emp24 domain trafficking protein 2; predicted gene 10698; predicted gene 7318	-1.234	0.031
NM_133794	glutaminyl-tRNA synthetase	-1.235	0.026
NM_008442	kinesin family member 2A	-1.237	0.049
NM_172674	PHD finger protein 20	-1.238	0.045
NM_026510	FtsJ homolog 2 (E. coli)	-1.242	0.048
NM_001033293	UDP-N-acteylglucosamine pyrophosphorylase 1-like 1	-1.253	0.026
NM_001081056	exportin, tRNA (nuclear export receptor for tRNAs)	-1.261	0.010
NM_009288	serine/threonine kinase 10	-1.263	0.029
NM_026474	SGT1, suppressor of G2 allele of SKP1 (S. cerevisiae)	-1.263	0.041
NM_008136	guanine nucleotide binding protein-like 1	-1.263	0.018
NM_026202	coiled-coil domain containing 50	-1.272	0.049
NM_028782	lon peptidase 1, mitochondrial	-1.282	0.025
NM_009373	transglutaminase 2, C polypeptide	-1.282	0.004
NM_001160319	ubiquitin protein ligase E3 component n-recognin 4	-1.284	0.046
NM_145506	erythrocyte protein band 4.1-like 5	-1.291	0.015
NM_144897	apolipoprotein A-I binding protein	-1.295	0.024
NM_145955	RIKEN cDNA 1110007A13 gene	-1.296	0.036
NP_001156418	pyruvate carboxylase	-1.305	0.034
NM_175372	retinol dehydrogenase 13 (all-trans and 9-cis)	-1.310	0.006
NM_001171582	methionine-tRNA synthetase	-1.316	0.013
NM_144818	non-SMC condensin I complex, subunit H	-1.316	0.045
NM_010562	integrin linked kinase; predicted gene 6263	-1.316	0.030
NM_025691	signal recognition particle 72	-1.318	0.012
NM_029635	COMM domain containing 9	-1.323	0.033
NM_013492	similar to clusterin; clusterin	-1.330	0.008
NM_013691	thrombospondin 3	-1.330	0.014
NM_029023	serine carboxypeptidase 1	-1.334	0.042
NM_013818	GTP binding protein 1	-1.334	0.032
NM_025515	similar to Coiled-coil domain containing 90B; coiled-coil domain containing 90B	-1.341	0.040
NM_008012	aldo-keto reductase family 1, member B8	-1.347	0.013
NM_028762	RNA binding motif protein 19	-1.349	0.007
NM_001164671	predicted gene 15542; predicted gene 7816; similar to DnaJ-like protein; predicted gene 6335; DnaJ (Hsp40) homolog, subfamily A, member 1, pseudogene; DnaJ (Hsp40) homolog, subfamily A, member 1	-1.350	0.003
NM_025544	mitochondrial ribosomal protein S15	-1.357	0.002
NM_018851	hypothetical protein LOC100045969; SAM domain and HD domain, 1	-1.358	0.010
NM_019564	HtrA serine peptidase 1	-1.359	0.011
NM_011486	similar to Stat3B; signal transducer and activator of transcription 3	-1.359	0.048
NM_010421	hexosaminidase A	-1.360	0.036
NM_008948	proteasome (prosome, macropain) 26S subunit, ATPase 3	-1.364	0.017
NM_198105	family with sequence similarity 120, member C	-1.365	0.024
NM_145507	aspartyl-tRNA synthetase	-1.368	0.047
NM_028198	exportin 5	-1.369	0.011
NM_007783	c-src tyrosine kinase	-1.371	0.036
NM_030238	dynein cytoplasmic 1 heavy chain 1	-1.379	0.009
NM_011414	secretory leukocyte peptidase inhibitor	-1.384	0.039
NM_020520	solute carrier family 25 (mitochondrial carnitine/acylcarnitine translocase), member 20	-1.385	0.047
NM_009190	similar to vacuolar protein sorting 4b; vacuolar protein sorting 4b (yeast)	-1.390	0.037

NM_008520	latent transforming growth factor beta binding protein 3	-1.394	0.010
NM_010546	inhibitor of kappaB kinase beta	-1.394	0.012
NM_009471	uridine monophosphate synthetase	-1.395	0.011
NM_001081066	DENN/MADD domain containing 3	-1.396	0.025
NM_024267	importin 4	-1.396	0.001
NM_024258	ubiquitin specific peptidase 16	-1.398	0.038
NM_027357	proteasome (prosome, macropain) 26S subunit, non-ATPase, 1	-1.400	0.012
NM_023525	carbamoyl-phosphate synthetase 2, aspartate transcarbamylase, and dihydroorotase	-1.404	0.016
NM_178719	Smith-Magenis syndrome chromosome region, candidate 7-like (human)	-1.404	0.026
NM_172990	pantothenate kinase 4	-1.405	0.035
NM_021295	LanC (bacterial lantibiotic synthetase component C)-like 1	-1.408	0.010
NM_024194	leucine rich repeat containing 40	-1.412	0.026
NP_001095925	amyloid beta (A4) precursor-like protein 2	-1.413	0.025
NP_001157185	predicted gene 9755; Tu translation elongation factor, mitochondrial	-1.421	0.005
NM_010106	predicted gene 5869; predicted gene 7161; predicted gene 7105; predicted gene 5822; similar to eukaryotic translation elongation factor 1 alpha 1; predicted gene 6192; predicted gene 6392; predicted gene 6767; predicted gene 6170; predicted gene 6548; pre	-1.423	0.001
NM_029293	phosphohistidine phosphatase 1	-1.433	0.048
NM_001038589	ubiquitin specific peptidase 14	-1.436	0.009
NM_178070	vacuolar protein sorting 33B (yeast)	-1.441	0.006
NM_021299	adenylate kinase 3	-1.443	0.004
NM_019812	sirtuin 1 (silent mating type information regulation 2, homolog) 1 (S. cerevisiae)	-1.444	0.009
NM_007643	CD36 antigen	-1.445	0.030
NM_152801	Rac/Cdc42 guanine nucleotide exchange factor (GEF) 6	-1.459	0.038
NM_177727	LSM14 homolog B (SCD6, S. cerevisiae)	-1.462	0.008
NM_009981	phosphate cytidylyltransferase 1, choline, alpha isoform	-1.463	0.031
NM_011723	xanthine dehydrogenase	-1.467	0.012
NM_016748	cytidine 5'-triphosphate synthase	-1.480	0.033
NM_008826	phosphofructokinase, liver, B-type	-1.480	0.031
NM_172404	cysteine conjugate-beta lyase 1	-1.483	0.026
NM_144915	diacylglycerol lipase, beta	-1.492	0.001
NM_001163126	component of oligomeric golgi complex 5	-1.494	0.024
NM_178337	tubulin-specific chaperone E	-1.500	0.000
NM_145578	ubiquitin-conjugating enzyme E2M (UBC12 homolog, yeast)	-1.501	0.020
NM_080708	predicted gene 4521; BMP2 inducible kinase	-1.504	0.009
NM_025921	chromatin modifying protein 1B; RIKEN cDNA 2610002M06 gene	-1.505	0.048
NM_144923	biliverdin reductase B (flavin reductase (NADPH))	-1.512	0.016
NM_026276	aminoadipate-semialdehyde dehydrogenase-phosphopantetheinyl transferase; hypothetical protein LOC100044211	-1.515	0.016
NP_808340	transmembrane protein 201	-1.516	0.004
NM_134079	adenosine kinase	-1.518	0.039
NM_026079	inhibitor of kappa light polypeptide enhancer in B-cells, kinase complex-associated protein	-1.522	0.007
NM_013792	alpha-N-acetylglucosaminidase (Sanfilippo disease IIIB)	-1.524	0.036
NM_027815	RIKEN cDNA 9030624J02 gene	-1.541	0.010
NM_177215	oculocerebrorenal syndrome of Lowe	-1.546	0.030
NM_025647	cytidine monophosphate (UMP-CMP) kinase 1; predicted gene 5867	-1.547	0.007
NM_001080748	general transcription factor II I; similar to transcription factor TFII-	-1.560	0.005

	I-gamma		
NM_023402	Myosin regulatory light chain 12B	-1.563	0.030
NM_025794	electron transferring flavoprotein, dehydrogenase	-1.575	0.004
NM_178376	Ras-related GTP binding A	-1.576	0.032
NM_016906	Sec61 alpha 1 subunit (S. cerevisiae)	-1.582	0.028
NM_053181	pyridoxal-dependent decarboxylase domain containing 1	-1.586	0.000
NM_013528	glutamine fructose-6-phosphate transaminase 1	-1.590	0.003
NM_173443	valosin containing protein (p97)/p47 complex interacting protein 1	-1.591	0.047
NM_009658	aldo-keto reductase family 1, member B3 (aldose reductase)	-1.592	0.001
NM_009755	bone morphogenetic protein 1	-1.601	0.009
NM_011340	serine (or cysteine) peptidase inhibitor, clade F, member 1	-1.606	0.009
NM_025918	coiled-coil domain containing 43	-1.617	0.000
NM_008826	phosphofructokinase, liver, B-type	-1.624	0.025
NM_029746	component of oligomeric golgi complex 2	-1.637	0.045
NM_001042501	RIKEN cDNA 5830415L20 gene	-1.637	0.001
NM_134138	proteasome (prosome, macropain) assembly chaperone 2; similar to Clast3 protein	-1.640	0.012
NM_010049	dihydrofolate reductase	-1.648	0.014
NM_011348	sema domain, immunoglobulin domain (Ig), short basic domain, secreted, (semaphorin) 3E; hypothetical protein LOC100044162	-1.650	0.008
NM_008325	iduronidase, alpha-L-	-1.653	0.039
NM_144804	DEP domain containing 7	-1.655	0.044
NM_144878	flavin containing monooxygenase 4	-1.656	0.018
NM_029005	mixed lineage kinase domain-like	-1.663	0.026
NM_011889	septin 3	-1.666	0.031
NM_008451	kinesin light chain 2	-1.681	0.022
NM_001004156	pleckstrin homology domain containing, family G (with RhoGef domain) member 5	-1.687	0.015
NM_021420	serine/threonine kinase 4	-1.690	0.004
NM_030201	heat shock protein 70 family, member 13	-1.695	0.015
NM_175465	SEC14 and spectrin domains 1; predicted gene 9165	-1.703	0.002
NM_001013380	dynein, cytoplasmic 1 light intermediate chain 2	-1.710	0.013
NP_001136216	RIKEN cDNA 2610110G12 gene	-1.712	0.011
NM_001127346	NADH dehydrogenase (ubiquinone) 1 alpha subcomplex, assembly factor 2	-1.714	0.010
NM_008776	platelet-activating factor acetylhydrolase, isoform 1b, subunit 3	-1.718	0.006
NM_175180	WD repeat domain 44	-1.723	0.003
NM_001033318	component of oligomeric golgi complex 7	-1.724	0.005
NM_011577	transforming growth factor, beta 1	-1.808	0.021

Table 1-C: Differentially regulated CHO DP-12 proteins determined in samples corresponding to culture using increased bioprocess media dissolved oxygen content of 110%.

RefSeq Annotation	Description	Fold Change	P-value
NM_025364	predicted gene 6563; SAP domain containing ribonucleoprotein	2.000	0.009
NM_011547	transcription factor AP-2, alpha	1.863	0.018
NM_007647	ectonucleoside triphosphate diphosphohydrolase 5	1.754	0.033
NM_021510	heterogeneous nuclear ribonucleoprotein H1	1.741	0.001
NM_144869	cDNA sequence BC021614	1.739	0.037
NP_001103618	mannoside acetylglucosaminyltransferase 1	1.732	0.004
NM_153516	BCL2-like 13 (apoptosis facilitator)	1.732	0.031

NM_027435	ATPase family, AAA domain containing 2	1.721	0.010
NM_146065	activating transcription factor 7	1.714	0.001
NM_024249	solute carrier family 38, member 10	1.706	0.047
NP_001157290	protein phosphatase 1, regulatory subunit 10	1.706	0.005
NM_172710	RIKEN cDNA 2310045A20 gene	1.705	0.014
NM_027434	regulation of nuclear pre-mRNA domain containing 1B	1.705	0.029
NP_001239458	Polyglutamine-binding protein 1	1.704	0.003
NM_011333	chemokine (C-C motif) ligand 2	1.700	0.019
NM_009624	adenylate cyclase 9	1.694	0.006
NM_019419	ADP-ribosylation factor-like 6 interacting protein 1	1.690	0.005
NM_008562	similar to myeloid cell leukemia sequence 1; myeloid cell leukemia sequence 1	1.690	0.022
NM_009833	cyclin T1	1.679	0.007
NM_007709	Cbp/p300-interacting transactivator with Glu/Asp-rich carboxy-terminal domain 1	1.665	0.038
NM_001163622	prolyl endopeptidase-like	1.662	0.001
NM_139291	cell division cycle 26; predicted gene 9174	1.661	0.013
NM_133196	cleavage stimulation factor, 3' pre-RNA subunit 2	1.660	0.034
NM_010724	proteasome (prosome, macropain) subunit, beta type 8 (large multifunctional peptidase 7)	1.655	0.006
NM_016709	AU RNA binding protein/enoyl-coenzyme A hydratase	1.654	0.001
NM_019821	glycolipid transfer protein	1.653	0.031
NM_025576	protein tyrosine phosphatase, mitochondrial 1	1.649	0.048
NM_026936	oxidase assembly 1-like	1.646	0.012
NM_019989	SH3-binding domain glutamic acid-rich protein like	1.637	0.002
NM_009739	branched chain ketoacid dehydrogenase kinase	1.636	0.012
NP_598452	poly-U binding splicing factor 60	1.631	0.001
NM_153168	leucyl-tRNA synthetase, mitochondrial	1.629	0.029
NM_133435	nicotinamide nucleotide adenylyltransferase 1	1.625	0.034
NM_010302	guanine nucleotide binding protein, alpha 12; similar to Guanine nucleotide-binding protein alpha-12 subunit (G alpha-12)	1.622	0.049
NM_028312	coiled-coil domain containing 12; predicted gene 8518	1.618	0.031
NM_025313	ATP synthase, H+ transporting, mitochondrial F1 complex, delta subunit	1.614	0.020
NM_172679	RIKEN cDNA 4932438A13 gene	1.611	0.028
NM_008704	similar to Nucleoside diphosphate kinase A (NDK A) (NDP kinase A) (Tumor metastatic process-associated protein) (Metastasis inhibition factor NM23) (NDPK-A) (nm23-M1); non-metastatic cells 1, protein (NM23A) expressed in	1.611	0.029
NM_133823	methylmalonic aciduria (cobalamin deficiency) type A	1.609	0.047
NM_011434	predicted gene 8566; superoxide dismutase 1, soluble; similar to Superoxide dismutase	1.609	0.028
NM_029078	cleavage and polyadenylation factor subunit homolog (S. cerevisiae)	1.607	0.048
NM_016794	vesicle-associated membrane protein 8	1.606	0.002
NM_134077	RNA binding motif protein 26	1.606	0.009
NM_007874	receptor accessory protein 5	1.605	0.021
NM_009032	RNA binding motif protein 4	1.602	0.037
NM_021563	Erbb2 interacting protein	1.601	0.007
NP_001003667	keratin 77	1.600	0.000
NM_029626	glycosyltransferase 8 domain containing 1	1.586	0.002
NM_172397	similar to epithelial protein lost in neoplasm; LIM domain containing 2	1.586	0.007

NM_008155	glucose phosphate isomerase 1	1.581	0.023
NM_134048	Casitas B-lineage lymphoma-like 1	1.576	0.032
NM_028767	forkhead box P4	1.574	0.031
NM_030561	cDNA sequence BC004004	1.574	0.026
NM_080556	transmembrane 9 superfamily member 2	1.574	0.005
NM_030004	crystallin, lambda 1	1.572	0.019
NM_133998	RIKEN cDNA 1810008A18 gene	1.569	0.015
NM_181407	malic enzyme 3, NADP(+)-dependent, mitochondrial	1.568	0.010
NM_009031	retinoblastoma binding protein 7; predicted gene 6382	1.563	0.045
NM_010176	fumarylacetoacetate hydrolase	1.563	0.041
NM_028754	RIKEN cDNA 0610037L13 gene	1.561	0.018
NM_175324	nephronophthisis 3 (adolescent); acyl-Coenzyme A dehydrogenase family, member 11	1.555	0.003
NM_153117	RIKEN cDNA 9530068E07 gene	1.554	0.033
NM_009883	CCAAT/enhancer binding protein (C/EBP), beta	1.552	0.040
NM_023041	peroxisomal biogenesis factor 19	1.549	0.035
NM_011528	transaldolase 1	1.548	0.050
NM_134063	cDNA sequence BC016423	1.546	0.013
NM_145553	predicted gene 7527; family with sequence similarity 76, member A	1.535	0.021
NM_027430	brain protein 44; similar to brain protein 44; predicted gene 3982	1.533	0.027
NM_023051	calsyntenin 1	1.533	0.040
NM_019791	melanoma antigen, family D, 1	1.525	0.021
NM_008881	plexin A1	1.524	0.005
NM_018858	phosphatidylethanolamine binding protein 1	1.523	0.002
NM_011933	2-4-dienoyl-Coenzyme A reductase 2, peroxisomal	1.523	0.013
NM_001024205	nuclear fragile X mental retardation protein interacting protein 2	1.521	0.002
NM_009242	secreted acidic cysteine rich glycoprotein; similar to Secreted acidic cysteine rich glycoprotein	1.521	0.033
NM_020618	similar to SWI/SNF related, matrix associated, actin dependent regulator of chromatin, subfamily e, member 1; predicted gene 1815; predicted gene 8494; SWI/SNF related, matrix associated, actin dependent regulator of chromatin, subfamily e, member 1; pred	1.521	0.009
NM_029169	RNA binding motif protein 6	1.520	0.002
NM_023733	carnitine O-octanoyltransferase	1.519	0.022
NM_172472	transcription factor E3	1.517	0.009
NM_009074	macrophage stimulating 1 receptor (c-met-related tyrosine kinase)	1.517	0.026
NM_001171052	metastasis associated 3	1.516	0.035
NM_007383	acyl-Coenzyme A dehydrogenase, short chain	1.516	0.021
NM_182939	similar to protein phosphatase 4, regulatory subunit 2; similar to Protein phosphatase 4, regulatory subunit 2; protein phosphatase 4, regulatory subunit 2	1.514	0.043
NM_009270	squalene epoxidase	1.514	0.008
NM_025952	magnesium transporter 1	1.513	0.002
NM_026068	mediator of RNA polymerase II transcription, subunit 31 homolog (yeast)	1.507	0.004
NM_011121	polo-like kinase 1 (Drosophila)	1.504	0.025
NM_008131	predicted gene 4949; glutamate-ammonia ligase (glutamine synthetase)	1.503	0.025
XP_619909	predicted gene 5449; small nuclear ribonucleoprotein D2; predicted gene 5848; predicted gene 10120	1.497	0.033
NM_001001932	early endosome antigen 1	1.497	0.022
NM_053014	1-acylglycerol-3-phosphate O-acyltransferase 3	1.496	0.035

NM_025797	cytochrome b-5	1.490	0.036
NM_027219	CDC42 effector protein (Rho GTPase binding) 1	1.488	0.037
NM_010191	predicted gene 6781; farnesyl diphosphate farnesyl transferase 1	1.488	0.011
NM_026420	polyadenylate-binding protein-interacting protein 2	1.485	0.040
NM_030732	transducin (beta)-like 1X-linked receptor 1	1.485	0.023
NM_025822	arginine/serine-rich coiled-coil 1	1.485	0.007
NM_078478	growth hormone inducible transmembrane protein	1.482	0.019
NM_010368	glucuronidase, beta	1.481	0.012
NP_001135450	TPX2, microtubule-associated protein homolog (Xenopus laevis)	1.474	0.026
NP_001164215	C-terminal binding protein 2	1.473	0.037
NM_028074	DEAD (Asp-Glu-Ala-Asp) box polypeptide 42	1.472	0.006
NM_013556	hypoxanthine guanine phosphoribosyl transferase 1	1.469	0.011
NM_024274	phenylalanine-tRNA synthetase 2 (mitochondrial)	1.469	0.001
NM_001098225	a disintegrin and metallopeptidase domain 22	1.469	0.010
NM_198937	hematological and neurological expressed 1-like	1.462	0.022
NM_001033534	layilin	1.460	0.034
NM_025682	paraspeckle protein 1	1.456	0.027
NM_144888	mitochondrial antiviral signaling protein	1.455	0.049
NM_009009	RAD21 homolog (S. pombe)	1.454	0.021
NM_010358	similar to Glutathione S-transferase Mu 1 (GST class-mu 1) (Glutathione S-transferase GT8.7) (pmGT10) (GST 1-1); predicted gene 5562; glutathione S-transferase, mu 1	1.446	0.006
NM_138758	trimethyllysine hydroxylase, epsilon	1.445	0.015
NM_177643	Zinc finger protein 281	1.442	0.002
NM_172205	suprabasin	1.441	0.026
NM_009832	cyclin K; similar to cyclin K	1.436	0.034
NM_008717	zinc finger, matrin-like	1.436	0.010
NM_008293	hydroxy-delta-5-steroid dehydrogenase, 3 beta- and steroid delta-isomerase 1	1.430	0.020
NM_013502	similar to CtBP1 protein; C-terminal binding protein 1	1.428	0.006
NM_019693	HLA-B-associated transcript 1A	1.426	0.030
NM_015735	damage specific DNA binding protein 1	1.425	0.002
NM_010070	docking protein 1	1.416	0.015
NM_021521	mediator of RNA polymerase II transcription, subunit 12 homolog (yeast)	1.411	0.030
NM_009033	RNA binding motif protein, X chromosome retrogene	1.408	0.021
NM_013534	leprecan-like 2	1.406	0.001
NM_009503	similar to Transitional endoplasmic reticulum ATPase (TER ATPase) (15S Mg(2+)-ATPase p97 subunit) (Valosin-containing protein) (VCP); valosin containing protein	1.403	0.003
NM_020520	solute carrier family 25 (mitochondrial carnitine/acylcarnitine translocase), member 20	1.402	0.038
NM_026170	endoplasmic reticulum-golgi intermediate compartment (ERGIC) 1	1.402	0.011
NM_001080981	DEAD (Asp-Glu-Ala-Asp) box polypeptide 23	1.400	0.035
NM_026512	biphenyl hydrolase-like (serine hydrolase, breast epithelial mucin-associated antigen)	1.396	0.016
NM_027373	actin filament associated protein 1	1.394	0.016
NM_025573	splicing factor, arginine/serine rich 9	1.391	0.046
NM_153412	pleckstrin homology-like domain, family B, member 2	1.387	0.027
NM_015816	LSM4 homolog, U6 small nuclear RNA associated (S. cerevisiae)	1.385	0.029
NM_007466	apoptosis inhibitor 5	1.383	0.039
NM_007749	similar to cytochrome c oxidase, subunit VIIc; predicted gene 3386; cytochrome c oxidase, subunit VIIc	1.377	0.008

NM_001081422	biorientation of chromosomes in cell division 1-like	1.375	0.002
NM_009409	topoisomerase (DNA) II beta	1.374	0.041
NM_026934	predicted gene 5909; zinc finger CCCH-type containing 15	1.373	0.004
NM_026141	peptidylprolyl isomerase (cyclophilin)-like 4	1.373	0.005
NM_010729	lysyl oxidase-like 1	1.361	0.042
NM_133803	dipeptidylpeptidase 3	1.360	0.032
NM_009774	budding uninhibited by benzimidazoles 3 homolog (S. cerevisiae)	1.358	0.034
NM_011327	sterol carrier protein 2, liver	1.358	0.017
NM_024200	mitofusin 1	1.357	0.015
NM_028793	acyl-Coenzyme A binding domain containing 5	1.357	0.050
NM_018871	tyrosine 3-monooxygenase/tryptophan 5-monooxygenase activation protein, gamma polypeptide	1.349	0.014
NM_011247	retinoblastoma binding protein 6	1.349	0.036
NM_001163570	exosome component 8	1.344	0.043
NM_011378	transcriptional regulator, SIN3A (yeast)	1.342	0.001
NM_023603	splicing factor proline/glutamine rich (polypyrimidine tract binding protein associated); similar to PTB-associated splicing factor	1.341	0.007
NM_146131	similar to Pre-B-cell leukemia transcription factor interacting protein 1; pre-B-cell leukemia transcription factor interacting protein 1	1.341	0.025
NM_001044384	tissue inhibitor of metalloproteinase 1	1.341	0.008
NM_139297	UDP-glucose pyrophosphorylase 2	1.338	0.007
NM_027375	GRIP and coiled-coil domain containing 2	1.336	0.005
NM_153552	THO complex 1	1.335	0.046
NM_008549	mannosidase 2, alpha 1	1.332	0.005
NM_007690	chromodomain helicase DNA binding protein 1	1.332	0.007
NM_001081251	polybromo 1	1.330	0.049
NM_175094	pyruvate dehydrogenase complex, component X; similar to pyruvate dehydrogenase complex, component X	1.326	0.001
NM_008402	integrin alpha V	1.325	0.008
NM_027226	forty-two-three domain containing 1	1.325	0.010
NM_011500	striatin, calmodulin binding protein	1.319	0.042
NM_010497	isocitrate dehydrogenase 1 (NADP+), soluble	1.315	0.013
NM_172266	lysophosphatidylglycerol acyltransferase 1	1.313	0.036
NM_011767	zinc finger RNA binding protein	1.310	0.007
NM_178592	HLA-B associated transcript 5	1.305	0.023
NM_001080926	low density lipoprotein receptor-related protein 8, apolipoprotein e receptor	1.305	0.034
NM_011479	serine palmitoyltransferase, long chain base subunit 2	1.304	0.045
NM_001077403	neuropilin 2	1.303	0.017
NM_001013389	MRS2 magnesium homeostasis factor homolog (S. cerevisiae)	1.302	0.007
NM_008305	perlecan (heparan sulfate proteoglycan 2)	1.302	0.007
NP_035681	upstream binding transcription factor, RNA polymerase I	1.297	0.047
NM_133947	nuclear mitotic apparatus protein 1	1.291	0.004
NM_016666	aryl-hydrocarbon receptor-interacting protein	1.290	0.020
NM_007981	acyl-CoA synthetase long-chain family member 1	1.287	0.013
NM_144831	DEAH (Asp-Glu-Ala-His) box polypeptide 8	1.284	0.014
NP_001185933	Golgin subfamily A member 5	1.281	0.025
NM_133957	nuclear factor of activated T-cells 5	1.280	0.024
NM_021507	sulfide quinone reductase-like (yeast)	1.276	0.023
NM_172965	Sin3A associated protein	1.276	0.023
NM_007840	DEAD (Asp-Glu-Ala-Asp) box polypeptide 5; predicted gene 12183	1.266	0.035
NM_001008422	SR-related CTD-associated factor 1	1.261	0.033

NM_001163300	scaffold attachment factor B	1.257	0.018
NM_021549	polynucleotide kinase 3'- phosphatase	1.256	0.016
NM_011078	PHD finger protein 2	1.256	0.035
NM_144846	family with sequence similarity 49, member B	1.256	0.005
NM_011623	topoisomerase (DNA) II alpha	1.256	0.002
NM_027213	mediator of RNA polymerase II transcription, subunit 6 homolog (yeast)	1.255	0.010
NM_010357	glutathione S-transferase, alpha 4	1.255	0.020
NM_025794	electron transferring flavoprotein, dehydrogenase	1.253	0.020
NM_019869	RNA binding motif protein 14	1.253	0.021
NM_012042	cullin 1	1.253	0.011
NM_138747	NOP2 nucleolar protein homolog (yeast)	1.249	0.043
NM_026644	1-acylglycerol-3-phosphate O-acyltransferase 4 (lysophosphatidic acid acyltransferase, delta)	1.245	0.047
NM_198249	RIKEN cDNA E130112L23 gene	1.243	0.004
NM_008765	origin recognition complex, subunit 2-like (S. cerevisiae)	1.238	0.029
NM_025988	acyl-Coenzyme A binding domain containing 4	1.229	0.040
NM_145991	cell division cycle 73, Paf1/RNA polymerase II complex component, homolog (S. cerevisiae)	1.229	0.035
NM_001166406	kinesin family member 20A	1.227	0.049
NM_011716	Wolfram syndrome 1 homolog (human)	1.226	0.002
NM_021305	Sec61, alpha subunit 2 (S. cerevisiae)	1.223	0.006
NM_010561	interleukin enhancer binding factor 3	1.222	0.006
NM_009011	RAD23b homolog (S. cerevisiae)	1.213	0.039
NM_008612	menage a trois 1	1.213	0.006
NM_009388	transketolase	1.205	0.031
NM_013830	PRP4 pre-mRNA processing factor 4 homolog B (yeast)	1.203	0.034
NM_010515	insulin-like growth factor 2 receptor	-1.201	0.031
NM_019816	apoptosis antagonizing transcription factor	-1.204	0.024
NM_013559	heat shock 105kDa/110kDa protein 1	-1.207	0.043
NM_013492	similar to clusterin; clusterin	-1.209	0.011
NM_008927	mitogen-activated protein kinase kinase 1	-1.211	0.035
NM_001033293	UDP-N-acteylglucosamine pyrophosphorylase 1-like 1	-1.217	0.046
NM_025959	proteasome (prosome, macropain) 26S subunit, ATPase, 6	-1.218	0.029
NM_012010	eukaryotic translation initiation factor 2, subunit 3, structural gene X-linked; similar to translation initiation factor eIF-2 gamma subunit; predicted gene 2223	-1.219	0.042
NM_153125	SEC16 homolog A (S. cerevisiae)	-1.220	0.026
NM_013647	predicted gene 8731; predicted gene 7504; similar to Rps16 protein; ribosomal protein S16	-1.221	0.039
NM_008872	plasminogen activator, tissue	-1.224	0.041
NM_024261	RIKEN cDNA 1700052N19 gene	-1.229	0.016
NM_023060	eukaryotic elongation factor, selenocysteine-tRNA-specific	-1.232	0.005
NP_001070732	adaptor protein complex AP-2, alpha 1 subunit	-1.233	0.034
NM_024242	RIO kinase 1 (yeast)	-1.234	0.029
NM_010615	kinesin family member 11	-1.235	0.002
NM_021514	phosphofructokinase, muscle	-1.258	0.018
NM_025691	signal recognition particle 72	-1.264	0.025
NM_023247	NADH dehydrogenase (ubiquinone) 1 alpha subcomplex, assembly factor 3	-1.267	0.036
NM_027896	Coenzyme A synthase	-1.272	0.008
NM_172381	expressed sequence AI314180	-1.281	0.015
NM_008788	procollagen C-endopeptidase enhancer protein	-1.283	0.011

NM_133360	predicted gene 5182; acetyl-Coenzyme A carboxylase alpha	-1.283	0.004
NM_133993	PWP1 homolog (S. cerevisiae)	-1.289	0.036
NM_139302	SH3-domain GRB2-like endophilin B2	-1.290	0.024
NM_146200	eukaryotic translation initiation factor 3, subunit C; similar to Eukaryotic translation initiation factor 3, subunit 8	-1.293	0.008
NM_134137	leucyl-tRNA synthetase	-1.297	0.006
NM_007508	ATPase, H+ transporting, lysosomal V1 subunit A	-1.298	0.009
NM_001105667	deoxythymidylate kinase	-1.298	0.006
NM_025648	phenylalanyl-tRNA synthetase, alpha subunit	-1.299	0.021
NM_138315	microtubule associated monoxygenase, calponin and LIM domain containing 1	-1.303	0.009
NM_011942	lysophospholipase 2	-1.317	0.032
NM_020009	mechanistic target of rapamycin (serine/threonine kinase)	-1.320	0.030
NM_026000	proteasome (prosome, macropain) 26S subunit, non-ATPase, 9	-1.324	0.006
NM_025919	predicted gene 10288; predicted gene 7589; ribosomal protein L11; predicted gene 10036; predicted gene 7384; predicted gene 6745; predicted gene 5093	-1.328	0.039
NM_145139	eukaryotic translation initiation factor 3, subunit L	-1.331	0.000
NM_145938	ribonuclease P 40 subunit (human)	-1.332	0.021
NM_028071	coactosin-like 1 (Dictyostelium)	-1.337	0.029
NM_026969	Sec31 homolog A (S. cerevisiae)	-1.337	0.014
NM_172265	eukaryotic translation initiation factor 2B, subunit 5 epsilon	-1.339	0.050
NM_138603	coiled-coil domain containing 22	-1.347	0.049
NM_013755	glycogenin	-1.351	0.023
NM_019827	glycogen synthase kinase 3 beta	-1.352	0.039
NM_029735	similar to Bifunctional aminoacyl-tRNA synthetase; glutamyl-prolyl-tRNA synthetase	-1.357	0.009
NM_183029	insulin-like growth factor 2 mRNA binding protein 2	-1.357	0.020
NM_030238	dynein cytoplasmic 1 heavy chain 1	-1.364	0.016
NM_019703	phosphofructokinase, platelet	-1.368	0.031
NM_001164677	programmed cell death 6 interacting protein	-1.370	0.036
NM_008996	RAB1, member RAS oncogene family	-1.372	0.019
NM_001081056	exportin, tRNA (nuclear export receptor for tRNAs)	-1.373	0.011
NM_007638	chaperonin containing Tcp1, subunit 7 (eta)	-1.374	0.040
NM_026195	5-aminoimidazole-4-carboxamide ribonucleotide formyltransferase/IMP cyclohydrolase; similar to 5-aminoimidazole-4-carboxamide ribonucleotide formyltransferase/IMP cyclohydrolase	-1.376	0.007
NM_009091	similar to 40S ribosomal protein S15 (RIG protein); predicted gene 6921; similar to insulinoma protein (rig); predicted gene 8460; predicted gene 7121; predicted gene 5781; predicted gene 5508; predicted gene 6867; ribosomal protein S15	-1.377	0.033
NM_173013	microtubule-associated protein 1S	-1.379	0.011
NM_026295	CTD (carboxy-terminal domain, RNA polymerase II, polypeptide A) phosphatase, subunit 1	-1.381	0.016
NM_146217	alanyl-tRNA synthetase	-1.384	0.026
NM_009674	annexin A7	-1.385	0.009
NM_001081255	leucine-rich repeats and calponin homology (CH) domain containing 3	-1.397	0.005
NM_007620	predicted gene 5678; carbonyl reductase 1	-1.397	0.019
NM_009673	annexin A5	-1.398	0.014
NM_028450	GULP, engulfment adaptor PTB domain containing 1	-1.402	0.032
NM_013469	annexin A11; predicted gene 2260; predicted gene 2274	-1.409	0.018
NM_028243	prolylcarboxypeptidase (angiotensinase C)	-1.410	0.048

NM_001081028	signal-induced proliferation-associated 1 like 3	-1.412	0.003
NM_001146023	Protein Fam98c	-1.414	0.002
NM_011125	phospholipid transfer protein	-1.416	0.034
NM_007509	ATPase, H+ transporting, lysosomal V1 subunit B2	-1.419	0.006
NM_008325	iduronidase, alpha-L-	-1.420	0.031
NM_011400	solute carrier family 2 (facilitated glucose transporter), member 1	-1.420	0.008
NM_001045489	milk fat globule-EGF factor 8 protein	-1.427	0.048
NM_013529	Glutamine--fructose-6-phosphate aminotransferase [isomerizing] 2	-1.428	0.010
NM_178644	OAF homolog (Drosophila)	-1.434	0.016
NM_146229	dynein cytoplasmic 1 light intermediate chain 1	-1.435	0.030
NM_009190	similar to vacuolar protein sorting 4b; vacuolar protein sorting 4b	-1.441	0.050
NM_009194	similar to solute carrier family 12, member 2; solute carrier family 12, member 2	-1.441	0.025
NM_011811	phenylalanyl-tRNA synthetase, beta subunit	-1.443	0.006
NM_010546	inhibitor of kappaB kinase beta	-1.445	0.006
NM_001163126	component of oligomeric golgi complex 5	-1.446	0.000
NM_024218	ribosomal protein L24; predicted gene 9385; predicted gene 7380	-1.447	0.027
NM_001033318	component of oligomeric golgi complex 7	-1.455	0.031
NM_172015	isoleucine-tRNA synthetase	-1.456	0.006
NM_133786	structural maintenance of chromosomes 4	-1.457	0.010
NM_030678	glycogen synthase 1, muscle	-1.457	0.014
NM_181072	myosin IE	-1.462	0.019
NM_033074	threonyl-tRNA synthetase	-1.463	0.028
NP_001107603	protein phosphatase 4, regulatory subunit 1	-1.463	0.028
NM_133972	armadillo repeat containing 6	-1.467	0.017
NM_013581	component of oligomeric golgi complex 1	-1.477	0.034
NM_028181	cell cycle progression 1	-1.478	0.027
NM_009296	predicted gene 3258; suppressor of Ty 4 homolog 1 (S. cerevisiae)	-1.480	0.003
NM_011051	programmed cell death 6	-1.480	0.031
NM_029720	cysteine-rich with EGF-like domains 2	-1.483	0.048
NM_178599	COMM domain containing 8	-1.491	0.039
NM_008509	lipoprotein lipase; similar to Lipoprotein lipase precursor (LPL)	-1.498	0.030
NM_178389	galactose-4-epimerase, UDP	-1.501	0.047
NM_001038589	ubiquitin specific peptidase 14	-1.503	0.012
NM_016905	galactokinase 1	-1.507	0.017
NM_008481	laminin, alpha 2	-1.508	0.016
NM_017397	DEAD (Asp-Glu-Ala-Asp) box polypeptide 20	-1.512	0.000
NM_027182	thyroid hormone receptor interactor 13	-1.516	0.040
NM_010233	fibronectin 1	-1.517	0.007
NM_015751	ATP-binding cassette, sub-family E (OABP), member 1	-1.518	0.013
NM_008826	phosphofructokinase, liver, B-type	-1.520	0.010
NM_001160163	neuraminidase 2	-1.521	0.007
NM_016748	cytidine 5'-triphosphate synthase	-1.522	0.004
NM_013507	eukaryotic translation initiation factor 4, gamma 2	-1.522	0.013
NM_001033375	RIKEN cDNA A230046K03 gene	-1.526	0.001
NM_011829	inosine 5'-phosphate dehydrogenase 1	-1.529	0.023
NM_028072	sulfatase 2	-1.529	0.044
NM_026742	NADH dehydrogenase (ubiquinone) 1 alpha subcomplex, assembly factor 4	-1.532	0.000
NM_024267	importin 4	-1.537	0.002
NM_026441	penta-EF hand domain containing 1	-1.540	0.028

NM_009795	calpain, small subunit 1	-1.546	0.046
NM_007908	eukaryotic elongation factor-2 kinase	-1.558	0.042
NM_133255	hook homolog 2 (Drosophila)	-1.559	0.029
NM_023290	makorin, ring finger protein, 2	-1.562	0.009
NM_015805	ATPase, class II, type 9B	-1.563	0.047
NM_026437	RIKEN cDNA 1810055E12 gene	-1.565	0.005
NM_018740	retinoic acid induced 12	-1.565	0.032
NM_133973	component of oligomeric golgi complex 4	-1.569	0.047
NM_001037746	mirror-image polydactyly gene 1 homolog (human); phosphoribosyl pyrophosphate synthetase 1; phosphoribosyl pyrophosphate synthetase 1-like 1	-1.580	0.016
NM_028262	SET domain containing 3; similar to CG32732-PA; predicted gene 7114; predicted gene 14026	-1.581	0.016
NM_027769	copine III	-1.583	0.019
NM_021343	spermatogenesis associated 5	-1.584	0.001
NM_025816	Tax1 (human T-cell leukemia virus type I) binding protein 1	-1.588	0.008
NM_026364	phosphoribosyl pyrophosphate synthetase-associated protein 1	-1.590	0.046
NM_007510	ATPase, H+ transporting, lysosomal V1 subunit E1	-1.591	0.018
NM_007926	aminoacyl tRNA synthetase complex-interacting multifunctional protein 1	-1.594	0.006
NM_001163567	family with sequence similarity 102, member B	-1.603	0.016
NM_001031667	glycogen synthase kinase 3 alpha	-1.605	0.001
NM_008826	phosphofructokinase, liver, B-type	-1.614	0.012
NM_007544	BH3 interacting domain death agonist	-1.616	0.035
NM_001081132	UPF2 regulator of nonsense transcripts homolog (yeast)	-1.616	0.019
NM_013471	annexin A4	-1.622	0.020
NM_013562	interferon-related developmental regulator 1	-1.624	0.004
NM_019437	riboflavin kinase	-1.627	0.025
NM_011956	nucleotide binding protein 2	-1.631	0.005
NM_145380	eukaryotic translation initiation factor 3, subunit M	-1.637	0.014
NM_028811	elongation protein 3 homolog (S. cerevisiae)	-1.640	0.013
NM_025304	leucine carboxyl methyltransferase 1	-1.643	0.023
NM_028304	pseudouridylate synthase 10	-1.644	0.016
NM_010851	myeloid differentiation primary response gene 88	-1.646	0.015
NM_183106	tetratricopeptide repeat domain 17	-1.655	0.008
NM_011348	sema domain, immunoglobulin domain (Ig), short basic domain, secreted, (semaphorin) 3E; hypothetical protein LOC100044162	-1.661	0.023
NP_001258788	Beta-adducin	-1.681	0.008
NM_010217	connective tissue growth factor	-1.682	0.028
NM_198613	adaptor-related protein complex 2, sigma 1 subunit	-1.684	0.011
NM_178710	salt inducible kinase 2	-1.707	0.001
NM_144877	methyltransferase like 13	-1.712	0.013
NM_007783	c-src tyrosine kinase	-1.719	0.007
NM_144818	non-SMC condensin I complex, subunit H	-1.752	0.007
NM_178883	golgin, RAB6-interacting	-1.753	0.002

Table 1-D: Differentially regulated CHO DP-12 proteins determined in samples corresponding to culture using decreased bioprocess media dissolved oxygen content of 60%.

RefSeq Annotation	Description	Fold Change	P-Value
NM_001126047	sema domain, immunoglobulin domain (Ig), transmembrane domain (TM) and short cytoplasmic domain, (semaphorin) 4C	1.894	0.015
NM_175242	RIKEN cDNA 2310014H01 gene	1.852	0.000
NP_001103618	mannoside acetylglucosaminyltransferase 1	1.802	0.000
NM_008681	N-myc downstream regulated gene 1	1.786	0.046
NM_020010	cytochrome P450, family 51	1.742	0.010
NM_010015	defender against cell death 1	1.739	0.035
NM_008562	similar to myeloid cell leukemia sequence 1; myeloid cell leukemia sequence 1	1.728	0.014
NM_001080926	low density lipoprotein receptor-related protein 8, apolipoprotein e receptor	1.720	0.004
NM_130862	brain-specific angiogenesis inhibitor 1-associated protein 2	1.706	0.015
NM_001166024	ADP-ribosylation factor GTPase activating protein 2	1.701	0.005
NM_001081376	chromodomain helicase DNA binding protein 5	1.701	0.002
NM_028767	forkhead box P4	1.699	0.006
NM_145553	predicted gene 7527; family with sequence similarity 76, member A	1.698	0.020
NP_001157290	protein phosphatase 1, regulatory subunit 10	1.694	0.006
NM_080556	transmembrane 9 superfamily member 2	1.688	0.007
NM_010302	guanine nucleotide binding protein, alpha 12; similar to Guanine nucleotide-binding protein alpha-12 subunit (G alpha-12)	1.686	0.025
NM_001024205	nuclear fragile X mental retardation protein interacting protein 2	1.685	0.016
NM_172710	RIKEN cDNA 2310045A20 gene	1.680	0.027
NM_134063	cDNA sequence BC016423	1.680	0.020
NM_010511	interferon gamma receptor 1	1.678	0.031
NM_011333	chemokine (C-C motif) ligand 2	1.678	0.031
NM_010191	predicted gene 6781; farnesyl diphosphate farnesyl transferase 1	1.676	0.006
NM_016666	aryl-hydrocarbon receptor-interacting protein	1.673	0.004
NM_027373	actin filament associated protein 1	1.673	0.022
NM_011284	replication protein A2	1.660	0.045
NM_145946	Fanconi anemia, complementation group I	1.650	0.007
NM_175394	predicted gene 14292; Wilms' tumour 1-associating protein	1.647	0.024
NM_024229	phosphate cytidylyltransferase 2, ethanolamine	1.647	0.037
NM_009125	ataxin 2	1.642	0.045
NM_027435	ATPase family, AAA domain containing 2	1.627	0.012
NM_146065	activating transcription factor 7	1.625	0.001
NM_029078	cleavage and polyadenylation factor subunit homolog (S. cerevisiae)	1.618	0.007
NM_011623	topoisomerase (DNA) II alpha	1.614	0.014
NM_027219	CDC42 effector protein (Rho GTPase binding) 1	1.613	0.032
NM_030743	ring finger protein 114	1.608	0.003
NM_028793	acyl-Coenzyme A binding domain containing 5	1.608	0.027
NM_009242	secreted acidic cysteine rich glycoprotein; similar to Secreted acidic cysteine rich glycoprotein	1.607	0.033
NM_144804	DEP domain containing 7	1.604	0.050
NM_145942	similar to Hmgcs1 protein; 3-hydroxy-3-methylglutaryl-Coenzyme A synthase 1	1.598	0.004
NM_134081	DnaJ (Hsp40) homolog, subfamily C, member 9	1.595	0.028

NM_001081359	ubiquitin protein ligase E3 component n-recognin 5	1.587	0.047
NP_001135450	TPX2, microtubule-associated protein homolog (Xenopus laevis)	1.568	0.021
NM_011121	polo-like kinase 1 (Drosophila)	1.568	0.023
NM_145611	KN motif and ankyrin repeat domains 2	1.567	0.033
NM_009624	adenylate cyclase 9	1.565	0.047
NM_172472	transcription factor E3	1.563	0.021
NM_030561	cDNA sequence BC004004	1.563	0.030
NM_001163570	exosome component 8	1.558	0.005
NM_028390	anillin, actin binding protein	1.555	0.000
NM_008402	integrin alpha V	1.554	0.000
NM_001171052	metastasis associated 3	1.554	0.039
NM_028283	uveal autoantigen with coiled-coil domains and ankyrin repeats	1.553	0.025
NM_172205	suprabasin	1.552	0.031
NM_016963	tropomodulin 3	1.549	0.007
NM_009103	ribonucleotide reductase M1	1.548	0.005
NM_009007	RAS-related C3 botulinum substrate 1	1.547	0.025
NM_008139	guanine nucleotide binding protein, alpha q polypeptide	1.547	0.004
NM_009270	squalene epoxidase	1.543	0.017
NM_144901	predicted gene 5064; cold shock domain containing E1, RNA binding	1.543	0.007
NM_153808	similar to Structural maintenance of chromosomes 5; structural maintenance of chromosomes 5	1.538	0.010
NM_133435	nicotinamide nucleotide adenylyltransferase 1	1.538	0.021
NM_053090	family with sequence similarity 126, member A	1.536	0.038
NM_001044384	tissue inhibitor of metalloproteinase 1	1.535	0.002
NM_028044	similar to calponin 3, acidic; predicted gene 4815; calponin 3, acidic	1.528	0.009
NM_172397	similar to epithelial protein lost in neoplasm; LIM domain containing 2	1.520	0.016
NM_010708	lectin, galactose binding, soluble 9	1.517	0.042
NM_019813	drebrin 1	1.514	0.027
NP_001128624	solute carrier family 39 (zinc transporter), member 14	1.513	0.044
NM_021563	Erbb2 interacting protein	1.513	0.010
NM_009655	activated leukocyte cell adhesion molecule	1.507	0.003
NM_010931	ubiquitin-like, containing PHD and RING finger domains, 1; predicted gene 5648; similar to nuclear zinc finger protein Np95	1.501	0.005
NM_026936	oxidase assembly 1-like	1.501	0.030
NM_012025	Rac GTPase-activating protein 1; predicted gene 1859	1.500	0.034
NM_147201	nuclear receptor binding protein 1	1.497	0.007
NM_028074	DEAD (Asp-Glu-Ala-Asp) box polypeptide 42	1.496	0.000
NM_153117	RIKEN cDNA 9530068E07 gene	1.495	0.046
NM_175313	RIKEN cDNA A130022J15 gene	1.495	0.036
NM_008364	interleukin 1 receptor accessory protein	1.491	0.041
NM_007840	DEAD (Asp-Glu-Ala-Asp) box polypeptide 5; predicted gene 12183	1.490	0.021
NM_198249	RIKEN cDNA E130112L23 gene	1.489	0.001
NM_009074	macrophage stimulating 1 receptor (c-met-related tyrosine kinase)	1.487	0.013
NM_001163622	prolyl endopeptidase-like	1.487	0.039
NM_144788	HECT domain containing 1	1.487	0.021
NP_031641	catenin (cadherin associated protein), delta 1	1.482	0.046
NM_133781	calcium binding protein 39	1.481	0.047
NM_007709	Cbp/p300-interacting transactivator with Glu/Asp-rich carboxy-terminal domain 1	1.476	0.012

NM_029169	RNA binding motif protein 6	1.474	0.002
NM_007602	calpain 5	1.469	0.028
NM_001081251	polybromo 1	1.455	0.017
NM_008567	minichromosome maintenance deficient 6 (MIS5 homolog, S. pombe) (S. cerevisiae)	1.455	0.018
NM_019975	2-hydroxyacyl-CoA lyase 1	1.453	0.044
NM_026101	hect domain and RLD 4	1.447	0.016
NM_007394	activin A receptor, type 1	1.444	0.025
NM_177643	Zinc finger protein 281	1.444	0.001
NP_733486	RNA binding motif protein 12	1.441	0.016
NM_021519	predicted gene 11964; endothelial differentiation-related factor 1	1.440	0.009
NM_025952	magnesium transporter 1	1.437	0.006
NM_008565	minichromosome maintenance deficient 4 homolog (S. cerevisiae)	1.436	0.040
NM_013863	BCL2-associated athanogene 3	1.429	0.024
NM_145139	eukaryotic translation initiation factor 3, subunit L	1.429	0.004
NM_008047	follistatin-like 1	1.429	0.017
NM_010070	docking protein 1	1.428	0.006
NM_028760	centrosomal protein 55	1.427	0.013
NM_026305	predicted gene 11401; similar to transcription elongation factor B (SIII), polypeptide 2; predicted gene 8971; transcription elongation factor B (SIII), polypeptide 2	1.419	0.026
NM_026934	predicted gene 5909; zinc finger CCCH-type containing 15	1.418	0.024
NM_009881	chromodomain protein, Y chromosome-like; predicted gene 7584	1.415	0.049
NM_030113	Rho GTPase activating protein 10	1.414	0.005
NM_146131	similar to Pre-B-cell leukemia transcription factor interacting protein 1; pre-B-cell leukemia transcription factor interacting protein 1	1.412	0.026
NP_001104536	FK506 binding protein 8	1.412	0.004
NM_025682	paraspeckle protein 1	1.409	0.031
NM_197982	DEAD (Asp-Glu-Ala-Asp) box polypeptide 39	1.404	0.024
NM_172666	alkylglycerone phosphate synthase	1.402	0.043
NM_175127	F-box protein 28	1.402	0.040
NM_023063	LIM domain and actin binding 1	1.396	0.015
NM_001166406	kinesin family member 20A	1.396	0.007
NM_146239	PCTAIRE-motif protein kinase 2	1.396	0.005
NP_001239458	Polyglutamine-binding protein 1	1.388	0.016
NM_144831	DEAH (Asp-Glu-Ala-His) box polypeptide 8	1.386	0.040
NM_023603	splicing factor proline/glutamine rich (polypyrimidine tract binding protein associated); similar to PTB-associated splicing factor	1.382	0.001
NM_172679	RIKEN cDNA 4932438A13 gene	1.381	0.015
NM_029402	cullin 2	1.381	0.017
NM_001048267	predicted gene 6493; transportin 1	1.379	0.016
NM_009510	ezrin; hypothetical protein LOC100044177	1.378	0.022
NM_175021	sterile alpha motif domain containing 4B	1.378	0.028
NM_025364	predicted gene 6563; SAP domain containing ribonucleoprotein	1.375	0.005
NP_598452	poly-U binding splicing factor 60	1.371	0.013
NM_016794	vesicle-associated membrane protein 8	1.368	0.018
NM_019408	nuclear factor of kappa light polypeptide gene enhancer in B-cells 2, p49/p100	1.366	0.008
NM_001081242	talin 2	1.364	0.017
NM_028242	HIV TAT specific factor 1	1.361	0.008

NM_146078	ubiquitin protein ligase E3 component n-recognin 2	1.361	0.041
NM_008619	Moloney leukemia virus 10; predicted gene 7357	1.360	0.036
NM_011767	zinc finger RNA binding protein	1.359	0.040
NM_139291	cell division cycle 26; predicted gene 9174	1.357	0.018
NM_020022	replication factor C (activator 1) 2	1.356	0.032
NM_025822	arginine/serine-rich coiled-coil 1	1.355	0.036
NM_183417	cyclin-dependent kinase 2	1.352	0.048
NM_027434	regulation of nuclear pre-mRNA domain containing 1B	1.351	0.048
NM_031165	similar to heat shock protein 8; heat shock protein 8	1.351	0.034
NM_008861	polycystic kidney disease 2	1.344	0.038
NM_015760	NADPH oxidase 4	1.343	0.022
NM_019811	acyl-CoA synthetase short-chain family member 2	1.341	0.006
NM_026653	replication protein A1	1.340	0.017
NM_009283	signal transducer and activator of transcription 1	1.340	0.045
NM_008881	plexin A1	1.330	0.030
NM_080793	SET domain containing (lysine methyltransferase) 7	1.320	0.031
NM_001048267	predicted gene 6493; transportin 1	1.319	0.039
NM_011486	similar to Stat3B; signal transducer and activator of transcription 3	1.318	0.005
NM_177296	transportin 3	1.314	0.016
NM_026497	nudix (nucleoside diphosphate linked moiety X)-type motif 12	1.313	0.008
NM_011716	Wolfram syndrome 1 homolog (human)	1.311	0.016
NM_145937	sulfatase modifying factor 1	1.310	0.016
NM_026872	ubiquitin-associated protein 2	1.305	0.034
NM_007988	fatty acid synthase	1.298	0.012
NM_018748	golgi autoantigen, golgin subfamily a, 4	1.293	0.018
NM_008549	mannosidase 2, alpha 1	1.288	0.018
NP_001005331	eukaryotic translation initiation factor 4, gamma 1	1.288	0.028
NM_015735	damage specific DNA binding protein 1	1.286	0.002
NM_172391	AHA1, activator of heat shock protein ATPase homolog 2 (yeast)	1.285	0.024
NM_207176	testis derived transcript	1.284	0.013
NM_024245	kinesin family member 23	1.280	0.008
NM_010235	fos-like antigen 1	1.277	0.021
NM_007896	predicted gene 8545; microtubule-associated protein, RP/EB family, member 1; similar to Microtubule-associated protein RP/EB family member 1 (APC-binding protein EB1) (End-binding protein 1) (EB1)	1.268	0.013
NM_011378	transcriptional regulator, SIN3A (yeast)	1.267	0.009
NM_133952	unc-45 homolog A (C. elegans)	1.264	0.038
NM_021521	mediator of RNA polymerase II transcription, subunit 12 homolog (yeast)	1.263	0.033
NM_001163540	plectin 1	1.251	0.014
NM_001003909	ankyrin repeat and IBR domain containing 1	1.250	0.019
NM_007798	cathepsin B	1.249	0.015
NM_153774	importin 9	1.245	0.010
NM_008684	neogenin	1.242	0.018
NM_001081255	leucine-rich repeats and calponin homology (CH) domain containing 3	1.237	0.012
NM_008566	minichromosome maintenance deficient 5, cell division cycle 46 (S. cerevisiae)	1.234	0.042
NM_133947	nuclear mitotic apparatus protein 1	1.230	0.001
NM_029582	thioredoxin domain containing 11	1.230	0.048
NP_963910	GNAS (guanine nucleotide binding protein, alpha stimulating)	1.219	0.025

	complex locus		
NM_021549	polynucleotide kinase 3'- phosphatase	1.219	0.003
NM_027226	forty-two-three domain containing 1	1.216	0.009
NM_146145	Janus kinase 1	1.211	0.042
NM_012056	FK506 binding protein 9	1.203	0.007
NM_134077	RNA binding motif protein 26	1.202	0.046
NM_011150	lectin, galactoside-binding, soluble, 3 binding protein	-1.203	0.026
NM_138597	predicted gene 5436; similar to ATP synthase, H+ transporting, mitochondrial F1 complex, O subunit; ATP synthase, H+ transporting, mitochondrial F1 complex, O subunit	-1.205	0.009
NM_026688	similar to NADH dehydrogenase (ubiquinone) Fe-S protein 3; NADH dehydrogenase (ubiquinone) Fe-S protein 3; predicted gene 12251	-1.208	0.016
NM_053119	enoyl Coenzyme A hydratase, short chain, 1, mitochondrial	-1.209	0.042
NP_001123951	nucleobindin 2	-1.211	0.027
NM_007509	ATPase, H+ transporting, lysosomal V1 subunit B2	-1.213	0.027
NM_013792	alpha-N-acetylglucosaminidase (Sanfilippo disease IIIB)	-1.215	0.037
NM_007643	CD36 antigen	-1.216	0.017
NM_025591	RIKEN cDNA 2010309E21 gene; similar to CG5323-PA; predicted gene 6396; predicted gene 6624	-1.219	0.009
NM_007653	CD63 antigen	-1.221	0.015
NM_172678	acyl-Coenzyme A dehydrogenase family, member 9	-1.222	0.047
NM_029103	mesencephalic astrocyte-derived neurotrophic factor	-1.224	0.040
NM_153559	quiescin Q6 sulfhydryl oxidase 2	-1.228	0.024
NM_001085493	RIKEN cDNA 2310030N02 gene	-1.231	0.047
NM_024242	RIO kinase 1 (yeast)	-1.240	0.014
NP_033778	A kinase (PRKA) anchor protein 1	-1.240	0.003
NM_029735	similar to Bifunctional aminoacyl-tRNA synthetase; glutamyl-prolyl-tRNA synthetase	-1.241	0.043
NM_007949	excision repair cross-complementing rodent repair deficiency, complementation group 2	-1.244	0.003
NM_007533	branched chain ketoacid dehydrogenase E1, alpha polypeptide	-1.244	0.032
NM_023646	DnaJ (Hsp40) homolog, subfamily A, member 3	-1.247	0.035
NM_009296	predicted gene 3258; suppressor of Ty 4 homolog 1 (S. cerevisiae)	-1.248	0.043
NM_028599	WD repeat domain 75	-1.249	0.030
NM_022410	myosin, heavy polypeptide 9, non-muscle	-1.251	0.006
NM_021607	nicastrin	-1.252	0.007
NM_024434	leucine aminopeptidase 3	-1.253	0.032
NM_026114	similar to Eukaryotic translation initiation factor 2 subunit 1 (Eukaryotic translation initiation factor 2 alpha subunit) (eIF-2-alpha) (EIF-2alpha) (EIF-2A); eukaryotic translation initiation factor 2, subunit 1 alpha; predicted gene 7459	-1.253	0.002
NM_020045	NFU1 iron-sulfur cluster scaffold homolog (S. cerevisiae); predicted gene 7859	-1.257	0.001
NM_027569	sperm associated antigen 9	-1.258	0.010
NM_008828	phosphoglycerate kinase 1; predicted gene, EG668435	-1.262	0.014
NM_153065	DEAD (Asp-Glu-Ala-Asp) box polypeptide 27	-1.268	0.013
NM_029720	cysteine-rich with EGF-like domains 2	-1.268	0.037
NM_026011	ADP-ribosylation factor-like 8B	-1.275	0.039
NM_027869	similar to polynucleotide phosphorylase-like protein; polyribonucleotide nucleotidyltransferase 1	-1.279	0.021
NM_013536	EMG1 nucleolar protein homolog (S. cerevisiae)	-1.284	0.036
NM_019736	acyl-CoA thioesterase 9	-1.286	0.017
NM_011811	phenylalanyl-tRNA synthetase, beta subunit	-1.289	0.024

NM_008149	glycerol-3-phosphate acyltransferase, mitochondrial	-1.293	0.033
NM_175121	solute carrier family 38, member 2	-1.301	0.027
NM_029673	inner membrane protein, mitochondrial	-1.301	0.032
NM_021460	lysosomal acid lipase A	-1.302	0.034
NM_023060	eukaryotic elongation factor, selenocysteine-tRNA-specific	-1.304	0.030
NP_034918	methyl CpG binding protein 2	-1.304	0.021
NM_018739	retinitis pigmentosa 9 (human)	-1.305	0.017
NM_029556	citrate lyase beta like	-1.314	0.041
NM_133217	beta-carotene oxygenase 2	-1.315	0.034
NM_007997	ferredoxin reductase	-1.316	0.049
NM_019734	N-acylsphingosine amidohydrolase 1	-1.319	0.040
NM_008482	laminin B1 subunit 1	-1.319	0.004
NM_027244	NADH dehydrogenase (ubiquinone) 1 alpha subcomplex 11	-1.320	0.000
NM_010233	fibronectin 1	-1.342	0.004
NM_030225	dihydrolipoamide S-succinyltransferase (E2 component of 2-oxo-glutarate complex)	-1.344	0.026
NM_028243	prolylcarboxypeptidase (angiotensinase C)	-1.345	0.011
NM_016763	hydroxysteroid (17-beta) dehydrogenase 10	-1.346	0.027
NM_027906	RIKEN cDNA 1300010F03 gene	-1.350	0.001
NM_172015	isoleucine-tRNA synthetase	-1.351	0.030
NM_011594	tissue inhibitor of metalloproteinase 2	-1.354	0.027
NM_009264	small proline-rich protein 1A	-1.358	0.004
NM_007510	ATPase, H+ transporting, lysosomal V1 subunit E1	-1.359	0.029
NM_026995	carbohydrate kinase domain containing	-1.364	0.001
NM_008929	DnaJ (Hsp40) homolog, subfamily C, member 3	-1.369	0.027
NM_013671	superoxide dismutase 2, mitochondrial	-1.371	0.040
NM_008231	hepatoma-derived growth factor	-1.373	0.009
NM_001030014	similar to mitochondrial malonyltransferase isoform b precursor; malonyl CoA:ACP acyltransferase (mitochondrial)	-1.374	0.020
NM_133895	solute carrier family 15, member 4	-1.377	0.039
NM_008325	iduronidase, alpha-L-	-1.378	0.004
NM_026192	calcium binding and coiled coil domain 1	-1.379	0.022
NM_145595	carbonyl reductase 4	-1.380	0.036
NM_134151	tyrosyl-tRNA synthetase	-1.388	0.039
NM_008323	isocitrate dehydrogenase 3 (NAD+), gamma	-1.397	0.040
NM_133826	ATPase, H+ transporting, lysosomal V1 subunit H	-1.401	0.013
NM_178619	predicted gene 5747; RIKEN cDNA 1810026J23 gene	-1.401	0.019
NM_016804	metaxin 2	-1.402	0.049
NM_019816	apoptosis antagonizing transcription factor	-1.407	0.029
NM_175287	RIKEN cDNA A430005L14 gene; hypothetical protein LOC676530; predicted gene 12247	-1.407	0.009
NM_015805	ATPase, class II, type 9B	-1.410	0.026
NM_025816	Tax1 (human T-cell leukemia virus type I) binding protein 1	-1.414	0.009
NM_030678	glycogen synthase 1, muscle	-1.417	0.045
NM_011414	secretory leukocyte peptidase inhibitor	-1.417	0.046
NM_026969	Sec31 homolog A (S. cerevisiae)	-1.429	0.006
NM_025403	NOP10 ribonucleoprotein homolog (yeast)	-1.430	0.046
NM_016709	AU RNA binding protein/enoyl-coenzyme A hydratase	-1.434	0.024
NM_028900	golgi coiled coil 1	-1.434	0.032
NM_144897	apolipoprotein A-I binding protein	-1.436	0.003
NM_024197	NADH dehydrogenase (ubiquinone) 1 alpha subcomplex 10	-1.440	0.027
NM_024201	coiled-coil domain containing 127	-1.449	0.048

NM_172436	solute carrier family 25 (mitochondrial carrier, Aralar), member 12	-1.451	0.035
NM_010239	ferritin heavy chain 1	-1.451	0.013
NM_029364	glucosamine (N-acetyl)-6-sulfatase	-1.455	0.024
NM_001177602	Adenylate kinase 4, mitochondrial	-1.457	0.039
NM_001171582	methionine-tRNA synthetase	-1.457	0.015
NM_001081056	exportin, tRNA (nuclear export receptor for tRNAs)	-1.464	0.034
NM_025304	leucine carboxyl methyltransferase 1	-1.472	0.026
NM_001113356	complement component 1, r subcomponent; predicted gene 8551	-1.473	0.042
NM_134007	CDGSH iron sulfur domain 1	-1.473	0.021
NM_008605	matrix metallopeptidase 12	-1.474	0.007
NM_010764	mannosidase 2, alpha B1	-1.481	0.002
NM_013657	sema domain, immunoglobulin domain (Ig), short basic domain, secreted, (semaphorin) 3C	-1.481	0.012
NM_001127338	aldehyde dehydrogenase family 7, member A1	-1.481	0.015
NM_001111121	coiled-coil domain containing 6	-1.485	0.024
NM_172745	predicted gene 9755; Tu translation elongation factor, mitochondrial	-1.487	0.030
NM_026742	NADH dehydrogenase (ubiquinone) 1 alpha subcomplex, assembly factor 4	-1.489	0.022
NM_026452	coenzyme Q9 homolog (yeast)	-1.489	0.047
NM_029956	methylmalonic aciduria (cobalamin deficiency) type B homolog (human)	-1.489	0.017
NM_183106	tetratricopeptide repeat domain 17	-1.492	0.014
NM_033074	threonyl-tRNA synthetase	-1.505	0.005
NM_011695	similar to Voltage-dependent anion-selective channel protein 2 (VDAC-2) (mVDAC2) (mVDAC6) (Outer mitochondrial membrane protein porin 2); predicted gene 7832; voltage-dependent anion channel 2	-1.507	0.002
NM_145501	phosphatidylinositol 4-kinase type 2 alpha	-1.507	0.013
NM_146229	dynein cytoplasmic 1 light intermediate chain 1	-1.511	0.023
NM_134147	MACRO domain containing 1	-1.518	0.011
NM_013768	protein arginine N-methyltransferase 5	-1.521	0.020
NM_008212	hydroxyacyl-Coenzyme A dehydrogenase	-1.524	0.033
NM_029023	serine carboxypeptidase 1	-1.524	0.023
NM_030026	methylcrotonoyl-Coenzyme A carboxylase 2 (beta)	-1.534	0.006
NM_019758	mitochondrial carrier homolog 2 (C. elegans); predicted gene, 100039384; predicted gene, 100039506	-1.534	0.015
NP_001156418	pyruvate carboxylase	-1.534	0.029
NM_008788	procollagen C-endopeptidase enhancer protein	-1.535	0.008
NM_023247	NADH dehydrogenase (ubiquinone) 1 alpha subcomplex, assembly factor 3	-1.542	0.022
NM_008131	predicted gene 4949; glutamate-ammonia ligase (glutamine synthetase)	-1.552	0.025
NM_025835	propionyl Coenzyme A carboxylase, beta polypeptide	-1.555	0.002
NM_001163126	component of oligomeric golgi complex 5	-1.555	0.000
NM_010438	hexokinase 1	-1.558	0.017
NM_026295	CTD (carboxy-terminal domain, RNA polymerase II, polypeptide A) phosphatase, subunit 1	-1.566	0.011
NM_008509	lipoprotein lipase; similar to Lipoprotein lipase precursor (LPL)	-1.569	0.041
NM_024243	fucosidase, alpha-L- 1, tissue	-1.570	0.002
NM_007383	acyl-Coenzyme A dehydrogenase, short chain	-1.574	0.025
NM_010261	Rab acceptor 1 (prenylated)	-1.576	0.023

NM_026744	mitochondrial ribosomal protein L53	-1.580	0.015
NM_029884	heparan-alpha-glucosaminide N-acetyltransferase	-1.581	0.004
NM_175109	ribosomal protein S19 binding protein 1	-1.585	0.001
NM_011400	solute carrier family 2 (facilitated glucose transporter), member 1	-1.586	0.002
NM_007861	dihydrolipoamide dehydrogenase	-1.591	0.029
NM_008095	glioblastoma amplified sequence	-1.593	0.015
NM_001160163	neuraminidase 2	-1.596	0.021
NM_013492	similar to clusterin; clusterin	-1.599	0.000
NM_201642	similar to UDP glycosyltransferase 1 family polypeptide A13; similar to UGT1.6; UDP glucuronosyltransferase 1 family, polypeptide A1; UDP glucuronosyltransferase 1 family, polypeptide A2; UDP glycosyltransferase 1 family, polypeptide A10; UDP glucuronosyl	-1.601	0.002
NM_053071	predicted gene 6265; similar to cytochrome c oxidase, subunit VIc; cytochrome c oxidase, subunit VIc	-1.613	0.028
NM_024220	NADH dehydrogenase (ubiquinone) 1, subcomplex unknown, 2; similar to NADH dehydrogenase (ubiquinone) 1, subcomplex unknown, 2	-1.617	0.023
NM_026364	phosphoribosyl pyrophosphate synthetase-associated protein 1	-1.617	0.029
NM_016918	nudix (nucleoside diphosphate linked moiety X)-type motif 5	-1.619	0.005
NM_028876	transmembrane emp24 protein transport domain containing 5; similar to Transmembrane emp24 protein transport domain containing 5	-1.620	0.002
NM_007544	BH3 interacting domain death agonist	-1.620	0.001
NM_025859	ADP-ribosylation factor-like 1	-1.623	0.000
NM_010421	hexosaminidase A	-1.624	0.001
NM_009194	similar to solute carrier family 12, member 2; solute carrier family 12, member 2	-1.626	0.024
NM_026432	transmembrane protein 66	-1.628	0.002
NM_013556	hypoxanthine guanine phosphoribosyl transferase 1	-1.630	0.001
NM_001045489	milk fat globule-EGF factor 8 protein	-1.636	0.005
NM_153561	nudix (nucleoside diphosphate linked moiety X)-type motif 6	-1.643	0.014
NM_009731	aldo-keto reductase family 1, member B7	-1.649	0.037
NM_007639	CD1d1 antigen; CD1d2 antigen	-1.655	0.020
NM_008481	laminin, alpha 2	-1.664	0.014
NM_178644	OAF homolog (Drosophila)	-1.670	0.001
NM_011348	sema domain, immunoglobulin domain (Ig), short basic domain, secreted, (semaphorin) 3E; hypothetical protein LOC100044162	-1.671	0.031
NM_025369	predicted gene 10078; predicted gene 3544; similar to mitochondrial ribosomal protein S36; mitochondrial ribosomal protein S36; predicted gene 7258; predicted gene 4676	-1.684	0.003
NM_026512	biphenyl hydrolase-like (serine hydrolase, breast epithelial mucin-associated antigen)	-1.686	0.004
NM_011125	phospholipid transfer protein	-1.692	0.010
NM_028181	cell cycle progression 1	-1.702	0.016
NM_053179	N-acetylneuraminic acid synthase (sialic acid synthase)	-1.704	0.029
NM_017393	caseinolytic peptidase, ATP-dependent, proteolytic subunit homolog (E. coli)	-1.711	0.005
NM_028152	MMS19 (MET18 S. cerevisiae)	-1.714	0.010
NM_011942	lysophospholipase 2	-1.715	0.001
NM_013562	interferon-related developmental regulator 1	-1.751	0.006

Table 1-E: Differentially regulated CHO DP-12 proteins determined in samples corresponding to culture using an increased bioprocess media pH of 7.2.

RefSeq Annotation	Description	Fold Change	P-value
NM_011638	transferrin receptor	1.893	0.017
NM_010736	lymphotoxin B receptor	1.776	0.014
NM_011019	oncostatin M receptor	1.725	0.002
NM_144930	expressed sequence AU018778	1.706	0.005
NM_021895	actinin alpha 4	1.650	0.012
NM_009201	solute carrier family 1 (neutral amino acid transporter), member 5	1.648	0.018
NM_010235	fos-like antigen 1	1.644	0.020
NM_009418	tripeptidyl peptidase II	1.623	0.005
NM_026693	gamma-aminobutyric acid (GABA) A receptor-associated protein-like 2; predicted gene 3724	1.620	0.015
NM_011886	secretory carrier membrane protein 3	1.617	0.024
NM_011296	predicted gene 10027; hypothetical protein LOC674425; predicted gene 6794; predicted gene 9175; similar to ribosomal protein S18; similar to ribosomal protein; ribosomal protein S18; predicted gene 11230; predicted gene 5321; predicted gene 10260; predict	1.605	0.003
NM_001024205	nuclear fragile X mental retardation protein interacting protein 2	1.603	0.003
NM_026497	nudix (nucleoside diphosphate linked moiety X)-type motif 12	1.603	0.023
NM_016797	syntaxin 7	1.599	0.028
NM_030248	CDK5 regulatory subunit associated protein 3	1.588	0.003
NP_035863	cold shock domain protein A	1.577	0.013
NM_001081378	kinase D-interacting substrate 220	1.570	0.030
NM_011563	peroxiredoxin 2	1.567	0.003
NM_009842	CD151 antigen	1.563	0.010
NM_001037847	CCR4-NOT transcription complex, subunit 2	1.559	0.016
NM_198631	zinc finger CCCH-type containing 4	1.558	0.012
NM_007643	CD36 antigen	1.556	0.046
NM_007932	endoglin	1.555	0.005
NP_001003667	keratin 77	1.552	0.002
NM_028450	GULP, engulfment adaptor PTB domain containing 1	1.526	0.002
NM_181348	RIKEN cDNA A230083H22 gene	1.525	0.030
NM_029565	transmembrane protein 59	1.517	0.004
NM_016714	nucleoporin 50	1.515	0.030
NM_001111279	WD repeat and FYVE domain containing 1	1.514	0.032
NM_181848	optineurin	1.504	0.002
NM_008684	neogenin	1.500	0.001
NM_009370	transforming growth factor, beta receptor I	1.483	0.033
NM_026842	ubiquilin 1	1.474	0.014
NM_030116	mitochondrial ribosomal protein L9	1.473	0.007
NM_146090	zinc binding alcohol dehydrogenase, domain containing 2	1.463	0.028
NM_007513	solute carrier family 7 (cationic amino acid transporter, y+ system), member 1	1.462	0.020
NP_034336	fibroblast growth factor receptor 1	1.461	0.031

NM_010730	annexin A1	1.459	0.030
NM_009074	macrophage stimulating 1 receptor (c-met-related tyrosine kinase)	1.457	0.038
NM_133900	phosphoserine phosphatase	1.456	0.000
NM_024287	similar to Rab6 protein; predicted gene 13082; RAB6, member RAS oncogene family	1.452	0.035
NM_008410	integral membrane protein 2B	1.444	0.048
NM_009643	AHNAK nucleoprotein (desmoyokin)	1.443	0.018
NM_021895	actinin alpha 4	1.434	0.040
NM_016696	glypican 1	1.428	0.024
NM_019813	drebrin 1	1.428	0.036
NP_001128624	solute carrier family 39 (zinc transporter), member 14	1.425	0.004
NM_026911	signal peptidase complex subunit 1 homolog (S. cerevisiae)	1.414	0.015
NM_011930	chloride channel 7	1.399	0.017
NM_010655	similar to ribosomal protein L38; predicted gene 13020; ribosomal protein L38; predicted gene 4991; karyopherin (importin) alpha 2; predicted gene 9028; predicted gene 8129; predicted gene 7123; predicted gene 5832; predicted gene 10184; predicted gene 73	1.394	0.049
NM_153680	sorting nexin 17	1.392	0.023
NM_027927	integrator complex subunit 12	1.389	0.008
NM_011197	prostaglandin F2 receptor negative regulator	1.385	0.040
NM_009371	transforming growth factor, beta receptor II	1.384	0.012
NM_007475	predicted gene 9625; predicted gene 14165; similar to acidic ribosomal phosphoprotein P0; predicted gene 8730; predicted gene 9093; ribosomal protein, large, P0	1.365	0.022
NM_025374	glyoxalase 1	1.353	0.020
NM_028817	acyl-CoA synthetase long-chain family member 3	1.339	0.019
NM_013933	vesicle-associated membrane protein, associated protein A	1.338	0.002
NM_021895	actinin alpha 4	1.334	0.002
NM_139001	chondroitin sulfate proteoglycan 4	1.328	0.045
NM_031165	similar to heat shock protein 8; heat shock protein 8	1.327	0.003
NM_133738	anthrax toxin receptor 2	1.324	0.026
NM_173784	ubiquitin domain containing 2	1.321	0.041
NM_025816	Tax1 (human T-cell leukemia virus type I) binding protein 1	1.307	0.007
NM_026029	glyoxalase domain containing 4	1.306	0.022
NM_026159	retinol saturase (all trans retinol 13,14 reductase)	1.306	0.026
NM_172666	alkylglycerone phosphate synthase	1.305	0.007
NM_019661	YKT6 homolog (S. Cerevisiae)	1.302	0.015
NM_026752	zinc finger, FYVE domain containing 21	1.293	0.014
NM_027168	HD domain containing 2	1.292	0.012
NP_083142	WD repeat domain 33	1.288	0.035
NM_010833	moesin	1.280	0.035
NM_009503	similar to Transitional endoplasmic reticulum ATPase (TER ATPase) (15S Mg(2+)-ATPase p97 subunit) (Valosin-containing protein) (VCP); valosin containing protein	1.279	0.009
NM_028390	anillin, actin binding protein	1.277	0.017
NM_008377	leucine-rich repeats and immunoglobulin-like domains 1	1.272	0.020
NM_028779	adenosine monophosphate deaminase 2 (isoform L)	1.269	0.010
NM_016677	hippocalcin-like 1	1.263	0.043

NM_001001932	early endosome antigen 1	1.257	0.012
NM_009628	activity-dependent neuroprotective protein	1.251	0.038
NM_133807	leucine rich repeat containing 59	1.251	0.016
NM_019961	peroxisomal biogenesis factor 3	1.251	0.045
NM_009081	predicted gene 13226; predicted gene 15435; ribosomal protein L28; predicted gene 12938	1.250	0.045
NM_008676	neighbor of Brca1 gene 1	1.248	0.008
NM_008525	aminolevulinate, delta-, dehydratase	1.245	0.050
NM_019650	golgi SNAP receptor complex member 2	1.238	0.015
NM_009078	predicted gene 5202; predicted gene 14449; predicted gene 6975; predicted gene 9188; predicted gene 6196; predicted gene 7801; similar to ribosomal protein L19; predicted gene 8936; ribosomal protein L19; predicted gene 15360; predicted gene 15424	1.235	0.025
NP_083939	predicted gene 11675; eukaryotic translation elongation factor 1 delta (guanine nucleotide exchange protein)	1.231	0.015
NM_011968	proteasome (prosome, macropain) subunit, alpha type 6	1.230	0.017
NM_021557	retinol dehydrogenase 11	1.221	0.027
NM_007874	receptor accessory protein 5	1.207	0.024
NM_053170	tripartite motif-containing 33	1.204	0.000
NM_009795	calpain, small subunit 1	-1.201	0.048
NM_008565	minichromosome maintenance deficient 4 homolog (S. cerevisiae)	-1.201	0.008
NM_133952	unc-45 homolog A (C. elegans)	-1.207	0.004
NM_007879	developmentally regulated GTP binding protein 1	-1.208	0.038
NM_011654	predicted gene 3756; tubulin, alpha 1B; predicted gene 5620; similar to alpha-tubulin isotype M-alpha-2; predicted gene 14150; predicted gene 3226	-1.220	0.043
NM_133350	microtubule-associated protein, RP/EB family, member 3	-1.223	0.026
NM_022332	suppression of tumorigenicity 7	-1.227	0.005
NM_025982	tetraspanin 31	-1.233	0.024
NM_177680	YTH domain containing 1	-1.238	0.049
NM_026876	RIKEN cDNA 1190005F20 gene	-1.240	0.003
NM_010106	predicted gene 5869; predicted gene 7161; predicted gene 7105; predicted gene 5822; similar to eukaryotic translation elongation factor 1 alpha 1; predicted gene 6192; predicted gene 6392; predicted gene 6767; predicted gene 6170; predicted gene 6548; pre	-1.241	0.028
NM_026154	mitochondrial ribosomal protein L10	-1.248	0.050
NM_025440	mitochondrial ribosomal protein S16; predicted gene 9173	-1.257	0.014
NM_025647	cytidine monophosphate (UMP-CMP) kinase 1; predicted gene 5867	-1.259	0.019
NM_010360	glutathione S-transferase, mu 5	-1.260	0.002
NM_144901	predicted gene 5064; cold shock domain containing E1, RNA binding	-1.267	0.035
NM_008567	minichromosome maintenance deficient 6 (MIS5 homolog, S. pombe) (S. cerevisiae)	-1.273	0.006
NM_147778	COMM domain containing 3	-1.282	0.009
NM_172832	prenylcysteine oxidase 1 like	-1.283	0.015
NM_027852	retinoic acid receptor responder (tazarotene induced) 2	-1.284	0.015
NM_001025156	coiled-coil domain containing 93	-1.294	0.026
NM_008628	mutS homolog 2 (E. coli)	-1.300	0.026

NM_134023	TBC1 domain family, member 10a	-1.306	0.009
NM_025392	BRCA2 and CDKN1A interacting protein	-1.306	0.004
NM_026318	RIKEN cDNA 2310003F16 gene	-1.310	0.005
NP_001186624	Alpha-taxilin	-1.313	0.015
NM_025922	inosine triphosphatase (nucleoside triphosphate pyrophosphatase)	-1.316	0.002
NM_008927	mitogen-activated protein kinase kinase 1	-1.317	0.018
NM_026934	predicted gene 5909; zinc finger CCCH-type containing 15	-1.318	0.009
NM_144923	biliverdin reductase B (flavin reductase (NADPH))	-1.318	0.015
NM_013559	heat shock 105kDa/110kDa protein 1	-1.320	0.010
NM_015765	heat shock protein 14	-1.326	0.044
NM_001009947	dedicator of cytokinesis 11	-1.333	0.025
NM_016682	ubiquitin-like modifier activating enzyme 2	-1.346	0.006
NM_028761	poly(A)-specific ribonuclease (deadenylation nuclease)	-1.353	0.033
NP_001070830	four and a half LIM domains 1	-1.355	0.043
NM_019758	mitochondrial carrier homolog 2 (C. elegans); predicted gene, 100039384; predicted gene, 100039506	-1.362	0.009
NM_027276	CDC16 cell division cycle 16 homolog (S. cerevisiae)	-1.365	0.047
NM_025996	translocase of outer mitochondrial membrane 34	-1.375	0.023
NM_173443	valosin containing protein (p97)/p47 complex interacting protein 1	-1.375	0.042
NM_028299	RIKEN cDNA 2700029M09 gene	-1.377	0.017
NM_009755	bone morphogenetic protein 1	-1.381	0.008
NM_009097	ribosomal protein S6 kinase polypeptide 1	-1.387	0.021
NM_001033259	coiled-coil domain containing 109A	-1.388	0.016
NM_027475	ecdysoneless homolog (Drosophila)	-1.413	0.010
NM_023716	Tubulin beta-2B chain	-1.416	0.032
NM_013492	similar to clusterin; clusterin	-1.422	0.007
NM_001029979	scaffold attachment factor B2	-1.441	0.014
NM_026512	biphenyl hydrolase-like (serine hydrolase, breast epithelial mucin-associated antigen)	-1.442	0.032
NM_198622	H1 histone family, member X	-1.451	0.007
NM_011131	polymerase (DNA directed), delta 1, catalytic subunit	-1.458	0.010
NM_010106	predicted gene 5869; predicted gene 7161; predicted gene 7105; predicted gene 5822; similar to eukaryotic translation elongation factor 1 alpha 1; predicted gene 6192; predicted gene 6392; predicted gene 6767; predicted gene 6170; predicted gene 6548; pre	-1.469	0.034
NM_011340	serine (or cysteine) peptidase inhibitor, clade F, member 1	-1.483	0.002
NM_138587	family with sequence similarity 3, member C	-1.485	0.015
NM_007620	predicted gene 5678; carbonyl reductase 1	-1.485	0.010
NM_019464	SH3-domain GRB2-like B1 (endophilin)	-1.486	0.047
NM_134078	CHMP family, member 7	-1.488	0.005
NM_021412	matrix metallopeptidase 19	-1.488	0.022
NM_008872	plasminogen activator, tissue	-1.489	0.043
NM_013529	Glutamine--fructose-6-phosphate aminotransferase [isomerizing] 2	-1.501	0.048
NM_001081130	oxoglutarate dehydrogenase-like	-1.509	0.007
NM_009398	similar to TNF-stimulated gene 6 protein; tumor necrosis factor alpha induced protein 6	-1.511	0.007

NM_025599	RIKEN cDNA 2610528E23 gene	-1.517	0.016
NM_146171	non-SMC condensin I complex, subunit D2	-1.524	0.026
NM_029023	serine carboxypeptidase 1	-1.538	0.008
NM_173441	IWS1 homolog (S. cerevisiae)	-1.540	0.036
NM_147201	nuclear receptor binding protein 1	-1.547	0.038
NM_008605	matrix metallopeptidase 12	-1.552	0.030
NM_181414	phosphoinositide-3-kinase, class 3	-1.553	0.018
NM_001080773	3-phosphoinositide dependent protein kinase-1	-1.560	0.032
NM_008921	DNA primase, p49 subunit	-1.569	0.033
NM_011871	protein kinase, interferon inducible double stranded RNA dependent activator	-1.576	0.017
NM_178708	PCI domain containing 2	-1.577	0.003
NM_172703	eukaryotic translation initiation factor 4 gamma, 3; similar to Eukaryotic translation initiation factor 4 gamma 3 (eIF-4-gamma 3) (eIF-4G 3) (eIF4G 3) (eIF-4-gamma II) (eIF4GII)	-1.618	0.021
NM_008788	procollagen C-endopeptidase enhancer protein	-1.638	0.045
NM_010217	connective tissue growth factor	-1.641	0.015
NM_178919	lipase maturation factor 2	-1.652	0.046
NM_009713	arylsulfatase A	-1.652	0.006
NM_007620	predicted gene 5678; carbonyl reductase 1	-1.654	0.028
NM_011198	prostaglandin-endoperoxide synthase 2	-1.685	0.007
NM_183417	cyclin-dependent kinase 2	-1.686	0.001
NM_021605	NIMA (never in mitosis gene a)-related expressed kinase 7	-1.703	0.007
NM_025692	ubiquitin-like modifier activating enzyme 5	-1.711	0.002
NM_080445	similar to UDP-Gal:betaGal beta 1,3-galactosyltransferase, polypeptide 6; UDP-Gal:betaGal beta 1,3-galactosyltransferase, polypeptide 6	-1.770	0.003

Table 1-F: Differentially regulated CHO DP-12 proteins determined in samples corresponding to culture using a decreased bioprocess media pH of 6.8.

RefSeq Annotation	Description	Fold Change	P-value
NM_009075	ribose 5-phosphate isomerase A	1.815	0.004
NM_025797	cytochrome b-5	1.803	0.035
NM_009321	tubulin cofactor A; predicted gene 4374; predicted gene 6142; similar to cofactor A	1.752	0.048
NM_144930	expressed sequence AU018778	1.738	0.012
NM_029556	citrate lyase beta like	1.737	0.004
NM_138587	family with sequence similarity 3, member C	1.721	0.003
NM_010893	neuraminidase 1	1.720	0.036
NM_026842	ubiquilin 1	1.717	0.008
NM_146090	zinc binding alcohol dehydrogenase, domain containing 2	1.716	0.012
NM_011341	stromal cell derived factor 4	1.716	0.018
NM_144896	PET112-like (yeast)	1.716	0.008
NM_026013	transmembrane protein 77	1.716	0.009

NM_009632	poly (ADP-ribose) polymerase family, member 2	1.715	0.008
NM_008548	mannosidase 1, alpha	1.711	0.017
NM_145630	pyruvate dehydrogenase kinase, isoenzyme 3	1.707	0.039
NM_016797	syntaxin 7	1.697	0.004
NM_027430	brain protein 44; similar to brain protein 44; predicted gene 3982	1.696	0.005
NM_146108	3-hydroxyisobutyryl-Coenzyme A hydrolase	1.695	0.028
NM_015753	zinc finger E-box binding homeobox 2	1.693	0.021
NM_021895	actinin alpha 4	1.689	0.018
NM_024166	coiled-coil-helix-coiled-coil-helix domain containing 2; predicted gene 13202; similar to coiled-coil-helix-coiled-coil-helix domain containing 2; predicted gene 12350	1.688	0.025
NM_057172	far upstream element (FUSE) binding protein 1	1.687	0.025
NM_175103	bolA-like 2 (E. coli)	1.686	0.023
NM_023625	phospholipase B domain containing 2	1.682	0.016
NM_016844	similar to 40S ribosomal protein S28; predicted gene 10443; predicted gene 12943; predicted gene 13192; similar to ribosomal protein S28; predicted gene 10263; predicted gene 3511; ribosomal protein S28	1.676	0.028
NP_001104536	FK506 binding protein 8	1.675	0.018
NM_010931	ubiquitin-like, containing PHD and RING finger domains, 1; predicted gene 5648; similar to nuclear zinc finger protein Np95	1.675	0.009
NM_027435	ATPase family, AAA domain containing 2	1.673	0.024
NM_001081130	oxoglutarate dehydrogenase-like	1.669	0.001
NM_153406	cytospin A	1.669	0.021
NP_001157089	threonyl-tRNA synthetase 2, mitochondrial (putative)	1.668	0.009
NM_029840	RIKEN cDNA 2610029I01 gene	1.667	0.024
NM_009264	small proline-rich protein 1A	1.666	0.038
NM_001033242	ceroid-lipofuscinosis, neuronal 5	1.666	0.030
NM_177231	arrestin, beta 1	1.664	0.015
NM_027168	HD domain containing 2	1.659	0.001
NM_001163501	RIKEN cDNA C130039O16 gene	1.658	0.021
NM_023130	RIKEN cDNA C130057N11 gene; hnRNP-associated with lethal yellow	1.658	0.015
NM_016690	heterogeneous nuclear ribonucleoprotein D-like	1.657	0.017
NM_133435	nicotinamide nucleotide adenylyltransferase 1	1.656	0.014
NM_001111279	WD repeat and FYVE domain containing 1	1.654	0.021
NM_134147	MACRO domain containing 1	1.652	0.006
NM_010368	glucuronidase, beta	1.651	0.043
NM_134042	aldehyde dehydrogenase family 6, subfamily A1	1.646	0.009
NM_025334	thioredoxin domain containing 12 (endoplasmic reticulum)	1.646	0.044
NM_019711	RNA binding motif, single stranded interacting protein 2	1.644	0.011
NM_023065	interferon gamma inducible protein 30	1.640	0.016
NM_019813	drebrin 1	1.639	0.007
NM_026410	cell division cycle associated 5	1.639	0.034
NM_016722	galactosamine (N-acetyl)-6-sulfate sulfatase	1.637	0.003
NM_025700	phosphoglucomutase 1	1.637	0.012
NM_201639	synemin, intermediate filament protein	1.635	0.002
NM_011638	transferrin receptor	1.620	0.047

NM_024249	solute carrier family 38, member 10	1.619	0.038
NM_028767	forkhead box P4	1.618	0.009
NM_026497	nudix (nucleoside diphosphate linked moiety X)-type motif 12	1.617	0.013
NM_029872	heterogeneous nuclear ribonucleoprotein A0	1.613	0.039
NM_009211	SWI/SNF related, matrix associated, actin dependent regulator of chromatin, subfamily c, member 1; predicted gene 7004	1.611	0.010
NM_007803	cortactin; predicted gene 8786	1.609	0.033
NM_177592	transmembrane protein 164	1.607	0.019
NM_025305	mitchondrial ribosomal protein S7	1.607	0.045
NM_025526	IscU iron-sulfur cluster scaffold homolog (E. coli); similar to nitrogen fixation cluster-like	1.607	0.006
NM_010729	lysyl oxidase-like 1	1.606	0.017
NM_001163622	prolyl endopeptidase-like	1.603	0.001
NM_023063	LIM domain and actin binding 1	1.600	0.021
NM_010027	D-dopachrome tautomerase	1.596	0.042
NM_013463	galactosidase, alpha	1.595	0.000
NM_010023	dodecenoyl-Coenzyme A delta isomerase (3,2 trans-enoyl-Coenzyme A isomerase)	1.593	0.006
NM_008562	similar to myeloid cell leukemia sequence 1; myeloid cell leukemia sequence 1	1.591	0.002
NM_023733	carnitine O-octanoyltransferase	1.589	0.015
NM_011035	p21 protein (Cdc42/Rac)-activated kinase 1	1.588	0.008
NP_001191902	Bromodomain-containing protein 2	1.587	0.013
NM_080445	similar to UDP-Gal:betaGal beta 1,3-galactosyltransferase, polypeptide 6; UDP-Gal:betaGal beta 1,3-galactosyltransferase, polypeptide 6	1.586	0.005
NM_138753	hexamethylene bis-acetamide inducible 1	1.585	0.004
NM_153561	nudix (nucleoside diphosphate linked moiety X)-type motif 6	1.583	0.045
NM_026080	mitochondrial ribosomal protein S24	1.582	0.033
NM_026988	parathymosin	1.581	0.040
NM_175251	AT rich interactive domain 2 (ARID, RFX-like); RIKEN cDNA 1700124K17 gene	1.578	0.044
NM_008917	palmitoyl-protein thioesterase 1	1.577	0.010
NM_153176	spastic paraplegia 7 homolog (human)	1.574	0.005
NM_027289	5'-nucleotidase domain containing 2	1.571	0.031
NM_011933	2-4-dienoyl-Coenzyme A reductase 2, peroxisomal	1.570	0.001
NM_009074	macrophage stimulating 1 receptor (c-met-related tyrosine kinase)	1.569	0.025
NM_008305	perlecan (heparan sulfate proteoglycan 2)	1.569	0.005
NM_025988	acyl-Coenzyme A binding domain containing 4	1.569	0.001
NM_026672	glutathione S-transferase, mu 7	1.568	0.016
NM_016786	ubiquitin-conjugating enzyme E2K (UBC1 homolog, yeast)	1.567	0.017
NM_008549	mannosidase 2, alpha 1	1.567	0.000
NM_011296	predicted gene 10027; hypothetical protein LOC674425; predicted gene 6794; predicted gene 9175; similar to ribosomal protein S18; similar to ribosomal protein; ribosomal protein S18; predicted gene 11230; predicted gene 5321; predicted gene 10260; predict	1.561	0.010
NM_021278	thymosin, beta 4, X chromosome; similar to thymosin beta-4	1.552	0.035
NM_001045523	bromo adjacent homology domain containing 1	1.551	0.040
NM_009270	squalene epoxidase	1.549	0.002

NP_001135450	TPX2, microtubule-associated protein homolog (Xenopus laevis)	1.545	0.016
NM_009054	tripartite motif-containing 27	1.545	0.031
NM_013782	phosphatidylserine synthase 2	1.544	0.012
NM_008669	N-acetyl galactosaminidase, alpha	1.540	0.003
NM_015734	collagen, type V, alpha 1	1.540	0.004
NM_023128	paralemmin	1.540	0.023
NM_030749	endoplasmic reticulum chaperone SIL1 homolog (S. cerevisiae)	1.538	0.026
NM_026933	TP53 regulated inhibitor of apoptosis 1	1.533	0.001
NM_001024205	nuclear fragile X mental retardation protein interacting protein 2	1.532	0.000
NM_025657	leucine rich repeat containing 57	1.530	0.004
NP_001171340	Ras-responsive element-binding protein 1	1.528	0.028
NM_153053	predicted gene 7935; splicing factor 3b, subunit 4	1.526	0.019
NM_181348	RIKEN cDNA A230083H22 gene	1.524	0.020
NM_053158	mitochondrial ribosomal protein L1	1.523	0.001
NM_138670	mercaptopyruvate sulfurtransferase	1.521	0.022
NM_026329	polymerase (RNA) II (DNA directed) polypeptide G	1.521	0.006
NM_001076554	spectrin alpha 2	1.521	0.001
NM_021460	lysosomal acid lipase A	1.521	0.023
NM_144846	family with sequence similarity 49, member B	1.520	0.005
NM_026004	5'-nucleotidase, cytosolic III	1.517	0.004
NM_134076	abhydrolase domain containing 4	1.515	0.007
NM_026159	retinol saturase (all trans retinol 13,14 reductase)	1.511	0.005
NP_035863	cold shock domain protein A	1.509	0.032
NM_011421	sphingomyelin phosphodiesterase 1, acid lysosomal	1.509	0.016
NM_133998	RIKEN cDNA 1810008A18 gene	1.509	0.013
NM_013897	translocase of inner mitochondrial membrane 8 homolog b (yeast)	1.509	0.021
NM_009533	X-ray repair complementing defective repair in Chinese hamster cells 5	1.508	0.035
NM_019734	N-acylsphingosine amidohydrolase 1	1.504	0.017
NM_021299	adenylate kinase 3	1.503	0.005
NM_173371	hexose-6-phosphate dehydrogenase (glucose 1-dehydrogenase)	1.503	0.020
NP_001003667	keratin 77	1.502	0.006
NM_030597	LSM2 homolog, U6 small nuclear RNA associated (S. cerevisiae)	1.502	0.023
NP_444310	Aldehyde dehydrogenase family 1 member A3	1.501	0.007
NM_011586	myosin XVIIIA	1.499	0.008
NM_133716	stromal membrane-associated GTPase-activating protein 2	1.498	0.026
NM_016677	hippocalcin-like 1	1.498	0.042
NM_175489	oxysterol binding protein-like 8	1.496	0.005
NM_007415	poly (ADP-ribose) polymerase family, member 1	1.496	0.016
NM_144870	NADH dehydrogenase (ubiquinone) Fe-S protein 8	1.491	0.005
NM_183144	inositol polyphosphate-5-phosphatase A	1.491	0.041
NM_025537	Ts translation elongation factor, mitochondrial	1.491	0.024
NM_025948	LSM14 homolog A (SCD6, S. cerevisiae)	1.491	0.016
NM_029909	RIKEN cDNA C330018D20 gene	1.490	0.017
NM_139001	chondroitin sulfate proteoglycan 4	1.490	0.020
NM_172736	leukocyte receptor cluster (LRC) member 8	1.490	0.008

NM_001080775	similar to nuclear myosin I beta; myosin IC	1.487	0.009
NM_172472	transcription factor E3	1.486	0.013
NM_025587	predicted gene 5963; ribosomal protein S21	1.484	0.027
NM_008512	low density lipoprotein receptor-related protein 1	1.482	0.002
NM_172532	aldhehyde dehydrogenase family 5, subfamily A1	1.482	0.003
NM_178605	NOP16 nucleolar protein homolog (yeast)	1.480	0.003
NM_027434	regulation of nuclear pre-mRNA domain containing 1B	1.479	0.035
NM_001163481	FK506 binding protein 10	1.478	0.031
NM_028611	RIKEN cDNA 2410091C18 gene	1.478	0.006
NM_026444	citrate synthase	1.477	0.036
NM_030116	mitochondrial ribosomal protein L9	1.477	0.021
NM_001033136	family with sequence similarity 82, member A2	1.477	0.040
NM_030225	dihydrolipoamide S-succinyltransferase (E2 component of 2-oxo-glutarate complex)	1.476	0.031
NP_598452	poly-U binding splicing factor 60	1.476	0.018
NM_078478	growth hormone inducible transmembrane protein	1.475	0.003
NM_028390	anillin, actin binding protein	1.475	0.041
NM_007647	ectonucleoside triphosphate diphosphohydrolase 5	1.473	0.002
NM_010135	enabled homolog (Drosophila)	1.471	0.015
NP_064426	molybdenum cofactor synthesis 1	1.466	0.025
NM_021895	actinin alpha 4	1.465	0.025
NM_007383	acyl-Coenzyme A dehydrogenase, short chain	1.463	0.039
NM_009752	galactosidase, beta 1	1.462	0.005
NM_010299	GM2 ganglioside activator protein	1.462	0.024
NM_030721	acyl-Coenzyme A oxidase 3, pristanoyl	1.461	0.044
NM_010436	H2A histone family, member X	1.459	0.010
NM_024434	leucine aminopeptidase 3	1.457	0.031
NM_021604	agrin	1.455	0.023
NM_025835	propionyl Coenzyme A carboxylase, beta polypeptide	1.455	0.003
NM_023645	KDEL (Lys-Asp-Glu-Leu) containing 1	1.455	0.035
NM_011563	peroxiredoxin 2	1.454	0.018
NM_207625	acyl-CoA synthetase long-chain family member 4	1.454	0.002
NM_009502	vinculin	1.453	0.017
NM_007840	DEAD (Asp-Glu-Ala-Asp) box polypeptide 5; predicted gene 12183	1.449	0.003
NM_027216	similar to Solute carrier family 39 (metal ion transporter), member 11; solute carrier family 39 (metal ion transporter), member 11	1.446	0.009
NM_026732	mitochondrial ribosomal protein L14	1.438	0.042
NM_008986	polymerase I and transcript release factor	1.437	0.022
NM_007996	ferredoxin 1	1.435	0.038
NM_027314	predicted gene 7684; membrane-associated ring finger (C3HC4) 5	1.430	0.038
NM_001177464	Zinc finger protein 516	1.427	0.048
NM_015735	damage specific DNA binding protein 1	1.426	0.007
NM_146234	membrane magnesium transporter 1	1.426	0.035
NM_024233	REX2, RNA exonuclease 2 homolog (S. cerevisiae)	1.426	0.037
NM_019961	peroxisomal biogenesis factor 3	1.425	0.047
NM_008402	integrin alpha V	1.424	0.011
NM_001081034	F-box protein 11	1.423	0.035

NM_026964	coiled-coil domain containing 124	1.423	0.029
NM_001080794	GTPase activating protein (SH3 domain) binding protein 2	1.419	0.030
NM_027906	RIKEN cDNA 1300010F03 gene	1.418	0.015
NM_021895	actinin alpha 4	1.418	0.003
NM_020050	TMEM9 domain family, member B	1.418	0.011
NM_026170	endoplasmic reticulum-golgi intermediate compartment (ERGIC) 1	1.418	0.028
NM_134080	filamin, beta	1.418	0.000
NM_013671	superoxide dismutase 2, mitochondrial	1.417	0.020
NM_020520	solute carrier family 25 (mitochondrial carnitine/acylcarnitine translocase), member 20	1.416	0.015
NM_011490	staufen (RNA binding protein) homolog 1 (Drosophila)	1.416	0.015
NM_029023	serine carboxypeptidase 1	1.412	0.001
NM_001163662	nucleobindin 1	1.410	0.003
NM_133798	exonuclease 3'-5' domain containing 2	1.410	0.038
NM_026819	dehydrogenase/reductase (SDR family) member 1	1.407	0.043
NM_144784	acetyl-Coenzyme A acetyltransferase 1	1.407	0.007
NM_133947	nuclear mitotic apparatus protein 1	1.406	0.008
NM_027159	coiled-coil domain containing 115; predicted gene 7774	1.406	0.042
NM_010948	nuclear distribution gene C homolog (Aspergillus), pseudogene 1; nuclear distribution gene C homolog (Aspergillus)	1.404	0.002
NM_013604	metaxin 1	1.404	0.006
NM_001033759	transmembrane protein 2	1.402	0.009
NM_009295	syntaxin binding protein 1	1.402	0.001
NM_016710	predicted gene 11914; nucleosome binding protein 1	1.401	0.040
NM_133823	methylmalonic aciduria (cobalamin deficiency) type A	1.400	0.009
NP_001156418	pyruvate carboxylase	1.400	0.012
NM_177319	zinc finger, FYVE domain containing 27	1.400	0.049
NM_009784	calcium channel, voltage-dependent, alpha2/delta subunit 1	1.398	0.012
NM_011414	secretory leukocyte peptidase inhibitor	1.398	0.031
NP_001095925	amyloid beta (A4) precursor-like protein 2	1.394	0.011
NM_010302	guanine nucleotide binding protein, alpha 12; similar to Guanine nucleotide-binding protein alpha-12 subunit (G alpha-12)	1.392	0.031
NM_001001932	early endosome antigen 1	1.384	0.038
NM_011197	prostaglandin F2 receptor negative regulator	1.383	0.030
NM_026373	Cyclin-dependent kinase 2-associated protein 2	1.381	0.024
NM_173011	isocitrate dehydrogenase 2 (NADP+), mitochondrial	1.380	0.023
NM_197982	DEAD (Asp-Glu-Ala-Asp) box polypeptide 39	1.378	0.027
NM_153807	acyl-CoA synthetase family member 2	1.375	0.000
NM_008650	methylmalonyl-Coenzyme A mutase	1.368	0.041
NM_001163540	plectin 1	1.368	0.011
NM_010888	similar to NADH dehydrogenase (ubiquinone) Fe-S protein 6; NADH dehydrogenase (ubiquinone) Fe-S protein 6; predicted gene 6415	1.368	0.004
NM_001033284	cDNA sequence BC026585	1.367	0.009
NM_011507	succinate-Coenzyme A ligase, GDP-forming, beta subunit	1.366	0.026
NM_001040026	SCO cytochrome oxidase deficient homolog 1 (yeast)	1.363	0.024
NM_019736	acyl-CoA thioesterase 9	1.363	0.001
NM_008095	glioblastoma amplified sequence	1.362	0.003

NM_021559	zinc finger protein 191	1.361	0.014
NP_001035493	flotillin 2	1.360	0.001
NM_025500	mitochondrial ribosomal protein L37	1.360	0.021
NM_026512	biphenyl hydrolase-like (serine hydrolase, breast epithelial mucin-associated antigen)	1.358	0.004
NM_026175	splicing factor 3a, subunit 1	1.349	0.017
NM_019767	actin related protein 2/3 complex, subunit 1A	1.344	0.037
NM_138601	similar to es1 protein; DNA segment, Chr 10, Johns Hopkins University 81 expressed	1.343	0.037
NP_001157185	predicted gene 9755; Tu translation elongation factor, mitochondrial	1.339	0.046
NM_134089	scribbled homolog (Drosophila)	1.339	0.034
NM_194342	unc-84 homolog B (C. elegans)	1.334	0.038
NM_030717	similar to lactamase, beta; lactamase, beta	1.332	0.050
NM_009503	similar to Transitional endoplasmic reticulum ATPase (TER ATPase) (15S Mg(2+)-ATPase p97 subunit) (Valosin-containing protein) (VCP); valosin containing protein	1.332	0.032
NM_008576	ATP-binding cassette, sub-family C (CFTR/MRP), member 1	1.327	0.038
NM_198608	alanyl-tRNA synthetase 2, mitochondrial (putative)	1.326	0.047
NM_010837	microtubule-associated protein 6	1.325	0.028
NM_027862	predicted gene 10250; hypothetical protein LOC676483; predicted gene 5051; ATP synthase, H+ transporting, mitochondrial F0 complex, subunit d; predicted gene 4953; similar to ATP synthase, H+ transporting, mitochondrial F0 complex, subunit d	1.323	0.031
NM_024181	DnaJ (Hsp40) homolog, subfamily C, member 10	1.320	0.016
NM_001039179	bicaudal D homolog 2 (Drosophila)	1.317	0.004
NM_029759	family with sequence similarity 54, member B	1.316	0.048
NP_001258827	Peroxisomal acyl-coenzyme A oxidase 1	1.314	0.015
NM_026095	small nuclear ribonucleoprotein D3	1.314	0.013
NM_007838	dolichyl-di-phosphooligosaccharide-protein glycotransferase	1.312	0.049
NM_019402	poly(A) binding protein, nuclear 1	1.311	0.035
NM_001038492	cathepsin A	1.310	0.016
NM_011876	twinfilin, actin-binding protein, homolog 2 (Drosophila)	1.304	0.040
NM_016739	cell cycle associated protein 1	1.302	0.002
NM_025814	serpine1 mRNA binding protein 1	1.301	0.024
NM_007757	coproporphyrinogen oxidase	1.300	0.007
NM_022314	predicted gene 7848; predicted gene 7839; predicted gene 4157; similar to tropomyosin 3, gamma; tropomyosin 3, gamma; predicted gene 4903	1.300	0.016
NP_036122	reticulocalbin 2	1.299	0.023
NM_013511	erythrocyte protein band 4.1-like 2	1.296	0.004
NM_023054	UTP3, small subunit (SSU) processome component, homolog (S. cerevisiae)	1.295	0.047
NM_172666	alkylglycerone phosphate synthase	1.295	0.029
NM_145575	caldesmon 1	1.291	0.046
NM_198653	isoleucine-tRNA synthetase 2, mitochondrial; similar to isoleucine-tRNA synthetase 2, mitochondrial	1.291	0.021
NM_008149	glycerol-3-phosphate acyltransferase, mitochondrial	1.290	0.015
NM_054081	similar to metastasis-associated protein; metastasis associated 1; similar to MTA1	1.290	0.043

NM_013651	splicing factor 3a, subunit 2	1.289	0.036
NM_001081260	tankyrase 1 binding protein 1	1.288	0.014
NM_172698	RIKEN cDNA 4732418C07 gene	1.284	0.022
NM_053123	SWI/SNF related, matrix associated, actin dependent regulator of chromatin, subfamily a, member 1	1.280	0.004
NM_025366	coiled-coil-helix-coiled-coil-helix domain containing 1	1.279	0.019
NM_011378	transcriptional regulator, SIN3A (yeast)	1.276	0.002
NM_026172	2,4-dienoyl CoA reductase 1, mitochondrial	1.274	0.004
NM_146176	CCR4-NOT transcription complex, subunit 3	1.269	0.003
NM_011173	protein S (alpha)	1.266	0.032
NM_019783	leprecan 1	1.265	0.032
NM_172591	FCH domain only 2	1.261	0.043
NM_021345	protein tyrosine phosphatase-like A domain containing 1	1.261	0.036
NM_025429	serine (or cysteine) peptidase inhibitor, clade B, member 1a	1.256	0.040
NM_016804	metaxin 2	1.249	0.000
NM_146034	CTAGE family, member 5	1.248	0.018
NM_146211	glycosyltransferase 25 domain containing 1	1.248	0.012
NM_016714	nucleoporin 50	1.243	0.044
NM_138747	NOP2 nucleolar protein homolog (yeast)	1.236	0.011
NM_011431	elongation factor Tu GTP binding domain containing 2	1.230	0.006
NM_175372	retinol dehydrogenase 13 (all-trans and 9-cis)	1.226	0.024
NM_019823	cytochrome P450, family 2, subfamily d, polypeptide 22	1.224	0.033
NM_008638	methylenetetrahydrofolate dehydrogenase (NAD+ dependent), methenyltetrahydrofolate cyclohydrolase	1.219	0.005
NM_009409	topoisomerase (DNA) II beta	1.217	0.020
NM_011333	chemokine (C-C motif) ligand 2	1.214	0.018
NM_009315	TAF6 RNA polymerase II, TATA box binding protein (TBP)-associated factor	1.212	0.001
NM_198326	NSFL1 (p97) cofactor (p47)	1.212	0.031
NM_007798	cathepsin B	1.210	0.010
NM_023409	Niemann Pick type C2	1.207	0.005
NM_172205	suprabasin	1.205	0.011
NM_019584	beclin 1, autophagy related	-1.202	0.045
NM_009418	tripeptidyl peptidase II	-1.202	0.011
NM_178405	ATPase, Na+/K+ transporting, alpha 2 polypeptide	-1.204	0.013
NM_178347	CDC23 (cell division cycle 23, yeast, homolog)	-1.207	0.038
NM_007414	ADP-ribosylarginine hydrolase	-1.208	0.025
NM_007700	conserved helix-loop-helix ubiquitous kinase	-1.210	0.025
NM_010546	inhibitor of kappaB kinase beta	-1.212	0.035
NM_010890	neural precursor cell expressed, developmentally down-regulated 4	-1.213	0.004
NM_024172	HSPA (heat shock 70kDa) binding protein, cytoplasmic cochaperone 1	-1.216	0.041
NM_011099	predicted gene 6560; predicted gene 2124; predicted gene 6992; pyruvate kinase, muscle; similar to M2-type pyruvate kinase	-1.221	0.009
NM_198249	RIKEN cDNA E130112L23 gene	-1.228	0.010
NM_007638	chaperonin containing Tcp1, subunit 7 (eta)	-1.230	0.042
NM_001081193	LEM domain containing 3	-1.248	0.025

NM_181848	optineurin	-1.249	0.016
NM_133708	GDP-mannose pyrophosphorylase A	-1.250	0.037
NM_183417	cyclin-dependent kinase 2	-1.266	0.007
NM_134014	exportin 1, CRM1 homolog (yeast)	-1.266	0.002
NM_153800	Rho GTPase activating protein 22	-1.269	0.041
NM_008684	neogenin	-1.279	0.014
NM_001081011	SLIT-ROBO Rho GTPase activating protein 2	-1.279	0.012
NP_001116240	leucine rich repeat containing 8D	-1.281	0.005
NM_013560	heat shock protein 1	-1.283	0.030
NM_001160319	ubiquitin protein ligase E3 component n-recognin 4	-1.287	0.047
NM_001163126	component of oligomeric golgi complex 5	-1.291	0.016
NM_025647	cytidine monophosphate (UMP-CMP) kinase 1; predicted gene 5867	-1.296	0.014
NM_001077363	polypyrimidine tract binding protein 1; predicted gene 4900	-1.302	0.023
NM_144913	methylphosphate capping enzyme	-1.304	0.001
NM_133884	GPN-loop GTPase 2	-1.304	0.050
NM_029332	A kinase (PRKA) anchor protein 13	-1.304	0.019
NM_015765	heat shock protein 14	-1.306	0.015
NM_172277	sorting nexin 8	-1.310	0.022
NM_008302	heat shock protein 90 alpha (cytosolic), class B member 1	-1.310	0.017
NM_011018	sequestosome 1	-1.310	0.024
NM_008563	minichromosome maintenance deficient 3 (S. cerevisiae)	-1.314	0.003
NM_008300	heat shock protein 4	-1.314	0.044
NM_001146268	platelet derived growth factor receptor, beta polypeptide	-1.315	0.032
NM_133794	glutaminyl-tRNA synthetase	-1.318	0.010
NM_133714	RIKEN cDNA 2310037I24 gene	-1.318	0.015
NM_027350	asparaginyl-tRNA synthetase	-1.319	0.009
NM_178616	predicted gene 14048; proteasome (prosome, macropain) 26S subunit, non-ATPase, 11	-1.319	0.037
NM_021884	tumor susceptibility gene 101	-1.319	0.041
NM_025599	RIKEN cDNA 2610528E23 gene	-1.319	0.036
NM_146229	dynein cytoplasmic 1 light intermediate chain 1	-1.323	0.049
NM_145942	similar to Hmgcs1 protein; 3-hydroxy-3-methylglutaryl-Coenzyme A synthase 1	-1.328	0.045
NM_008328	similar to Interferon-activatable protein 203 (Ifi-203) (Interferon-inducible protein p203); similar to interferon activated gene 203; interferon activated gene 203	-1.339	0.013
NM_133838	EH-domain containing 4	-1.348	0.039
NM_023294	NDC80 homolog, kinetochore complex component (S. cerevisiae)	-1.349	0.026
NM_009398	similar to TNF-stimulated gene 6 protein; tumor necrosis factor alpha induced protein 6	-1.351	0.009
NM_133360	predicted gene 5182; acetyl-Coenzyme A carboxylase alpha	-1.353	0.015
NM_130862	brain-specific angiogenesis inhibitor 1-associated protein 2	-1.354	0.017
NM_033444	chloride intracellular channel 1	-1.354	0.032
NM_022410	myosin, heavy polypeptide 9, non-muscle	-1.355	0.035
NM_008826	phosphofructokinase, liver, B-type	-1.356	0.007
NM_026114	similar to Eukaryotic translation initiation factor 2 subunit 1 (Eukaryotic translation initiation factor 2 alpha subunit) (eIF-2-alpha) (EIF-2alpha) (EIF-2A); eukaryotic translation initiation factor	-1.357	0.017

	2, subunit 1 alpha; predicted gene 7459		
NM_025691	signal recognition particle 72	-1.364	0.029
NM_011035	p21 protein (Cdc42/Rac)-activated kinase 1	-1.364	0.022
NM_026370	MYST histone acetyltransferase 1	-1.365	0.036
NM_009673	annexin A5	-1.371	0.011
NM_026879	chromatin modifying protein 2B	-1.371	0.001
NM_008565	minichromosome maintenance deficient 4 homolog (S. cerevisiae)	-1.377	0.023
NM_012025	Rac GTPase-activating protein 1; predicted gene 1859	-1.383	0.000
NM_009840	chaperonin containing Tcp1, subunit 8 (theta)	-1.384	0.029
NM_022022	ubiquitination factor E4B, UFD2 homolog (S. cerevisiae)	-1.391	0.046
NM_009272	spermidine synthase	-1.391	0.008
NM_180678	glycyl-tRNA synthetase	-1.394	0.014
NM_009097	ribosomal protein S6 kinase polypeptide 1	-1.395	0.015
NM_030238	dynein cytoplasmic 1 heavy chain 1	-1.396	0.015
NM_001029895	arginyltransferase 1	-1.398	0.024
NM_144923	biliverdin reductase B (flavin reductase (NADPH))	-1.400	0.031
NM_080638	major vault protein	-1.400	0.002
NM_025304	leucine carboxyl methyltransferase 1	-1.403	0.016
NM_027236	eukaryotic translation initiation factor 1A domain containing	-1.403	0.038
NM_027807	cullin 5	-1.403	0.043
NM_008410	integral membrane protein 2B	-1.410	0.034
NM_011830	predicted gene 15210; inosine 5'-phosphate dehydrogenase 2	-1.410	0.020
NM_145139	eukaryotic translation initiation factor 3, subunit L	-1.411	0.025
NM_133826	ATPase, H+ transporting, lysosomal V1 subunit H	-1.415	0.003
NM_001009947	dedicator of cytokinesis 11	-1.417	0.038
NM_025380	eukaryotic translation elongation factor 1 epsilon 1	-1.418	0.029
NM_016843	ataxin 10	-1.418	0.019
NM_013854	ATP-binding cassette, sub-family F (GCN20), member 1	-1.421	0.004
NM_007835	dynactin 1	-1.422	0.024
NM_029735	similar to Bifunctional aminoacyl-tRNA synthetase; glutamyl-prolyl-tRNA synthetase	-1.423	0.000
NM_201226	leucine rich repeat containing 47; similar to leucine rich repeat containing 47	-1.425	0.020
NM_009481	ubiquitin specific peptidase 9, X chromosome	-1.426	0.011
NM_024267	importin 4	-1.426	0.011
NM_013477	ATPase, H+ transporting, lysosomal V0 subunit D1	-1.427	0.040
NM_026007	predicted gene 4462; similar to eukaryotic translation elongation factor 1 gamma; predicted gene 9276; predicted gene 5525; eukaryotic translation elongation factor 1 gamma; similar to Elongation factor 1-gamma (EF-1-gamma) (eEF-1B gamma); predicted gene	-1.427	0.010
NM_139144	O-linked N-acetylglucosamine (GlcNAc) transferase (UDP-N-acetylglucosamine:polypeptide-N-acetylglucosaminyl transferase)	-1.428	0.039
NM_013559	heat shock 105kDa/110kDa protein 1	-1.429	0.023
NM_025864	transmembrane protein 206	-1.430	0.034
NM_022563	discoidin domain receptor family, member 2	-1.431	0.007
NM_152801	Rac/Cdc42 guanine nucleotide exchange factor (GEF) 6	-1.432	0.013
NM_027498	similar to Serine/threonine-protein kinase QSK; cDNA sequence	-1.433	0.033

	BC033915		
NM_008567	minichromosome maintenance deficient 6 (MIS5 homolog, S. pombe) (S. cerevisiae)	-1.435	0.001
NM_009842	CD151 antigen	-1.435	0.008
NM_028864	zinc finger CCCH type, antiviral 1	-1.437	0.003
NM_027896	Coenzyme A synthase	-1.439	0.043
NM_019780	vacuolar protein sorting 29 (S. pombe)	-1.440	0.045
NM_021473	aldo-keto reductase family 1, member A4 (aldehyde reductase)	-1.444	0.025
NP_663401	Microfibril-associated glycoprotein 3	-1.445	0.021
NM_010724	proteasome (prosome, macropain) subunit, beta type 8 (large multifunctional peptidase 7)	-1.447	0.008
NM_173010	ubiquitin protein ligase E3A	-1.449	0.014
NM_146171	non-SMC condensin I complex, subunit D2	-1.451	0.024
NM_025697	RIKEN cDNA 6330409N04 gene	-1.453	0.022
NM_016966	predicted gene 7669; predicted gene 5207; predicted gene 9252; predicted gene 8096; predicted gene 13337; predicted gene 9210; predicted gene 8341; predicted gene 5847; predicted gene 7901; predicted gene 9347; predicted gene, EG627427; similar to 3-phosp	-1.453	0.013
NM_012010	eukaryotic translation initiation factor 2, subunit 3, structural gene X-linked; similar to translation initiation factor eIF-2 gamma subunit; predicted gene 2223	-1.455	0.001
NM_172265	eukaryotic translation initiation factor 2B, subunit 5 epsilon	-1.457	0.017
NM_177045	coiled-coil and C2 domain containing 1B	-1.460	0.002
NM_026693	gamma-aminobutyric acid (GABA) A receptor-associated protein-like 2; predicted gene 3724	-1.468	0.007
NM_030210	acetoacetyl-CoA synthetase	-1.468	0.018
NM_009072	Rho-associated coiled-coil containing protein kinase 2	-1.468	0.006
NM_028198	exportin 5	-1.471	0.005
NM_008084	predicted gene 4691; predicted gene 6944; predicted gene 10290; predicted gene 10566; predicted gene 10291; predicted gene 3200; predicted gene 12070; predicted gene 7286; predicted gene 6946; predicted gene 8825; predicted gene 9081; glyceraldehyde-3-pho	-1.476	0.012
NM_026295	CTD (carboxy-terminal domain, RNA polymerase II, polypeptide A) phosphatase, subunit 1	-1.478	0.006
NM_008605	matrix metallopeptidase 12	-1.478	0.028
NM_145527	MAP-kinase activating death domain	-1.480	0.032
NM_008921	DNA primase, p49 subunit	-1.486	0.048
NM_130862	brain-specific angiogenesis inhibitor 1-associated protein 2	-1.488	0.026
NM_134078	CHMP family, member 7	-1.491	0.021
NM_013471	annexin A4	-1.492	0.005
NM_021504	N-glycanase 1	-1.493	0.015
NM_177876	vacuolar protein sorting 37B (yeast)	-1.494	0.007
NM_033074	threonyl-tRNA synthetase	-1.494	0.007
XM_001479591	similar to Eukaryotic translation initiation factor 5; eukaryotic translation initiation factor 5	-1.495	0.036
NM_025816	Tax1 (human T-cell leukemia virus type I) binding protein 1	-1.495	0.012
NM_028032	protein phosphatase 2 (formerly 2A), regulatory subunit B (PR 52), alpha isoform	-1.496	0.022
NM_001031667	glycogen synthase kinase 3 alpha	-1.497	0.035

NM_013472	annexin A6	-1.497	0.011
NM_016721	IQ motif containing GTPase activating protein 1	-1.501	0.047
NM_015760	NADPH oxidase 4	-1.501	0.009
NM_145605	kelch domain containing 4	-1.501	0.043
NM_011596	ATPase, H+ transporting, lysosomal V0 subunit A2	-1.502	0.032
NM_018799	eukaryotic translation initiation factor 3, subunit I	-1.504	0.026
NM_138745	methylenetetrahydrofolate dehydrogenase (NADP+ dependent), methenyltetrahydrofolate cyclohydrolase, formyltetrahydrofolate synthase	-1.506	0.050
NM_133685	RAB31, member RAS oncogene family	-1.507	0.008
NM_009674	annexin A7	-1.507	0.015
NM_001162870	spastin	-1.508	0.013
NM_027815	RIKEN cDNA 9030624J02 gene	-1.508	0.016
NM_011654	predicted gene 3756; tubulin, alpha 1B; predicted gene 5620; similar to alpha-tubulin isotype M-alpha-2; predicted gene 14150; predicted gene 3226	-1.512	0.002
NM_010620	kinesin family member 15	-1.515	0.018
NM_138315	microtubule associated monoxygenase, calponin and LIM domain containing 1	-1.516	0.009
NM_001164677	programmed cell death 6 interacting protein	-1.516	0.048
NM_016807	similar to syntenin; syndecan binding protein	-1.519	0.050
NM_177152	leucine-rich repeats and immunoglobulin-like domains 3	-1.521	0.007
NM_008136	guanine nucleotide binding protein-like 1	-1.522	0.001
NM_025550	proteasome (prosome, macropain) 26S subunit, non-ATPase, 6	-1.523	0.005
NM_010562	integrin linked kinase; predicted gene 6263	-1.524	0.009
NM_133758	ubiquitin specific peptidase 47	-1.526	0.001
NM_001025156	coiled-coil domain containing 93	-1.528	0.002
NM_009837	chaperonin containing Tcp1, subunit 4 (delta)	-1.529	0.000
NM_020578	EH-domain containing 3	-1.529	0.025
NM_148945	ribosomal protein S6 kinase polypeptide 3	-1.531	0.006
NM_028811	elongation protein 3 homolog (S. cerevisiae)	-1.534	0.013
NM_028632	predicted gene 11221; similar to Protein C14orf111 homolog; predicted gene 4893; FCF1 small subunit (SSU) processome component homolog (S. cerevisiae)	-1.535	0.013
NM_013507	eukaryotic translation initiation factor 4, gamma 2	-1.540	0.004
NM_134037	ATP citrate lyase	-1.540	0.006
NM_153569	cyclin G associated kinase	-1.545	0.004
NM_001146023	Protein Fam98c	-1.546	0.034
NM_173443	valosin containing protein (p97)/p47 complex interacting protein 1	-1.548	0.027
NM_022309	core binding factor beta	-1.549	0.023
NM_013492	similar to clusterin; clusterin	-1.552	0.003
NM_016748	cytidine 5'-triphosphate synthase	-1.555	0.005
NM_146217	alanyl-tRNA synthetase	-1.556	0.016
NM_007988	fatty acid synthase	-1.560	0.004
NM_008468	karyopherin (importin) alpha 6	-1.564	0.030
NM_019942	septin 6	-1.568	0.019
NM_010615	kinesin family member 11	-1.569	0.008
NM_001037746	mirror-image polydactyly gene 1 homolog (human);	-1.573	0.001

	phosphoribosyl pyrophosphate synthetase 1; phosphoribosyl pyrophosphate synthetase 1-like 1		
NM_080555	phosphatidic acid phosphatase type 2B	-1.575	0.032
NM_013818	GTP binding protein 1	-1.575	0.042
NM_024281	ribosome binding protein 1	-1.576	0.004
NM_133786	structural maintenance of chromosomes 4	-1.578	0.035
NM_009370	transforming growth factor, beta receptor I	-1.584	0.012
NM_008927	mitogen-activated protein kinase kinase 1	-1.584	0.035
NM_175195	RIKEN cDNA 3110056O03 gene	-1.585	0.017
NM_023716	Tubulin beta-2B chain	-1.590	0.029
NM_028724	similar to Ras and Rab interactor 2; Ras and Rab interactor 2	-1.592	0.015
NM_178376	Ras-related GTP binding A	-1.592	0.004
NM_019795	DnaJ (Hsp40) homolog, subfamily C, member 7	-1.593	0.005
NM_009371	transforming growth factor, beta receptor II	-1.600	0.009
NM_008788	procollagen C-endopeptidase enhancer protein	-1.603	0.026
NM_029565	transmembrane protein 59	-1.605	0.000
NM_013529	Glutamine--fructose-6-phosphate aminotransferase [isomerizing] 2	-1.609	0.039
NM_030201	heat shock protein 70 family, member 13	-1.610	0.024
NM_001080773	3-phosphoinositide dependent protein kinase-1	-1.611	0.039
NM_172558	gem (nuclear organelle) associated protein 5	-1.616	0.013
NM_026662	phosphoribosyl pyrophosphate synthetase 2	-1.619	0.024
NM_153680	sorting nexin 17	-1.621	0.031
NM_008708	N-myristoyltransferase 2	-1.622	0.016
NM_025664	similar to Sorting nexin 9; sorting nexin 9	-1.624	0.000
NM_134100	major facilitator superfamily domain containing 5	-1.630	0.010
NM_009068	receptor (TNFRSF)-interacting serine-threonine kinase 1	-1.631	0.011
NM_009795	calpain, small subunit 1	-1.632	0.006
NM_198710	synaptophysin-like protein	-1.645	0.022
NM_010233	fibronectin 1	-1.646	0.001
NM_007502	ATPase, Na+/K+ transporting, beta 3 polypeptide	-1.649	0.010
NM_024229	phosphate cytidylyltransferase 2, ethanolamine	-1.651	0.050
NM_013562	interferon-related developmental regulator 1	-1.653	0.006
NM_013469	annexin A11; predicted gene 2260; predicted gene 2274	-1.654	0.002
NM_147778	COMM domain containing 3	-1.661	0.024
NM_015747	solute carrier family 20, member 1	-1.662	0.022
NM_026969	Sec31 homolog A (S. cerevisiae)	-1.663	0.007
NM_008668	Ngfi-A binding protein 2	-1.665	0.039
NM_146121	RAB GTPase activating protein 1	-1.666	0.009
NM_001102565	neural regeneration protein; alkB, alkylation repair homolog 1 (E. coli)	-1.671	0.009
NM_022332	suppression of tumorigenicity 7	-1.674	0.002
NM_010217	connective tissue growth factor	-1.678	0.014
NM_007653	CD63 antigen	-1.680	0.026
NM_028181	cell cycle progression 1	-1.681	0.006
NM_010684	lysosomal-associated membrane protein 1	-1.687	0.020
NM_153774	importin 9	-1.687	0.015

NM_007620	predicted gene 5678; carbonyl reductase 1	-1.697	0.020
NM_001159519	phosphoribosylformylglycinamidine synthase (FGAR amidotransferase)	-1.703	0.045
NM_026441	penta-EF hand domain containing 1	-1.710	0.027
NM_177304	ectonucleotide pyrophosphatase/phosphodiesterase 6	-1.712	0.000
NM_175121	solute carrier family 38, member 2	-1.714	0.011
NM_025343	required for meiotic nuclear division 1 homolog (S. cerevisiae); predicted gene 5512	-1.715	0.001
NM_012032	serine incorporator 3	-1.719	0.008
NM_181414	phosphoinositide-3-kinase, class 3	-1.720	0.007
NM_010169	coagulation factor II (thrombin) receptor	-1.720	0.007
NM_010106	predicted gene 5869; predicted gene 7161; predicted gene 7105; predicted gene 5822; similar to eukaryotic translation elongation factor 1 alpha 1; predicted gene 6192; predicted gene 6392; predicted gene 6767; predicted gene 6170; predicted gene 6548; pre	-1.721	0.005
NP_062718	Nuclear receptor coactivator 4	-1.726	0.018
NM_018737	cytidine 5'-triphosphate synthase 2	-1.752	0.040
NM_010212	four and a half LIM domains 2	-1.754	0.011
NM_008676	neighbor of Brca1 gene 1	-1.771	0.005
NM_011930	chloride channel 7	-1.787	0.040
NM_153507	copine II	-1.787	0.012

Appendix B

CHO K1 proteins determined to be significantly differentially regulated in CHO K1 cultures prepared using spent media from CHO DP-12 cells cultured at altered Bioprocessing conditions when compared to CHO K1 cells cultured using spent media from CHO DP-12 cells cultured using standard Bioprocessing conditions. Proteomic samples were analysed using 2D-LC-MS[3] and data analysed using Thermo Fisher Scientific[TM] Proteome Discoverer[TM] version 2.1.0.81 and InfernoRDN version 1.1.5970.31895.

Table 2-A: Differentially regulated CHO K1 proteins determined in samples corresponding to culture using spent media from CHO DP-12 cells prepared under an increased bioprocess temperature of 39.5°C.

RefSeq Annotation	Description	Fold Change	P-value
NM_008669	N-acetyl galactosaminidase, alpha	1.809	0.002
NM_009082	similar to ribosomal protein; predicted gene 6344; predicted gene 11449; predicted gene 13841; predicted gene 8210; hypothetical protein LOC675793; ribosomal protein L29; predicted gene 12704; predicted gene 7252; predicted gene 8965; predicted gene 13213	1.768	0.026
NM_007737	collagen, type V, alpha 2	1.761	0.005
NM_015734	collagen, type V, alpha 1	1.751	0.005
NM_021519	predicted gene 11964; endothelial differentiation-related factor 1	1.749	0.011
NM_172262	amine oxidase, flavin containing 1	1.745	0.035
NM_177068	olfactomedin-like 2B	1.742	0.014
NM_028266	collagen, type XVI, alpha 1	1.718	0.003
NM_008047	follistatin-like 1	1.717	0.002
NM_207298	cerebral endothelial cell adhesion molecule	1.717	0.005
NM_009981	phosphate cytidylyltransferase 1, choline, alpha isoform	1.711	0.001
NM_011146	peroxisome proliferator activated receptor gamma	1.708	0.000
NP_001020788	calcium activated nucleotidase 1	1.706	0.015
NM_133886	expressed sequence AU040320	1.702	0.003
NM_001003949	open reading frame 61	1.698	0.014
NM_010191	predicted gene 6781; farnesyl diphosphate farnesyl transferase 1	1.692	0.008
NM_011341	stromal cell derived factor 4	1.691	0.015
NM_023232	diablo homolog (Drosophila)	1.686	0.027
NM_008675	neuroblastoma, suppression of tumorigenicity 1	1.683	0.028
NP_080444	ERGIC and golgi 2	1.681	0.030
NM_025571	predicted gene 9803; mitochondria-associated protein involved in granulocyte-macrophage colony-stimulating factor signal transduction	1.678	0.001
NM_026560	cell division cycle associated 8	1.677	0.011
NM_009346	TEA domain family member 1	1.671	0.035
NM_010756	similar to mafG; v-maf musculoaponeurotic fibrosarcoma	1.671	0.015

	oncogene family, protein G (avian)		
NM_133766	EFR3 homolog A (S. cerevisiae)	1.669	0.022
NM_011333	chemokine (C-C motif) ligand 2	1.669	0.006
NM_172205	suprabasin	1.664	0.031
NM_011173	protein S (alpha)	1.659	0.001
NP_663432	polyadenylate binding protein-interacting protein 1; similar to poly(A) binding protein interacting protein 1	1.659	0.012
NM_145606	chromatin modifying protein 1A; predicted gene 8515	1.650	0.038
NM_010517	insulin-like growth factor binding protein 4	1.646	0.042
NM_027478	RIKEN cDNA 5730494N06 gene; predicted gene 7368	1.644	0.000
NM_175021	sterile alpha motif domain containing 4B	1.633	0.004
NM_007801	cathepsin H	1.628	0.020
NM_010516	cysteine rich protein 61	1.624	0.003
NP_082223	zinc finger and BTB domain containing 43	1.624	0.037
NM_010380	histocompatibility 2, D region; histocompatibility 2, D region locus 1	1.623	0.014
NM_026752	zinc finger, FYVE domain containing 21	1.623	0.016
NM_008689	nuclear factor of kappa light polypeptide gene enhancer in B-cells 1, p105	1.623	0.043
NM_009101	Harvey rat sarcoma oncogene, subgroup R	1.621	0.006
NM_027852	retinoic acid receptor responder (tazarotene induced) 2	1.620	0.045
NM_010917	similar to Nidogen precursor (Entactin); nidogen 1; similar to Nid1 protein	1.616	0.016
NM_146065	activating transcription factor 7	1.616	0.040
NM_008305	perlecan (heparan sulfate proteoglycan 2)	1.615	0.003
NM_028945	DNA segment, Chr 14, Abbott 1 expressed	1.614	0.010
NM_144857	cDNA sequence BC011248	1.608	0.016
NM_130888	nuclear RNA export factor 7	1.606	0.015
NM_020010	cytochrome P450, family 51	1.604	0.034
NM_010592	Jun proto-oncogene related gene d	1.602	0.043
NM_012056	FK506 binding protein 9	1.601	0.019
NM_001039644	ER degradation enhancer, mannosidase alpha-like 3	1.596	0.016
NM_008139	guanine nucleotide binding protein, alpha q polypeptide	1.596	0.044
NM_022985	zinc finger, AN1-type domain 6	1.594	0.025
NM_028017	N-ethylmaleimide sensitive fusion protein attachment protein gamma	1.592	0.003
NM_015804	ATPase, class VI, type 11A	1.588	0.002
NM_181070	RAB18, member RAS oncogene family	1.583	0.013
NM_181278	RIKEN cDNA B230219D22 gene	1.577	0.015
NM_010931	ubiquitin-like, containing PHD and RING finger domains, 1; predicted gene 5648; similar to nuclear zinc finger protein Np95	1.576	0.010
NM_017478	coatomer protein complex, subunit gamma 2	1.574	0.024
NM_001037166	predicted gene 4925	1.574	0.016
NM_029658	family with sequence similarity 101, member B	1.572	0.015
NM_013866	zinc finger protein 385A	1.553	0.019
NM_025573	splicing factor, arginine/serine rich 9	1.550	0.020
NM_011961	procollagen lysine, 2-oxoglutarate 5-dioxygenase 2	1.548	0.040
NM_022328	myeloid/lymphoid or mixed-lineage leukemia (trithorax homolog,	1.548	0.001

	Drosophila); translocated to, 1		
NM_025673	golgi phosphoprotein 3	1.546	0.009
NM_183417	cyclin-dependent kinase 2	1.536	0.027
NM_001113573	bromodomain containing 3	1.536	0.006
NM_026844	RIKEN cDNA 2310061C15 gene	1.535	0.035
NM_172272	prolyl-tRNA synthetase (mitochondrial)(putative)	1.535	0.005
NM_007552	Bmi1 polycomb ring finger oncogene	1.532	0.024
NM_009270	squalene epoxidase	1.526	0.002
NM_001134717	RIKEN cDNA 2810006K23 gene	1.525	0.001
NP_034835	lectin, galactose binding, soluble 3	1.520	0.008
NM_019832	G kinase anchoring protein 1	1.520	0.010
NM_194342	unc-84 homolog B (C. elegans)	1.516	0.009
NM_145985	similar to Archain 1; archain 1; similar to coat protein delta-cop; predicted gene 8752; predicted gene 8750; similar to archain	1.516	0.019
NM_007725	calponin 2	1.512	0.021
NM_054078	bromodomain adjacent to zinc finger domain, 2A	1.510	0.033
NM_010299	GM2 ganglioside activator protein	1.505	0.020
NM_029619	methionine sulfoxide reductase B2	1.504	0.050
NM_001001932	early endosome antigen 1	1.501	0.009
NM_001013786	zinc finger protein 187	1.500	0.015
NM_018774	polyhomeotic-like 2 (Drosophila)	1.494	0.045
NM_027307	golgi membrane protein 1	1.492	0.007
NM_011871	protein kinase, interferon inducible double stranded RNA dependent activator	1.492	0.031
NM_025657	leucine rich repeat containing 57	1.485	0.043
NM_010312	guanine nucleotide binding protein (G protein), beta 2	1.481	0.015
NM_001081218	host cell factor C2	1.479	0.005
NM_008619	Moloney leukemia virus 10; predicted gene 7357	1.478	0.035
NP_033030	kinesin family member 20A	1.478	0.024
NM_007792	cysteine and glycine-rich protein 2	1.473	0.003
NM_172120	vacuolar protein sorting 41 (yeast)	1.473	0.027
NM_201642	similar to UDP glycosyltransferase 1 family polypeptide A13; similar to UGT1.6; UDP glucuronosyltransferase 1 family, polypeptide A1; UDP glucuronosyltransferase 1 family, polypeptide A2; UDP glycosyltransferase 1 family, polypeptide A10; UDP glucuronosyl	1.473	0.021
NM_021604	agrin	1.471	0.001
NM_010398	histocompatibility 2, T region locus 23; similar to RT1 class Ib, locus H2-Q-like, grc region	1.463	0.016
NM_008408	STT3, subunit of the oligosaccharyltransferase complex, homolog A (S. cerevisiae)	1.461	0.024
NM_031874	RAB3D, member RAS oncogene family	1.461	0.039
NM_013902	FK506 binding protein 3	1.455	0.037
NM_153150	solute carrier family 25 (mitochondrial carrier, citrate transporter), member 1	1.451	0.000
NM_022325	cathepsin Z	1.449	0.006
NM_146211	glycosyltransferase 25 domain containing 1	1.448	0.009
NM_009003	RAB4A, member RAS oncogene family	1.442	0.026
NM_013885	chloride intracellular channel 4 (mitochondrial)	1.440	0.020
NM_008684	neogenin	1.438	0.025

NM_008774	poly(A) binding protein, cytoplasmic 1	1.435	0.026
NM_010655	similar to ribosomal protein L38; predicted gene 13020; ribosomal protein L38; predicted gene 4991; karyopherin (importin) alpha 2; predicted gene 9028; predicted gene 8129; predicted gene 7123; predicted gene 5832; predicted gene 10184; predicted gene 73	1.433	0.011
NM_008138	guanine nucleotide binding protein (G protein), alpha inhibiting 2; similar to Guanine nucleotide-binding protein G(i), alpha-2 subunit (Adenylate cyclase-inhibiting G alpha protein)	1.433	0.008
NM_133983	CD276 antigen	1.431	0.031
NM_021310	junction-mediating and regulatory protein	1.431	0.000
NM_011306	retinoid X receptor beta	1.430	0.034
NM_009983	cathepsin D	1.430	0.048
NM_010864	myosin VA	1.430	0.024
NM_010580	integrin beta 5	1.427	0.019
NM_019783	leprecan 1	1.425	0.024
NM_010189	Fc receptor, IgG, alpha chain transporter	1.422	0.003
NM_001039137	short coiled-coil protein	1.416	0.012
NM_007379	ATP-binding cassette, sub-family A (ABC1), member 2	1.415	0.040
NM_009655	activated leukocyte cell adhesion molecule	1.414	0.039
NM_019821	glycolipid transfer protein	1.409	0.033
NM_019642	ribophorin II	1.405	0.006
NM_011197	prostaglandin F2 receptor negative regulator	1.395	0.002
NM_175933	peroxisomal biogenesis factor 5	1.391	0.008
NM_019776	staphylococcal nuclease and tudor domain containing 1	1.387	0.002
NM_028262	SET domain containing 3; similar to CG32732-PA; predicted gene 7114; predicted gene 14026	1.381	0.008
NM_024181	DnaJ (Hsp40) homolog, subfamily C, member 10	1.379	0.001
NM_010015	defender against cell death 1	1.378	0.000
NM_028295	protein disulfide isomerase associated 5	1.374	0.024
NM_007481	ADP-ribosylation factor 6	1.372	0.002
NM_183270	coiled-coil-helix-coiled-coil-helix domain containing 8	1.369	0.032
NM_133350	microtubule-associated protein, RP/EB family, member 3	1.369	0.030
NM_010235	fos-like antigen 1	1.369	0.007
NM_015827	coatomer protein complex, subunit beta 2 (beta prime)	1.366	0.001
NM_011029	predicted gene 9323; predicted gene 7516; ribosomal protein SA pseudogene; predicted gene 9819; predicted gene 6339; predicted gene 9083; ribosomal protein SA; predicted gene 13374; predicted gene 12595; similar to laminin receptor 1 (ribosomal protein SA	1.359	0.001
NM_007879	developmentally regulated GTP binding protein 1	1.359	0.030
NM_010421	hexosaminidase A	1.356	0.047
NM_023040	growth factor, erv1 (S. cerevisiae)-like (augmenter of liver regeneration)	1.355	0.020
NM_026666	ubinuclein 1	1.355	0.006
NM_144861	regulation of nuclear pre-mRNA domain containing 1A	1.353	0.007
NM_013531	guanine nucleotide binding protein (G protein), beta 4	1.337	0.023
NM_009153	sema domain, immunoglobulin domain (Ig), short basic domain, secreted, (semaphorin) 3B	1.335	0.007
NM_001111279	WD repeat and FYVE domain containing 1	1.334	0.002
NM_183250	multiple EGF-like-domains 8; similar to coiled-coil domain	1.331	0.029

	containing 72; coiled-coil domain containing 72; predicted gene 7526; predicted gene 9613; predicted gene 15235; predicted gene 14200		
NM_007798	cathepsin B	1.330	0.034
NM_001076554	spectrin alpha 2	1.321	0.017
NM_008686	nuclear factor, erythroid derived 2,-like 1	1.319	0.018
NM_019734	N-acylsphingosine amidohydrolase 1	1.318	0.031
NM_133808	high density lipoprotein (HDL) binding protein	1.318	0.045
NM_026533	similar to ribosomal protein S13; predicted gene 12270; predicted gene 6834; predicted gene 15483; predicted gene 6573; ribosomal protein S13; predicted gene 10159	1.311	0.016
NM_009033	RNA binding motif protein, X chromosome retrogene	1.307	0.015
NM_178628	predicted gene 3086; atlastin GTPase 1; similar to Spg3a protein	1.300	0.006
NM_010368	glucuronidase, beta	1.297	0.021
NM_011127	paired related homeobox 1	1.296	0.048
NM_010757	v-maf musculoaponeurotic fibrosarcoma oncogene family, protein K (avian)	1.293	0.018
NP_001029138	similar to adenylate kinase 2; adenylate kinase 2	1.286	0.011
NM_010435	histone cell cycle regulation defective homolog A (S. cerevisiae)	1.286	0.016
NM_033370	coatomer protein complex, subunit beta 1	1.280	0.001
NM_008064	glucosidase, alpha, acid	1.270	0.016
NM_007475	predicted gene 9625; predicted gene 14165; similar to acidic ribosomal phosphoprotein P0; predicted gene 8730; predicted gene 9093; ribosomal protein, large, P0	1.269	0.044
NM_020296	RNA binding motif, single stranded interacting protein 1	1.264	0.022
NM_001163481	FK506 binding protein 10	1.262	0.018
NP_001164011	predicted gene 9308; basic transcription factor 3; predicted gene 3531; predicted gene 7973	1.256	0.026
NM_178660	RNA binding motif, single stranded interacting protein	1.254	0.016
NM_145553	predicted gene 7527; family with sequence similarity 76, member A	1.251	0.041
NM_007602	calpain 5	1.250	0.007
NM_001168488	multiple endocrine neoplasia 1	1.247	0.030
NM_019806	vesicle-associated membrane protein, associated protein B and C	1.242	0.021
NM_175115	IKAROS family zinc finger 5	1.239	0.017
NM_009784	calcium channel, voltage-dependent, alpha2/delta subunit 1	1.239	0.008
NM_173371	hexose-6-phosphate dehydrogenase (glucose 1-dehydrogenase)	1.237	0.006
NM_023348	synaptosomal-associated protein 29	1.229	0.021
NM_133933	ribophorin I	1.228	0.026
NM_207176	testis derived transcript	1.228	0.039
NM_009938	coatomer protein complex subunit alpha	1.225	0.002
NM_007886	dystrobrevin, beta	1.223	0.028
NM_022997	vacuolar protein sorting 35	1.222	0.022
NM_011289	predicted gene 6599; predicted gene 6199; predicted gene 6341; predicted gene 6301; predicted gene 11518; similar to ribosomal protein L27; ribosomal protein L27; predicted gene 7053; predicted gene 11552; predicted gene 15730	1.222	0.036
NM_008416	Jun-B oncogene	1.212	0.040
NM_026620	family with sequence similarity 98, member B	1.211	0.032

NM_025846	related RAS viral (r-ras) oncogene homolog 2	1.209	0.041
NM_009075	ribose 5-phosphate isomerase A	1.207	0.033
NM_207625	acyl-CoA synthetase long-chain family member 4	1.205	0.010
NM_001081288	TAF2 RNA polymerase II, TATA box binding protein (TBP)-associated factor	1.202	0.005
NM_009212	immunoglobulin mu binding protein 2	-1.205	0.005
NM_007842	DEAH (Asp-Glu-Ala-His) box polypeptide 9	-1.206	0.048
NM_011189	predicted gene 7776; proteasome (prosome, macropain) 28 subunit, alpha	-1.208	0.019
NM_008379	karyopherin (importin) beta 1	-1.210	0.039
NM_172456	endo/exonuclease (5'-3'), endonuclease G-like	-1.210	0.007
NM_009838	chaperonin containing Tcp1, subunit 6a (zeta)	-1.211	0.006
NM_178610	KRR1, small subunit (SSU) processome component, homolog (yeast)	-1.212	0.035
NM_180678	glycyl-tRNA synthetase	-1.212	0.010
NM_146066	G1 to S phase transition 1	-1.215	0.039
NM_012019	apoptosis-inducing factor, mitochondrion-associated 1	-1.221	0.018
NM_010438	hexokinase 1	-1.232	0.024
NM_007637	chaperonin containing Tcp1, subunit 5 (epsilon)	-1.238	0.014
NM_009418	tripeptidyl peptidase II	-1.242	0.030
NM_028812	general transcription factor II E, polypeptide 1 (alpha subunit)	-1.244	0.000
NM_009048	RalBP1 associated Eps domain containing protein	-1.249	0.026
NP_001185796	Dynactin subunit 1	-1.251	0.040
NM_010360	glutathione S-transferase, mu 5	-1.252	0.033
NM_007907	predicted gene 13050; eukaryotic translation elongation factor 2	-1.254	0.000
NM_026894	RIKEN cDNA 1500001M20 gene	-1.255	0.036
NM_130867	kin of IRRE like (Drosophila)	-1.255	0.000
NM_009466	UDP-glucose dehydrogenase	-1.256	0.036
NM_152807	coiled-coil domain containing 137	-1.259	0.027
NM_024281	ribosome binding protein 1	-1.265	0.037
NM_027236	eukaryotic translation initiation factor 1A domain containing	-1.266	0.005
NM_028074	DEAD (Asp-Glu-Ala-Asp) box polypeptide 42	-1.269	0.009
NM_053069	autophagy-related 5 (yeast)	-1.270	0.023
NM_001171582	methionine-tRNA synthetase	-1.270	0.011
NM_011240	RAN binding protein 2	-1.271	0.003
NM_028276	UTP14, U3 small nucleolar ribonucleoprotein, homolog A (yeast)	-1.277	0.026
NM_024220	NADH dehydrogenase (ubiquinone) 1, subcomplex unknown, 2; similar to NADH dehydrogenase (ubiquinone) 1, subcomplex unknown, 2	-1.278	0.006
NM_016661	similar to Adenosylhomocysteinase (S-adenosyl-L-homocysteine hydrolase) (AdoHcyase) (Liver copper-binding protein) (CUBP); S-adenosylhomocysteine hydrolase	-1.281	0.017
NM_134123	RNA binding motif protein 16	-1.286	0.043
NM_028597	THO complex 3	-1.287	0.000
NM_011655	tubulin, beta 5	-1.288	0.030
NM_177367	gem (nuclear organelle) associated protein 4	-1.290	0.010
NM_019805	anaphase promoting complex subunit 7	-1.290	0.027
NM_053183	predicted gene 8228; DEAD (Asp-Glu-Ala-Asp) box polypeptide 50	-1.290	0.010

NM_025824	predicted gene 11652; predicted gene 5191; basic leucine zipper and W2 domains 1	-1.291	0.002
NM_011680	similar to USF2; upstream transcription factor 2	-1.292	0.033
NM_001039474	transcription elongation regulator 1 (CA150)	-1.293	0.022
NM_010173	fatty acid amide hydrolase	-1.296	0.043
NM_029525	phosphatidylinositol-3,4,5-trisphosphate-dependent Rac exchange factor 2	-1.297	0.004
NM_178700	G-rich RNA sequence binding factor 1	-1.298	0.005
NM_007687	cofilin 1, non-muscle; similar to Cofilin-1 (Cofilin, non-muscle isoform); predicted gene 6180	-1.299	0.001
NM_026114	similar to Eukaryotic translation initiation factor 2 subunit 1 (Eukaryotic translation initiation factor 2 alpha subunit) (eIF-2-alpha) (EIF-2alpha) (EIF-2A); eukaryotic translation initiation factor 2, subunit 1 alpha; predicted gene 7459	-1.301	0.007
NM_016799	serine/arginine repetitive matrix 1	-1.303	0.018
NM_025692	ubiquitin-like modifier activating enzyme 5	-1.303	0.019
NM_030035	golgi autoantigen, golgin subfamily b, macrogolgin 1	-1.304	0.003
NM_011319	seryl-aminoacyl-tRNA synthetase	-1.307	0.007
NM_017379	tubulin, alpha 8	-1.307	0.020
NM_178213	histone cluster 2, H2ab	-1.308	0.014
NM_009088	polymerase (RNA) I polypeptide A	-1.311	0.012
NM_134125	thyroid hormone receptor interactor 10	-1.313	0.026
NM_008014	protein phosphatase 1G (formerly 2C), magnesium-dependent, gamma isoform	-1.319	0.027
NM_133925	RNA binding motif protein 28	-1.323	0.008
NM_175294	nuclear casein kinase and cyclin-dependent kinase substrate 1	-1.329	0.036
NM_008481	laminin, alpha 2	-1.335	0.035
NM_001081247	polymerase (RNA) III (DNA directed) polypeptide A	-1.335	0.030
NM_030238	dynein cytoplasmic 1 heavy chain 1	-1.339	0.030
NM_198303	eukaryotic translation initiation factor 5B	-1.339	0.022
NM_026171	nuclear VCP-like	-1.340	0.005
NM_028782	lon peptidase 1, mitochondrial	-1.344	0.006
NM_026816	general transcription factor IIF, polypeptide 2	-1.345	0.001
NM_133716	stromal membrane-associated GTPase-activating protein 2	-1.346	0.039
NM_152803	heparanase	-1.349	0.004
NM_009933	collagen, type VI, alpha 1	-1.358	0.042
NM_146229	dynein cytoplasmic 1 light intermediate chain 1	-1.358	0.010
NM_172381	expressed sequence AI314180	-1.359	0.020
NM_011714	bromodomain adjacent to zinc finger domain, 1B	-1.364	0.018
NM_007858	diaphanous homolog 1 (Drosophila)	-1.367	0.035
NM_023119	predicted gene 4735; enolase 1, alpha non-neuron; similar to enolase 1, alpha non-neuron; hypothetical protein LOC100044223; predicted gene 5506; predicted gene 5855; hypothetical protein LOC100045967	-1.371	0.015
NM_009388	transketolase	-1.374	0.003
NM_026662	phosphoribosyl pyrophosphate synthetase 2	-1.376	0.002
NM_008826	phosphofructokinase, liver, B-type	-1.380	0.030
NM_007949	excision repair cross-complementing rodent repair deficiency, complementation group 2	-1.380	0.017

NM_007530	B-cell receptor-associated protein 29	-1.381	0.006
NM_008537	alpha-methylacyl-CoA racemase	-1.388	0.023
NM_019869	RNA binding motif protein 14	-1.395	0.000
NM_144825	TAO kinase 1	-1.396	0.033
NM_145625	eukaryotic translation initiation factor 4B	-1.397	0.006
NM_021884	tumor susceptibility gene 101	-1.401	0.008
NM_172407	CDKN2A interacting protein	-1.412	0.001
NP_001106817	similar to Transcriptional repressor p66 alpha (GATA zinc finger domain-containing protein 2A); GATA zinc finger domain containing 2A	-1.414	0.042
NM_015728	solute carrier family 33 (acetyl-CoA transporter), member 1	-1.417	0.041
NM_021511	predicted gene 5067; RRS1 ribosome biogenesis regulator homolog (S. cerevisiae)	-1.420	0.025
NM_144731	UDP-N-acetyl-alpha-D-galactosamine: polypeptide N-acetylgalactosaminyltransferase 7	-1.422	0.012
NM_145416	KRI1 homolog (S. cerevisiae)	-1.426	0.002
NM_001081043	protein tyrosine phosphatase, non-receptor type 23	-1.429	0.008
NM_010830	mutS homolog 6 (E. coli)	-1.432	0.028
NM_019763	SPEN homolog, transcriptional regulator (Drosophila)	-1.433	0.038
NM_027016	SEC62 homolog (S. cerevisiae)	-1.439	0.017
NM_011076	ATP-binding cassette, sub-family B (MDR/TAP), member 1A	-1.441	0.009
NM_013768	protein arginine N-methyltransferase 5	-1.442	0.006
NM_029437	cytoskeleton associated protein 5	-1.442	0.005
NM_026476	RIKEN cDNA 2610101N10 gene	-1.448	0.016
NM_028083	chromatin assembly factor 1, subunit B (p60)	-1.450	0.013
NM_011574	cirrhosis, autosomal recessive 1A (human)	-1.457	0.007
NM_144543	thymocyte nuclear protein 1	-1.457	0.004
NM_133921	nuclear transcription factor, X-box binding-like 1	-1.457	0.007
NM_009481	ubiquitin specific peptidase 9, X chromosome	-1.461	0.004
NM_029600	ATP-binding cassette, sub-family C (CFTR/MRP), member 3	-1.462	0.007
NM_027379	fatty acyl CoA reductase 1	-1.464	0.025
NM_026370	MYST histone acetyltransferase 1	-1.465	0.038
NM_027346	coiled-coil domain containing 44	-1.468	0.009
NM_011654	predicted gene 3756; tubulin, alpha 1B; predicted gene 5620; similar to alpha-tubulin isotype M-alpha-2; predicted gene 14150; predicted gene 3226	-1.470	0.025
NM_178923	splicing factor, arginine/serine-rich 15	-1.479	0.035
NP_001258788	Beta-adducin	-1.481	0.018
NM_019553	DEAD (Asp-Glu-Ala-Asp) box polypeptide 21	-1.481	0.002
NM_013507	eukaryotic translation initiation factor 4, gamma 2	-1.482	0.009
NM_011830	predicted gene 15210; inosine 5'-phosphate dehydrogenase 2	-1.483	0.014
NM_010925	ribosomal RNA processing 1 homolog (S. cerevisiae)	-1.488	0.001
NM_013700	ubiquitin specific peptidase 5 (isopeptidase T)	-1.489	0.019
NM_025959	proteasome (prosome, macropain) 26S subunit, ATPase, 6	-1.489	0.003
NM_145358	calcium/calmodulin-dependent protein kinase kinase 2, beta	-1.490	0.021
NM_023871	predicted gene, EG625349; predicted gene 5789; predicted gene 7085; predicted gene 5708; predicted gene 6847; SET translocation; cDNA sequence BC085271; predicted gene 7239; similar to protein phosphatase 2A inhibitor-2 I-2PP2A; predicted	-1.490	0.012

	gene 9531		
NM_134188	acyl-CoA thioesterase 2	-1.492	0.000
NP_997603	widely-interspaced zinc finger motifs	-1.504	0.008
NM_145954	aldehyde dehydrogenase 16 family, member A1	-1.504	0.011
NM_028032	protein phosphatase 2 (formerly 2A), regulatory subunit B (PR 52), alpha isoform	-1.518	0.002
NM_080287	engulfment and cell motility 2, ced-12 homolog (C. elegans)	-1.522	0.028
NM_025623	nipsnap homolog 3A (C. elegans)	-1.527	0.028
NM_029746	component of oligomeric golgi complex 2	-1.530	0.012
NM_172712	ubiquitin-like modifier activating enzyme 6	-1.531	0.022
NM_178883	golgin, RAB6-interacting	-1.534	0.036
NM_133702	nucleolar protein 11	-1.542	0.008
NM_198411	subacute ozone induced inflammation; RIKEN cDNA 2610204M08 gene	-1.543	0.004
NM_016721	IQ motif containing GTPase activating protein 1	-1.549	0.005
NM_026160	microtubule-associated protein 1 light chain 3 beta	-1.558	0.036
NM_134151	tyrosyl-tRNA synthetase	-1.563	0.002
NM_007714	CDC like kinase 4	-1.569	0.015
NM_030678	glycogen synthase 1, muscle	-1.571	0.043
NM_021505	anaphase-promoting complex subunit 5; similar to anaphase-promoting complex subunit 5	-1.575	0.006
NM_177992	guanosine monophosphate reductase 2	-1.575	0.006
NM_026550	PAK1 interacting protein 1	-1.576	0.015
NM_133826	ATPase, H+ transporting, lysosomal V1 subunit H	-1.576	0.009
NM_145147	GTP binding protein 6 (putative)	-1.590	0.024
NM_029775	DCN1, defective in cullin neddylation 1, domain containing 5 (S. cerevisiae)	-1.599	0.000
NM_025816	Tax1 (human T-cell leukemia virus type I) binding protein 1	-1.604	0.040
NM_001039388	WD repeat domain 37	-1.607	0.006
NM_133806	UDP-N-acetylglucosamine pyrophosphorylase 1	-1.611	0.013
NM_028181	cell cycle progression 1	-1.613	0.008
XM_001479591	similar to Eukaryotic translation initiation factor 5; eukaryotic translation initiation factor 5	-1.621	0.035
NM_024436	RAB22A, member RAS oncogene family	-1.627	0.030
NM_011723	xanthine dehydrogenase	-1.642	0.016
NM_019746	predicted gene 3837; programmed cell death 5	-1.645	0.047
NM_023554	nucleolar protein 7	-1.648	0.029
NM_011018	sequestosome 1	-1.649	0.037
NP_001240821	Anion exchange protein 2	-1.650	0.010
NM_026432	transmembrane protein 66	-1.651	0.047
NM_009254	serine (or cysteine) peptidase inhibitor, clade B, member 6a	-1.651	0.003
NM_020587	splicing factor, arginine/serine-rich 4 (SRp75)	-1.666	0.001
NM_001033293	UDP-N-acteylglucosamine pyrophosphorylase 1-like 1	-1.673	0.004
NM_172952	gephyrin	-1.675	0.019
NM_010442	heme oxygenase (decycling) 1	-1.678	0.016
NP_001107603	protein phosphatase 4, regulatory subunit 1	-1.679	0.014
NM_009288	serine/threonine kinase 10	-1.691	0.012
NM_175121	solute carrier family 38, member 2	-1.702	0.017

NM_013678	surfeit gene 2	-1.709	0.013
NM_009628	activity-dependent neuroprotective protein	-1.710	0.017
NM_027371	brix domain containing 5	-1.730	0.001
NM_016766	microspherule protein 1; predicted gene 13127	-1.731	0.000
NM_144806	predicted gene 13651; phosphoribosyl pyrophosphate synthetase-associated protein 2	-1.734	0.022
NM_010685	lysosomal-associated membrane protein 2	-1.738	0.012
NM_001081045	hypothetical protein LOC100043982; RIKEN cDNA 1700081L11 gene	-1.744	0.014
NM_001080928	recombination signal binding protein for immunoglobulin kappa J region	-1.748	0.007
NM_001111288	SCO cytochrome oxidase deficient homolog 2 (yeast)	-1.760	0.014
NM_183106	tetratricopeptide repeat domain 17	-1.760	0.002
NM_019965	DnaJ (Hsp40) homolog, subfamily B, member 12	-1.846	0.025
NM_001029895	arginyltransferase 1	-1.875	0.019

Table 2-B: Differentially regulated CHO K1 proteins determined in samples corresponding to culture using spent media from CHO DP-12 cells prepared under a reduced bioprocess temperature of 32.0°C.

RefSeq Annotation	Description	Fold Change	P-Value
NM_028266	collagen, type XVI, alpha 1	1.676	0.019
NM_009810	caspase 3	1.594	0.039
NM_025700	phosphoglucomutase 1	1.554	0.005
NM_011127	paired related homeobox 1	1.499	0.031
NM_007406	adenylate cyclase 7	1.489	0.016
NM_001003949	open reading frame 61	1.470	0.019
NM_009939	COP9 (constitutive photomorphogenic) homolog, subunit 2 (Arabidopsis thaliana)	1.450	0.021
NM_146252	TBC1 domain family, member 13	1.442	0.020
NM_146258	StAR-related lipid transfer (START) domain containing 13; similar to serologically defined colon cancer antigen 13	1.435	0.026
NM_010906	nuclear factor I/X	1.428	0.010
NM_175115	IKAROS family zinc finger 5	1.400	0.018
NM_007392	actin, alpha 2, smooth muscle, aorta	1.400	0.046
NM_175113	tRNA methyltransferase 6 homolog (S. cerevisiae)	1.396	0.043
NM_001009818	septin 11	1.363	0.049
NM_019542	N-acetylglucosamine kinase	1.347	0.043
NM_025968	prostaglandin reductase 1	1.331	0.016
NM_022988	Ngg1 interacting factor 3-like 1 (S. pombe)	1.327	0.007
NM_022653	thimet oligopeptidase 1	1.301	0.023
NM_001077529	predicted gene 7730; non-metastatic cells 2, protein (NM23B) expressed in; predicted gene 5566; predicted gene 5425; similar to Nucleoside diphosphate kinase B (NDK B) (NDP kinase B) (P18)	1.296	0.016
NM_144846	family with sequence similarity 49, member B	1.294	0.045
NM_001037166	predicted gene 4925	1.285	0.024

NM_009289	STE20-like kinase (yeast)	1.268	0.003
NM_025958	cullin-associated and neddylation-dissociated 2 (putative)	1.268	0.029
NM_001033533	coiled-coil domain containing 102A	1.247	0.045
NM_023248	Shwachman-Bodian-Diamond syndrome homolog (human)	1.240	0.028
NM_009075	ribose 5-phosphate isomerase A	1.223	0.023
NM_011862	protein kinase C and casein kinase substrate in neurons 2	1.215	0.033
NM_028975	transmembrane protein 33	-1.204	0.025
NM_010303	guanine nucleotide binding protein, alpha 13	-1.217	0.047
NM_028083	chromatin assembly factor 1, subunit B (p60)	-1.218	0.002
NM_175094	pyruvate dehydrogenase complex, component X; similar to pyruvate dehydrogenase complex, component X	-1.225	0.001
NP_001106817	similar to Transcriptional repressor p66 alpha (GATA zinc finger domain-containing protein 2A); GATA zinc finger domain containing 2A	-1.230	0.049
NM_022018	family with sequence similarity 129, member A	-1.235	0.028
NM_024220	NADH dehydrogenase (ubiquinone) 1, subcomplex unknown, 2; similar to NADH dehydrogenase (ubiquinone) 1, subcomplex unknown, 2	-1.241	0.024
NM_001081252	UDP-glucose ceramide glucosyltransferase-like 2	-1.246	0.015
NM_001033293	UDP-N-acteylglucosamine pyrophosphorylase 1-like 1	-1.268	0.028
NM_024281	ribosome binding protein 1	-1.272	0.017
NM_012025	Rac GTPase-activating protein 1; predicted gene 1859	-1.276	0.001
NM_013495	carnitine palmitoyltransferase 1a, liver	-1.283	0.014
NM_130867	kin of IRRE like (Drosophila)	-1.291	0.002
NM_175212	transmembrane protein 65	-1.315	0.006
NM_001111279	WD repeat and FYVE domain containing 1	-1.320	0.001
NM_025816	Tax1 (human T-cell leukemia virus type I) binding protein 1	-1.333	0.030
NM_027371	brix domain containing 5	-1.352	0.029
NM_133983	CD276 antigen	-1.365	0.016
NM_020587	splicing factor, arginine/serine-rich 4 (SRp75)	-1.366	0.014
NM_020003	RIKEN cDNA 0610031J06 gene	-1.420	0.044
NM_145541	predicted gene 9392; similar to Raichu404X; RAS-related protein-1a	-1.432	0.001
NM_001111288	SCO cytochrome oxidase deficient homolog 2 (yeast)	-1.433	0.037
NM_176849	arginine and glutamate rich 1	-1.434	0.021
NM_024245	kinesin family member 23	-1.502	0.000
NM_146145	Janus kinase 1	-1.508	0.002
NM_152803	heparanase	-1.566	0.002
NM_027213	mediator of RNA polymerase II transcription, subunit 6 homolog (yeast)	-1.582	0.030
NM_023056	transmembrane protein 176B	-1.607	0.034
NM_026160	microtubule-associated protein 1 light chain 3 beta	-1.647	0.003
NM_024436	RAB22A, member RAS oncogene family	-1.684	0.028
NM_028181	cell cycle progression 1	-1.723	0.003
NM_183106	tetratricopeptide repeat domain 17	-1.896	0.001

Table 2-C: Differentially regulated CHO K1 proteins determined in samples corresponding to culture using spent media from CHO DP-12 cells prepared using a media dissolved oxygen content of 110%.

RefSeq Annotation	Description	Fold Change	p-value
NM_028975	transmembrane protein 33	1.826	0.020
NM_025538	alkB, alkylation repair homolog 7 (E. coli)	1.821	0.035
NM_011594	tissue inhibitor of metalloproteinase 2	1.803	0.004
NM_011333	chemokine (C-C motif) ligand 2	1.776	0.002
NM_009105	Ras suppressor protein 1	1.770	0.001
NM_146015	epidermal growth factor-containing fibulin-like extracellular matrix protein 1	1.751	0.014
NM_021528	carbohydrate sulfotransferase 12	1.728	0.002
NM_009103	ribonucleotide reductase M1	1.727	0.003
NM_133804	transmembrane protein 132A	1.727	0.003
NM_183016	CDC42 binding protein kinase beta	1.726	0.020
NM_145376	lysophosphatidylcholine acyltransferase 1	1.726	0.003
NM_177592	transmembrane protein 164	1.723	0.001
NM_001039644	ER degradation enhancer, mannosidase alpha-like 3	1.722	0.000
NM_009861	cell division cycle 42 homolog (S. cerevisiae); predicted gene 7407	1.721	0.006
NM_010517	insulin-like growth factor binding protein 4	1.719	0.001
NM_011961	procollagen lysine, 2-oxoglutarate 5-dioxygenase 2	1.718	0.006
NM_001013786	zinc finger protein 187	1.712	0.012
NM_001013616	tripartite motif-containing 6; similar to Tripartite motif protein 6	1.710	0.004
NM_011341	stromal cell derived factor 4	1.707	0.002
NM_001081357	mitogen-activated protein kinase kinase kinase kinase 3; similar to mitogen-activated protein kinase kinase kinase kinase 3	1.706	0.005
NP_067263	thymidylate synthase	1.705	0.015
NM_172769	sterol-C5-desaturase (fungal ERG3, delta-5-desaturase) homolog (S. cerevisae)	1.698	0.018
NM_030743	ring finger protein 114	1.698	0.016
NM_026186	coiled-coil domain containing 49	1.698	0.028
NM_011258	replication factor C (activator 1) 1	1.697	0.014
NM_011497	aurora kinase A	1.697	0.002
NM_199032	centrosomal protein 135	1.697	0.007
NM_009873	cyclin-dependent kinase 6	1.695	0.024
NM_001003949	open reading frame 61	1.693	0.022
NM_021519	predicted gene 11964; endothelial differentiation-related factor 1	1.688	0.031
NM_025364	predicted gene 6563; SAP domain containing ribonucleoprotein	1.688	0.012
NM_025788	nucleus accumbens associated 1, BEN and BTB (POZ) domain containing	1.688	0.011
NM_007838	dolichyl-di-phosphooligosaccharide-protein glycotransferase	1.688	0.005
NM_001033192	expressed sequence C78339	1.687	0.024
NM_029730	motile sperm domain containing 2	1.685	0.002
NM_011870	calcium and integrin binding 1 (calmyrin)	1.682	0.010
NM_025436	sterol-C4-methyl oxidase-like	1.680	0.009

NM_008562	similar to myeloid cell leukemia sequence 1; myeloid cell leukemia sequence 1	1.679	0.018
NM_011521	syndecan 4	1.679	0.002
NM_022985	zinc finger, AN1-type domain 6	1.678	0.022
NM_026560	cell division cycle associated 8	1.677	0.032
NM_025800	predicted gene 5490; protein phosphatase 1, regulatory (inhibitor) subunit 2; predicted gene 2780; predicted gene 7749; predicted gene 2802; hypothetical protein LOC639433	1.677	0.021
NM_018794	ATPase, H+ transporting, lysosomal accessory protein 1	1.675	0.005
NM_011068	peroxisomal biogenesis factor 11 alpha	1.674	0.011
NM_027194	TM2 domain containing 2	1.674	0.024
NM_144959	helicase-like transcription factor	1.669	0.040
NM_008163	growth factor receptor bound protein 2; predicted gene 12791	1.668	0.033
NM_007924	elongation factor RNA polymerase II	1.667	0.019
NM_177386	Scm-like with four mbt domains 2	1.665	0.039
NM_010189	Fc receptor, IgG, alpha chain transporter	1.664	0.037
NM_145150	protein regulator of cytokinesis 1	1.663	0.020
NM_009842	CD151 antigen	1.663	0.009
NM_009404	tumor necrosis factor (ligand) superfamily, member 9	1.658	0.001
NM_020010	cytochrome P450, family 51	1.658	0.043
NM_009177	ST3 beta-galactoside alpha-2,3-sialyltransferase 1	1.656	0.005
NM_054078	bromodomain adjacent to zinc finger domain, 2A	1.651	0.006
NM_144807	RIKEN cDNA 7120451J01 gene; choline phosphotransferase 1	1.650	0.006
NM_177619	MYST histone acetyltransferase 2	1.650	0.047
NM_020586	HERPUD family member 2	1.646	0.019
NM_001033533	coiled-coil domain containing 102A	1.646	0.033
NM_025401	predicted gene 5955; predicted gene 6803; ubiquitin-like 5; predicted gene 2001; similar to beacon	1.645	0.034
NM_176963	galactose mutarotase	1.644	0.047
NM_026176	phosducin-like	1.644	0.015
NM_028127	predicted gene 5780; FERM domain containing 6	1.642	0.008
NM_020559	aminolevulinic acid synthase 1	1.641	0.039
NP_001135450	TPX2, microtubule-associated protein homolog (Xenopus laevis)	1.639	0.008
NP_001104536	FK506 binding protein 8	1.637	0.005
NM_010917	similar to Nidogen precursor (Entactin); nidogen 1; similar to Nid1 protein	1.634	0.016
NM_010027	D-dopachrome tautomerase	1.626	0.006
NM_008684	neogenin	1.626	0.033
NM_025740	coiled-coil domain containing 104	1.625	0.003
NM_013615	outer dense fiber of sperm tails 2; similar to outer dense fiber of sperm tails 2	1.624	0.017
NM_201245	myosin phosphatase Rho interacting protein; predicted gene 8086	1.622	0.005
NP_032723	ninein	1.622	0.030
NM_008139	guanine nucleotide binding protein, alpha q polypeptide	1.619	0.036
NM_011173	protein S (alpha)	1.618	0.012
NM_172205	suprabasin	1.618	0.005
NM_138596	mediator of RNA polymerase II transcription, subunit 10 homolog (NUT2, S. cerevisiae)	1.618	0.001

NM_001033534	layilin	1.616	0.042
NP_001095925	amyloid beta (A4) precursor-like protein 2	1.615	0.028
NM_001163622	prolyl endopeptidase-like	1.613	0.005
NM_010015	defender against cell death 1	1.613	0.020
NP_001258682	DNA (cytosine-5)-methyltransferase 3A	1.612	0.020
NM_146211	glycosyltransferase 25 domain containing 1	1.611	0.003
NM_001143689	MHC class I like protein GS10	1.610	0.008
NM_144516	zinc finger, MYND domain containing 11	1.600	0.006
NM_011879	IK cytokine	1.596	0.009
NM_010117	rhomboid family 1 (Drosophila)	1.594	0.036
NM_010176	fumarylacetoacetate hydrolase	1.587	0.011
NM_025872	golgi transport 1 homolog B (S. cerevisiae)	1.579	0.046
NM_026950	OCIA domain containing 2	1.577	0.021
NM_021535	smu-1 suppressor of mec-8 and unc-52 homolog (C. elegans)	1.577	0.009
NM_133957	nuclear factor of activated T-cells 5	1.575	0.002
NM_145542	S-adenosylhomocysteine hydrolase-like 1	1.574	0.020
NM_053272	24-dehydrocholesterol reductase	1.573	0.044
NM_019883	predicted gene 5928; predicted gene 12617; predicted gene 4802; similar to ribosomal protein S27a; predicted gene 13215; predicted gene 6111; predicted gene 7808; predicted gene 6014; predicted gene 8317; ubiquitin C; ubiquitin B; similar to fusion protei	1.571	0.035
NM_013659	sema domain, immunoglobulin domain (Ig), transmembrane domain (TM) and short cytoplasmic domain, (semaphorin) 4B	1.565	0.046
NM_197980	COX19 cytochrome c oxidase assembly homolog (S. cerevisiae)	1.565	0.027
NM_001001932	early endosome antigen 1	1.563	0.004
NP_663432	polyadenylate binding protein-interacting protein 1; similar to poly(A) binding protein interacting protein 1	1.558	0.028
NM_175251	AT rich interactive domain 2 (ARID, RFX-like); RIKEN cDNA 1700124K17 gene	1.558	0.025
NM_008408	STT3, subunit of the oligosaccharyltransferase complex, homolog A (S. cerevisiae)	1.558	0.027
NM_175096	starch binding domain 1	1.558	0.040
NM_133913	RIKEN cDNA 2010209O12 gene	1.558	0.027
NM_024200	mitofusin 1	1.556	0.023
NM_012056	FK506 binding protein 9	1.554	0.002
NM_018864	inositol (myo)-1(or 4)-monophosphatase 1	1.546	0.021
NM_007841	DEAD (Asp-Glu-Ala-Asp) box polypeptide 6	1.545	0.000
NM_001039200	RIKEN cDNA C230096C10 gene	1.535	0.023
NM_008305	perlecan (heparan sulfate proteoglycan 2)	1.532	0.034
NM_019642	ribophorin II	1.532	0.011
NM_133662	immediate early response 3	1.530	0.019
NM_009883	CCAAT/enhancer binding protein (C/EBP), beta	1.524	0.040
NM_007659	cell division cycle 2 homolog A (S. pombe)	1.523	0.019
NM_139139	DnaJ (Hsp40) homolog, subfamily C, member 17; predicted gene 6257	1.522	0.032
NM_011414	secretory leukocyte peptidase inhibitor	1.516	0.014
NM_020050	TMEM9 domain family, member B	1.508	0.039
NM_027434	regulation of nuclear pre-mRNA domain containing 1B	1.504	0.002
NM_008539	MAD homolog 1 (Drosophila)	1.503	0.019

NM_146131	similar to Pre-B-cell leukemia transcription factor interacting protein 1; pre-B-cell leukemia transcription factor interacting protein 1	1.503	0.005
NM_028762	RNA binding motif protein 19	1.502	0.015
NM_018888	ubiquinol-cytochrome c reductase complex chaperone, CBP3 homolog (yeast)	1.500	0.011
NM_145997	lysine (K)-specific demethylase 5A	1.499	0.013
NM_197991	RIKEN cDNA 2310044H10 gene	1.499	0.012
NM_013885	chloride intracellular channel 4 (mitochondrial)	1.497	0.036
NM_001033297	predicted gene 561	1.497	0.009
NM_212450	CTD (carboxy-terminal domain, RNA polymerase II, polypeptide A) small phosphatase like 2	1.497	0.005
NM_172276	splicing factor, arginine/serine-rich 8	1.495	0.008
NM_013626	peptidylglycine alpha-amidating monooxygenase	1.493	0.022
NM_133900	phosphoserine phosphatase	1.490	0.000
NP_001034283	apoptosis-inducing factor, mitochondrion-associated 2	1.489	0.012
NM_133669	retinitis pigmentosa 2 homolog (human)	1.489	0.007
NM_133803	dipeptidylpeptidase 3	1.487	0.004
NM_172266	lysophosphatidylglycerol acyltransferase 1	1.486	0.017
NM_019693	HLA-B-associated transcript 1A	1.481	0.002
NM_011711	formin-like 3	1.474	0.014
NM_016786	ubiquitin-conjugating enzyme E2K (UBC1 homolog, yeast)	1.473	0.025
NM_009145	neuroplastin	1.471	0.030
NM_019832	G kinase anchoring protein 1	1.470	0.014
NM_007471	amyloid beta (A4) precursor protein	1.464	0.006
NM_172528	leucine rich repeat containing 1	1.462	0.040
NM_018768	syntaxin 8	1.458	0.004
NM_001001738	inositol 1,4,5-triphosphate receptor interacting protein	1.457	0.004
NM_053252	EH domain binding protein 1-like 1	1.457	0.009
NM_026964	coiled-coil domain containing 124	1.457	0.044
NM_010577	integrin alpha 5 (fibronectin receptor alpha)	1.453	0.033
NM_011962	procollagen-lysine, 2-oxoglutarate 5-dioxygenase 3	1.448	0.001
NM_009833	cyclin T1	1.444	0.033
NM_013790	ATP-binding cassette, sub-family C (CFTR/MRP), member 5	1.443	0.035
NM_145500	ubiquitin domain containing 1	1.442	0.039
NM_011693	vascular cell adhesion molecule 1	1.437	0.019
NM_175414	tetraspanin 9	1.433	0.023
NM_007886	dystrobrevin, beta	1.431	0.049
NM_019773	RAB9, member RAS oncogene family; predicted gene 9181	1.424	0.012
NM_011083	phosphatidylinositol 3-kinase, C2 domain containing, alpha polypeptide	1.420	0.040
NM_021548	cAMP-regulated phosphoprotein 19	1.420	0.025
NM_001004140	cytoskeleton associated protein 2	1.418	0.005
NM_009941	cytochrome c oxidase subunit IV isoform 1	1.417	0.002
NM_145553	predicted gene 7527; family with sequence similarity 76, member A	1.417	0.008
NM_207625	acyl-CoA synthetase long-chain family member 4	1.416	0.019
NM_207298	cerebral endothelial cell adhesion molecule	1.411	0.038

NM_001164663	hypothetical protein LOC639171; RIKEN cDNA 9830001H06 gene; similar to C34E11.3	1.409	0.016
NM_011218	protein tyrosine phosphatase, receptor type, S	1.405	0.036
NM_207209	similar to SEC24 related gene family, member B (S. cerevisiae); Sec24 related gene family, member B (S. cerevisiae)	1.404	0.020
NM_008875	phospholipase D1	1.398	0.035
NM_019975	2-hydroxyacyl-CoA lyase 1	1.396	0.015
NM_010755	v-maf musculoaponeurotic fibrosarcoma oncogene family, protein F (avian)	1.395	0.033
NM_008255	3-hydroxy-3-methylglutaryl-Coenzyme A reductase	1.387	0.028
NM_026130	signal recognition particle receptor ('docking protein')	1.385	0.028
NM_008047	follistatin-like 1	1.385	0.020
NM_026252	cytoplasmic polyadenylation element binding protein 4	1.382	0.008
NM_027450	GLI pathogenesis-related 2	1.381	0.049
NM_025594	zinc finger, matrin type 2	1.379	0.030
NM_008972	predicted gene 12504; predicted gene 9800; predicted gene 4617; predicted gene 6625; predicted gene 7614; similar to prothymosin alpha; prothymosin alpha; predicted gene 9009	1.371	0.042
NM_027238	tetratricopeptide repeat domain 39B	1.370	0.009
NM_001123371	purine-nucleoside phosphorylase 2	1.370	0.007
NM_010833	moesin	1.369	0.019
NM_015804	ATPase, class VI, type 11A	1.364	0.015
NM_197982	DEAD (Asp-Glu-Ala-Asp) box polypeptide 39	1.363	0.012
NM_010516	cysteine rich protein 61	1.361	0.030
NM_025463	hypothetical protein LOC100048454; RIKEN cDNA 1810009A15 gene	1.358	0.029
NM_021460	lysosomal acid lipase A	1.358	0.037
NM_199199	transmembrane protein 199	1.350	0.044
NM_010580	integrin beta 5	1.349	0.018
NP_031641	catenin (cadherin associated protein), delta 1	1.349	0.006
NM_001166450	solute carrier family 25 (mitochondrial carrier, brain), member 14	1.347	0.035
NM_053257	predicted gene 10191; predicted gene 7689; predicted gene 9401; similar to ribosomal protein L31; hypothetical protein LOC675768; predicted gene 13004; predicted gene 9228; predicted gene 10072; predicted gene 5437; predicted gene 9154; ribosomal protein	1.344	0.021
NM_030252	cDNA sequence BC003266	1.344	0.017
NM_010356	glutathione S-transferase, alpha 3	1.342	0.046
NM_009480	upstream transcription factor 1	1.341	0.004
NM_025983	ATP synthase, H+ transporting, mitochondrial F1 complex, epsilon subunit	1.339	0.045
NM_053075	Ras homolog enriched in brain; similar to RAS-homolog enriched in brain	1.338	0.009
NM_025846	related RAS viral (r-ras) oncogene homolog 2	1.337	0.000
NM_153807	acyl-CoA synthetase family member 2	1.331	0.016
NP_001186624	Alpha-taxilin	1.330	0.002
NM_133933	ribophorin I	1.326	0.003
NM_175512	dehydrogenase/reductase (SDR family) member 9	1.326	0.018
NM_194342	unc-84 homolog B (C. elegans)	1.325	0.012
NM_033320	glucuronyl C5-epimerase	1.322	0.008

NM_007404	a disintegrin and metallopeptidase domain 9 (meltrin gamma)	1.319	0.014
NM_007879	developmentally regulated GTP binding protein 1	1.318	0.041
NM_133808	high density lipoprotein (HDL) binding protein	1.318	0.005
NM_007840	DEAD (Asp-Glu-Ala-Asp) box polypeptide 5; predicted gene 12183	1.317	0.033
NM_001081282	inhibitor of Bruton agammaglobulinemia tyrosine kinase	1.316	0.025
NM_019640	phosphatidylinositol transfer protein, beta	1.316	0.041
NM_001045529	microrchidia 3	1.315	0.004
NM_026420	polyadenylate-binding protein-interacting protein 2	1.313	0.010
NM_001081251	polybromo 1	1.313	0.013
NM_134063	cDNA sequence BC016423	1.311	0.019
NM_019972	sortilin 1	1.309	0.040
NM_009825	serine (or cysteine) peptidase inhibitor, clade H, member 1	1.305	0.007
NM_007616	caveolin 1, caveolae protein	1.298	0.039
NM_021412	matrix metallopeptidase 19	1.293	0.012
NM_025516	ERGIC and golgi 3	1.290	0.029
NM_175021	sterile alpha motif domain containing 4B	1.290	0.012
NM_145959	DNA segment, Chr 15, ERATO Doi 621, expressed	1.289	0.035
NP_001153413	potassium channel tetramerisation domain containing 10	1.288	0.035
NM_144937	ubiquitin specific peptidase 3	1.283	0.008
NM_011116	phospholipase D family, member 3	1.283	0.025
NM_032008	sarcolemma associated protein	1.280	0.002
NM_021336	small nuclear ribonucleoprotein polypeptide A'	1.279	0.014
NM_021414	S-adenosylhomocysteine hydrolase-like 2	1.275	0.000
NM_027153	pirin	1.270	0.004
NM_133943	hydroxy-delta-5-steroid dehydrogenase, 3 beta- and steroid delta-isomerase 7	1.259	0.013
NM_175646	thioredoxin-like 4B	1.258	0.027
NM_134077	RNA binding motif protein 26	1.256	0.034
NM_009153	sema domain, immunoglobulin domain (Ig), short basic domain, secreted, (semaphorin) 3B	1.255	0.025
NM_001033136	family with sequence similarity 82, member A2	1.255	0.040
NM_175226	ring finger protein 139	1.253	0.049
NM_053187	golgi associated PDZ and coiled-coil motif containing	1.243	0.024
NM_013502	similar to CtBP1 protein; C-terminal binding protein 1	1.242	0.046
NM_009273	signal recognition particle 14	1.237	0.035
NM_011738	tyrosine 3-monooxygenase/tryptophan 5-monooxygenase activation protein, eta polypeptide	1.233	0.008
NP_001258827	Peroxisomal acyl-coenzyme A oxidase 1	1.233	0.030
NM_017478	coatomer protein complex, subunit gamma 2	1.219	0.028
NM_024459	protein phosphatase 3, regulatory subunit B, alpha isoform (calcineurin B, type I)	1.216	0.050
NP_001123951	nucleobindin 2	1.211	0.024
NM_026844	RIKEN cDNA 2310061C15 gene	1.209	0.032
NM_025429	serine (or cysteine) peptidase inhibitor, clade B, member 1a	1.207	0.016
NM_011035	p21 protein (Cdc42/Rac)-activated kinase 1	1.206	0.014
NM_019663	protein inhibitor of activated STAT 1	1.203	0.011
NM_019783	leprecan 1	1.202	0.011

NM_001039162	CAP-GLY domain containing linker protein 2	-1.203	0.019
NM_133826	ATPase, H+ transporting, lysosomal V1 subunit H	-1.203	0.004
NM_180678	glycyl-tRNA synthetase	-1.207	0.019
NM_177474	DNA segment, Chr 19, Brigham & Women's Genetics 1357 expressed	-1.210	0.017
NM_024281	ribosome binding protein 1	-1.211	0.026
NM_013676	suppressor of Ty 5 homolog (S. cerevisiae)	-1.212	0.001
NM_001163026	DnaJ (Hsp40) homolog, subfamily C, member 13	-1.212	0.005
NM_025996	translocase of outer mitochondrial membrane 34	-1.215	0.010
NM_181072	myosin IE	-1.218	0.020
NM_138579	TRIO and F-actin binding protein	-1.222	0.036
NM_010546	inhibitor of kappaB kinase beta	-1.227	0.013
NM_001035854	adaptor-related protein complex 2, beta 1 subunit	-1.230	0.014
NM_153569	cyclin G associated kinase	-1.231	0.025
NM_001080775	similar to nuclear myosin I beta; myosin IC	-1.232	0.013
NM_133771	mediator of cell motility 1; similar to Memo1 protein	-1.233	0.028
NM_057171	HLA-B-associated transcript 3	-1.234	0.023
NM_022811	polymerase (RNA) I polypeptide E	-1.235	0.036
NM_011150	lectin, galactoside-binding, soluble, 3 binding protein	-1.239	0.012
NM_025513	exosome component 3	-1.239	0.029
NM_175155	SAM and SH3 domain containing 1; predicted gene 2082	-1.242	0.032
NM_029103	mesencephalic astrocyte-derived neurotrophic factor	-1.243	0.026
NM_145354	NOL1/NOP2/Sun domain family member 2	-1.248	0.019
NM_153774	importin 9	-1.256	0.006
NM_133692	polymerase (DNA-directed), delta 3, accessory subunit	-1.256	0.009
NM_028162	TBC1 domain family, member 5	-1.259	0.021
NM_138745	methylenetetrahydrofolate dehydrogenase (NADP+ dependent), methenyltetrahydrofolate cyclohydrolase, formyltetrahydrofolate synthase	-1.260	0.016
NM_007803	cortactin; predicted gene 8786	-1.260	0.003
NM_021888	queuine tRNA-ribosyltransferase 1	-1.260	0.046
NM_027604	ubiquitin specific peptidase 15	-1.267	0.005
NM_023912	SCY1-like 1 (S. cerevisiae)	-1.267	0.045
NM_007508	ATPase, H+ transporting, lysosomal V1 subunit A	-1.269	0.004
NM_026833	open reading frame 19	-1.280	0.017
NM_011874	proteasome (prosome, macropain) 26S subunit, ATPase, 4	-1.284	0.010
NM_023644	methylcrotonoyl-Coenzyme A carboxylase 1 (alpha)	-1.284	0.047
NM_022018	family with sequence similarity 129, member A	-1.286	0.013
NM_153585	CCR4-NOT transcription complex, subunit 10	-1.295	0.023
NM_009439	proteasome (prosome, macropain) 26S subunit, non-ATPase, 3	-1.298	0.002
NM_134137	leucyl-tRNA synthetase	-1.304	0.020
NM_001030307	dyskeratosis congenita 1, dyskerin homolog (human)	-1.304	0.016
NM_021552	predicted gene 15596; RIKEN cDNA 5730427N09 gene; similar to TGF beta-inducible nuclear protein 1 (L-name related LNR42); predicted gene 7966; predicted gene 5515; predicted gene 9722; predicted gene 6451; predicted gene 9634	-1.307	0.046
NM_054056	PRKC, apoptosis, WT1, regulator	-1.308	0.039
NM_030210	acetoacetyl-CoA synthetase	-1.314	0.030

NP_001005331	eukaryotic translation initiation factor 4, gamma 1	-1.315	0.042
NM_009837	chaperonin containing Tcp1, subunit 4 (delta)	-1.316	0.031
NM_001160319	ubiquitin protein ligase E3 component n-recognin 4	-1.317	0.015
NM_026658	mitochondrial translation optimization 1 homolog (S. cerevisiae)	-1.322	0.012
NM_026653	replication protein A1	-1.328	0.018
NM_022027	synaptic nuclear envelope 1	-1.329	0.043
NM_022410	myosin, heavy polypeptide 9, non-muscle	-1.344	0.029
NM_027250	RIKEN cDNA 2010305A19 gene	-1.345	0.050
NM_016748	cytidine 5'-triphosphate synthase	-1.346	0.018
NP_033778	A kinase (PRKA) anchor protein 1	-1.346	0.005
NM_015787	histone cluster 1, H1e	-1.348	0.031
NM_009679	predicted gene 8717; adaptor protein complex AP-2, mu1	-1.349	0.009
NM_011811	phenylalanyl-tRNA synthetase, beta subunit	-1.354	0.013
NM_021315	nucleolar complex associated 3 homolog (S. cerevisiae)	-1.354	0.004
NM_198645	coiled-coil domain containing 58	-1.354	0.033
NP_705782	aldehyde dehydrogenase 18 family, member A1	-1.355	0.012
NM_007509	ATPase, H+ transporting, lysosomal V1 subunit B2	-1.359	0.001
NM_011654	predicted gene 3756; tubulin, alpha 1B; predicted gene 5620; similar to alpha-tubulin isotype M-alpha-2; predicted gene 14150; predicted gene 3226	-1.359	0.003
NM_011777	zyxin	-1.360	0.018
NM_029878	tubulin-specific chaperone d	-1.360	0.004
NM_133916	hypothetical protein LOC100047993; eukaryotic translation initiation factor 3, subunit B	-1.362	0.010
NM_001033375	RIKEN cDNA A230046K03 gene	-1.370	0.019
NP_001185796	Dynactin subunit 1	-1.371	0.041
NM_011049	PCTAIRE-motif protein kinase 1	-1.371	0.038
NM_001164677	programmed cell death 6 interacting protein	-1.377	0.033
NM_026396	brix domain containing 2	-1.380	0.016
NM_019966	malonyl-CoA decarboxylase	-1.384	0.007
NM_027815	RIKEN cDNA 9030624J02 gene	-1.385	0.046
NM_139063	muted	-1.387	0.028
XP_003085306	Polyadenylate -binding protein 1-like 2	-1.390	0.005
NM_138593	similar to La ribonucleoprotein domain family, member 7; La ribonucleoprotein domain family, member 7	-1.391	0.010
NM_021473	aldo-keto reductase family 1, member A4 (aldehyde reductase)	-1.393	0.010
NM_019553	DEAD (Asp-Glu-Ala-Asp) box polypeptide 21	-1.394	0.033
NM_021514	phosphofructokinase, muscle	-1.395	0.010
NM_080463	protein O-fucosyltransferase 1	-1.398	0.010
NM_080445	similar to UDP-Gal:betaGal beta 1,3-galactosyltransferase, polypeptide 6; UDP-Gal:betaGal beta 1,3-galactosyltransferase, polypeptide 6	-1.398	0.006
NM_029633	CLIP associating protein 2	-1.401	0.041
NM_021303	nucleolar complex associated 2 homolog (S. cerevisiae)	-1.411	0.019
NM_001128601	5, 10-methenyltetrahydrofolate synthetase; predicted gene 2372; predicted gene 2382	-1.427	0.046
NM_199447	ribosomal RNA processing 12 homolog (S. cerevisiae)	-1.427	0.018
NM_146200	eukaryotic translation initiation factor 3, subunit C; similar to Eukaryotic translation initiation factor 3, subunit 8	-1.427	0.019

NM_011714	bromodomain adjacent to zinc finger domain, 1B	-1.430	0.029
NM_023525	carbamoyl-phosphate synthetase 2, aspartate transcarbamylase, and dihydroorotase	-1.434	0.005
NM_009703	v-raf murine sarcoma 3611 viral oncogene homolog	-1.435	0.014
NM_175287	RIKEN cDNA A430005L14 gene; hypothetical protein LOC676530; predicted gene 12247	-1.435	0.041
NM_017379	tubulin, alpha 8	-1.436	0.022
NM_025536	COMM domain containing 5	-1.449	0.033
NM_030238	dynein cytoplasmic 1 heavy chain 1	-1.451	0.001
NM_009288	serine/threonine kinase 10	-1.453	0.018
NM_018799	eukaryotic translation initiation factor 3, subunit I	-1.456	0.020
NM_026825	leucine rich repeat containing 16A	-1.457	0.034
NM_199068	forkhead box K1	-1.457	0.034
NM_011125	phospholipid transfer protein	-1.460	0.008
NM_025706	TBC1 domain family, member 15	-1.461	0.010
NM_016905	galactokinase 1	-1.461	0.008
NM_013507	eukaryotic translation initiation factor 4, gamma 2	-1.463	0.029
NM_010123	eukaryotic translation initiation factor 3, subunit A	-1.464	0.003
NM_033074	threonyl-tRNA synthetase	-1.467	0.000
NM_147778	COMM domain containing 3	-1.468	0.040
NM_026969	Sec31 homolog A (S. cerevisiae)	-1.481	0.018
NM_001033293	UDP-N-acteylglucosamine pyrophosphorylase 1-like 1	-1.482	0.000
NM_146066	G1 to S phase transition 1	-1.482	0.029
NM_026473	tubulin, beta 6	-1.485	0.024
NM_146217	alanyl-tRNA synthetase	-1.485	0.013
NM_007408	adipose differentiation related protein	-1.486	0.021
NM_028003	RNA polymerase II associated protein 3; predicted gene 5697	-1.496	0.028
NM_022314	predicted gene 7848; predicted gene 7839; predicted gene 4157; similar to tropomyosin 3, gamma; tropomyosin 3, gamma; predicted gene 4903	-1.505	0.009
NM_177644	RAS protein activator like 2	-1.510	0.004
NM_175109	ribosomal protein S19 binding protein 1	-1.515	0.034
NM_021312	WD repeat domain 12; predicted gene 4879	-1.517	0.009
NM_008892	polymerase (DNA directed), alpha 1	-1.523	0.040
NM_153065	DEAD (Asp-Glu-Ala-Asp) box polypeptide 27	-1.524	0.015
NP_001165617	aminoacyl tRNA synthetase complex-interacting multifunctional protein 2	-1.526	0.001
NM_027000	GTP binding protein 4	-1.530	0.005
NM_025595	mitochondrial ribosomal protein L51	-1.535	0.015
NP_733469	copine I	-1.538	0.004
NM_153119	pleckstrin homology domain containing, family O member 2	-1.542	0.005
NM_025310	FtsJ homolog 3 (E. coli)	-1.545	0.018
NM_080638	major vault protein	-1.546	0.002
NM_145620	RRP9, small subunit (SSU) processome component, homolog (yeast)	-1.566	0.008
NM_025664	similar to Sorting nexin 9; sorting nexin 9	-1.567	0.010
NM_027375	GRIP and coiled-coil domain containing 2	-1.578	0.043
NM_007510	ATPase, H+ transporting, lysosomal V1 subunit E1	-1.579	0.005

NM_011830	predicted gene 15210; inosine 5'-phosphate dehydrogenase 2	-1.579	0.017
NM_145507	aspartyl-tRNA synthetase	-1.585	0.015
NM_013742	cysteinyl-tRNA synthetase	-1.585	0.024
NM_011829	inosine 5'-phosphate dehydrogenase 1	-1.593	0.016
NP_001107603	protein phosphatase 4, regulatory subunit 1	-1.594	0.017
NM_010212	four and a half LIM domains 2	-1.596	0.001
NM_008033	farnesyltransferase, CAAX box, alpha; similar to farnesyltransferase alpha subunit	-1.603	0.025
NM_001038589	ubiquitin specific peptidase 14	-1.605	0.007
NM_026788	methylenetetrahydrofolate dehydrogenase (NADP+ dependent) 2-like	-1.607	0.008
NM_021448	elongation protein 2 homolog (S. cerevisiae)	-1.610	0.020
NM_025918	coiled-coil domain containing 43	-1.618	0.022
NM_027498	similar to Serine/threonine-protein kinase QSK; cDNA sequence BC033915	-1.621	0.007
NM_025380	eukaryotic translation elongation factor 1 epsilon 1	-1.625	0.000
NM_025494	ATPase, H+ transporting, lysosomal V1 subunit C1	-1.636	0.005
NM_013562	interferon-related developmental regulator 1	-1.636	0.006
NM_001033318	component of oligomeric golgi complex 7	-1.645	0.043
NM_133775	interleukin 33	-1.647	0.041
NM_153125	SEC16 homolog A (S. cerevisiae)	-1.659	0.027
NM_134188	acyl-CoA thioesterase 2	-1.660	0.021
NM_029005	mixed lineage kinase domain-like	-1.663	0.040
NM_178623	RIKEN cDNA 2010005J08 gene	-1.663	0.018
NM_019795	DnaJ (Hsp40) homolog, subfamily C, member 7	-1.667	0.018
NM_153116	GTP-binding protein 10 (putative); predicted gene 6877	-1.675	0.029
NM_013752	nibrin	-1.686	0.018
NM_001037746	mirror-image polydactyly gene 1 homolog (human); phosphoribosyl pyrophosphate synthetase 1; phosphoribosyl pyrophosphate synthetase 1-like 1	-1.688	0.028
NM_181348	RIKEN cDNA A230083H22 gene	-1.696	0.010
NM_153164	predicted gene 6158; CCR4-NOT transcription complex, subunit 1	-1.707	0.033
NM_028427	transmembrane protein 192	-1.711	0.011
NM_172582	coenzyme Q6 homolog (yeast)	-1.714	0.011
NM_054102	influenza virus NS1A binding protein	-1.718	0.001
NM_054099	RIKEN cDNA 1110038F14 gene	-1.729	0.001
NM_138603	coiled-coil domain containing 22	-1.731	0.012

Table 2-D: Differentially regulated CHO K1 proteins determined in samples corresponding to culture using spent media from CHO DP-12 cells prepared using a media dissolved oxygen content of 60%.

RefSeq Annotation	Description	Fold Change	p-value
NM_011333	chemokine (C-C motif) ligand 2	1.761	0.004
NM_054078	bromodomain adjacent to zinc finger domain, 2A	1.749	0.010

NM_133957	nuclear factor of activated T-cells 5	1.730	0.017
NP_001258682	DNA (cytosine-5)-methyltransferase 3A	1.728	0.002
NM_021528	carbohydrate sulfotransferase 12	1.707	0.014
NM_028945	DNA segment, Chr 14, Abbott 1 expressed	1.701	0.018
NM_009103	ribonucleotide reductase M1	1.699	0.029
NM_199032	centrosomal protein 135	1.692	0.007
NM_001013616	tripartite motif-containing 6; similar to Tripartite motif protein 6	1.691	0.011
NM_011341	stromal cell derived factor 4	1.690	0.001
NM_010235	fos-like antigen 1	1.685	0.027
NM_011961	procollagen lysine, 2-oxoglutarate 5-dioxygenase 2	1.683	0.005
NM_025788	nucleus accumbens associated 1, BEN and BTB (POZ) domain containing	1.678	0.010
NM_001033534	layilin	1.665	0.045
NM_001081357	mitogen-activated protein kinase kinase kinase kinase 3; similar to mitogen-activated protein kinase kinase kinase kinase 3	1.656	0.007
NM_001039644	ER degradation enhancer, mannosidase alpha-like 3	1.653	0.005
NP_067263	thymidylate synthase	1.644	0.040
NM_133804	transmembrane protein 132A	1.641	0.011
NM_010117	rhomboid family 1 (Drosophila)	1.637	0.047
NM_197999	RIKEN cDNA 2210023G05 gene	1.621	0.049
NM_172205	suprabasin	1.620	0.018
NM_009186	transformer 2 beta homolog (Drosophila); predicted gene 6439	1.612	0.016
NM_001039522	Leo1, Paf1/RNA polymerase II complex component, homolog (S. cerevisiae)	1.611	0.038
NM_001080931	mediator complex subunit 13	1.611	0.047
NM_012056	FK506 binding protein 9	1.610	0.008
NM_024459	protein phosphatase 3, regulatory subunit B, alpha isoform (calcineurin B, type I)	1.608	0.002
NM_001081163	similar to mKIAA0990 protein; chondroitin sulfate synthase 1	1.601	0.039
NM_028762	RNA binding motif protein 19	1.595	0.030
NM_028975	transmembrane protein 33	1.595	0.024
NM_009177	ST3 beta-galactoside alpha-2,3-sialyltransferase 1	1.590	0.006
NM_009404	tumor necrosis factor (ligand) superfamily, member 9	1.584	0.003
NM_146211	glycosyltransferase 25 domain containing 1	1.577	0.013
NM_029730	motile sperm domain containing 2	1.569	0.007
NM_212450	CTD (carboxy-terminal domain, RNA polymerase II, polypeptide A) small phosphatase like 2	1.567	0.001
NM_029581	mitochondrial translational initiation factor 3	1.561	0.013
NM_011962	procollagen-lysine, 2-oxoglutarate 5-dioxygenase 3	1.560	0.000
NM_144814	REST corepressor 3	1.544	0.031
NM_010517	insulin-like growth factor binding protein 4	1.540	0.028
NM_023645	KDEL (Lys-Asp-Glu-Leu) containing 1	1.525	0.045
NM_021460	lysosomal acid lipase A	1.519	0.002
NM_008255	3-hydroxy-3-methylglutaryl-Coenzyme A reductase	1.516	0.049
NM_001033297	predicted gene 561	1.490	0.044
NM_001033533	coiled-coil domain containing 102A	1.482	0.023
NM_172266	lysophosphatidylglycerol acyltransferase 1	1.481	0.040
NM_010516	cysteine rich protein 61	1.479	0.004

NP_001106817	similar to Transcriptional repressor p66 alpha (GATA zinc finger domain-containing protein 2A); GATA zinc finger domain containing 2A	1.477	0.016
NM_026950	OCIA domain containing 2	1.465	0.020
NM_011580	thrombospondin 1; similar to thrombospondin 1	1.444	0.012
NM_025740	coiled-coil domain containing 104	1.433	0.016
NP_001159505	general transcription factor IIIC, polypeptide 4	1.433	0.007
NM_010799	predicted gene 12818; multiple inositol polyphosphate histidine phosphatase 1	1.432	0.023
NM_011879	IK cytokine	1.423	0.000
NM_001146296	adenosine deaminase, RNA-specific	1.421	0.044
NM_027658	similar to hexamthylene bis-acetamide inducible 2; hexamthylene bis-acetamide inducible 2	1.409	0.012
NM_029620	procollagen C-endopeptidase enhancer 2	1.390	0.047
NM_008917	palmitoyl-protein thioesterase 1	1.389	0.040
NM_026186	coiled-coil domain containing 49	1.386	0.048
NM_153421	polyhomeotic-like 3 (Drosophila)	1.384	0.039
NM_080558	sperm specific antigen 2	1.379	0.010
NM_001081340	SET domain containing 2	1.373	0.002
NM_007392	actin, alpha 2, smooth muscle, aorta	1.371	0.027
NM_138596	mediator of RNA polymerase II transcription, subunit 10 homolog (NUT2, S. cerevisiae)	1.371	0.002
NM_010580	integrin beta 5	1.365	0.024
NM_026252	cytoplasmic polyadenylation element binding protein 4	1.364	0.030
NM_001163741	RIKEN cDNA 1110021J02 gene	1.361	0.032
NM_025554	polymerase (RNA) II (DNA directed) polypeptide E	1.358	0.008
NM_144954	peptidylprolyl isomerase (cyclophilin)-like 2	1.352	0.016
NM_027373	actin filament associated protein 1	1.344	0.001
NM_145619	poly (ADP-ribose) polymerase family, member 3	1.343	0.003
NM_026130	signal recognition particle receptor ('docking protein')	1.341	0.013
NM_178367	DEAH (Asp-Glu-Ala-His) box polypeptide 33	1.341	0.038
NM_145215	abhydrolase domain containing 11	1.339	0.024
NM_172276	splicing factor, arginine/serine-rich 8	1.338	0.011
NM_025783	vacuolar protein sorting 24 (yeast); predicted gene 7464	1.332	0.041
NP_001104536	FK506 binding protein 8	1.326	0.011
NM_153783	polyamine oxidase (exo-N4-amino)	1.322	0.003
NM_001164663	hypothetical protein LOC639171; RIKEN cDNA 9830001H06 gene; similar to C34E11.3	1.321	0.001
NM_175153	RIKEN cDNA 2010321M09 gene	1.314	0.026
NM_009825	serine (or cysteine) peptidase inhibitor, clade H, member 1	1.303	0.006
NM_146239	PCTAIRE-motif protein kinase 2	1.302	0.049
NM_007840	DEAD (Asp-Glu-Ala-Asp) box polypeptide 5; predicted gene 12183	1.300	0.047
NM_153412	pleckstrin homology-like domain, family B, member 2	1.284	0.002
NM_018774	polyhomeotic-like 2 (Drosophila)	1.280	0.042
NM_023403	mesoderm development candidate 2	1.272	0.018
NM_001163622	prolyl endopeptidase-like	1.266	0.003
NM_145553	predicted gene 7527; family with sequence similarity 76, member A	1.262	0.037

NM_018888	ubiquinol-cytochrome c reductase complex chaperone, CBP3 homolog (yeast)	1.257	0.004
NM_029365	mediator of RNA polymerase II transcription, subunit 25 homolog (yeast)	1.250	0.006
NM_153559	quiescin Q6 sulfhydryl oxidase 2	1.237	0.012
NM_028017	N-ethylmaleimide sensitive fusion protein attachment protein gamma	1.233	0.029
NM_021412	matrix metallopeptidase 19	1.218	0.028
NM_177592	transmembrane protein 164	1.214	0.013
NM_019975	2-hydroxyacyl-CoA lyase 1	1.213	0.019
NM_033320	glucuronyl C5-epimerase	1.208	0.029
NM_172259	myosin, light polypeptide 6B	1.208	0.016
NM_198160	SWI/SNF related, matrix associated, actin dependent regulator of chromatin, subfamily c, member 2	1.207	0.038
NM_011521	syndecan 4	1.207	0.028
NM_001033136	family with sequence similarity 82, member A2	1.202	0.020
NM_019966	malonyl-CoA decarboxylase	-1.202	0.035
NM_028276	UTP14, U3 small nucleolar ribonucleoprotein, homolog A (yeast)	-1.204	0.044
NM_146200	eukaryotic translation initiation factor 3, subunit C; similar to Eukaryotic translation initiation factor 3, subunit 8	-1.205	0.050
NM_010442	heme oxygenase (decycling) 1	-1.206	0.020
NM_017379	tubulin, alpha 8	-1.209	0.025
XP_003085306	Polyadenylate-binding protein 1-like 2	-1.211	0.012
NM_138745	methylenetetrahydrofolate dehydrogenase (NADP+ dependent), methenyltetrahydrofolate cyclohydrolase, formyltetrahydrofolate synthase	-1.212	0.027
NM_170669	predicted gene 13048; predicted gene 11968; predicted gene 13253; predicted gene 14166; predicted gene 10196; similar to ribosomal protein S15a; predicted gene 5623; ribosomal protein S15A; similar to hCG1994130; predicted gene 7263	-1.214	0.031
NM_011654	predicted gene 3756; tubulin, alpha 1B; predicted gene 5620; similar to alpha-tubulin isotype M-alpha-2; predicted gene 14150; predicted gene 3226	-1.216	0.042
NM_011291	predicted gene 4754; ribosomal protein L7; predicted gene 12174; LOC100049084; predicted gene 6543; predicted gene 7059; predicted gene 4734	-1.223	0.015
NM_023060	eukaryotic elongation factor, selenocysteine-tRNA-specific	-1.227	0.021
NM_018829	adaptor-related protein complex 3, mu 1 subunit; similar to Adapter-related protein complex 3 mu 1 subunit (Mu-adaptin 3A) (AP-3 adapter complex mu3A subunit)	-1.239	0.021
NP_705782	aldehyde dehydrogenase 18 family, member A1	-1.244	0.019
NM_025380	eukaryotic translation elongation factor 1 epsilon 1	-1.256	0.036
NM_019808	PDZ and LIM domain 5	-1.257	0.024
NM_026545	proteasome (prosome, macropain) 26S subunit, non-ATPase, 8	-1.262	0.037
NM_172735	zinc finger, C3HC type 1	-1.267	0.038
NM_146217	alanyl-tRNA synthetase	-1.268	0.014
NM_013507	eukaryotic translation initiation factor 4, gamma 2	-1.280	0.046
NM_134137	leucyl-tRNA synthetase	-1.283	0.036
NM_013742	cysteinyl-tRNA synthetase	-1.299	0.010
NM_011975	predicted gene 14439; predicted gene 8213; predicted gene 13981; predicted gene 8451; predicted gene 6378; predicted gene	-1.315	0.001

	8667; predicted gene 4923; predicted gene 5908; ribosomal protein L27a; predicted gene 14044; predicted gene 7536; predicted gene 144		
NM_145546	general transcription factor IIB	-1.318	0.009
NM_009082	similar to ribosomal protein; predicted gene 6344; predicted gene 11449; predicted gene 13841; predicted gene 8210; hypothetical protein LOC675793; ribosomal protein L29; predicted gene 12704; predicted gene 7252; predicted gene 8965; predicted gene 13213	-1.318	0.002
NM_023525	carbamoyl-phosphate synthetase 2, aspartate transcarbamylase, and dihydroorotase	-1.320	0.025
NM_013454	ATP-binding cassette, sub-family A (ABC1), member 1	-1.321	0.040
NM_028636	mannosidase, alpha, class 2C, member 1	-1.321	0.029
NM_198007	activating signal cointegrator 1 complex subunit 3	-1.324	0.023
NM_053181	pyridoxal-dependent decarboxylase domain containing 1	-1.329	0.009
NM_023372	similar to ribosomal protein L38; predicted gene 13020; ribosomal protein L38; predicted gene 4991; karyopherin (importin) alpha 2; predicted gene 9028; predicted gene 8129; predicted gene 7123; predicted gene 5832; predicted gene 10184; predicted gene 73	-1.330	0.040
NM_028032	protein phosphatase 2 (formerly 2A), regulatory subunit B (PR 52), alpha isoform	-1.347	0.011
NM_021514	phosphofructokinase, muscle	-1.350	0.006
NP_001135450	TPX2, microtubule-associated protein homolog (Xenopus laevis)	-1.352	0.037
NM_080638	major vault protein	-1.360	0.006
NM_133973	component of oligomeric golgi complex 4	-1.368	0.027
NM_026969	Sec31 homolog A (S. cerevisiae)	-1.370	0.043
NM_009391	RAS-like, family 2, locus 9; RAN, member RAS oncogene family; similar to RAN, member RAS oncogene family	-1.379	0.019
NM_019581	GTP binding protein 2	-1.386	0.011
NM_008388	eukaryotic translation initiation factor 3, subunit E	-1.393	0.010
NM_011889	septin 3	-1.395	0.014
NM_028390	anillin, actin binding protein	-1.402	0.012
NM_033074	threonyl-tRNA synthetase	-1.406	0.004
NM_027815	RIKEN cDNA 9030624J02 gene	-1.408	0.007
NM_016905	galactokinase 1	-1.409	0.025
NM_153058	microtubule-associated protein, RP/EB family, member 2	-1.409	0.046
NM_028427	transmembrane protein 192	-1.409	0.043
NM_025494	ATPase, H+ transporting, lysosomal V1 subunit C1	-1.409	0.006
NM_011874	proteasome (prosome, macropain) 26S subunit, ATPase, 4	-1.421	0.004
NM_001045489	milk fat globule-EGF factor 8 protein	-1.422	0.021
NM_001080929	cerebellar degeneration-related protein 2-like	-1.431	0.021
NM_133900	phosphoserine phosphatase	-1.435	0.009
NM_011484	signal transducing adaptor molecule (SH3 domain and ITAM motif) 1	-1.444	0.032
NP_001165617	aminoacyl tRNA synthetase complex-interacting multifunctional protein 2	-1.455	0.048
NM_012003	COP9 (constitutive photomorphogenic) homolog, subunit 7a (Arabidopsis thaliana)	-1.458	0.001
NP_955769	Protein FAM63A	-1.458	0.030
NM_008033	farnesyltransferase, CAAX box, alpha; similar to farnesyltransferase alpha subunit	-1.468	0.001
NM_007386	aconitase 1	-1.470	0.019

NM_010123	eukaryotic translation initiation factor 3, subunit A	-1.485	0.002
NM_024281	ribosome binding protein 1	-1.488	0.015
NM_018799	eukaryotic translation initiation factor 3, subunit I	-1.498	0.012
NM_010212	four and a half LIM domains 2	-1.509	0.010
NM_025344	eukaryotic translation initiation factor 3, subunit F	-1.509	0.030
NM_031248	roadblock domain containing 3	-1.516	0.003
NM_025536	COMM domain containing 5	-1.524	0.006
NM_028633	similar to UCH37-interacting protein 1; HAUS augmin-like complex, subunit 7	-1.533	0.018
NM_054102	influenza virus NS1A binding protein	-1.535	0.024
NM_001038589	ubiquitin specific peptidase 14	-1.540	0.019
NM_001033293	UDP-N-acteylglucosamine pyrophosphorylase 1-like 1	-1.541	0.003
NM_001128601	5, 10-methenyltetrahydrofolate synthetase; predicted gene 2372; predicted gene 2382	-1.543	0.041
NM_023912	SCY1-like 1 (S. cerevisiae)	-1.544	0.004
NM_027188	SET and MYND domain containing 3	-1.548	0.011
NP_001192260	Microtubule-associated protein 4	-1.549	0.026
NM_053273	tweety homolog 2 (Drosophila); similar to tweety homolog 2	-1.555	0.007
NM_021473	aldo-keto reductase family 1, member A4 (aldehyde reductase)	-1.572	0.009
NM_024433	methylthioadenosine phosphorylase	-1.576	0.013
NM_145507	aspartyl-tRNA synthetase	-1.578	0.013
NM_011369	Shc SH2-domain binding protein 1	-1.586	0.022
NM_010239	ferritin heavy chain 1	-1.586	0.017
NM_207670	GRIP1 associated protein 1	-1.592	0.034
NM_021888	queuine tRNA-ribosyltransferase 1	-1.600	0.003
NM_011125	phospholipid transfer protein	-1.605	0.021
NM_138603	coiled-coil domain containing 22	-1.613	0.017
NM_007408	adipose differentiation related protein	-1.622	0.020
NM_183021	thyroid adenoma associated	-1.636	0.032
NP_058665	myeloid-associated differentiation marker	-1.642	0.005
NP_001107603	protein phosphatase 4, regulatory subunit 1	-1.674	0.007
NM_181348	RIKEN cDNA A230083H22 gene	-1.707	0.005
NM_011777	zyxin	-1.718	0.031
NM_026825	leucine rich repeat containing 16A	-1.753	0.007

Table 2-E: Differentially regulated CHO K1 proteins determined in samples corresponding to culture using spent media from CHO DP-12 cells prepared using media maintained at pH 7.2.

RefSeq Annotation	Description	Fold Change	P-Value
NM_029576	RAB1B, member RAS oncogene family	1.750	0.001
NM_198645	coiled-coil domain containing 58	1.721	0.005
NM_015782	predicted gene 8655; predicted gene 5145; predicted gene 8587; small nuclear ribonucleoprotein polypeptide A; predicted gene 5161	1.682	0.014

NM_010442	heme oxygenase (decycling) 1	1.670	0.006
NM_001033534	layilin	1.633	0.020
NM_145073	histone cluster 1, H3i; histone cluster 1, H3h; histone cluster 1, H3g; predicted gene 12260; histone cluster 1, H3a	1.606	0.002
NM_001136075	numb gene homolog (Drosophila)	1.604	0.046
NM_025562	fission 1 (mitochondrial outer membrane) homolog (yeast)	1.558	0.001
NM_010756	similar to mafG; v-maf musculoaponeurotic fibrosarcoma oncogene family, protein G (avian)	1.557	0.016
NM_133804	transmembrane protein 132A	1.554	0.033
NM_024166	coiled-coil-helix-coiled-coil-helix domain containing 2; predicted gene 13202; similar to coiled-coil-helix-coiled-coil-helix domain containing 2; predicted gene 12350	1.533	0.044
NM_025740	coiled-coil domain containing 104	1.519	0.014
NM_007639	CD1d1 antigen; CD1d2 antigen	1.516	0.048
NM_008416	Jun-B oncogene	1.516	0.042
NM_008097	glutaryl-Coenzyme A dehydrogenase	1.495	0.004
NM_010288	gap junction protein, alpha 1	1.483	0.002
NM_027430	brain protein 44; similar to brain protein 44; predicted gene 3982	1.478	0.014
NM_022310	heat shock protein 5	1.457	0.014
NM_053115	acyl-Coenzyme A oxidase 2, branched chain	1.413	0.009
NM_144800	metastasis suppressor 1	1.409	0.020
NM_139001	chondroitin sulfate proteoglycan 4	1.400	0.026
NM_010046	diacylglycerol O-acyltransferase 1	1.391	0.007
NM_178112	integrator complex subunit 8	1.389	0.037
NM_029437	cytoskeleton associated protein 5	1.388	0.012
NM_016786	ubiquitin-conjugating enzyme E2K (UBC1 homolog, yeast)	1.363	0.001
NM_007830	diazepam binding inhibitor	1.356	0.026
NM_010655	similar to ribosomal protein L38; predicted gene 13020; ribosomal protein L38; predicted gene 4991; karyopherin (importin) alpha 2; predicted gene 9028; predicted gene 8129; predicted gene 7123; predicted gene 5832; predicted gene 10184; predicted gene 73	1.336	0.011
NP_080965	mitochondrial ubiquitin ligase activator of NFKB 1	1.331	0.015
NM_010485	ELAV (embryonic lethal, abnormal vision, Drosophila)-like 1 (Hu antigen R)	1.323	0.024
NM_026573	reproductive homeobox 3B; UPF3 regulator of nonsense transcripts homolog B (yeast); reproductive homeobox 1; NFKB activating protein	1.320	0.013
NM_025833	BAI1-associated protein 2-like 1	1.317	0.025
NM_026009	coiled-coil domain containing 47	1.307	0.013
NM_175318	SPT2, Suppressor of Ty, domain containing 1 (S. cerevisiae)	1.303	0.001
NM_028876	transmembrane emp24 protein transport domain containing 5; similar to Transmembrane emp24 protein transport domain containing 5	1.300	0.006
NM_007451	solute carrier family 25 (mitochondrial carrier, adenine nucleotide translocator), member 5; similar to ADP/ATP translocase 2 (Adenine nucleotide translocator 2) (ANT 2) (ADP,ATP carrier protein 2) (Solute carrier family 25 member 5); predicted gene 5529;	1.287	0.027
NM_027307	golgi membrane protein 1	1.285	0.002
NM_019734	N-acylsphingosine amidohydrolase 1	1.283	0.005

NM_178772	arylacetamide deacetylase-like 1	1.283	0.005
NM_024452	leucine zipper protein 1	1.278	0.024
NM_010875	neural cell adhesion molecule 1	1.275	0.049
NM_001037166	predicted gene 4925	1.274	0.018
NM_172471	inter-alpha (globulin) inhibitor H5	1.273	0.019
NM_025994	similar to EF hand domain containing 2; EF hand domain containing 2	1.269	0.003
NM_026184	ERO1-like beta (S. cerevisiae)	1.269	0.017
NM_013771	YME1-like 1 (S. cerevisiae)	1.258	0.027
NM_001082961	small nuclear ribonucleoprotein N; SNRPN upstream reading frame; predicted gene 5802; similar to SNRPN upstream reading frame protein	1.258	0.018
NM_145605	kelch domain containing 4	1.251	0.008
NM_026487	ATPase family, AAA domain containing 1	1.246	0.034
NM_020000	mediator of RNA polymerase II transcription, subunit 8 homolog (yeast)	1.242	0.031
NP_083142	WD repeat domain 33	1.234	0.013
NM_010833	moesin	1.231	0.014
NM_175229	serine/arginine repetitive matrix 2; similar to Serine/arginine repetitive matrix protein 2; similar to retinitis pigmentosa GTPase regulator	1.228	0.009
NM_145706	nucleoporin 43	1.222	0.006
NM_023053	twisted gastrulation homolog 1 (Drosophila)	1.220	0.039
NM_021895	actinin alpha 4	1.208	0.001
NM_009101	Harvey rat sarcoma oncogene, subgroup R	1.208	0.005
NM_001033375	RIKEN cDNA A230046K03 gene	-1.208	0.007
NM_001038589	ubiquitin specific peptidase 14	-1.218	0.016
NM_009097	ribosomal protein S6 kinase polypeptide 1	-1.218	0.032
NM_019703	phosphofructokinase, platelet	-1.219	0.011
NM_172712	ubiquitin-like modifier activating enzyme 6	-1.219	0.050
NP_001157290	protein phosphatase 1, regulatory subunit 10	-1.225	0.026
NM_145925	pituitary tumor-transforming 1 interacting protein	-1.233	0.016
NM_008950	protease (prosome, macropain) 26S subunit, ATPase 5	-1.237	0.025
NM_152801	Rac/Cdc42 guanine nucleotide exchange factor (GEF) 6	-1.239	0.038
NM_011029	predicted gene 9323; predicted gene 7516; ribosomal protein SA pseudogene; predicted gene 9819; predicted gene 6339; predicted gene 9083; ribosomal protein SA; predicted gene 13374; predicted gene 12595; similar to laminin receptor 1 (ribosomal protein SA	-1.252	0.041
NM_178616	predicted gene 14048; proteasome (prosome, macropain) 26S subunit, non-ATPase, 11	-1.253	0.043
NM_008017	structural maintenance of chromosomes 2	-1.261	0.046
NM_019564	HtrA serine peptidase 1	-1.269	0.001
NM_001033300	guanine monphosphate synthetase; predicted gene 7282	-1.273	0.007
NM_009457	ubiquitin-like modifier activating enzyme 1	-1.287	0.002
NM_133823	methylmalonic aciduria (cobalamin deficiency) type A	-1.288	0.017
NM_175115	IKAROS family zinc finger 5	-1.292	0.028
NM_153116	GTP-binding protein 10 (putative); predicted gene 6877	-1.303	0.031
NM_009439	proteasome (prosome, macropain) 26S subunit, non-ATPase, 3	-1.314	0.020

NM_008567	minichromosome maintenance deficient 6 (MIS5 homolog, S. pombe) (S. cerevisiae)	-1.314	0.015
NM_080554	proteasome (prosome, macropain) 26S subunit, non-ATPase, 5	-1.317	0.048
NM_009462	ubiquitin specific peptidase 10	-1.335	0.006
NM_017380	septin 9	-1.337	0.007
NM_023248	Shwachman-Bodian-Diamond syndrome homolog (human)	-1.341	0.002
NM_025382	transmembrane protein 57	-1.342	0.016
NM_133786	structural maintenance of chromosomes 4	-1.344	0.006
NM_025706	TBC1 domain family, member 15	-1.348	0.002
NM_009794	calpain 2	-1.352	0.021
NM_030678	glycogen synthase 1, muscle	-1.352	0.030
NM_008481	laminin, alpha 2	-1.355	0.048
NM_175126	zinc finger, CCHC domain containing 3	-1.358	0.037
NM_019771	destrin	-1.368	0.015
NM_138584	spastic paraplegia 21 homolog (human); similar to spastic paraplegia 21 homolog	-1.369	0.038
NM_021523	HECT, UBA and WWE domain containing 1	-1.372	0.017
NM_146093	UBX domain protein 1	-1.380	0.012
NM_023871	predicted gene, EG625349; predicted gene 5789; predicted gene 7085; predicted gene 5708; predicted gene 6847; SET translocation; cDNA sequence BC085271; predicted gene 7239; similar to protein phosphatase 2A inhibitor-2 I-2PP2A; predicted gene 9531	-1.383	0.015
NM_177364	SH3 and PX domains 2B	-1.405	0.003
NM_173379	leprecan-like 1	-1.406	0.010
NM_018859	aldo-keto reductase family 1, member E1	-1.408	0.000
NM_009120	SAR1 gene homolog A (S. cerevisiae)	-1.421	0.019
NM_010220	FK506 binding protein 5	-1.423	0.005
NM_001033191	ARD1 homolog B (S. cerevisiae)	-1.429	0.009
NM_026277	NIN1/RPN12 binding protein 1 homolog (S. cerevisiae)	-1.430	0.040
NM_145564	F-box protein 21	-1.435	0.023
NM_008708	N-myristoyltransferase 2	-1.438	0.042
NM_007388	acid phosphatase 5, tartrate resistant	-1.441	0.038
NM_026969	Sec31 homolog A (S. cerevisiae)	-1.448	0.028
NM_015765	heat shock protein 14	-1.466	0.002
NM_025864	transmembrane protein 206	-1.478	0.029
NM_010239	ferritin heavy chain 1	-1.486	0.007
NM_001077687	LPS-responsive beige-like anchor	-1.489	0.018
NM_013472	annexin A6	-1.491	0.010
NM_146041	GDP-mannose 4, 6-dehydratase	-1.492	0.003
NM_001166024	ADP-ribosylation factor GTPase activating protein 2	-1.496	0.024
NM_029005	mixed lineage kinase domain-like	-1.511	0.041
NM_016710	predicted gene 11914; nucleosome binding protein 1	-1.526	0.004
NM_029839	TruB pseudouridine (psi) synthase homolog 1 (E. coli)	-1.543	0.002
NM_145836	similar to polyglutamine-containing protein; RIKEN cDNA 6430527G18 gene	-1.549	0.022
NM_028152	MMS19 (MET18 S. cerevisiae)	-1.562	0.014
NM_001045528	FK506 binding protein 15	-1.596	0.009

NP_733469	copine I	-1.596	0.030
NM_178726	protein phosphatase 1 (formerly 2C)-like	-1.602	0.018
NM_021354	hypothetical protein LOC674305; predicted gene 8918; developmentally regulated GTP binding protein 2	-1.623	0.001
NM_001164559	TRM1 tRNA methyltransferase 1 homolog (S. cerevisiae)	-1.669	0.028
NM_025692	ubiquitin-like modifier activating enzyme 5	-1.689	0.025

Table 2-F: Differentially regulated CHO K1 proteins determined in samples corresponding to culture using spent media from CHO DP-12 cells prepared using media maintained at pH 6.8.

RefSeq Annotation	Description	Fold Change	p-value
NM_010708	lectin, galactose binding, soluble 9	1.663	0.027
NM_138589	ubiquitin family domain containing 1	1.650	0.048
NM_133775	interleukin 33	1.648	0.006
NM_001081218	host cell factor C2	1.648	0.008
NM_025740	coiled-coil domain containing 104	1.589	0.038
NM_009242	secreted acidic cysteine rich glycoprotein; similar to Secreted acidic cysteine rich glycoprotein	1.520	0.027
NM_133804	transmembrane protein 132A	1.512	0.041
NM_011127	paired related homeobox 1	1.485	0.002
NM_013558	heat shock protein 1B; heat shock protein 1A; heat shock protein 1-like	1.465	0.007
NM_023232	diablo homolog (Drosophila)	1.458	0.028
NM_001033534	layilin	1.456	0.039
NM_011961	procollagen lysine, 2-oxoglutarate 5-dioxygenase 2	1.443	0.003
NM_009811	caspase 6	1.406	0.036
NM_177068	olfactomedin-like 2B	1.392	0.028
NM_010302	guanine nucleotide binding protein, alpha 12; similar to Guanine nucleotide-binding protein alpha-12 subunit (G alpha-12)	1.390	0.006
NP_080965	mitochondrial ubiquitin ligase activator of NFKB 1	1.386	0.001
NM_031185	A kinase (PRKA) anchor protein (gravin) 12	1.371	0.037
NM_027373	actin filament associated protein 1	1.307	0.026
NM_026267	NECAP endocytosis associated 1	1.296	0.027
NM_011862	protein kinase C and casein kinase substrate in neurons 2	1.295	0.045
NM_015782	predicted gene 8655; predicted gene 5145; predicted gene 8587; small nuclear ribonucleoprotein polypeptide A; predicted gene 5161	1.292	0.005
NM_016706	RIKEN cDNA 2210409E12 gene; coilin	1.288	0.019
NM_026184	ERO1-like beta (S. cerevisiae)	1.282	0.003
NM_007803	cortactin; predicted gene 8786	1.277	0.036
NM_026623	nudix (nucleoside diphosphate linked moiety X)-type motif 21	1.259	0.026
NM_010288	gap junction protein, alpha 1	1.256	0.034
NM_021493	RIKEN cDNA 4933428G20 gene	1.216	0.039
NM_207625	acyl-CoA synthetase long-chain family member 4	1.209	0.012
NP_001156986	exostoses (multiple)-like 2	1.201	0.023

NM_134037	ATP citrate lyase	-1.205	0.008
NM_008388	eukaryotic translation initiation factor 3, subunit E	-1.231	0.014
NP_001159610	armadillo repeat containing 8	-1.238	0.045
NM_008017	structural maintenance of chromosomes 2	-1.242	0.037
NM_008788	procollagen C-endopeptidase enhancer protein	-1.256	0.017
NM_027375	GRIP and coiled-coil domain containing 2	-1.311	0.014
NM_183016	CDC42 binding protein kinase beta	-1.315	0.003
XP_483949	predicted gene 6807; predicted gene 6136; predicted gene 6883; predicted gene 5428; similar to ribosomal protein L6; predicted gene 5247; ribosomal protein L6	-1.333	0.038
NM_001004436	wings apart-like homolog (Drosophila)	-1.337	0.014
NM_017380	septin 9	-1.338	0.002
NP_705782	aldehyde dehydrogenase 18 family, member A1	-1.339	0.036
NM_133786	structural maintenance of chromosomes 4	-1.342	0.007
NM_001081122	centrosomal protein 63	-1.346	0.020
NM_001015507	Vpr (HIV-1) binding protein	-1.347	0.017
NM_015765	heat shock protein 14	-1.353	0.025
NM_001033231	cDNA sequence BC003940	-1.417	0.031
NM_012053	ribosomal protein L8; similar to 60S ribosomal protein L8	-1.427	0.001
NM_011125	phospholipid transfer protein	-1.436	0.050
NM_001037166	predicted gene 4925	-1.453	0.038
NM_008605	matrix metallopeptidase 12	-1.466	0.005
NM_177884	expressed sequence AW146020	-1.508	0.035
NM_021354	hypothetical protein LOC674305; predicted gene 8918; developmentally regulated GTP binding protein 2	-1.536	0.003
NM_009120	SAR1 gene homolog A (S. cerevisiae)	-1.538	0.033
NM_145925	pituitary tumor-transforming 1 interacting protein	-1.541	0.020
NM_175294	nuclear casein kinase and cyclin-dependent kinase substrate 1	-1.548	0.001
NM_026539	chromodomain helicase DNA binding protein 1-like	-1.582	0.042
NM_145836	similar to polyglutamine-containing protein; RIKEN cDNA 6430527G18 gene	-1.685	0.014
NM_138315	microtubule associated monoxygenase, calponin and LIM domain containing 1	-1.726	0.044